"THE CRYSTAL STRUCTURE OF LAYER SILICATE MINERALS"

E.W. Radoslovich M.Sc.(Adel.), Ph.D.(Cambridge)

being a thesis submitted in fulfilment of the requirements for the degree of Doctor of Science in the University of Adelaide.

May 1967.

CONTENTS

2 - 3 "Surface symmetry and cell dimensions of layer silicates".

2 - 4 "Cell dimensions and inter-atomic forces in layer silicates".

2 - 5 "Some structural considerations".

2 - 6 "Regression relations".

2 - 7 "Octahedral ordering".

2 - 8 "Interatomic forces".

2 - 9 "Composition limits".

2 - 10 "Serpentine and kaolin morphology".

2 - 11 "Cell dimension studies on layer silicates".

2 - 12 "Some relations between composition, cell dimensions and structure of layer silicates".

2 - 13 Micas and Soil Science.

Part III. Supporting papers in X-ray crystallography, diffraction and spectrography.

3 - 1 "A geometrical construction in reciprocal space".

3 - 2 "Calculation of geometrical structure factors. I."

3 - 3 "Calculation of geometrical structure factors. II."

3 - 4 "Calculation of geometrical structure factors. III."

3 - 5 "The structure of anorthite, $CaAl_2Si_2O_8$. I. Structure analysis".

3 - 6 "The structure of anorthite. II. Description and discussion."

3 - 7 "X-ray studies of the alteration of soda felspar".

3 - 8 "Effect of biotite on the firing characteristics of weathered schists".

3 - 9 "Clay mineralogy of some Australian red-brown earths".

3 - 10 "A curved-crystal fluorescence X-ray spectrograph".

3 - 11 Felspars and Soil Science.

ACKNOWLEDGEMENTS

The published and unpublished papers presented in this D.Sc. thesis have been the author's own original work, except where the collaboration or assistance of others is explicitly acknowledged in the papers themselves. None of the work submitted in Parts I and II has been presented for any other degree. Two of the supporting papers in Part III, however, contain some such work. Paper 3-10 represents the development, jointly with K. Norrish, of the work on the fluorescent X-ray spectrograph originally submitted for my M.Sc. Paper 3-5 represents a considerable extension, mainly by Helen D. Megaw and C.J.E. Kempster of my original Ph.D. thesis work on the crystal structure of anorthite; paper 3-6, however, does not include any material which was part of my Ph.D. thesis.

It is a pleasure to record that the main part of this work (especially Parts I and II) has been carried out as part of the general research program of the Division of Soils, Commonwealth Scientific and Industrial Research Organisation. For this reason the author is sincerely indebted to a number of

C.S.I.R.O. colleagues for stimulating discussion and constructive criticism. In particular Dr. K. Norrish (Division of Soils, C.S.I.R.O.) and Mr. L.G. Veitch (Division of Mathematical Statistics, C.S.I.R.O.) not only shared joint authorship of papers 2-5 and 2-7 but were generous in discussion and criticism of related ideas as these developed. Their contribution is gratefully acknowledged at this point, whilst at the same time it is emphasised that the over-riding responsibility for the initiation and for the continued planning and development of this field of research has been entirely the author's own.

(Signed) E.W. Radoslovich.

SUMMARY

Three detailed determinations of the crystal structures of mica minerals have clearly shown that future studies of this kind on layer silicates should only be based on experimental X-ray data of high accuracy, analysed by large-scale high-speed computing facilities. The first of these studies led to a critical review of the currently accepted ideas about the crystal structures of layer silicates. After re-assessing in an empirical way the relative importance of various forces within these minerals it became possible to predict structural details with considerable confidence, simply on the basis of chemical composition and unit cell dimensions, i.e. by using data which are relatively easily obtained. Furthermore it has been possible to postulate some sensible limiting conditions for certain common structural configurations, and to examine whether these limits are compatible or coincident with independent data, e.g. the observed range of chemical composition for naturally-occurring specimens of a given mineral species. Some accepted ideas about physical properties such as micro-morphology have also been shown to require at least substantial modification and/or re-investigation.

Finally, this kind of critical review of a large group of related minerals whose structures can be predicted in detail allows the experienced crystallographer to make a much better choice of those individual structures most worthy of precise and detailed analysis in the future.

This study has been important because it has demonstrated very thoroughly, and possibly for the first time, just how much can be gained by studying a wide group of related minerals, bearing in mind the reasonably expected limits to given interatomic distances and angles for structural units and groups such as silica tetrahedra, aluminium octahedra etc. At the same time the rather rigid models previously developed for these mineral structures have been replaced by more dynamic models in which the overall adjustments to specific internal changes (such as an isomorphous substitution) may be taken into account. The result is that our crystallographic ideas about layer silicates are now far more realistic, and hence more useful in other studies.

PREFACE.

The two main objectives of almost all of the research work described in the papers submitted in this thesis have been the determination of the crystal structures of layer silicate minerals with progressively increased precision, together with such further interpretation of known physical and chemical properties of these minerals as this increased crystallographic insight may allow. To assess the merit of an individual author's contribution to this field it is necessary to ask several questions, such as the following. Why should we study layer silicate minerals? What kind of information about these minerals should structure analysis yield? What was the status of the subject when these particular studies began, what were the inherent difficulties then, and how much has this area of knowledge advanced? What new general ideas and what shifts of emphasis in understanding has the author given which others in this field recognise as important forward steps?

The purpose of this preface is to discuss questions of this kind briefly, and in general terms, for the whole of the research work in this thesis. The introductory statements at the beginning of each of the

three main parts then attempt to summarise the particular place of the separate papers.

The layer silicate minerals include a wide range of very commonly occurring minerals which are of great importance both in modern agricultural and industrial technology, and in a number of areas of fundamental geological and geochemical studies. They include the "clay minerals" which are (by agreed definition) less than two microns in effective particle diameter. These are inherently highly reactive because of their enormous surface area, and especially because many "internal" surfaces are available for physico-chemical reactions, as a result of their structural crystallography. That is, the clay mineral structures can be modified to a very considerable extent, either consciously by the technologist (e.g. in processing clays for use as catalysts in oil refining), or unconsciously as in any agricultural management of soils with high cation exchange capacities. Whilst many advances in the manipulation of these minerals have been made semi-empirically it has become clear in recent years that major long-term advances will require a detailed

knowledge of their crystal chemistry (especially of their surfaces).

In the more fundamental areas of geology a detailed knowledge of the layer silicate crystal structures is rapidly becoming essential to the further progress of other studies. These minerals, together with the closely related fibrous and framework silicates, are most important components of all kinds of rock systems. To any geologist studying the phase relations, the pressure-temperature-composition limits of stability fields, or the partition of various elements between different minerals in alteration zones, a reliable knowledge of the strong and weak forces within the crystal structures may help greatly in explaining experimental results. This is particularly true for studies of mineral transformations, and of the relative ease with which different transformations occur. Furthermore, the layer silicates are late-stage products of geological weathering processes, and an adequate understanding of such processes will eventually require real insight into their structural crystallography - e.g. how do the atomic structures of these minerals protect them against further rapid degradation?

What, then, is the specific information to be sought through a detailed crystal structure analysis of selected layer silicates, and what is its application? As a first step the general pattern of atomic arrangements may be discovered, and this was in fact the situation when my researches began early in 1956. For this step a limited amount of poor X-ray data, very modest calculating facilities and a high order of creative imagination were the prerequisites. These pioneering studies by men such as Bragg, Pauling, Jackson and West, Hendricks and others left us with rather formal "idealised geometrical models" of these structures, in which for example the surface networks of oxygen anions were neatly hexagonal. Whilst these simple models were sufficient to explain gross properties such as tabular morphology they were, in 1956, widely recognized as inadequate for most current research problems. An increasing number of people wished to know the actual values of the interatomic distances, with meaningful precision, as a measure of the nature and strength of the interatomic forces within these minerals. The variations in bond angles and the extent to which interatomic bonds are "directed bonds"; the nature and amount of long-range and short-range

order, especially in cation sites subject to isomorphous substitution; the presence and effectiveness of hydrogen bonds, especially at interfaces in these structures where no other bonds appear to play a part; the extent of local charge balance; the relationships of cell dimensions to chemistry, polymorphic type, pressure and temperature of formation; the effective co-ordination around large cations; the accessibility of large cations to chemical leaching; the manner of attachment of organic molecules when these form clay-organic complexes on "internal" surfaces; the explanation of some infra-red absorption results in terms of internal modes of vibrational freedom; the nature of the forces controlling polymorphism in layer silicates -- these were among the questions posed which a serious program of structure analysis of layer silicates should attempt to answer.

When this work was begun seriously, early in 1956, the amount of precise structural data about layer silicates in the literature was very limited indeed, and <u>detailed</u> structural ideas over the whole mineral group were almost non-existent. This is shown, for example, by a quick review of the detailed structural information presented in the definitive monograph, "X-ray Identification

and Crystal Structures of Clay Minerals" (Second Edition) published in 1961 by the Mineralogical Society, London, and edited by G. Brown. (The available literature is, of course, also reviewed in Paper 1 - 1 of this thesis.) By contrast G. Brown has contributed an Invited Review paper to Clay Minerals, vol. 6, 73, 1965 on the "Significance of Recent Structure Determinations of Layer Silicates for Clay Studies" which begins :-

> "In the last 10 years or so much work has been done to determine the crystal structures of layer silicates more precisely than previously and, as a result, ideas about these structures have had to be revised".

It is claimed in this thesis that the author's accurate re-determination of the muscovite structure (and particularly my discussion of the results of that analysis) provided a major impetus for this overall change. Furthermore the author's subsequent development of ideas about the controlling forces within layer silicates has quite clearly influenced many of the crystallographers involved in more recent accurate structure analyses of other key layer silicates. As Brown (1965) has put it :- "Despite limitations caused by too few structure determinations, Radoslovich's

work has gone a considerable way to providing a new general model for layer silicates". Brown goes on at this point to discuss the further development of "a prediction model" for one-layer trioctahedral micas by Donnay et al (1964). In the present context it is interesting to note that during my stay at the Geophysical Laboratory, Washington, in 1962-63 I discussed the progress of the ferriannite structure extensively with Prof. J.D.H. Donnay and Dr.G. Donnay (who is on the staff of the Geophysical Laboratory). These discussions centred around my recent predictions about the details of the ferriannite structure (see, e.g. Paper 2-5); and the Donnays' subsequent development of their own prediction formula arose directly from these discussions with me.

This, then, emphasises the claim that the research work submitted in this thesis has made a major contribution by defining very much more clearly the goals of present and future structure analyses of layer silicates. The critical questions still to be resolved have been delineated in a new way, and attention has been drawn to the structure determinations most likely to provide unambiguous solutions to these problems. It is

particularly this element of forward prediction -- already amply confirmed in many details -- about structures and/or cell dimensions (or variations in cell dimensions, with changing conditions) which has, in the writer's opinion, been a significant contribution. Implicit in my approach, too, has been the abandonment of relatively rigid geometrical models, and the preparedness to think about each layer silicate structure in detail in a more dynamic way than has previously been possible. Whilst this is hardly new to crystallography as a whole the very recent clay mineral literature does suggest that this new freedom of thought (as developed in Parts I and II) has made a considerable impact. Brown's (1965) Review Paper enlarges on this, and this is developed a little further in the introductions to individual papers in this thesis.

This work can only be set properly in perspective if the current state and rate of development of X-ray crystallography is also borne in mind. Due primarily to the impact of electronic digital computers and of sophisticated single crystal goniometers (with solid state counting equipment) the whole art of structure analysis has been (and still is) making very rapid progress. But this development is very recent.

Papers 3-5 and 3-6 amply illustrate that leading laboratories such as the Crystallographic Laboratory, Cavendish Laboratory, Cambridge, were -- as late as 1955 -- still using visual photographic techniques and a low-powered, half-Hollerith, half-EDSAC computer system for very complex mineral structures. (This, indeed, is the reason for Papers 3-2, 3-3 and 3-4 which would hardly have been written at all, even three years later!) In 1956, however, and especially in Australia, it was a large undertaking to commence a structure analysis such as that in Paper 1-1. The major practical difficulty centred around computing which must either be done at a large distance by correspondence (e.g. on SILLIAC), or on digital computers such as WREDAC to which access was severely restricted for security reasons, and for which we had extremely low priority of use, and lacked any general symbolic language to allow the crystallographer to write his own programs. For all major calculations -- structure factors, Fourier synthesis, least squares analysis, function and error problems etc. -- there were severe limitations either of computer speed or memory capacity, or of specialised and limited programs

generally written in two-dimensions for certain space-groups only. The contrast between the accuracy of the results in Paper 1-1 with those in Papers 1-2 and 1-3 is quite striking for this reason; and it is not altogether surprising that some errors were eventually found in the published results in Paper 1-1 (see Paper 1-3).

My previous experience with the felspar, anorthite (Papers 3-5 and 3-6), had convinced me that at least partially three-dimensional methods (such as bounded Fourier projections) would be needed to ensure that a refinement of layer silicate structures at this time would yield significant new information and ideas. This was essential in order to resolve all atoms clearly, and to increase the accuracy of the positional parameters to the point where, for example, it might be meaningful to look for Si-Al ordering tetrahedrally on the basis of differences in measured bond lengths. Papers 1-2 and 1-3 again emphasise this, and also point out the importance of detailed and reliable information about the vibrational parameters in layer silicates. This view of the structure analysis of layer silicates was not then generally held (e.g. Paper 1-5) but has been fully vindicated by the most recent work in this field.

One other development of modest account in the papers presented, but of great future importance, is the application of microchemical analytical techniques to small single crystals. In Papers 1-2 and 1-3 the actual single crystal studied, or a very closely adjacent crystal, was examined by X-ray microprobe analysis for Na and K content. In any future crystallographic studies on layer silicates concerned with bond lengths, cation ordering, structural defects, substitutional disorder and the like, elemental microprobe results should be obtained, if possible on the crystal used for structural studies, at least for those elements of particular interest.

This preface should, perhaps, conclude with a review of the current status of layer silicate structure analysis, but since this topic is rather large I have simply included Paper 2-13, which is in fact an invited article for the new "Handbuck der Bodenkunde", yet to be published. This paper summarises current structure analyses on micas, and of course briefly alludes to similar work on other layer silicates.

PART I. CRYSTAL STRUCTURES OF MICACEOUS MINERALS.

In beginning a program of crystallographic research on layer silicates within the Division of Soils, C.S.I.R.O., the choice of minerals studied reflects both the interests of this Division and the relative scientific merit and feasibility for study of various minerals. This Division has had a long-standing interest in the micaceous clay minerals, including illites deficient in structural potassium, a problem in which I had already been involved (Paper 3-9). Furthermore the micas had at least been studied in the 1930's, and they are of very widespread academic and applied-technological interest. Finally, it seemed likely that suitable crystals of different micas could be obtained in Adelaide more easily than of minerals from any other layer silicate group.

The number of mica structures analysed since 1956 has been disappointingly small. Nevertheless our understanding of these has now made it pointless to continue with structure analyses of micas without first-class computing and single-crystal goniometer facilities. The former have recently become available and I have now checked out a network of interlinked

programs; it is hoped that new research funds will soon allow the purchase of the counter-goniometer necessary to improve the experimental data.

Paper 1-1. "The structure of muscovite, $KAl_2(Si_3Al)O_{10}(OH)_2$"

E.W. Radoslovich

This paper already has been cited frequently in a wide variety of studies published by other scientists, so that it appears to have become a prime reference in this field. As far as the author himself can judge there are several reasons for this. In the first place this was one of the earliest "precise" structure analyses on a layer silicate; at publication Mathieson's refinement of vermiculite was the only comparable precise study. But whereas Dr. Mathieson (quite rightly) was pre-occupied with the interlayer-water region in vermiculite, the attention in the muscovite analysis is focussed on the nature of the layers themselves. Each part of the structure was looked at critically (including such well-accepted "facts" as the supposed twelve-fold co-ordination of interlayer potassium). This fresh look at micas

showed that no part of the simple model for these minerals is inviolate to adjustment in the real structures, and it seems fair to say that this helped considerably to trigger off the spate of structure determinations now in progress on layer silicates.

The whole analysis clearly demonstrated the need for precise structural information to clarify our ideas, the need for accurate experimental data (even for scattering factors, or for cell dimensions or for tests for centrosymmetry), and the value for all clay studies of some key structure analyses in this group.

Papers 1-2 and 1-3. "Refinement of the crystal structures of coexisting muscovite and paragonite".

Charles W. Burnham and E.W. Radoslovich

There have, at the present time, been very few structure analyses of complex silicates reported in which the final precision in both the positional and thermal parameters has been better. This alone marks these as notable papers because of the wide current interest in highly refined bond lengths and bond angles for the silicate minerals (e.g. see J.V. Smith and S.W. Bailey, Acta Cryst. 16, 801, 1963). Secondly there is the

important innovation that two coexisting minerals have been studied simultaneously which have very similar structures, and which have occurred naturally in apparent equilibrium with each other chemically. This has provided a unique opportunity to study the structural effects of isomorphous replacement, and to attempt to relate closely accurate crystallographic information and detailed knowledge of the asymmetric curve of solid-solution versus temperature of quenching.

This work was begun entirely on my initiative, and it was my recent general studies (Papers 2-3 to 2-12) which clearly defined the problems to be answered. It was also my decision to proceed with both structural analyses when it was discovered, fortuitously, that good crystals of both minerals had been successfully oriented on the goniometer. On the other hand the experimental methods were Dr. Burnham's, since one purpose of my visit to the Geophysical Laboratory was to learn these -- though I personally performed all the experimental work up to and including the final measurement of intensities.

At that stage my sabbatical leave expired, and Dr. Burnham then offered to continue immediately with the computational analysis of the data. He had not

previously been involved in the analysis of layer silicate structures, but he and I had discussed the problems associated with them extensively during my preliminary work on muscovite and paragonite. Furthermore Dr. Burnham already had the necessary computer programs operational, whereas C.S.I.R.O. was only then calling tenders for its own computer network. The refinement of the raw data and the writing of the first drafts of these papers was therefore done entirely by Dr. Burnham in Washington.

Paper 1-4. "Transparent packing models of layer-lattice silicates based on the observed structure of muscovite"

E.W. Radoslovich and J.B. Jones.

Whilst the construction of easily understood and fairly realistic models is desirable for teaching purposes the real point of this short paper is to reinforce visually for research workers in clay mineralogy some of the new and more subtle features of the mica structures. For this purpose Figs. 2 and 4 are quite striking. The paper does also show how our whole thinking about three-dimensional structures is

conditioned by the models -- actual, mathematical and mental -- which we customarily use. The subsequent papers in Part II grew out of the efforts put in to making the packing model described here.

The models were made on the initiative of Dr. J.B. Jones (because of his teaching responsibilities) and he provided the technician and workshop facilities. The ideas for the jigs were my own, however.

Paper 1-5. "Accuracy in structure analysis of layer silicates".

A.L. Mathieson, E.W. Radoslovich and G.F. Walker.

Dr. Steinfink's papers (which triggered off this warning note) were published during the final stages of the muscovite analysis. Some of his conclusions and deductions were so obviously at variance with my own developing ideas that I sought Dr. Mathieson's advice and discussed the points of disagreement with him extensively. Paper 1-5 was, however, primarily drafted by Mathieson from that point onwards.

Ironically enough, my own subsequent difficulties with the muscovite data (Gatineau, Bull. Soc. Frac.Mineral.Crist. 87(3), 321, 1964) illustrate still further the main point of the present note!

PART II. SOME GENERALISATIONS ABOUT THE STRUCTURES AND PROPERTIES OF OTHER LAYER SILICATES.

Chronologically this work followed directly on from my analysis of muscovite, and in fact some of Part II is fore-shadowed in the discussion section of Paper 1 - 1. One of the less scientific reasons for this development was the sheer frustration and slowness of the muscovite analysis under the current conditions of computing. Moreover the total body of relevant knowledge had increased to the point where a first attempt could be made at an analysis and synthesis of new ideas about the whole family of layer silicate structures. Finally, any continuation of a research program in layer silicates demanded that the next several minerals chosen for a full structure analysis should offer the highest potential return of significant new information for the considerable efforts expended — and this required thought about which features of which structures should depart most obviously from the general model for layer silicates. The subject grew rather unexpectedly from this point, however.

Paper 2-1. "Structural control of polymorphism in micas."

E.W. Radoslovich.

This is simply a short note about an inspired guess on a problem which had bothered many people for a long time. However, the hypothesis has been very amply borne out by a large amount of recent work (e.g. Ross, Takeda and Wones; Science, 151, 191, 1966).

Paper 2-2. "Hydromuscovite with the $2M_2$ structure -- a criticism."

E.W. Radoslovich.

A short exercise in the application of the developing ideas; Dr. Threadgold accepted the criticism as a valid one. The close similarity of the relevant powder data made it difficult for Threadgold to avoid this apparent mis-identification without some more general principles about what to expect amongst mica polymorphs.

Paper 2-3. "Surface symmetry and cell dimensions in layer lattice silicates."

E.W. Radoslovich.

A bare statement of new ideas, partly to establish priority in a rapidly developing field.

Paper 2-4. "Cell dimensions and interatomic forces in layer lattice silicates".

E.W. Radoslovich.

A bare statement of new ideas, partly to establish priority in a rapidly developing field.

Paper 2-5. "The cell dimensions and symmetry of layer lattice silicates. I. Some structural considerations".

E.W. Radoslovich and K. Norrish.

In retrospect this paper seems quite simple and straightforward. At the time, however, it represented a radical departure from most current thinking in which the ideas of regular geometrical arrangements and of unrelieved misfit between the tetrahedral and octahedral dimensions were strongly entrenched. We were not, of course, the first to suggest that the tetrahedral groups may articulate in some way to accommodate any natural misfit. Our claim is that in Paper 2-5 the structural basis for these ideas is much more thoroughly developed, and the supporting facts more adequately marshalled than by any earlier authors. Furthermore we were not discussing just a particular mineral (or small number of minerals) but our arguments were

extended logically to the whole field of layer silicates, including those of "extreme" composition, or "anomalous" cell dimensions. When we developed the use of multiple regression analysis for this purpose I was unaware of Hey's use of this technique to study certain physical properties of chlorites. Indeed it may be claimed that this statistical technique has (in Papers 2-5, 2-6 and 2-7) been applied so thoroughly that this in itself is a noteworthy innovation in structural mineralogy. This approach has given considerable confidence in explaining a large number of apparent anomalies, and indeed in predicting, confirming and explaining anomalies of which others were previously unaware. More recently others have successfully used the same general predictions to explain dynamic changes occurring during laboratory studies such as heat treatments, hydrothermal synthesis or chemical weathering. This same new outlook on the "structural model" also showed some matters to be more subtle than they were previously believed to be, e.g. the "prohibited" 061, 1 odd reflections in dioctahedral micas.

Dr. Norrish is the co-author of this paper because he and I had discussed these problems

increasingly enthusiastically during the drafting of Paper 1-1, so that it became impossible clearly to assign the ultimate responsibility for any new ideas. The prime initiative in this field, however, was my own throughout Papers 2-5 to 2-12, and indeed Dr. Norrish went overseas on sabbatical leave before Paper 2-5 was properly drafted.

Paper 2-6. "The cell dimensions and symmetry of layer-lattice silicates. II. Regression relations."

E.W. Radoslovich.

This is a detailed outworking of the ideas in Paper 2-5. It is a significant publication because it provides the best available practical formulae connecting structural chemical formulae and cell dimensions, and also because it enhances our understanding of the physical realities behind these empirical formulae.

Paper 2-7. "The cell dimensions and symmetry of layer-lattice silicates.
II. Octahedral ordering".

L.G. Veitch and E.W. Radoslovich.

I had developed a "hunch" that the cations in the octahedral layers of these minerals would very

generally be found to be crystallographically ordered. This paper is an attempt to validate this hunch statistically, ahead of individual structure analyses. The attempt failed in the rigorous statistical sense, though the hypothesis of octahedral ordering is now being substantiated by recent structure analyses. However Paper 2-7 serves two purposes, firstly of showing how -- with more adequate data of a simple kind -- general crystallographic ideas may be able to be tested over whole mineral groups; and secondly, of drawing out very explicitly the separate components of the physical model (for the octahedral layers) which clay mineralogists had accepted uncritically so far. This led quite directly to Paper 2-8.

Mr. Veitch is justifiably senior author. The initiative for the analysis was mine, since Mr. Veitch is a statistician who knew nothing of the chemical crystallography of layer silicates; and as the analysis developed I had continually to try to relate the results to some physically sensible situation. But the enterprise is trying to extract by statistics the confirmation of the hypothesis, and the clear delineation of the geometrical assumptions in our model is entirely due to my co-author.

Papers 2-6 and 2-7 unified our ideas on "b-axis formulae", e.g. by showing how the base constant is almost identical for all groups of minerals, and that Li does fit into the general pattern if rightly understood. Paper 2-7 also led to some real understanding, for the first time, of the several factors which control the c-axis dimension in these minerals -- previously there seemed to be little orderliness in the way this dimension changed with composition.

Paper 2-8. "The cell dimensions and symmetry of layer-lattice silicates.
IV. Interatomic forces".
E.W. Radoslovich.

Paper 2-8 was written using an admittedly empirical and pragmatic approach to the discussion of interatomic forces in layer silicates. In my view any more sophisticated development (e.g. using ligand field theory) would be totally unjustified in terms of the quality and quantity of available data -- in fact it would probably be impossible at present. On the other hand a clear statement or restatement of the principles on which sensible approximate guesses may

be made about the relative strength of different forces in these structures has undoubtedly been useful -- even if the forces themselves are not altogether understood in detail.

In retrospect some errors have occurred in this paper, especially when the bond-length data have knowingly been "interpreted" well beyond the points allowed by their inherent inaccuracies. This simply bears out the several warnings that this was a first attempt at such an analysis, and reiterates the need for future precise structure analyses.

I believe that the importance of Paper 2-8 lies in the way in which I drew attention to the detailed variations in observed values of bond-lengths and bond-angles, and to departures from regularity of ionic groups such as tetrahedra and octahedra. These departures are only partly due to random experimental errors, and there should be increasing attempts at their interpretation as the structural data for these minerals becomes more precise. Many of the observed physical properties of most interest are related to structural detail of this kind. For this reason Paper 2-8 is probably a rather pioneering effort to carry modern structural clay mineralogy beyond the prosaically descriptive stage.

Paper 2-9. "The cell dimensions and symmetry of layer-lattice silicates.
V. Composition limits."
E.W. Radoslovich.

As with Paper 2-8 this is a departure from the usual kinds of crystallographic or mineralogical studies. It is true that others have speculated that given minerals are unstable because of some obvious strains in their structure. I am not aware, however, of any other extensive study which attempts to relate observed composition limits to some postulated limits of adjustments, structurally, in the way that Paper 2-9 has done over a major group of minerals. Yet surely our observational knowledge of composition limits -- either naturally or synthetically -- must eventually be found compatible with our structural insight. Already Paper 2-9 has been surprisingly successful in confirming or predicting limits of compatibility between composition and structure for the layer silicates -- despite the crude and inadequate data on which it had to be based.

Paper 2 - 10. "The cell dimensions and symmetry of layer-lattice silicates.
VI. Serpentine and kaolin morphology."
E.W. Radoslovich.

This brief paper simply challenges the basic ideas on which the current explanations of tubular morphology are based. The discovery of other morphological forms (such as tabular halloysite) more recently appears to confirm that the published explanations prior to Paper 2 - 10 are at least inadequate, if not strongly suspect.

Paper 2 - 11. "Cell dimension studies on layer-lattices silicates : A summary."
E.W. Radoslovich.

A review of the work in Papers 2 - 1 to 2 - 10 delivered orally as the main paper of the general session of the Eleventh Clay Conference, Ottawa. Most of the material in Paper 2 - 11 was "in press" at the date of the Conference.

Paper 2-12. "Some relations between composition, cell dimensions and structure of layer silicates."
E.W. Radoslovich.

This was the invited lead-paper in "Section 1. Clay mineral structures and compositions" of the International Clay Conference, Stockholm, 1963; it was apparently very well received.

Paper 2-13. "Micas" E.W. Radoslovich.

This is an invited article for the new "Encyclopedia of Soil Science" now in preparation by Springer-Verlag, Berlin. The article of course is directed towards soil scientists and their needs rather than structural crystallographers or mineralogists.

PART III. SUPPORTING PAPERS IN X-RAY CRYSTALLOGRAPHY, DIFFRACTION AND SPECTROGRAPHY.

This group of papers covers other work carried out by the author in fields relating either to the use of X-rays in scientific investigations, or to the structure analysis of silicate minerals. In addition to showing the general competence and experience of the author as an independent investigator some of these papers describe work which formed an essential foundation of experience and skill on which to base the main work of this thesis found in Parts I and II.

Paper 3-1. "A construction giving the projection of the point h00 on the 0kl plane in reciprocal space for non-orthogonal axes."
E.W. Radoslovich.

A time-saving device when working with triclinic crystals.

Paper 3-2. "Calculation of geometrical structure factors for space groups of low symmetry. I. "

E.W. Radoslovich and (in part) Helen D. Megaw.

This little aid to crystallographic calculations done by hand speeded these up very considerably. It was,

in fact, manufactured commercially in small numbers by Crystal Structures Ltd., Cambridge. Its main "fault" lay in being too late, historically, in that shortly after it was designed the large all-purpose electronic digital computer started to become available to most crystallographers. In simplicity and flexibility of use it had many advantages over other similar devices.

Paper 3-3. "Calculations of geometrical structure factors for space groups of low symmetry. II.

E.W. Radoslovich.

This extension of the previous device was not really a success. It lacked the extreme simplicity and cheapness of construction and could not compete with the incoming digital computers. It is, however, probably fair to say that it would have been extensively used if it had preceded digital computers by another ten years.

Paper 3-4. "Calculation of geometrical structure factors for space groups of low symmetry. III."

E.W. Radoslovich.

This further development of the device described in Paper 3-2 does represent a highly useful accessory to any crystallographer who uses hand-calculation and desk calculating machines for triclinic and monoclinic space groups. Although the number of people doing structure analyses this way must be very rapidly decreasing there are marginal studies (e.g. in clay mineralogy) for which this device should represent quite a sophisticated aid to hand calculation, achieved quite simply mechanically.

Papers 3-5 and 3-6. "The structure of anorthite $CaAl_2Si_2O_8$."

C.J.E. Kempster, Helen D. Megaw and E.W. Radoslovich.

As stated in the Acknowledgements section of this thesis, Paper 3-5 includes all the material of my Ph.D. thesis accepted in 1955 by the University of Cambridge. Dr. Megaw was my research supervisor, and Dr. Kempster post-dated me by two years as a Ph.D. student;

in fact he continued the research on anorthite, which had turned out to be far too difficult as a Ph.D. project considering the current state of digital computers in the early 1950's.

I cannot claim to have made any further contribution to this research, beyond that for which I have already received credit by my Ph.D. degree, until it had reached the drafting stage of writing-up. This happened at the same time as I was preparing Papers 2-5 to 2-10, and it is my belief that I was able to add significantly to the final manuscript at several points because of the ways in which I was then thinking about the layer silicate structures. It is practically impossible to itemize any contribution of this kind now, however.

Paper 3-7. "X-ray studies of the alteration of soda felspar."

G.W. Brindley and E.W. Radoslovich.

This was only intended as an exploratory study over a limited period of an admittedly difficult though important field of clay mineral investigations. The positive achievements are small, though the problems were probably defined more clearly.

The writer's contribution consisted of doing all the experimental work, bringing to bear on the problem up-to-date experience of crystal structure analysis (on anorthite) and of jointly framing the problem as being of interest in soil mineralogy. Dr. Brindley contributed his wide knowledge of clay mineralogy in day-by-day discussion and planning. I wrote and delivered the paper to the Fourth National Clay Conference.

Paper 3 - 8. "Effect of biotite on the firing characteristics of certain weathered schists."

K. Norrish and E.W. Radoslovich.

A little piece of useful practical ad hoc research carried out experimentally by me under the guidance of Dr. Norrish, during my first year as a graduate scientist. As a measure of scientific success it is a pleasure to record, sixteen years later, that the Onkaparinga Brick Works are still in business successfully!

Paper 3-9. "Clay mineralogy of some Australian red-brown earths."

E.W. Radoslovich.

This is an early piece of fundamental research seeking to relate the classification of soils by pedologists, primarily on their field observations, with their clay mineralogy as determined by X-ray powder diffraction analysis with supplementary chemistry. It is related to the subject matter of this thesis by showing the importance of micaceous clay minerals, structurally deficient in potassium, in an Australian Great Soil Group which is of great consequence agriculturally.

Paper 3-10. "A curved-crystal fluorescence X-ray spectrograph."

K. Norrish and E.W. Radoslovich.

I have made no further contribution experimentally to this subject beyond that for which I received credit in my M.Sc. degree, whereas Dr. Norrish developed my original instrument substantially during my three years overseas. This work would not, however, have been published at all if I had not exerted considerable pressure in writing the preliminary drafts

of this paper. The instrument included some notable features of simplicity of construction and operation when it was designed and the publication of Paper 3 - 10, largely on my initiative, has brought this piece of developmental research to a worthwhile conclusion. It is to be regretted that the co-author did not go on to publish his sophisticated analytical methods as a sequel to Paper 3 - 10.

Paper 3 - 11. "Felspars" E.W. Radoslovich.

Like Paper 2 - 13 this also is an invited article for the new "Encyclopedia of Soil Science" to be published by Springer-Verlag, Berlin. It is purposely directed towards the needs of soils workers and for that reason is far from comprehensive in discussing felspar structures.

Paper 1-1

Reprinted from *Acta Crystallographica*, Vol. 13, Part 11, November 1960

PRINTED IN DENMARK

Acta Cryst. (1960). **13**, 919

The Structure of Muscovite, $KAl_2(Si_3Al)O_{10}(OH)_2$

BY E. W. RADOSLOVICH

Division of Soils, Commonwealth Scientific and Industrial Research Organization, Adelaide, Australia

(*Received* 27 *October* 1959)

The structure of the $2M_1$ polymorph of muscovite, originally described by Jackson & West (1930, 1933), has been refined. The new atomic parameters show the structure to be considerably distorted from the ideal structure, especially by a departure from hexagonal symmetry on the surfaces of the silicate sheets. A number of difficulties concerning muscovite can now be resolved, and tentative explanations offered for properties of other layer silicates.

Though the structures of the micaceous minerals have been known in their main features for many years there is now considerable interest in the precise details of these and related layer-lattice silicate structures, especially the clay minerals.

The unit cells and symmetries of the micas were first investigated by Mauguin (1928). Their general structural scheme was then proposed by Pauling (1930) from a consideration of these dimensions, and of the known layer structures of the related minerals hydrargillite (i.e. gibbsite) $Al(OH)_3$, brucite $Mg(OH)_2$, β-tridymite SiO_2 and β-cristobalite SiO_2. Pauling showed that the micas also are layer structures, with an octahedral Al–O layer between two tetrahedral Si–O layers.* At the same time Jackson & West (1930, 1933) studied muscovite ($KAl_2(Si_3Al)O_{10}(OH)_2$) further, investigating the relative positions of the layers in the x and y directions. Their structure, based on symmetry and packing considerations, was confirmed by a general comparison of the observed and calculated intensities of a limited number of *hkl* reflections. This work was not claimed to give atomic parameters accurately, however, the structure being essentially an 'ideal' one.

No other analyses of mica structures appear to have been made since that of Jackson & West; and indeed it is only recently that structure analyses have been made of any layer-lattice silicates. Of these analyses the most accurate work is that on vermiculite by Mathieson & Walker (1954), and by Mathieson (1958). Less precise analyses have also been reported of amesite (Steinfink & Brunton, 1956), dickite (Newnham & Brindley, 1956), chloritoid (Harrison & Brindley, 1957), prochlorite (Steinfink, 1958*a*) and corundophillite (Steinfink, 1958*b*).

The ideal muscovite structure of Jackson & West (1930) leaves several problems unsolved, viz.:

(*a*) For the accepted space group ($C2/c$) and ideal structure, reflections of the kind $06l$, with l odd, are forbidden; but such reflections are observed.

(*b*) The measured monoclinic angles for many layer-lattice silicates (e.g. muscovite) do not agree with the ideal angles, $\beta = \cos^{-1}(-a/3c)$.

(*c*) There is a known misfit between the dimensions of a 'free' tetrahedral Si–O (or a $Si_{\frac{3}{4}}Al_{\frac{1}{4}}$–O) layer and a 'free' octahedral Al–O layer, and this misfit must somehow be accommodated in muscovite.

(*d*) Jackson & West gave the K–O bondlength as 3·09 Å, which is rather larger than the sum of their ionic radii, 2·95 Å approx. if the K^+ is 12-coordinated.

(*e*) In the tetrahedral layers the four cation sites are occupied by 3 Si and 1 Al ion; are these in an ordered arrangement?

(*f*) Hendricks & Jefferson (1939), and later Levinson (1953) and others, have demonstrated extensive polymorphism amongst the micas, whilst Smith & Yoder (1956) have recently suggested a theory to predict possible polymorphs. Some of these are either rare or not yet observed, but there appears to be no satisfactory explanation either of this or of the relative abundance of the common polymorphs.

Hendricks & Jefferson (1939) suggested that muscovite is unique among the micas in possessing only one form, the two-layer monoclinic form ($2M_1$) studied by Jackson & West (1930). This is no longer accepted, but since the $2M_1$ polymorph is the most common it is the one chosen for the present re-examination of the muscovite structure. Yoder & Eugster (1955) give cell dimensions for a synthetic $2M_1$ muscovite as

$$a = 5{\cdot}189 \pm 0{\cdot}010,\ b = 8{\cdot}995 \pm 0{\cdot}020,$$
$$c = 20{\cdot}097 \pm 0{\cdot}005\ \text{Å},\ \beta = 95^\circ\ 11' \pm 5'.$$

This contains four formula units, $KAl_2(Si_3Al)O_{10}(OH)_2$. The systematically absent reflections are consistent with either the space-group $C2/c$ or the non-centrosymmetric equivalent, Cc; and in absence of evidence for asymmetry Jackson & West chose $C2/c$. (Pabst (1955) has recently proposed that the one-layer micas are best described as $C2/m$, not Cm). The density is $2{\cdot}83_1$ g.cm.$^{-3}$, calculated from the unit-cell dimensions and molecular weight.

* The structural features of micas are adequately described by Bragg (1937).

Experimental

The sample of muscovite studied was from the Spotted Tiger Mine, Central Australia. The hand specimen consists of felspar crystals and of hexagonal muscovite books, 3 to 4 cm. across, which had grown into a cority. The muscovite is attached to the felspar, which is corroded in places. The books are clear at the edges, but show greenish iron stains in cleavage planes toward the centre. A suitable flake ($0{\cdot}4 \times 0{\cdot}5 \times 0{\cdot}1$ mm. approx.) was cut parallel to the true a-axis, from the edge of one book; the orientation was checked by the interfacial angles on the book, by percussion figures, and by Laue photographs. The true a-axis may be chosen optically and is confirmed by an oscillation photo after aligning the crystal about c, normal to the flake. (A 5° tilt towards $-a$ gives layer-lines for a 20 Å c-axis, but a tilt towards a pseudo a-axis gives layer-lines for a 60 Å spacing, given by the larger orthorhombic cell).

The refractive indices have the values

$$\beta = 1{\cdot}594 \pm 0{\cdot}001, \quad \gamma = 1{\cdot}598 \pm 0{\cdot}001$$

which suggests a fairly pure muscovite. A chemical analysis on a powdered sample, obtained by filing a mica book, gave the results in Table 1.

Table 1. *Chemical analysis of muscovite from Harts Range, Central Australia*

	%	No. of metal ions	No. of oxygens	Metal ions* (22 oxygens)	
K_2O	10·91	0·2316	0·1158	1·872	1·987
Na_2O	0·44	0·0142	0·0071	0·115	
SiO_2	46·20	0·7675	1·5350	6·220	8·000
Al_2O_3	34·28	0·6722	1·0083	5·450	
Fe_2O_3	2·29	0·0288	0·0432	0·237	4·018
MgO	0·60	0·0149	0·0149	0·121	
H_2O	5·0			4	
	99·72				

Analyst: R. Bond, Division of Soils, C.S.I.R.O., Adelaide.

* Calculated on the basis of 22 oxygens in the unit cell, ignoring H_2O. The percentage of Fe_2O_3 is difficult to determine, since there is a marked variability across any mica book, due to the iron stains. An estimate of 2·6% Fe_2O_3 was formed from the value of the refractive indices. Fluorescent X-ray spectrography on the powdered sample gave 2·1%, though values from 1·5% to 2·5% were found on scanning a 'book' of mica with a fine beam.

It is quite difficult to prepare a small muscovite crystal which is free from distortion or attached fragments, and it is not possible (due to the marked cleavage) to grind such a crystal to an ideal shape. The crystal used is sufficiently small, however, for the absorption not to vary seriously for different reflections (using Mo $K\alpha$ radiation for which $\mu/\varrho = 4{\cdot}8$ approx.). A diffractometer pattern of the powdered specimen was compared with the curves of Yoder & Eugster (1955) to confirm that this muscovite is a $2M_1$ polymorph.

Weissenberg photographs were taken on a Nonius integrating goniometer about the a-axis (zero to 7th layer lines), b-axis (zero, 1st, 3rd, and 5th) and c-axis (zero layer). On these photographs about 900 independent reflections are permissible for space group $C2/c$, of which 550 were observed. About 200 of these were measured on both a- and b-axis photographs. The integrated intensities were measured using a microphotometer in which the slits were adjusted to be smaller than the flat plateau of density on the integrated reflections; the film density is then proportional to the integrated intensity. Two independent measurements of the $0kl$ intensities, some weeks apart, gave agreement to better than 10%; a pack of three films, interleaved with tin foil, was used for each photograph. The a-axis photographs were correlated using the b-axis photographs, though due to the systematic absences the $0kl$ reflections could only be correlated by taking a *combined* $0kl$ and $1kl$ photograph, with a wide slot in the layer-line screen. The Lorentz and polarization corrections were applied to the correlated intensities graphically. Since the weakest reflections were hard to measure after integration the a-axis photographs were repeated using long exposures, without integration, from which reflections could be assessed as 'weak-but-present' or as absent. The systematic absences were therefore confirmed; no hkl reflections of the kind $(h+k)$ odd are observed. A powdered sample of the Spotted Tiger muscovite, mixed with a standard quartz sample, was photographed on a carefully calibrated 19 cm vacuum powder camera, for comparison with the unit-cell dimensions reported for synthetic muscovite. The b- and c-axes were determined as $8{\cdot}996 \pm 0{\cdot}006$ Å and $20{\cdot}096 \pm 0{\cdot}02$ Å respectively, assuming $\beta = 95°\ 11'$.

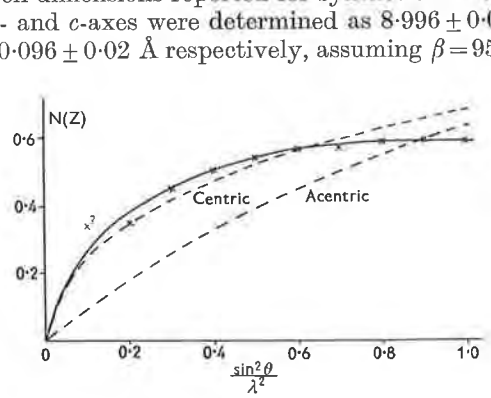

Fig. 1. Wilson's N(2) test for centrosymmetry, applied to one zone of general reflections for muscovite.

Two statistical tests for centrosymmetry due to Wilson were applied to some general hkl reflections. For two such zones containing many reflections the Wilson ratio, $(\overline{F})^2/\overline{F^2}$, was 0·507 and 0·455. Whilst this is not good agreement with the theoretical value for centrosymmetry (0·637), these figures are still further removed from the acentric value (0·785). It was hoped to avoid effects due to hypersymmetry in the $N(Z)$ test (Steinfink & Brunton, 1956) by applying it to one zone of general (rather than $0kl$) reflections

(Fig. 1). Though the departure from the theoretical curve at high values of $\sin^2\theta/\lambda^2$ may indicate some effect of hypersymmetry the results show that muscovite is probably centrosymmetric. The intensities were placed on an absolute scale by Wilson's method, the factor being adjusted in later calculations.

Calculations

Jackson & West (1930) proposed that the space group of muscovite is $C2/c$, though they pointed out that the symmetry must be lower than this if the tetrahedral cations are fully ordered. The possibilities then are either Cc or $P2/c$, of which Cc is acentric and $P2/c$ would allow *all* hkl reflections, contrary to observation. The maximum order possible in the tetrahedral ions for $C2/c$ (assumed correct) is 2 $Si_{\frac{1}{2}}Al_{\frac{1}{2}}$ with 2 Si.* There are eight general positions in this space group, related by the symmetry operations of face-centring, a glide of $c/2$ after reflection across the plane at $y=0$, and a centre of symmetry at the origin. A suggested system of nomenclature for each atom is illustrated (for Si_1) in Table 2.

Table 2. *System of nomenclature.*

System of nomenclature for atoms

Si_1	(000)	x	y	z	Si_1	(0g0)	$\bar{x}$	y	$\frac{1}{2}-z$
Si_1	(00c)	$\bar{x}$	$\bar{y}$	$\bar{z}$	Si_1	(0gc)	x	$\bar{y}$	$\frac{1}{2}+z$
Si_1	(f00)	$\frac{1}{2}+x$	$\frac{1}{2}+y$	z	Si_1	(fg0)	$\frac{1}{2}-x$	$\frac{1}{2}+y$	$\frac{1}{2}-z$
Si_1	(f0c)	$\frac{1}{2}-x$	$\frac{1}{2}-y$	$\bar{z}$	Si_1	(fgc)	$\frac{1}{2}+x$	$\frac{1}{2}-y$	$\frac{1}{2}+z$

Atoms in special positions

K	(000)	0	y	$\frac{1}{4}$	K	(f00)	0	$\frac{1}{2}+y$	$\frac{1}{4}$
K	(00c)	0	$\bar{y}$	$-\frac{1}{4}$	K	(f0c)	0	$\frac{1}{2}-y$	$-\frac{1}{4}$

Atomic scattering factors were obtained from the empirical curves of Bragg & West (1929) for silicate structures, modified somewhat by the data of Viervoll & Øgrim (1949). These factors were tabulated before the more recent data of MacGillavry *et al.* (1955) were published, and a change to the latter data is difficult and not warranted at this stage. The effective values of the temperature factors were: Al and Si, $B=0{\cdot}3$ Å^2; O, $B=1{\cdot}5$ Å^2; and K, $B=0{\cdot}4$ Å^2. The value of B for potassium is obviously too low, as is shown by the final difference maps. The curves of Bragg & West do not correspond to fully ionised atoms, and since Verhoogen (1958) has suggested that alumino-silicates can be considered as largely ionic the present work would be capable of further refinement by using MacGillavry's data for K^+, Si^{4+}, Al^{3+} and O^{2-}, allowing for anisotropic temp. factors if necessary.

Values of the atomic scattering factors at the points hkl (tabulated graphically from the appropriate reciprocal nets) were transferred to punched tape as the input for a structure-factor programme on WREDAC,* for which an additional short tape specified parameters at each cycle. The parameters of Jackson & West were used as a trial structure and refinement proceeded by means of two-dimensional and bounded Fourier and difference syntheses. Bounded projections were partially summed by hand to reduce them to the standard two-dimensional Fourier programme on SILLIAC.†

The major difficulty in the structure analysis of any layer-lattice silicate is the lack of resolution in two-dimensional projections. In the (0kl) projection two of the three crystallographically distinct oxygens in the layer surface (O_D and O_E) are partially superimposed on the Si_1 and Si_2 contours; little improvement was achieved in several refinements. The $h0l$ projection shows Si_1 and Si_2, and O_D and O_E, and O_A, O_B and OH as superimposed, and the x-coordinate of the Al atom is difficult to determine. The $hk0$ projection shows very poor resolution. For these reasons it was necessary to use the following methods.

Bounded Fourier projections

Increased resolution was obtained by using bounded Fourier projections (Lipson & Cochran (1953), p. 80) in which the slabs were $a/2$ and $b/2$ thick (for the projections along [100] and [010]) to restrict the labour of computation. (Only the 0kl, $h0l$, 1kl, 3kl, 5kl and 7kl data were needed to divide the cell into slabs $a/2$ and $b/2$ thick.) Final computations were at 1/128ths of the unit-cell edge; the plane groups of bounded projections differ from those of the two-dimensional projections.

Two cycles of bounded Fourier projections were plotted for the slabs from $a/2$ to a along [100], and $b/2$ to b along [010]. Certain symmetry-related atoms whose centres lie in the slab 0 to $a/2$ project partially into the slab $a/2$ to a, notably the oxygens, which

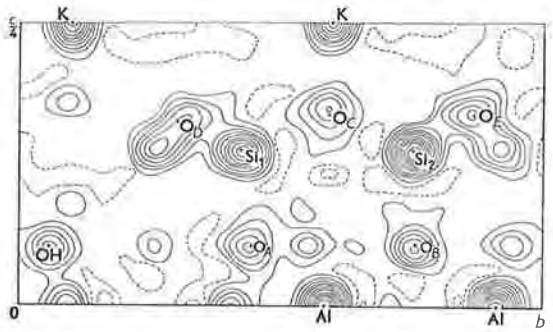

Fig. 2. Bounded Fourier projection along the a-axis for the slab between planes at $x=a/2$ and $x=a$. Contours plotted at intervals of 4 e.Å^{-2}—zero contour broken.

* Complete ordering within $C2/c$ is possible if the unit cell is doubled in size with some kind of disorder present; but no additional reflections indicating this have been observed.

* Weapons Research Establishment Digital Automatic Computer, Salisbury, Sth. Aust. Programme kindly designed and calculations supervised by Mr P. N. L. Goddard and Mr R. Byron-Scott.

† Digital computer, University of Sydney.

have an ionic diameter of 2·8 Å compared with a slab thickness of 2·6 Å. These overlapping atoms do not superimpose on atoms within the slab, except for a portion of an Si_2 atom, which partially masks the O_D atom (Fig. 2). The position of a related Si_2 atom is established elsewhere in the projection, and by subtracting a reasonable fraction of the full electron density from the composite peak fairly circular contours are obtained for O_D.

The overlap of atoms between 0 and $b/2$ into the slab from $b/2$ to b is less but is far more serious since separate x-coordinates cannot be immediately deduced for O_A, O_B and OH (Fig. 4). Furthermore there are two symmetry-related Al atoms, Al(f00) and Al(00c), which superimpose to give a pseudo-centre of symmetry at $x=\frac{3}{4}a$, $z=0$. If Al(000) has coordinates very near $(\frac{1}{4}, y, 0)$ then these composite contour lines are practically circular, and the x and z parameters can hardly be determined. The projection from $3b/4$ to $b/4$ was, however, fairly rapidly calculated from the data for $b/2$ to b, and in this projection Al(000) is completely resolved.

The progress of refinement was followed by calculating $R=\Sigma||F_o|-|F_c||/\Sigma|F_o|$ for the reflections actually observed; after the second cycle of bounded projections this was 0·25. At this stage the bond lengths for the tetrahedral Si_1–O and Si_2–O groups suggested that there may be ordering of the kind $Si_{\frac{1}{2}}Al_{\frac{1}{2}}$ in Si_1 positions and Si in Si_2 positions.

Difference, or (F_o-F_c), syntheses

The parameters of the cations were now sufficiently near their final positions for difference 0kl syntheses to be used to improve the y and z parameters, with much less computation. The R-factor, after four (F_o-F_c) cycles, was 0·12. One $h0l$ difference synthesis was computed, for which the R-factor was 0·19, and it was obvious that the x-parameters of O_AO_B and OH (which are superimposed) needed adjustment. This adjustment could not be made from a difference synthesis of the $hk0$ data which was difficult to interpret because of the direct superposition of O_B on Si_2, and close overlap of O_A, O_C and Si_1.

Most of the interatomic distances and bond lengths were reasonable, except Al–O_A, Al–O_B and Al–OH, but these could be improved by adjusting the x-parameters for O_A, O_B and OH. These could not be easily adjusted otherwise, and nothing is assumed about the tetrahedral bonds by this. At the same time the O–Si–O tetrahedral bond angles all assumed more reasonable values.

Final syntheses

The following projections were computed as the final Fourier syntheses:

(1) A bounded projection along the a-axis, between planes at $x=a/2$ and $x=a$ (Fig. 2).

(2) An (F_o-F_c) two-dimensional projection along the a-axis (Fig. 3).

(3) A bounded projection along the b-axis, between planes at $x=b/2$ and $x=b$ (Fig. 4).

(4) A bounded (F_o-F_c) projection along the b-axis, between planes at $x=b/2$ and $x=b$ (Fig. 5).

Fig. 2 shows all atoms clearly resolved except O_D; the additional unmarked peaks >4e.Å^{-2} are all due to symmetry-related atoms whose centres lie outside the bounds of the slab. The peak heights are quite satisfactorily high, though due to the partial projection of these atoms out of the slab (and also to the somewhat unsatisfactory scattering and temperature factors) the peak values of electron density cannot be discussed in detail. It should be noted that in Fig. 2

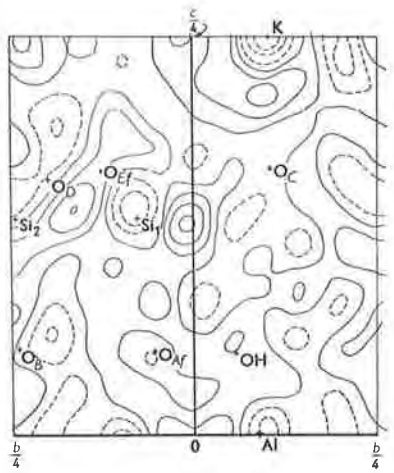

Fig. 3. Two-dimensional (F_o-F_c) map, projected along a-axis. Contours at 1 e.Å^{-2}—negative levels broken.

the centre of the K^+ ion lies in the face of the slab, and therefore the K^+ peak is only at half-height. When Fig. 2 is considered in relation to Fig. 3 it is seen that the K and Al ions are correctly placed but probably need larger temperature factors; that the oxygen atoms are correctly placed, being on flat areas

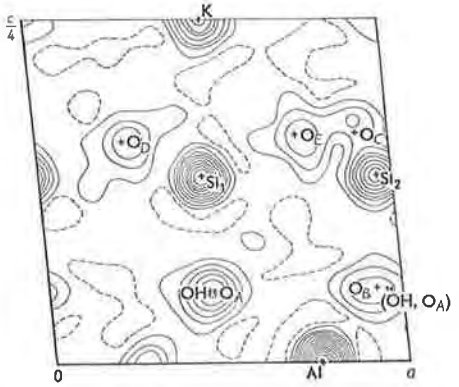

Fig. 4. Bounded Fourier projection along the b-axis for the slab between planes at $y=b/2$ and $y=b$. Contours plotted at intervals of 4 e.Å^{-2}—zero contour broken.

Table 3. *Observed and calculated structure factors*

hkl	F_o	F_c
000	†	+810
2	†	+50
4	89	−70
6	179	+181
8	77	+74
10	237	−229
12	37	+52
14	88	+87
16	129	+126
18	†	+16
20	82	+84
22	101	+89
24	80	+63
26	77	−76
020	41	+23
1	38	+31
2	63	+60
3	119	+106
4	133	+113
5	167	−146
6	18*	−23
7	47	+52
8		+6
9	26	+17
10	37	+31
11	18*	+8
12	36	+34
13	77	−86
14	18*	−10
15	43	+46
16	33	+34
17		−12
18	41	+32
19		+1
20	18*	+36
040	34	−42
1	52	−45
2	71	+61
3	55	+43
4	89	−89
5	18*	−39
6	57	−48
7	41	−44
8	26	−44
9		+16
0,4,10	50	−42
11	60	+52
12	144	−133
13	82	−87
14	44	+43
15	18*	+26
16		−19
17	45	+36
18	37*	−33
19		−26
20		−26
060	275	−258
1	57	+57
2	57	−44
3	18*	+4
4		+14
5	18*	+2
6	57	−65
7	28	−16
8	118	−126
9	60	+51
10	59	+76
11	18*	−33
12	18*	0
13	18*	−8
14	78	−90
15		−11
16	111	−106
17	37	+26
18	18	+32
19	28	−24
20	49	−58
21		+13
22	80	−86
080	18*	−9
1	18*	+3
2	50	−46
3	43	−56
4	18*	−18
5	44	+52
6	18*	−15
7	18*	−8
8	18*	+12
9	18*	−12
10		−12
0,8,11	18*	−21
12		+3
13	64	+75
0,10,0	18*	+9
1		−10
2	27*	−23
3		−3
4	64	+69
5	9*	+23
6	18*	+13
7	9*	+26
8	18*	+35
9		−25
10	37*	+34
11		−4
12	81	+91
110	68	−53
1	47	−38
2	36	−39
3	34	+36
4	161	+137
5	157	−123
6	80	−81
7	10*	+11
8		−11
9	10*	−18
10		−4
11	10*	−21
12	61	+49
13	54	−69
14	55	−67
15	10*	−12
16	9*	−3
17	45	−36
18		−1
19		0
20	32	+29
21	52	−52
22	49	−57
11$\bar{1}$	110	−95
$\bar{2}$		0
$\bar{3}$	110	−105
$\bar{4}$	134	+121
$\bar{5}$	51	+44
11$\bar{6}$	138	−117
$\bar{7}$	62	−77
$\bar{8}$	23	+19
$\bar{9}$	10*	−27
$\bar{10}$	26	+26
$\bar{11}$	49	−35
$\bar{12}$	28	+42
$\bar{13}$	28	+25
$\bar{14}$	59	−58
$\bar{15}$	52	−58
$\bar{16}$	19*	+35
$\bar{17}$	58	−35
$\bar{18}$	10*	+20
$\bar{19}$	29*	−31
$\bar{20}$	29*	+30
$\bar{21}$		+7
$\bar{22}$	38*	−42
$\bar{23}$	48*	−57
130	50	+40
1	191	−212
2	18	+13
3	142	−127
4		−10
5	197	−150
6		+13
7	59	−38
8	31	−18
9	202	−206
10	37	+25
11	109	−68
12		−2
13	67	+56
14		+7
15	69	+20
16		−17
17	141	−150
18		+13
13$\bar{1}$	140	+114
$\bar{2}$	15	+7
$\bar{3}$	143	+109
$\bar{4}$	2	+1
$\bar{5}$	70	−74
$\bar{6}$	30	+21
$\bar{7}$	170	−127
$\bar{8}$	49	−29
13$\bar{9}$	151	+139
$\bar{10}$	15*	+30
$\bar{11}$	197	−183
$\bar{12}$	27	+4
$\bar{13}$	246	−218
$\bar{14}$	24*	−11
$\bar{15}$	60	−32
$\bar{16}$	41	−18
$\bar{17}$	49	+40
$\bar{18}$	44	+25
$\bar{19}$	144	−144
$\bar{20}$		−18
$\bar{21}$	30	−13
$\bar{22}$	27	−3
$\bar{23}$	49	+31
150	38	+40
1	38	−10
2		+14
3	58	−52
4	82	−76
5	61	−53
6	76	+76
7	57	−47
8	10*	−21
9	29*	−26
10	10*	+18
11		−5
12	29*	−45
13		−15
14	29*	+41
15	10*	−17
15$\bar{1}$	38	−25
$\bar{2}$	38	+36
$\bar{3}$	8*	−21
$\bar{4}$	128	−126
$\bar{5}$	38*	+30
$\bar{6}$	81	+79
$\bar{7}$		+5
$\bar{8}$	8*	+1
$\bar{9}$	19*	−50
$\bar{10}$	8*	−36
$\bar{11}$		−18
$\bar{12}$	51	−50
$\bar{13}$	38	−20
$\bar{14}$	77	+76
$\bar{15}$	72	−48
$\bar{16}$		−40
1,5,$\bar{17}$	19*	−33
$\bar{18}$	10*	−12
$\bar{19}$	10*	−5
170	30	+31
1	41	+46
2	14*	+27
3	105	−84
4	79	−83
5	77	+83
6	10*	+23
7		−5
8	19*	+54
9	29*	−13
10	14*	−25
11		+15
12	10*	−19
13	106	+108
14	38*	+53
17$\bar{1}$	116	+92
$\bar{2}$	38	−45
$\bar{3}$	82	+84
$\bar{4}$	10*	−18
$\bar{5}$		−2
$\bar{6}$	38*	+46
$\bar{7}$	93	+101
$\bar{8}$		−7
$\bar{9}$		0
$\bar{10}$		−3
$\bar{11}$		+27
$\bar{12}$		−15
$\bar{13}$	29	−35
190	60	+53
1	66	+85
2		−11
3	106	+107
4	14*	0
5		+2
6		−24
7		−16
8	19*	+45
9	115*	+137

Table 3 (*cont.*)

hkl	F_o	F_c
10	10*	−38
11	14*	+38
12	10*	−8
191	67*	−55
2	29*	−28
19$\bar{3}$	14*	−28
$\bar{4}$	10*	+1
$\bar{5}$	68	+83
$\bar{6}$		−14
$\bar{7}$	38*	+47
$\bar{8}$	38*	+39
$\bar{9}$	10*	−30
$\bar{10}$	24*	−45
$\bar{11}$	57	+68
$\bar{12}$		+5
$\bar{13}$	77	+86
310	†	−15
1	29	−27
2	85	−87
3	82	+96
4	117	+112
5	22	+7
6	10*	−14
7	15	+8
8	38	−31
9	35	+47
10		+3
11	90	+79
12	65	+65
13		−22
14	46	−49
15	31	+35
16		+6
17	48	+26
31$\bar{1}$	†	−10
$\bar{2}$	35	+27
$\bar{3}$	80	+40
$\bar{4}$	29	+24
$\bar{5}$	124	+83
$\bar{6}$	78	−86
$\bar{7}$		+2
$\bar{8}$	35	+35
$\bar{9}$	60	+57
$\bar{10}$		−7
$\bar{11}$	31*	+24
$\bar{12}$	31*	+24
$\bar{13}$	15*	+52
$\bar{14}$	59	−57
$\bar{15}$	31*	−15
$\bar{16}$		+15
$\bar{17}$	15*	+17
$\bar{18}$	21*	+5
3,1,$\bar{19}$		+16
$\bar{20}$		−1
$\bar{21}$	15*	+41
$\bar{22}$	60	−60
330	32	−21
1	73	+45
2		+0
3	10*	−23
4		−10
5	46	+38
6	31	+22
7	153	+126
8	36	−24
9	89	−91
10		+7
11	42	−2
12	40	+12
13	95	+100
14		+6
15	135	+122
16	41*	−24
17	31*	−34
18	10*	+18
19	67	+70
20		−5
21	92	+81
33$\bar{1}$	263	+281
$\bar{2}$	38	+7
$\bar{3}$	54	+53
$\bar{4}$		−1
$\bar{5}$		−10
$\bar{6}$	10*	+5
$\bar{7}$	67	+73
$\bar{8}$		−13
$\bar{9}$	146	+132
$\bar{10}$	31	+29
$\bar{11}$	96	−101
$\bar{12}$	15*	−14
$\bar{13}$	15*	−4
$\bar{14}$		−3
$\bar{15}$	106	+84
$\bar{16}$		−4
$\bar{17}$	122	−102
$\bar{18}$		+13
$\bar{19}$	20*	−33
$\bar{20}$		−14
$\bar{21}$	74	+73
3,3,$\bar{22}$		+7
$\bar{23}$	89	+84
$\bar{24}$		−3
$\bar{25}$	40	+40
350		+2
1		+17
2	99	+101
3	31*	+35
4	121	−106
5	10*	−12
6		+18
7	31*	−18
8	59	+44
9	10*	+28
10		−5
11	31*	+20
12	56	−73
13	43	+16
14	61	+55
15	36*	+26
16	10*	−19
17	26*	+28
18		−4
35$\bar{1}$	46	+8
$\bar{2}$	57	−43
$\bar{3}$	108	+66
$\bar{4}$		−17
$\bar{5}$	71	+50
$\bar{6}$	78	+75
$\bar{7}$	31*	+17
$\bar{8}$	52	−57
$\bar{9}$	31*	+16
$\bar{10}$	10*	+26
$\bar{11}$		+11
$\bar{12}$		−16
$\bar{13}$		−3
$\bar{14}$	31*	+47
370	10*	+18
1	10*	+14
2		+8
3	78	−84
4	21*	−34
5		−7
6		−9
377	15*	−49
8		+11
9	46*	−34
10		+12
11	95	−80
12	31*	−31
37$\bar{1}$		+7
$\bar{2}$		+2
$\bar{3}$		+21
$\bar{4}$	46	−26
$\bar{5}$	94	−75
$\bar{6}$	31*	+43
$\bar{7}$		+3
$\bar{8}$		+22
$\bar{9}$		−39
$\bar{10}$		−31
$\bar{11}$	66	−40
$\bar{12}$		−9
$\bar{13}$	82	−87
$\bar{14}$	31*	+45
$\bar{15}$	31*	+25
390	31*	+42
1	15*	−10
2		−11
3	15*	−9
4		+9
5	15*	−38
6	15*	−26
7	75	−82
8	31*	+36
9		+9
10		−15
39$\bar{1}$	97	−116
$\bar{2}$	31*	−34
$\bar{3}$	46*	−43
$\bar{4}$	20*	−4
$\bar{5}$	31*	+28
$\bar{6}$	31*	−2
$\bar{7}$		−37
$\bar{8}$	46*	+29
$\bar{9}$	120	−112
$\bar{10}$	61*	−53
510	14*	−27
1	10*	−15
2	36	+46
3	25	−16
4	25	−30
5	15*	−14
6	10*	−4
7	59	−40
8		+0
9	70	−29
10	47	+48
11		−1
12	41	−52
51$\bar{1}$	†	−19
$\bar{2}$	†	+3
$\bar{3}$	†	−14
$\bar{4}$	†	+21
$\bar{5}$	†	+20
$\bar{6}$	44	−43
$\bar{7}$	50	−45
$\bar{8}$	10*	+30
$\bar{9}$	14	−15
$\bar{10}$	14*	+17
$\bar{11}$	44	−23
$\bar{12}$	10*	+23
$\bar{13}$	14*	−6
$\bar{14}$	48*	−44
$\bar{15}$	58*	−63
530	10*	−21
1	30	−25
2		+5
3	70	−62
4		−2
5	74	−71
6	10*	+6
7	36	+32
8	10*	−10
9	58	−86
10		+8
11	109	−97
12		−6
13	61	−43
14		+14
15	53	+52
16		−11
17	65	−80
18		+1
53$\bar{1}$	64	+84
$\bar{2}$	20	+21
$\bar{3}$	88	−90
$\bar{4}$		−2
$\bar{5}$	99	−95
$\bar{6}$		−6
$\bar{7}$		−18
$\bar{8}$		−5
$\bar{9}$	10*	+11
$\bar{10}$	14*	+20
$\bar{11}$	147	−166
$\bar{12}$		−17
$\bar{13}$	41	−32
$\bar{14}$		+0
$\bar{15}$	43	+30
$\bar{16}$		−1
550	14*	−27
1	10*	−15
2	36	+46
3	25	−16
4	25	−30
5	15*	−14
6	10*	−4
7	59	−40
8		+0
9	70	−29
10	47	+48
11		−1
12	41	−52
55$\bar{1}$	24*	−2

Table 3 (*cont.*)

hkl	F_o	F_c	*hkl*	F_o	F_c	*hkl*	F_o	F_c	*hkl*	F_o	F_c
$\bar{2}$	†	+5	590	29*	+30	200	119		10	20*	+3
$\bar{3}$	30	+6	1	19*	+14	2	123	+116	12	10*	−30
$\bar{4}$	27	−28	2		−1	4	56	−75	14		−7
$\bar{5}$	10*	+1				6	140	−146	16	80	+101
$\bar{6}$	40	+44	59$\bar{1}$	39*	−43	8	125	+111			
$\bar{7}$	39	−17	$\bar{2}$	58*	−42	10	161	−192	40$\bar{2}$	122	−121
$\bar{8}$		−18	$\bar{3}$	92	+85	12	224	−211	$\bar{4}$		+7
$\bar{9}$	34	−33	$\bar{4}$		+13	14	73	−43	$\bar{6}$	117	+98
$\bar{10}$		−14	$\bar{5}$	69	+59	16	56	+56	$\bar{8}$	46	+35
$\bar{11}$	47	−17				18	95	−129	$\bar{10}$	83	−88
$\bar{12}$	20	−22	730		−3	20	30*	−15	$\bar{12}$	142	+142
$\bar{13}$	66	−23	1	68	+65	22	47	+31	$\bar{14}$	128	+119
$\bar{14}$	60	+56	2		−3	24	40	+11	$\bar{16}$	47	+42
$\bar{15}$	46	−36	3		+5	26	88	−103	$\bar{18}$	10*	−18
$\bar{16}$	34	−52	4		−6				$\bar{20}$	95	+106
			5		−4	20$\bar{2}$	194	−190	$\bar{22}$	41	+25
570		+6	6		+16	$\bar{4}$	119	−100	$\bar{24}$	10*	−17
1	78	+80	7	74	+93	$\bar{6}$	181	−161			
2	39	+28				$\bar{8}$	70	−64	600	52	−43
3	43	−28	73$\bar{1}$	90	+96	$\bar{10}$	218	−222	2	47	+30
4	39*	−34	$\bar{2}$		+14	$\bar{12}$	98	−89	4		−8
5	19*	+39	$\bar{3}$	42	−56	$\bar{14}$	52	+45	6	117	−119
6	14*	−17	$\bar{4}$		−12	$\bar{16}$	73	+51	8	30*	+57
7	52	+26	$\bar{5}$		+25	$\bar{18}$	142	−150	10	10*	+3
8	19*	+21	$\bar{6}$		+4	$\bar{20}$		+31	12	73	−84
			$\bar{7}$	78	+65	$\bar{22}$	45	+20			
57$\bar{1}$	39*	+35	$\bar{8}$		−1	$\bar{24}$	83	−88	60$\bar{2}$	115	−141
$\bar{2}$	19*	−26	$\bar{9}$		+24				$\bar{4}$		−7
$\bar{3}$		+21	$\bar{10}$		+9	400	153	+186	$\bar{6}$	20*	−35
$\bar{4}$		+6	7,3,$\bar{11}$	43	−48	2	123	+137	$\bar{8}$	47	−36
$\bar{5}$		−12	$\bar{12}$		−11	4	10*	+33	$\bar{10}$	83	−90
$\bar{6}$	39*	+29	$\bar{13}$	57	+73	6	20*	+25	$\bar{12}$		+33
$\bar{7}$	64	+57	$\bar{14}$		+6	8	153	+175	$\bar{14}$	10*	+9
			$\bar{15}$	45	+49				$\bar{16}$	33	−45

* Those reflections are visually estimated since they are too weak for satisfactory measurement.
† These reflections were not photographed.

of Fig. 3; and that Si_1 (and possibly Si_2) need a shift of $<0{\cdot}012$ Å (apparently in the $+\delta y$ and $-\delta z$ direction) together with some adjustment of the temperature factor.

Fig. 4 does not completely resolve the octahedral oxygens, nor does it separate two related octahedral Al ions which are practically superimposed in this projection. These Al ions and the K ion are only partly within this slab, and symmetry related atoms to O_A and OH partly project on to O_B. All unlabelled peaks >4 e.Å^{-2} are due to atoms whose centres lie outside the slab. The peaks of the atoms are satisfactorily high, except for Si_2 which is sharp but shows a low peak electron density.

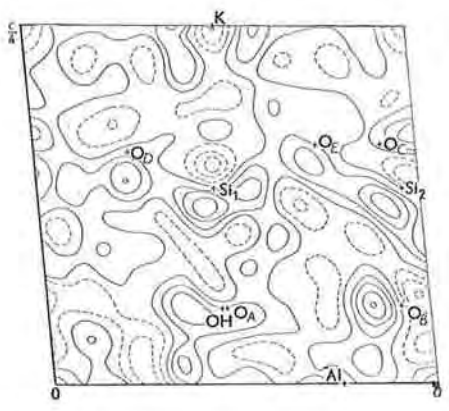

Fig. 5. Bounded (F_o-F_c) map, projected along b-axis for the slab between planes at $y=b/2$ and $y=b$. Contours plotted at intervals of 1 e.Å^{-2}—negative levels broken.

Fig. 5, on a scale of 1 e.Å^{-2}, suggests that very small adjustments in certain parameters may help further. In particular it had not been possible from any previous map—either the bounded electron-density or the $h0l$ difference map—to determine which x-parameters for O_A, O_B and OH needed adjustment. Fig. 5, however, shows quite clearly that (O_A+OH) lie on a flat part of this (F_o-F_c) map; and they cannot therefore contribute at all (through the *partly* protruding symmetry related atoms) to the *difference* density in the region of O_B. The bounded difference map therefore suggests that the x-coordinate for O_B should be reduced by about 0·04 Å. The tetrahedral oxygens appear to be correctly placed, but Si_1 and Si_2 may require small shifts (of $<0{\cdot}012$ Å along slope).

Results

The observed and the calculated structure factors (F_o and F_c) suitably scaled, are given in Table 3,

Table 4. *Initial and final atomic parameters*

(as decimal fractions of unit-cell dimensions)

	Jackson & West			Final coordinates			Shift (Å)		
Atom	x	y	z	x	y	z	$\|\delta x\|$	$\|\delta y\|$	$\|\delta z\|$
Al(000)	250	083	000	2484	0871	0016	0·008	0·036	0·032
O_A(000)	438	917	055	4650	9450	0527	0·140	0·252	0·046
O_B(000)	438	250	055	4250	2600	0542	0·016	0·090	0·016
OH(000)	438	583	058	4530	5580	0520	0·078	0·225	0·120
Si_1(000)	467	917	135	4625	9242	1372	0·023	0·065	0·044
Si_2(000)	467	250	135	4593	2550	1365	0·040	0·045	0·030
O_C(000)	480	083	164	4080	0960	1680	0·374	0·117	0·080
O_D(000)	228	833	164	2450	8020	1620	0·088	0·279	0·040
O_E(000)	228	333	164	2629	3713	1674	0·181	0·344	0·068
K(000)	000	083	250	0000	1016	2500	0	0·167	0

from which it is seen that these agree satisfactorily. The R-factors (measured intensities only) have the following values: $R(0kl)=0{\cdot}12$; $R(h0l)=0{\cdot}13$; R (all measured reflections) $=0{\cdot}17$.

The final values of the atomic parameters, together with the 'ideal' parameters, are given in Table 4, and the bond lengths, interatomic distances and bond angles are recorded in Table 5. The Si_1–O bond lengths (mean $=1{\cdot}69_5$ Å) are clearly different from the Si_2–O bonds (mean $=1{\cdot}61_2$ Å); and within each tetrahedron the bond to the apical oxygen, within the layer, is rather larger than the others. The difference is possibly significant for Si_2–O_B (where $\delta l/\sigma=2{\cdot}2$) and may reflect the different coordination and therefore different ionic radius of the apical oxygens. The K–O bonds also clearly fall into two groups of three, the average K–O distance for one group being $2{\cdot}81_2$ Å, and for the remainder $3{\cdot}39_0$ Å; the symmetry operations bring the total oxygen group around the K^+ to 12. For the O–O interatomic distances (fixed by packing) around the tetrahedral groups the six distances around Si_1 are close to the mean value, $2{\cdot}76_9$ Å, as are the O–O distances from the apical oxygen to the three basal oxygens around Si_2. The three O–O distances in the base of the Si_2 group, however, have values very close to their mean, $2{\cdot}58_7$; and the corre-

Table 5. *Bond lengths, interatomic distances and bond angles*

(1) Tetrahedral groups

Si_1–O_C	$1{\cdot}69_5$ Å	Si_2–O_C	$1{\cdot}59_6$ Å
Si_1–O_D	$1{\cdot}68_2$	Si_2–O_D	$1{\cdot}58_1$
Si_1–O_E	$1{\cdot}68_9$	Si_2–O_E	$1{\cdot}62_3$
(Mean $=1{\cdot}69_0$)		(Mean $=1{\cdot}60_0$)	
Si_1–O_A*	$1{\cdot}71_0$	Si_2–O_B*	$1{\cdot}64_8$
Mean $=1{\cdot}69_5$ Å		Mean $=1{\cdot}61_2$ Å	

* Apical oxygens.

Around Si_1

O_C–O_D	$2{\cdot}77_5$ Å	O_A*–O_C	$2{\cdot}74_3$ Å
O_C–O_E	$2{\cdot}73_3$	O_A*–O_D	$2{\cdot}87_0$
O_D–O_E	$2{\cdot}74_9$	O_A*–O_E	$2{\cdot}74_1$
Mean $=2{\cdot}76_9$ Å			

* Apical oxygens.

Around Si_2

O_C–O_D	$2{\cdot}58_3$ Å	O_B*–O_C	$2{\cdot}74_3$ Å
O_C–O_E	$2{\cdot}58_8$	O_B*–O_D	$2{\cdot}80_6$
O_D–O_E	$2{\cdot}59_1$	O_B*–O_E	$2{\cdot}73_2$
(Mean $=2{\cdot}58_7$)		(Mean $=2{\cdot}76_0$)	
Mean $=2{\cdot}67_4$ Å			

* Apical oxygens.

O_C–Si_1–O_D	110° 24′	O_A–Si_1–O_C	106° 16′
O_C–Si_1–O_E	108° 15′	O_A–Si_1–O_D	115° 33′
O_D–Si_1–O_E	111° 52′	O_A–Si_1–O_E	107° 22′
Mean $=109°\ 58'$			

O_C–Si_2–O_D	107° 14′	O_B–Si_2–O_C	114° 35′
O_C–Si_2–O_E	107° 3′	O_B–Si_2–O_D	109° 8′
O_D–Si_2–O_E	107° 49′	O_B–Si_2–O_E	109° 32′
(Mean $=107°\ 22'$)			
Mean $=109°\ 13'$			

Table 5 (*cont.*)

Si_1–O_C–Si_2	129° 22′	Si_1–O_D–Si_2	135° 24′
Si_1–O_E–Si_2	128° 42′		
Mean $=131°\ 9'$			

(2) Octahedral groups

Al–O_A	$1{\cdot}93_5$ Å	Al–O_A	$1{\cdot}94_4$ Å
Al–O_B	$1{\cdot}93_2$	Al–O_B	$2{\cdot}04_8$
Al–OH	$1{\cdot}93_9$	Al–OH	$1{\cdot}93_0$
Mean $=1{\cdot}95_4$ Å			

Around Al

O_A–O_A	$2{\cdot}39_6$ Å*	OH–O_A	$2{\cdot}73_1$ Å
O_A–O_B	$2{\cdot}90_9$	OH–O_B	$2{\cdot}80_7$
O_A–O_B	$2{\cdot}92_6$	OH–O_B	$3{\cdot}04_6$
O_A–O_B	$2{\cdot}84_1$	OH–O_B	$2{\cdot}68_4$
O_A–OH	$2{\cdot}73_4$	OH–OH	$2{\cdot}51_1$*
O_A–OH	$2{\cdot}88_1$	O_B–O_B	$2{\cdot}76_8$*
Mean $=2{\cdot}76_9$ Å			

* These oxygen–oxygen distances correspond to shared edges of neighbouring octahedra.

(3) Interlayer cation

K–O_C	$2{\cdot}79_9$ Å	K–O_C	$3{\cdot}35_7$ Å
K–O_D	$2{\cdot}77_5$	K–O_D	$3{\cdot}51_1$
K–O_E	$2{\cdot}86_2$	K–O_E	$3{\cdot}30_3$
Mean $=2{\cdot}81_2$ Å		Mean $=3{\cdot}39_0$ Å	

sponding bond angles are consistent with this. There is more variation in the interatomic O–O and O–OH distances in the octahedral configuration around the Al atom. The mean, 2·76$_9$ Å, is close to the oxygen diameter; one O–O distance is rather small (2·40 Å). The O–Si–O angles are all close to the tetrahedral angle of 109° 28′.

Accuracy

The accuracy of the positional parameters and certain bond lengths determined in this analysis has been computed as recommended by Lipson & Cochran (1953), using the final ϱ_0 bounded projections and the a-axis ($F_o - F_c$) projection. The standard deviations of these bond-lengths have been used to determine the significance of bond length differences between the two silicon tetrahedral groups, as suggested by Cruickshank (1949). The standard deviations $\sigma(x_n)$ have been computed over the whole unit cell, which is a slight over-estimate of error; computational errors are not allowed for. Since there is little evidence of asymmetry (except possibly for the K atom) the standard deviations have been assumed equal in all directions. The values of the curvatures and $\sigma(x_n)$ are given in Table 6, together with the standard deviations of bond lengths and mean bond lengths. The significance test shows that the bond lengths in the two silicon tetrahedra are significantly different; and the standard deviations of the mean Si_1–O and Si_2–O bond lengths are consistent with the hypothesis that Si_2 is fully occupied by silicon, whilst Si_1 is occupied by $Si_{\frac{1}{2}}Al_{\frac{1}{2}}$, within the limits of Smith's (1954) curve.

Table 6. *Accuracy of atomic parameters and bond lengths*

	p	$-C_n$ (e.Å^{-4})	$\sigma(x)$ (Å)
K	7·0	1036	0·0048 Å
Al	7·7	740	0·0067
Si_1	7·5	585	0·0085
Si_2	7·5	720	0·0069
O_A	6·5	260	0·0192
O_B	6·0	288	0·0173
O_C	4·5	171	0·0292
O_D	7·0	294	0·0170
O_E	5·5	264	0·0189
OH	6·5	300	0·0166

Mean $\sigma(x)$ for oxygens = 0·0197 Å
$\sigma(\varrho)$ over whole unit cell = 1·15 e.Å^{-2}

Bond lengths

$\sigma(Si_1–O_C)$ = 0·030 Å	$\sigma(Si_2–O_C)$ = 0·030 Å
$\sigma(Si_1–O_D)$ = 0·019	$\sigma(Si_2–O_D)$ = 0·018
$\sigma(Si_1–O_E)$ = 0·021	$\sigma(Si_2–O_E)$ = 0·020
$\sigma(Si_1–O_A)$ = 0·021	$\sigma(Si_2–O_B)$ = 0·019
Mean $\sigma(Si_1–O)$ = 0·023 Å	Mean $\sigma(Si_2–O)$ = 0·022 Å
Mean σ(Al–O) = 0·019 Å	Mean σ(K–O) = 0·020 Å
Mean σ(O–O) = 0·028 Å	

Standard deviations of mean bond lengths

σ(mean Si_1–O) = 0·012 Å	σ(mean Si_2–O) = 0·011 Å
σ(mean Al–O) = 0·012 Å	σ(mean O–O) around Si_1 = 0·011 Å

For the difference between the mean Si_1–O and mean Si_2–O bond lengths

$\delta l/\sigma = 5{\cdot}19$ (highly significant)

For the difference between the mean Si_1–O and $Si_{\frac{1}{2}}Al_{\frac{1}{2}}$–O = 1·69 ± 0·015

$\delta l/\sigma = 0{\cdot}20$ (not significant)

For the difference between the mean Si_2–O and Si–O = 1·60 ± 0·01

$\delta l/\sigma = 0{\cdot}54$ (not significant)

For the difference between the mean Si_2–O = $1{\cdot}60_0$ and Si_2–O_B = $1{\cdot}64_8$

$\delta l/\sigma = 2{\cdot}22$ (possibly significant)

Discussion

The present analysis has yielded new atomic parameters which depart significantly from the 'ideal' coordinates of Jackson & West (1931, 1933). Certain of these 'distortions' appear to be a common feature of the layer-lattice silicates, and will be discussed in the next section in relation to other recently published structures. Some of the difficulties of the ideal muscovite structure can now be resolved as follows.

(*a*) *Forbidden reflections*

Reflections of the kind 06l, l odd are no longer forbidden since the actual y parameters in muscovite are not multiples of $b/12$ (Table 4). The departures from ideal parameters account for the observed intensities.

(*b*) *Monoclinic angle*

The monoclinic angle for the various layer silicates can be predicted theoretically by considering the packing of the octahedral O and OH sheets, together with the packing of the O and OH surface layers in minerals such as the kaolins (Brindley, 1951). The monoclinic angle for a number of idealized structures is given by $\beta = \cos^{-1}(-a/3c)$, even though the number of layers and their type varies from structure to structure. The $-a/3$ shift for 1M muscovite is across the octahedral layer, the surface layers packing together without stagger. For the ideal $2M_1$ muscovite each octahedral layer shows a shift of $-a/3$, but this is now at $\pm 60°$ to the a-axis—a net shift of $-a/3$, so that $\beta = 94° 55'$ theoretically. Direct superposition of one layer on the next is assumed, the K^+ ions being symmetrically placed in the hexagonal 'holes' in the oxygen surface sheet.

A diagrammatic projection normal to the a–b plane clearly shows that this is not so. The K^+ ion is no longer at the geometric centre of the oxygen network, but is displaced from it, towards the unfilled octahedral sites above and below the K^+ ion; this displacement from the geometric centre of the oxygens is in the reverse direction on the opposite side of the 10 Å layer.

If we assume that $\beta = 95° 11'$ then the interlayer K–K vectors (Smith & Yoder, 1956) are at $\pm 63° 36'$ to the a-axis, rather than $\pm 60°$. The displacement of the K^+ ion from the geometric centre of the oxygens is largely the reason for the departure of β from the theoretical value. Ideally the K–K vector has a length in normal projection of $a/3 = 1{\cdot}72$ Å; and if all the layer stagger occurs in the octahedral layer then certain Si–Si vectors, in normal projection, will also be 1·72 Å. The observed values are 1·85 Å for the appropriate Si–Si vectors, but 2·04 Å for the K–K vector, which confirms that the O–K–O sheets (as well as the octahedral layers) contribute to the observed monoclinic angle.

(*c*) *Distortion and tilt of surface oxygen network from hexagonal*

In the ideal triphormic layer silicate structures the surface of each layer consists of an open hexagonal network of basal oxygen atoms of the Si–O tetrahedra. In several structures examined recently this hexagonal network has been shown to be distorted, usually to an approximately ditrigonal configuration, as in crocidolite (Whittaker, 1949), Mg-vermiculite (Mathieson & Walker, 1954), dickite (Newnham & Brindley, 1956), amesite (Steinfink & Brunton, 1956) and prochlorite (Steinfink, 1958*a*). Mathieson & Walker described the distortion in vermiculite as the net effect of rotations of whole Si–O tetrahedra of about $\pm 5\frac{1}{2}°$. A similar distortion is evident in muscovite, but appears to be greater than for the minerals previously examined, since the basal triads in muscovite have rotated about 13° from the ideal positions, compared with 4°–6° for other minerals. The six oxygens of any hexagon are now at the corners of two interpenetrating triangles which are approx. equilateral and coplanar, with sides 3·9 Å and 5·1 Å respectively. The surfaces thus have a marked ditrigonal rather than hexagonal symmetry. The octahedral layer is less distorted from the ideal hexagonal packing; 'shared edges' of octahedra are shortened in conformity with Pauling's Rules.

Several hypotheses have been advanced to account for this apparently characteristic distortion of the hexagonal layer-lattice silicate surface. Mathieson & Walker (1954) suggested the presence of residual charges on surface oxygens and octahedral cations which, if present, would produce a torque in the right direction. Whittaker (1956) pointed out that this explanation cannot apply to clino-chrysotile, due to the distortion alternating in direction in this two-layer structure. Newnham & Brindley (1956) explain the distortion in dickite as due to the considerable misfit between the tetrahedral and octahedral layers. Bradley (1957) has discussed the possible relationships (for layer silicates) between the 'free' dimensions of the tetrahedral and octahedral layers, the decrease in these dimensions achieved either by ordering or by the rotation of the tetrahedral groups through small angles, and the thickness of the octahedral layer in relation to the strain imposed on it.

In the case of the micas the distortions in the oxygen network are apparently primarily due to misfit between the tetrahedral and octahedral layers. Brindley & MacEwan (1953) have proposed formulae for calculating the b-axes of 'free' tetrahedral and octahedral layers with various cationic substitutions. (The b-dimension only need be considered since $a = b/\sqrt{3}$ very nearly.) For a tetrahedral layer with all sites occupied by Si the b-axis is about 9·10 Å, but for a net with Si:Al = 3:1 the b-axis is about 9·27 Å ($9{\cdot}30 \pm 0{\cdot}06$, Smith & Yoder, 1956). The gibbsite, $Al(OH)_3$, b-axis is 8·64 Å. In muscovite* ($b = 8{\cdot}995$ Å) there must be a considerable contraction of the tetrahedral layer to fit the octahedral layer, which must be correspondingly stretched. Bradley (1957) has pointed out that a stretched octahedral layer probably reduces in thickness; for gibbsite the layer thickness is 2·53 Å, but the octahedral layer in muscovite is approximately 2·12 Å thick.

A rotation of the tetrahedra of about 13°—which is quite feasible—allows the necessary contraction of the silicate layer. This fitting together of different sized layers does not, however, dictate the *direction* in which any given tetrahedra will rotate. It may be that small residual charges on the surface oxygens and octahedral aluminiums govern the direction of rotation. (Such attractive forces would, it is to be noted, initiate rotations in the directions observed).

The parameters (Table 4) show that the Si–O tetrahedra in muscovite are slightly tilted, this being seen more readily in a normal projection on to the a–b face. The tilt of the triad of basal oxygens is matched by the displacement of the apical oxygens O_A and O_B from vertically below Si_1 and Si_2 respectively. The oxygen O_A (and O_B) is ideally sited equidistant from three possible octahedral cation positions. The displacement of O_A (and of O_B) is away from the unoccupied, and towards the two occupied Al sites as expected. Gatineau & Mering (1958) in a one-dimensional structural analysis of muscovite (using 27 00l terms(!)) proposed a 'static disorder of the oxygen network in the c-direction'. It would appear that for such data the effect of temperature and statistical disorder would be difficult to differentiate. The present parameters do not agree with their data nor does their hypothesis of complete ordering of 3 Si and 1 Al fit the accepted space group, $C2/c$.

(*d*) *Oxygen configuration around interlayer cation*

In the ideal muscovite structure the K^+ ion is in 12-coordination with equidistant oxygens, six above and six (symmetry-related) below the K^+ plane. In the real structure the K^+ is still on a two-fold axis but the six independent oxygens are no longer equi

* For $2M_1$ muscovite the b-axis of the separate 10 Å layer is still 8·995 Å approx.

distant (Fig. 6). Fig. 6 also clearly shows the K^+ ion to be closely surrounded by six oxygens at an average distance of 2·81$_2$ Å, and then by an outer shell of six, at a mean distance of 3·39$_0$ Å. Since the sum of the ionic radii for K^+ and O^- in 12-coordination is about 2·95 Å it is clear that the six inner oxygens (three above, interleaved with three below) must be in close contact with the K^+ ion—indeed a bond of 2·81 Å suggests a lower K^+ coordination than 12. These surface oxygens appear to be so displaced from hexagonal symmetry by the strains in the structure that the 'hole' left for the K^+ is too small for this ion to fit into completely. It therefore holds the layers slightly apart, and this is confirmed by the interatomic distance between two oxygens (across the K^+ layer) being 3·4 Å, whereas the expected O–O distance is approximately 2·8 Å.

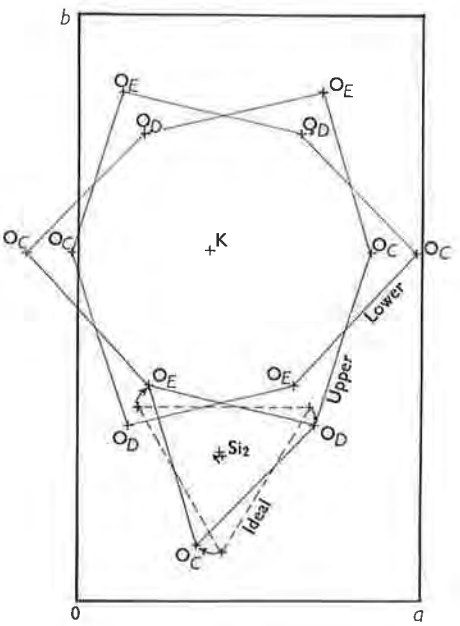

Fig. 6. *Normal* projection on to the *a*–*b* face of some of the atoms in muscovite. This clearly shows the di-trigonal character of the oxygen network, the inner ring of six oxygens around K^+, and the rotation of the tetrahedra from the ideal structure.

The six outer oxygens around the K^+ are still at reasonable distances, except possibly the pair at 3·51 Å away from the K^+ ion; the latter may have little effective bonding to the K^+.

(e) Silicon–aluminium ordering

Ordering of Si and Al atoms—either partial or complete—in tetrahedral 'Si' sites has been observed recently for a number of silicate structures (e.g. felspars). Ordering is usually established by a comparison of observed bondlengths with the data, summarized by Smith (1954), showing the essentially linear increase in 'Si'–O bondlength as the average Al occupancy of the tetrahedral sites is increased. For the pure Si–O bond the distance is close to 1·60 Å; the Al–O bondlength is rather less well-established as 1·78 Å. The bondlengths in muscovite (Table 5) show that the tetrahedral positions are partially ordered, the 'Si_2' sites being almost fully occupied by Si atoms, and the 'Si_1' positions by $Si_{\frac{1}{2}}Al_{\frac{1}{2}}$ atoms on the average. The Si_2–O_B bond (Table 2) may be larger than 1·60 Å because O_B is an apical oxygen, whereas the short O–O distance in the Si_2 tetrahedral base reflects the Si occupancy of this site. This is the maximum ordering possible within the space group ($C2/c$) requirements, and no evidence of lower symmetry—allowing higher ordering—has been found. Further ordering would no doubt cause sufficient displacements of the oxygen atoms to give additional reflections. Nevertheless the result is a little surprising in view of the number of reliable muscovite analyses in which there are exactly three Si and three Al atoms per unit cell; complete ordering might be expected as a possible structural mechanism to ensure this exact 3:1 ratio of Si to Al tetrahedrally.

A satisfying explanation of the ordering of Si and Al in these structures has not been found. Since the tetrahedral cations all have equivalent octahedral configurations in their neighbourhood ordering can hardly be due to muscovite being dioctahedral. It appears, however, that one, or possibly two, oxygens in any surface hexagon are sufficiently distant from the K^+ ion (3·51 Å, and 3·36 Å) to give some local lack of charge balance. Though this may aid any ordering process it is difficult to see how such charge unbalance could *cause* the trigonal symmetry shown by the alternation of Si and $Si_{\frac{1}{2}}Al_{\frac{1}{2}}$ sites around the hexagons.

(f) Polymorphism of muscovite

Polymorphism in the micas arises because an $a/3$ stagger in the octahedral region of each 10 Å layer is combined with the (ideal) hexagonal symmetry of the surface oxygen network. Smith & Yoder (1956), in a discussion of mica polymorphism both theoretically and experimentally, predicted that six simple polymorphs should be observed. For muscovite only the $1M$, $2M_1$, and (less commonly) 3T polymorphs have been found; but the $2M_2$ polymorph has also been observed (for lepidolites) though 20 and 6H micas have yet to be found. Radoslovich (1959) has suggested that the reason for this lies in the trigonal rather than hexagonal symmetry of the actual layer surfaces of micas. Such surfaces can fit together most readily in ways which correspond to no rotation, or to rotations which are multiples of 120°, between layers. Those polymorphs which correspond to rotations between layers which are multiples of 60° (2O, $2M_2$ and 6H) should only be observed in micas showing little or no distortion of the oxygen network.

This hypothesis—if substantiated by several structural analyses—explains the abundance of the $1M_1$,

$2M_1$ and 3T micas, but does not suggest why 3T occurs less frequently than $2M_1$, to which it is converted at high temperature (Smith & Yoder, 1956). For the following discussion of a possible 'mechanism' of structural control it is assumed that

(i) the trigonal symmetry precludes 180° rotations between layers;
(ii) the K^+ ion is displaced from the centre of the oxygen network by some small force;
(iii) the two potassium ions on opposite sides of one layer tend to move as far apart as possible.

Now suppose that K_1^+ at the top of layer A is acted on by a small force in one direction (away from O_D?) within its surrounding oxygen network. In the $1M$ structure the same K_1^+ experiences an opposing force from the bottom of layer B (Fig. 7(a)). A more stable state may be reached, however, if these two forces act as nearly as possible in the same direction. The nearest permissible approach to this, because of the trigonal symmetry, is at 60° to each other; and the resultant force on K_1^+ will lie between the two (Fig. 7(b)). The force on K_2^+ at the top of layer B is

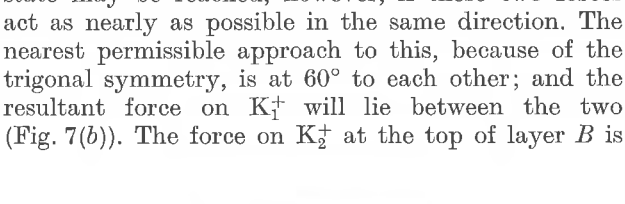

Fig. 7. (a) Forces on the K^+ ions in the $1M$ structure, from successive layers A and B. (b) Forces on the K^+ ions in the $2M_1$ structure, from successive layers A, B and C. (c) ditto in $3T$ structure.

then at 120° to that on K_1^+ at the top of layer A. If layer C also rotates relative to B (to likewise reach a more stable position) then this rotation may be either a further +120°, or else −120°. Of these the latter results in a net force on, and displacement of, K_2^+ which is directly opposite the resultant force on K_1^+. If assumption (iii) is correct then this is the more stable arrangement; and it is seen that the net effect is an alternating ±120° rotation between layers, as required for the $2M_1$ structure (Fig. 7(b)). The alternative position of layer C (Fig. 7(c)) corresponds to the 3T structure. This does not remove K_2^+ as far as possible from K_1^+, and would not be so likely to occur as the $2M_1$ arrangement.

Other layer silicate structures—some hypotheses

The above conclusions lead to interesting speculations concerning structures related to $2M_1$ muscovite.

(a) *Structure of* $1M$ *muscovite*

It is easily shown that the β-angle of the separate 10 Å layers (Smith & Yoder, 1956) in $2M_1$ muscovite is 101° 28′, assuming the layers to be rotated through ±63° 36′ to the a-axis of the $2M_1$ unit cell and using the observed K^+ parameters. This will also be the β-angle of $1M$ muscovite if this has a closely similar layer structure but differs in the stacking of the layers. The *observed* value of β is 101° 35′ ± 5′, and the theoretical value is 100° 0′; so that we may conclude that the $1M$ structure is very similar to one layer of the $2M_1$ structure. Bradley (1957) has also deduced a similar monoclinic angle for $1M$ muscovite, from a hypothetical ordering, based on packing considerations, of the tetrahedral Si and Al ions. His arrangement, however, predicts that the K displacement will be at approx. 15° to the $1M$ a-axis, and requires complete ordering of Si and Al. Neither suggestion is permissible within the space group $C2/m$ suggested by Pabst (1955) for $1M$ micas since the K^+ ion is at 0, ½, 0 and the Si and Al must be completely disordered. (There can only be one, not four, general positions in the unit cell for all the tetrahedral ions). The present hypothesis sets the additional K^+ displacement along the b-axis direction, as required for $C2/m$.

The writer suggests that the unit cell for $1M$ muscovite as proposed for $1M$ micas by Pabst (1955) should be shifted by $c/2$, for convenience in comparing $1M$ and $2M_1$ micas. This places the K^+ at 0, ½, ½ instead of 0, ½, 0, but these special positions are comparable in $C2/m$. For $2M_1$ muscovite ($C2/c$) the K^+ is at 0, y, ¼, the counterpart of 0, ½, ½ in the larger cell, whereas there is no counterpart of 0, ½, 0, which does not fix y.

If the space group proposed recently by Pabst (1955) for the $1M$ structure is correct then the tetrahedral sites must be completely disordered (i.e. four $Si_{\frac{3}{4}}Al_{\frac{1}{4}}$ sites) since there are eight tetrahedral cations and only eight general positions in the unit cell for $C2/m$. For the five other simple polymorphs (Smith & Yoder 1956) there are twice as many general positions as there are tetrahedral cations. Hence partial ordering up to ($Si_{\frac{1}{2}}Al_{\frac{1}{2}}$ and Si) is the maximum possible, if these space groups are correct.

(b) *Trioctahedral layer silicates*

For the trioctahedral micas there is less misfit between the tetrahedral and octahedral layers than for dioctahedral micas, due to their larger octahedral dimensions. The brucite, $Mg(OH)_2$, lattice corresponds to a b-axis of about 9·36 Å (Brindley & MacEwan 1953) and the tetrahedral layer to 9·30 ± 0·06 Å. The b-axis of phlogopite (and biotite) is 9·23 Å, but both

this and the octahedral layer dimensions will vary with ionic substitutions in the latter. The absence of 06*l* reflections with *l* odd confirms that there is less distortion from the ideal structures.

Lepidolite ($K.LiAl_2.Si_4O_{10}(OH)_2$) is particularly interesting because it is the only mica for which the tetrahedral positions are completely occupied by Si. This layer ($b=9{\cdot}10$ Å) should therefore fit easily to an octahedral layer containing some larger Li^+ as well as Al^{+++}; and the value of $b=9{\cdot}07$ Å (Levinson, 1953) is consistent with this. Lepidolite should therefore show little distortion of the hexagonal layer surface; and Levinson (1953) has reported the gradual disappearance of the sensitive 06*l* reflections with *l* odd as the lithium content of muscovite increases.

The analogous structure, pyrophyllite,

$$Al_2Si_4O_{10}(OH)_2\,,$$

which contains no Li^+ in the octahedral position, has a *b*-axis of 8·90 Å, and may therefore be expected to show moderate rotations of the Si–O tetrahedra. In contrast to this the talc structure, $Mg_3Si_4O_{10}(OH)_2$, with $b=9{\cdot}10$ Å appears to be one in which the Si–O tetrahedral layer ($b=9{\cdot}16$ Å) controls the structure by causing some compression of the Mg–O, OH octahedral layer ($b=9{\cdot}36$ Å approx.). The silica sheet in talc is therefore probably fully extended and undistorted.

(*c*) *Brittle micas*

In the brittle micas

(e.g. margarite, $CaAl_2.Al_2Si_2O_{10}(OH)_2$)

which are less common than normal micas, the Si:Al ratio of 1:1 in the tetrahedral layer implies a 'natural' *b*-axis for this layer of $9{\cdot}58\pm0{\cdot}06$ Å (Brindley & MacEwan, 1953). There must be considerable strain between this and the octahedral layer, and since $b=8{\cdot}92$ Å (Mauguin, 1928) even greater rotation of the tetrahedra would be expected than for muscovite.

(*d*) *Paragonite structure*

Suppose that the K^+ of muscovite could be removed and the layers collapsed without pronounced changes in the latter. An approximate calculation shows that a monovalent ion with radius less than 0·93 Å could be accommodated within the six inner oxygens. The Na^+ ion has a radius of 0·95 Å, and paragonite, $NaAl_2(Si_3Al)O_{10}(OH)_2$, is the sodium analogue of muscovite, with closely similar *a*- and *b*-axes, and giving 06*l*, *l* odd reflections. The *c*-axis of paragonite is $19{\cdot}28_5$ Å, and of muscovite is 20·09 Å, which clearly suggests that the paragonite layers have a closely similar structure to muscovite, but that the layers are in contact about the (smaller) Na^+ ion. The β-angle of paragonite is 94° 05′, approximately—not too different from muscovite for this hypothesis.

Pyrophyllite, $Al_2Si_4O_{10}(OH)_2$, with no interlayer ion also has a smaller *c*-axis (18·55 Å) than muscovite.

(*e*) *Prochlorite and corundophillite*

Steinfink (1958*a*, *b*) has discussed certain features of the prochlorite and corundophillite structures on the basis of layer dimensions, but the arguments appear to be inconsistent. It appears incorrect to state (Steinfink, 1958*b*) that 'the dimensions of the octahedral talc layer in the monoclinic polymorph are larger than in the triclinic structure, and the tetrahedral layer has to undergo a larger distortion to fit itself to its octahedral neighbour. The larger value of b_0 in prochlorite also reflects this expansion of the octahedral talc layer'. The implication is that the tetrahedral layer is distorted because it is *smaller* than the octahedral talc layer. But if we compute 'free' layer dimensions by Brindley & MacEwan's approximate formulae (1953), we find

(1) for an $Si_{\frac{1}{2}}Al_{\frac{1}{2}}$–O tetrahedral layer, $b=9{\cdot}58\pm0{\cdot}06$;
(2) for the brucite layer in prochlorite, $b=9{\cdot}06$;
(3) for the talc layer in prochlorite, $b=9{\cdot}50$.

In the *talc* layer, therefore, there should be practically no misfit between the octahedral and tetrahedral layers. It is the *brucite* layer which controls the prochlorite *b*-axis, because there is a limit to the amount which it can be stretched. The tetrahedral distortion occurs to allow the talc layer to *contract* somewhat towards the brucite layer. This is confirmed by the fact that the brucite layer is 1·85 Å thick, against 2·10 Å for brucite itself. The *c*-axis for corundophillite ($14{\cdot}36\pm0{\cdot}02$) may be significantly greater than in prochlorite ($14{\cdot}25\pm0{\cdot}02$) for this reason, and the β-angle of prochlorite may depart from the theoretical value because of the stretching of the brucite layer. It seems unlikely that ordering in these minerals can be due to the very slight dimensional difference between a network of, say, 3 Si–O and 1 Al–O tetrahedra, and of 4 $Si_{\frac{3}{4}}Al_{\frac{1}{4}}$–O tetrahedra. The explanation more probably depends on some local balance-of-charge effect (as proposed for albcites by Ferguson *et al.* (1958)) consequent upon distortion of the lattice.

A detailed structure analysis of the layer silicates should explain any departure of the observed monoclinic angle from the theoretical values, and it is therefore surprising to note some discrepancy in the data for prochlorite. Brindley, Oughton & Robinson (1950) obtained a theoretical angle of 97° 8′ 42″, and a measured angle of 97° 6′ for monoclinic chlorite. Steinfink (1958*a*), however, gives data for a monoclinic chlorite from which β(observed) = 96° 17′ ± 10′ but β(theoretical) = $\cos^{-1} -a/3/c = 97°\ 13'$.

The observed $\beta=97°\ 22'\pm6'$ and the theoretical $\beta=97°\ 8'$ for triclinic chlorite (Steinfink, 1958*b*) are in reasonable agreement, however.

Conclusion

These speculations concerning mica structures can only be tested by precise structure analyses of some or all of these minerals. For this purpose it is important

to apply adequate significance tests (Lipson & Cochran, 1953, p. 309) to bondlengths, especially if detailed interpretations are given to results obtained from few data (as, e.g. in the prochlorite analysis). The present discussion suggests that trial structures for layer silicates may now be proposed which include some degree of distortion, the amount depending on the calculated misfit of the layers, and the direction on the attractive forces due to assumed residual charges.

The mica specimen was kindly supplied by Dr A. W. Kleeman, the refractive indices determined by Dr E. R. Segnit, both of the Department of Geology, University of Adelaide. It is a pleasure to acknowledge helpful discussions with Dr K. Norrish and other colleagues during this work.

References

Berghuis, J., Haanappel, IJ. M., Potters, M., Loopstra, B. O., MacGillavry, C. H. & Veenendaal, A. L. (1955). *Acta Cryst.* **8**, 478.

Bradley, W. F. (1957). *Sixth Nat. Clay Conference Proceedings.*

Bragg, W. L. (1937). *Atomic Structure of Minerals.* London: Oxford University Press.

Bragg, W. L. & West, J. (1929). *Z. Kristallogr.* **69**, 118.

Brindley, G. W. (1951). *X-ray Identification of Clay Minerals*, p. 35. London: The Mineralogical Soc.

Brindley, G.W. & MacEwan, D.M.C. (1953). Ceramics; a symposium, *Brit. Cer. Soc.* p. 15.

Brindley, G. W., Oughton, B. M. & Robinson, K. (1950). *Acta Cryst.* **3**, 408.

Cruickshank, D. W. J. (1949). *Acta Cryst.* **2**, 65.

Ferguson, R. B., Traill, R. J. & Taylor, W. H. (1958). *Acta Cryst.* **11**, 331.

Gatineau, L. & Méring, J. (1958). *Clay Min. Bull.* **3**, 238.

Harrison, F. W. & Brindley, G. W. (1957). *Acta Cryst.* **10**, 77.

Hendricks, S. B. & Jefferson, M. E. (1939). *Amer. Min.* **24**, 729.

Jackson, W. W. & West, J. (1930). *Z. Kristallogr.* **76**, 211.

Jackson, W. W. & West, J. (1933). *Z. Kristallogr.* **85**, 160.

Levinson, A. A. (1953). *Amer. Min.* **38**, 88.

Lipson, H. & Cochran, W. (1953). *The Determination of Crystal Structures.* London: Bell.

Mathieson, A. McL. (1958). *Amer. Min.* **43**, 216.

Mathieson, A. McL. & Walker, G. F. (1954). *Amer. Min.* **94**, 231.

Mauguin, C. (1928). *C. R. Acad. Sci. Paris*, **185**, 288.

Newnham, R. E. & Brindley, G. W. (1956). *Acta Cryst.* **9**, 759.

Pabst, A. (1955). *Amer. Min.* **40**, 967.

Pauling, L. (1930). *Proc. Nat. Acad. Sci. Wash.* **16**, 123.

Radoslovich, E. W. (1959). *Nature, Lond.* **183**, 253.

Smith, J. V. (1954). *Acta Cryst.* **7**, 479.

Smith, J. V. & Yoder, H. S. (1956). *Min. Mag.* **XXXI**, 209.

Steinfink, H. (1958*a*). *Acta Cryst.* **11**, 191.

Steinfink, H. (1958*b*). *Acta Cryst.* **11**, 195.

Steinfink, H. & Brunton, G. (1956). *Acta Cryst.* **9**, 487.

Verhoogen, J. (1958). *Amer. Min.* **43**, 552.

Viervoll, H. & Øgrim, O. (1949). *Acta Cryst.* **2**, 277.

Whittaker, E. J. W. (1949). *Acta Cryst.* **2**, 312.

Whittaker, E. J. W. (1956). *Acta Cryst.* **9**, 855.

Yoder, H. S. & Eugster, H. P. (1955). *Geochim. Cosmochim. Acta* **8**, 225.

Printed in Denmark at Fr. Bagges kgl. Hofbogtrykkeri, Copenhagen

Paper 1-2

REFINEMENT OF THE CRYSTAL STRUCTURES OF COEXISTING MUSCOVITE AND PARAGONITE

by

CHARLES W. BURNHAM and E. W. RADOSLOVICH*

Geophysical Laboratory
Carnegie Institution of Washington,
Washington, D.C.

EXTENDED ABSTRACT

THE CRYSTAL structures of specimens of muscovite and paragonite coexisting in a mica–kyanite schist from Alpe Sponda, Switzerland, have been refined using three-dimensional least-squares techniques. Anisotropic thermal models yield identical R values of 0.038 for 619 muscovite observations and 558 paragonite observations. Refinement of the occupancies of K and Na in the interlayer cation positions gives compositions corresponding to $Mu_{66}Pa_{34}$ for muscovite and $Mu_{13}Pa_{87}$ for paragonite; these results agree with compositions calculated from electron-microprobe analyses of these materials.

Direct comparison of atomic co-ordinates shows that the two crystallographically independent tetrahedral cations are coplanar in both structures, as are the two independent tetrahedral apical oxygen atoms. Within the surface oxygen layer, two of the three independent oxygen atoms are coplanar in both structures. The differing z-co-ordinates of the third oxygens correspond to departures from coplanarity normal to the sheet of 0.266Å (muscovite) and 0.238Å (paragonite). Thus the basal oxygen layer is rippled, or corrugated, by the tilting of each tetrahedron. The extent of corrugation is slightly, but probably significantly, greater in paragonite than muscovite.

Average T—O (T = tetrahedral cation) interatomic distances are 1.645Å and 1.645Å in muscovite, 1.652Å and 1.651Å in paragonite. These averages demonstrate conclusively that, in both structures, each tetrahedron contains a disordered arrangement of Si and Al atoms corresponding to the composition (Si_3Al). The difference of 0.006Å between the muscovite and paragonite averages, results from slight rearrangement of the surface oxygen layers as Na substitutes for K in the interlayer cation position. In muscovite the average of six alkali—O distances is 2.793Å; this decreases to 2.641Å in paragonite.

Structural differences between the two minerals are primarily restricted to the surface oxygen layers. The dioctahedral layers have average Al–O distances of 1.923Å in muscovite and 1.913Å in paragonite; and average O—O distances of 2.824Å (muscovite) and 2.807Å (paragonite) for nine unshared edges, and 2.420Å (muscovite) and 2.417Å (paragonite) for three shared edges.

Thermal models for both structures are very similar. Substitutional disorder in the tetrahedral and interlayer cation positions causes abnormally large rms displacements of co-ordinating oxygen atoms toward these cations.

* Permanent address: Division of Soils, Commonwealth Scientific and Industrial Research Organization, Adelaide, Australia.

Lattice constants and individual interatomic distances have been given previously (Burnham and Radoslovich, 1964). A detailed report of this study is now in preparation. *

REFERENCE

BURNHAM, C. W., and RADOSLOVICH, E. W. (1964) The crystal structures of coexisting muscovite and paragonite, Carnegie Inst. Washington Year Book 63, pp. 232–6.

* Still in preparation by Dr. Burnham
May 1967.

Paper 1-3

Crystal Structures of Coexisting Muscovite and Paragonite

Charles W. Burnham and E. W. Radoslovich

Sound explanations of structural control over polymorphism and isomorphism in the micas are of considerable importance to the metamorphic petrologist. Very few micas have been sufficiently studied by modern crystallographic methods to allow detailed analysis of structural parameters. Since one of the better known mica structures is that of muscovite (Radoslovich, 1960), we thought that an analysis of paragonite, the sodium analogue of muscovite, would provide significant insight into the structural changes accompanying isomorphous replacement in sheet silicates.

Last year one of us reported that excellent single crystals of $2M_1$ paragonite had been obtained from a kyanite schist from Alpe Sponda, Switzerland. Since this specimen also contains $2M_1$ muscovite, presumably formed in equilibrium with paragonite, we considered it worth while to carry out full three-dimensional refinements of both structures. This would provide the first known structural analysis of two similar coexisting minerals from the same hand specimen and would, we hoped, allow detailed evaluation of any variations in tetrahedral aluminum-silicon distribution resulting from the change of K/Na ratio in the interlayer cation positions. Reexamination of the muscovite structure assumed critical importance after Gatineau (1963) presented results,

based on least-squares analysis of Radoslovich's (1960) muscovite data, that differed from those reported by Radoslovich (1960), particularly with respect to aluminum-silicon distribution within the tetrahedral layers.

Full three-dimensional refinements have been carried out with 557 observable *hkl* reflections for paragonite and 619 observable *hkl* reflections for muscovite; data for both crystals were measured using a single-crystal diffractometer with Ni-filtered CuKα radiation and a scintillation detector associated with pulse-height analysis circuitry adjusted to accept 90 per cent of the diffracted characteristic radiation. Unit-cell dimensions of both specimens are listed in table 30. Least-squares refinement of anisotropic thermal models reduced the discrepancy factors, R, to 0.038 (unweighted) and 0.034 (weighted) for paragonite and 0.038 (unweighted) and 0.038 (weighted) for muscovite. The standard error of fit $(= [\Sigma w(F_{obs} - F_{cal})^2/(m - n)]^{1/2})$ is 0.971 for paragonite and 1.305 for muscovite.[21] At this stage no attempt has been made to locate hydrogen, and the refinement has not been biased by any predetermined tetrahedral cation distribution; both crystallographically distinct positions have been assigned the scattering power of fully ionized silicon.

A partial electron-microprobe analysis of both mica specimens for potassium, calcium, and aluminum was kindly undertaken by J. V. Smith. His preliminary results show the paragonite to contain 1.80 to 1.85 weight per cent K_2O and the muscovite to contain approximately 7.8 weight per cent K_2O, with no appreciable calcium present (J. V. Smith, personal communication). Assuming ideal Al/Si ratios, these results correspond to the formulas

Paragonite $(K_{0.15}Na_{0.85})Al_2(Si_3Al)O_{10}(OH)_2$

Muscovite $(K_{0.65}Na_{0.35})Al_2(Si_3Al)O_{10}(OH)_2$

Our refinements were carried through to the final stages assuming incorrect compositions corresponding to Mu_{17} for paragonite and Mu_{74} for muscovite. During the final stage of each refinement, the occupancy of the interlayer alkali positions was allowed to vary, subject to the restriction that the total occupancy of the positions is 100 per cent. The refinements converged to occupancies corresponding to $K_{0.15}Na_{0.85} \pm 0.02$ for paragonite and $K_{0.66}Na_{0.34} \pm 0.02$ for muscovite.

Comparison of the final atomic coordinates shows that the two crystallographically independent tetrahedral cations are coplanar in both structures. The two apical oxygen atoms, O_a and O_b, are also coplanar in both structures. Two of the three oxygen atoms (O_c, O_c) making up the basal triad of each tetrahedron are coplanar, whereas the differing z coordinate of the third oxygen (O_d) causes the basal plane of each tetrahedron to be tilted slightly. The equivalent isotropic temperature factors, B, are remarkably similar atom for atom in the two structures, and the equality of temperature factors for all four tetrahedral cations (0.65, 0.65, 0.62, 0.63) immediately suggests that the aluminum-silicon distribution is identical in all four positions.

Important interatomic distances are listed in table 31. The T_1-O and T_2-O distances demonstrate conclusively that the distribution of tetrahedral cations is disordered and the same in both tetrahedra in both structures. In muscovite the two crystallographically distinct tet-

TABLE 30. Unit-Cell Dimensions of Coexisting Muscovite (Mu_{66}) and Paragonite (Mu_{15}), Alpe Sponda, Switzerland*

	Muscovite	Paragonite
a, Å	5.174 ± 0.001	5.134 ± 0.001
b, Å	8.976 ± 0.001	8.907 ± 0.001
c, Å	19.875 ± 0.003	19.376 ± 0.002
β	95.590 ± 0.006	94.625 ± 0.006

* Values determined by least-squares analysis of precision Weissenberg film measurements.

[21] The expected value of this quantity is 1.0 for a converged least-squares analysis carried out using proper absolutely scaled weights for the observations.

TABLE 31. Interatomic Distances (Å) in $2M_1$ Muscovite (Mu_{88}) and Paragonite (Mu_{15})

Atom Pair	Muscovite	Paragonite
T_1 tetrahedron		
T_1-O_a (apical)	1.642 ± 0.004	1.648 ± 0.002
T_1-O_c	1.645 ± 0.004	1.655 ± 0.004
T_1-O_d	1.643 ± 0.004	1.642 ± 0.004
T_1-O_e	1.649 ± 0.004	1.664 ± 0.003
Mean T_1-O	1.645	1.652
O_a-O_c	2.694 ± 0.005	2.706 ± 0.004
O_a-O_d	2.725 ± 0.005	2.720 ± 0.004
O_a-O_e	2.701 ± 0.005	2.709 ± 0.004
O_c-O_d	2.696 ± 0.005	2.707 ± 0.005
O_c-O_e	2.654 ± 0.005	2.685 ± 0.005
O_d-O_e	2.639 ± 0.005	2.656 ± 0.005
Mean O-O	2.685	2.697
T_2 tetrahedron		
T_2-O_b (apical)	1.644 ± 0.004	1.652 ± 0.003
T_2-O_c	1.648 ± 0.004	1.656 ± 0.004
T_2-O_d	1.644 ± 0.004	1.653 ± 0.003
T_2-O_e	1.645 ± 0.004	1.644 ± 0.004
Mean T_2-O	1.645	1.651
O_b-O_c	2.702 ± 0.005	2.709 ± 0.005
O_b-O_d	2.726 ± 0.005	2.726 ± 0.005
O_b-O_e	2.699 ± 0.005	2.707 ± 0.005
O_c-O_d	2.647 ± 0.005	2.677 ± 0.005
O_c-O_e	2.647 ± 0.005	2.650 ± 0.005
O_d-O_e	2.695 ± 0.005	2.709 ± 0.005
Mean O-O	2.686	2.696
Al octahedron		
Al-O_a	1.943 ± 0.004	1.933 ± 0.002
Al-O_a'	1.920 ± 0.004	1.914 ± 0.002
Al-O_b	1.917 ± 0.004	1.906 ± 0.004
Al-O_b'	1.946 ± 0.004	1.938 ± 0.004
Al-OH	1.907 ± 0.004	1.891 ± 0.004
Al-OH′	1.907 ± 0.004	1.899 ± 0.004
Mean Al-O	1.923	1.913
Mean of 9 unshared O-O	2.824	2.807
Mean of 3 shared O-O	2.420	2.417
Interlayer cation		
K,Na-O_c	2.762 ± 0.004	2.531 ±0. 004
K,Na-O_d	2.823 ± 0.004	2.726 ±0. 004
K,Na-O_e	2.795 ± 0.004	2.668 ±0. 004
Mean K,Na-O	2.793	2.641

(Burnham and Radoslovich, 1963)

rahedra are identical within the precision of the determination. The two tetrahedra in paragonite, although having identical average interatomic distances, are individually somewhat distorted as evidenced by comparing T_1-O_d, T_1-O_e, T_2-O_d, and T_2-O_e distances. The average T-O distances are less than the value of approximately 1.655 Å expected for tetrahedra containing 75 per cent Si and 25 per cent Al (Smith and Bailey, 1963).

Comparison of interatomic distances in the aluminum octahedra shows that this layer is practically unaffected by the change of K/Na ratio in the interlayer cation position. The OH-OH shared octahedral edges are significantly shorter in both structures than the shared O_a-O_a and O_b-O_b edges: 2.370 Å versus 2.448 Å and 2.443 Å in muscovite, and 2.362 Å versus 2.450 Å and 2.439 Å in paragonite. These aluminum octahedra show no unusual distortions attributable to "stresses" arising in the tetrahedral layers or due to the presence of interlayer alkalies. The average Al-O distances correspond closely to those found in other silicates, and distortions from ideality are primarily due to octahedral edge sharing resulting in the expected shared-edge contraction (see, for example, Burnham, 1963*b*).

Because of the marked ditrigonal nature of the tetrahedral sheets (fig. 100), the effective alkali coordination is six rather than twelve. The average of six alkali-O distances reflects the change of K/Na ratio. This composition change has little or no effect on the relative orientations of surface oxygens (O_c, O_d, O_e) between layers.

Of critical importance, then, is the question: What changes *do* take place in the mica framework when sodium is substituted for potassium? In an overall sense, the answer is that there are *no* changes corresponding to first-order effects but that there are some slight shifts corresponding to second-order effects. These manifest themselves primarily as a contraction of the surface oxygen

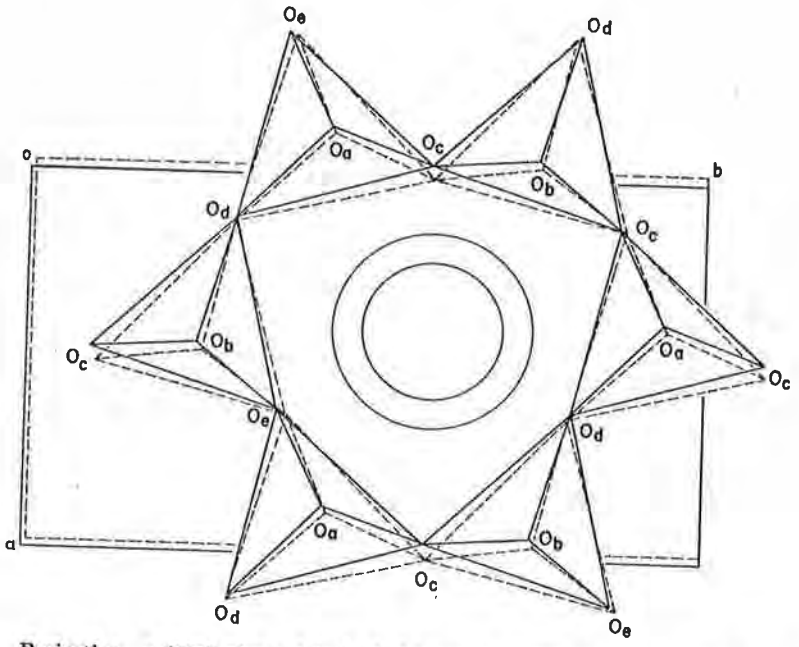

Fig. 100. Projection on (001) of one tetrahedral layer of muscovite (solid lines) and paragonite (dashed lines). The basis for superposition of layers is exact coincidence of alkali atoms. Concentric circles show the relative sizes of K (outer) and Na (inner) atoms.

network and a reduction in the interlayer separation. Note, in table 31, that, of the changes in T-O distances, the greatest is in some of the T-$O_{surface}$ distances, whereas increases in the T-O_{apical} distances are about equivalent to the standard errors. Adjustment of the surface oxygen network to accommodate more Na and less K is seen in the significant changes in some $O_{surface}$-$O_{surface}$ distances; the simultaneous decrease in interlayer separation results in minor increases in only three of the six distinct O_{apical}-$O_{surface}$ distances.

Muscovite-paragonite solid solution. Stability relations within the pseudobinary system muscovite-paragonite have been investigated experimentally by Eugster and Yoder (*Year Book 54*, p. 125) and Nicol and Roy (1964). Both studies have demonstrated that complete solid solution does not exist between muscovite and paragonite within the temperature-pressure regions investigated. A recent study of coexisting muscovites and paragonites by Zen and Albee (1964) shows that the solvus is extremely asymmetric and that the solubility of muscovite in paragonite is very limited. These authors suggest that the maximum on the solvus will lie at approximately 80 mole per cent paragonite.

From a structural point of view, the asymmetric solid solution limits are easily explained by considering the variation of average alkali-oxygen interatomic distances with changing K/Na atomic ratio. In figure 101 the averages obtained in our structure refinements are plotted versus composition. The expected average distances for pure alkalies (in octahedral coordination) are given by the *International Tables for Crystallography* (vol. 3, p. 258) as 2.83 Å for K-O and 2.44 Å for Na-O; Radoslovich (1960) reported an average K-O distance of 2.81 Å for pure muscovite. Figure 101 shows that substitution of Na for K does not result in a linear variation of alkali-oxygen distance, but that the change as Na replaces K is gradual, whereas only a small amount of

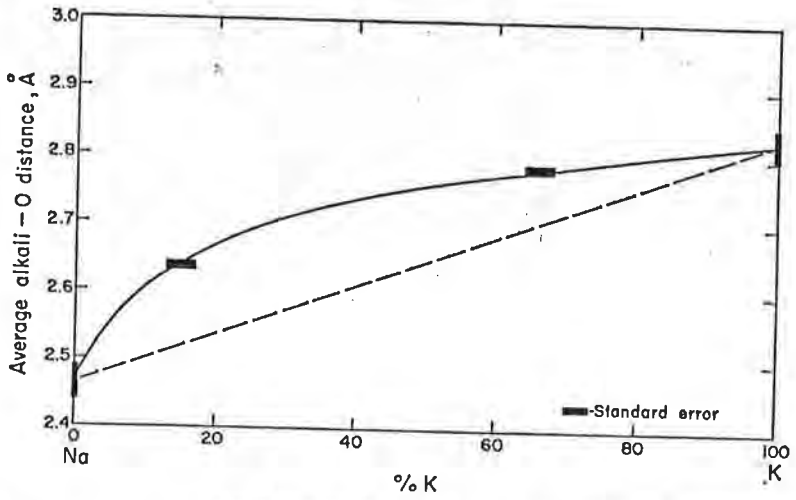

Fig. 101. Effect of Na-K atomic substitution on average six-coordinated alkali-oxygen interatomic distances. Two intermediate points represent average distances in muscovite (Mu_{66}) and paragonite (Mu_{15}). The straight dashed line emphasizes the nonlinearity of the change of average distance with composition.

K substituting for Na causes an appreciable increase in the average distance. This is, of course, an expected result, since an Na ion is considerably smaller than a K ion (Wells, 1962, p. 71), and may fit easily into a K coordination polyhedron, whereas substitution of K for Na requires expansion of the coordination polyhedron. For this reason alone, solid solution involving these atomic species can hardly be ideal.

These structural relations lead to the conclusion that, at room temperature and pressure, paragonite will accept only a very small amount of K substituting for Na, but that muscovite will allow a considerably larger amount of Na to substitute for K, in agreement with the results of Nicol and Roy (1964) and Zen and Albee (1964). The variation of average alkali-oxygen distances furthermore suggests that, in view of the minor changes in the mica framework between Mu_{66} and Mu_{15}, the structural differences between Mu_{66} and Mu_{100} will be negligible. On the other hand, the most significant structural changes will exist between Mu_{15} and Mu_0 (pure paragonite).

Throughout this discussion we have assumed that K and Na are truly disordered in both structures. There is, however, the possibility that the alkalies might be ordered within each interlayer plane. If K ions were restricted to certain planes, Na to others, and the sequence were random in the c direction, there would be no visible superstructure. Evidence for such an arrangement might be found by analyzing the apparent anisotropic thermal motion of the surface oxygens; if each interlayer plane contained only one kind of alkali, the largest apparent rms displacement of the oxygens should be normal to the layers (along c^*), representing this random change in interlayer separation from layer to layer. Although a room-temperature determination is not conclusive, the rms displacements of O_c, O_d, and O_e toward the alkali are larger than they are toward the disordered Si_3Al positions, and none of the longest principal axes is directed parallel to c^*. The large rms displacements toward the alkali tend to uphold a completely random arrangement of alkalies.

COMMONWEALTH OF AUSTRALIA
COMMONWEALTH SCIENTIFIC AND INDUSTRIAL RESEARCH ORGANIZATION

Reprinted from *Clay Minerals Bulletin*, Vol. 4, No. 26, pp. 318-322, (1961).

TRANSPARENT PACKING MODELS OF LAYER-LATTICE SILICATES BASED ON THE OBSERVED STRUCTURE OF MUSCOVITE

By E. W. RADOSLOVICH
Division of Soils, C.S.I.R.O., Adelaide, Australia
and J. B. JONES
Department of Geology, University of Adelaide, Australia

[Received 29th May, 1961]

ABSTRACT

A simple jig is described for the construction of a model of the muscovite structure in which the distorted hexagonal, *i.e.*, ditrigonal, arrangement of the basal oxygens of the tetrahedra is accurately represented. The model is of the *packing* kind as opposed to the *ball-and-spoke* kind and demonstrates the advantages of this type of model, which would be more generally used if transparent plastic balls were available commercially.

INTRODUCTION

Whilst the majority of atomic structure models used both for teaching and research purposes are of the *ball-and-spoke* kind, *packing* models may be far more realistic for teaching and may assist considerably in research. This has been emphasised previously by Hatch, Comeforo and Pace (1952), who also described techniques for making models of hollow, transparent, tinted plastic balls, and pointed out the several notable advantages of such models.

Previous models of the *ideal* mica structure (Jackson and West, 1930) have necessitated the use of enlarged octahedral ions (in order to make this layer close-packed whilst allowing the surface oxygens of the tetrahedral layer to remain in a hexagonal network) together with enlarged potassium ions to produce the deduced separation between layers.

A detailed determination of the structure of muscovite (Radoslovich, 1960) shows that (*a*) the octahedral anions are not in contact with each other, (*b*) the layer surfaces are not hexagonal but ditrigonal due to rotation of the tetrahedra, and (*c*) the holes so produced are smaller than the diameter of the potassium ion. Other micas are probably similar in some of these respects (Radoslovich, 1961).

JIG FOR CONSTRUCTING MUSCOVITE MODEL

A simple jig allows the rapid construction of a muscovite model having such features. Suppose the scale is $\frac{1}{2}$ in.$=1$Å, the oxygen

diameter being 2·6 Å. For $b_{obs}=9{\cdot}0$ Å and $b_{tetr.}=9{\cdot}3$ Å the tetrahedral rotation, $\alpha=13\frac{1}{2}^\circ$ (Radoslovich, 1961). In the *ideal* structure the silicon ions are on a hexagonal grid of side $2{\cdot}6\times\frac{2}{\sqrt{3}}$ Å, which becomes in the ditrigonal model $\frac{2{\cdot}6}{2}\times\frac{9{\cdot}0}{9{\cdot}3}\times\frac{2}{\sqrt{3}}=1{\cdot}45$ in.

The jig consists of a piece of wood with paper attached inscribed with a hexagonal grid, sides 1·45 in. The tetrahedral cations will lie vertically above the centres of some of these hexagons; and where this is so a nail (*N*, Fig. 1) with a $\frac{1}{4}$ in. diameter head is partly driven

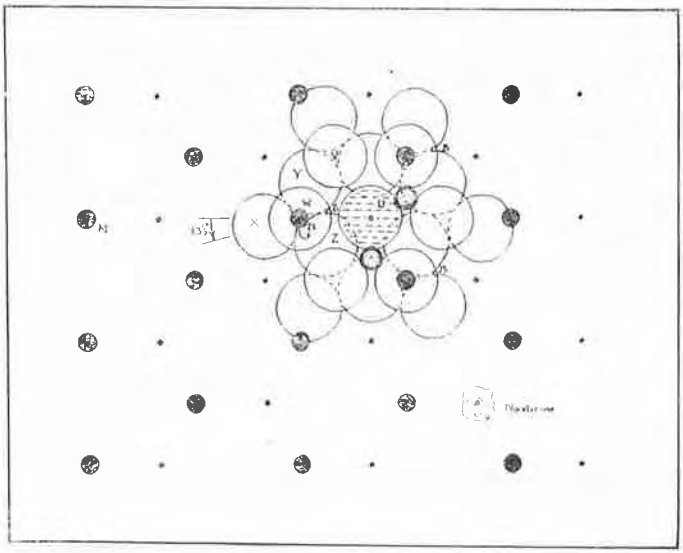

FIG. 1—Diagram of jig for constructing muscovite model. Large circles are oxygens; *X*, *Y*, *Z* are basal and *V*, *W* apical. Shaded circle is hydroxyl, spotted circles are octahedral aluminium; tetrahedral silicon not shown. Solid spots are nails and brads.

in. The height of the nail is adjusted until a tetrahedron constructed of oxygen balls will just sit on its base (*X*, *Y* and *Z*, Fig. 1) over the nail, without wobbling or movement other than rotation. The twist of $13\frac{1}{2}^\circ$ is set out with a protractor at a number of these nail points, and thin brads (*B*, Fig. 1) are fixed so that when a tetrahedral group is placed over the nail the brad lies between two oxygens, *Y* and Z, to give the group its twist. In fact three brads will fix one ditrigonal ring (Fig. 1), and all other tetrahedra will, with careful construction, adjust themselves to make the whole model ditrigonal.

The hydroxyls (*U*, Fig. 1) are situated above the centres of the ditrigonal holes, but not touching *X*, *Y*, and *Z*, so that they must be supported by being glued to the octahedral cations only, which are in turn glued to the apical oxygens, *V*, *W*, etc. Thin nails are therefore fixed at the centres of the ditrigons, and covered with lumps of plasticine, on to which the hydroxyls are pressed until they are level with *V* and *W*. The octahedral cations may now be inserted and glued, after which the whole layer may be lifted free of the jig. A second tetrahedral layer is then constructed on the same jig.

At this point one must decide how the model is to be dissected, if at all. Our model can be split at the octahedral layer because the

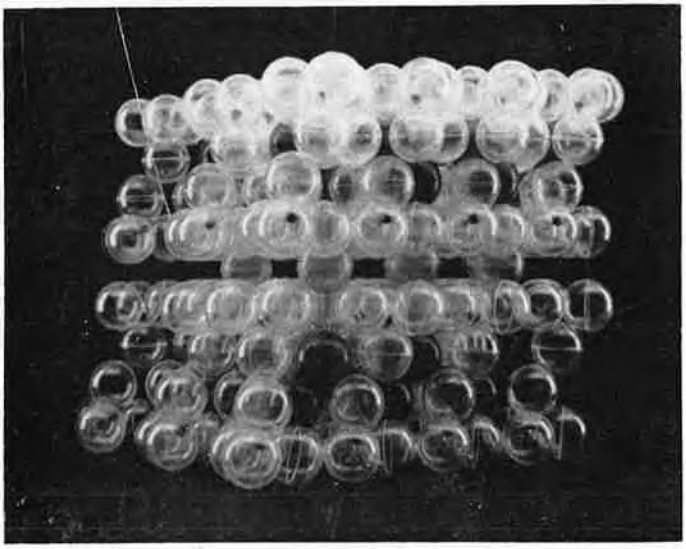

FIG. 2—Edge view of muscovite model.

hydroxyls for the top tetrahedral layer have been glued on the top of the previously constructed layer; thus, they are correctly attached to the octahedral cations. The second tetrahedral layer fits this layer readily because of the gaps between neighbouring octahedral anions. The model is completed by glueing (or loosely positioning) tinted spheres for the potassiums (Fig. 2).

This model and jig may be used for other structures quite readily. Thus, for kaolinite loose hydroxyls can be added to the layer constructed first and for chlorite the inter-layer potassium ions are omitted and replaced by a brucite layer (Fig. 3). In constructing the brucite layer the second tetrahedral layer should begin using oxygen

triads only; when this triad sheet has been glued it forms a jig on which to place hydroxyls for the construction of brucite, on the same scale as muscovite. Other micas, such as trioctahedral micas, can obviously be formed using extra cations, and micas with different twists can be made by changing α in the above.

Discussion

These models effectively illustrate several features of the mica structures. (*a*) The rotations in the tetrahedral layer force the interlayer potassium out of the surface (Fig. 2) sufficiently to keep successive muscovite layers clearly separated (Radoslovich, 1960).

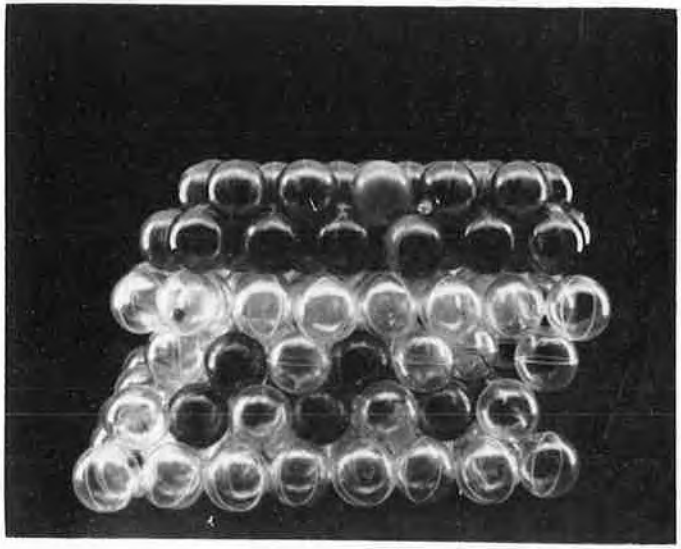

Fig. 3—Edge view of chlorite model.

(*b*) Larger octahedral cations will increase the space between the anions, thereby expanding this layer and untwisting the tetrahedral layers (Radoslovich, 1961). (*c*) The ditrigonal symmetry of the surface networks is obvious (Figs. 1 and 4) and this can be related to mica polymorphism (Radoslovich, 1959) by superimposing layers across the interlayer region. These figures should be compared with those of Hatch, Comeforo and Pace (1952).

Need for a Source of Spheres

The construction of silicate models would be much easier if hollow spheres (or hemispheres) of diameter 1·3 in., as described above, were available commercially. The present model requires 300-400

oxygen balls which also serve (when tinted) as hydroxyls, fluorines, potassiums or bariums; with the scale adjusted they would represent sulphurs in sulphide models. Making these balls takes the major part of the construction time; the smaller opaque balls present little difficulty. It is therefore suggested, in support of the plea by Hatch, Comeforo and Pace (1952), that, if the demand were sufficient,*

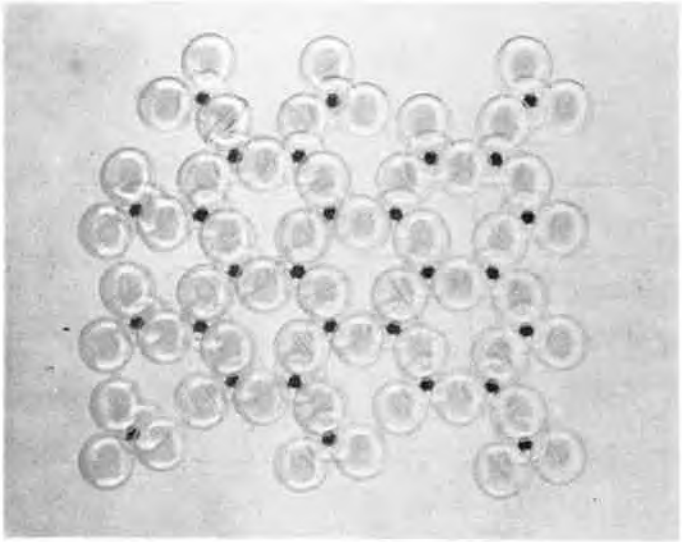

FIG. 4—Face view of tetrahedral layer of muscovite model, showing ditrigonal network of oxygens.

some manufacturer of plastics should produce clear transparent spheres of this one size at a moderate cost; on a minimum order of 10,000 spheres (which is a very small order for injection moulding of perspex) an appropriate cost of eightpence, sterling, each has been quoted to the authors.

Acknowledgements.—The thanks of the authors are due to Mr R. Welfare and Mr R. B. Major for technical assistance in the construction of the models.

REFERENCES

HATCH, R. E., COMEFORO, J. E., and PACE, N. A., 1952. *Amer. Min.*, **37**, 58.
JACKSON, W. W., and WEST, J., 1930. *Z. Kristallogr.*, **76**, 211.
RADOSLOVICH, E. W., 1959. *Nature, Lond.*, **183**, 253.
RADOSLOVICH, E. W., 1960. *Acta Cryst.*, **13**, 919.
RADOSLOVICH, E. W., 1961. *Nature, Lond.*, **191**, 67.

*It might be possible to assess demand and organize production through one of the professional societies; meantime, the authors would be glad to hear from others interested.

Paper 1-5

COMMONWEALTH OF AUSTRALIA
COMMONWEALTH SCIENTIFIC AND INDUSTRIAL RESEARCH ORGANIZATION

Reprinted from *Acta Crystallographica*, Vol. 12, Part 11, November 1959
PRINTED IN DENMARK

Acta Cryst. (1959). **12**, 937

Accuracy in structure analysis of layer silicates.

By A. McL. Mathieson,* E. W. Radoslovich† and G. F. Walker*, *Commonwealth Scientific and Industrial Research Organization, Melbourne, Australia.*

(*Received* 12 *August* 1958 *and in revised form* 8 *May* 1959)

In several of the analyses of layer silicates reported during recent years, it is claimed that small departures from the high symmetry of the 'ideal' structures have been demonstrated. In addition to displacements of atoms, variations in the filling of, or substitution in, tetrahedral and octahedral sites have been inferred.

In order to justify these claims, diffraction data which are sufficiently accurate and extensive both in angular (θ) and amplitude (F) range are an essential prerequisite, for minor details of the final stage of the refinement can hardly be considered significant unless the number of structure amplitudes measured is considerably in excess

* Chemical Research Laboratories, Melbourne.
† Division of Soils, Adelaide.

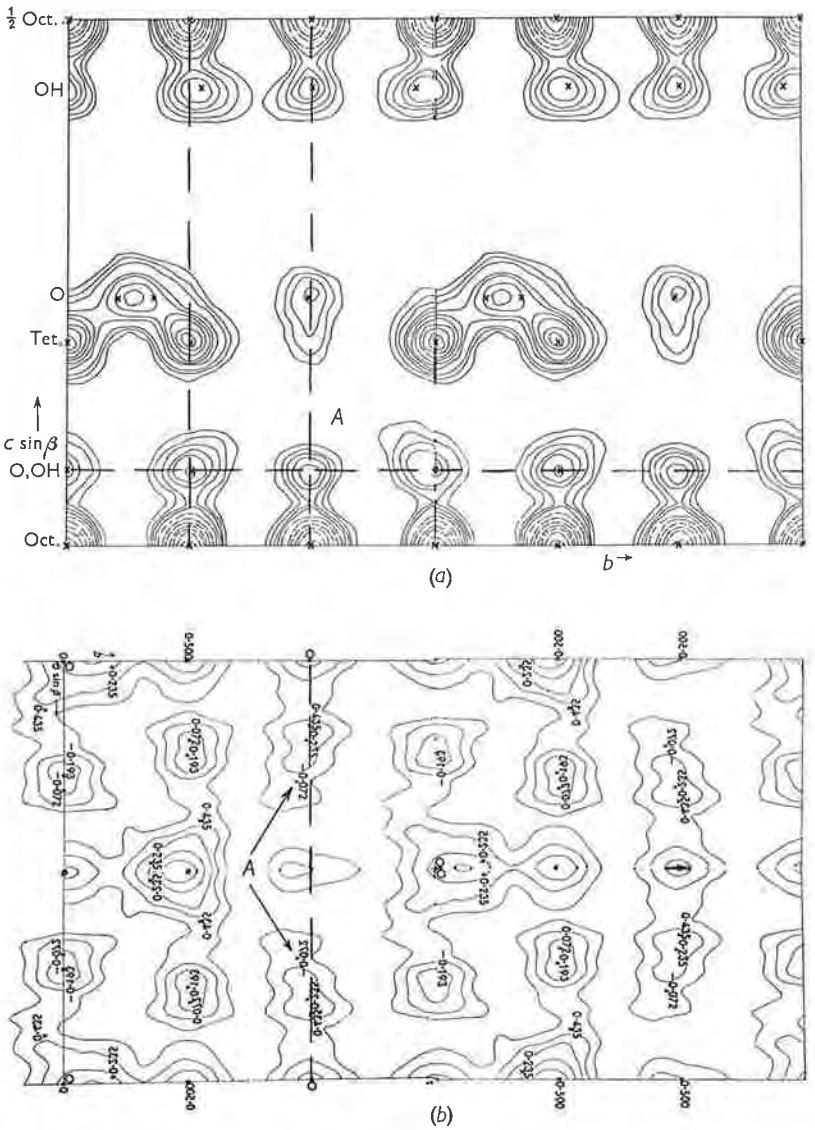

Fig. 1. (*a*) An extended reproduction of the (0*kl*) projection of Steinfink's paper with dashed lines superimposed at $y = \frac{1}{6}$, $\frac{1}{3}$ and $z = 0{\cdot}072$. *A* refers to atom OH_1. (*b*) An extended reproduction of the (*hk*0) projection of Steinfink's paper, adjusted so that the *b* axis is on the same scale as Fig. 1(*a*).

of the number of parameters deduced.* Extensive overlap of atoms in the two-dimensional projections generally used and the high symmetry of the 'ideal' structures require that deviations from special positions be supported by unambiguous evidence. The methods currently employed for assessing the accuracy of the electron-density distributions, atomic parameters and the significance of differences in bond lengths at each stage of the refinement (Lipson & Cochran, 1953; Jeffrey & Cruickshank, 1953) are hence of particular importance in the analysis of layer silicates. Where no recourse to these criteria has been made, plausible but unwarranted structural features have been proposed.

As an obvious example of the effects of inadequate data, the recent analysis of a chlorite by Steinfink (1958) may be cited. In this analysis, 51 positional parameters, as well as hidden parameters involved in loading the atomic scattering curves, are claimed to have been derived from 28 *hk*0 and 50 0*kl* structure amplitudes, with an accuracy, implied by the later discussion, of considerably better than $\pm 0{\cdot}05$ Å, although no actual limits are quoted. The suspect nature of the atomic parameters and inter-atomic distances derived from these data is immediately apparent from a comparison of the tabulated atomic parameters (Table 2 of the paper) with the contoured electron-density maps (Figs. 1 and 2 of the paper). In our Fig. 1, we have placed in juxtaposition extended reproductions of Steinfink's (0*kl*) and (*hk*0) electron-density projections. Inspection reveals the following, more obvious, points of criticism:

(i) The displacement of atoms OH_2 and OH_4 (Fig. 1(*a*)) from 'ideal' positions is justified by Steinfink on the basis of the asymmetry of their peak distributions. Atom O_2, however, which shows equally marked asymmetry of distribution, is assigned an 'ideal' position.

(ii) No account is taken of the ridge extending from O_5 in the *z*-direction, while a displacement of the *y*-parameter of this atom is held to be significant. The latter displacement involves a shift of $\Delta y = 0{\cdot}333 - 0{\cdot}328 \equiv 0{\cdot}046$ Å.

(iii) The selected *y* parameter of atom OH_1, as indicated in the (*hk*0) projection at *A* (Fig. 1(*b*)) is clearly inconsistent with the observed peak distribution in the more reliable (0*kl*) projection* (Fig. 1(*a*)). In this connection, it should be pointed out that the projection corresponding to the (*hk*0) contour map is inherently extremely complex due to overlap. With typical peak heights of individual octahedral, tetrahedral and oxygen sites of the order of 46, 50 and 20 e.Å^{-2} respectively (derived from Mathieson, 1958), it is evident that this projection is so crowded by the heavier scattering units that exact deductions regarding oxygen positions cannot be expected from 28 structure amplitudes.

These considerations lead us to the conclusion that the probable errors in this analysis are much greater than would be required to substantiate a real deviation from the 'ideal' structure and hence, to support the subsequent detailed argument put forward by Steinfink.

In view of the increasing interest presently being shown in the analysis of layer silicates, we are of the opinion that a general plea for caution in the interpretation of minor details in such analyses is called for, more particularly in the interests of those not fully conversant with the methods of structure analysis and hence unable to judge the strength of the evidence presented.

References

Jeffrey, G. A. & Cruickshank, D. W. J. (1953). *Quart. Rev.* **7**, 335.

Lipson, H. & Cochran, W. (1953). *The Crystalline State*, Vol. III. London: Bell.

Mathieson, A. McL. (1958). *Amer. Min.* **43**, 216.

Steinfink, H. (1958). *Acta Cryst.* **11**, 191.

* Because it is implicit in the Fourier technique of structure refinement using data of the normal measured accuracy e.g. by eye-estimation, this condition should be self-evident; however, its significance appears to be frequently overlooked or under-estimated.

* Although neither projection is based on adequate data, *y* parameters derived from the (0*kl*) projection with 50 terms will be more trustworthy than those from the (*hk*0) projection with 28 terms.

Printed in Denmark at Fr. Bagges kgl. Hofbogtrykkeri, Copenhagen

COMMONWEALTH OF AUSTRALIA
COMMONWEALTH SCIENTIFIC AND INDUSTRIAL
RESEARCH ORGANIZATION

(*Reprinted from Nature, Vol.* 183, *p.* 253 *only, Jan.* 24, 1959)

Structural Control of Polymorphism in Micas

THE extensive polymorphism shown to exist among the mica minerals by Hendricks and Jefferson[1] has been confirmed by a number of workers in more recent years[2,3]. Polymorphism similarly has been clearly demonstrated for other layer lattice silicates, for example, for the chlorites by Brindley, Oughton and Robinson[4].

It is well known that micaceous minerals can form polymorphs principally because the surfaces of the individual silicate layers are composed of oxygen atoms arranged in hexagonal networks. Thus the successive layers can be superimposed or stacked in a number of different ways, in each of which the two hexagonal layer surfaces pack together identically, oxygen to oxygen ; but these different ways of layer stacking can give rise to different symmetries and unit cells in the total structure. The successive layers may be regarded as being related to each other by regular rotations between layers, this being geometrically equivalent to regular translations of successive layers along either the *a*-axis or the *b*-axis or both. (The concept of rotations between layers is geometrically simpler, but that of translations may be more acceptable physically.)

Smith and Yoder[5] have developed a theory based on these ideas to predict all the possible polymorphs of micas which may occur. They have shown that there are six simple ways of stacking mica layers in an ordered manner, these being based on "inter-layer stacking angles" as follows : $1M$ (one-layer monoclinic) on 0° stacking angles, $2M_1$ on alternating 120° and 240° angles, $3T$ (three-layer trigonal) on 120°, $2O$ (two-layer orthorhombic) on 180°, $2M_2$ on alternating 60° and 300°, and $6H$ (six-layer hexagonal) on 60° angles. While Smith and Yoder discussed the possible factors governing the growth of various polymorphs (including forces due to distortions of the hexagonal oxygen networks) it was not possible to explain, on the evidence then available, their observed relative abundance. It was noted, however, that only the $1M$, $2M_1$, and $3T$ polymorphs are

common in Nature, and that $2O$ and $6H$ specimens had not been found at all. Lepidolite specimens crystallizing with the $2M_2$ structure have been described by Levinson[2] and others.

The rarity or non-occurrence of the $2O$, $2M_2$ and $6H$ mica polymorphs appears to me to be explained fairly satisfactorily by the observed departures of layer-lattice silicates from their idea structures as reported in several recent analyses (of vermiculite[6], of dickite[7] and of amesite[8]). In each of these the oxygen network is distorted from a hexagonal array to one in which the oxygen atoms are arranged on two interpenetrating triangles of different sizes. For vermiculite these are two isosceles triangles with the equal sides 4·35 and 4·84 A. respectively; but it is to be noted that both triangles are very nearly equilateral. Mathieson and Walker point out that the distortion can be viewed as due to a rotation of triads of oxygen of about $5\frac{1}{2}°$. I am at present re-investigating the $2M_1$ muscovite structure; and while the atomic parameters are not finally fixed it is clear that a similar—though probably greater—distortion of the oxygen network exists in this mica.

The net effect of such distortions is to lower the symmetry of the surface layer from hexagonal to approximately, though not precisely, trigonal. Those polymorphs which result from interlayer stacking angles of 0°, 120° or 240° may therefore occur fairly readily, though their relative abundance may depend on how nearly trigonal the oxygen network is in a given mineral. But those polymorphs based on angles of 60°, 180° or 300° may be expected to occur infrequently (and only as fine-grained specimens), since considerable adjustments of oxygen positions on each layer face would be necessary.

The above argument seems to be supported by the fact that the $2M_2$ mica structure has only been observed for lepidolites. Smith and Yoder[5] pointed out the controlling effect of the linked array of SiO_4 and AlO_4 tetrahedra on the dimensions of the micas; and Newnham and Brindley[7] have attributed the rotations of these tetrahedra in dickite to the misfit of the 'oversize' tetrahedral layer on to the smaller octahedral layer. The lepidolites have less tetrahedral aluminium-for-silicon substitution than other micas, and this layer will thus have dimensions more nearly equal to the (smaller) octahedral layer.

It may be expected that there will therefore be less strain in lepidolites due to tetrahedral–octahedral misfit. This suggests that the oxygen configuration will show a smaller degree of distortion from the ideal hexagonal symmetry, thus allowing a polymorph based on 60° rotations (such as $2M_2$) to occur.

This hypothesis can, of course, only be tested

satisfactorily by an accurate analysis of the $2M_2$ lepidolite structure.

For micas other than lepidolites and brittle micas the tetrahedral layer has cation composition $Si_{3/4}Al_{1/4}$, and this network, according to Smith and Yoder[5], should have b-dimensions of $9{\cdot}30 \pm 0{\cdot}06$ A. There will be little distortion of the oxygen hexagons in those micas having a b-axis close to this value (for example, phlogopites and some biotites). If the above argument is valid then the $2O$, $2M_2$ and $6H$ polymorphs may occur among these micas.

E. W. RADOSLOVICH

Division of Soils,
Commonwealth Scientific and
Industrial Research Organization,
Adelaide.

[1] Hendricks, S. B., and Jefferson, M. E., *Amer. Min.*, **24**, 729 (1939).
[2] Levinson, A. A., *Amer. Min.*, **38**, 88 (1953); **40**, 41 (1955).
[3] Yoder, H. S., and Eugster, H. P., *Geochim. and Cosmochim. Acta*, **8**, 225 (1955).
[4] Brindley, G. W., Oughton, Beryl M., and Robinson, K., *Acta Cryst.*, **3**, 408 (1956).
[5] Smith, J. V., and Yoder, H. S., *Min. Mag.*, **31**, 209 (1956).
[6] Mathieson, A. L., and Walker, G. F., *Amer. Min.*, **94**, 231 (1954).
[7] Newnham, R. E., and Brindley, G. W., *Acta Cryst.*, **9**, 759 (1956).
[8] Steinfink, Hugo, and Brunton, George, *Acta Cryst.* **9**, 487 (1956).

Printed in Great Britain by Fisher, Knight & Co., Ltd., St Albans

"HYDROMUSCOVITE WITH THE $2M_2$ STRUCTURE—A CRITICISM"

BY

E. W. RADOSLOVICH

Reprinted from American Mineralogist, **45**: (1960)
Pages 894-898

THE AMERICAN MINERALOGIST, VOL. 45, JULY-AUGUST, 1960

"HYDROMUSCOVITE WITH THE $2M_2$ STRUCTURE—A CRITICISM"

E. W. RADOSLOVICH, *Division of Soils, Commonwealth Scientific and Industrial Research Organization, Adelaide, Australia.*

A recent paper by Threadgold (1959) has reported chemical, differential thermal and x-ray diffraction data on a hydromuscovite from Mt. Lyell in Tasmania. Threadgold gives data which are claimed to show that this hydromuscovite has the $2M_2$ structure, a mica polymorph previously only found amongst the lepidolites (Levinson, 1953). Radoslovich (1959) has recently suggested, however, that the theoretical polymorphs 2O, $2M_2$ and 6H, which are based on 60° rotations between layers (Smith

and Yoder, 1956) may be expected to be rare or non-existent among the muscovites, because of the markedly ditrigonal symmetry of the oxygen network (Radoslovich, 1960, in press).

Since this specimen is the first reported $2M_2$ mica other than lepidolite it was decided to re-examine it. A careful survey did not reveal any material sufficiently coarse-grained for single crystal methods, so that powder diffraction techniques must be used. For this purpose a 19 cm. diameter evacuated powder camera was used to record consecutively (under the same conditions) the diffraction patterns of various polymorphs and mixtures of polymorphs. The camera is equipped with knife-edges, and has been carefully calibrated using a quartz standard. A Hilger film-measuring rule was used for obtaining θ values, and the corresponding d spacings were determined by extrapolation from the table published by Rose (1957).

The following mica specimens were photographed under standard conditions.

(a) Hydromuscovite from Lyell Comstock Mine, Mt. Lyell, Tasmania; kindly supplied by I. Threadgold, C.S.I.R.O., Melbourne.
(b) 1M muscovite from Iron Monarch quarries, Sth. Australia; kindly supplied by E. R. Segnit, University of Adelaide.
(c) $2M_1$ muscovite from Spotted Tiger Mine, Central Australia as studied by Radoslovich (in press, 1960).
(d) A 2:1 mixture of (b) and (c).
(e) $2M_2$ lepidolite from the Brown Derby pegmatite, Gunnison County, Colorado, described as #505 by Levinson (1953); kindly supplied by Prof. E. Wm. Heinrich, Univ. of Michigan.

The d spacings for each of these micas are given in Table 1, with the visually estimated intensities.[1] By direct comparison of the photographs—which show high resolution—it is clear that the Mt. Lyell hydromuscovite is not identical with the $2M_2$ lepidolite specimen, but in fact shows considerably better agreement with the 2:1 mixture of 1M and $2M_1$ polymorphs. These are, of course, subtle variations in relative line intensities, but these are not unexpected in layer-silicates, both because of orientation effects and because the hydromuscovite differs a little chemically from the 1M and $2M_1$ specimens. A print of the photographs of specimens (*a*), (*d*) and (*e*) is given in Fig. 1; the detail does not reproduce well.

In view of the slight intensity discrepancies between the Mt. Lyell hydromuscovite and the authentic muscovite polymorphs examined it cannot be claimed categorically that this hydromuscovite is a mixture

[1] Victor (1957) has also given data for a mixture of 70% 2M, and 30% 1M muscovite.

TABLE 1. *X*-RAY POWDER PHOTOGRAPH DATA FOR FIVE MICAS

(*d* values in Å)

a		*b*		*c*		*d*		*e*	
9.96	s	10.07	s	10.02	s	9.97	s	9.93	m
4.97	m	5.00	w-m	4.99	m-s	4.98	m	4.97	m
4.448	vs	4.487	s	4.453	vs	4.460	vs	4.465	s
4.342	w	4.342	w-m			4.343	w	4.327	w
4.258	w			4.278	w	4.268	w		
4.093	vw (br.)	4.093	w-m	4.089	w	4.087	w-m		
				3.951	vw			3.969	w
3.868	m			3.868	m	3.866	w-m	3.855	m
3.780	vw								
3.713	vw			3.721	m	3.718	w-m	3.710	vw
3.647	m-s	3.647	s			3.640	m-s	3.611	m-s
				3.575	vvw				
3.478	m-s	3.482	vvw	3.480	s (br.)	3.478	m	3.473	m-s
3.316	vs	3.337	s	3.326	vs	3.327	vs	3.314	m-s
		3.208	vvw	3.250	vw	3.245	vvw		
3.1820	m			3.190	m-s	3.1836	w	3.195	m-s
3.1180	vw			3.0830	vw			3.0710	m
3.0382	m	3.0593	s	3.0480	vw	3.0570	m		
2.9675	w-m			2.9798	m-s	2.9728	w-m	2.9714	vw
2.9145	w-m	2.9211	w			2.9142	w		
								2.8860	m
2.8454	m			2.8542	m-s	2.8475	w-m	2.8490	m
2.7818	m			2.7818	m	2.7769	w	2.7700	w-m
2.6986	vw	2.6772	w-m			2.6736	w		
2.5745	vs	2.5875	w-m	2.5820	m	2.5783	m	2.5686	vs
2.5495	(br.)	2.5585	v.s. (br.)	2.5530	vs	2.5528	vs		
2.4800	vw	2.4773	vvw	2.4922	vw (br.)	2.4986	vvw	2.4780	vw
				2.4540	w	2.4530	vw		
2.4336	w (br.)	2.4327	w	2.4313	w	2.4319	w		
2.4083	w			2.4075	vvw			2.4148	m (br.)
2.3834	w (br.)	2.3918	w	2.3887	vw	2.3890	w		
				2.3720	m	2.3708	w	2.3744	vw
2.3249	vvw	2.3509	w			2.3525	vw		
2.2934	vvw							2.3006	vw (br.)
2.2666	vvw	2.2440	w						
2.2381	w-m			2.2401	w-m (br.)	2.2384	w	2.2438	m
2.1999	w	2.2096	vw	2.1982	w-m			2.2156	vw
		2.1901	vvw					2.2027	vw
2.1730	w			2.1752	w			2.1733	w
2.1372	w			2.1429	w-m				
2.1180	w	2.1020	vw	2.1224	m-s	2.1236	w-m	2.1230	vw
2.0727	w-m (br.)	2.0766	w-m	2.0590	vw	2.0766	w	2.0902	vw
2.0402	w			2.0475	w			2.0551	w
2.0314	w							2.0266	
2.0144	w								
1.9912	w-m	2.0022	w-m (br.)	1.9944	m (br.)	1.9945	m (v. br.)	1.9824	m-s
1.9628	vvw			1.9658	w-m	1.9637	w		
1.9390	vvw	1.9454	v.w. (br.)	1.9440	w	1.9436	w		
1.9102	vvw								
				1.8881	vw				
				1.8161	vw				
				1.7420	vvw				
				1.7269	w	1.7274	vvw		
1.7079	vw			1.7084	vw	1.7081	vw		
1.6942	vw			1.6947	vw				
1.6821	vw	1.6856	vvw	1.6862	vw	1.6871	vvw	1.6884	m
				1.6723	vvw			1.6731	w-m
1.6581	w (br.)	1.6662	w-m	1.6627	w	1.6629	w (br.)		
1.6407	vw			1.6439	m	1.6423	vw		
1.6302	w-m	1.6307	m (v.br.)			1.6307	w		
				1.6237	w			1.6296	w
				1.6104	w				
1.6011	w			1.5980	w-m	1.5919	vw (br.)	1.6041	w
1.5783	w	1.5717	w			1.5681	vw	1.5856	w
								1.5707	

a Hydromuscovite, Mt. Lyell, Tasmania
b 1M muscovite
c $2M_1$ muscovite
d 2:1 mixture of (b) and (c)
e $2M_2$ lepidolite

vs very strong
s strong
m-s medium to strong
m medium
w-m weak to medium

w weak
vw very weak
vvw just discernible
br broad
bracket = band

TABLE 1 (*continued*)

a		*b*		*c*		*d*		*e*	
1.5594	w			1.5531	w-m	1.5491	vvw		
				1.5406					
								1.5377	vw (br.)
				1.5228	w-m	1.5225	vw		
				1.5065	vw				
1.4947	s	1.4978	vs (br.)	1.4959	vs	1.4955	s	1.4985	s
		1.4791	w	1.4804	vvw	1.4794	w		
				1.4678	vvw				
1.4465	vvw			1.4521	w				
1.4220	w (v.br.)	1.4299	vw	1.4289	vw				
		1.4234	vw	1.3938	vvw				
		1.3746	w (br.)	1.3712	vvw	1.3722	w. band		
1.3483	w	1.3405	w (br.)	1.3516	m				
1.3346	vw			1.3374	w-m	1.3377	w (br.)		
1.3220	vw	1.3293	vvw	1.3206	vw band			1.3123	w (v.br.)
1.2949	w	1.2972	w	1.2923	m band	1.2947	w	1.2957	m-s
1.2904		1.2880				1.2868			
1.2745	vw band			1.2760	w				
				1.2707	w				
1.2463	w-m	1.2484	vw	1.2459	w-m	1.2436	w band		
1.2426		1.2414		1.2369	w-m				
				1.2181	w (br.)	1.2173	w band		
		1.1878	vw						
		1.1624							
1.1694	w-m								
1.1173									
		1.1118	vvw	1.1118	w (br.)				
		1.1015	vw	1.1017	w (br.)				
		1.0923	w (v.br.)						
1.0930	w								
1.0870									
1.0124	v.w.	1.0136	v.w.						
1.0085		1.0087							

of 1M and $2M_1$ polymorphs, though the diffraction data are in better agreement with this mixture than with $2M_2$ lepidolite. It should be further remarked that the pattern of a $2M_2$ muscovite (when found) will not necessarily be identical with the observed pattern of $2M_2$ lepidolite. This re-examination therefore clearly shows that the Mt. Lyell hydromuscovite has not been proved to be a $2M_2$ polymorph. Indeed it will be very difficult to demonstrate conclusively that the $2M_2$ polymorph of muscovites exists at all, by powder methods. For this reason it will, in the writer's opinion, first be necessary to find a $2M_2$ muscovite (if such exists) by single crystal methods, in order to provide standard $2M_2$ muscovite powder data, against which unknown polymorphs can be compared with certainty.

FIG. 1. *X*-ray powder photographs. (Above) 2:1 mixture of 1M muscovite and $2M_1$ muscovite, (*d*). (Middle) Hydromuscovite from Mt. Lyell, Tasmania, (*a*). $2M_2$ lepidolite (*e*).

References

Levinson, A. A. (1953), Studies in the mica group: *Am. Mineral.*, **38**, 88–107.

Radoslovich, E. W. (1959), Structural control of polymorphism in micas: *Nature*, **183**, 253.

Radoslovich, E. W. (1960), The structure of muscovite: *Acta Cryst.* In press.

Rose, A. J. (1957), Tables permettant le dépouillement des diagrammes de rayons X, C.N.R.S. Paris.

Smith, J. V. and Yoder, H. S. (1956), Studies of the mica polymorphs: *Min. Mag.*, **31**, 209.

Threadgold, I., (1959), Hydromuscovite with the $2M_2$ structure; *Am. Mineral.*, **44**, 488.

Victor, Iris. (1957), Burnt Hill Wolframite Deposit, Canada. *Econ. Geol.*, **52**, 149.

Paper 2-3

COMMONWEALTH OF AUSTRALIA
COMMONWEALTH SCIENTIFIC AND INDUSTRIAL
RESEARCH ORGANIZATION

(*Reprinted from Nature, Vol.* 191, *No.* 4783, *pp.* 67–68, *July* 1, 1961)

Surface Symmetry and Cell Dimensions of Layer Lattice Silicates

In a previous communication[1] it was pointed out that the ditrigonal surface symmetry observed for a number of layer lattice silicates probably plays an important part in determining polymorphism among the micas. This idea has now been extended considerably by theoretical and experimental studies to be reported elsewhere. It appears to me that the ideal layer lattice structures must have ditrigonal, rather than hexagonal, surface symmetry. That is, the tetrahedral groups apparently can rotate quite readily about axes normal to the sheets to allow the tetrahedral sheets to contract to the dimensions of the octahedral sheets.

These concepts have several important implications. For example: (1) it is shown easily that the average tetrahedral rotation is given by $\alpha = \cos^{-1}(b_{obs.}/b_{tetr.})$, where $b_{obs.}$ is observed b-axis, and $b_{tetr.}$ is b-dimension which the given tetrahedral layer would assume, if unconstrained. This gives reasonable agreement to $\alpha_{obs.}$ for those structures for which the latter is known. Values of $\alpha_{calc.}$ for a large number of layer lattice silicate structures show that almost all these minerals have more or less ditrigonal surface networks, for example, α for micas = 6–23°.

(2) The substitution of aluminium for silicon in the tetrahedral layer will not increase $b_{obs.}$ but merely increase α, that is, change the surface configuration. Previous unit cell formulæ giving $b_{obs.}$ in terms of composition[2] are therefore wrong in this respect. Multiple regression analyses, of b against composition, computed separately for experimental data for kaolins, micas and chlorites have each yielded non-significant regression coefficients for tetrahedral Al^{iv}, confirming the theoretical predictions.

(3) In the case of the micas, the interlayer cations play a major part in determining the unit-cell dimensions, a direct contradiction of current concepts. In general the 'Si'–O tetrahedra rotate until the nearer six oxygens (of the twelve) are 'in contact' with the interlayer cation, as I[3] have shown in the particular case of $2M_1$ muscovite. A large interlayer cation therefore contributes significantly to the value

of $b_{obs.}$; interlayer K^+ has a greater effect than octahedral Fe^{++} for micas. This physical concept has been confirmed by the multiple regression analyses mentioned. A single relation obtained from the mica data, giving b in terms of composition, fits both normal and brittle micas adequately, and both dioctahedral and trioctahedral types. For example, the unusual brittle mica xanthophyllite has $b_{obs.} = 9{\cdot}01$ Å and $b_{calc.} = 9{\cdot}016$, whereas earlier formulæ break down altogether[2].

(4) It is obvious that the relative rigidity of the Si–O tetrahedral group takes control of the b-axis dimensions of those layer minerals for which the octahedral layer would be significantly larger than the tetrahedral layer. It is for this reason that $b_{obs.} = 9{\cdot}15$ for talc, rather than $\approx 9{\cdot}3$; and the same factor is possibly an important one in distinguishing the chrysotile from the antigorite structures.

Necessary experimental results to support these ideas are now being submitted for publication. Some of these data have been kindly supplied by Dr. K. Norrish of this Division, with whom I have had very profitable discussions of this work.

E. W. Radoslovich

Division of Soils,
Commonwealth Scientific and
Industrial Research Organization,
Adelaide.

[1] Radoslovich, E. W., *Nature*, **183**, 253 (1959).
[2] Brindley, G. W., and MacEwan, D. M. C., *Ceramics Symp., Brit. Cer. Soc.*, 15 (1953).
[3] Radoslovich, E. W., *Acta Cryst.*, **13**, 919 (1960).

Printed in Great Britain by Fisher, Knight & Co., Ltd., St. Albans.

COMMONWEALTH OF AUSTRALIA
COMMONWEALTH SCIENTIFIC AND INDUSTRIAL RESEARCH ORGANIZATION

(*Reprinted from Nature, Vol.* 195, *No.* 4838, *p.* 276 *only, July* 21, 1962)

Cell Dimensions and Interatomic Forces in Layer Lattice Silicates

THE factors which control the sheet dimensions of the layer lattice silicates have been carefully re-examined recently[1], both from a structural point of view[2], and by the methods of multiple regression analysis[3]. This has led to a new, more explicit geometrical model[4] for the octahedral layers of these minerals, and thence to a detailed study of the balance of forces which must be involved. The results of the latter are outlined here.

Megaw, Kempster and Radoslovich[5] have attempted to understand the felspar structure, anorthite, by treating the network of bonds and bond-angles rather as a problem in statics, comparable with the design of bridge trusses. The same kind of approach is profitable for the layer lattice silicates, with the following general conclusions.

(1) The primary control of all three dimensions, *a*, *b* and *c*, is vested in the octahedral layer. In this layer the highly charged cations are only partly shielded electrostatically from each other across the shared octahedral edges. There is a strong mutual repulsion which is balanced by the limit of stretching of the cation–anion bonds, and the limit of compression towards each other of pairs of anions in these shortened shared edges (in accordance with Pauling's rules).

(2) Other factors exert control at a secondary level, or in extreme cases in an over-riding fashion. These factors include: (*a*) interlayer cation-surface oxygen bonds; (*b*) net surface charge (for example, cation exchange capacity effects); (*c*) net octahedral layer charge; (*d*) polarization of anions, particularly surface hydroxyls; (*e*) interlayer hydrogen bonding; (*f*) surface hydroxyl–hydroxyl bonding; (*g*) limitations of tetrahedral deformation, governed by bond-lengths and anion–anion compression. I believe that detailed examples of each may be found in various layer silicate structures already determined accurately.

(3) For several quite accurate structures the reported minor variations in bond-lengths—both within one structure, and between structures—appear to be consistent with these general concepts. The variations apparently may be 'explained' by treating these minerals as essentially ionic structures and then considering the effects on the bonds of small but known variations in effective electrostatic valency. Very similar arguments have been used by other authors in discussing several rather unrelated inorganic structures determined with notable precision recently.

(4) If these ideas are substantially correct then they: will allow much better prediction of trial structures of layer lattice silicates; should give convincing explanations for observed composition limits for the naturally occurring minerals[6]; cause considerable rethinking about the forces governing the morphology of kaolins and serpentines[7]; and have real bearing on the relative stability under weathering, and on the observed polymorphism, of the micas.

I thank Dr. K. Norrish, Division of Soils, and Mr. L. G. Veitch, Division of Mathematical Statistics, C.S.I.R.O., for their assistance.

E. W. Radoslovich

Division of Soils,
Commonwealth Scientific and
Industrial Research Organization,
Adelaide.

[1] Radoslovich, E. W., *Nature*, **191**, 67 (1961).
[2] Radoslovich, E. W., and Norrish, K., *Amer. Min.* (in the press).
[3] Radoslovich, E. W., *Amer. Min.* (in the press).
[4] Veitch, L. G., and Radoslovich, E. W. (in preparation).
[5] Megaw, H. D., Kempster, C. J. E., and Radoslovich, E. W., *Acta Cryst.* (in the press).
[6] Radoslovich, E. W. (in preparation).
[7] Radoslovich, E. W. (in preparation).

Printed in Great Britain by Fisher, Knight & Co., Ltd., St. Albans.

THE AMERICAN MINERALOGIST, VOL. 47, MAY–JUNE, 1962

THE CELL DIMENSIONS AND SYMMETRY OF LAYER-LATTICE SILICATES

I. SOME STRUCTURAL CONSIDERATIONS

E. W. RADOSLOVICH AND K. NORRISH, *Division of Soils, Commonwealth Scientific and Industrial Research Organisation, Adelaide, Australia.*

ABSTRACT

The theoretical basis underlying accepted *b*-axis formulae (giving the sheet dimensions of layer-lattice silicates in terms of composition) has been re-examined. It is now proposed that in general the *b*-axis is determined by the octahedral layer together with (for micas) the interlayer cation. As a consequence of this most layer silicates will have ditrigonal, not hexagonal, surface networks; and the surface rotations may be easily calculated from b_{obs} and the known Al-for-Si substitution tetrahedrally. These ideas have implications for all layer structures; these implications are examined in detail for the micas and brittle micas.

INTRODUCTION

Various attempts have been made to predict the unit cell dimensions of the layer silicates, especially the *b* axes, from certain observations and assumptions about their structures, allowing for the expected differences due to different ionic radii. Cell sizes calculated from recent formulae generally agree well with experimental values; there are, however, some notable anomalies, especially among the micas and brittle micas.

A detailed analysis of the muscovite structure (Radoslovich, 1960), and other data, suggest that the previous *b*-axis formulae have been wrongly based for the micas, and also that the accepted "ideal" mica structure may usefully be modified (Radoslovich, 1961). New *b*-axis formulae for all the layer silicates, including the micas, are presented in Part II.

The most recent attempt to set up general formulae relating lattice parameters to composition in layer silicates appears to be that of Brindley and MacEwan (1953), who also summarize earlier work. Their semi-empirical formulae are based on the observed increase in the cell dimensions (with change of cation) of the hydroxides, $Al(OH)_3$, $Fe(OH)_3$, $Mg(OH)_2$ and $Fe(OH)_2$, though similar results may also be obtained by considering ionic radii. Brindley and MacEwan give several different formulae, *viz.*

(a) for the expected *b* dimensions of various tetrahedral networks, if they were not constrained.
(b) for the expected *b* dimensions of various di-octahedral and tri-octahedral layers, if they were not constrained.
(c) for the *b* axis of the unit cell, by considering the combined tetrahedral and octahedral layers.

TABLE 1

b dimension (Å)	Celadonite[1]	Xanthophyllite[2]
Tetrahedral, calculated[3]	9.20	9.84
Octahedral, calculated	9.19	9.19
Overall, calculated[3]	9.14	9.49
Observed	9.02	9.00

[1] *vide* Zviagin, 1957.
[2] *vide* Takéuchi and Sadanaga, 1959.
[3] Adjusted to the values, Si-O = 1.60 Å, Al-O = 1.78 Å (Smith, 1954).

When (c) is applied to some representative minerals (Table 2, Brindley and MacEwan) the results are surprisingly good; and more recent studies (*e.g.* Faust, 1957) have confirmed the general applicability of the formulae, within the limits of their premises. Recently, however, there has been increased interest in applying (a) and (b) to various minerals as a means of predicting strains between the layers, since such strains will cause departures from ideal structures and may account partially for observed properties such as polymorphism and morphology. When detail of this kind is sought some factors omitted by Brindley and MacEwan become important. In their formulation, for example,

(1) no account was taken of the effect of interlayer cations.
(2) no factor was introduced for varying octahedral layer thicknesses (Bradley, 1957).
(3) some correction may be required because the charge balanced by the interlayer cation is sometimes in the tetrahedral, and sometimes in the octahedral sites.
(4) the expansion due to increased ionic size is computed by comparing *e.g. di*octahedral $Al(OH)_2$, with two *tri*valent cations, with *trio*ctahedral $Mg(OH)_2$, with three *di*valent cations, whereas some minerals either are intermediate in the number of octahedral cations, or differ in octahedral charge, or both.
(5) the three octahedral sites (per one-layer cell) are treated as similar, whereas the accepted space groups imply that they are crystallographically distinct for the common mica polymorphs.

The inadequacy of these formulae for micas is clearly shown by celadonite and xanthophyllite, for both of which the calculated tetrahedral, octahedral and overall *b* dimensions are each considerably larger than the observed *b* axis (Table 1).

The present paper is concerned with the structural model which is accepted by implication as the theoretical basis for calculating *b*-axis formulae; basic alterations to previous models are proposed. These alterations imply a number of changes in the current ideas of the mica structures especially, which are therefore discussed in the latter part of this paper.

Adequate *b*-axis formulae consistent with the new model have been constructed by trial and error, but somewhat better results are obtained by the regression analysis of *b* against composition, as Hey (1954) also has shown for the chlorites. In addition one aspect of the new model can be tested *only* by multiple regression analyses of an adequate number of minerals in each of the main groups. Such analyses are reported in Part II, in which the new *b*-axis formulae for the kaolins, chlorites, micas and montmorillonites (which follow from the regression analyses) are presented.

Calculation of the Rotation of "Silica" Tetrahedra in Layer Silicates

For most of the layer silicate structures now known in some detail the network of "silica" tetrahedra—ideally hexagonal—is "distorted" to a ditrigonal surface symmetry, by the opposed rotation of alternate tetrahedra. The amount of this rotation varies from a few degrees to near the theoretical maximum of 30°. Minerals for which this has been reported include dickite, kaolinite, amesite, Mg-vermiculite, muscovite, celadonite, xanthophyllite, prochlorite, corundophyllite, and clinochrysotile. (Similar rotations have also been reported for the silicate network structures, tourmaline, crocidolite and hexagonal $BaAl_2Si_2O_8$ and $CaAl_2Si_2O_8$.)

The tetrahedral rotation is generally accepted as due to the misfit of a larger tetrahedral layer onto a smaller octahedral layer (*e.g.* Newnham and Brindley, 1956). The strain between these two layers is supposedly relieved by expansion of the octahedral layer, with an accompanying contraction in thickness, and partly by contraction of the tetrahedral layer by the rotation of the basal triads.

The average tetrahedral rotation from hexagonal symmetry, α, may be predicted from the observed *b* axis and known Al-for-Si substitution tetrahedrally. Let the actual 'Si'-O bond have an average length λ in projection along c^* (Fig. 1). The hexagon of 'Si' atoms has sides $= 2SO' = 2\lambda \cos \alpha$, and it is easily shown that the observed *b* axis, b_{obs}, is three times this length, *i.e.* $6\lambda \cos \alpha$. The value of *b* for the same tetrahedral layer with zero rotations would be $b_{tetr} = 6\lambda$, whence

$$\alpha = \arccos (b_{obs}/b_{tetr}) \qquad (1)$$

This equation applies to all layer silicates; the only assumptions are that the tetrahedra are approximately regular, and that contraction occurs simply by tetrahedral rotation. Calculated and observed values of α are discussed below for micas and in Part II for other layer silicates.

It is noteworthy that calculated rotations of $<7°$ approx. are uncom-

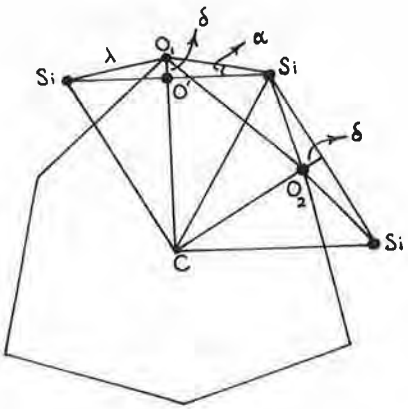

FIG. 1. Calculations of angle, α, of rotation of tetrahedra.

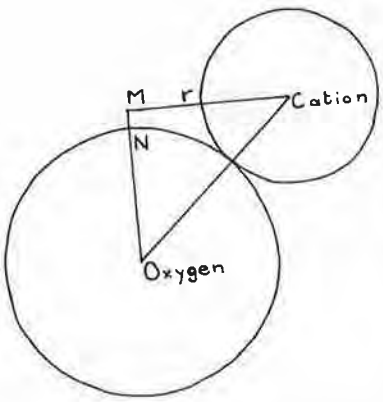

FIG. 2. Calculation of layer separation.

mon for micas, although this requires caution, since the expression for α is very sensitive to small errors in b_{obs} and b_{tetr} when α is in this range.

The value of b_{tetr} may be calculated from the expected 'Si'-O bond length for a given Al-for-Si substitution from the curve by Smith (1954). If x is the number of Al atoms in *four* tetrahedral sites, T, and τ is the O_{apex}-T-O_{basal} angle, then

$$b_{tetr} = 6\lambda = 6\left(1.60 + \frac{0.18x}{4}\right)\sin(180 - \tau) = (9.60 + 0.18x)\sin\tau \qquad (2)$$

which becomes, for the ideal value of $\tau = 109°28'$,

$$b_{tetr} = (9.051 + 0.254x) \qquad (2a)$$

Since τ can only be determined by a structure analysis (which also determines α), the validity of equation (1) rests on how far τ may depart from 109°28'. A literature survey gave values from 107° for celadonite to 112° for dickite, *i.e.* $\pm 2\frac{1}{2}°$ from theoretical, which is serious when α is small but less important for $\alpha > 7$–8°. Observed values of α agree quite well with calculated values, *e.g.* muscovite, 13.7° (14°42'); dickite, 7.5° (8°56'); kaolinite, 10.9° (10°48'); kaolinite, 9° (9°18'); xanthophyllite, 23.2° (23°19'); and chrome chlorite, 6° (5°58'). The agreement is not quite so close for several other minerals, but in each case the O-Si-O angle is known to depart from 109°28' in the correct direction to account for any marked discrepancy. The observed values above have been obtained by plotting out the atomic parameters from the structure analyses, to which references are given in Table 3 and in Part II.

Factors Controlling the *b*-axis Dimension in Layer-Lattice Silicates

Recent structural analyses of micas strongly suggest that the tetrahedral layers play a secondary role in determining the *b* axis, not the dominant role previously assumed (*e.g.* Smith and Yoder, 1956). The *cell dimensions* of micas appear to be controlled largely by the octahedral layer and the interlayer actions, though micas for which the tetrahedral layer is smaller than the octahedral layer form (rare) exceptions to this. The *surface configuration*, however, depends primarily on the size of the "free" tetrahedral layer relative to the actual *b* axis.

This view of the mica structures led to a reconsideration of the role of the tetrahedral layer in determining the *b* axis of the other layer-lattice silicates. Whereas previous *b*-axis formulae (*e.g.* Brindley and MacEwan, 1953) have included a factor for the substitution of Al for Si tetrahedrally, the following hypothesis is now advanced, *viz.*

a) In *all the layer silicates* the "silica" tetrahedra can rotate fairly freely to *reduce* the dimensions of this layer; but the rigidity of the tetrahedral group prevents significant extension of the layer as, *e.g.* in the serpentine structures.

b) In *all the layer silicates* the octahedral layer can be extended or contracted with somewhat more difficulty, by changes in bond angles rather than bond lengths, and therefore with accompanying changes in thickness.

c) *For the micas* in particular the surface oxygen triads rotate until some (probably half) of the cation-oxygen bonds have normal bond-lengths, *i.e.* until half the oxygens "lock" onto the interlayer cation.

Note that if the octahedral layer of a mica tends to be *much* smaller than the tetrahedral layer the tetrahedra may rotate beyond this point (c); normal bond-lengths from the surface oxygens to the interlayer cation are then attained by the latter being held with its center slightly above the top of the oxygen layer, *i.e.* the oxygen surfaces are no longer in contact, *e.g.* muscovite (Radoslovich 1960).

The separate parts of this hypothesis may be supported as follows:

a) The inclusion of a tetrahedral term in the *b*-axis formulae was justified originally (*e.g.* Brown, 1951, p. 160) by comparing *b* for pyrophyllite (8.90 Å) and muscovite (9.00 Å). This was invalid as may be seen by likewise comparing pyrophyllite with paragonite (8.90 Å); the interlayer cation is the important factor in both cases. In fact it is not possible to find a mineral pair which differ *only* in tetrahedral substitution, since the necessity for charge balance requires an accompanying change either in the octahedral cations or interlayer region or both. The null effect of the tetrahedral layer may be inferred, however, if it is accepted that Li octahedrally does not increase *b*. Muscovite and polylithionite, both with

$b = 9.00$ Å, then effectively differ only in tetrahedral composition; and likewise for cookeite and kaolinite, both with $b = 8.92$ Å. In neither case does the substitution of Si_3Al for Si_4 change b.

The hypothesis is only *proved*, however, by determining by the multiple regression analysis of an adequate number of minerals the size and significance level of the coefficient for the tetrahedral Al term. This has been done (Part II); the coefficient is not significantly different from zero for each mineral group, kaolins, chlorites, and micas. The conclusion is that the tetrahedra rotate *so* freely that this layer does not effectively increase b at all, except possibly for the montmorillonites.

b) As a necessary consequence of a) it is now seen that the octahedral layers of only a minority of layer-lattice silicates are being stretched. For the dioctahedral micas the interlayer cation (especially the large K^+) appears to stretch the octahedral layer, and this may also happen in certain chlorites with pronounced ordering between octahedral layers. But for other layer-lattice silicates the regression analyses indicate virtually no stretching of this layer.

Octahedral layers are not generally contracted either, but the serpentines, saponites, talc and some talc analogues are exceptions to this. For all these except the saponites the octahedral layer so greatly exceeds the tetrahedral layer that the b axis is determined solely by the limit of stretching of the latter. For the saponites the octahedral layer only slightly exceeds the tetrahedral layer, and in this case the octahedral layer apparently contracts to the undistorted tetrahedral dimension; this is discussed further in Part II.

Bradley's discussion (1957) of octahedral layer thicknesses appears to be valid only under rather special circumstances, if the present hypothesis is correct.

c) Evidence to support this idea is found in the observed cation-oxygen bond lengths for muscovite, celadonite and xanthophyllite. In each case half of the total bonds are close to values predicted from ionic radii, the remainder being so great that these oxygens effectively are not bonded to the interlayer cation (Table 2).

TABLE 2. INTERLAYER CATION—OXYGEN BOND LENGTHS

Muscovite, K-O[1]	2.79_9	2.77_5	2.86_2	3.35_7	3.51_1	3.30_3
Celadonite, K-O	2.77	2.85	2.77	3.27	3.27	3.34
Xanthophyllite, Ca-O[1]	2.35	2.39	2.39	3.49	3.49	3.52

[1] A reasonable value for the K-O bond is 2.81 Å, and for the Ca-O bond 2.35 Å.

Takéuchi and Donnay (1959) have shown that in the hexagonal framework structures $CaAl_2Si_2O_8$ and $BaAl_2Si_2O_8$ the networks are ditrigonal, with the nearer Ca-O bonds = 2.39 Å (contact distance for the effectively six-fold co-ordination); the rotation in α—$BaAl_2Si_2O_8$ is less than in $CaAl_2Si_2O_8$, because Ba is larger than Ca.

Separation of Successive Layers in Micas

It is possible to use the calculated α to make plausible predictions about the separation of the layers and/or the value of the O-T-O angle for individual micas as follows.

Let the interlayer cation-oxygen bond have length r (= CO_2 in Fig. 1) in projection along c^*, for an oxygen in contact with the cation, irrespective of whether the latter has its center at the surface of the oxygen layer or not. Then

$$r = CO' - \delta = (SiO' \cot 30°) - \delta = (b_{tetr}/6)(\sqrt{3}\cos\alpha - \sin\alpha) \qquad (3)$$

For the general case (Fig. 2) the separation of the basal planes of successive layers will be

$$\eta = 2MO = 2(CO^2 - CM^2)^{1/2} = 2((\text{cation-oxygen bond})^2 - r^2)^{1/2} \qquad (4)$$

Though equation (4) gives reasonable values of η for some micas it leads to an impossibly close approach of successive layers for other micas if the O-T-O angle is required to be 109°28′ and the interlayer cation in contact with six oxygens. Where this occurs it may reasonably be assumed that the O-T-O angle changes and the layers are in contact, since the oxygen sheets can only interleave about 0.06 Å for $\alpha = 10°$, and for larger rotations than this the normal interlayer cations prevent any appreciable interleaving. On this basis new values of b_{tetr}, α, and τ are derived. From (1) and (3),

$$b_{tetr} = \left[36\left(\frac{\sqrt{3}}{6}b_{obs} - r\right)^2 + b_{obs}^2\right]^{1/2} \qquad (5)$$

in which r is given by (4) with $\eta = 0$. Corrected values of α and τ are then given by (1) and (2).

The "Ideal" Mica Structure

The observed layer silicate structures are usually discussed in relation to an "ideal" structure in which the surface oxygen configuration has hexagonal symmetry, *e.g.* the muscovite structure proposed by Jackson and West (1930) for which the y parameters are all multiples of $b/12$. In their classic work on the polymorphism of micas Hendricks and Jefferson (1939) pointed out that $2M_1$ muscovite departs considerably from this

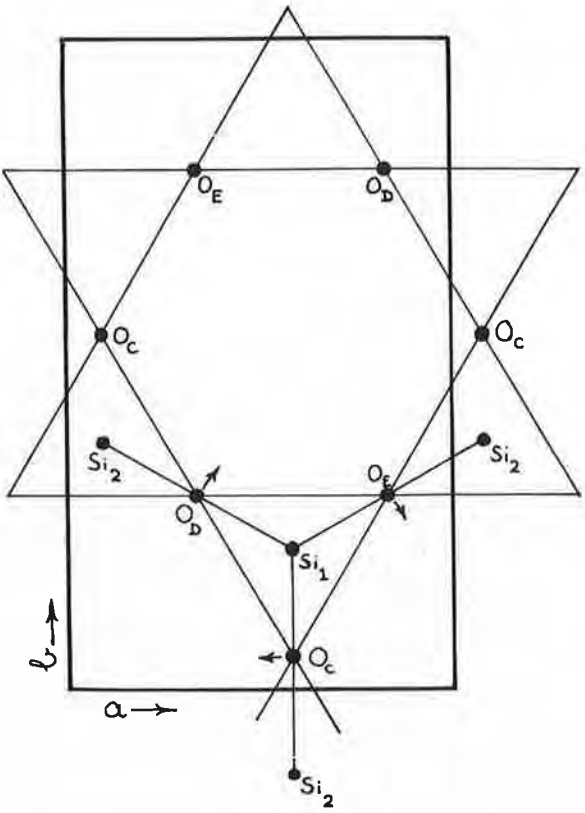

FIG. 3. Non-appearance of *o6l*, *l* odd reflections with tetrahedral rotations only.

arrangement because the *o6l*, *l* odd reflections (which are thereby forbidden with spacegroup $C2/c$) are observed; this has been confirmed by Radoslovich (1960).

The erroneous implication, however, has been that two-layer micas for which the *o6l*, *l* odd reflections are *not* observed must have approximately hexagonal symmetry. A simple calculation shows that the triads of oxygens on the mica surfaces may have all rotations from zero to the maximum of 30° without the *o6l*, *l* odd reflections appearing, provided that the tetrahedral centers are not displaced from their $y = nb/12$ positions.

In the ideal hexagonal network (Fig. 3) any triad of oxygens consists of two oxygen atoms, O_D and O_E on the line in projection joining two silicons which lie at $\pm 60°$ to the *b* axis, together with O_C on such a line

parallel to the *b* axis. It is assumed that all triads are equal in size, and that their centers remain at $y = nb/12$ when *b* is decreased by tetrahedral rotations. The parameters of O_D and O_E before and after rotation are:

$$O_D,\ x,\ y,\ z \rightarrow x + \delta x,\ y + \delta y,\ z \text{ and } O_E,\ x + \tfrac{1}{2},\ y,\ z \rightarrow x + \tfrac{1}{2} + \delta x,\ y - \delta y,\ z.$$

The y parameter of O_C remains at $y = nb/12$, since Si_1 and Si_2 also maintain $y = nb/12$; and hence the *o6l*, *l* odd reflections are solely due to O_D and O_E. For space group $C2/c$, the geometrical structure factor is

$$\begin{aligned} A &= -8 \sin 2\pi lz\{\sin 2\pi k(y - \delta y) + \sin 2\pi k(y + \delta y)\} \\ &= 16 \sin 2\pi lz \cdot \sin 2\pi ky \cdot \sin 2\pi k \cdot \delta y \cdot \\ &= 0 \text{ for } k = 6 \text{ and } y = \frac{n}{12} \end{aligned}$$

For the 1M polymorph, spacegroup $C2/m$, these reflections may be present for all $y = nb/12$.

It appears probable that the tetrahedral networks in layer silicates may *readily* contract to a ditrigonal symmetry. Radoslovich (1961) has therefore suggested that the "ideal" mica structure be redefined as having ditrigonal surface symmetry, with the tetrahedral cations having $y = nb/12$; a hexagonal network is thus a special case of this structure. Muscovite is then a "distorted" structure because of tetrahedral displacements (due to the *partly*-filled octahedral layer).

Application to Various Micas

Calculated values of the rotation, α, and the expected interlayer separation η are given in Table 3; for several minerals average experimental values of α and η are also available for comparison. Since η_{calc} depends on the assumed bond length from the interlayer cation to the near oxygens, this is given in column 10, with the known observed average values in column 11.

(a) Biotites (no. 1–24), and phlogopites (no. 25–29)

It is noteworthy that α_{calc} varies between the narrow limits of 7–9½° approx., for these biotites having a considerable composition range (Table 4). Likewise the calculated separation η lies between 2.5 and 2.9 Å, suggesting that successive layers are generally in contact—in contrast with muscovites and lepidolites. This cannot be tested experimentally, however, because η cannot be estimated from $d(001)$, and the tetrahedral and octahedral thickness, since the latter is not precisely known for biotites and phlogopites. The substitution of F^- for OH^- introduces a further difficulty because Yoder and Eugster (1954) have shown

TABLE 3. TETRAHEDRAL ROTATIONS AND INTERLAYER DISTANCES IN SOME MICAS

No.	Mineral	b Å		$\alpha°$		η Å		Cation-oxygen Å	
		obs.	tetr.	obs.	calc.	obs.	calc.	Obs.	Assume
1	Biotite, J-56-1	9.265*	9.355		7°57′		2.65		2.81
2	Biotite, J-56-1b	9.247*	9.355		8°42′		2.81		2.81
3	Biotite, J-56-5	9.268*	9.350		7°36′		2.68		2.81
4	Biotite, J-56-9	9.251*	9.320		7° 0′		2.64		2.81
5	Biotite, J-56-10	9.261*	9.358		8°15′		2.75		2.81
6	Biotite, J-56-11	9.251*	9.305		6°12′		2.55		2.81
7	Biotite, J-56-11b	9.257*	9.305		5°48′		2.51		2.81
8	Biotite, J-56-11b1	9.225*	9.305		7°30′		2.72		2.81
9	Biotite, J-56-12	9.254*	9.391		9°48′		2.91		2.81
10	Biotite, J-56-12b	9.265*	9.391		9°24′		2.86		2.81
11	Biotite, J-56-13	9.262*	9.360		8°18′		2.76		2.81
12	Biotite, J-56-13b	9.206*	9.360		10°24′		2.93		2.81
13	Biotite, J-56-20	9.308*	9.410		8°21′		2.72		2.81
14	Biotite, J-56-21	9.246*	9.371		9°22′		2.87		2.81
15	Biotite, J-56-21b	9.255*	9.371		9° 1′		2.83		2.81
16	Biotite, J-56-22	9.253*	9.353		8°23′		2.67		2.81
17	Biotite, J-56-22b	9.215*	9.353		9°53′		2.99		2.81
18	Biotite, J-56-23	9.328*	9.360		4°51′		2.31		2.81
	For $\eta=2.60, \tau=108°41'$	9.328*	9.41		7°21′		2.60		2.81
19	Biotite, EL-38-134	9.266*	9.353		7°48′		2.63		2.81
20	Biotite, EL-38-167	9.300*	9.307		2°12′		2.00		2.81
	For $\eta=2.60, \tau=108°19'$	9.300*	9.37		7°41′		2.60		2.81
21	Biotite, EL-38-265	9.323*	9.305						
	For $\eta=2.60, \tau=107°49'$	9.323*	9.40		7°19′		2.60		2.81
22	Biotite, EL-230	9.260*	9.335		7°16′		2.66		2.81
23	Biotite, SLR-138	9.271*	9.360		7°54′		2.71		2.81
24	Biotite, Ra 135	9.265*	9.301		5° 2′		2.41		2.81
	For $\eta=2.60, \tau=109°2'$	9.265*	9.33		6°46′		2.60		2.81
25	Phlogopite, J-56-14	9.241*	9.292		6° 0′		2.54		2.81
26	Phlogopite	9.22	9.30		7°30′		2.72		2.81
27	Phlogopite	9.204	9.305		8°28′		2.83		2.81
28	Fluorophlogopite	9.195	9.395		8°48′		2.86		2.81
29	Fluorophlogopite	9.188	9.30		8°54′		2.88		2.81
30	Muscovite	8.995*	9.30	13.7°	14°42′	3.37	3.49	2.81	2.81
31	Iron-muscovite	9.06	9.24		11° 3′		3.17		2.81
32	Paragonite	8.90	9.30		16°52′		2.34		2.42
	For $\eta=2.60, \tau=106°51'$	8.90	9.45		19°36′		2.60		2.42
33	Lepidolite	9.006*	9.16		10°25′		3.16		2.81
34	Lepidolite	8.97	9.25		14°36′		3.51		2.81
35	Celadonite	9.02	9.12	12.0°	8°33′	3.30	3.12	2.78	2.81
	For $r_{obs}=107°0'$	9.02	9.28	12.0°	13°43′	3.30	3.30		2.78
36	Celadonite	9.05	9.05		0°		2.07		2.81
	For $\eta=2.60, \tau=108°58'$	9.05	9.08		4°30′		2.60		2.81
37	Celadonite	9.06	9.09		4°14′		2.55		2.81
38	Celadonite	9.08	9.09		2°42′		2.36		2.81
	For $\eta=2.60, \tau=109°33'$	9.08	9.11		4°54′		2.60		2.81
39	Zinnwaldite	9.12	9.23		9° 8′		2.97		2.81
40	Zinnwaldite	9.06	9.19		9°31′		3.04		2.81
41	Lithium biotite	9.21	9.32		8°44′		2.81		2.81
42	Lithium biotite	9.09	9.29		10°40′		3.08		2.81
43	Gümbelite	9.04	9.25		12°14′		3.28		2.81
44	Lepidomelane	9.29	9.41		9°10′		2.82		2.81
45	Margarite	8.92	9.56		21° 4′		2.57		2.38
46	Ephesite	8.896*	9.57		21°36′		2.78		2.42
47	Xanthophyllite	9.00	9.80	23.2°	23°19′	2.69	2.72	2.38	2.38
48	Xanthophyllite	9.01	9.77		22°45′		2.66		2.38
49	Xanthophyllite	9.00	9.76		22°46′		2.72		2.38
50	Xanthophyllite	9.02	9.77		22°36′		2.65		2.38
51	Bityite	8.713*	9.225		19°10′		2.55		2.38
52	Bityite	8.67	9.455		23°30′		2.93		2.38

* Original data, obtained using CoKα radiation, quartz internal standard, 19 cm diam. camera.

This table contains data on a few representative specimens of each of the micas, except for the biotites for which Dr. Jones supplied excellent data on twenty five specimens. All these data are included, partly to allow a discussion of interlayer separation, and partly because the same data are used subsequently in a regression analysis (Part II).

No.	Reference	K	Na	Ca		Fe^{2+}	Mg	Li	Mn	Fe^{3+}	Ti	Al^{VI}	Al^{IV}	Si	OH	F	Cl	O
1	Jones (1958) J-56-1	0.93	0.02	0.03		1.30	1.03		0.03	0.15	0.10	0.33	1.20	2.80	1.55	0.21	0.01	10.29
2	Jones (1958) J-56-1b	0.93	0.02	0.03		0.01	1.03		0.03	1.44	0.10	0.33	1.20	2.80	0.27	0.21	0.01	11.51
3	Jones (1958) J-56-5	0.85	0.02	0.04	0.01[1]	1.33	0.84	0.10	0.03	0.20	0.10	0.27	1.18	2.82	1.67	0.21	0.01	10.11
4	Jones (1958) J-56-9	0.80	0.10	0.01		0.37	2.37	0.04		0.02	0.15	0.07	1.06	2.94	1.57	0.13	0.01	10.29
5	Jones (1958) J-56-10	0.92		0.02	0.01[2]	1.13	1.11	0.03		0.18	0.15	0.25	1.21	2.79	1.72	0.09		10.19
6	Jones (1958) J-56-11	0.92	0.01	0.02		1.06	1.54	0.07	0.06	0.11	0.13	0.01	1.00	3.00	0.84	0.84	0.02	10.33
7	Jones (1958) J-56-11b	0.92	0.01	0.02		0.85	1.54	0.07	0.06	0.30	0.13	0.01	1.00	3.00	0.67	0.84	0.02	10.47
8	Jones (1958) J-56-11b$_1$	0.92	0.01	0.02		0.18	1.54	0.07	0.06	0.97	0.13	0.01	1.00	3.00		0.84	0.02	11.16
9	Jones (1958) J-56-12	0.92	0.04			1.33	0.68	0.02	0.02	0.08	0.17	0.50	1.34	2.66	1.76	0.06	0.01	10.17
10	Jones (1958) J-56-12b	0.92	0.04			0.01	0.68	0.02	0.02	1.41	0.17	0.50	1.34	2.66	0.43	0.06	0.01	11.50
11	Jones (1958) J-56-13	0.93	0.01	0.01		1.34	0.94	0.01	0.02	0.18	0.16	0.26	1.22	2.78	1.61	0.18	0.01	10.20
12	Jones (1958) J-56-13b	0.93	0.01	0.01		0.01	0.94	0.01	0.02	1.53	0.16	0.26	1.22	2.78	0.08	0.18	0.01	11.73
13	Jones (1958) J-56-20	0.95		0.03		1.42	0.51		0.14	0.76	0.06		1.43	2.54	1.87	0.04		10.09
14	Jones (1958) J-56-21	0.92	0.03	0.01	0.01[2]	1.27	0.88	0.03	0.02	0.16	0.12	0.38	1.26	2.74	1.80	0.08	0.01	10.11
15	Jones (1958) J-56-21b	0.92	0.03	0.01	0.01[2]	0.20	0.88	0.03	0.02	1.20	0.12	0.38	1.26	2.74	1.02	0.08	0.01	10.89
16	Jones (1958) J-56-22	0.88	0.01	0.01		1.19	1.24	0.01	0.01	0.09	0.14	0.24	1.27	2.73	1.76	0.13	0.02	10.09
17	Jones (1958) J-56-22b	0.88	0.01	0.01			1.24	0.01	0.01	1.25	0.14	0.24	1.27	2.73	0.95	0.13	0.02	10.90
18	Jones (1958) J-56-23	0.73	0.01	0.04	0.21[3]	1.72	0.28	0.04	0.03	0.44	0.18	0.13	1.22	2.78	1.62	0.09	0.02	10.27
19	Jones (1958) EL-38-134	0.90	0.03			1.05	1.05			0.26	0.19	0.36	1.19	2.81	1.01	0.33		10.66
20	Jones (1958) EL-38-167	0.92	0.08	0.05		1.82	0.69			0.09	0.33	0.40	1.01	2.99	0.60	0.06		11.34
21	Jones (1958) EL-38-265	0.85	0.02	0.01		1.80	0.51			0.23	0.19	0.37	1.01	2.99	0.72	0.22		11.06
22	Jones (1958) EL-230	0.80	0.08	0.11		1.00	1.18			0.26	0.31		1.12	2.88	0.31	0.31		11.39
23	Jones (1958) SLR-138	0.71	0.07	0.20		1.09	1.27			0.19	0.17	0.38	1.12	2.88	0.70	0.05		11.25
24	Jones (1958) Ra-135	0.83	0.08	0.08		1.33	0.93		0.01	0.23	0.21	0.30	0.99	3.01	0.85	0.08		11.07
25	Jones (1958) J-56-14	0.99	0.02	0.01	0.01[2]	0.23	2.15			0.12	0.48		0.95	2.99	0.92	0.15		10.93
26	Nagelschmidt (1937)	0.78	0.06	0.03		0.04	2.98			0.02		0.16	0.98	3.02	0.55	1.19		10.26
27	Yoder and Eugster (1954)[4]	1.0					3.0						1.0	3.0	2.0			10.0
28	Yoder and Eugster (1954)[4]	1.0					3.0						1.0	3.0		2.0		10.0
29	Kohn and Hatch (1955)	0.98	0.01				3.00						1.01	3.01		2.05		10.0
30	Radoslovich (1960)	0.94	0.06				0.06			0.12		1.84	0.89	3.11	1.9			10.1
31	Foster *et al.* (1960)	0.94	0.02			0.15	0.19			0.42		1.27	0.73	3.27	2.0			10.0
32	Yoder (1958)[4]		1.0									2.0	1.0	3.0	2.0			10.0
33	Stevens (1938) no. 6	0.82	0.10	0.01	0.07[1]	0.01	0.02	1.36	0.03			1.32	0.42	3.58	0.57	1.55		9.95
34	Nagelschmidt (1937)	0.87	0.13			0.02	0.02	1.35		0.09		0.82	0.79	3.21	4.34			9.66
35	Zviagin (1957)	0.82					0.7			1.4			0.4	3.6	2.0			10.0
36	Foster (1956) no. 17	0.98				0.24	0.77			0.93		0.07		4.00	2.0			10.0
37	Maegdefrau and Hoffman (1937)	0.83		0.03		0.20	0.68			0.36		0.75	0.14	3.86	2.0			10.0
38	Malkova (1956) no. 41M	0.72		0.05	0.25[1]	0.57	0.57			1.0	0.01	0.18	0.26	3.74	2.0			10.0
39	Cundy *et al.* (1960)	0.94	0.07			0.60		1.05	0.02	0.06		1.08	0.72	3.28	2.0			10.0
40	Cundy *et al.* (1960)	0.91	0.04			0.33	0.02	1.15	0.03	0.05	0.02	1.16	0.54	3.46	2.0			10.0
41	Cundy *et al.* (1960)	0.90	0.05	0.11		1.19	0.06	0.45	0.02	0.03	0.02	0.95	1.05	2.95	2.0			10.0
42	Mauguin (1913)	0.92	0.11	0.03		0.60	0.02	1.01	0.08	0.03		1.00	0.77	3.23	2.0			10.0
43	Aruja (1944)	0.68	0.05				0.40				0.04	1.48	0.77	3.19	2.82			9.18
44	Nagelschmidt (1937)	0.81	0.13	0.02		1.46	0.68			0.35	0.23	0.07	1.43	2.57	2.01			9.99
45	Takéuchi and Sadanaga (1959)			1.0								2.0	2.0	2.0	2.0			10.0
46	Phillips (1931)		1.11	0.10		0.02	0.04	0.40		0.03		1.90	2.05	1.95	2.34	0.04		9.62
47	Takéuchi and Sadanaga (1959)			1.1			2.18					0.72	2.95	1.05	2.0			10.0
48	Forman (1951)			0.98		0.02	2.09			0.15		0.70	2.83	1.17	2.10			9.92
49	Forman (1951)	0.01	0.12	1.00		0.06	2.23			0.04		0.72	2.78	1.22	1.92			10.16
50	Forman (1951)			0.98		0.04	2.14			0.08		0.76	2.84	1.16	2.07			9.97
51	Rowledge and Hayton (1948)		0.04	1.01	1.14[5]			0.63				2.09	0.69	2.17	2.42			10.0
52	Strunz (1956)	0.01	0.05	0.99	0.35[5]		0.01	0.71				1.58	1.59	2.06	2.06			10.0

[1] Rb [2] Ba [3] $(H_3O)^+$ [4] Synthetic specimen [5] Be tetrahedrally [6] Plus 0.8 H

that this substitution in phlogopite decreases $d(001)$, and Jones (1958) has suggested that similarly the substitution of both O^{2-} and F^- for OH^- in biotite decreases $d(001)$.

When b_{oct} is nearly as large as b_{tetr} the tetrahedra may not be sufficiently rotated for half the oxygens to be in contact with the interlayer cation. For these biotites (*e.g.* EL-38-167, Table 3) the tetrahedral angle is probably $<109°28'$, and has therefore been adjusted to maintain both cation-oxygen contact and oxygen-oxygen contact across the interlayer region. It can be shown (*vide* Part II) that the ratio

$$\frac{Fe^{2+} + 0.853Fe^{3+} + 0.455Mg + 0.43Ti}{Al_{tetrahedral}}$$

(where Fe^{2+} etc. are the ionic proportions in the structural formulae) is a good measure of the ratio, b_{oct}/b_{tetr}. This ratio has been plotted against the η_{calc} in Figure 4, with values for muscovite, Fe-muscovite and three zinnwaldites added for comparison. The general trend (dotted line) shows that as the octahedral layer becomes smaller relative to the tetrahedral layer the increased tetrahedral rotation forces the layers apart.

There is a little evidence to confirm this trend for η_{calc}. The separation, η_{obs}, is known for muscovite; and if biotites are usually in interlayer contact this leads to the dashed line (Fig. 4). Secondly, $d(001)$ for muscovite, Fe-muscovite and the zinnwaldites is plotted on the same scale and shows a similar trend. Since, on the simplest hypotheses, the octahedral substitution of Fe^{3+}, etc. for Al^{3+} should *increase* $d(001)$ this observed *decrease* supports the present calculations of interlayer separations.

(For muscovite at least the substitution of F^- for OH^- does not decrease $d(001)$ (Yoder and Eugster, 1955). This may be expected if the decrease with the substitutions depends on the directed nature of the OH bond in relation to the K^+ ion. Bassett (1960) and others have shown by infrared spectroscopy that these bonds are normal to the sheets in phlogopite, nearly so in biotite, and at a low angle in muscovite. Zinnwaldite should be similar to muscovite; and this comparison of $d(001)$ with η_{calc} should be valid for these micas.)

(b) Muscovite, Fe-muscovite, paragonite (no. 30–32)

The correlation between $d(001)$ decreasing from 20.097 to 19.991, and the closer approach of successive layers due to the smaller tetrahedral rotation (*i.e.* greater K^+ penetration) is obvious for muscovite and iron muscovite.

For paragonite $\eta_{calc}=2.34$ is far too small, since oxygen layers across the interlayer region can scarcely interleave. It appears that the tetrahedra in paragonite must be somewhat "flattened," to give a greater ro

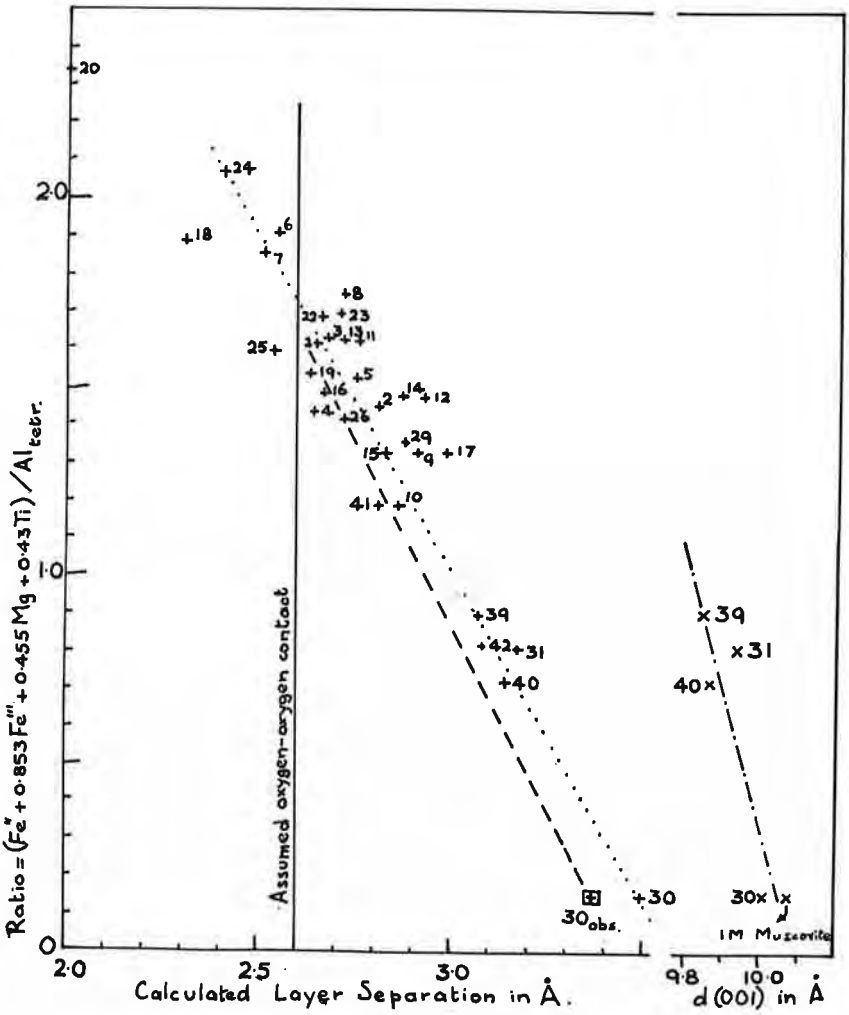

FIG. 4. Calculated layer separation as a function of composition; also (001) spacing as same function.

tation than ideal; and $\tau_{calc} = 106°51'$, close to $\tau_{obs} = 107°0'$ for celadonite (Zviagin, 1957).

An error in the discussion of the muscovite structure (Radoslovich, 1960) should be noted here. The octahedral layer in gibbsite was assumed to have a thickness equal to half the cell height (*i.e.* 2.53 Å), and the octahedral layer in muscovite (thickness, 2.12 Å) was supposed to be thinner because it was "stretched," *i.e.* $b = 8.995$ against 8.64 for gibbsite.

Megaw (1934) has studied gibbsite in detail, and gives the layer thickness as 2.12 Å, which is the same as that in muscovite. This, of course, is to be expected on the present hypothesis, that the tetrahedral layer exerts very little stretching force on the octahedral layer in micas. The b axis of gibbsite is shorter than that of muscovite because the surface OH-OH bonds result in a small contraction of the Al-O bonds (by 0.06 Å) and of the vacant site ("site"—0 distance less by 0.05 Å); and these contractions in bond length shorten the b axis *without* thickening the layer.

(c) Lepidolite (no. 33)

This lepidolite is a $2M_2$ polymorph (Levinson, 1953) which is surprising since $\alpha = 10\frac{1}{2}°$, and ditrigonal surfaces should not allow this polymorph (Radoslovich, 1959).

The surface would be nearly hexagonal ($\alpha = 2°8'$), if the layers were in contact at 2.6 Å, and the K-O bonds were 2.86 Å; then $\tau = 111°54'$, which is reasonable. But this lepidolite has the same c^* as $2M_1$ muscovite, so that the layers are probably separated by a similarly large distance. Crystallization in the $2M_2$ form is therefore very surprising; and a structural analysis of this is now being undertaken.

(d) Celadonite (no. 35)

The observed and calculated values of α and η do not agree well. Zviagin's structural analysis, however, shows that the O-T-O angle, $\tau = 107°0'$, instead of $109°28'$, which gives $\alpha_{calc} = 13°43'$, in better agreement with $\alpha_{obs} = 12°$ (aver. of 13.3°, 13° and 10°). Using α_{obs} and the observed K-O bond of 2.78 Å gives a calculated separation of layers of 3.30°, as observed.

This structure shows several unusual features for which tentative explanations may now be offered, *viz:*

(1) the observed octahedral layer thickness is 2.48 Å, compared with 2.12 Å for muscovite and 2.10 Å for brucite, $Mg(OH)_2$. This layer in celadonite is deficient in cationic charge, however, and can therefore more readily increase in thickness than other micas. This increased thickness completely accommodates the increase in octahedral cation-oxygen bonds in passing from muscovite to celadonite, by changing the bond angles; and the isomorphous replacement of Fe^{2+}, Mg^{2+} and Fe^{3+} for Al^{3+} does *not* therefore increase the b axis in this case.

(2) the O-T-O angle is 107°, rather than 109°28′. The oxygen surfaces are separated (as in muscovite); this may possibly be a consequence of some mutual repulsion due to the K^+ charge being satisfied by the *octahedral* oxygens. For the nearer oxygens to maintain

TABLE 5. INTERATOMIC DISTANCES, OCTAHEDRAL CATION SITE TO OXYGENS

Celadonite		$2M_1$ Muscovite	
$Fe_{1.4}^{+3}$, $Mg_{0.6}^{2+}$-O (two sites)	2.06, 2.12, 2.15 Å	Al-O (two sites)	1.93_5, 1.93_2, 1.93_9 1.94_4, 2.04_8, 1.93_0
$Mg_{0.1}^{2+}$-O	2.11, 2.14, 2.14 Å	vacant-O	2.28_7, 2.23_3, 2.09

contact with the K^+ ion the tetrahedra must "over-rotate," which requires the basal triads to be enlarged; and since bond angles are changed more readily than bond lengths the tetrahedra "flatten out" by reducing τ to 107°0′.

(3) the β angle of celadonite is 100°6′, nearly equal to $\beta = \cos^{-1}(-a/3c) = 99°44'$, and therefore contrasting with 1M muscovite for which $\beta_{obs} = 101°30'$ and $\beta_{calc} = 100°0'$. This is surprising since both structures are dioctahedral, with similar tetrahedral rotations (12° and $14\frac{1}{2}$°). In celadonite, however, the octahedral sites are similar in size, whereas in 1M muscovite (by deduction from $2M_1$ muscovite) the unoccupied site is significantly larger than the other two (Table 5). This leads to asymmetry in muscovite, *i.e.* to displacement of K^+ (and Si) from $y = nb/12$. The K^+ displacement contributes to the departure of β from theoretical for the 1M polymorph in muscovite, but does not occur in celadonite.

(e) Celadonite (no. 36)

Although this one mica theoretically has hexagonal symmetry this implies an impossibly close approach of successive layers (1.07 Å). If a more reasonable approach of 2.6 Å is assumed then $\alpha_{calc} = 4°30'$ (*c.f.* celadonite, ref. 5) with $b_{tetr} = 9.08$ and $\tau = 109°58'$, which is acceptable. A mica having $\alpha = 0$ may be expected to occur amongst the end-member celadonites, if at all; and this specimen suggests that micas with hexagonal surfaces do not occur in nature.

(f) Margarite, no. 45

The value of η_{calc} can be confirmed by comparison with muscovite and xanthophyllite for which structural data is available. The layers of margarite and xanthophyllite have the same thickness (9.56 and 9.59 Å); and the octahedral layer of margarite, $CaAl_2(Si_2Al_2)O_{10}(OH)_2$, should be comparable with muscovite, $KAl_2(Si_3Al)O_{10}(OH)_2$, *i.e.* 2.12 Å, which is close to that of xanthophyllite 2.20 Å. Hence the interlayer distances of margarite and xanthophyllite should be comparable, which they are, *viz.* 2.57 and 2.69 Å.

(g) Ephesite, no. 46

The regression analyses (Part II) suggested that the original value of b (=8.81 Å) was far too small, and it was noted that ($\sqrt{3}$ a) (=8.95 Å) was rather larger. An ephesite specimen from Postmasburg (U.S.N.M. 104815, kindly donated by the U. S. National Museum) was found to have $b = 8.896$ Å, using a 19 cm camera.

(h) Xanthophyllite, nos. 47–50

Even though xanthophyllite has an *excess* cationic charge octahedrally, the octahedral layer is nevertheless thicker (2.20 Å) than in brucite (2.10 Å). This confirms the dominant role of the interlayer cation-oxygen bonds in determining b axes in micas—in this case the Ca-O bonds apparently shorten the b axis to the extent of compressing and slightly thickening the octahedral layer against its excess charge effects.

(i) Bityite, nos. 51–52

Although the Be-O bond length in a layer-lattice silicate is not accurately known, this bond is quoted by Wyckoff (1948) for BeO, which has 4–4 tetrahedral co-ordination, as 1.64 Å. As an approximation, then, Be is treated as equivalent to Si in calculating b_{tetr}. For bityite no. 51 ("bowleyite") successive layers are in contact. For no. 52 the data suggest a small separation across the interlayer region. Strunz (1956) used a 5.73 cm diam. camera, however, and b_{obs} may easily be in error. A value of 8.77 Å, *e.g.*, makes $\alpha = 22°$ and $\eta = 2.75$ Å, and it is noteworthy that all the other brittle micas (nos. 45–51) are virtually in contact across the interlayer region. It is also interesting that the tetrahedral rotations are about 20° for each of the brittle micas, as would be expected because of their greater tetrahedral Al, and the dominating influence of Ca. The latter is illustrated by bityite in which the Ca contracts the octahedral layers from 8.9 Å to 8.7 Å, even against the excess charge effects on this layer. The comparable octahedral contraction in xanthophyllite (to which bityite is closely analogous) is from 9.2 Å to 9.0 Å, also due to interlayer Ca.

Summary

The hypotheses on which b-axis formulae for layer-lattice silicates have previously been based have been modified in ways suggested by the results of recent structure analyses. The new hypothesis carries structural implications for all these minerals; these are discussed in detail for the micas. This hypothesis also allows new b-axis formulae to be proposed (in Part II) which remove several anomalies, especially for the brittle micas.

More than ten structures are now known in which the tetrahedral

layers contract by the rotation of individual tetrahedra. The simple formula, $\alpha = \text{arc cos } (b_{obs}/b_{tetr})$ predicts the average rotation satisfactorily, though uncertainties arise in b_{tetr} when the O-Si-O angle departs from 109°28′.

It is proposed that the sheet dimensions of layer-lattice silicates are controlled by the octahedral layer, and (for micas) the interlayer cation, except for those few minerals for which the tetrahedral layer is unduly stretched. Evidence is accumulating that the tetrahedral dimensions merely govern the surface configuration of these minerals.

A tentative formula is suggested for the separation of successive layers of micas across the interlayer region, and some evidence given for its general correctness.

A new ideal mica structure is proposed which has ditrigonal surface symmetry; this is consistent with the accepted space groups.

The new hypothesis is discussed in detail in relation to the micas and brittle micas, for which there are sufficient data to test its validity in some detail. A number of anomalies are explained thereby. It is emphasized, however, that the full validity of the model can be assessed only by comparison with the detailed analyses of key structures in the future.

Acknowledgments

The writers acknowledge with thanks the gifts of celadonite specimens from Margaret D. Foster and B. B. Zviagin, of biotite specimens from J. B. Jones, of ephesite from P. E. Desautels and of lepidolite specimens from A. A. Levinson. Extended discussions of the biotite data with J. B. Jones have been most helpful.

References

Aruja, E. (1944), An *x*-ray study on the crystal structure of gümbelite. *Mineral. Mag.*, **27,** 11.

Bassett, W. A. (1960), Role of hydroxyl orientation in mica alteration. *Bull. Geol. Soc. Am.*, **71,** 449.

Bradley, W. F. (1957), Current progress in silicate structures. *Clays and Clay Minerals, 7th. Nat. Conf.*, 18.

Brindley, G. W. and D. M. C. MacEwan (1953), Structural aspects of the mineralogy of clays and related silicates. *Ceramics; a symposium, Brit. Cer. Soc.*, 15.

Brown, G. (1951), *in* "*X*-ray Identification of Clay Minerals." Mineral. Soc., London.

Cundy, E. K., W. Windle and I. H. Warren (1960), The occurrence of zinnwaldite in Cornwall. *Clay Mineral. Bull.*, **4,** 151.

Faust, G. T. (1957), The relation between lattice parameters and composition for montmorillonite-group minerals. *Jour. Wash. Acad. Sci.*, **45,** 146.

Forman, S. A. (1951), Xanthophyllite. *Am. Mineral.*, **36,** 450.

Foster, M. D. (1956), Correlation of dioctahedral potassium micas on the basis of their charge relations. *U. S. Geol. Survey Bull.* **1036-D,** 57.

——— B. Bryant and J. Hathaway (1960), Iron-rich muscovite mica from the Grandfather Mountain area, N. Carolina. *Am. Mineral.*, **45,** 839.

Hendricks, S. B. and M. E. Jefferson (1939), Polymorphism of the micas. *Am. Mineral.*, **24,** 729.

Hey, M. H. (1954), A new review of the chlorites. *Mineral. Mag.* **XXX,** 277.

Jackson, W. W. and J. West (1930), The structure of muscovite. *Zeit. Krist.*, **76,** 211 and **85,** 160.

Jones, J. B. (1958), Dispersion in trioctahedral micas. Ph.D. thesis, Univ. Wisconsin.

Kohn, J. A. and R. A. Hatch (1955), Synthetic mica investigations. VI. *X*-ray and optical data on fluorophlogopites. *Am. Mineral.*, **40,** 10.

Levinson, A. A. (1953), Studies in the mica group, relationship between polymorphism and composition in the muscovite-lepidolite series. *Am. Mineral.*, **38,** 88.

Maegdefrau, E. and U. Hoffman (1938), Glimmerartige Mineralien als Tonsubstanzen. *Zeit. Krist.*, **98,** 31.

Malkova, K. M. (1956), Celadonite from Pobuzhé. *Min. sb. L'vov Geol. Ob-vo*, **305.**

Mauguin, C. (1913), Comptes Rendus, **156,** 1246.

Megaw, H. D. (1934), The crystal structure of hydrargillite, $Al(OH)_3$. *Zeit Krist*, **87,** 185.

Nagelschmidt, G. (1937), *X*-ray investigation on clays. III. The differentiation of micas by *X*-ray powder photographs. *Zeit. Krist.*, **97,** 514.

Newnham, R. E. and G. W. Brindley (1956), The crystal structure of dickite. *Acta. Cryst.*, **9,** 759.

Rowledge, H. P. and J. D. Hayton (1948), Two new beryllium minerals from Londonderry. *Jour. Roy. Soc. West. Aust.*, **33,** 45.

Phillips, F. C. (1931), Ephesite (soda margarite) from the Postmasburg district, Sth. Africa. *Mineral. Mag.*, **22,** 482.

Radoslovich, E. W. (1960), The structure of muscovite, $KAl_2(Si_3Al)O_{10}(OH)_2$. *Acta. Cryst.*, **13,** 919.

——— (1961), Surface symmetry and cell dimensions of layer-lattice silicates. *Nature*, **191,** 67.

Smith, J. V. (1954), A review of the Al-O and Si-O distances. *Acta Cryst.*, **7,** 479.

——— and H. S. Yoder (1956), Experimental and theoretical studies of the mica polymorphs. *Mineral. Mag.*, **XXXI,** 209.

Stevens, R. E. (1938), New analyses of lepidolites and their interpretation. *Am. Mineral.*, **23,** 607.

Strunz, H. (1956), Bityit, ein Berylliumglimmer. *Zeit. Krist.* **107,** 325.

Takéuchi, Y. and G. Donnay (1959), The crystal structure of hexagonal $CaAl_2Si_2O_8$. *Acta Cryst.*, **12,** 465.

——— and R. Sadanaga (1959), The crystal structure of xanthophyllite, *Acta. Cryst.*, **12,** 945.

Wyckoff, R. W. G. (1948), "Crystal Structures, Vol. I." Interscience, New York.

Yoder, H. S. (1958), Priv. Comm.

——— and H. P. Eugster (1954), Phlogopite synthesis and stability range. *Geochim. Cosmochim. Acta*, **6,** 157.

——— (1955), Synthetic and natural muscovites. *Geochim. Cosmochim. Acta*, **8,** 155.

Zviagin, B. B. (1957), Determination of the structure of celadonite by electron diffraction. *Soviet Physics, Crystallography*, **2,** 388 (in transl).

Manuscript received, June 15, 1961.

THE AMERICAN MINERALOGIST, VOL. 47, MAY–JUNE, 1962

THE CELL DIMENSIONS AND SYMMETRY OF LAYER-LATTICE SILICATES

II. REGRESSION RELATIONS

E. W. RADOSLOVICH, *Division of Soils, Commonwealth Scientific and Industrial Research Organisation, Adelaide, Australia.*

ABSTRACT

New formulae connecting the sheet dimensions (*b* axes) of layer-silicates with their chemical composition are proposed; the theoretical basis for these was described earlier (Part I). The new formulae are obtained by the multiple regression analysis of unit cell *x*-ray data and ionic proportions as given by the structural formulae. Kaolinite and serpentine minerals, chlorites, micas and montmorillonites are treated as separate groups. Tetrahedral aluminum does not increase *b* for kaolin and serpentine minerals, chlorites and micas, and only slightly increases *b* for the montmorillonites. The interlayer cation has a major effect on the cell dimensions of micas. The present *b*-axis formulae appears to be sufficiently precise to allow a number of conclusions to be drawn about individual mineral structures, and also to suggest errors in some older data in the literature.

INTRODUCTION

It has long been apparent that a close relationship exists between cell dimensions and composition for the layer-lattice silicates. In particular the sheet dimensions, b (or $a = b/\sqrt{3}$), apparently depend in a simple way on composition, so that many "*b*-axis" formulae have appeared in the literature. These have been shown in Part I (Radoslovich and Norrish, 1962) to be based on partially incorrect hypotheses. New formulae consistent with the new hypotheses were established satisfactorily by trial-and-error methods. However, it was also highly desirable to establish the significance or non-significance of certain coefficients in the formulae. For this reason the best available data have been analysed statistically (by multiple regression analysis), and new formulae for predicting "*b*" from composition were derived on this basis. Since it is now obvious that micas must be treated independently, because of the interlayer cation, it was decided to keep separate all four groups, *viz.* kaolin and serpentine minerals, micas, chlorites and montmorillonites.

Although the theoretical predictions in Part I indicated that tetrahedral Al should not appear in the formulae it was considered essential to insert the Al_{tetr} figures to check that the contribution made by Al in the tetrahedral sites is effectively zero. For each group of minerals the variation of b with composition was computed as a multiple regression equation,

$$b = b_0 + \sum a_i x_i,$$

where a_i are the required regression coefficients for cations 1, 2, . . . i . . . and x_i are the ionic proportions of the various substituting cations in the

appropriate structural formulae. In order to keep all of the coefficients a_i positive the equations were set up so that b_0 should correspond to the end member mineral with the smallest dimensions, in each case the member with only Al octahedrally and only Si tetrahedrally coordinated. (The latter condition is, of course, unnecessary if Al_{tetr} makes no contribution, as is now known to be true for very many minerals.)

It is not easy to find data in the literature for layer-lattice silicates for which the particular sample is undoubtedly pure, the chemical analysis is sufficiently accurate, the basis for calculating the structural formula is known and acceptable, and the x-ray data are of assessable and high accuracy. Within limits the data available have been selected rather critically; data which are suspected to be inadequate have merely been checked against the new regression equations, and not used in computing them originally.

It is, of course, impossible on the simple premises proposed here to distinguish between polymorphs of the same composition, although it is known for example that kaolinite, dickite and nacrite differ slightly in b. Likewise the development of a single regression relation to cover many minerals of a given structural type does not necessarily imply the existence of a complete isomorphous series between member minerals. For example one regression relation applies to both muscovite and phlogopite despite a probable structural discontinuity between them; and similarly one relation applies (with one restriction only) to kaolins and their trioctahedral analogues (variously called serpentines, septochlorites etc.)[1] though a structural discontinuity has been claimed here by Nelson and Roy (1954).

During the course of this study it became necessary or desirable to place certain limits on the samples included in the various regression analyses. In particular, for those compositions for which $b_{oct} > b_{tetr}$, if both layers were unconstrained, the octahedral layer may or may not contract before the tetrahedral layer expands. For this reason the data used in the final regression analyses did not include those minerals for which $b_{obs} \geq b_{tetr}$; these minerals were merely compared with the results obtained. This is discussed later in relation to the saponites and serpentines.

Kaolins[1]

The final regression relations for these minerals were first computed to give the increase in b when substitutions occur in $Al_2Si_2O_5(OH)_4$ of Al^{3+} tetrahedrally, and of Mg^{2+}, Fe^{2+} and Fe^{3+} octahedrally. This calculation

[1] There is no generally accepted nomenclature yet which describes concisely the kaolin minerals and their trioctahedral analogues; for the sake of brevity only, the words "kaolin, kaolins" will be used in this paper to refer to all these minerals collectively.

TABLE I. REGRESSION COEFFICIENTS FOR KAOLINS, CHLORITES, MICAS AND MONTMORILLONITES

Group	No. of Specimens	R^2	b_0	Variate	Regression Coefficient	Standard Deviation	Significance Level %
Kaolins $Al_2Si_2O_5(OH)_4$	12	0.994	8.9226	Mg	0.1248	±0.0053	0.1
				Fe^{2+}	0.2290	±0.0078	0.1
				Fe^{3+}	0.0794	±0.0099	0.1
Chlorites $Al_4Si_4O_{10}(OH)_8$	21	0.765	9.23	Fe^{2+}	0.03	±0.0035	0.1
Micas Na $Al_2(Si_2Al)O_{10}(OH)_2$	45	0.941	8.9245	K	0.0992	±0.0344	1
				Ca	−0.0685	±0.0335	5
				Mg	0.0621	±0.0062	0.1
				Fe^{2+}	0.1160	±0.0094	0.1
				Fe^{3+}	0.0976	±0.0127	0.1
				Ti	0.1655	±0.0563	1
Montmorillonites $Al_2Si_4O_{10}(OH)_2$	30	0.987	8.9442	Mg	0.0957	±0.0062	0.1
				Fe^{3+}	0.0957	±0.0048	0.1
				Al_{tetr}	0.0367	±0.0118	1.0

gave a non-significant regression coefficient for $Al_{tetr.}$, so that the assumption that Al_{tetr} does not affect "*b*" for these minerals is fully justified. The regression analysis was therefore recalculated omitting this variate (Table 1). The very high value of the square of the multiple regression coefficient, $R^2(=0.994)$, confirms that the variations in "*b*" are almost completely explained by the regression of "*b*" on the ionic substitutions.[1]

It is assumed that the regression coefficients are linearly proportional to the difference between the ionic radii r_i and the hole filled r_h by the substituting cations, *i.e.* $(r_i - r_h) = k \cdot a_i$ where for Mg, for example, $(0.65 - r_h) = k \cdot 0.125$. A least squares determination of k also yields values for r_h (Table 2), which are highly self consistent, and close to the ionic radius of Al. On the strong probability that Mn and Ti will behave similarly regression coefficients may be predicted from their ionic radii as follows:

Mn	$0.80 - 0.52 = 0.995a$	whence	$a = 0.28$
Ti	$0.69 - 0.52 = 0.995a$	whence	$a = 0.17$

A regression analysis which also included the two antigorites and grovesite in Table 4 gave a coefficient for Mn of 0.269 with $R^2 = 0.996$. The mica analysis gives a Ti coefficient of 0.165 with $k \fallingdotseq 1.18 = 1$. These predicted coefficients are therefore reasonable.

The recommended regression equation to be used for predicting *b* axes for kaolin minerals is given in Table 3, and in Table 4 the observed values of *b* are compared with values calculated by this equation. Minerals in-

[1] See any textbook on mathematical statistics, *e.g.* "Regression Analysis," by E. J. Williams, John Wiley & Sons, N. Y., 1959, p. 25.

TABLE 2. RELATIONS BETWEEN REGRESSION COEFFICIENTS AND IONIC RADII

$(r_i - r_h) = k \cdot a_i$

Group	Variate	Radius, r_i	Coefficient, a_i	"Hole, r_h"	k
Kaolins	Mg	0.65	0.125	0.521	0.995
	Fe^{2+}	0.75	0.229	0.522	
	Fe^{3+}	0.60	0.079	0.526	
	Al	0.50	—	0.50	
Micas	K	1.33	0.099	1.130	2.03
	Ca	0.99	−0.069	1.130	
	Mg	0.65	0.062	0.535	1.86
	Fe^{2+}	0.75	0.116	0.535	
	Fe^{3+}	0.60	0.098	0.484	1.18
	Ti	0.68	0.166	0.484	
	Al	0.50	—	0.50	
Montmorillonites	Mg	0.65	0.096	0.554	Put k = 1
	Fe^{3+}	0.60	0.096	0.504	Put k = 1
	Al	0.50	—	0.50	
	Si	0.41		0.41	
	$Al_{tetr.}$	0.50	0.074[1]	0.43	Put k = 1

[1] For a valid comparison with the other a_i this coefficient has been doubled because there are two tetrahedral layers per cell.

cluded in the first part of Table 4 were those used to compute the regression coefficients; the remaining b_{obs} were simply compared with the regression relation. Table 4 also gives the calculated and available observed values of the tetrahedral twist, α (see Part I), except where b_{obs} exceeds b_{tetr}, when the twist is assumed to be zero. The agreement for the two kaolinites is excellent.

Certain minerals in Table 4 merit further discussion. For dickite Newnham (1960) gives the Si-O bonds as 1.62 Å, rather than 1.60 Å,

TABLE 3. RECOMMENDED PREDICTION RELATIONS FOR CALCULATING b

Kaolins	$b = (8.923 + 0.125\ Mg + 0.229\ Fe^{2+} + 0.079\ Fe^{3+} + 0.28\ Mn^{2+} + 0.17\ Ti) \pm 0.014$ Å
Chlorites	$b = (9.23 + 0.03\ Fe^{2+}) \pm 0.03$ Å
Micas	$b = (8.925 + 0.099\ K - 0.069\ Ca + 0.062\ Mg + 0.116\ Fe^{2+} + 0.098\ Fe^{3+} + 0.166\ Ti) \pm 0.03$ Å
Montmorillonites	$b = (8.944 + 0.096\ Mg + 0.096\ Fe^{3+} + 0.037\ Al_{tetr.}) \pm 0.012$ Å

TABLE 4. CELL DIMENSIONS AND TETRAHEDRAL ROTATIONS FOR KAOLINS

Mineral	Reference	Composition										b_{ob} Å	b_{calc} Å	b_{tetr} Å	α_{obs} °	α_{calc} °
		Al^{VI}	Mg	Fe^{2+}	Fe^{3+}		Al^{IV}	Si	Fe^{3+}	OH	O					
Kaolinite	Author	2.0						2.0		4.0	5.0	8.924	8.924	9.05		9°34′
Dickite	Author	2.0						2.0		4.0	5.0	8.929	8.924	9.05		9°42′
Halloysite	Author	2.0						2.0		4.0	5.0	8.904	9.924	9.05		10°18′
Dickite	Newnham (1961)	2.0						2.0		4.0	5.0	8.940	8.924	9.05	7½°	8°36′
Nacrite	Brammall *et al.* (1937)	2.0						2.0		4.0	5.0	8.95	8.924	9.05		8°36′
Serpentine	Gillery (1959)	0.75	2.25				0.75	1.25		4.0	5.0	9.193	9.204	9.432		12°54′
Serpentine	Gillery (1959)	0.375	2.62				0.375	1.625		4.0	5.0	9.245	9.250	9.242		0°
Amesite	Steinfink & Brunton (1956)	1.0	2.0				1.0	1.0		4.0	5.0	9.20	9.174	9.56	11°30′	15°48′
Amesite	Brindley *et al.* (1951)	1.06	1.50	0.41			0.99	1.01		4.0	5.0	9.19	9.205	9.56		16°0′
Chamosite	Brindley (1951)	0.76	0.16	1.73	0.02	0.15[2]	0.76	1.24		4.0	5.0	9.333	9.366	9.437		8°12′
Chamosite	Brindley *et al.* (1953)	0.81	0.22	0.02	1.83		0.68	1.32		1.02	7.3	9.10	9.100	9.397		14°28′
Chamosite	Brindley *et al.* (1953)	0.83	0.23	1.82	0.01		0.68	1.32		3.96	5.0	9.379	9.369	9.397		4°24′
Antigorite	Brindley *et al.* (1954)		2.869	0.006	0.060	0.002[3]	0.005	1.954	0.041	4.102	4.898	9.219[1]	9.288	9.052		—
Grovesite	Bannister *et al.* (1955)	0.67	0.07		0.18	2.21[3]	0.68	1.32		3.57	5.42	9.54	9.565	9.391		—
Antigorite	Zussman *et al.* (1957)	0.31	2.73	0.03	0.03		0.102	1.898		3.58	5.42	9.26	9.273	9.11		—
Hydroamesite	Erdelyi *et al.* (1959)	0.203	2.329		0.20		0.448	1.552		3.881	5.12	9.20	9.230	9.164		—
Greenalite	Gruner (1936)			2.2	0.5			2.0		4.0	5.0	9.56	9.467	9.05		—
Cronstedite	Hendricks (1939)			2.3	0.5			1.0	1.0	4.5	5.0	9.49[1]	9.490	10		18°
Cronstedite	Gossner (1935)			2.28	0.60	0.09[4]	0.07	1.07	0.86	4.41	5.59	9.50[1]	9.450	10		18°
Chrysotile	Zussman *et al.* (1957)	0.222	2.704		0.042		0.189	1.811		3.98	4.02	9.21	9.265	9.15		—
Lizardite	Zussman *et al.* (1957)	0.12	2.75		0.02			2.04		3.92	4.08	9.2	9.268	9.05		—
Colerainite	A.S.T.M. index	0.26	2.51		0.04	0.04[4]	0.30	1.70		4.26	4.74	9.20	9.240	9.20		—
Kaolinite	Zviagin (1960)	2.0						2.0		4.0	5.0	8.89	8.924	9.05	10.9°	10.8°
Kaolinite	Drits and Kashaev (1960)	2.0						2.0		4.0	5.0	8.93	8.924	9.05	9°	9°18′
Pyrophyllite	19 cm camera	2.0						4.0		2.0	10.0	8.924	8.924	9.05		9°35′
Talc	19 cm camera		3.0					4.0		2.0	10.0	9.158	9.293	9.05		—
Minnesotaite	Gruner (1944)		0.66	1.96			0.05	3.57	0.10	2.0	10.0	9.40?	9.45	<9.05		?

[1] Assuming Fe^{3+} tetrahedrally does not contribute to b_{calc}, by analogy with Al tetrahedrally. [2]Ti. [3]Mn. [4]Ca.

which should increase α_{obs} relative to α_{calc}; but the average O-Si-O angle, τ is 111.9° approx., which rather more than compensates for the larger bond length. Detailed data for τ are not quoted for amesite, for which there is a larger discrepancy between α_{obs} and α_{calc}.

The values of α for the two serpentines are interesting when compared with their symmetries. One serpentine, with $\alpha = 0$, is a one-layer orthoserpentine, the other, with $\alpha = 12°54'$, is a six-layer orthoserpentine. It is tempting to suppose that it is the regular surface network of the former which allows this serpentine to form an orthohexagonal cell repeating through only one layer, rather than three or six.

Grovesite and antigorite (Zussman *et al.* 1957) are examples of kaolins in which the tetrahedral layer appears to have stretched to the limit without effectively contracting the octahedral layer; this is shown by the close agreement between b_{calc} and b_{obs}. The angle τ is 106°50′ for grovesite and 106°32′ for the antigorite, *i.e.* at the apparent lower limit of 106½–107° for this angle. The other "antigorite" (Brindley *et al.*, 1954) is clearly one in which the tetrahedral layer has set the limit to expansion; $b_{obs} = 9.219$ Å is noticeably less than $b_{calc} = 9.288$ Å, even after making $\tau = 106°47'$ to allow the tetrahedral layer to stretch to 9.219 Å. In fact this specimen was later called an orthoserpentine. There is, indeed, some evidence suggesting that antigorites have b determined by the octahedral layer, and chrysotiles have b determined by the tetrahedral layer;[1] the chrysotile and lizardite specimens are consistent with this.

The rotation $\alpha = 18°$ for cronstedite can only be roughly calculated since the increase in tetrahedral dimensions due to Fe^{3+}- for -Si substitution is not known precisely. The rotation will certainly exceed that for most other kaolins.

The data on greenalite are unsatisfactory. Gruner (1936) gives $b = 2 \times 9.3$ Å, though Brindley and MacEwan (1953) used another spacing of Gruner's data giving $b = 9.56$. Neither of these can be accepted in relation to the quoted structural formula since for the tetrahedral layer to stretch even to 9.32 Å τ drops to 104½°. However if the tetrahedral composition were $(Si_{1.75}\ Fe_{0.25}^{3+})$ and $\tau \doteqdot 107°$ then b_{tetr} will be about 9.3 Å. Gruner pointed out the considerable difficulty in obtaining a satisfactory analysis of greenalite, and data on this mineral obviously need revision.

Pyrophyllite, talc and minnesotaite may be expected to conform to the kaolin b-axis formula, since these layers carry no charge. The calculated and observed values of b for pyrophyllite agree precisely. For talc, however, b corresponds to two Si-O layers with Si-O bonds of 1.60 Å and $\tau = 107°27'$, the minimum expected value for τ when *two* tetrahedral layers

[1] It is hoped to discuss these results, in relation to kaolin morphology, in a later paper.

are fully stretched by *one* octahedral layer, which is itself contracted from 9.29 Å to 9.16 Å. The minnesotaite data are probably wrong, since the observed tetrahedral layer could hardly stretch to 9.40 Å. Gruner (1944) recorded lines at 1.567 Å (intensity 1.0) and 1.514 Å (intensity 0.5), and by these hypotheses the latter is the 060 line, *i.e.* $b = 9.08$ Å. That is, the octahedral layer is greatly contracted, from 9.45 to 9.08 Å. This is not impossible (sauconite contracts a comparable amount octahedrally), and the layers of minnesotaite are 9.55 Å thick, compared with 9.26 Å for talc which is similarly compressed and thickened. This mineral also requires re-investigation.

Chlorite group

Six variates were used initially to compute the regression of b when substitutions occur in $Al_4Si_4O_{10}(OH)_8$, *viz.* Al^{3+} and Cr^{3+} tetrahedrally, and Mg^{2+}, Fe^{2+}, Fe^{3+} and Cr^{3+} octahedrally. Of these only the coefficient for Fe^{2+} was significant, and the overall fit was considerably less satisfactory than for the kaolins. Several two-variate relations were then computed, but the best relation obtainable from the present data is

$$b = 9.23 + 0.03Fe^{2+} \pm 0.0285 \qquad (1)$$

This should be compared with the regression relation proposed by Hey (1954), *viz.*

$$b = 9.202 + 0.028Fe(\text{total}) + 0.047Mn^{2+}$$

The available published data on manganiferous chlorites are not sufficiently extensive or reliable to include Mn^{2+} as a variate in (1) above, but when such a term can be computed the coefficient should exceed that for Fe^{2+}, because of the larger ionic radius. The present analysis disagrees with Hey's result in that Fe^{3+} at no stage showed a significant regression coefficient. A comparison of ripidolite and thuringite data (Table 5 Nos. 1 and 3) confirms that Fe^{2+} and Fe^{3+} have quite different effects on b, and suggests that Fe^{2+} (not total Fe) should be used, as in (1).

The relative independence of the b-dimension of chlorites with respect to the smaller cations is rather less surprising when considered in relation to their structures and composition range. Normal chlorites (*e.g.* as defined by Hey, 1954) contain moderate proportions of Mg^{2+} (radius 0.65 Å) and/or Fe^{3+} (0.60 Å) and/or Cr^{3+} (0.64 Å). The analyses by Steinfink (1958) of the prochlorite and corundophillite structures suggest that the various octahedral cations may well be ordered between the two octahedral layers of normal chlorites generally. Hence it is quite possible that even in chlorites with moderate Al content one octahedral layer may contain very little Al. If so then the presence of Al (0.50 Å) in the other layer would not necessarily lead to a smaller overall b axis. That is, the

presence of *two* octahedral layers and some Mg or Fe^{3+} in chlorites effectively buffers the b axis against variations, except those due to substitutions by much larger cations such as Fe^{2+} (0.75 Å) and Mn^{2+} (0.80 Å); Brindley and Gillery (1956) have put forward similar arguments.

Calculated and observed b values are compared in Table 5, which also gives the calculated tetrahedral rotations, α. The observed average rotation is given for prochlorite and corundophillite, from a plot of Steinfink's parameters. Though the agreement between α_{obs} and α_{calc} is only moderate the calculated prochlorite angle exceeds the corundophillite angle as observed. Steinfink reported the O-Si-O angle for prochlorite to be 110.8°, however, and this increases α_{calc} to $9\frac{1}{2}°$, close to $\alpha_{obs} = 10°$; the same angle is not given for corundophillite.

The unusual "chlorite" mineral, cookeite (Norrish, 1952), cannot be considered according to the regression relation above for normal chlorites, since it does not contain Fe^{3+} or Mg. It is therefore the more interesting that for cookeite $b = 8.918$ (Table 5) which is very close to b for kaolins and micas (Table 1). This is certainly to be expected since Li behaves much as Al in the variation of b with composition.

Several papers have recently reported dioctahedral chlorites, though with insufficient data for inclusion in this regression analysis. Bailey and Tyler (1960) have noted a dioctahedral chlorite for which no analysis is yet available, but which contains some magnesium. The b axis, 9.03 Å, is consistent with the present hypotheses. This suggests that if enough data on dioctahedral chlorites eventually become available, then the variation in b for all chlorites may be described by a regression relation closely similar to that for the kaolins. As a crude test of this the kaolin relation was applied to the chlorites in Table 5, assuming that the octahedral cations are equally divided between the two octahedral layers. The values of b calculated in this way (Table 5) are sufficiently close to b_{obs} to give considerable weight to the suggestion above.

Micas

The following conditions were imposed on the final regression analysis, as a result of extensive preliminary studies.

1. The analysis was computed to give the increase in b when K and Ca, and Mg, Fe^{2+}, Fe^{3+} and Ti are substituted in the paragonite composition, $NaAl_2(Si_3Al)O_{10}(OH)_2$. Micas must contain an interlayer cation, and coefficients for *both* Na and K cannot be satisfactorily determined because these cations are very highly correlated. The early studies had confirmed that tetrahedral Al does not have a significant coefficient, and this variate was omitted.

2. The data were chosen to be sufficiently representative and numerous to give satisfactory average values of the coefficients for prediction pur-

TABLE 5. CELL DIMENSIONS AND TETRAHEDRAL ROTATIONS FOR CHLORITES

Mineral	Reference	Composition									b_{obs} Å	b_{calc} Å	b "kaolin" Å	α_{obs} °	α_{calc} °
		Mg	Fe^{2+}	Fe^{3+}	Al^{VI}		Al^{IV}	Si	OH	O					
Ripidolite	Gillery (A.S.T.M. index)	2.8	1.7		1.3		1.2	2.8	8.0	10.0	9.283	9.28	9.29		7°6′
Bavalite	Gillery (A.S.T.M. index)	0.4	4.2		1.5		1.4	2.6	8.0	10.2	9.365	9.36	9.43		5°24′
Thuringite	Gillery (A.S.T.M. index)	2.2	0.7	1.4	1.2		1.5	2.5	7.7	10.2	9.192	9.25	9.19		13°
Grochanite	Gillery (A.S.T.M. index)	4.2	0.22		1.22		1.4	2.6	8.0	10.0	9.227	9.23	9.21		11°12′
Diabantite	Gillery (A.S.T.M. index)	2.9	2.2	0.2	0.7		1.1	2.9	7.7	10.7	9.305	9.30	9.36		4°12′
Kammererite	Gillery (A.S.T.M. index)	5.1	0.2		0.2	0.6[3]	0.9	3.1	6.6	10.8	9.242	9.24	9.26		5°6′
Sheridanite	Gillery (A.S.T.M. index)	4.3	0.1		1.6		1.5	2.5	7.9	10.1	9.226	9.23	9.20		12°
Chrome Chlorites	Lapham (1958)	Eight similar analyses and x-ray data									9.222	9.23–9.25			
Mg-Chamosite	Bannister & Whittard (1945)	1.84	2.82		1.21		1.12	2.87	7.7	10.3	9.33	9.32	9.36		0°
Pennantite	Structure Reports, 10, 157.	0.25		0.37	1.18	3.82[4]	1.38	2.62	7.3	10.1	9.40	9.36[1]	9.47		0°
Thuringite	Structure Reports, 10, 157.	0.70	3.70	0.75	0.85		1.60	2.40	8.0	10.0	9.30	9.34	9.42		10°27′
Thuringite	Structure Reports, 10, 157.		3.85	0.75	1.40		1.30	2.70	8.6	10.3	9.31	9.35	9.39		7°
Bavalite	Structure Reports, 10, 157.	0.35	4.75	0.05	0.80		1.75	2.25	7.0	10.0	9.35	9.37	9.49		10°
Diabantite	Bannister & Whittard (1945)	2.53	2.16	0.18	0.76	0.12[5]	0.58	3.42	8.0	10.0	9.29	9.29	9.34		
		$b_{tetr.}$ = 9.20; tetr. layer stretched, O-Si-O < 109°28′													
Daphnite	Bannister & Whittard (1945)	0.92	3.37	0.18	1.35	0.04[4]	1.29	2.71	8.0	10.0	9.38	9.33	9.38		0°
Chamosite	Bannister & Whittard (1945)	0.75	3.23	0.56	1.12		1.01	2.99	8.0	10.0	9.36	9.33	9.36		—
		$b_{tetr.}$ = 9.31; O-Si-O < 109°28′													
Thuringite	Bannister & Whittard (1945)	0.72	3.68	0.76	0.83		1.58	2.42	8.0	10.0	9.32	9.34	9.42		9°45′
Corundophillite	Steinfink (1958)	4.9	0.07	0.17	0.75	0.18[3]	1.4	2.6	8.0	10.0	9.27	9.23	9.24	7.5°	9°30′
Prochlorite	Steinfink (1958a)	2.6	0.2	1.5	1.2		1.8	2.2	8.0	10.0	9.30	9.24	9.17	10°	11°48′
Chamosite	von Wolff (1942)	0.75	3.35	0.6	1.3		0.9	3.1	8.8	10.0	9.36	9.33	9.38		—
		$b_{tetr.}$ = 9.28; O-Si-O < 109°28′													
Leuchtenbergite	McMurchy (1934)	5.2			0.82		1.1	2.9	8.0	10.0	9.19	9.23	9.24		9°55′
Sheridanite	McMurchy (1934)	4.6	0.02	0.10	1.30		1.4	2.6	8.0	10.0	9.21	9.23	9.21		11°42′
Chlorite	McMurchy (1934)	3.9	0.70		1.40		1.4	2.6	8.0	10.0	9.21	9.25	9.24		11°42′
Prochlorite	McMurchy (1934)	2.7	2.3		1.01		1.58	2.42	8.0	10.0	9.27	9.30	9.36		11°24′
Cookeite	Norrish (1952)	3.79				1.36[6]	0.85	3.15	8.16	9.84	8.918		8.924		14°10′
Chrome Chlorite	Brown and Bailey (1960)	5.05	0.11	0.04	0.17	0.71[3]	0.97	3.03	7.9	10.0	9.250	9.23[2]	9.29[2]	6°	5°58′

[1] Assuming a coefficient for Mn = 0.033. [2] Assuming same coefficient for Cr as for Mg. [3] Cr. [4] Mn. [5] Ca. [6] Li.

TABLE 6. CELL DIMENSIONS FOR MICAS

Mineral	No.[1]	b_{obs}	b_{cal}	b_{kaolin}	Mineral	No.[1]	b_{obs}	b_{calc}	b_{kaolin}
Biotite	1	9.265	9.261	9.39	Biotite	24	9.265	9.271	9.40
Biotite	2	9.247	9.238	9.19	Phlogopite	25	9.241	9.185	9.34
Biotite	3	9.268	9.249	9.37	Phlogopite	26	9.22	9.195	9.31
Biotite	4	9.251	9.220	9.33	Phlogopite	27	9.204	9.210	9.30
Biotite	5	9.261	9.257	9.36	Fluorophlogopite	28	9.195	9.210	9.30
Biotite	6	9.251	9.266	9.41	Fluorophlogopite	29	9.188	9.208	9.30
Biotite	7	9.257	9.260	9.37	Muscovite	30	8.995	9.034	8.94
Biotite	8	9.225	9.248	9.27	Iron Muscovite	31	9.06	9.077	9.01
Biotite	9	9.254	9.249	9.35	Paragonite	32	8.90	8.925	8.92
Biotite	10	9.265	9.226	9.16	Lepidolite	33	9.006	9.008	8.94
Biotite	11	9.262	9.274	9.39	Lepidolite	34	8.97	9.024	8.94
Biotite	12	9.206	9.252	9.20	Zinnwaldite	39	9.12	9.094	9.07
Biotite	13	9.308	9.298	9.42	Zinnwaldite	40	9.06	9.063	9.02
Biotite	14	9.246	9.253	9.36	Lithium biotite	41	9.21	9.155	9.21
Biotite	15	9.255	9.231	9.20	Lithium biotite	42	9.09	9.088	9.09
Biotite	16	9.253	9.258	9.38	Gümbelite	43	9.04	9.017	8.97
Biotite	17	9.215	9.234	9.20	Lepidomelane	44	9.29	9.288	9.41
Biotite	18	9.328	9.284	9.43	Margarite	45	8.92	8.925	8.92
Biotite	19	9.266	9.258	9.35	Xanthophyllite	47	9.00	8.984	9.20
Biotite	20	9.300	9.330	9.49	Xanthophyllite	48	9.01	9.004	9.20
Biotite	21	9.323	9.303	9.45	Xanthophyllite	49	9.00	9.005	9.22
Biotite	22	9.260	9.262	9.37	Xanthophyllite	50	9.02	9.003	9.21
Biotite	23	9.271	9.234	9.37					
Celadonite	35	9.02	9.185	9.12	Celadonite	38	9.08	9.192	9.21
Celadonite	36	9.05	9.188	9.15	Ephesite	46	8.896	8.926	8.93
Celadonite	37	9.06	9.106	9.08	Bityite	51	8.713	8.856	8.92
					Bityite	52	8.67	8.859	8.93

[1] These numbers correspond with those in Table 4 of Part I, in which the structural formulae are listed.

poses. This is important because the linear model cannot be completely obeyed by all cations for all micas, and in particular the interlayer cations will sometimes increase b (*e.g.* muscovite *cf.* paragonite) and sometimes decrease b (*e.g.* xanthophyllite). The regression coefficients therefore will depend somewhat on the data analysed; the exclusion of all dioctahedral micas, for example, would probably considerably decrease the coefficient for K^+. Likewise the coefficients for the octahedral cations are not independent of the effects of the interlayer cations, and their values will not be as precise for the micas as for the kaolins.

3. The micas ephesite, bityite and celadonite were not included in the analysis, and data on these minerals (Table 6) were simply checked against the prediction relation. The new value of b for ephesite (Part I) was not available in time to include in the analysis. No precise account can be taken for Be tetrahedrally, so that bityite was omitted. Celadonites are also excluded, because the octahedral layer of this mineral is charge deficient, and it is therefore probably disproportionately thick. The preliminary regression analyses showed a marked improvement in R^2 when nos. 35–38 were omitted. No. 37 (Table 6), which has an appre-

ciable amount of Al octahedrally and probably should not be named a celadonite, may be expected to conform more readily to the model. For this mineral b_{obs} and b_{calc} differ by less than two standard errors, but for nos. 35, 36 and 38 this difference is between 4 and 6 standard errors. Lepidolites (which also are charge deficient octahedrally) conform to the regression relation simply because $b_{calc} = b_0$, *i.e.* the Li^+ does not effectively increase the volume of their octahedral layers.

The regression analysis of 45 micas (Table 6) yielded coefficients showing several interesting features (Table 1). The surprisingly high value of R^2 shows that condition 2 (above) was observed. The value of b_0 is effectively identical with that for the kaolins, which suggests that Na^+ neither increases nor decreases the dimensions set by the dioctahedral Al layer. (This is consistent with the discussion of paragonite, Part I.) The Ca^{2+} coefficient is negative, even though Ca^{2+} (0.99 Å) exceeds Na^+ (0.90 Å) in size, but this coefficient depends considerably on the xanthophyllite data, whose composition ensures that Ca^{2+} markedly contracts *b*.

The sizes of the holes filled, r_h, and the constants of proportionality, k, were determined from three pairs of simultaneous equations (Table 2). The coefficients for both the interlayer cations and the divalent and trivalent octahedral cations were analysed separately, since there is considerable evidence of ordering of these in the mica structures. The high values of k for the interlayer cations (=2.03) and divalent ions (=1.86) confirms that the model is not invariant for either of these groups whereas the smaller value (*viz.* 1.18) for the trivalent ions shows that these obey the model more closely. Physically the latter appear to substitute directly into Al sites, and in fact the "hole" size (r_h=0.48 Å) approximates the Al radius (0.50 Å). The interlayer cation sometimes increases and sometimes decreases *b* (2., above), and hence k is high. It appears probable that small amounts (<1.0) of divalent cations occupy mainly the unique octahedral sites, whereas larger amounts (<2.0) tend to occupy the two symmetry-related sites. (In muscovite the former is vacant and considerably larger than the Al-occupied sites.) Ordering of this kind, which under some circumstances could lead to an inconsistent model for the divalent cations (*i.e.* higher k) will be discussed in a later paper.

The effect of the interlayer cation on *b* may be estimated in general terms by comparing b_{obs} with b_{kaolin} (Table 6), *i.e.* with *b* computed for the micas using the *kaolin* relation. Since b_{kaolin} generally exceeds b_{obs} for phlogopites and biotites the K^+ apparently contracts b_{oct} in these minerals. But the high iron biotites, before and after heating to convert Fe^{2+} to Fe^{3+}, now form an interesting group. For nos. 2, 10 and 15 $b_{kaolin} < b_{obs}$, and of these the *b* axes of 10 and 15 represent a slight *increase*, and of 2 only a very small decrease relative to *b* for the unheated specimens

(9, 14 and 1, respectively). For nos. 12 and 17 $b_{kaolin} \doteqdot b_{obs}$, and b_{obs} is noticeably less than b_{obs} for nos. 11 and 16 respectively (the unheated specimens). This is to be expected with normal biotites since Fe^{3+} (0.60 Å) is smaller than Fe^{2+} (0.75 Å). These data suggest that in normal biotites interlayer K decreases *b* slightly, or has no effect, but for the very unusual "biotites," nos. 10 and 15, K is increasing *b;* this again indicates the varying role of the interlayer cations.

Montmorillonites

The interpretation of chemical analyses of montmorillonites is much more difficult than of kaolins and micas, as Kelley (1945) has especially pointed out. The acid dissolution studies of Osthaus (1956) and others clearly show the problem of obtaining really pure specimens. The readiness with which Fe^{2+} is oxidised to Fe^{3+} in the minerals also suggests that structural formulae must be viewed cautiously. Errors in these formulae may therefore occur due to impurities, or else to more systematic errors inherent in the chemical techniques.

The final regression analysis for montmorillonites was computed to give the increase in *b* when substitutions occur in $Al_2Si_4O_{10}(OH)_2$ essentially, of Al^{3+} tetrahedrally and Mg and Fe^{3+} octahedrally. The omission of Fe^{2+} points to the restricted range of montmorillonite compositions which can be included in the regression analysis, a serious disadvantage statistically. Ferrous iron occurs in insignificant proportions in montmorillonite formulae, of course; but montmorillonites high in Mg, Fe^{3+}, Mn, Zn and other larger cations equally must be excluded. For these montmorillonites the overall composition ensures that $b_{tetr} \leq b_{obs} < b_{oct}$ which is not permitted (*v.* introduction). It is, however, reasonable to suppose that vermiculites will behave in a closely similar way to montmorillonites, and several have been included to widen the range of compositions analysed for multiple regression.

The results of the regression analysis of the minerals in Table 7a (excepting volchonskoite) are given in Table 1, the relations between ionic radii and regression coefficients in Table 2, and the recommended prediction relation in Table 3. The very high value of $R^2 = 0.987$, confirms that variations in "*b*" for these data are almost completely explained by the regression of "*b*" on the ionic substitutions. The base constant, 8.944 Å is very close to 8.923 Å for kaolins and 8.925 Å for micas. Although most minerals in Table 7a are dioctahedral, both cardenite and the vermiculites are more nearly trioctahedral; it is an artifact that the relation cannot cover more trioctahedral minerals.

It is immediately obvious that the coefficient for tetrahedral Al is significant, contrary to prediction. This may be regarded in two ways

TABLE 7. A. CELL DIMENSIONS AND TETRAHEDRAL ROTATIONS FOR MONTMORILLONITES

Mineral	Reference	Composition (cations only)								b_{obs} Å	b_{calc} Å	b_{tetr} Å	b "kaolin" Å	α_{calc} °
		Al^{VI}	Fe^{2+}	Fe^{3+}	Mg	Zn		Si	Al^{IV}	Fe^{3+}					
Montmorillonites:														
Santa Rita, N.M.	Osthaus (1956)	1.460		0.059	0.487			4.00			8.993	8.996	9.051	8.989	6°30′
Belle Fourche, S.D.	Osthaus (1956)	1.550		0.213	0.232			3.804	0.196		8.993	8.994	9.101	8.969	8°49′
Merritt, B.C.	Osthaus (1956)	1.513		0.271	0.231			3.776	0.224		9.000	9.000	9.108	8.973	8°50′
Clay Spur, Wyo.	Osthaus (1956)	1.583		0.180	0.254			3.866	0.117	0.017	9.001	8.991	9.087	8.969	7°53′
Polkville, Miss.	Osthaus (1956)	1.465		0.000	0.489			4.000			9.002	8.997	9.051	8.989	5°55′
Amory, Miss.	Osthaus (1956)	1.458		0.181	0.310			3.912	0.088		9.004	8.994	9.074	8.976	7°6′
Plymouth, Utah	Osthaus (1956)	1.418		0.187	0.406			3.877	0.077	0.046	9.011	9.006	9.083	8.989	7°12′
Otay, Calif.	Osthaus (1956)	1.281		0.062	0.705			4.000			9.014	9.018	9.051	9.016	5°8′
Little Rock, Ark.	Earley *et al.* (1953)	1.507		0.307	0.201			3.799	0.201		8.996	9.000	9.102	8.985	8°46′
Chambers, Ariz.	Earley *et al.* (1953)	1.374		0.192	0.465			3.846	0.154		9.004	9.013	9.090	8.996	7°53′
Upton, Wyo.	Foster (1953)	1.55		0.20	0.25			3.90	0.10		8.997[1]	8.991	9.076	8.970	7°36′
Belle Fourche, S.D.	Foster (1953)	1.57	0.02	0.18	0.23			3.91	0.09		8.988[1]	8.989	9.074	8.971	7°54′
Lemon, Miss.	Foster (1951)	1.45	0.01	0.16	0.44			3.89	0.11		9.019[1]	9.008	9.079	8.993	6°37′
Rideout, Utah	Foster (1953)	1.55		0.06	0.39			3.97	0.03		8.994[1]	8.988	9.059	8.976	6°53′
San Antonio, Texas	Foster (1953)	1.57		0.12	0.30			3.99	0.01		8.997[1]	8.985	9.054	8.968	6°25′
Honeycomb, Utah	Sand and Regis (1960)	1.45			0.58		0.16[2]	4.00			8.979[1]	8.999	9.051	8.996	7°13′
Unter-Rupsroth	Nagelschmidt (1938)	1.77		0.03	0.20			3.74	0.26		9.00	8.976	9.117	8.950	9°12′
Black Jack, Idaho	Nagelschmidt (1938)	1.96		0.04				3.46	0.54		8.94	8.950	9.188	8.926	13°10′
Black Jack, Idaho	Weir (1960)	1.98		0.02	0.01			3.48	0.52		8.978[1]	8.966	9.183	8.926	12°0′
Nontronites:															
Manito, Wash	Kerr *et al.* (1950)	0.03		2.02	0.005			3.50	0.50		9.155[1]	9.145	9.178	9.083	4°0′
Garfield, Wash.	Kerr *et al.* (1950)	0.05		1.93	0.12			3.50	0.50		9.175[1]	9.159	9.178	9.090	0°
Nontron	Nagelschmidt (1938)	0.08		1.84	0.08			3.72	0.28		9.12	9.139	9.122	9.078	0°
Behenjy	Nagelschmidt (1938)	0.08	0.04	1.79	0.08			3.57	0.43		9.13	9.141	9.160	9.084	4°30′
Batavite	Weiss *et al.* (1955)	0.33			2.64			2.99	1.01		9.22	9.235	9.308	9.253	8°18′
Cardenite	MacEwan (1954)	0.45	0.15	0.69	1.50		0.12[3]	3.09	0.91		9.20	9.207	9.283	9.200	7°40′
Galapektite	Faust (1957)	1.56		0.11	0.39			3.88	0.12		8.988	8.996	9.080	8.980	8°10′
Vermiculite	Mathieson and Walker (1954)	0.16		0.48	2.36			2.73	1.27		9.262[1]	9.264	9.373	9.256	8°42′
Vermiculite	Walker (1961)	0.22	0.08	0.46	1.92		0.11[4]	2.72	1.28		9.222[1]	9.239	9.376	9.236	10°24′
Vermiculite	Walker (1961)	0.170	0.023	0.232	2.239			2.837	1.163		9.244[1]	9.226	9.348	9.226	8°35′
Vermiculite	Walker (1961)		0.037	0.365	2.238		0.056[4]	2.853	1.024	0.123	9.253[1]	9.247	9.312	9.250	6°27′
Volchonskoite	Weiss *et al.* (1954)	0.40		0.58	0.82		0.35[5]	3.82	0.18		8.94	9.119	9.097	9.099	

TABLE 7. B. CELL DIMENSIONS FOR SAPONITES, SAUCONITES, HECTORITES ETC.

Mineral	Reference	Composition (cations only)									b_{obs} Å	b_{calc} Å	b_{tetr} Å	b "kaolin" Å	O-Si-O angle
		Al^{VI}	Fe^{2+}	Fe^{3+}	Mg	Zn		Si	Al^{IV}	Fe^{3+}					
Saponite	Faust (1957)		0.26	0.45	2.29			3.19	0.75	0.06	9.258	9.268	9.259	9.304	109°28′
Saponite	Cahoon (1954)	0.04		0.01	2.85			3.70	0.30		9.165[1]	9.230	9.127	9.280	108°12′
Saponite	Weiss *et al.* (1955)	0.03		0.02	2.95			3.38	0.62		9.218[1]	9.253	2.209	9.293	109°28′
Saponite	Schmidt and Heystek (1953)			0.01	2.99			3.63	0.37		9.198[1]	9.246	9.145	2.298	108°31′
Saponite	Mackenzie (1957)	0.15		0.04	2.92		0.005[6]	3.495	0.505		9.178[1]	9.251	9.179	9.293	109°28′
Saponite	Midgley and Gross (1956)	0.05	0.05		2.91			3.38	0.52	0.10	9.197[1]	9.255	9.20	9.298	109°28′
Griffithite	Faust (1957)	0.04	0.52	0.44	1.88			3.19	0.81		9.246	9.264	9.256	9.312	109°28′
Sauconite	Ross (1946)	0.79		0.02	0.14	1.85		3.30	0.70		9.228[1]		9.229	9.366	109°30′
Sauconite	Ross (1946)	0.78		0.23	0.15	1.54		3.39	0.61		9.220[1]		9.206	9.313	109°14′
Sauconite	Ross (1946)	0.12		0.13	0.11	2.64		3.27	0.73		9.251[1]		9.237	9.552	109°14′
Sauconite	Ross (1946)	0.04		0.02	0.10	2.89	0.01[6]	3.35	0.65		9.247[1]		9.216	9.599	108°56′
Sauconite	Ross (1946)	0.17		0.58	0.12	1.95		3.39	0.61		9.259[1]		9.206	9.430	108°30′
Sauconite	Ross (1946)	0.22		0.17	0.18	2.40		3.47	0.53		9.252[1]		9.186	9.509	108°16′
Hectorite	Kerr *et al.* (1950)	0.008			2.71		0.34[2]	4.00			9.119[1]	9.204	9.051	9.262	108°12′
Stevensite	Faust (1957)			0.02	2.88		0.02[6]	4.00			9.136	9.221	9.051	9.290	107°30′
Talc	Stemple & Brindley (1960)				3.0			4.0			9.158	9.230	9.051	9.298	107°30′
Talc	Author				3.0			4.0			9.171[1]	9.230	9.051	9.298	107°12′
Hectorite	Nagelschmidt (1938)				2.73		0.33[2]	3.89	0.05		9.18	9.208	9.064	9.264	107°17′

[1] Original data, obtained using CoKα radiation, calibrated 19 cm diam. camera. [2]Li. [3]Ca. [4]Ti. [5]Cr. [6]Mn.

viz. (1) as real for these data, but that the data are systematically erroneous, or (2) as real for montmorillonites. As stated above, the first possibility cannot be entirely dismissed for montmorillonites; and in fact the *b*-axis formula for *kaolins* works very well for most minerals in Table 7a. It requires only small changes in certain structural formulae to make the Al_{tetr} coefficient non-significant.

The tetrahedral Al may really increase *b* for montmorillonites, however. The value of the coefficient then is very reasonable, and such an increase is not entirely incompatible with the non-significant coefficient found for Al_{tetr} for kaolins and micas. Suppose that in all the layer silicates the tetrahedral layers exert a *very* small expansive force (when $\alpha > 0$). In kaolins there is only one tetrahedral layer per octahedral layer, and in micas the interlayer cation dominates the tetrahedral twist. But in montmorillonites the small forces due to *two* tetrahedral layers per octahedral layer may just have a noticeable effect. In this case the coefficient will be small for tetrahedral Al; and in fact the observed coefficient is rather smaller than that suggested by the difference in ionic radii of Si and Al (Table 2).

The coefficients for Mg and Fe^{3+} are identical, and assuming a proportionality constant $k = 1$ for these two octahedral cations then the "hole" for Mg, 0.554, is larger than that for Fe^{3+}, 0.504, which is very close to the Al radius, 0.50. This again suggests, as for the micas, the possibility of ordering in the way in which divalent Mg and Fe^{3+} enter the octahedral sites.

If the coefficient for Al_{tetr} is real, then the base constant for montmorillonites will be slightly greater than for kaolins and micas (as observed), since montmorillonites always contain some Mg, Fe and/or Al_{tetr}.

It is worth noting that nontronites have rather smaller tetrahedral twists than montmorillonites. For vermiculite $\alpha_{obs} = 5\frac{1}{2}°$ (Mathieson and Walker, 1954) compared with $\alpha_{calc} = 8°42'$. Their paper quotes $b = 9.18$ Å, and $\sqrt{3}a = 9.23$ Å; from a 19 cm powder photograph $b = 9.262$ Å, giving $\alpha = 8°42'$. The Si-O bonds to the basal oxygens are shorter than predicted from Smith's (1954) curve, accounting for the smaller actual α.

The omission of volchonskoite raised R^2 for the regression analysis from 0.8 approx. to 0.987, confirming the doubts felt about the data for this mineral, which is very rarely pure. The value of b_{obs} seems far too low.

Table 7b gives *b*-axis data on montmorillonites for which $b_{tetr} \leq b_{obs}$. It is assumed that b_{kaolin} is close to the dimension which the octahedral layers of these minerals would have if free.

Considering the saponite data first, these clearly suggest that the $b_{obs.}$ values are determined by the dimensions of the tetrahedral layers, to which the octahedral layers contract; $b_{obs} = b_{tetr} < b_{oct}$ for four out of the

six saponites. This contrasts with the serpentines; the saponites are 2:1 minerals, compared with the 1:1 serpentines.

The tetrahedral layers of sauconites are somewhat stretched, which decreases the O-Si-O angle to about $108\frac{1}{2}°$. The octahedral layers are considerably contracted (by 0.20 to 0.25 Å) to meet the tetrahedral dimensions. Contractions in this layer will occur primarily by changes in the oxygen-cation-oxygen bond angles, and such changes will occur more easily as the radius ratio, cation/oxygen, increases. This ratio for Zn is 0.53 (*cf.* 0.46 for Mg and 0.36 for Al), so that octahedral layers of sauconites can contract further if necessary than those of, say, hectorites.

Hectorite, stevensite and talc are 2:1 minerals in which a fully siliceous tetrahedral layer is stretched to its limit by a fully magnesic octahedral layer. The O-Si-O angle is reduced to $107\frac{1}{2}°$ or slightly less. The chrysotiles, which are the 1:1 analogue, do not show a comparable octahedral contraction. The presence of only one tetrahedral layer allows the strain between octahedral and tetrahedral sheets to be relieved by curling and by adopting non-stoichiometric compositions.

Discussion

The *b*-axis formulae proposed in this paper as a result of the multiple regression analyses of kaolin, chlorite, mica and montmorillonite data separately appear to be more soundly based theoretically (see Part I) and to yield better predictions in practice than previous formulae.

There are few minerals which do not conform to the model implicit in these formulae, *viz.* (1) chrysotiles for which b_{oct} so exceeds b_{tetr} that the latter takes control; (2) celadonite, with excess octahedral layer charge; (3) dioctahedral chlorites, for which there are insufficient data to adjust the regression relations suitably; and (4) trioctahedral montmorillonites and talc, for which the tetrahedral layers again take control.

The availability of considerably more and better data in the future may alter the basis for calculating these relationships in only one major way. If many data become available on dioctahedral chlorites, then their inclusion may change the present equation to one closely similar to the kaolin relation. However, the coefficient for tetrahedral Al for montmorillonites may no longer be significant when more good data can be analysed. If so, then the prediction relations for kaolins, chlorites and montmorillonites may be sufficiently close to each other so that one relationship will serve to predict *b* axes for all these minerals. The micas, however, not only require additional terms for the interlayer cations but these cations may be indirectly affecting the coefficients for octahedral cations, so preventing the proposal of one total prediction relationship for all layer silicates.

A prediction relation for minerals for which the tetrahedral layers are

hexagonal ($\alpha=0$) can scarcely be proposed because of the variety of mechanisms involved in adjusting the layer dimensions to each other.

It is instructive to reconsider the pairs of minerals from which the coefficients have been derived for previous *b*-axis formulae.

a) Pyrophyllite-muscovite. MacEwan (1951) and Brown (1951) both considered this pair in order to arrive at a contribution for tetrahedral Al. As discussed in Part I it is equally valid to consider pyrophyllite-paragonite, which gives a zero coefficient; therefore it is not valid to deduce a coefficient for tetrahedral Al in this way.

b) Pyrophyllite-talc. MacEwan (1951) and Brown (1951) deduced a coefficient for Mg from this pair of minerals, and coefficients for other ions were then taken as proportional to the ionic radii. This is very likely to be invalid since the *b* axis of talc is determined solely by the maximum limit to which a purely Si-O tetrahedral layer can be stretched (by a decrease in the O-Si-O angles).

c) Gibbsite-brucite-$Fe(OH)_2$. Brindley and MacEwan (1953) based their coefficients on the *b* dimensions of the hydroxides. Bernal and Megaw (1935), who studied the metallic hydroxides in detail, pointed out that cations with the polarizing power of Al and higher induce hydroxyl bonding on the surface of their hydroxides, with a clear shortening effect on the *b* axis. It is therefore invalid to deduce coefficients for *b*-axis formulae by considering the pair gibbsite-brucite.

d) Si-O bond lengths. Brindley and MacEwan (1953) based their tetrahedral term on the known Si-O and Al-O bond lengths, but this has now been shown to be irrevelant to the *b* dimension.

Previous *b*-axis formulae (e.g. Brown, 1951) have omitted a term for Li because better agreement with b_{obs} is obtained by treating Li, radius 0.60 Å, as if it were Al, radius 0.50 Å. The implied reason has been that since Li is more readily polarized it may be squeezed more easily into a small site. This cannot, however, be readily settled since Li does not occur in moderate ionic proportions except in hectorite, cookeite, lepidolite and zinnwaldite. No information is obtainable from hectorite in which $b_{obs}=9.16$ Å is determined by the tetrahedral layer which is stretched to the limit. Nor can deductions be made from cookeite, which is probably comparable structurally to kaolinite and dickite. In the latter the vacant site is much bigger than the Al sites, and is sufficiently large to accommodate the Li ion, so that deductions about the Li coefficient cannot be soundly based on cookeite alone.

Similar arguments do not seem to apply to lepidolites high in Li, yet the *b* dimensions of lepidolites vary surprisingly little from 9.00 Å. This suggests that Li does not increase *b*, but it would be interesting to know the Li-O bond lengths in a lepidolite. The two zinnwaldites in Table 6 also

give good agreement between b_{obs} and b_{calc} when Li is equated to Al. White *et al.* (1960) have claimed to have inserted Li into the muscovite structure experimentally and state that this does not increase b. The vacant site is, of course, quite large enough to accept Li (0.60 Å) readily (Radoslovich, 1960).

Acknowledgments

This work follows closely on that in Part I, and detailed discussions of the results with Dr. K. Norrish have therefore been most helpful. Dr. J. Jones kindly made his biotite specimens available and discussed aspects of these data; thanks are also due to M. Foster, L. B. Sand, P. F. Kerr, G. F. Walker, H. C. Cahoon, R. C. MacKenzie and C. S. Ross for analysed specimens. The multiple regression analyses were calculated at the Division of Mathematical Statistics, C.S.I.R.O., under the direction of Mr. L. G. Veitch, without whose help this work would not have been possible.

References

Bailey, S. W. and S. A. Tyler (1960), Clay minerals associated with the Lake Superior iron ores. *Econ. Geol.*, **55,** 150.

Bannister, F. A., M. H. Hey, and W. Campbell-Smith (1955), Grovesite, the manganese-rich analogue of berthierine. *Mineral. Mag.*, **30,** 645.

——— and W. F. Whittard (1945), A magnesium chamosite from Gloucestershire: *Mineral Mag.*, **27,** 99.

Bernal, J. D. and H. D. Megaw (1935), The function of hydrogen in intermolecular forces. *Proc. Roy. Soc. London*, A, **151,** 384.

Brammall, A., J. G. C. Leech and F. A. Bannister (1937), The paragenesis of cookeite at Ogofau, Carmathenshire. *Mineral Mag.*, **24,** 507.

Brindley, G. W. (1951), The crystal structure of some chamosite minerals. *Mineral. Mag.*, **29,** 502.

——— and F. H. Gillery (1956), *X*-ray identification of chlorite species. *Am. Mineral.*, **41,** 169.

——— and O. von Knorring (1954), Orthoantigorite from Unst, Shetland Islands. *Am. Mineral.*, **39,** 794.

——— and D. M. C. MacEwan (1953), Structural aspects of the mineralogy of clays. *Brit. Ceram. Soc. Symp.*, **15.**

Brown, B. E. and S. W. Bailey (1960), Denver Meeting, *Geol. Soc. Am.*

Brown, G. (1951), *in* *X*-ray Identification and Crystal Structures of Clay Minerals. *Mineral. Soc., London.*

Cahoon, H. C. (1954), Saponite from Milford, Utah. *Am. Mineral.*, **39,** 222.

Drits, V. A. and A. A. Kashaev (1960), An *x*-ray study of a single crystal of kaolinite. *Kristallografiya*, **5,** 224.

Earley, J. W., B. Osthaus and I. H. Milne (1953), Purification and properties of montmorillonite. *Am. Mineral.*, **38,** 707.

Erdelyi, J., V. Kablenez and N. S. Varga (1959), Hydroamesite. *Acta Geol. Acad. Sci. Hung.*, **6,** 95.

Faust, G. T. (1957), The relation between lattice parameters and composition for montmorillonites. *Jour. Wash. Acad. Sci.*, **47,** 146.

FOSTER, M. D. (1951), Exchangeable magnesium in montmorillonitic clays. *Am. Mineral.*, **36,** 717.

——— (1953), Relation between ionic substitution and swelling in montmorillonites. *Am. Mineral.*, **38,** 994.

GILLERY, F. H. (1959), The *x*-ray study of synthetic Mg-Al serpentines and chlorites. *Am. Mineral.*, **44,** 143.

GOSSNER, B. (1935), Cronstedite. *Strukt. Ber.*, **3,** 556.

GRUNER, J. W. (1936), The structure and chemical composition of greenalite. *Am. Mineral.*, **21,** 449.

——— (1944), The composition and structure of minnesotaite. *Am. Mineral.*, **29,** 363.

HENDRICKS, S. B. (1939), Random structures of layer minerals—cronstedite (2 FeO Fe_2O_3 $\cdot SiO_2 \cdot 2H_2O$). *Am. Mineral.*, **24,** 529.

HEY, M. H. (1954), A new review of the chlorites. *Mineral. Mag.*, **30,** 277.

KERR, P. F. *et al.* (1950), Analytical data on reference clay materials. *Am. Petrol. Inst.* Project 49, Rept. **7.**

KELLEY, W. P. (1945), Calculating formulae for fine grained minerals on the basis of chemical analyses. *Am. Mineral.*, **30,** 1.

LAPHAM, D. M. (1958), Structural and chemical variation in chrome chlorites. *Am. Mineral.*, **43,** 921.

MACEWAN, D. M. C. (1951), *in* *X*-ray Identification and Crystal Structures of Clay Minerals. *Mineral. Soc.*, London.

——— (1954), "Cardenite," a trioctahedral montmorillonite derived from biotite. *Clay Mineral. Bull.*, **2,** 120.

MACKENZIE, R. C. (1957), Saponite from Allt. Ribhein, Fiskavaig Bay, Skye. *Mineral. Mag.*, **31,** 672.

MCMURCHY, R. C. (1934), The crystal structure of the chlorite minerals. *Zeit. Krist.*, **88,** 420.

MATHIESON, A. MCL. AND G. F. WALKER (1954), Crystal structure of Mg-vermiculite. *Am. Mineral.*, **39,** 231.

MIDGLEY, H. G. AND K. A. GROSS (1956), Thermal reactions of smectites. *Clay Mineral. Bull.*, **3,** 79.

NAGELSCHMIDT, G. (1938), On the atomic arrangement and variability of the members of the montmorillonite group. *Mineral. Mag.*, **25,** 140.

NELSON, B. W. AND R. ROY (1954), New data on the composition and identification of the chlorites. *Second Nat. Clay Conf. Proc.*, 335.

NEWNHAM, R. E. (1961), A refinement of the dickite structure. *Mineral. Mag.*, **32,** 683.

NORRISH, K. (1952), The crystal structure of cookeite. Part of Ph.D. thesis, Univ. London.

OSTHAUS, B. (1956), Kinetic studies on montmorillonites by acid-dissolution. *Fourth Nat. Clay Conf. Proc.*, 301.

RADOSLOVICH, E. W. (1960), The structure of muscovite, $KAl_2(Si_3Al)O_{10}(OH)_2$. *Acta Cryst.*, **13,** 919.

——— AND NORRISH, K. (1962), The cell dimensions of layer-lattice silicates. I. Some structural considerations. *Am. Mineral.*, **47,** 599–616.

ROSS, C. S. (1946), Sauconite—a clay mineral of the montmorillonite group. *Am. Mineral.*, **31,** 411.

SAND, L. B. AND A. J. REGIS (1960), *Bull. Geol. Soc. Am.* (abs.), **71,** 1965.

SCHMIDT, E. R. AND H. HEYSTEK (1953), A saponite from Krugersdorp district, Transvaal. *Mineral. Mag.*, **30,** 201.

STEINFINK, H. (1958), The crystal structure of prochlorite. *Acta Cryst.*, **11,** 191.

——— (1958a), The crystal structure of corundophillite. *Acta Cryst.*, **11,** 195.

——— AND G. BRUNTON (1956), The crystal structure of amesite. *Acta Cryst.*, **9**, 487.

STEMPLE, I. S. AND G. W. BRINDLEY (1960), A structural study of talc and talc-tremolite relations. *Jour. Amer. Ceram. Soc.*, **43**, 34.

WALKER, G. F. (1961), *Priv. comm.*

WEIR, A. (1960), Beidellite. *Priv. comm.*

WEISS, VON A., G. KOCH AND U. HOFFMANN (1954), Zur Kenntnis von Wolchonskoit. *Sond. Ber. Deut. Ker. Ges.*, **31**, 301.

——— 1955), Zur Kenntnis von Saponit. *Sond. Ber. Deut. Ker. Ges.*, **32**, 12.

WHITE, J. L., G. W. BAILEY, C. B. BROWN AND J. L. ALRICHS (1960), Infra-red investigation of the migration of lithium ions into empty octahedral sites in muscovite and montmorillonite. *Nature*, **190**, 342.

WOLF, E. VON (1942), Die Strukturen von Thuringit, Bavalit und Chamosit und ihre Stellung in der Chloritgruppe. *Zeit. Krist.*, **104**, 142.

ZUSSMAN, J., G. W. BRINDLEY AND J. J. COMER (1957), Electron diffraction studies of serpentine minerals. *Am. Mineral.*, **42**, 133.

ZVIAGIN, B. B. (1960), Electron diffraction determination of the structure of kaolinite. *Kristallografiya*, **5**, 40.

Manuscript received, August 14, 1961.

THE CELL DIMENSIONS AND SYMMETRY OF LAYER-LATTICE SILICATES. III. OCTAHEDRAL ORDERING

BY

L. G. VEITCH AND E. W. RADOSLOVICH

Commonwealth of Australia
COMMONWEALTH SCIENTIFIC AND INDUSTRIAL RESEARCH ORGANIZATION

Reprinted from American Mineralogist, **48**:
Pages 62-75
(1963)

THE AMERICAN MINERALOGIST, VOL. 48, JANUARY–FEBRUARY, 1963

THE CELL DIMENSIONS AND SYMMETRY OF LAYER-LATTICE SILICATES. III. OCTAHEDRAL ORDERING

L. G. Veitch and E. W. Radoslovich, *Division of Mathematical Statistics and Division of Soils, Commonwealth Scientific and Industrial Research Organization, Adelaide, Australia.*

Abstract

The 3n octahedral sites in the unit cells of the layer silicates are accepted as being topologically distinct from each other, and the octahedral cations are known to be largely ordered for several published structures. The present study sought to determine quantitatively any differences between divalent and trivalent octahedral sites, by a suitable form of regression analysis of dimensional and composition data; and with this there is the implication of widespread ordering. Certain difficulties inherent in this statistical analysis of clay mineral data have thereby become obvious. Moreover the initial results made it essential to reconsider the model by which regression coefficients commonly have been related to ionic radii in unit cell formulae.

It has been necessary to abandon the simplest geometrical model (which assumes that the octahedra remain essentially regular) for one in which the expansion due to the subsitution of larger ions is several-fold greater in the direction normal to the layers than it is in the a–b plane. The new regression analyses confirm the results of the previous study and lead to simpler prediction relations for unit cell dimensions.

The new geometrical model is readily justified physically by considering several structures already accurately determined.

Introduction

Layer silicates are classified as trioctahedral or dioctahedral according to whether nearly all, or only two-thirds of the possible sites for cations in the octahedral layer are occupied. The unit cell of such a mineral may contain 6n (n = integer) sites per unit cell, but the overall symmetry generally reduces the number of octahedral sites in the asymmetric unit to three. Of these, two sites are generally symmetry-related or at least topologically equivalent, and the third site is distinct. For example, in $2M_1$ muscovite (Radoslovich, 1960) the two octahedral aluminum cations (hereafter Al^{VI}) are in symmetry-related sites, whereas the larger and vacant third site is a center of symmetry for the structure as a whole.

As the layer structures have become increasingly well understood the evidence has grown that ordering of the octahedral cations according to valency and radius may be widespread, and fairly complete in many minerals. Evidence for such ordering is in general only circumstantial, but the structural analysis of several layer silicates has already shown that ordering exists, at least in those minerals—for example celadonite (Zviagin, 1957), prochlorite (Steinfink, 1958), xanthophyllite (Takéuchi

and Sadanaga, 1959), muscovite (Radoslovich, 1960), kaolinite (Drits and Kashaev, 1960) and dickite (Newnham, 1961).

The general hypothesis, however, seemed worthwhile testing statistically over a wide range of minerals if possible, without determining each structure in detail. As the simplest initial hypothesis it is supposed that there are two kinds of octahedral sites, A and B, such that A is smaller than B, and that there are either two A sites and one B site, or vice versa, for each three octahedral sites. It is further supposed that the trivalent (and quadrivalent) cations tend to occupy A sites and the divalent (and monovalent) cations tend to be in the B sites. This is obviously an approximation to the actual structural characteristics of these minerals. For example, the two small (A) sites in dioctahedral minerals may differ from the single small site in the trioctahedral minerals. Furthermore, some trioctahedral minerals *cannot* obey this model strictly, *e.g.* phlogopites. If such minerals nevertheless are assumed to have (2B+1A) sites then the excess of *divalent* cations (over 2.00) must occupy a "wrong" A site. For the purposes of this statistical analysis the excess of divalent cations is "transferred" to the trivalent group, smallest cations first.

Our previous study of the variation of sheet dimensions with composition (Radoslovich, 1962; hereafter Part II) suggested the possibility of establishing (by suitable statistical methods) whether there are two different kinds of octahedral sites into which cations substitute. Of the four major mineral groups the micas are the most amenable to analysis of this kind. The chlorites cannot be studied this way because there are two octahedral layers in the stacking unit, and ordering may also occur *between* these. The montmorillonites are difficult to study, not only because of uncertainties in the structural formulae (Part II), but also because of unsuspected complexities in these structures (Cowley and Goswani, 1961). Furthermore, most of the trioctahedral montmorillonites must be excluded because they follow a different model (Part II). This severely restricts the range of values for the *b*-axis and ionic proportions, increasing the difficulties statistically. The available data in the literature for the kaolin minerals are likewise restricted. In addition some of the more reliable data (Part II) have been obtained from synthetic or heated specimens, and there is some doubt whether these can have reached an equilibrium state of ordering in laboratory times. The importance of some of these restrictions only became apparent as the analysis proceeded.

A further major difficulty—with implications beyond the present study—has become increasingly obvious. For any expression connecting sheet dimensions and ionic proportions (*e.g.* Part II) each coefficient should be related to the appropriate ionic radius by a factor depending explicitly on

the geometry of the structures. Brindley and MacEwan (1953), and Brown (1951), implied this in stating that "very similar results (to the empirical coefficients) are obtained if the argument is based on ionic radii." The form of regression analysis used (see below) may not only test for two significantly different "hole sizes" but yield estimates of the geometrical factor. The values obtained for this factor should agree, within their fiducial limits, with the theoretical value for the model used.

In the simplest model for the octahedral layers of these minerals the octahedra are assumed on the average to remain geometrically regular in shape. The anions may only be in mutual contact when the cation is sufficiently small; when larger cations are substituted the anions move apart, but the bond angles for a regular octahedron are preserved. Under these conditions the increase in b for an increase in cation radius from r_i to r_j is

$$\delta b = \sqrt{2}\,(r_j - r_i)x_j \qquad 1.1$$

where x_j = ionic proportions, of j^{th} atoms, in three sites—*i.e.* as expressed in most structural formulae (*e.g.* Part II). The relation between the regression coefficients, b_j and the ionic radii, r_j is, therefore,

$$b_j = \sqrt{2}\,(r_j - r_i) \qquad 1.2$$

and the predicted geometrical factor is $g = \sqrt{2}$, where (for convenience in writing) g is the inverse of the constant k as discussed in Part II, and the a_i in that paper have been re-named b_j.

Even in the preliminary calculations the statistical value of this factor was considerably less than $\sqrt{2}$. As the analysis was refined it became clear that the value statistically is close to half this figure. This required the formulation of the more general *geometrical* model—*i.e.* with less severe restraints—which is developed below. The new choice of restraints is then justified by some simple physical arguments from known structures and the statistical analysis follows.

The development of a satisfactory geometrical model, and the physical justification of this in general terms, has led to a detailed re-examination of the interatomic forces in layer silicates. These are to be discussed in Part IV, in which it is shown that the earlier hypotheses (Parts I and II) and the present model of the octahedral layers follow as reasonable consequences of the total balance of interatomic forces in these minerals.

New Geometrical Model for the Octahedral Layers

Restraints

The preservation of completely regular octahedra has been abandoned in favor of the following set of restraints:

(1) centers of octahedral cations lie in a plane,
(2) there are two A sites for each B site,[1]
(3) centers of anions lie in two planes parallel to the cation plane, and distant t/2 above and below it,
(4) anions are constrained to remain on the surfaces of spheres about the cations as centers,
(5) the radius of such a sphere is the accepted cation-anion bondlength, *i.e.*, either l_A or l_B,
(6) the network of cation sites is hexagonal.

As a corollary of these restraints it follows that only two kinds of cations (*i.e.* for A and for B sites) may be accepted by an ideal structure. In actual structures both A and B sites accept cations of several different radii; the most probable compromise is in condition (3).

When substitutions of various cations occur in A and B sites the bondlengths change by amounts of dl_A and dl_B respectively, and the thickness t by dt. It is then assumed that:

(7) $dt = \lambda db$ where λ is some proportionality "constant."

This is simply for descriptive convenience, and λ is only a "constant" in the sense of having some average value over many minerals. Assumption (7) implies that these layers may become thicker at some rate disproportionate to their increase in sheet dimensions.

Calculation of the b-axis of unit cell (b_U)

From (6) the *b*-axis is three times any cation-cation distance. From (2), (3) and (6) the cation-anion bondlengths must have a common value, l_A, for both A sites. If such an octahedral layer is projected on to a plane through the cations (Fig. 1) then the common value for l_A means that the anions around B have, in projection, hexagonal symmetry and hence BCD is an equilateral triangle (Fig. 1). [The upper equilateral triad of anions around an A site is, however, rotated relative to the corresponding lower equilateral triad.] From (5) the spheres around A and B sites have radii l_A and l_B; let the same spheres cut the anion planes in circles of radii ρ_A and ρ_B respectively. Then it follows that

$$\rho_A = \left(l_A^2 - \frac{t^2}{4}\right)^{1/2} = AC: \qquad \rho_B = \left(l_B^2 - \frac{t^2}{4}\right)^{1/2} = BC$$

$$AB = \left(\rho_A^2 - \frac{\rho_B^2}{4}\right)^{1/2} + \left(\rho_B^2 - \frac{\rho_B^2}{4}\right)^{1/2}$$

whence the *b*-axis dimension becomes

$$b_U = \frac{3}{2}\left[4l_A^2 - l_B^2 - \frac{3t^2}{4}\right]^{1/2} + \frac{3\sqrt{3}}{2}\left[l_B^2 - \frac{t^2}{4}\right]^{1/2}. \qquad 2.1$$

[1] All subsequent formulae hold good by interchanging A and B for the cases where the ratio is 2B sites for each A site.

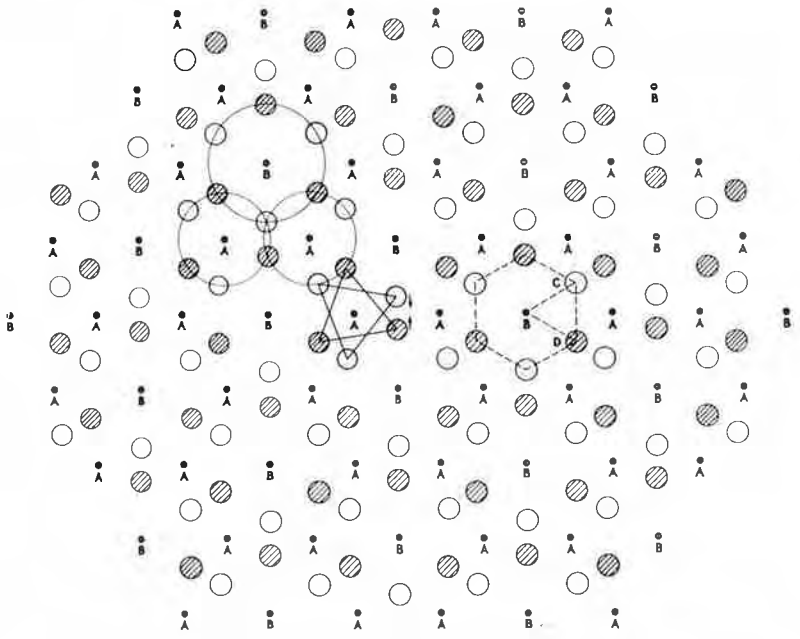

FIG. 1. Schematic drawing of a geometrically ideal octahedral layer, showing two small A sites for each large B site. Note triads of oxygens above (unshaded) and below (shaded) cations. These triads are counter-rotated about any A site, but have hexagonal symmetry, in projection, about any B site. Cations A and B are also on a hexagonal grid in this model.

Average values for muscovite (Radoslovich, 1960) are $1_A = 1.95_4$, $1_B = 2.20$, $t = 2.12$ from which $b_{calc} = 8.99_6$ compared with $b_{obs.} = 8.99_8$ Å. The agreement is fortuitously close, since not all the conditions (1) to (7) are fulfilled precisely; nevertheless equation 2.1 seems to be a very good approximation for real octahedral layers.

Variations in b_U as l_A, l_B and t vary

Totally differentiating equation 2.1 with respect to 1_A, 1_B and t gives

$$db_U = 6l_A\left(4l_A^2 - l_B^2 - \frac{3t^2}{4}\right)^{-1/2} dl_A + \frac{3\sqrt{3}}{2} l_B\left[\left(l_B^2 - \frac{t^2}{4}\right)^{-1/2} - \frac{1}{\sqrt{3}}\left(4l_A^2 - l_B^2 - \frac{3t^2}{4}\right)^{-1/2}\right] dl_B - \frac{3\sqrt{3}}{8} t\left[\sqrt{3}\left(4l_A^2 - l_B^2 - \frac{3t^2}{4}\right)^{-1/2} + \left(l_B^2 - \frac{t^2}{4}\right)^{-1/2}\right] dt. \qquad 2.2$$

The earlier model, in which the octahedra remain regular, has the special conditions that

$$dt = \frac{\sqrt{2}\, db}{3\sqrt{3}};\ 1_A = 1_B = 1;\ \text{and}\ t = 21/\sqrt{3}.$$

Substitution in equation 2.2 gives

$$db_U = \sqrt{2}\,(2dl_A + dl_B)$$

or, assuming that the anion radius is constant,

$$db_U = \sqrt{2}\,(dr_A + dr_B)$$

for the three octahedra in an asymmetric unit. Taking the average, as required by the definition of the x_j, gives

$$db = \sqrt{2} \sum dr_j x_j \qquad 2.3$$

which is, in fact, equation 1.1.

Dioctahedral micas

Substituting muscovite data in equation 2.2,

$$db_U = 4.422dl_A + 1.718dl_B - 1.616dt$$

and if condition (7) is obeyed then

$$db_U = (0.4523 + 0.7309\lambda)^{-1}2dl_A + (0.5821 + 0.9406\lambda)^{-1}dl_B \qquad 2.4$$

Trioctahedral micas

No accurate determinations of t are yet published, but trioctahedral micas may reasonably be assumed to have regular octahedra initially, if cell dimensions are considered in relation to ionic radii. That is,

$$db_U = \frac{3}{\sqrt{2}}(2dl_B + dl_A) - \frac{3\sqrt{3}}{2\sqrt{2}}dt$$

or

$$db_U = (0.4714 + 0.8661\lambda)^{-1}(2dl_B + dl_A) \qquad 2.5$$

Relation between geometrical constant g and λ

Consider the dependence of the separate geometrical constants on λ for the two extreme cases immediately above. From the calculated factors in Table 1 it is clear that, provided λ remains the same for the total suite of micas, the geometrical factor g does not vary seriously between A and B sites or between di- and trioctahedral minerals. This produces a considerable simplification in the model for statistical analysis.

Physical Plausibility of New Geometrical Model

It is sufficient, for a valid discussion of the present statistical analysis, to show that the geometrical model now adopted is readily acceptable physically. In the following paper the interatomic forces are considered in more detail; and again the conclusions support this model. Of the seven restraints listed previously, several may be regarded as axiomatic, viz. (1), (3), (4), (5), and these are seen to be quite closely obeyed by structures already accurately determined. The second restraint, (2), is in fact

TABLE 1. SEPARATE GEOMETRICAL FACTORS[1] AT A AND B SITES IN MICAS, CALCULATED FOR A RANGE OF VALUES OF λ

λ	Dioctahedral		Trioctahedral	
	A sites	B sites	A sites	B sites
0.2	1.671[1]	1.298[1]	1.551[1]	1.551[1]
0.4	1.343	1.043	1.223	1.223
0.6	1.123	0.872	1.009	1.009
0.8	0.964	0.749	0.859	0.859
1.0	0.845	0.657	0.748	0.748
1.2	0.752	0.585	0.662	0.662
1.4	0.678	0.527	0.594	0.594

[1] The factors in columns 2–5 correspond to the coefficients of $2d1_A$, $d1_B$, $2d1_B$ and $d1_A$ in equations 2.4 and 2.5.

the postulated characteristic which the statistical analysis was designed to test.

Implicit in restraints (1) to (6), taken together, is the requirement that if there *are* two kinds of sites (as in (2)) then they are in an ordered arrangement. It is emphasized again that this analysis tests for different hole sizes only; but in so far as this geometrical model appears to conform to real structures (*e.g.* in leading to geometrical factors consistent with experimental data) it lends support to the hypothesis of ordering. The restraint (6) is, in any case, fairly closely followed by known structures. It is a highly probable consequence of the controlling forces in the layer silicates. Again, the counter-rotation of triads around A sites—deduced as a consequence of (2), (3) and (6)—is observed experimentally; for example, in kaolinite (Drits and Kashaev, 1960) the upper and lower triads around Al sites rotate $+6\frac{1}{2}°$ and $-4°$ respectively.

The final restraint (7) needs rather more discussion. The concept of octahedral layers varying in thickness according to externally applied constraints is not entirely new (*e.g.* Bradley, 1957). The writers, however, are not aware of any attempt to calculate an average rate by which the thickness varies with sheet dimensions, over a wide range of minerals, using valid statistical methods.

A simple comparison of observed sheet dimensions with those calculated on the assumption of three equal and regular octahedral sites (Table 2) shows the necessity for some moderately large factor, λ. Taking the micas particularly, case 3 shows that many Fe^{2+} biotites may have approximately *regular* octahedral layers. For these $b_{obs.} \approx 9.3$ Å, and the radius of Fe^{2+} (0.75 Å) is not too different from 0.79 Å. There are no data yet available for t, but their octahedral layers must be considerably thicker than that of muscovite (2.12 Å), since the *total* layer thickness is

TABLE 2. OCTAHEDRAL DIMENSIONS[1] FOR VARIOUS IONIC RADII, r_i

	Case 1	Case 2	Case 3
r_i in Å	0.58	0.70	0.79
t in Å	2.29	2.42	2.53
b in Å	8.4	8.91	9.3

1 Assuming regular, and equal, octahedra; and that the anion radius is constant at 1.40 Å (Ahrens, 1952).

very similar (d(001) = 10.0 Å for each) yet muscovite alone should have (Part I) a large interlayer separation ($\approx$0.6 Å). An observed t $\approx$ 2.53 Å would, therefore, be expected.

The dioctahedral micas have sheet dimensions comparable with case 2, yet the radius of the cations is nearer 0.50 than 0.70, and the thickness will typically be about 2.1 Å (muscovite 2.12 Å) rather than 2.42 Å. For the micas, then, we may predict that b increases from 8.9 to 9.3 as t goes from 2.1 to 2.5, *i.e.* if $dt = \lambda d\mathit{b}$ then $\lambda \approx 1.0$. Since $\mathit{b} \approx 4.5t$ this means that the percentage increase in thickness is, on the average, more than four times the percentage increase in sheet dimensions. This is confirmed by the analysis which follows.

Less definite information is available for the kaolins and montmorillonites, but for both groups it is known that 8.9 and 9.3 are the lower and upper limits to b, and that for the former dimension r_i is much less than 0.7 and for the latter r_i is near 0.79. Moreover dickite has a thickness t = 2.06 Å, *i.e.* much less than 2.42 Å. Gibbsite, $Al(OH)_3$ (Megaw, 1934) is much thinner (2.12 Å) than an array of regular octahedra with the same b(= 8.64 Å).

Case 1 shows that oxygens of radius 1.40 Å can be close packed (*i.e.*, 0–0 distances = 2.80 Å) to form regularly-shaped octahedral layers with interstices easily large enough (0.58 Å) to accommodate Al ions (0.50 Å). In three aluminum-bearing minerals *average* 0–0 distances in the planes of the sheets are 2.93 Å (gibbsite), 2.997 Å (dickite) and 2.99$_4$ Å (muscovite).

It is concluded that for the micas, kaolins and montmorillonites at least, the dioctahedral layers are noticeably stretched and thin, but that the corresponding trioctahedral layers are more nearly regular. That is, restraint (7) appears acceptable physically.

STATISTICAL ANALYSIS FOR TWO DISTINCT KINDS OF OCTAHEDRAL SITES

The regression coefficients of Part II are expressed as

$$b_j = g_i(r_j - r_i) \qquad 4.1$$

where

r_i = characteristic radius of the ith site
g_i = geometrical factor for the ith site (= 1/k in Part II)
r_j = radius of the cation substituting in that site
b_j = corresponding regression coefficient (= a_i in Part II).

The subscript i, which typically refers to octahedral sites, may if necessary refer to interlayer and tetrahedral sites. The average sheet dimensions which are given by

$$b = b_0 + \sum_{j=1}^{p} b_j x_j \qquad 4.2$$

for an average proportion x_j substituting in ith sites, then becomes

$$b = b_0 + \sum_i \left[g_i \sum_{j=1}^{p_i} r_j x_j - g_i r_i \sum_{j=1}^{p_i} x_j \right] \qquad 4.3$$

where p_i = number of different cations substituting in the ith site.

$$\text{Denote } \sum_{j=1}^{p_i} r_j x_j \text{ by } u_{1i} \quad \text{and} \quad \sum_{j=1}^{p_i} x_j \text{ by } u_{2i}.$$

Then the regression coefficient of u_{1i} estimates the geometrical factor g_i at the ith site, and the regression coefficient of u_{2i} estimates $(-g_i r_i)$ from which the characteristic radius r_i is obtained.
Let

i = 1 for interlayer sites
i = 2 for larger octahedral sites (B), occupied by R^{2+}.
i = 3 for smaller octahedral sites (A), occupied by R^{3+},
i = 4 for tetrahedral sites.

The first geometrical model and physical considerations (Part II) led us to expect that $g_1 = 1.5$, $g_2 = g_3 = \sqrt{2}$, $g_4 = 0$ except for the montmorillonites possibly, $r_1 = 0.95$ Å, $r_2 > r_3$, $r_2 = 0.65$ Å, $r_3 = 0.50$ Å, and $r_4 = 0.41 \times 0.88 = 0.36$ Å. The actual results contradicted some of these expectations so strongly that the model based on effectively regular octahedra has been discarded.

In the following analyses an excess over 2.00 of x_j at B sites has been arbitrarily transferred to A sites. This may introduce errors into the u variates which would cause the regression coefficients to bias towards zero. If, however, g_2 is made equal to g_3 the appropriate variate to be used for estimating a common g_0 is $(u_{12} + u_{13})$, which is independent of such transfers.

Mica minerals

A set of 39 micas was used initially, which involved 12 different cat-

ions. Since a preliminary analysis had indicated that g_2 was not significantly different from g_3 the restriction was imposed of a common $g = g_0$ at both kinds of octahedral sites. The appropriate variates are given in Table 3, in which u_4 owes its form to the fact that in the structural formulae $(x_{Al^{IV}} + x_{Si}) = 4$ always, so that there is effectively only one variate and this depends on the difference $r_{Al} - r_{Si} = 0.09$ Å. The ex-

TABLE 3. FORMS OF VARIATES USED FOR DIFFERENT CALCULATIONS

1. *Set of 39 micas*

$u_{11} = 1.33x_K + 0.95x_{Na} + 0.99x_{Ca}$

$u_1 = (u_{12} + u_{13}) = 0.75x_{Fe^{2+}} + 0.65x_{Mg} + 0.60x_{Li} + 0.80x_{Mn} + 0.68x_{Ti} + 0.50x_{Al} + 0.65x_{\hat{M}g}$

$u_4 = 0.09x_{Al^{IV}}$

$u_{21} = x_K + x_{Na} + x_{Ca}$

$u_{22} = x_{Fe^{2+}} + x_{Mg} + x_{Li} + x_{Mn}$

$u_{23} = x_{Fe^{3+}} + x_{Ti} + x_{Al} + x_{\hat{M}g}$

2. *Set of 15 kaolin and serpentine minerals*

$u_{12} = 0.08x_{Mn} + 0.65x_{Mg} + 0.75x_{Fe^{2+}} + 0.60x_{F\hat{e}^{3+}}$

$u_{13} = 0.50x_{Al} + 0.60x_{F\hat{e}^{3+}} + 0.65x_{\hat{M}g} + 0.75x_{F\hat{e}^{3+}}$

$u_1 = u_{12} + u_{13}$

$u_{22} = x_{Mn} + x_{Mg} + x_{Fe^{2+}} + x_{Fe^{3+}}$

$u_{23} = x_{Al} + x_{Fe^{3+}} + x_{M\hat{g}} + x_{F\hat{e}^{2+}}$

3. *Set of 28 montmorillonite minerals*

$u_1 = 0.75x_{Fe^{2+}} + 0.65x_{Mg} + 0.60x_{Li} + 0.60x_{Fe^{3+}} + 0.68x_{Ti} + 0.50x_{Al} + 0.65x_{M\hat{g}}$

$u_4 = 0.09x_{Al^{IV}}$

$u_{22} = x_{Fe^{2+}} + x_{Mg} + x_{Li}$

$u_{23} = x_{Fe^{3+}} + x_{Ti} + x_{Al} + x_{M\hat{g}}$

The accent $\hat{T}$ refers to proportions of various cations which have been transferred as discussed in the Introduction.

pected non-significance of u_4 (Parts I and II) was confirmed and this variate then omitted in obtaining the final regression relation (Table 4).

The least squares estimates of r_2 and r_3 are 0.62 Å and 0.54 Å respectively. Although these values are encouragingly close to the predicted "hole sizes," and also the value for $g_0 = 0.811$ corresponds to $\lambda \approx 1.0$ and seems reasonable, they are nevertheless suspect because the other values, *viz.* $g_1 = 0.285$, $r_1 = 1.48$ Å contrast strongly with expected values, indicating the possibility that the interlayer cations in such a set of micas behave heterogeneously (Parts I and II). Hence a subset of 23 trioctahedral micas was studied. For these the interlayer cation should have little effect, or at least behave homogeneously. The results (Table 4) show that the interlayer cations do not affect the *b*-axis; this confirms the earlier hypotheses (Parts I and II) and proves the heterogeneity of the first set of 39 micas. However, a new difficulty arises because the

TABLE 4. REGRESSION RELATIONS AND CORRESPONDING ANALYSES OF VARIANCE

1. *Set of 39 micas*

$$b = 9.114 + 0.2849(\pm 0.03789)u_{11} + 0.8106(\pm 0.0493)u_1 - 0.4207(\pm 0.06405)u_{21} - 0.5003(\pm 0.04315)u_{22} - 0.4402(\pm 0.04385)u_{23}$$

Variation	D.F.	S.S.	M.S.	V.R.	R^2
due to regression	5	0.594167	0.118833	231.64	0.9723
due to residuals	33	0.016945	0.000513		
Total	38	0.611112			

2. *Subset of 23 trioctahedral micas*

$$b = 8.927 - 0.2017(\pm 0.1596)u_{11} + 0.7034(\pm 0.08393)u_1 + 0.1128(\pm 0.2163)u_{21} - 0.2603(\pm 0.3739)u_{22} - 0.4221(\pm 0.05583)u_{23}$$

2.1 *Prediction relation, from subset of 23 trioctahedral micas*

$$b = 8.244 + 0.7071(\pm 0.08728)u_1 - 0.4116(\pm 0.05716)u_{23}$$

Variation	D.F.	S.S.	M.S.	V.R.	R^2
due to regression	2	0.0212019	0.0106009	32.88	0.7668
due to residuals	20	0.0064487	0.0003224		
Total	22	0.0276506			

3. *Set of 15 kaolin and serpentine minerals*

$$b = 9.012 + 0.9197(\pm 0.05335)u_1 - 0.4892(\pm 0.04176)u_{22} - 0.5042(\pm 0.03875)u_{23}$$

Variation	D.F.	S.S.	M.S.	V.R.	R^2
due to regression	3	0.839569	0.279856	874.55	0.9958
due to residuals	11	0.003521	0.000320		
Total	14	0.843090			

4. *Set of 28 montmorillonite and vermiculite minerals*

$$b = 9.114 + 0.8375(\pm 0.07761)u_1 + 0.6664(\pm 0.1548)u_4 - 0.5170(\pm 0.06439)u_{22} - 0.5068(\pm 0.06213)u_{23}$$

Variation	D.F.	S.S.	M.S.	V.R.	R^2
due to regression	4	0.336929	0.084232	427.57	0.9867
due to residuals	23	0.004528	0.000197		
Total	27	0.341457			

[1] In table 4 the number of asterisks refers to the statistical significance (3, 2 and 1 refer to 0.1%, 1% and 5% levels respectively, N.S. = not significant at 5%). The numbers in brackets are the standard errors of the regression coefficients. D.F. = degrees of freedom, S.S. = sums of squares, M.S. = mean square, V.R. = Variance ratio F, R^2 = square of multiple correlation coefficient (Part II).

variate u_{22} has a very nearly constant value of 2.0 in such a set, so that it is not possible to estimate r_2 (*i.e.* r_B). The estimation of r_2 requires a suitable set of dioctahedral micas which unfortunately is not available.

The best relation to use for predicting *b*-axes for trioctahedral micas is also given in Table 4. This result, with an s^2 (=mean square due to residuals) of 0.00032, is appreciably better than for the analysis of 45 micas in Part II, in which $s^2=0.00091$. The improvement reflects the choice of a more homogeneous set of micas. The value for $k_0=0.707$ is highly significantly different from the earlier prediction that $g_0=\sqrt{2}$. The least squares estimate of $r_3=0.58$ Å is somewhat higher than expected. The low $b=8.244$ is due to the fact that the variation in u_{22} does produce a real physical effect, but its value is virtually fixed at 2.0 by the choice of data. [For example, putting the value of -0.5003 for the regression coefficient of u_{22} (*i.e.*, from set of 39 micas) changes *b* to 9.244.]

It has not been possible to select a homogeneous set of micas which will give satisfactory estimates of both r_2 and r_3 or even of r_2 above. Hence it cannot be shown statistically whether r_2 is significantly different from r_3.

Kaolin and serpentine minerals

The variates (Table 3) and regression relations (Table 4) refer to a set of 15 minerals selected from Part II. Since g_2 and g_3 were shown not to differ significantly a common g_0 was estimated by combining u_{12} and u_{13}; at $g_0=0.92$ it is highly significantly different from $\sqrt{2}$. The least squares estimates of r_2 and r_3 are 0.53 Å and 0.54 Å, so that ordering is not proven. The possibility of heterogeneous behavior cannot be excluded, but no satisfactory subset could be chosen.

A subset of 11 minerals in Part II (Mg, Fe^{2+} and Fe^{3+} substituting for Al) gave a value for s^2 of 0.000271, slightly better than 0.000320 obtained here.

Montmorillonite minerals

The choice of minerals is severely restricted (see Introduction) leading to a very high correlation between u_{12} and u_{13}; the reasonable restriction, as in 3.3 and 3.4, that $g_2=g_3=g_0$ (*i.e.* $u_1=u_{12}+u_{13}$, Table 3) overcame this difficulty. The results (Table 4) confirm the significant contribution of Al^{IV}, shown in Part II. Again $g_0(=0.84)$ is much less than $\sqrt{2}$, and the least squares estimates of r_2 and r_3, *viz.* 0.62 Å and 0.61 Å, are inconclusive. The value of $s^2=0.000197$ is slightly higher than 0.000153 obtained in Part II.

Discussion

The results over the three sets of minerals indicate that for studies of this kind the problem of obtaining statistically adequate sets of data which behave in a homogeneous manner within a set has considerable difficulties. In addition the montmorillonite data suffered from very high correlation between determining variates which gives results unduly sensitive to small sampling differences; and the mica subset did not have an adequate range of variation in the determining variates.

Only in the kaolin data was it possible to show that g_2 was not significantly different from g_3, and there still remains some doubt about the physical homogeneity of a set containing heated and synthetic minerals.

Statistically the *strong* results of the analysis are to show that:

(1) g_0 is about 0.8 for the three sets, highly different from $\sqrt{2}$,

(2) the regression coefficients of the octahedral cations can be usefully and simply approximated to

$$b_j = 0.8(r_j - C)$$

where C = 0.55 to 0.60.

Although the values of g_0 do not differ *significantly* from each other for the micas, kaolins and montmorillonites,[1] their differences are self-consistent with the regression coefficients in Part II. The b-axes of the Al-dioctahedral minerals (*e.g.*, paragonite, kaolinite and Al mont-

Table 5. Regression Coefficients in Relation to Geometrical Constants

	g	Mg[1]	Fe^{2+}	Fe^{3+}
Kaolins	0.92	0.125	0.229	0.079
Montmorillonites	0.84	0.096	—	0.096
Micas	0.811	0.062	0.116	0.096

[1] These values for the regression coefficients are taken from Table 1, Part II.

morillonite) are all close to 8.92. The largest individual regression coefficients b_j should, therefore, be found for the mineral group in which the sheet thickness increases least rapidly, *i.e.* λ is smallest, or g is greatest. The regression coefficients for Mg, Fe^{2+} and Fe^{3+} (taken from Part II) are given in Table 5. The coefficients for Mg and Fe^{2+} are consistent with the relative size of g for these three groups. The coefficient for Fe^{3+} for the kaolins is anomalously low. This coefficient depends entirely on the data (Part II) for a heated Fe^{2+}-chamosite, and may well

[1] To test the homogeneity of the estimates of g_0 between the three groups we used the procedure given by Williams (1959, pp. 131–2) which resulted in a value for F on 2 and 54 degrees of freedom being equal to 2.62. This contradicts homogeneity at a level between 5% and 10%, *i.e.* the level is not quite significant. The greatest contribution towards heterogeneity comes from the mica estimate.

be suspect. A value of about 0.1 seems more consistent. It is interesting that the "hole size" for Fe^{3+} (Table 2, Part II) is then 0.50, as for Al, again hinting at ordering of the octahedral cations in this group.

If the differences in g (*i.e.* λ) are indeed real then the external constraints resisting marked expansion in the *a-b* planes are strongest in micas and weakest in the kaolins. This is discussed further in the following paper on the interatomic forces.

The postulate (2) that there are two hole sizes, A and B, is not proven statistically primarily because of insurmountable limitations in the published—and probably in the potentially available—data. However, the present explicit geometrical model seems to be essentially correct. In so far as this is true octahedral ordering follows as a consequence.

Acknowledgements

The helpful advice of Dr. E. A. Cornish and Dr. E. J. Williams, both of the Division of Mathematical Statistics, C.S.I.R.O., is gratefully acknowledged. Dr. F. Chayes, Geophysical Laboratory, Washington, has kindly read the manuscript.

References

Ahrens, L. H. (1952) The use of ionisation potentials, Part I. Ionic radii of the elements. *Geochim. Cosmochim. Acta*, **2**, 155.

Bernal, J. D. and H. D. Megaw (1935) The function of hydrogen in intermolecular forces. *Proc. Roy. Soc. London, A*, **151**, 184.

Bradley, W. F. (1957) Current progress in silicate structures. *Sixth National Clay Conference Proc.*, p. 18.

Brindley, G. W. and D. M. C. MacEwan (1953) Structural aspects of the mineralogy of clays and related silicates. Ceramics; a symposium, *Brit. Cer. Soc.*, **15**.

Brown, G. (1951), in "*X-ray Identification of Clay Minerals*." Mineral. Soc., London.

Cowley, J. M. and A. Goswani (1961) Electron diffraction patterns from montmorillonite. *Acta Cryst.* **14**, 1071.

Drits, V. A. and A. A. Kashaev (1960) An X-ray study of a single crystal of kaolinite. *Kristallografiya* (in transl.), **5**, 207.

Megaw, H. D. (1934) The crystal structure of hydrargillite, $Al(OH)_3$. *Zeit. Krist.* **87**, 185.

Newnham, R. E. (1961) A refinement of the dickite structure. *Mineral. Mag.* **32**, 683.

Radoslovich, E. W. (1960) The structure of muscovite, K $Al_2(Si_3Al)O_{10}(OH)_2$. *Acta Cryst.* **13**, 919.

——— (1962), The cell dimensions and symmetry of layer-lattice silicates, II. Regression relations. *Am. Mineral.*, **47**, 617–636.

——— and K. Norrish (1962) The cell dimensions and symmetry of layer-lattice silicates, I. Some structural considerations. *Am. Mineral.*, **47**, 599–616.

Steinfink, H. (1958) The crystal structure of prochlorite. *Acta Cryst.* **11**, 191.

Takéuchi, Y. and R. Sadanaga (1959) The crystal structure of xanthophyllite. *Acta Cryst.* **12**, 945.

Williams, E. J. (1959) *Regression Analysis*, John Wiley & Sons, Inc., New York.

Zviagin, B. B. (1957) Determination of the structure of celadonite by electron diffraction *Kristallografiya* (in transl.), **2**, 388.

Manuscript received, July 27, 1962; accepted for publication, October 12, 1962.

THE CELL DIMENSIONS AND SYMMETRY OF LAYER-LATTICE SILICATES. IV. INTERATOMIC FORCES

BY

E. W. RADOSLOVICH

Commonwealth of Australia
COMMONWEALTH SCIENTIFIC AND INDUSTRIAL RESEARCH ORGANIZATION

Reprinted from American Mineralogist, 48:
Pages 76-99
(1963)

THE AMERICAN MINERALOGIST, VOL. 48, JANUARY–FEBRUARY, 1963

THE CELL DIMENSIONS AND SYMMETRY OF LAYER-LATTICE SILICATES IV. INTERATOMIC FORCES

E. W. RADOSLOVICH, *Division of Soils, Commonwealth Scientific and Industrial Research Organisation, Adelaide, Australia.*

ABSTRACT

The relative importance of different kinds of interatomic forces in controlling the layer silicate structures has been roughly assessed, from a review of bond lengths and angles in published structures. This has lead to some simple rules, consistent with current ideas in structural inorganic chemistry, from which detailed explanations may be deduced of many observed variations in bond lengths and angles from the expected values.

The main postulates are that bond angles are more readily changed under stress than bond lengths, that bond lengths vary inversely as electrostatic bond strengths, and that forces due to cation-cation repulsion across shared octahedral edges are of comparable importance to the stronger bonds in these structures.

It is deduced in general that forces within the octahedral layers control major features of the layer silicate structures, that these forces tend to produce ordering of the octahedral cations, and that individual octahedra cannot be geometrically regular. Tetrahedral layers may be distorted to limits set by O—O approach distances rather than by O—Si—O bond angles in the tetrahedral groups. The importance of bonds between interlayer cations and surface oxygens is greater than is usually recognized.

The specific postulates are applied firstly to some simple structures containing octahedral groups, thereby explaining several apparent anomalies in earlier data. The published dickite and the $2M_1$ muscovite structures are then critically reviewed, and satisfactory reasons proposed for many observed variations in bond lengths and angles, in terms of local forces on particular atoms. Some less accurately determined layer silicate structures are briefly reviewed in a similar way.

The successful application of these rules to known structures gives the author confidence that the atomic parameters for other layer silicate structures can now be predicted much more closely than previous "ideal structures" for these minerals allowed. The detailed understanding of local stresses in accurately known structures is beginning to suggest means of structural control over properties such as polymorphism. The probability of extensive ordering of octahedral cations should be noted in considering the limits of composition, and other physical properties of these minerals.

INTRODUCTION

The surface oxygen networks of layer silicates often have approximately ditrigonal rather than hexagonal symmetry, a characteristic which Radoslovich and Norrish (1962)[1] have recognized in proposing that the sheet dimensions of micas are controlled largely by the octahedral layers and the interlayer cations. Radoslovich (1962a)[2] has confirmed this suggestion by showing the negligible effect of Al—for—Si substitution tetrahedrally in new "*b*-axis formulae" computed by

[1] Hereafter Part I.

[2] Hereafter Part II.

multiple regression analysis. Veitch and Radoslovich (1962)[1] subsequently proposed an explicit geometrical model of the octahedral layers in these minerals, during an investigation into the possible degree of ordering of the octahedral cations. These studies together have led to the following more detailed examination of the forces within the sheets of the layer silicates, the broad conclusions of which have already been reported (Radoslovich, 1962b). The present study has sought an understanding about which forces dominate in the layer silicate structures, and which forces generally have a secondary effect only. Such an analysis cannot begin until highly accurate parameters have have been published for several comparable structures, a situation only just reached for this mineral group; future accurate structural analyses should enable the refinement of the present ideas. Though very few layer silicate structures currently have been published the general concepts developed should of course be consistent with, or applicable to, other allied structures such as the feldspars to which passing reference is made. The mental approach is similar to that successfully adopted for anorthite and other feldspars in which Megaw *et al.* (1962) have considered the structures effectively as a network of forces comparable to the "Theory of Frames" used in designing bridge trusses.

Terms of Reference, Limitations, Restrictions

Standard deviations in bond lengths. Standard deviations in bond lengths, σ, have been adequately calculated for the structures of vermiculite, dickite and muscovite, but scarcely for any other relevant structures. It is, moreover, clearly necessary to make inferences from reported bond length differences which the known (or unknown) σ do not strictly allow—a severe limitation. Such inferences can be supported in part, however, by observing that a number of previous anomalies disappear and that the concepts developed are at least in the right direction for the reported differences. It is essential that, where the minerals studied allow, future structure analyses be of a high, known and stated accuracy (Mathieson *et al.* 1959).

Ionic and covalent bonds. The length of a given cation—anion bond depends on whether it is fully ionic, fully covalent or has some of both characteristics. In discussing individual structures (below) it is assumed that reported differences in the electrostatic strength of individual bonds can be correlated reasonably with observed variations in bond lengths. Although this ignores the possibility of some change in the "ionic versus

[1] Hereafter Part III.

covalent" character of a given bond this is tolerable provided that small variations in strictly comparable bonds alone are involved.

For example, in a tetrahedral group an Al—O bond appears to be largely ionic—observed Al—O distances are consistent with the ionic radii of Al and oxygen, corrected for a ligancy of 4 and Born number = 7 (Pauling, 1960). But the tetrahedral Si—O bond may well be up to 50% covalent in character, as Pauling (1960) and others have calculated. Alternatively it may be largely ionic in character, as Verhoogen (1958) has maintained, and the effective co-ordination correction is then somewhat different from that for Al^{IV}—O bonds, "due to the higher polarizing power of the Si^{4+} towards the oxygens."

If, however, two structures are compared which have similar Al—for—Si substitutions then it is reasonable to compare the cation—oxygen bond lengths in relation to the charge available at the oxygens to form such a bond.

Indeed, to a first approximation the layer lattice structures may be compared with each other as if they are purely ionic structures, on the assumption that for the differences discussed below there is little change in the character of the bonds involved, and that these are largely ionic anyway. This is, of course, the customary way of treating complex silicate minerals.

Electrostatic bond strengths and shortening of bonds. Although there are experimental errors in all reported bond lengths there are undoubtedly variations in comparable ionic bond lengths due to differences in electrostatic bond strengths in different structural environments. Observed bond lengths are here assumed to be approximately inversely proportional to actual electrostatic bond strengths (*e.g.* Burnham and Buerger, 1961; Buerger, 1961; Jones and Taylor, 1961).

Petch *et al.* (1956) and others have explicitly pointed out, however, that although a weak bond is generally assumed to be long (and a strong bond short) this is not universally true. Particular steric effects may result in short interatomic distances where the bond strength is low or negligible; several examples of such fortuitously short bonds are mentioned below. Possible mechanisms of bond shortening with increased electrostatic bond strength are not relevant here.

Local charge balance and stability. The stability of the feldspars has been examined recently in terms of the local balance of charge structurally, by Ferguson *et al.* (1959), and others. There is, as yet, no agreement on a general theory, because of difficulties arising from the partially covalent character of some bonds, because of uncertainties about the range of electrostatic forces, and for other reasons.

Although departures from local charge balance will be briefly discussed it is not possible or desirable at present to consider the relative stabilities of the layer silicates in these or similar terms.

Pauling's rules. It is assumed that for these structures Pauling's Rules are widely applicable and indeed they appear to be obeyed in detail in most cases. In particular the Electrostatic Valence Rule (or an equivalent rule for partly covalent bonds, Pauling, 1960, p. 547) is satisfied, and deviations exceeding $\pm 1/6$ seem rare for layer silicates, as for other minerals. In so far as steric effects will allow, the shared edges between polyhedra are shortened, as they should be in ionic structures.

Tetrahedral Si—O and Al—O bond lengths. The expected lengths for Si—O and Al—O bonds in tetrahedral groups have been discussed by Smith (1954) and Smith and Bailey (1962). These values are important for layer lattice silicate structures, not only in estimating the amount of Si—Al ordering during the initial structure determination, but in assessing the magnitude of other effects (below) when the parameters are known.

Smith and Bailey (1962) suggest values of 1.61$_4$ Å for Si—O and 1.75 Å for Al—O for the framework structures, plus 0.01 to 0.02 Å for layer silicates. Values of 1.62 Å for Si—O bonds with an electrostatic bond strength of one, and 1.77 Å for Al—O bonds with an electrostatic bond strength of 0.75 may therefore be anticipated for the layer silicates.[1] Though these figures may be slightly adjusted later, this paper is largely limited to a comparison of tetrahedral bond lengths within the group of layer lattice silicates only and these comparisons should remain valid.

General Theory of Layer Lattice Silicate Structures

"Balance of forces" rather than "packing structures." Pauling (1960), Bragg (1937) and many others have commented that the scale of various silicate structures is mainly determined by the packing together of the large anions, notably oxygen, whereas electrical neutrality is maintained by cations of suitable size and charge in the interstices. Alternatively, the silicates can be classified according to the types of linkage adopted by the tetrahedral groups.

Although these are still very useful generalisations their too ready application forms barriers to a detailed understanding of any particular mineral group. Thus the layer silicates are not simply close packed layers of anions, with cations of the right size stuffed in the interstices, rather passively maintaining neutrality. Each mineral, indeed, represents a

[1] The Al-O bond length is less precisely defined and values as high as 1.80 Å have been reported for recent structures.

"stable" equilibrium, at the lowest possible internal energy, of bonds under "tension" or "compression," of atoms pushed into close proximity against their mutual repulsion, and (infrequently) of directed bonds under "torsion." Interstices are of the "right size" for certain cations only in the sense that with those cations present the increased strains in the other bonds, distances and angles do not lead to obvious instability.

Structural elements in layer silicates. The assumptions on which the later discussion of particular structures is to be based cannot be rigorously proven, but they appear to be valid generally for complex ionic (*e.g.* mineral) structures. They are:

(1) Bond lengths in general vary inversely with electrostatic bond strengths.

(2) Bonds are effectively non-directional, with occasional O—H bonds as exceptions.

(3) Bonds increase in compliance (see Megaw, Kempster and Radoslovich, 1962) from Si—O, through Al^{IV}—O, octahedral cation—O, to interlayer cation—O bonds.

(4) Bond angles are more compliant than bond lengths, the T—O—T angles more than O—T—O (T=tetrahedral cation), as shown by Megaw, Kempster and Radoslovich (1962).

(5) Mutual repulsion between anions increases very rapidly as interatomic distances fall below the sum of their ionic radii. In particular, the minimum observed O—O distances—*e.g.* 2.25 Å in andalusite (Burnham and Buerger, 1961) or 2.29 Å in $Rb_2Ti_6O_{13}$ (Andersson and Wadsley, 1962)—are "probably close to the lower limit attainable without the formation of detectable homopolar bonds."

(6) The mutual repulsion of multivalent cations only partly shielded electrostatically from each other may be of comparable strength to the strongest bonds. More specifically, trivalent cations sharing octahedral edges exert a mutual repulsion which is one of the dominant forces in layer silicates.

(7) Adjacent anions whose valencies are not fully satisfied by immediate bonds will mutually repel each other, due to their charge.

(8) The charges on silicate layers and interlayer cations cannot be too far separated, due to increased Coulomb energy.

Octahedral layers.[1] The cell dimensions of such a layer correspond to an equilibrium between three different kinds of forces, *viz.* (i) cation—cation repulsion across shared octahedral edges, (ii) anion—anion repulsion along shared edges and (iii) cation—anion bonds within octahedra (Fig. 1). On all the available evidence these forces result in severe deformation of all octahedral layers, except for minerals in which they are opposed by additional and strong external forces. That is, the balance of forces *within* the octahedral layer usually dominates in layer silicates.

Of these forces the cation—cation repulsion is the most influential in causing individual departures from ideal structures, for several reasons. The octahedral cations are only partly shielded from each other elec-

[1] These arguments apply equally to separate octahedral layers, as in the metal hydroxides, or to octahedral layers combined with tetrahedral layers, as in the clay minerals.

trostatically, they vary considerably in environment, valency and size, and the undirected nature of the cation—anion bonds allows wide variations in the shapes of individual octahedral layers.

If an octahedron in such a layer be viewed as an upper and lower triad of oxygens around the cation then the shortening of O—O edges shared with neighbouring octahedra results in the counter-rotation of these

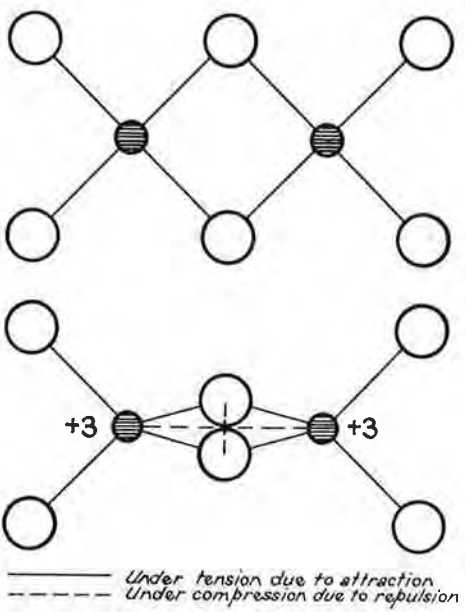

FIG. 1. Deformation of unconstrained octahedral layers to some equilibrium between (i) cation-anion bonds, (ii) cation-cation repulsion, and (iii) anion-anion mutual compression, across shared edges (diagrammatic).

triads (Part III). The operation of a "cation avoidance rule"—due to their mutual repulsion—has several implications, *viz*:

(i) Dioctahedral structures will show strong tendencies toward regular hexagonal arrangements of cations around vacant sites (Part III).

(ii) Sheet dimensions become as large as the cation—anion bonds and O—O approach will allow; major expansions to occur along edges of triads enclosing vacant sites. For example, equilibrium in pure Al^{3+} dioctahedral minerals corresponds to $b=8.92$–8.94 Å; and strong forces external to the octahedral layer are needed to cause any marked variation from this.

(iii) In trioctahedral minerals containing ≈ 2.0 R^{2+} and some R^{3+} the R^{2+} cations tend to be disposed hexagonally around the R^{3+}, to separate adjacent R^{3+} as much as possible.

(iv) Shared octahedral edges in layers with very different cations should be shortened to about the same minimum distance, below which the anions become more incompres-

sible very rapidly. Again, this minimum distance is not always attained, due to forces external to some layers.

Tetrahedral layers. Unperturbed tetrahedra in the layer silicates seem to have T—O lengths close to values to be predicted from their average cation occupancy, T; individual bonds, however, can be slightly stretched under severe external stress. The T—O bonds also appear to vary systematically with the net charge available at the anion, after allowing for the bond strengths from that anion to other cations. If, for example, a given oxygen has less than one of its charges satisfied by other cations then that Si—O bond will be correspondingly stronger and hence shorter than the expected 1.62 Å approx.

Although the Si—O bonds are partly covalent the O—T—O angles appear to depart readily from the ideal 109°28′ to limits which are set by the minimum O—O approach along tetrahedral edges rather than by any directed nature of the T—0 bonds. A review of these distances and angles in recent accurate analyses of felspar structures confirms this (*e.g.* Megaw, Kempster and Radoslovich, 1962). In six felspar structures the individual angles vary at least from 99° to 119°, whereas the O—O edges are always >2.48 Å and mostly >2.55 Å—indicating that tetrahedra can be deformed fairly easily until edge lengths approach 2.55 Å. Donnay *et al.* (1959), Jones and Taylor (1961) and others have previously noted that tetrahedra need not be perfectly regular.

In layer silicates tetrahedra share corners only. This, combined with the low radius ratio Si/O, ensures fairly good electrostatic shielding of Si's from each other—at least when compared with octahedral cations. The T—O—T angles are therefore among the most compliant elements of the layer structures as of the felspars (Megaw *et al.* 1962). More generally they may increase from the average 138° to at least 160° (Liebau, 1961).

Interlayer cations; net surface charges. Important details of the layer structures are actively controlled by the bonds between interlayer cations and surface oxygens; the common concept that "cations of the right size occupy holes to maintain over-all neutrality" underestimates their influence. Indeed, even the T—O bonds appear to be influenced by any discrepancy between the bond strengths to, and valency of, the interlayer cations. Likewise unexpected variations in T—O bonds seem to be correlated with the net surface charge on the layers of minerals with high exchange capacities.

It is noteworthy that a given interlayer cation (*e.g.* K^+) can produce opposing structural effects in two micas having appreciably different octahedral layers.

Some Octahedral Layers Controlled by External Forces

Corundum,[1] Al_2O_3. This consists of successive dioctahedral layers, with the anions shared between two layers. The Al^{3+} cations are arranged so that each unoccupied site is surrounded by occupied sites. Accurate unit cell data on corundum (A.S.T.M. *X*-ray Data Card 10–173) refers this structure to a trigonal cell with $a=4.758$ Å, equivalent to a "*b*-axis" of 8.241 Å if corundum is being compared with layer silicate dimensions.

Corundum obeys Pauling's Rules—single shared O—O edges are shortened to 2.61 Å, and shared O—O edges of shared octahedral faces to 2.49 Å. Despite this evidence of strong cation—cation repulsion the octahedral layers are both thin (2.16 Å; *vide* Part III) and have sheet dimensions very small in comparison with comparable dioctahedral layers, *i.e.*, 8.24 Å as against 8.94 Å, for example. The reason for this is that no expansion can occur around the unoccupied sites. Both triads of oxygens which together form the corners of a given unoccupied octahedra are also triads of the neighbouring occupied octahedra. Their expansion is thereby severely restricted, except for the small difference between 2.49 and 2.61 noted above. That is, the cation—cation repulsion in any one layer is restrained from increasing the sheet dimensions by the fact that the interatomic O—O distances which should become much longer are themselves, in corundum, already shortened shared edges. This same kind of structural restraint is evident in diaspore and chloritoid.

Diaspore,[2] AlO.OH This can be viewed as a stack of infinite ribbons two octahedra wide and one octahedra high, alternating with channels of these dimensions. The mineral has most recently been studied by Busing and Levy (1961) using neutron diffraction to locate the protons accurately. Their discussion does not resolve an anomaly noted earlier by Bernal and Megaw (1935).[3] This concerns the relation between the O—OH distances across the channels, Ewing's suggested long hydrogen bond here, and the fact that infra-red analysis suggests the existence of independent OH's, not hydrogen bonds.

When the principles stated earlier are applied to the diaspore data it is clear that the O_I—O_{II} distances are short almost entirely for *steric* reasons—the balance of forces within and between occupied octahedra ensure that O_I—O_{II} is "shortened" to 2.65_0 Å. Very little hydrogen or hydroxyl bonding is required or allowable, to make the observed data

[1] See, *e.g.*, Bragg, 1937, p. 93.
[2] See, *e.g.*, Wells, 1962, p. 556.
[3] Note that O_I in B. and L.=O_{II} in B. and M.; and *vice versa*.

self-consistent, *viz.*

(i) the O_{II}'s give I.—R. spectra of free hydroxyls.
(ii) the protons belong to O_{II}; observed O_{II}—H = 0.990 Å, and O_I—H = 1.694 Å.
(iii) the O_I's are bound to 3 Al's, with bond strengths therefore of $\frac{2}{3}$; and the O_{II}'s to 3 Al's, strengths $\frac{1}{3}$.

These bond lengths, Al—O and Al—OH, in diaspore may then be compared with predicted bond lengths for (a) no O—OH bond, as above *or* (b) a "hydroxyl" O—OH bond (Bernal and Megaw, 1935). Bond-lengths to be expected for various bond strengths may be estimated from the normal octahedral and tetrahedral Al—O bonds. Five co-ordinated Al in andalusite (Burnham and Buerger, 1961) provides a check with values 1.82, 1.82, 1.82, 1.86, 1.88 Å. The observed values (Table 1) are more

Table 1. Expected and Observed Al—O Bonds in Diaspore

Al—O bond lengths in relation to bond strengths[1]			Diaspore		
			O_I-O_{II} bond proposed		Observed (Busing and Levy, 1958)
Type	Strength	Length	None	Hydroxyl	
—	0.33	1.99 Å	Al-O_{II}[1]	Al-O_I and O_{II}	1.977 Å
Octah.	0.50	1.91			
5-coord	0.60	1.86			
—	0.66	1.83	Al-O_I		1.854 Å
Tetrah.	0.75	1.78			

[1] These average values are proposed from an empirical consideration of a number of other structures.
[2] That is, with no hydrogen bonding the expected Al-O_{II} bond length will be 1.99 Å.

closely comparable with values predicted on the assumption of *no* O_I–O_{II} bond. The angle of 12.1° which O_{II}—H makes with O_{II}—O_I (Busing and Levy, 1958) is no longer unexpected.

If the octahedral ribbons in diaspore are compared with octahedral layers in clay minerals then the ribbons have a thickness ≈2.2 Å (*i.e.* $a/2$) and sheet dimensions of "b" ≈8.53 Å (*i.e.* $3c$). This confirms that the unoccupied octahedra cannot expand because they share all faces with occupied octahedra—analogous to corundum.

Chloritoid, $[(Fe^{2+}, Mg)_2Al](OH)_4Al_3[O_2(SiO_4)_2]$ Harrison and Brindley (1957) have discussed in detail the relations between the chloritoid, mica and corundum structures. In chloritoid rather incomplete tetrahedral layers alternate with two different octahedral layers, one of

which is closely similar to, and has very nearly the same dimensions as an octahedral layers in corundum.

This octahedral layer should have expanded markedly in the triads of anions about the unoccupied sites (see above), if unconstrained externally. In chloritoid, however, these triads are also the base triads of the separate tetrahedral groups, above and below (Fig. 2, Harrison and Brindley, 1957). Their maximum size is therefore fixed, and this in

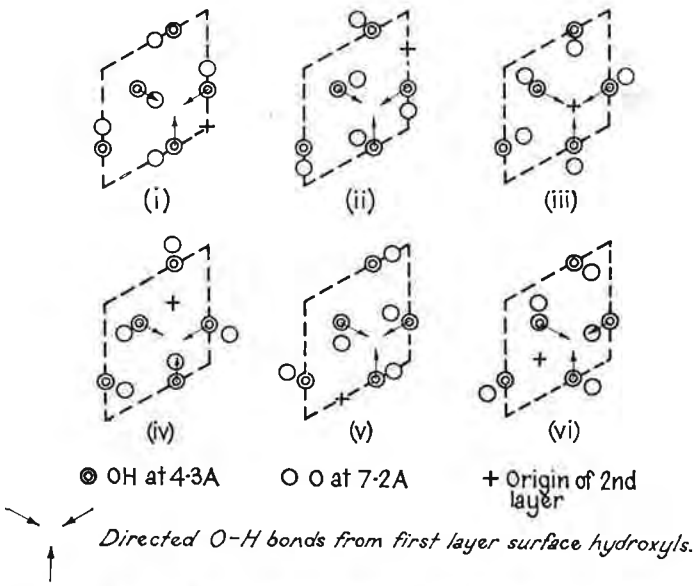

FIG. 2. Six ways of placing the oxygen layer over the hydroxyl layer (Fig. 6, N.), but with the preferred directions of the O—H bonds also shown.

fact allows practically no octahedral expansion. The octahedral sheet dimensions in chloritoid and corundum are closely comparable, controlled, respectively, by neighbouring tetrahedral faces and octahedral faces shared with the vacant octahedra.

The other octahedral layer in chloritoid is of course constrained to these short dimensions, despite being trioctahedral and containing larger cations.

Harrison and Brindley (1957) have argued that the sheet dimensions of chloritoid (*viz.* $a = 9.52$ Å) *exceed* those of micas with similar Fe^{2+} content because, they imply, the discontinuous tetrahedral layers allows more ready expansion. Unfortunately they did not compare the same orientation of the octahedral cations in chloritoid (and corundum) as in micas giving $b \approx 9.3$ Å. The appropriate chloritoid dimension is 8.24 Å,

not 9.52 Å; and this is very much *smaller* than the *b*-axes of biotites, due to the overriding restraints exerted by the discontinuous tetrahedral layers!

Gibbsite,[1] $Al(OH)_3$. Bernal and Megaw (1935) clearly demonstrated the existence of hydroxyl bonds, both between sheets and also *along the surfaces* of sheets around unoccupied sites. They specifically stated that these OH—OH bonds decreased the sheet dimensions to 8.624 Å (*i.e.* "*a*"). These bonds are not very strong, and only modify the octahedral strains as a secondary effect. Thus the average O—O distances in triads enclosing an unoccupied site, 3.20 Å, are much larger than surface O—O distances around occupied sites, 2.79 Å (Megaw, 1934). (The difference is still larger in dickite and muscovite which lack the OH—OH bonds.)

Dioctahedral kaolins and micas. In these minerals dioctahedral Al—layers appear to have dimensions virtually unaffected by constraints from the structure as a whole, *viz.* $b = 8.92$–8.94 Å. Dickite, a kaolin polymorph, is discussed below. The interlayer Na in paragonite probably does not perturb the *b*-axis set by its octahedral layer (Parts I, II). Interlayer K in muscovite (5.2) is the exception, in actively increasing the overall dimensions to 8.995 Å.

Brucite, $Mg(OH)_2$ *and phlogopite*, $K\ Mg_3\ (Si_3\ Al)\ O_{10}(OH)_2$. Although Mg (0.65 Å) is larger in radius than Al (0.51 Å) brucite and gibbsite layers have a comparable thickness, around 2.1 Å, set for both by the limit of O—O approach along shared octahedral edges (see above). The longer Mg—O bonds allow Mg—Mg repulsion to extend the *b*-axis to 9.44 Å, greater than for almost all other trioctahedral layer lattice silicates. That is, most such layers—except brucite—have some constraint applied by the rest of the structure. For example the K—O bonds in phlogopite probably limit the overall expansion to the observed 9.2 Å; both the tetrahedral and octahedral layers could have gone to ≈9.44 Å.

Accurately Determined Layer Structures[1]

Dickite, $Al_2Si_2O_5(OH)_4$. *Newnham, 1961.*[2] Newnham's highly accurate data fully confirm the concepts stated earlier, just as these enable his careful discussion of the dickite structure to be extended or amended at some points.

The very short shared octahedral edges (2.37 Å), which Newnham

[1] In standard texts, *e.g.* Wells, 1962.

[2] In this section references are, for brevity, given to tables and figures in the original papers, *e.g.* "Table 1, N."

noted, result from the uninhibited Al—Al repulsion which produces, in dickite, a maximum expansion for such a layer. Average O—O distances in one anion layer are much larger around unoccupied sites (3.43 Å) than occupied sites (2.78 Å). The corresponding counter-rotation of the octahedral triads (Part III) is $-3°$ and $+8°$, as Brindley and Nakahira (1958) observed.

The average Al—"O" bonds also fall into two groups, *viz.* Al—(surface) OH = 1.85_7 Å and Al—(interior), O, OH = 1.94_8 Å; the Al—"O"—Al angles are consistent with this difference. Both distances should be compared with an expected 1.91 Å, and with an observed mean in muscovite of 1.93_6 Å (omitting Al—O_B = 2.04_8 Å). Newnham commented on the closer approach of the Al's to the surface hydroxyls, but he has apparently misunderstood the diaspore structure in quoting diaspore and dickite as "very similar" in this respect. The relevant bonds are in direct contrast (Table 2). In dickite the surface hydroxyls form long hydrogen bonds to tetrahedral oxygens on the adjacent surfaces (Newnham,

TABLE 2. AVERAGE Al-"O" BONDS IN DIASPORE AND DICKITE, IN Å

Diaspore[1]		Dickite[2]	
Al_1-O_{II} (*i.e.* OH)	1.98_0 Å	Al_1-OH (surface)	1.85 Å
Al_2-O_{II} (*i.e.* OH)	1.97_5	Al_2-OH (surface)	1.86
Al_1-O_I	1.85_8	Al_1-(2O, OH)	1.96
Al_2-O_I	1.85_1	Al_2-(2O, OH)	1.94

[1] Busing and Levy, 1958
[2] Newnham, 1961.

1961). This bond formation is assisted by the high polarization induced in each OH by the two Al^{3+} to which it is bonded internally. Thus the protons of the OH's are strongly directed away from the Al's, so that in each OH

(i) the O—H bond shows a marked tendency to be coplanar with the two Al—OH bonds (see below), and
(ii) there is considerable asymmetry of charge, with increased negative charge towards the Al's.

As a result of (ii) the electrostatic strength of the Al—OH bonds significantly exceeds the expected $\frac{1}{2}$, and these bonds are shortened from 1.91 Å to 1.86 Å; from Table 1 the strengths are about 0.6–0.65.

The excess strength of the Al—OH bonds is confirmed by their marked contraction despite the strong Al—Al and O—O repulsions with which they are in equilibrium. In diaspore, however, each Al—OH bond has an expected strength of $\frac{1}{3}$ (see above) and should, according to Bernal and

Megaw (1935), cause relatively little OH polarization; their length of 1.98 Å agrees with this.

If the valency of the Al^{3+} is to be closely satisfied in dickite the remaining bonds must have strengths $< \frac{1}{2}$, which the average Al—O, OH distances of 1.95 Å, rather than 1.91 Å, confirm. In diaspore, however, the expected Al—O bond strength is $\frac{2}{3}$; (*i.e.* $> \frac{1}{2}$) and three such bonds to each oxygen will inhibit any further bonding to the opposing OH's. For further comparison the surface OH—OH bonding in gibbsite (Megaw, 1934) ensures a strength near $\frac{1}{2}$ in all Al—OH bonds, and the average bondlength of 1.89 Å is close to an expected 1.91 Å.

The Al distribution determines the pattern of counter rotations in the octahedral layer (Part III). The directions of the required tetrahedral rotations (Parts I and II) are therefore set by the octahedral layers so that basal oxygens are matched to surface hydroxyls (N., 1961) to shorten the O—H—O bonds to 2.94, 2.97 and 3.14 Å. These rotations are less than ideal (Part II) because the tetrahedra are "contracted in the oxygen basal plane and elongated along c^*." This basal compression, which Newnham attributed to general misfit, may be explained in detail by observing that

(i) the Si—O and O—H—O bonds are not very compliant,
(ii) the O—H bonds are strongly directed, at an angle inclined to c^* (see above), and
(iii) the O—Si—O angles are quite compliant.

It follows from (i) and (ii) that although the basal oxygens of one layer are bound at about 3 Å from the opposing OH's they will not be vertically above them (see Fig. 3, N.). The directed O—H—O bonds are acting to reduce the size of the tetrahedral base triads, which is achieved—in agreement with (i) and (iii)—by τ increasing from 109°28′ to an average 111.8° (Table 2, N.). The final tetrahedral configuration is a balance between the Si—O bond lengths, the inclined and directed O—H—O bonds, and the O—O compression in the basal triads, shown by $O_1—O_3 = 2.58$ Å and $O_2—O_3 > O_1—O_2 = 2.59$ Å.

This is linked with the buckles in dickite surfaces whereby OH_3 protrudes from the layers and O_3 is depressed into them. Newnham's explanation in terms of tetrahedral tilting (by the apex oxygens, O_4 and O_5) is inadequate in view of the high compliance of tetrahedral angles. Rather, the directed bonds from OH_2 and OH_4 largely fix the positions of O_1 and O_2, whereas O_3—which is above an unoccupied octahedral site—is pushed into its own layer by the compression along $O_1—O_3$ and $O_2—O_3$. This depression of O_3 stretches $OH_3—O_3$, but only to 3.12 Å, because OH_3 can be (and is) elevated above OH_2 and OH_4. The shortness of the shared edge $OH_3—OH_1$ is easily maintained since OH_1 (unlike the corresponding O_4 and O_5) is not firmly held by the rest of the structure.

The elevation of OH_3 fully explains other variations observed by Newnham, *viz.*

$Al_1—O_4 = 1.93$ Å	$Al_2—O_4 = 1.98$ Å
$Al_1—O_5 = 2.01$	$Al_2—O_5 = 1.94$
$Al_1—OH_1 = 1.93$	$Al_2—OH_1 = 1.90$

The bonds to OH_1 should have strength $\frac{1}{2}$ because the OH_1 charge is satisfied, and their lengths are close to the predicted 1.91 Å. Each Al now has four bonds to OH's with a total strength of about $(3\times0.6+0.5) = 2.3$ approx., leaving only 0.7 as the combined strengths for the two Al—O bonds in each case. The observed lengths are consistent with strengths $<\frac{1}{2}$, with one bond of each pair noticeably longer than the other. From Fig. 3, N., it is obvious that the long bonds, $Al_1—O_5$ and $Al_2—O_4$ are the bonds directly opposite the bonds $Al_1—OH_3$ and $Al_2—OH_3$ in their respective octahedra, whereas $Al_1—O_4$ and $Al_2—O_5$ are at about 90° to the Al—OH_3 bonds. On the understanding (above) that the overall structure holds the O_4, O_5 fairly firmly then clearly the elevation of the OH_3 (and the strong Al—OH_3 bonds) mainly stretches $Al_1—O_5$ and $Al_2—O_4$, as observed. Moreover the OH_3 are attracted to O_3's in such a way (Fig. 3, N.) that $Al_1—O_5$ should exceed $Al_2—O_4$, and Al_1 should be lifted relative to Al_2; both these consequences are observed.

In both tetrahedra the external distribution of bond strengths should lead to $Si—O_{basal}$ bonds of strengths <1.0 (due to interlayer O—H—O) and $Si—O_{apex}$ bonds >1.0 (due to asymmetric Al—O, OH groups). The mean 1.619 Å agrees with Smith and Bailey's (1962) predictions for an Si—O group with external bonds exactly balancing to strength 4, as expected. It is, however, likewise to be expected that *within* each group the $Si_1—O_4$ and $Si_2—O_5$ bonds would be rather shorter than the other three, and the lack of any such trend in the observed bonds is a little surprising.

There appears to be no alternative explanation for the tetrahedral distortion, for the lack of direct superposition of O on OH, and for the small tetrahedral twists, other than the directed nature of the O—H—O bonds. This surface property obviously bears on the polymorphism of the kaolins and its recognition allows Newnham's detailed discussion to be both simplified and extended. The six ways of placing the oxygen surface over the hydroxyl surface (Fig. 6, N.) are no longer equivalent, if O—H bonds are directed (Fig. 2). Although all six ways lead to some torsion of these bonds the strains involved in (ii) and (v) are less than in (i), (iv) and (vi), whilst (iii) is quite unlikely to occur at all.

Amongst the single layer structures in Table 7, N., the most probable are therefore nos. 7 and 25—the same conclusion, but a more explicit argument than that from the Coulomb energy. The two layer structures

in Table 8, N., must now (a) minimise the Coulomb energy, (b) satisfy the pucker conditions *and* (c) minimise the angular strain in the O—H bonds. The sequence 11, 27, 11, 27 . . . (superpositions ii, v) is more likely to occur as a stable mineral than 20, 36, 20, 36 . . . (superpositions iv, vi). That is, the abundance of dickite (11, 27, 11, 27 . . .) relative to nacrite (20, 36, 20, 36 . . .) is at least consistent with, if not explained by, control exerted by the directed O—H bonds.

These directed bonds are discussed further in relation to kaolinite (below) and kaolin morphology (Radoslovich, 1963b).

Muscovite, $K\ Al_2(Si_3Al)O_{10}(OH)_2$[1] *Radoslovich, 1960.* The previous discussion (R., 1960) can now be carried further.[2] Extension of the octahedral layer occurs mainly around the vacant site (3.3.2). For coplanar O's around these sites O—O = 3.34_1 Å aver. and (Vacant Site)—O = 2.20_4 Å aver. whereas for the two occupied sites O—O = 2.82_4 Å aver. and Al—O = 1.95_4 Å aver. Shared octahedral edges are shortened, but not equally so (Table 5, R.). One edge, $O_A - O_A = 2.39_6$ Å, close to the 2.37 Å in dickite. Another, OH—OH = 2.51_1 Å, possibly a little longer due to OH—OH repulsion following their polarization (below). The third edge O_B—$O_B = 2.76_8$ Å is apparently not shortened at all, but this is quite misleading. In fact all bonds to O_B are severely stretched (see below) and O_B—O_B edges *are* shortened, but only as far as the strong Si_2—O_B bonds will allow. The Si_2 are firmly held by the three bonds to O_C, O_D and O_E, aver. 1.60_0 Å, whereas Si_2—$O_B = 1.64_8$ Å. The differences between edges of 2.39_6, 2.51_1 and 2.76_8 Å are quite real, and the octahedral anions are not strictly coplanar (Part III). The Si_2—O_B bonds hold the O_B's above the plane of the O_A's and OH's, and also help to stretch one Al—O_B bond to 2.04_8 Å. The average Al—O = 1.93_6 for the remaining five bonds still exceeds the calculated 1.91 Å.[3] In muscovite the K^+ stretches the sheet dimensions (Part I) beyond the 8.92–8.94 Å set by the octahedral layer. Since two shared edges are held larger than the three edges in dickite (with $b = 8.94$ Å) the Al—O bonds must extend, as observed.

[1] These arguments become clearer from a true model (*e.g.* Radoslovich and Jones, 1961).

[2] Note that Radoslovich studied the $2M_1$ structure. In fact the detailed differences between the probable or known structures of the various polymorphs now have become more obvious and some structural factors controlling mica polymorphism will be described in a subsequent paper.

[3] In occupied octahedra in muscovite, therefore, several strong forces are in equilibrium, and it is not surprising to find that about 80% of these octahedra must be occupied by Al^{3+} in particular, in order to maintain a stable muscovite-type structure (Radoslovich, 1963a).

The two tetrahedral sites ("Si_2" and "Si_1") which alternate throughout the layer appear to contain, respectively, no Al^{IV} and—on the average—$Si_{1/2}$ $Al_{1/2}$. This is shown by the mean bond lengths, $Si_2-O = 1.61_2$ Å and $Si_1-O = 1.69_5$ Å. This ordering of cations means that neither the octahedral nor the surface anions can form fully coplanar networks, nor can both tetrahedra remain perfectly regular in shape—with the smaller (Si_2) tetrahedra showing the greater strains. The whole structure, however, adjusts to the mismatch of tetrahedral sizes—by "waves" in the planes of anions, by the tilting of both tetrahedra, and by the elongation of Si_2 groups along c^* with a very slight flattening of Si_1 groups. This elongation is shown by the basal edges around Si_2, compressed to 2.58_2, 2.58_8 and 2.59_1 Å, together with the $Si—O_{apex}$ bond, stretched to 1.64_8 Å; by contrast the six O—O edges around Si_2 are normal contact distances, mean 2.76_9 Å. The angles at Si_2 confirm this, with $O_{basal}—Si_2—O_{basal} = 107°22'$ (mean) but $O_{basal}—Si_2—O_{apex} = 111°5'$ (mean).

The disproportionate deformation of Si_2 rather than Si_1 groups is due to the overall control exercised jointly by the octahedral layers and interlayer K^+. Within the tetrahedral layer alone it would seem easier to flatten Si_1 groups a little more and thereby strain Si_2 groups less severely. This would immediately increase b_{tetr}, which the octahedral and interlayer forces totally prevent.

The forces in $2M_1$ muscovite are best discussed by comparing the observed atomic positions with the "ideal" positions of Jackson and West (1933). The configuration of the octahedral layers means that all $O_B—O_B$ shared octahedral edges are (in a projection along the c-axis) parallel to the a-axis, and all $O_A—O_A$ and OH—OH edges are at $\pm 120°$ to this. Moreover the lack of bonds from O_A, O_B and OH towards the vacant octahedral sites allows the anions to be pulled away from their "ideal" positions as the shared edges are shortened. Of the two kinds of apex oxygens each O_A, attached to the larger tetrahedra, can and does move much more freely than each O_B. The shift of O_A is directly away from O_D. The Si_1 groups adjust themselves a little by tilting (see below) and $Si_1—O_A = 1.71$ is slightly longer than $Si_1—O_{C,D,E}$; but the primary deformation is an increase in angle $O_A—Si_1—O_D$ from $109\frac{1}{2}°$ to $115\frac{1}{2}°$ (*i.e.* $O_A—O_D$ up to 2.87 Å), in agreement with the earlier postulates.

Each K^+ is surrounded by six O's at 2.81_2 Å (aver.) and six at 3.39_0 Å (aver.) and 2 OH's at 3.98_4 Å, so that effectively there are direct K—O bonds only to the six nearest oxygens which are approximately octahedrally arranged around it. These oygens can only form bonds of strength $\frac{1}{8}$, since they already have bonds to Si_1 and Si_2 of strength $\frac{7}{8}$ and 1. The sum of the K and O radii is 2.73, given for six-coordination which implies a strength of $\frac{1}{6}$. The expected bondlengths for six bonds of

strength $\frac{1}{8}$ should be close to $2.73 \times 1.04 = 2.84$ Å, where 1.04 is a correction factor for eight-coordination. The mean of 2.81 Å reflects the general compression of these weak bonds (Part I, and this paper) by the rest of the structure.

Each K^+ is hardly shielded at all electrostatically from O_A's, O_B's and OH's, above and below. The O_A's carry an unsatisfied charge of about $-\frac{1}{8}$, and the K^+ of $+2/8$. To a first approximation each K^+ is attracted towards, and its charge largely satisfied by, one O_A from each layer. For K's at the $c/4$ level these attractions give a resultant force which moves each K directly along $+b$; at the $3c/4$ level each K is moved along $-b$. The separate $K—O_A$ attractions through the $2M_1$ cell are in fact disposed just as shown in Fig. 7b, R., and these attractions clearly are the unknown forces postulated by Radoslovich (1960) as a possible "mechanism" for forming the $2M_1$ polymorph, and explaining the observed β.

This net attraction, *e.g.* towards $-b$, makes the $K—O_{C,D,E}$ bonds unsymmetrical. The total arrangement is such that the K is pulled towards an O_D, above and below, and away from an O_E, above and below. Thus $K—O_D = 2.77_5$ Å is really an ideal (weak) bond of 2.83—2.84 Å under compression, and this assists the depression of O_D. By contrast $K—O_E = 2.86_2$ Å is a similar bond under tension; O_E is restrained by $Si_2—O_E = 1.62_3$ Å ($Si_2—O_D = 1.59_6$ and $Si_2—O_C = 1.58_1$) and ultimately by the bonds from Si_2 through O_B to the Al network. The tension in $K—O_E$ and $Si—O_E$ explains why the Si_2 move a little in the same direction as an associated K.

The attraction and movement of K^+ by O_A compresses the bonds $Si_2—O_C = 1.59_6$ Å and $Si_2—O_D = 1.58_1$ Å for which Smith and Bailey (1962) would predict 1.62 Å. At the same time $Si_2—O_B$ is being severely stretched. This appears to redistribute the bond strengths in the Si_2 tetrahedra a little, so that O_B is left with a slight negative charge to be satisfied by the K^+. This would account for a movement of O_B towards K (even though this *lengthens* the shared octahedral edge $O_B—O_B$), and would correctly explain why one $Al—O_B$ bond (2.04_8 Å) is longer than the other (1.93_2 Å). This movement of O_B raises $O_B—Si_2—O_C$ from $109\frac{1}{2}°$ to $114\frac{1}{2}°$.

The O—H bonds in muscovite, as in dickite, should be directed at an expected inclination of about 65–70° to the sheets. Infrared studies (*e.g.* Serratosa, and Bradley 1958) point to an angle of $\approx 20°$ which is a likely compromise between the directed nature of the O—H bonds and the repulsion of the proton by the K^+ directly above. The shortening of the OH—OH edge further separates the proton from the K^+.

In $2M_1$ muscovite the interlayer K^+ is held in place by six bonds under compression, on the average. In detail, the K^+ occupies an

equilibrium position determined by a complex balanced system of interlocking strong bonds reaching right through the adjacent layers to K's at the next level, above and below. This system of bonds is a direct consequence of $2M_1$ muscovite being a dioctahedral mineral with 2 Al^{3+} octahedrally, and with an ordered arrangement of 2 Si and 2 $Si_{1/2}$ $Al_{1/2}$ tetrahedrally. It is hardly surprising that this polymorph is one of the most stable micas under natural weathering. This view of the role of K^+ in muscovite is far removed from the early concepts of an ion of the right charge flopping into a hole of comfortable size!

These two accurate structures illustrate in detail the factors previously discussed as general postulates.

Layer Silicate Structures Less Precisely Described

For several published structures the tables of bond lengths and angles are incomplete, or the accuracy is low, and only a brief comment is warranted in support of these ideas.

Vermiculite, $(Mg_{2.36}Fe^{3+}{}_{0.48}Al_{0.16})(Al_{1.28}Si_{2.72})O_{10}(OH)_2 \cdot 4.32\ H_2O$. Since Mathieson and Walker (1954) and Mathieson (1958) were primarily interested in the interlayer water they did not look for octahedral ordering or compute all individual bond lengths within the layers. The structure shows several anomalies. The T—O bonds are 1.63 ± 0.02 Å, whereas Smith and Bailey (1962) would have predicted 1.67 Å; such a discrepancy may possibly mean that the actual crystal has a composition differing from the bulk analysis. The octahedral layers are thin (*i.e.* stretched) but the shared edges are not short, 2.76 Å. The angles O_{apex}—T—$O_{basal} = 108°42'$ (mean) and the *b*-axis is longer than $b = 9.18$ Å for phlogopite K Mg_3 Si_3 Al O_{10} $(OH)_2$. Note the error in *b* for vermiculite, which is more nearly 9.26 Å, Part II.

These apparent contradictions are removed by applying the concepts in the earlier section and by noting that (a) the net tetrahedral charge is divided between octahedral and intercalated ions, and (b) "direct electrostatic interaction between cations and surface oxygens is unimportant" (Mathieson and Walker, 1954, p. 254). It is then reasonable that:

(i) T—O_{basal} bonds have excess strength and are noticeably shortened because their surface charge is not satisfied by *direct* bonds, as in micas. But O_{apex} should contribute excess charge to the octahedral bonds, if anything, and T—$O_{apex} = 1.67 \pm 0.01$ is nearer prediction.

(ii) All surface oxygens mutually repel each other because of their net negative charge. This explains why O_{apex}—T—$O_{basal} = 108°42'$ ($< 109\frac{1}{2}°$). Moreover this repulsion will tend to untwist the surface ditrigonal network, so that the substitution of Al^{IV}—for—Si increases *b* in vermiculites—but *not* because of the larger radius of Al^{IV}! The

shortening of T—O and decrease of τ to 108°42′ gives an $\alpha_{calc}=4°42'$, *c.f.* $\alpha_{obs.}=5\frac{1}{2}°$ and $\alpha_{calc.}=8°42'$ (Part II). The lack of K—O bonds allows (ii) to increase b for vermiculite to values $>b$ for phlogopite, even though the octahedral cations would suggest the reverse.

(ii) The apex oxygens carry a net negative charge which should shorten the bonds to the octahedral cations and prevent the shortening of shared edges; the latter is observed. The bonds have a length of 2.07 Å against an expected 2.05 Å, so that any shortening is balanced by an overall stretching from the tetrahedral layers.

Celadonite, $K_{0.8}(Mg_{0.7}Fe_{1.4}{}^{3+})(Al_{0.4}Si_{3.6})O_{10}(OH)_2$ (*Zviagin, 1957*). The key to this unusual structure is found in the fact that about half the $K_{0.8}{}^{+}$ charge is satisfied tetrahedrally and half octahedrally. The observed K—O bondlengths (Fig. 7, Z.) show that these bonds are (at 2.78 Å, mean) under compression due to the strong negative charge on the octahedral layer. The tetrahedra confirm this by being flattened (to $\tau=107°0'$) to a limit set by the limited expansion possible in the octahedral layer. Thus the T—O_{basal} bonds are strongly compressed and—as for Si_2 groups in muscovite—this appears to redistribute the tetrahedral charge to contract T—O_{basal} to 1.60–1.61 Å and lengthen T—O_{apex} to 1.71 Å, both from an expected 1.63–1.64 Å.

The apex oxygens carry the large net octahedral charge, plus a further charge due to this redistribution, all satisfied by the distant interlayer K^+. They therefore mutually repel each other strongly, so that shared edges are lengthened to about 3 Å and the octahedral layer is very thick, 2.48 Å (against 2.12 Å). (The distribution of charges on apex oxygens also ensures that celadonite is a 1M polymorph with $\beta_{obs}=\beta_{ideal}$). In agreement with previous sections the octahedral cations fill two out of three sites and leave only 0.1 Mg in the third site.

The final structure is an equilibrium between the strong O—O repulsion octahedrally, the stretched (Mg, Fe)—O bonds octahedrally (mean of 2.11 Å, against an expected 2.05 Å), the compressed and flattened tetrahedra, and the strong K—O_{apex} attraction. The result is a structure with three regular octahedra, one empty, with an abnormally thick octahedral layer, and with an otherwise unexpected interlayer separation and ditrigonal surface (Part I).

Xanthophyllite, $Ca(Mg_2Al)(SiAl_3)O_{10}(OH)_2$. Each Ca is six-coordinated with surface oxygens (Takéuchi and Sadanaga, 1959) and its charge is fully satisfied by them. The observed Ca—O bonds = 2.38 Å, very close to an expected 2.39 Å. This means that the real bond strength of T—O_{basal} is 0.843 instead of 0.813 and it is understood that these bonds are tending to be a little shorter than ideal in the refinement now in progress.

Lepidolites. No structural information is available but the fact that the

charge resides octahedrally should give comparable structural effects to celadonites. The short *b*-axis and apparently large interlayer separation have already been noted (Part I).

Kaolinite (*Zviagin, 1960*; *Drits and Kashaev, 1960*). These analyses are admittedly imprecise, especially when compared with the more crystalline polymorph, dickite. The results show comparable features to dickite, *e.g.* (a) shorten shared octahedral edges and counter-rotations of octahedral triads (*viz.* $+3°$, $-5°$; $+6.5°$, $-4°$), (b) O—H—O bonds of about 3 Å, (c) shortened Al—$OH_{surface}$ bonds, and (d) one OH raised out of surface. Some contrasts may be highly significant, when related to the directed interlayer bonds discussed for dickite. Thus the *c*-axis is bigger and the *b*-axis is smaller than in dickite, and the surface oxygen is *elevated* from the layer, not depressed into it. The accuracy of the kaolinite analyses do not justify further discussion of these interesting observations here.

Amesite (Mg_2Al)($Si\ Al$) O_5 $(OH)_4$ (*Steinfink and Brunton, 1956*). This kaolin-type mineral has excess charge on the octahedral cations, which results in longer T—O_{apex} bonds ($=1.71\pm0.03$ Å) and shorter T—O_{basal} bonds ($=1.67\pm0.02$ Å). These latter account for an observed $\alpha=11\frac{1}{2}°$ but a calculated $\alpha=16°$ (Part II).

Trioctahedral micas. No structures have been published, but the *b*-axis of phlogopite ($=9.22$ Å) versus brucite ($=9.44$ Å) shows how the K—O bonds act to inhibit the octahedral expansion. Bassett (1960) has proposed a repulsion of K^+ by the vertically directed OH proton in phlogopite. The smaller $b=9.188$ and smaller thickness of fluorophlogopite (with d (003) = 3.329 against 3.387 in phlogopite) are consistent with this. In phlogopite such a repulsion would increase *c*, and also shorten OH—OH shared edges, *i.e.* increase *b*.

Chlorites. Although these concepts should apply in full to chlorite structures it seems wise to await a really accurate analysis, in view of the complications caused by the additional octahedral layers.

Montmorillonite group. No structural data are available but some observations connected with Part II are pertinent. Thus the octahedral layers of saponites and hectorites can certainly conform to the smaller dimensions set by their tetrahedral layers, especially since only Mg^{2+}—Mg^{2+} repulsion is involved.

Beidellites and nontronites are unique amongst this group in that their

cation exchange capacity originates from tetrahedral substitutions almost entirely. That is, the surface oxygens themselves carry most of the net negative charge for these layers. In both cases there should be a comparable surface O—O repulsion to that postulated for vermiculite; and it is very interesting that these montmorillonites appear to have anomalous and high values for *b* (Table 7A, Part II). It is also notable that there appears to be a complete series between nontronites and beidellites (MacEwan, 1961) whereas nontronites and montmorillonites have separate composition fields (*e.g.* Radoslovich, 1963a).

Other Structures

The general concepts of this paper should apply to other minerals than layer lattice silicates, and they were therefore tested against a few comparable structures, as recorded very briefly below.

Lithiophorite (*Al, Li*) MnO_2 $(OH)_2$ (*Wadsley, 1952*). Although O—H——O bonds undoubtedly exist between the two octahedral layers they are not, as Wadsley suggested, the classical hydroxyl bonds of Bernal and Megaw (1935) between two OH's. In the Al, Li layer the $(Al_{0.68}\ Li_{0.32})$—OH bond strength is ideally 0.393, and predicted bondlength therefore 1.966, compared with observed bonds of 1.93 and 1.95 Å. In the Mn layer the ideal $(Mn_{0.17}{}^{2+}\ Mn_{0.82}{}^{4+})$—O bond strength is 0.603, giving a predicted 1.96 Å against an observed 1.93 and 1.97 Å. Moreover the hydroxyls can be fairly readily polarized, and hence 1.93 and 1.95 are both <1.966 Å. It is simply this polarization of the hydroxyls (*c.f.* dickite) which sets up O—H——O bonds of 2.76 Å between the layers. The bond strengths are too low $(0.39<\frac{1}{2})$ to tetrahedrally polarize the OH's, and the matching surface is an oxygen, not an hydroxyl surface, as in gibbsite.

Sanbornite, *Ba* Si_2O_5 (*Douglass, 1958*). The four different Si—O bondlengths are directly related to the Ba—O bonds and the Si—Si repulsion across shared tetrahedral edges. Each O_I, O_{II} and O_{II} has one Ba—O bond of strength about $\frac{2}{9}$ and therefore two Si—O bonds of strength $\frac{8}{9}$. Each O_{III} has three Ba—O bonds of strength $\frac{2}{9}$ each and hence one Si—O_{III} bond of strength $\frac{1}{9}^2$. Hence Si—$O_{III}=1.60$, *i.e.* less than an expected 1.62–1.63 Å, and Si—$O_{II}=1.64$ and 1.65, greater than 1.62–1.63. The combined Si—Si repulsion and Si—O_{III} attraction act together to stretch still further the weakened Si—O_I bonds and these are even greater than Si—O_{II}, *viz.* 1.68 Å.

Cummingtonite $(Mg_{4.05}\ Fe_{2.50}\ Mn_{0.17}\ Ca_{0.35})(Si_{7.9}\ Al_{0.1})O_{22}\ (OH)_2$. It is unnecessary to invoke a rather unlikely covalent Fe^{2+}—O bonding as

proposed by Ghose (1961) to explain the short bond of 2.04 Å between M_4—O_4 (Fig. 1, G.) The bond strengths from O_4 are about 1.0 to Si_2, $\frac{1}{6}$ to M_2, and hence $\frac{5}{6}$ to M_4 which is $Fe_{0.75}^{2+}$ $Mg_{0.25}$. The expected length for an $(Fe_{0.75}^{2+}$ $Mg_{0.25})$—O bond of strength $\frac{5}{6}$ is around 2.02 Å, close to the observed 2.04 Å. This distribution of bond strengths is the reason for the high proportion of Fe^{2+} in this site. If M_4 were occupied by Mg entirely for example, then these strong bonds would bring oxygens in neighbouring chains much closer together than 2.97 Å, and this is not tolerable.

These three examples help to confirm the general application of the present concepts, and suggest that a more critical look at bond strengths and lengths in accurate structure analyses of complex ionic minerals often would be profitable.

In this connection the structure of tilleyite (Smith, 1953) appears markedly to disobey Pauling's Valency Rule if due allowance is made for the totally covalent nature of the bonds in the carbonate radical (e.g. Wells, 1962). Perhaps this is to be expected for ionic structures containing such radicals, however.

Discussion of Consequences of Theory

It must be re-emphasised that, although the present concepts appear to be applicable with marked success to published data, it is most desirable that they be tested against further precisely determined structures as soon as possible. Any implications in other studies on clay minerals should be viewed with considerable reservations at present. Nevertheless some of these will be of wide interest.

It follows from the "cation avoidance rule" (above) that octahedral cations will tend to be largely ordered, in the way that Veitch and Radoslovich have sought to establish (Part III). Likewise the geometrical model adopted in that analysis is fully consistent with present theories about the actual structures—at least in as much as it is a geometrical model. The varying role of the interlayer cations, and the various restraints on the *b*-axis expansion (Parts I, II, III) also are fully consistent with present hypotheses. In particular the positive regression coefficient for Al^{IV} for montmorillonites is now thought to be understood, and is not due simply to the larger radius of Al^{IV} than Si. From Table 7A, Part II it is seen by comparing b_{obs} and b_{kaolin} that the coefficient for Al^{IV} has gained most weight from the beidellite, nontronite and vermiculite samples. In each of these minerals the tetrahedral location of the charge results in an expansion of the sheets, and is of course proportional to the Al—for—Si substitution. On this basis the coefficient for Al^{IV} is real but is of quite different origin from the other coefficients.

Problems of mica stability under weathering are so complex that they

must await some trioctahedral mica structures, but at least the position of K^+ in muscovite (the most resistant mica) is now seen to be unique in several significant ways.

The discussion of $2M_1$ muscovite has clearly linked that polymorph and its "distorted" structure with asymmetric forces between the K^+ and the apex oxygens, and also with the distribution of octahedral cations. The writer has already guessed at similar forces distributed rather differently which appear to control the formation of other mica polymorphs generally, and this subject is at present under more intensive study.

Acknowledgments

This work would never have been undertaken without the stimulus, encouragement and cooperation of Mr. L. G. Veitch, Division of Mathematical Statistics, C.S.I.R.O., Adelaide, to whom much thanks are due. Discussions with Dr. J. B. Jones, Geology Dept., University of Adelaide, have also been helpful. Drs. J. V. Smith and S. W. Bailey have very kindly loaned me an advance copy of their paper.

References

Andersson, Sten and A. D. Wadsley (1962) The structures of $Na_2Ti_6O_{13}$ and $Rb_2Ti_6O_{13}$ and the alkali metal titanates. *Acta Cryst.* **15,** 194.

Bassett, W. A. (1960) Role of hydroxyl orientation in mica alteration. *Bull. Geol. Soc. Amer.* **71,** 449.

Bernal, J. D. and H. D. Megaw (1935) The function of hydrogen in intermolecular forces. *Proc. Roy. Soc. London,* **A151,** 384.

Bragg, W. L. (1937) *Atomic Structure of Minerals,* Cornell University Press.

Brindley, G. W. and M. Nakahira (1958) Further consideration of the crystal structure of kaolinite. *Mineral. Mag.* **31,** 781.

Buerger, M. J. (1961) Polymorphism and phase transformations. *Fort. Mineral.* **39,** 9.

Burnham, Charles W. and M. J. Buerger (1961) Refinement of the crystal structure of andalusite. *Zeit. Krist.* **115,** 269.

Busing, W. R. and Henri A. Levy (1958) A single crystal neutron diffraction study of diaspore, Al O(OH). *Acta Cryst.* **11,** 798.

Donnay, Gabrielle, J. Wyart and G. Sabatier (1959) Structural mechanism of thermal and compositional transformations in silicates. *Zeit. Krist.* **112,** 161.

Douglass, Robert M. (1958) The crystal structure of sanbornite $BaSi_2O_5$. *Am. Mineral.* **43,** 517.

Drits, V. A. and A. A. Kashaev (1960) An *x*-ray study of a single crystal of kaolinite. *Kristallografiya* (in transl.), **5,** 207.

Ferguson, R. B., R. J. Traill and W. H. Taylor (1959) Charge balance and the stability of alkali felspars, a discussion. *Acta Cryst.* **12,** 716.

Ghose, Subrata (1961), The crystal structure of a cummingtonite. *Acta Cryst.* **14,** 622.

Harrison, F. W. and G. W. Brindley (1957) The crystal structure of chloritoid. *Acta Cryst.* **10,** 77.

Jackson, W. W. and J. West (1933) The crystal structure of muscovite—$KAl_2(AlSi_3)O_{10}(OH)_2$. *Zeit. Krist.* **85,** 160.

Jones, John B. and W. H. Taylor (1961) The structure of orthoclase. *Acta Cryst.* **14,** 443.

Liebau, von Friedrich (1961) Untersuchungen über die Grösse des Si—O—Si Valenzwinkels. *Acta Cryst.*, **14,** 1103.

MacEwan, D. M. C. (1961), p. 158 in *The X-ray Identification and Crystal Structures of Clay Minerals* 2nd ed., Min. Soc., London.

Mathieson, A. McL. (1958) Mg-Vermiculite, a refinement and re-examination of the crystal structure of the 14.36 Å phase. *Am. Mineral.* **43,** 216.

——— and G. F. Walker (1954) Crystal structure of magnesium-vermiculite. *Am. Mineral.* **39,** 231.

——— E. W. Radoslovich and G. F. Walker (1959) Accuracy in structure analysis of layer silicates. *Acta Cryst.* **12,** 937.

Megaw, H. D. (1934) The crystal structure of hydrargillite, $Al(OH)_3$. *Zeit. Krist.* **87,** 185.

——— C. J. E. Kempster and E. W. Radoslovich (1962) The structure of anorthite, $CaAl_2Si_2O_8$, II, Description and discussion. *Acta Cryst.* in press.

Newnham, Robert E. (1961) A refinement of the dickite structure and some remarks on polymorphism in kaolin minerals. *Mineral. Mag.* **32,** 683.

Pauling, Linus B. (1960) *Nature of the Chemical Bond,* Cornell University Press.

Petch, H. E., N. Sheppard and H. D. Megaw (1956) The infra-red spectrum of afwillite, $Ca_3(SiO_3OH)_2 \cdot 2H_2O$, in relation to the proposed hydrogen positions. *Acta Cryst.* **9,** 29.

Radoslovich, E. W. (1960) The structure of muscovite, $KAl_2(Si_3Al)O_{10}(OH)_2$. *Acta Cryst.* **13,** 919.

——— (1962a) The cell dimensions and symmetry of layer lattice silicates, II. Regression relations. *Am. Mineral.* **47,** 617.

——— (1962b) Cell dimensions and interatomic forces in layer lattice silicates. *Nature,* in press.

——— (1963a) The cell dimensions and symmetry of layer lattice silicates, V. Composition limits. *Am. Mineral.,* in press.

——— (1963b) The cell dimensions and symmetry of layer lattice silicates, VI. Serpentine and kaolin morphology. *Am. Mineral.,* in press.

——— and John B. Jones (1961) Transparent packing models of layer-lattice silicates based on the observed structure of muscovite. *Clay Min. Bull.* **4,** 318.

——— and K. Norrish (1962) The cell dimensions and symmetry of layer lattice silicates, I. Some structural considerations. *Am. Mineral.,* **47,** 599.

Serratosa, J. M. and F. W. Bradley (1958) Determination of the orientation of OH bond axes in layer silicates by infrared absorption. *Jour. Phys. Chem.* **62,** 1164.

Smith, J. V. (1953) The crystal structure of tilleyite. *Acta Cryst.* **6,** 9.

——— (1954) A review of the Al—O and Si—O distances. *Acta Cryst.* **7,** 479.

——— and S. W. Bailey (1962) Second review of Al—O and Si—O tetrahedral distances. *Acta Cryst.* in press.

Steinfink, Hugo and George Brunton (1956) The crystal structure of amesite. *Acta Cryst.* **9,** 487.

Takéuchi, Y. and R. Sadanaga (1959) The crystal structure of xanthophyllite. *Acta Cryst.* **12,** 945.

Veitch, L. G. and E. W. Radoslovich (1962) The cell dimensions and symmetry of layer lattice silicates, III. Octahedral ordering. *Am. Mineral.,* **48,** 62.

Verhoogen, John (1958) Physical properties and bond type in Mg—Al oxides and silicates. *Am. Mineral.* **43,** 552.

Wadsley, A. D. (1952) The structure of lithiophorite, $(Al_1Li)MnO_2(OH)_2$. *Acta Cryst.* **5,** 676.

Wells, A. F. (1962) *Structural Inorganic Chemistry,* Claredon Press, Oxford.

Zviagin, B. B. (1957) Determination of the structure of celadonite by electron diffraction. *Kristallografiya* (in translation), **2,** 388.

——— (1960) Electron diffraction determination of the structure of kaolinite. *Kristallografiya* (in translation), **5,** 32.

Manuscript received, July 27, 1962; accepted for publication, October 12, 1962.

THE CELL DIMENSIONS AND SYMMETRY OF LAYER-LATTICE SILICATES. V. COMPOSITION LIMITS

BY

E. W. RADOSLOVICH

Reprinted from American Mineralogist, 48:
Pages 348-367
(1963)

THE AMERICAN MINERALOGIST, VOL. 48, MARCH–APRIL, 1963

THE CELL DIMENSIONS AND SYMMETRY OF LAYER-LATTICE SILICATES. V. COMPOSITION LIMITS

E. W. RADOSLOVICH, *Division of Soils, Commonwealth Scientific and Industrial Research Organisation, Adelaide, Australia.*

ABSTRACT

The reported limits of stability (from synthesis studies) and also the observed ranges of compositions for natural specimens may be used as independent checks on the validity of current theoretical models of these structures. These models (Parts I–IV) allow broad limits to be set to the strains from preferred lengths and shapes which different structural components (bonds, polyhedral groups) can reasonably tolerate in adjusting to some local dimensional misfit. The formation of micas in which such strains should far exceed these limits should not be possible, even in the laboratory. Micas in which the strains would need to be unusually large may be expected to adjust their compositions rapidly, as soon as their environment allowed any change. They may therefore be synthesized but should—for at least this reason—be rare as natural specimens. It is not yet possible, of course, to predict precise composition limits for micas on structural grounds.

An examination of the detailed published composition limits for micas shows that the present structural models are not at all incompatible with these, nor is there any discrepancy with the rather less well defined limits of other layer silicates.

INTRODUCTION

A preliminary attempt has been made to relate recent theoretical models of structures of the layer silicates[1] to their reported limits of chemical composition. Although at this stage several severe restrictions must be observed it is still useful to review the structural concepts in relation to observed limits of composition for at least two reasons. Firstly, if the structural concepts are essentially correct then no minerals (natural or synthetic) should be found for which the internal stresses would appear to be totally incompatible with even a metastable existence at room temperature. The observance of such a "forbidden" structure would require re-appraisal of the structure models. Secondly, it now seems possible to suggest at what compositions the internal stresses and strains (due to increasing misfit within these structures) should start to become large. It seems reasonable to assume that minerals existing metastably but with very large internal stresses would undergo some change as soon as any factor in the local environment becomes at all conducive to change. That is, the probability of such minerals being found naturally should be small for this reason alone, in addition to any other controlling factors. Natural composition limits (*e.g.* those of Foster 1956, 1960 a, b, c) are not likely to include minerals for which large internal stresses would be predicted structurally. Again this is mainly a test of the compatibility of

[1] Discussed in Parts I–IV, *i.e.* Radoslovich and Norrish (1962), Radoslovich (1962a), Veitch and Radoslovich (1962), and Radoslovich (1962b).

present structural concepts with observed composition limits. There may, however, be some instance where there is no other acceptable explanation for an observed restriction of composition, and the suggested structural restraint then merits further study.

Since the studies defining composition limits have been of at least two distinct kinds it is necessary to set certain restrictions on the present discussion.

Foster (1956; 1960 a, b, c) has very carefully assessed the probable composition limits for naturally occurring micas from a critical review of published chemical analyses, essentially of specimens found by geologists exploring the earth's surface. Nothing is thereby implied about the possibilities for forming micas of more extreme composition either in the laboratory or in some quite unusual geological environment. The observed limits of natural micas include those imposed by the requirements that a given mica must exist at least metastably under near surface conditions (*e.g.* of temperature, pressure and chemical environment) for a sufficient period after formation, so that there can be a small but real probability of a specimen being found somewhere.

Yoder (1959) and others have, as an entirely different approach, studied experimentally the stability fields for the layer silicates for varying temperatures, pressures, known melt compositions and other parameters. Such laboratory studies not only define the appropriate stability fields, but also confirm that many layer silicates formed stably at elevated temperatures and pressures can be quenched and retained for indefinite periods metastably at atmospheric conditions. However, the stability fields of natural micas are probably more restricted, because more elements are available under geologic conditions (allowing alternative minerals to crystallize) and because the natural abundance of the elements may not be favorable for the formation of certain micas. Furthermore their formation temperatures and pressures may differ considerably from those at which the experimental studies have been made, *e. g.* by having a smaller range.

Any discussion of observed composition limits in relation to structural ideas must therefore take note of the nature of those reported limits. Moreover, there may well be no direct relation between structure and composition limits in many cases. For example a mica of a certain unusual composition may never be found naturally simply because nature never provides the right physical and chemical conditions of formation. Again, such a mica may not persist metastably at normal temperatures even though natural conditions have existed suitable for its formation; or if it persisted through quenching then it may break down extremely rapidly for physico-chemical rather than specifically structural reasons.

It is equally difficult to use the available structural data to predict an acceptable stability field for some unusual theoretical mica. Even if the available structure analyses permit sensible estimates of the internal stresses such a mineral would have at room temperature they do not allow satisfactory extrapolation of these estimates to the conditions of rock formation. There are virtually no direct studies of the variation of given bondlengths with temperature, except unpublished data by Young (1962) which show—within the moderate errors involved—no significant change in the Si-O bonds in quartz up to 600° C.

From the empirical study (Part IV) of various interatomic forces in the layer silicates it seems that micas should be rare whose compositions would contravene one or more of the following restraints.

(1) In the interlayer region structural adjustments should be possible which allow each cation to approach approximately to within contact distance (sum of ionic radii for the requisite coordination) with at least six surface oxygens (Part I). Also, two interlayer cations which would strongly influence the layers of a structure in opposing directions are unlikely to be found together in one mineral; the local strains would be too severe.

(2) For the tetrahedral layers there are limits to the stretching (in their own plane) which may be imposed by the rest of the structure. Any such stretching should not require the basal oxygens to approach intolerably close (aver. O-O not less than 2.55 Å) to the apex oxygens along tetrahedral edges.[1]

(3) For the octahedral layers there are limits both of dimensions and (probably) of arrangement. Such layers tend to be as large in the *a-b* plane as the shortening of shared octahedral edges to about 2.35 Å (with some slight lengthening of bonds) will allow (Part IV), but can be no larger. Conversely a contraction can be imposed on the *a-b* dimensions of octahedral layers, by lengthening shared edges, giving a closer approach of octahedral cations. Clearly the mutual repulsion of the cations will rise rapidly as they come closer together, especially since the intervening (and partially shielding) anions must move apart along shared edges at the same time. Thus any contraction which a given octahedral layer must undergo to fit into some hypothetical structure will be effectively limited by this increasing cation-cation repulsion.

The apparently general tendency towards the ordering of octahedral cations of different valency and size (Parts III and IV) implies further possible structural restraints on composition limits.

[1] This is discussed further in Part VI (Radoslovich, 1962c).

Foster's studies (1956, 1960a, b, c), which also summarize much other work, have shown that the layer compositions of micas are best discussed under the following headings:

Dioctahedral micas: muscovites, celadonites.
Trioctahedral micas: phlogopites, biotites, siderophyllites
Lithium micas: lithium muscovites, lepidolites, siderophyllites

Some Observed Composition Limits

Muscovite-paragonite. Eugster and Yoder (1955) studied the stability limits of solid solution between muscovite and paragonite. Their preliminary phase diagram for the subsolidus region of this join shows very limited solid solution at normal temperatures (about 3% paragonite in muscovite and vice versa) with a steady rise in solid solution with temperature. These results appear to be explained by the very different situation of K in muscovite and Na in paragonite (Parts I and IV). In $2M_1$ muscovite the K actively increases the sheet dimensions which the octahedral layers would otherwise adopt, and also props successive layers far apart. The average twist tetrahedrally is 13.7° and half the tetrahedra are forced to be elongated along c^*. In paragonite Na should affect neither the b nor c dimensions, but possibly causes a flattening of tetrahedra along c^*, along with rotations of about $19\frac{1}{2}°$. Opposing tetrahedral surfaces (of oxygen) also should be in contact.

If isolated Na ions are made to replace K in muscovite then the larger b-axis (8.995 Å) will require further tetrahedral flattening and rotation around these Na ions beyond that predicted for paragonite ($b=8.90$ Å). The difference in layer separation ($\eta=3.37$ Å observed for muscovite and $\eta=2.6$ Å predicted for paragonite, Part I) is especially important here. That is, the local strains and stresses around "impurity" Na ions would appear to be extremely severe; and excess of Na during muscovite formation should certainly lead to a mixture containing some paragonite. Likewise the amount of, say, Na tolerated by muscovite would be expected to rise with temperature as the increased thermal motions allow the muscovite structure to accommodate local strains more readily.

Sodium micas. Sodium analogues of the trioctahedral micas are not compatible with the proposed restraints. The most favorable hypothetical case in Na-phlogopite. If we allow the octahedral layer (which is 9.4 Å in brucite, Part IV) to be as short as 9.1 Å it is still impossible to establish six Na-O distances under 2.5 Å. To do so would require grossly flattened tetrahedra (τ about 99°, well below the limit of 106°, Part II) and a high rotation, α, of 22°.

Similar calculations show that in any hypothetical Na-lepidolite the weak Na-O bonds must grossly distort the tetrahedra (*i.e.* aver. $\tau<106°$)

and also contract the octahedral layers to some value below b = 8.8 Å. Even if such a structure could be synthesized it should be very rare naturally.

On the other hand the additional Al^{IV} in ephesite, $Na_{1.11}Ca_{0.10}$ $(Al_{1.90} \cdot Fe_{0.026}^{3+}Li_{0.40}Mg_{0.40}Mg_{0.04}Mg_{0.04}Fe_{0.02}'')(Si_{1.95}Al_{2.05})O_{0.63}(OH)_{2.34}F_{0.04}$ taken with the short b axis set by the dioctahedral layer ensures a high rotation ($\alpha = 21°36'$, Part I) which permits the appropriate Na-O contacts. This rare brittle mica, together with paragonite, seem to represent the only reasonable Na-mica compositions from a structural viewpoint.

Turning to the potassium trioctahedral micas, Foster (1960b) has critically examined the published analyses of more than 200 natural specimens, drawing detailed conclusions about their observed composition limits. Her results are summarized in Fig. 1, the two main areas of which are discussed below.

Trioctahedral micas very high in Fe^{2+}. The absence of such micas naturally is at least compatible with the marked contraction required in their octahedral layers. For example annite, $K\,Fe_3^{2+}(Si_3Al)O_{10}(OH)_2$ has not been observed naturally (Foster, 1960b) but has been studied extensively as a synthetic product (Eugster and Wones, 1962). It can, of course, only be assumed that annites synthesized in the presence of iron oxide at con-

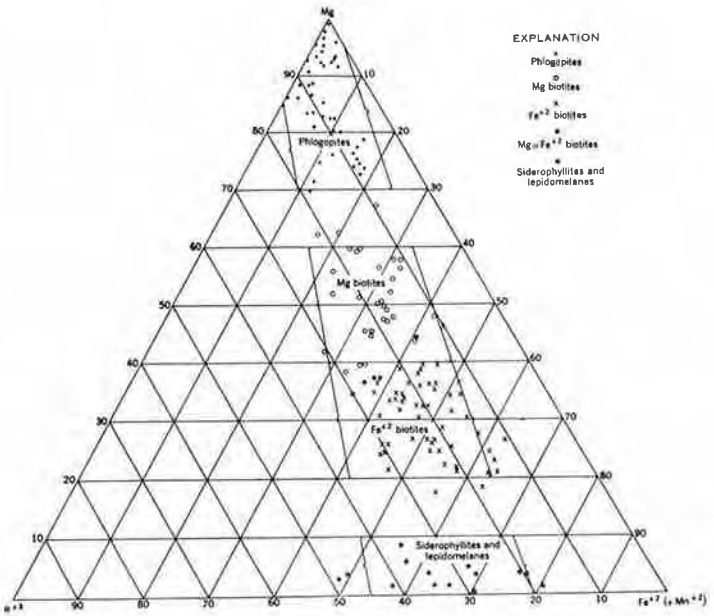

FIG. 1. Relation between Mg, Fe^{2+} (Mn^{2+}) and R^{3+} (Al, Fe^{3+} and Ti) in trioctahedral micas, from Foster (1960b).

ditions of high hydrogen fugacity represent a close approach to the ideal formula. Assuming also that the kaolin regression relation gives a usable estimate of the "unconstrained" octahedral dimensions (Parts II to IV) then b_{oct} is around 9.6 Å. The required contraction to b_{obs} (= 9.348 Å) is then quite large. Moreover, with $b_{tetr} = 9.31$ Å the tetrahedral layer must expand and rotate to establish K-O contact distances (≈ 2.8 Å); the estimated average O-Si-O angle $\tau = 107°10'$ and rotation $\alpha = 8°6'$ (Part I).

The analogue, ferri-annite, K Fe_3^{2+} $(Si_3Fe^{3+})O_{10}(OH)_2$ has also been synthesized, and cell dimensions determined by Donnay and Kingman (1958). This, too, should have flattened and slightly rotated tetrahedra, with τ about $107\frac{1}{2}°$ and $\alpha = 8°$, if K-O bonds around 2.8 Å are to be established.[1] In both these synthetic high Fe^{2+} micas the tetrahedra and octahedra must be severely distorted from their *preferred* shapes in layer structures, in order to fit together with each other and with the desired interlayer distances. Under most natural conditions a little Al, Fe^{3+} or Mg will be available, and it seems very likely that smaller cations such as these will enter the octahedral sites also, rather than Fe^{2+} cations alone, giving the naturally occurring siderophyllites, lepidomelanes and high iron biotites. Very little unit cell data are available on such minerals, but the regression relations (Parts I, II) may be used to estimate roughly the tetrahedral and octahedral distortions required to assemble such micas allowing six K-O bonds around 2.8 Å. Three specimens for which Foster (1960a) gives explicit structural formulae are particularly high in Fe^{2+}, and for these

	b_{oct}	b_{calc}	b_{tetr}	$b_{oct} - b_{calc}$	τ	α
siderophyllite, no. 132	9.44	9.29	9.31	0.15 Å	$108\frac{1}{2}°$	7°
lepidomelane, no. 126	9.48	9.33	9.32	0.15	$107\frac{1}{2}$	$7\frac{1}{2}$
biotite, no. 36	9.46	9.30	9.37	0.16	$109\frac{1}{2}$	7

where $(b_{oct} - b_{calc})$ is an estimated octahedral contraction, τ measures the tetrahedral flattening (aver. O-Si-O_{apix} angle), and α is the angle of tetrahedral rotation.

For each of these natural high Fe^{2+} micas the (estimated) octahedral contraction from the expected (usual) dimensions should not lead to unduly long shared edges octahedrally. Likewise the predicted tetrahedral adjustments are readily made, especially for the biotites which tend to have > 1.00 Al^{IV} (nearer 1.25 Al^{IV}, Foster, 1960b)—for these a simple tetrahedral rotation is sufficient.

These data obviously allow no rigorous conclusions, but suggest that

[1] The structure analysis in progress (Morimoto and Donnay, 1962) shows a small but definite tetrahedral rotation.

the structural strains will exceed tolerable limits for natural biotites at about those composition limits drawn in the high Fe^{2+} region by Foster (1960b).

Trioctahedral micas high in R^{3+}. Most biotites appear to be 1M polymorphs and presumably belong to space group C2/m (Smith and Yoder, 1956), in which one octahedral site is at a center of symmetry, and the remaining two are symmetry-related. It is believed that under these symmetry conditions for trioctahedral micas the R^{3+} (and R^{4+}) cations tend to substitute into the phlogopite structure mainly in the unique site. This hypothesis of considerable ordering was studied statistically in Part III, and has an acceptable physical basis in terms of interatomic forces (Part IV). If the substitution were $1R^{3+}$ for $1R^{2+}$ and entirely as above then the limit would be clearly 1.00 R^{3+} in the trioctahedral mica structures. In fact, as Foster points out, the charge relations mean that as little as 0.67 R^{3+} substitutes for $1R^{2+}$, and also some R^{3+} will, on the average, be found in the symmetry-related sites. Most biotites high in R^{3+} are therefore likely to be somewhat deficient in all three octahedral sites. Nevertheless Foster (1960 b) has shown conclusively that in the trioctahedral micas the essential upper limit to the number of R^{3+} and R^{4+} cations octahedrally is 1.00 $(R^{3+}+R^{4+})$ per three sites. A strong correlation with cation ordering structurally may reasonably be deduced.

There is, as yet, no direct structural evidence for ordering amongst the octahedral positions of biotites. Takéuchi and Sadanga (1959) have published a preliminary analysis of the xanthophyllite structure (space group $C2/m$) in which they place the $Al_{0.72}$ octahedrally at x, y, $z=0, \frac{1}{2}, \frac{1}{2}$ and the $Mg_{2.18}$ mainly at x, y, $z=\frac{1}{2}$, 0.328, $\frac{1}{2}$ and $\frac{1}{2}$, 0.672, $\frac{1}{2}$.

Foster also showed that the total occupancy octahedrally falls from three to about 2.6[1] as $(R^{3+}+R^{4+})$ rises from zero to one. The lower limit of $(1.6R^{2+}+1.0R^{3+})$ implies, however, that the corresponding trioctahedral mica structures require approximately 0.75 to 0.8 R^{2+} in each of the two symmetry related sites. This lower limit of, say, 0.75 R^{2+} in each related site cannot be predicted structurally, but in view of the necessary balance of forces octahedrally (Part IV) it is at least to be expected that a majority of sites should be occupied in specimens persisting naturally—as Foster has observed.

Muscovite—trioctahedral micas. It is well known that there is very little solid solution of muscovite towards the trioctahedral micas (*e.g.* Foster, 1960 b; Yoder, 1959); muscovite departs only slightly from dioctahedral status, by the addition or substitution of R^{2+} and R^{3+} octahedrally. In

[1] The criticism by Eugster and Wones (1962) implying that the octahedral occupancy is usually nearer 3.0 strengthens the present discussion.

discussing the possible solid solution of muscovite and phlogopite, biotite and siderophyllite the latter minerals impose the conditions that Al^{IV} lies between 1.00–1.50 cations and K between 0.90–1.00 cations per formula unit (Foster, 1960 b). A dioctahedral mica with $Al^{IV} < 1.00$ lies in the muscovite—celadonite join, discussed later. By considering two extreme cases it then becomes clear that the maximum octahedral occupancy in the muscovite structure (excepting Li-muscovite) is effectively <2.2 per three sites.

(1) Suppose that the structure retains 2.00 Al octahedrally but accepts R^{2+} or R^{3+} into the vacant and larger octahedral site. Then to maintain charge balance Al^{IV} increases at the rate of 2n Al^{IV} substituted for 2n Si, for each n R^{+2} added octahedrally; and this is more favorable than the addition of R^{3+}. For example the hypothetical muscovite

$$(Al_2Mg_{0.15})(Si_{2.70}Al_{1.30})O_{10}(OH)_2K_{1.00}$$

is a typical biotite tetrahedrally and in K content; but the additional 0.3 Al^{IV} would unduly strain the muscovite structure as follows. The 0.15 Mg would easily fit into vacant sites without effectively increasing $b = 9.0$ Å. Then $b_{tetr} = 9.38$ Å, $\alpha = 16°24'$ and $\eta = 3.60$ Å (Part I); i.e. the increased tetrahedral dimensions should require successive layers to be far out of contact even beyond the observed muscovite separation, $\eta = 3.37$ Å. The stresses in the interlayer region obviously are becoming critical very rapidly compared with the small increase in octahedral occupancy from 2.00 Al to 2.15 $(Al+R^{2+})$.

(2) The interlayer stresses are not increased if the tetrahedral composition is held constant at Si_3Al and R^{2+} (or less favourably R^{3+}) substitutes for Al chemically. There appears, however, to be a lower limit to the amount of Al^{3+}—or possibly $(Al^{3+}+R^{3+})$—required to maintain a stable muscovite structure. In a survey by the writer of 40 good muscovite analyses in the literature the total number of octahedral cations ranged from 1.9 to 2.2 and the *minimum* number of Al was 1.7 per three sites. Studies on Li-muscovites (below) also suggest a minimum of 1.7 Al octahedrally, for a stable muscovite structure.

It should be noted that in the $2M_1$ muscovite structure (Radoslovich, 1960) the occupied sites are symmetry related and the unoccupied site is crystallographically distinct, $\bar{1}$; and the average Al-O bond is 1.95 Å but the average "radius" of the vacant site is 2.2 Å. These facts support the proposed ordering of octahedral cations (Part III) by which the larger divalent ions (and Li) "substitute" for Al mainly into this distinct site rather than directly into the Al sites. The lower limit of 1.7 Al is equivalent to 85% of the occupied sites retaining Al in a stable muscovite structure, which at least is not surprising when the appropriate forces are considered in detail (Part IV). Below this level of R^{3+} occupancy (or with excessive replacement of Al directly by the larger Fe^{3+}) the muscovite structure is either unstable or open to rapid attack. This is interesting in relation to the similar level of occupancy by R^{2+} ions (about 75%) in the *same* sites, proposed above for trioctahedral micas.

If an effective limit of 1.6 cations octahedrally is accepted for Al (or possibly $Al+Fe^{3+}$) then this implies a maximum of 0.60 R^{2+} to maintain charge balance, and a total of 2.20 cations octahedrally.

These two extremes both lead to the conclusion that muscovites should not exceed approximately 2.20 cations octahedrally; and of course most muscovites will generally be nearer 2.00. The conclusion is still valid for the majority of specimens which simultaneously show some excess Al^{IV} and some deficiency of Al^{VI}. Muscovites therefore can show very little solid solution with the trioctahedral micas.

Muscovite-celadonite. Foster (1956) has studied the structural formulas and charge relations for the complete composition range of natural dioctahedral micas from muscovite, $KAl_2(Si_3Al)O_{10}$ $(OH)_2$ to celadonite, $K(Mg, Fe)Si_4$ $O_{10}(OH)_2$. Throughout this range the layer charge and potassium content remain effectively *constant;* the major change is in the shift of the charge from the tetrahedral to the octahedral layers. This suite of micas also remains strictly dioctahedral.

Yoder and Eugster (1955) have discussed four possible substitution schemes in muscovite, *viz.*

(a) $Si \rightarrow KAl$ (c) $MgSi \rightarrow 2Al$

(b) $(H_3O)^+ \rightarrow K$ (d) $2Mg \rightarrow KAl$

and have plotted (Fig. 2) the observed composition ranges of natural minerals. They point out that (a) is unlikely because "on Morey's evidence a given leaching of K_2O implies a six-fold loss of SiO_2;" and (d) which leads towards the trioctahedral micas is only possible to a limited extent.

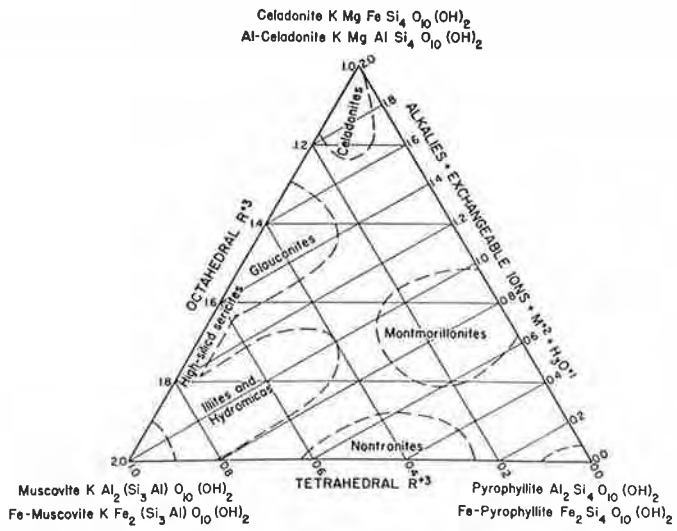

FIG. 2. Plot of tetrahedral R^{3+} and octahedral R^{3+} in atom proportions of dioctahedral micas and related minerals; from Yoder and Eugster (1955).

Yoder and Eugster suggested that some synthetic muscovites lie close to the muscovite-oxonium muscovite join, rather than the muscovite-montmorillonite join (substitution (b)). Substitution (c) leads to high-silica sericites, an observed solid solution effect.

Both of the hypothetical substitution schemes, $Si \rightarrow KAl^{IV}$ and $2Mg \rightarrow KAl^{IV}$, seem unlikely to occur to any extent when the bonding of K in muscovite is considered in detail (Part IV). Both substitutions result in fewer and weaker *direct* bonds between the remaining K and their six *nearest* anions. At the same time the surface anions around unoccupied K sites no longer have their valence charge fully satisfied by immediate bonds, and this should result in some anion-anion repulsion between layers at those sites. That is, although these substitutions preserve overall neutrality they appear to weaken the effective K-O bonds and to induce localised repulsions between layers at unoccupied cation sites. The net effect would seem to be that K-rich regions will hold any incoming K and K-poor regions are more readily able to lose their remaining K. (Such effects are masked in vermiculites because the intercalated ions are surrounded by hydration shells and do not form direct bonds in six-coordination.) The substitutions $Si \rightarrow KAl$ and $2Mg \rightarrow KAl$, which both lead to low-K muscovites, should be of very limited occurrence in unique structures for this reason alone; but the substitution $H_3O^+ \rightarrow K$ should be rather more possible because in this case K^+ is simply replaced by $(H_3O)^+$, with the *same* charge and similar size.

The substitution $MgSi \rightarrow 2Al$ is not of course limited in this way, and high-silica sericites (*i.e.* phengites) are well known. There is a limit to this substitution, however, which will be set by the lower limit of Al^{VI} required for the stable muscovite structure (see above), *viz.*

$$R^{3+}_{1.6}Mg_{0.4}(Si_{3.4}Al_{0.6})O_{10}(OH)_2K_{1.0}.$$

This is in fact a composition on the muscovite-celadonite join at the extreme limit of the high-silica sericites towards glauconites (Fig. 2). In the series of structural formulae quoted by Foster (1956) the Al-dominant micas with the least Al^{IV} are successively:

Phengite	$X_{0.96}(Al_{1.50}Fe^{+3}_{0.15}Fe^{+2}_{0.07}Mg_{0.28})(Si_{3.40}Al_{0.60})O_{10}(OH)_2$
	$K_{0.83}$
Metasericite	$X_{0.92}(Al_{1.45}Fe^{+2}_{0.33}Mg_{0.25})(Si_{3.57}Al_{0.43})O_{10}(OH)_2$
	$K_{0.82}$
Alurgite	$X_{1.01}(Al_{1.28}Fe^{+3}_{0.06}Mn_{0.04}Fe^{+2}_{0.01}Mg_{0.61})(Si_{3.59}Al_{0.41})O_{10}(OH)_2$
	$K_{0.96}$

Whereas phengites are known which have a unique structure it is possible that metasericite may refer only to mixed structures or mixtures, as

Yoder (1959) and Burst (1958) have suggested that the "glauconites" will also prove to be. Heinrich and Levinson (1955) have shown that alurgite may have the 2M or 3T structure, but the only analysis of unquestioned alurgite is very old (Penfield, 1893) and was a made on both uniaxial and biaxial material.

The celadonite structure (Zviagin, 1957) is different in important respects (Part IV) from the muscovite structure, although it is a 1M mica (Foster, 1956) with spacegroup $C2/m$. Zviagin examined a "celadonite" of composition

$$(Fe_{1.4}Mg_{0.7})(Si_{3.6}Al_{0.4})O_{10}(OH)_2K_{0.8}$$

in which the 1.4 Fe is all Fe^{3+} (by implication, to keep the charges balanced). Although the three octahedral sites are of equal size the two related sites contain (1.4 Fe^{3+}+0.6 Mg) and the unique site only 0.1 Mg. If the size of the "hole" available to the octahedral cations was the main factor in controlling their occupancy then for this celadonite an equal distribution of two cations between the three sites of equal size would be expected; this further supports the discussion in Part IV. The cation distribution for Foster's end member celadonite

$$K_{0.98}(Al_{0.07}Fe^{3+}_{0.93}Fe^{2+}_{0.24}Mg_{0.77})Si_{4.00}O_{10}(OH)_2$$

is not known but seems just as likely to include a practically vacant third octahedral site, with the implication that celadonite is stable with only 0.5 Fe^{3+} in the (related) sites.

Foster (1956) has observed that celadonites contain Fe^{3+} rather than Al^{3+}, and indeed the theoretical end member (see Yoder, 1959) K (AlMg) Si_4 O_{10} $(OH)_2$ has not yet been found or synthesized. The unsatisfied charge octahedrally leads to long shared edges in celadonite (Part IV), presumably due to increased anion-anion repulsion. If Al is substituted for Fe^{3+} then the average cation-oxygen bonds are correspondingly shortened, and the octahedral cations brought closer together—in fact unduly close. (A rough estimate suggests that an (Al, Mg) to (Al, Mg) distance of <2.65 Å is required, across a shared edge exceeding 3 Å, giving a large cation-cation repulsion.) The apparent discontinuity in the muscovite—celadonite series of minerals may therefore be due to this shift of charge from tetrahedral to octahedral anions which leads to a need for octahedral bonds to be as long as possible at the celadonite end.

Foster (1956) has discussed the composition range of hydrous micas and "illites," pointing out that "the fact that a rational formula can be derived from an analysis does not guarantee that there is only one mineral present." Yoder and Eugster (1955) and Yoder (1959) also have emphasized that most "illites" are mixtures or mixed-layer structures, which

"can be regarded only as composed of two or more phases." It is now shown that dioctahedral micas near to the muscovite composition cannot be expected to have single *unique* structures if they are K-deficient, except for the replacement, $(H_3O)^+ \rightarrow K^+$. The region "illites and hydromicas" on Fig. 2 must therefore represent mixed structures or mixtures, since a pure $(H_3O)\ Al_2\ (Si_3Al)\ O_{10}(OH)_2$ mica would be plotted coincident with muscovite in this diagram. A "structural compositional diagram" matching Fig. 2 may be drawn tentatively as in Fig. 3, in which the names refer to "structure type" specifically.

This further implies that mixed layer structures with dioctahedral mica layers as components must have the interlayer sites between successive mica layers largely occupied by K. Equally there should be little K between the remaining layers, except as loosely held exchangeable K. Hence it seems desirable to reserve the name "hydromica" for single phase minerals with the three-dimensional muscovite type of structure, in which an approximately 1:1 replacement of K^+ by $(H_3O)^+$ can be shown to have occurred.

Muscovite-lepidolite. Micas with compositions between muscovite and polylithionite have been extensively studied, *e.g.* Stevens (1938), by Levinson (1953) who particularly studied lepidolite polymorphism, and by Foster (1960 c) who has also discussed the relations between structural type and composition.

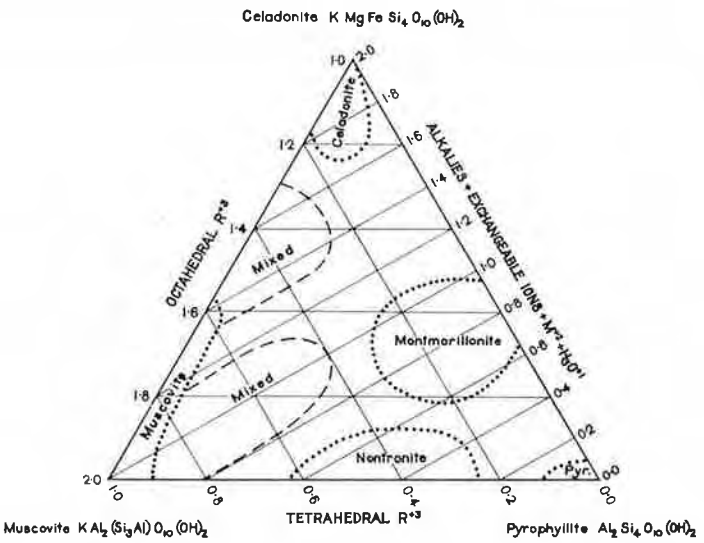

FIG. 3. Same plot as Fig. 2, showing suggested limits for various "structure types."

Foster (1960 c) has considered in detail chemically the ways in which Li can substitute for Al in muscovite, and has set composition limits by examining the structural formulae of 80 naturally-occurring aluminum lithium micas. It has been realized for some time that the trioctahedral lepidolite structures are quite distinct from the dioctahedral muscovite structures. Foster has therefore restated earlier work about their structural composition limits, reaching the conclusion that "both the compositional and structural continuity of the aluminum-lithium series is broken at the point in which change of structure takes place, and the isomorphous series that starts with muscovite extends only to an octahedral occupancy of about 2.45 sites and a Li occupancy just short of 1.00 octahedral site." Levinson (1953) suggested that the maximum Li occupancy compatible with the true muscovite structure is about 3.3% Li_2O, corresponding to about 0.85 Li per three sites. Further Li up to 4.3 % Li_2O (*i.e.* 1.1 Li per three sites) results in the so-called "lithian muscovite" structure.

Lithium can substitute for Al^{VI} in muscovite in all proportions from the simple addition of Li in the vacant site down to a ratio of 1 Li for 1 Al (Foster, 1960 c). Figure 4 shows that natural micas may only slightly exceed the replacement ratio of 3 Li:1 Al^{VI} for specimens low in Li, and otherwise not at all. This is due to the position of K in the muscovite (and presumably in the lepidolite) structure (Part IV). For higher ratios —*e.g.* simple addition of Li in the vacant site—the necessity for charge balance requires that Al^{IV} increases and Si^{IV} decreases. This means greater twists, α, and therefore even greater layer separation, η, than in muscovite; such structures should be readily changed, if they are formed at all.

On the other hand the substitution of Li in natural muscovites would hardly induce a disproportionate decrease in Al^{IV} rather than in Al^{IV} since this would shift the layer charge to the octahedral layer for a mica with essentially the *muscovite* structure. The theoretical mica $K(Al_{1.5}\ Li_{0.5})(Si_4)\ O_{10}\ (OH)_2$, which is the end member for the 1:1 replacement, represents such an unlikely structure leading to high anion-anion repulsion and close cation-cation approach octahedrally. Figure 4 in fact implies that Al^{IV} and Al^{VI} decrease equally (2:1 replacement ratio) or else Al^{IV} decreases by a smaller number of ions than Al^{VI}, *e.g.* a Li: Al^{VI} replacement ratio of 2.5:1. This keeps the layer charge largely tetrahedral which is very reasonable structurally for the muscovite arrangement of octahedral cations.

It was suggested above that the muscovite structure required about 0.8 Al in two sites. It is probable that such a muscovite could accept, on the average, a further 0.8–0.9 Li in the larger vacant site; and this leads

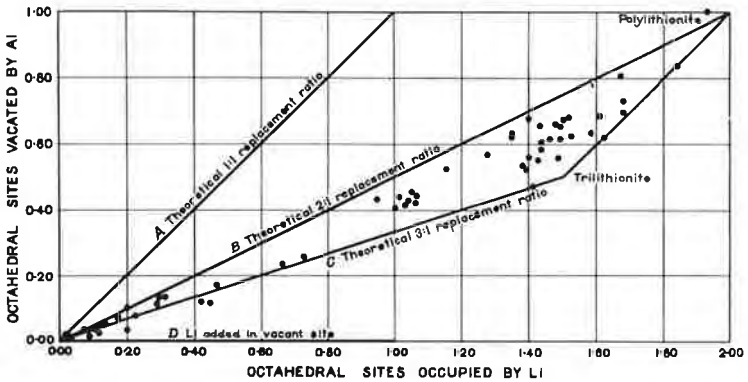

FIG. 4. Relation between octahedral sites occupied by Li and vacated by Al in aluminum lithium micas; after Foster (1960c).

to an acceptable decrease in Al^{IV} of 0.35, slightly smaller than the decrease in Al^{VI} of 0.40, *viz.*

$$(Al_{1.60}Li_{0.35})(Si_{3.35}Al_{0.65})O_{10}(OH)_2K_{1.00}$$

The lower limit to Al^{VI} appears to set a lower limit to Al^{IV}, *i.e.* an upper limit to Li, which is consistent, moreover with the structural requirements. This mica should represent about the maximum octahedral occupancy for *muscovites;* and the sum of the octahedral cations, 2.45, is the same as Foster's observed limit.

Lepidolites near polylithionite, $K(Al\,Li_2)\,Si_4\,O_{10}\,(OH)_2$, in composition will probably have highly ordered octahedral layers, with the Al in the unique site and the 2 Li in the symmetry related sites. Foster (1960 c) noted however that lepidolite structures may contain as much as 1.4 Al^{VI} (implied *e.g.* in Fig. 4) with an ideal composition,

$$(Al_{1.40}Li_{1.40})(Si_{3.60}Al_{0.40})O_{10}(OH)_2K_{1.00}$$

Although partial octahedral ordering of the above type *may* still remain the Al^{VI} obviously must occupy some of the symmetry-related sites. At present it can only be noted that such structures occur naturally, and that lepidolite structures show little-understood peculiarities in this as in some other aspects (Part I).

Trioctahedral micas-lepidolites. Foster (1960 c) has examined about 45 ferrous lithium micas ranging in composition between siderophyllites and lepidolites (Fig. 5). She also records data on taeniolite, ideally $(Mg_2\,Li)\,Si_4\,O_{10}\,(OH)_2\,K$, and on three Li-biotites; these data have been inserted as nos. 1–4 on Fig. 6. Foster comments:

"The prototype, siderophyllite, is structurally trioctahedral, and, as replacement tends to

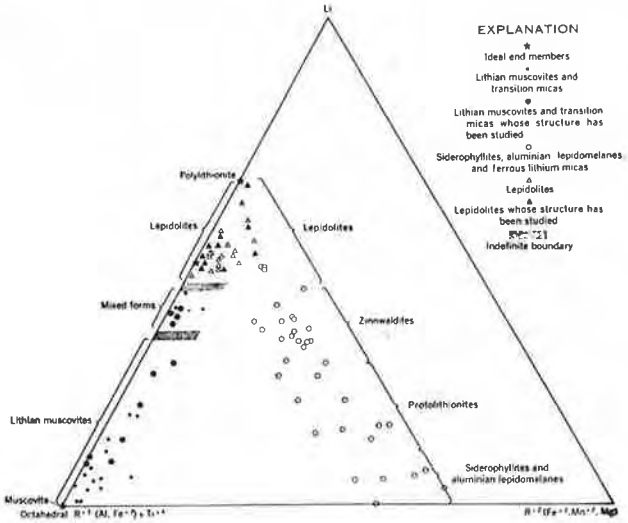

FIG. 5. Relation between Li, R^{2+} (Fe^{2+}, Mn^{2+}, Mg) and octahedral R^{3+} (Al, Fe^{3+})+Ti^{4+} in lithium micas; from Foster (1960c).

increase octahedral occupancy, the ferrous lithium micas are also trioctahedral and no structural adjustments are necessary. The ferrous lithium mica series is, therefore, not broken as is the aluminium lithium mica series."

On this basis a "structural composition diagram" is now proposed (Fig. 6) in which the trioctahedral and dioctahedral areas each correspond to *continuous* structural series. These composition limits are reasonable in terms of the structures involved, as follows. Taeniolite represents the maximum Li substitution possible in phlogopite to maintain charge ballance. Approximate sheet dimensions and other data for this and its iron analogue may be calculated (Part II) to be:

Composition	b_{calc}	b_{tetr}	τ	new b_{tetr}	α
$(Mg_2Li)Si_4O_{10}(OH)_2K$	9.14	9.05	107°	9.18	5°24′
$(Fe_2^{2+}Li)Si_4O_{10}(OH)_2K$	9.26	9.05	105.7°	9.32	6°42′

That is, in taeniolite (which is rare) the stretching required in the tetrahedral layers to meet the expected sheet dimensions is just within the acceptable limits ($\tau = 106\frac{1}{2}°$). In the ferrous analogue the misfit is excessive, and if such a mica were formed the octahedral layer would have to be quite unusually short and thick for a ferrous mica. Structurally this seems unlikely to be formed, and even less likely to persist naturally. Taeniolite

is reported to have the 1M structure (Foster, 1960 c) with which on ordered octahedral arrangement would be consistent. Similar arguments show that the present structural concepts are compatible with the other limits sketched for biotites (Fig. 6). Normal micas cannot of course have compositions in the blank upper right portion of this diagram where there would be an inherent lack of charge balance. The discontinuity between muscovite and siderophyllite was discussed earlier.

The join siderophyllite-lepidolite (Fig. 5) appears to be continuous from chemical data (Foster, 1960 c) which may be expected from structural considerations also. Foster gives as average formulae:

siderophyllite	$(R^{3+}_{1.05}Fe^{2+}_{1.50})(Si_{2.85}Al_{1.15})O_{10}(OH)_2K_{1.00}$
zinnwaldite	$(R^{3+}_{1.05}Fe^{2+}_{0.75}Li_{1.00})(Si_{3.35}Al_{0.65})O_{10}(OH, F)_2K_{1.00}$
lepidolite (ferroan)	$(R^{3+}_{1.05}Fe^{2+}_{0.37}Li_{1.50})(Si_{3.61}Al_{0.39})O_{10}(F, OH)_2K_{1.00}$

The octahedral layer is probably largely ordered throughout this range, with the $R_{1.05}^{3+}$ mainly in the unique site. The two related sites are then largely occupied by Fe^{2+} in siderophyllites and by Li in polylithionite; *i.e.* structurally the Li ions replace Fe^{2+} ions directly. (An interesting consequence is that the role of K changes continously from contracting siderophyllite layers to expanding lepidolite layers and propping them apart.) Though there is as yet no *direct* structural evidence the likelihood of octahedral ordering (Parts III, IV), and Foster's chemical data both strongly support this hypothesis. In the ferrous lithium micas "the octa-

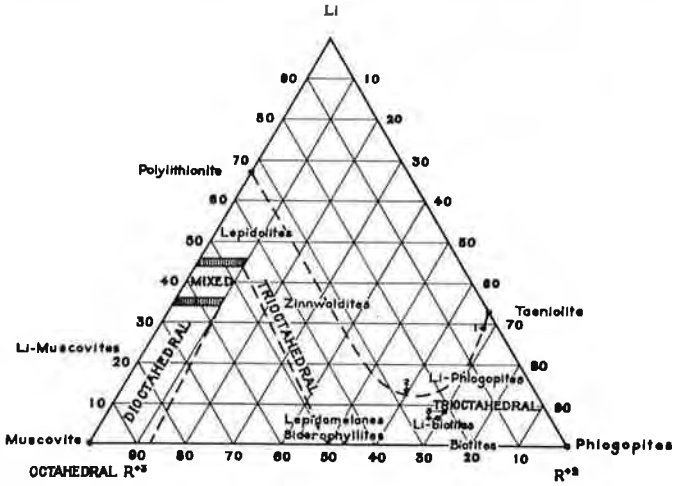

FIG. 6. Same plot as Fig. 5, showing suggested limits fo. various dioctahedral and trioctahedral structural series.

hedral R^{3+} content is remarkably constant over a range in Li_2O content of from 1.5% to 4.8% "suggesting that these cations are not involved in the addition of Li." But a study of the Li-Fe^{2+} relation shows an approximately linear decrease in Fe^{2+} with increase in Li "which is suggestive of replacement." The replacement ratio is about 1.3:1 rather than 1:1 because of other adjustments made in the number of vacant sites and in layer charge distribution. Chemically the range of R^{3+} for minerals between siderophyllites and lepidolites is $(1.15 \pm 0.10)R^{3+}$ approx., suggesting that most of the R^{3+} ions are in a particular octahedral site throughout this series.

Other clay mineral groups. At present the other clay mineral groups are generally less well defined chemically and structurally than the micas, and considerable restraint is needed in extending the present discussion of composition and structure to them. However, the study of interatomic forces (Part IV) and of the probable ordering of octahedral cations (Part III) applies to the layer silicate structures generally. It may therefore at least be noted here that these structural concepts are compatible with several broad conclusions about composition ranges in these other minerals. In particular a discontinuity between dioctahedral and trioctahedral minerals may be expected in other groups (as in micas) if octahedral ordering of cations is fairly widespread. The discontinuities will be more obvious if there are lower limits to the number of symmetry-related sites which must be occupied by certain cations (as discussed above for the micas).

MacEwan (1961) has noted that amongst the naturally occurring minerals in the montmorillonite group "there are two distinct series (dioctahedral and trioctahedral) with very limited solid solution." In dioctahedral montmorillonites there are between 2.0 and 2.2 cations per three sites. In the trioctahedral analogues Mg ranges from 1.8 to 3.0; or in the sauconites Zn ranges from 1.5 to 2.5 (Ross, 1946) with a total cation occupancy of 2.7 to 3.0. The present ideas about octahedral ordering are entirely consistent with these figures.[1]

[1] Roy and Roy (1955) have studied the system MgO-Al_2O_3-SiO_2-H_2O extensively. They state that due to considerable experimental difficulties "the present study appears to be fairly conclusive only insofar as it shows the existence of relatively pure "single" phase montmorillonites extending about 10 molar per cent into the diagram from each of the ternary systems" (*i.e.* from talc and pyrophyllite). It is also to be noted that their "ideally" stable montmorillonite has an octahedral composition of approximately $(Mg_{0.75}Al_{1.5})$, which is within the proposed structural limitations. If the present concept of octahedral ordering is widely applicable, then their assumption of a continuous series of montmorillonites (made "to greatly simplify the representation of the phase relations") is not in fact valid.

Nelson and Roy (1958) have argued strongly that there is a clear structural discontinuity between dioctahedral kaolins and their trioctahedral analogues, adding that "the crystal chemistry of kaolins admits no isomorphous substitutions in the ideal formula." The structure analysis of dickite (Newnham, 1961) and kaolinite (Zviagin, 1960) show no sign of Al in the third site, from which we may conclude that in these minerals the appropriate octahedral sites must be occupied and the arrangement a fully ordered one. In view of the tight network of octahedral forces, at least in dickite (Part IV), perhaps it is not too surprising that defects in the form of substituted ions of larger radius, or simply of occasionally unoccupied sites are not readily tolerated.

With the chlorites the additional octahedral layer per unit cell allows many more variations in cation ordering, and it is hardly possible to consider the observed composition ranges (Foster, 1962) until several structure analyses have been published. However the high degree of octahedral ordering in prochlorite (Steinfink, 1958) may be noted with interest. In the refinement of Mg-vermiculite Mathieson (1958) made no attempt to distinguish between the occupancy of the three crystallographically distinct sites. The Cr-chlorite structure recently determined by Brown and Bailey (1963) is fully ordered octahedrally in the sense predicted in Part III. All three sites in the talc layer are occupied by Mg; and in the brucite layer the unique site, $\bar{1}$, contains ($Cr_{0.7}Al_{0.2}$ $Mg_{0.1}$) and the related sites are occupied by Mg.

Discussion

The internal strains which the layer silicates can tolerate—in the form of stretched bonds and highly distorted polyhedra—are limited, and some broad physical limits can be suggested from the previous empirical study of their interatomic forces (Part IV). On this basis we may conclude that certain hypothetical micas are structurally prohibited (*e.g.* Na-biotites) or highly unlikely to be synthesized (*e.g.* Na and K equally in muscovite). In other cases it seems that should the particular structure be formed naturally then it would at least have large internal stresses at surface conditions (*e.g.* annite). It may be inferred that these minerals would be rather readily altered if a new environment favors any change, and natural specimens should be rare for this reason alone.

A review of observed composition limits for natural micas shows that the present structural ideas are at least compatible with these limits. It is not, of course, to be implied that the structural factors necessarily have controlled any of the observed limits because of the known importance of other factors during formation.

The need for detailed studies of bond lengths in known structures at elevated temperatures is again obvious.

Acknowledgments

Thanks are due to both Dr. Margaret D. Foster and Dr. Hatten S. Yoder, Jr., for their helpful comments on the original manuscript.

References

Brown, B. E. and S. W. Bailey (1963) Chlorite polytypism: II. Crystal structure of a one-layer Cr-chlorite. *Am. Mineral.*, **48,** 42.

Burst, J. F. (1958) Mineral heterogeneity in "glauconite" pellets. *Am. Mineral.* **43,** 481.

Donnay, G. and P. Kingman (1958) *Carnegie Inst. of Wash. Year Book No.* **57,** 252.

Eugster, H. P. and D. R. Wones (1962) *Jour. Petrology,* **3,** 82.

——— and H. S. Yoder (1955) *Carnegie Inst. of Wash. Year Book No.* **54,** 123.

Foster, M. D. (1956) Correlation of dioctahedral potassium micas on the basis of their charge relations. *U. S. Geol. Survey Bull.* **1036-D,** 57.

——— (1960a) Layer charge relations in the dioctahedral and trioctahedral micas. *Am. Mineral,* **45,** 383.

——— (1960b) Interpretation of the composition of trioctahedral micas. *U. S. Geol. Survey Prof. Paper,* **354-B,** 11.

——— (1960c) Interpretation of the composition of lithium micas. *U. S. Geol. Survey Prof. Paper,* **354-B,** 115.

——— (1962) Interpretation of the composition and a classification of the chlorites. *U. S. Geol. Survey Prof. Paper,* **414-A,** 1.

Heinrich, E. Wm. and A. A. Levinson (1955) Polymorphism among the high-silica sericites. *Am. Mineral.* **40,** 983.

Levinson, A. A. (1953) Relationship between polymorphism and composition in the muscovite-lepidolite series. *Am. Mineral.* **38,** 88.

McEwan, D. M. C. (1961) Montmorillonite minerals, in "*X-ray Identification and Crystal Structures of Clay Minerals,*" Mineral Soc., London.

Mathieson, A. Mc. L. (1958) Mg-Vermiculite: a refinement and re-examination of the 14.36 Å phase. *Am. Mineral.* **43,** 216.

Morimoto, N. and J. D. H. Donnay (1962) Private communication.

Nelson, B. W. and R. Roy (1958) Synthesis of the chlorites and their structural and chemical constitution. *Am. Mineral.* **43,** 707.

Newnham, R. E. (1961) A refinement of the dickite structure. *Mineral. Mag.* **32,** 683.

Penfield, S. L. (1893) On some minerals from the manganese mines of St. Marcel in Piedmont, Italy. *Am. Jour. Sci.* **46,** 288.

Radoslovich, E. W. (1960) The structure of muscovite, $KAl_2(Si_3Al)O_{10}(OH)_2$. *Acta Cryst.* **13,** 919.

——— (1962a) The cell dimensions and symmetry of layer lattice silicates; II, Regression relations. *Am. Mineral.* **47,** 617.

——— (1962b) The cell dimensions and symmetry of layer lattice silicates; IV, Interatomic forces. *Am. Mineral.* **48,** 76.

——— (1962c) The cell dimensions and symmetry of layer lattice silicates; VI, Serpentine and kaolin morphology. *Am. Mineral.* **48,** 368.

——— and K. Norrish (1962) The cell dimensions and symmetry of layer lattice silicates; I, Some structural considerations. *Am. Mineral.* **47,** 599.

Ross, C. S. (1946) Sauconite—a clay mineral of the montmorillonite group. *Am. Mineral.* **31,** 411.

SMITH, J. V. AND H. S. YODER (1956) Experimental and theoretical studies of the mica polymorphs. *Mineral. Mag.* **31,** 209.

STEINFINK, H. (1958) The crystal structure of prochlorite. *Acta Cryst.* **11,** 191.

STEVENS, R. E. (1938), New anlayses of lepidolites and their interpretation. *Am. Mineral.* **23,** 607.

TAKÉUCHI, Y. AND R. SADANAGA (1959) The crystal structure of xanthophyllite. *Acta Cryst.* **12,** 945.

VEITCH, L. G. AND E. W. RADOSLOVICH (1962) The cell dimensions and symmetry of layer lattice silicates; III, Octahedral ordering. *Am. Mineral.* **48,** 62.

YODER, H. S. (1959) Experimental studies on micas; a synthesis. *Clays and Clay Minerals, Sixth Conf. Proc.*, 42. Pergamon Press, N. Y.

——— AND H. P. EUGSTER (1955) Synthetic and natural muscovites. *Geochim. Cosmochim. Acta,* **8,** 155.

YOUNG, R. A. (1962) Private communication.

ZVIAGIN, B. B. (1957) Determination of the structure of celadonite by electron diffraction. *Kristallografiya,* **2,** 388 (in transl.).

——— (1960) Determination of the structure of kaolinite by electron diffraction. *Kristallografiya,* **5,** 32 (in transl.).

Manuscript received, July 27, 1962; accepted for publication, January 2, 1963.

THE CELL DIMENSIONS AND SYMMETRY OF LAYER-LATTICE SILICATES. VI. SERPENTINE AND KAOLIN MORPHOLOGY

BY

E. W. RADOSLOVICH

Reprinted from American Mineralogist, **48**:
Pages 368-378
(1963)

THE AMERICAN MINERALOGIST, VOL. 48, MARCH–APRIL, 1963

THE CELL DIMENSIONS AND SYMMETRY OF LAYER-LATTICE SILICATES. VI. SERPENTINE AND KAOLIN MORPHOLOGY

E. W. Radoslovich, *Division of Soils, Commonwealth Scientific and Industrial Research Organisation, Adelaide, Australia.*

Abstract

As a consequence of the hypotheses developed in earlier papers in this series the stresses between tetrahedral and octahedral layers in serpentines can be more precisely expressed in terms of bond lengths and bond angles. It is shown that the sheet dimensions of serpentines are compatible with a tetrahedral layer stretched, by changes in bond angles, to the maximum possible structurally. It is suggested that octahedral layers in chrysotiles must contract under constraints rather more than these layers in antigorites, and that the two groups may be separated on this basis. If the same hypotheses are right then endellite sheets do not curl because of forces due to misfit between the tetrahedral and octahedral layers, since these are negligible. Attention is drawn to earlier work on the surface hydroxyl bonds in basic hydroxide layer structures, and to the peculiarly sensitive position of the Al ion in the kaolin minerals.

The morphology of the serpentine minerals and kaolin minerals has been studied in many laboratories by techniques which include electron microscopy, electron diffraction, *x*-ray powder diffraction, single crystal structure analysis, chemical analysis, hydrothermal synthesis and infrared spectroscopy. The literature is extensive (*e.g.* the references herewith) but the explanations for the observed phenomena are still more often tentative rather than rigorous. In particular the dimensional misfit of various sheet structures is only discussed qualitatively in most published work.

It is widely agreed that both serpentines and kaolins adopt various morphological forms because of a misfit between the tetrahedral layer and the octahedral layer which together make up these 1:1 layer-lattice silicates. As a broad generalisation this "explains" the observed plates, plates with rolled edges, tubes and fibrils, and also the structural types such as rectified and alternating wave structures, orthohexagonal cells, etc. Bates (1959) has discussed this misfit in detail, suggesting the adoption of a 'morphological index, "M",' but this seems to the writer to be defined in a rather arbitrary manner. Moreover "M" is not explicitly related to the physical quantities which really determine the degree of misfit, *viz.* the average bond lengths and bond angles in the two layers thought to be under stress.

Different kinds of stress in layer structures are very probably relieved by several distinct structural adjustments. Hypotheses about the nature of these adjustments have been proposed recently by Radoslovich and Norrish (1962; hereafter Part I), by Veitch and Radoslovich (1963; *i.e.*

Part III) and by Radoslovich (1963a; *i.e.* Part IV). Confirmatory evidence has been obtained by the multiple regression analysis of sheet dimensions and composition *i.e.* *b*-axis data and structural formulae (Radoslovich 1962; hereafter Part II). These hypotheses are further supported by the fact that they may be satisfactorily correlated with the observed composition limits for the micas and possibly other minerals (Radoslovich 1963b; hereafter Part V).

If these ideas are essentially correct, and the present values of ionic radii, bond lengths and bond angles are reliable, then for the serpentines the limits of strain may be stated more clearly in structural terms and these limits should correspond to observed changes in morphology. On the other hand if the same ideas are right then the currently accepted explanation for curled and tubular morphology amongst the kaolins is only superficially correct and should at least be reviewed carefully. This short paper does not aim to explain all facets of serpentine and kaolin morphology, but merely to draw attention to several factors with which any rigorous theory eventually must be consistent.

Serpentine Minerals

Several writers have compared the morphology and crystal symmetry of synthetic serpentines of varying composition with that observed for natural serpentine minerals. Some caution is necessary, however, because the hypotheses in Part I imply that there are considerable differences in the surface symmetry (and also in the kind of layer misfit) between certain synthetic and natural serpentines.

Mg-Ge synthetic serpentine. Roy and Roy (1954) synthesised a serpentine wherein Ge fully replaces Si in the tetrahedral layer and for which Zussman and Brindley (1957) have given detailed *x*-ray data, including cell dimensions. Because of the larger ionic radius of Ge (0.53 Å) compared with either Si (0.41 Å) or Al (0.50 Å) the tetrahedral layer will be quite large. Although the exact Ge-O bondlength for such a layer is not known a value of 1.84 Å seems reasonable,[1] so that b_{tetr} (Part I) $\doteqdot 10.4$ Å. The octahedral dimensions, if unconstrained, may be calculated by the kaolin regression relation (Part II) as $b_{oct} = 9.3$ Å. Then $\cos\alpha = 0.894$ and $\alpha \doteqdot 26\frac{1}{2}°$. Although tetrahedral rotations as high as this are possible, the theoretical maximum is 30° and it is not surprising to find the octahedral layer stretching a little to 9.415 Å (Zussman and Brindley, 1957). For $b_{obs} = 9.415$ Å and $b_{tetr} = 10.4$ Å, $\alpha = 25°$.

This synthetic serpentine is therefore markedly ditrigonal in surface

[1] See *International Tabellen zur Bestimmung von Kristallstrukturen*, Vol. II, p. 610. G. Bell, London, 1935 (Pauling's values of radii).

symmetry, more than almost all other lattice silicates (Parts I, II, V). It should tend to crystallise in an orthogonal unit cell which is 3n layers thick in the *c* direction (Radoslovich, 1959). Gillery (1959) has pointed out that this Mg-Ge serpentine is a six-layer orthohexagonal structure which approximates to a two-layer cell; this is apparently the basic unit which then may be built up in a similar way to the 3T micas (Smith and Yoder, 1956).

It is quite evident that in surface properties, including the stacking of layers, this serpentine is notably different from natural serpentines in which the tetrahedral layer is invariably untwisted ($\alpha = 0°$) and often severely stretched. Zussman and Brindley (1957) confirmed that the Unst orthoserpentine has a six-layer cell by comparing its powder pattern with that of $Mg_6Ge_4O_{10}(OH)_8$. Though their independent evidence establishes a six-layer orthohexagonal cell and though the patterns are quite similar it is hardly valid to compare these minerals without qualification; the mechanism of forming six-layer polymorphs may be considerably different in the two minerals.

This synthetic serpentine is platey because the tetrahedral layer *contracts by rotations* to the octahedral layer with practically no resistance to deformation.

Mg-Al synthetic serpentines. Gillery (1959) has synthesised a range of such minerals with the general formula $(Si_{4-x}\ Al_x)(Mg_{6-x}\ Al_x)O_{10}(OH)_8$, and for x from 0 to 2.50. He observed that when $x = 0.75$ a platey one-layer orthoserpentine is formed, and when $x = 1.50$ a platey six-layer orthoserpentine is formed. The first decreases and the second increases as x goes from 0.75 to 1.50. In Part II it was shown that $\alpha = 0°$ and $12\frac{1}{2}°$ respectively, and this suggested that the Mg-Al serpentine higher in Al would most readily form an orthogonal cell through 3n layers. Gillery (1959) mentions that it approximates to a 3-layer cell. The increase in proportion of 6-layer structure with increasing Al—which Gillery could not explain at that time—therefore seems to be a direct result of the increasing tetrahedral rotation, α, as Al increases.

The morphology of these Mg-Al serpentines was shown by Gillery to be platey, except for a fibrous morphology when $x < 0.25$, *e.g.* $x = 0$. The above calculations show that there is no unrelieved stress between tetrahedral and octahedral layers for $x \geq 0.75$ at least, and hence these structures are platey.

Composition limits between platey and fibrous structures. In all natural serpentines the sheet dimensions of the octahedral layer would exceed those of the tetrahedral layer, if both were unconstrained. These structures re-

main platey, however, until those compositions are reached where the octahedral layer is excessively larger than the tetrahedral.

It seems reasonable to assume that dimensional adjustments are made largely by changes in bond angles rather than bond lengths. For example, the O-Si-O angles in an ideal tetrahedral layer are 109°28′. If such a layer is stretched the main effect probably will be to expand the basal triads of oxygens by decreasing the angles $\tau = O_{apex}$-Si-O_{basal} (Parts I, II, IV, V). Even though the individual angles τ are not known for a given structure the *average* value for τ should reach some fairly definite minimum for those tetrahedral layers which have been stretched as far as possible for a layer silicate.

It has been assumed (Parts I, II, V) that *average* values of τ do not fall below $106\frac{1}{2}°$ to 107°, and empirically all the calculated values of τ appear to equal or exceed this lower limit. This may also be supported theoretically as follows. The radius ratio of Si:O is too high (0.293) for the four oxygens to be in contact with each other (which implies a radius ratio = 0.225). Presumably the angles τ may be decreased easily until the basal oxygens O_B "touch" the apex oxygen O_A, when the resistance to further change in τ should increase very rapidly (Part IV). The average interatomic distances O_A–O_B are given in Table 1 for a range of angles τ, assuming Si-O bonds of 1.615 Å (Smith and Bailey, 1962). These dis-

TABLE 1. INTERATOMIC DISTANCES O_A–O_B FOR VARIOUS O-Si-O ANGLES

τ in degrees	105	105.5	106	106.5	107	107.5	108
O_A-O_B in Å	2.563	2.571	2.580	2.587	2.596	2.605	2.613

tances are to be compared with the effective oxygen radius *towards another oxygen*, for the particular type of co-ordination involved. In the present case this is neither the ionic radius nor the van der Waal radius. Moreover tables of ionic radii are given for ions in six-fold co-ordination and the exact correction to be applied to O_A and O_B is not clearly evident. In such a distorted tetrahedra the oxygens will certainly approach closer than an oxygen diameter, 2.80 Å. But they will *not* approach as closely as twice the effective radius of the oxygens towards the silicons, *viz.* $2 \times 1.40 \times 0.88 = 2.46$ Å (where 0.88 is the co-ordination correction for 4.2 co-ordination, Internationale Tabellen, *loc. cit.*). This short distance would require quite unusual compressive forces if it is to be the *average* tetrahedral edge throughout the sheets. Some value around 2.58–2.60 Å is therefore quite reasonable, though a precise figure cannot of course be calculated. This estimate is supported, for example, by the 48 inde-

pendent O–O distances around Si tetrahedra in anorthite (Megaw, *et al.* 1962). The *shortest* (even under stress) are 2.486, 2.518, 2.519, 2.520, 2.525, 2.535, 2.537 and 2.540 Å— and the other *40* are longer. A minimum average angle of $\tau \geq 106.5°$ approximately therefore seems quite acceptable. This limit may eventually need slight adjustment when more precise data on bond lengths and angles under strain have appeared in the literature. The limit will vary somewhat with the substitution of Al for Si tetrahedrally, but this substitution is quite restricted for natural serpentines.

As a useful check on these ideas interatomic distances were calculated for the clino-chrysotile structure which has been determined with moderate accuracy by Whittaker (1956). Using his preferred x parameter of 0.145 for O_x the "O_A–O_B" distances are approximately 2.62, 2.63, and 2.63 Å, for Si-O bonds of about 1.57, 1.63 and 1.63 Å. This confirms, within the limits of accuracy involved, that the basal oxygens are "touching" the apex oxygens of a fully stretched tetrahedral layer.

The detailed regression analysis of sheet dimensions and composition (Part II) strongly suggested that for the 1:1 minerals the tetrahedral layer will stretch until $\tau \approx 107°$, *before* the octahedral layer shows any significant contraction. Beyond this degree of misfit the stretched tetrahedral layer (with $\tau \approx 107°$) fixes the overall sheet dimensions and the octahedral layer must contract somewhat; *i.e.* very roughly, if $b'_{tetr} = b_{tetr} \times (\sin \tau / \sin 109°28')$ then

$$b'_{tetr} = b_{oct} = b_{kaolin} = b_{obs} \qquad \text{for } \tau > 107°$$
$$b_{obs} = b'_{tetr} < b_{oct}\,(=b_{kaolin}) \qquad \text{for } \tau = 107°$$

where b_{tetr} and b_{oct} are the *unconstrained* dimensions, and b_{kaolin} is the b axis as calculated by the kaolin regression relation.

The limit between platey and tubular serpentines may now be defined in terms of the above hypothesis and observations.

Serpentines whose composition leads to values of τ clearly greater than 107° should show very little stress due to misfit between the layers and therefore be platey. Serpentines whose composition leads to values of τ clearly less than $106\frac{1}{2}°$—as calculated (Part I) from $(9.60+0.27x) \sin \tau = b_{oct}$ (*i.e.* b_{kaolin})—must have very considerable stresses due to misfit between layers and therefore show strong tendencies to be fibrous or tubular, with an accompanying contraction octahedrally. Serpentines with τ around $106\frac{1}{2}°$—whether calculated from b_{obs} or b_{oct}—must be under various degrees of stress. These specimens should show quite variable morphology between plates and tubes, and possibly even show variations between different areas of the one specimen, due to subtle changes in chemistry.

These limits should apply quite generally, irrespective of the particular substitutions or deficiencies in the tetrahedral and octahedral layers. For example, in his study of the Mg-Al synthetic serpentines $(Si_{4-x}\ Al_x)\ (Mg_{6-x}\ Al_x)\ O_{10}\ (OH)_8$ Gillery (1959) concluded that these minerals are fibrous for $x<0.25$, and cited evidence by Nagy and Faust (1956) to support a limit at $x\geq 0.2$. Olsen (1961) has argued that "the break point between fibrous and platey polytypes might more properly lie around $x=0.1\ R_2O_3$." For these limits the corresponding angles τ are

$x = 0.1$	0.2	0.25
$\tau = 105°$	106°	$106\frac{1}{4}°$

so that the higher value of x is more acceptable.

Chrysotile, lizardites, antigorites. Zussman *et al.* (1957) have summarized electron microscope data on the morphology of serpentines, concluding that chrysotiles are either tubes or laths, antigorites are plates or broad laths (with various super-lattice parameters), and lizardites are plates. As Bates (1959) has pointed out in discussing his morphological index "M" all the serpentines are so closely similar that a clear-cut division at some value of "M" would not be expected, though some trend should be observed which distinguishes platey from tubular morphology. Furthermore the strength of the hydrogen bonds between the layers will certainly influence the particular morphology by which misfit stresses are relieved in a given specimen. Nevertheless the preceding discussion suggests that chrysotiles should tend to have lower values of τ than antigorites when τ is calculated from $(9.60+0.27x)\sin\tau=b_{oct}$. In view of the known stresses in antigorites—resulting in a non-stoichiometric wave structure (Zussman, 1954)—the expected values of τ should be somewhat less than the lower limit of $106\frac{1}{2}°$, which corresponds to relatively little octahedral compression.

It is difficult to test this in detail because there are not many good analyses of chrysotiles and antigorites in the literature, and even some of these have been made on specimens inadequately characterised by *x*-ray analysis (Whittaker and Zussman, 1956). Moreover there is, at present, no agreed method for calculating structural formulae from serpentine assays. For this reason the values of τ in Table 2 have mostly been calculated from the structural formulae given by Bates (1959), since these are all computed by the same method and should at least provide a suitable basis for comparison. In several cases which were checked the alternative formulae of other workers lead to very similar τ to those in Table 2. (Some of Bates' platey serpentine specimens which have been criticized by others are omitted.)

It seems fair to conclude from Table 2 that τ for chrysotiles does in

fact tend to be lower than for the platey minerals, especially when the average analyses are compared, *i.e.* for C-5 (25 chrysotiles) $\tau = 105°$ but for P-5 (14 antigorites) $\tau = 106°$.

It is notable that natural chrysotiles have practically no substitution tetrahedrally, so that their *b*-axes should all be close to $b = 9.60 \times \sin 106\frac{1}{2} = 9.20$ Å. Whittaker and Zussman (1956) have given accurate d values for four chrysotiles and nine lizardites (which are found with chrysotiles, but not with antigorites) and these lie between $b = 9.186$ and 9.222 Å. Antigorites, which may have some tetrahedral Al, have average *b*-axes of 9.241 Å. These results confirm the present arguments.

The notion of a "strain-free" layer in tubular chrysotile structures (*e.g.* Whittaker, 1957) is misleading since it is probably only a layer of *minimal* strain which is involved. For smaller radii of curvature the octahedral strains (in bond angles) should increase sharply, and for larger radii of curvature the tetrahedral strains (*i.e.* smaller τ) should do likewise; but no layer will be "strain-free."

TABLE 2. AVERAGE O_{apex}—Si—O_{basal} ANGLES, τ, CALCULATED FOR SOME SERPENTINES

Specimen	Locality	(from τ/b_{kaolin})	(from τ/b_{obs})
C—1[1]	Quebec	104°42′	
C—2[1]	Delaware Co., Pa.	104°43′	
C—3[1]	Aboutville, N. Y.	104°46′	
C—4[1]	Montville, N. J.	105°5′	
C—5[1]	Aver. of 29 chrys.	105°	
C—6[1]	Gila Co., Ariz.	105°	
C—7[1]	Transvaal	105°15′	
C—8[1]	Woodsreef, N.S.W.	105°14′	
P—5[1]	Aver. of 14 antig.	106°2′	
P—6[1]	Val Antigorio	106°16′	107°12′
P—8[1]	Mikonni, N. Z.	105°2′	106°10′
P—9[1]	Caracas	105°7′	106°22′
P—12[1]	"Deweylite"	105°21′	
P—13[1]	"Williamsite"	105°17′	
P—14[1]	"Baltimoreite"	105°55′	
P—15[1]	"Yu Yen Stone"	104°50′	
Lizardite[2]	Kennack Cove	105°16′	106°36′
6-layer orthohexagonal	Unst[2]	105°15′	106°44′
6-layer orthohexagonal	Quebec[3]	107°9′	107°50′

[1] *v.* Bates (1959).

[2] *v.* Zussman, Brindley and Comer (1957).

[3] *v.* Olsen (1961).

Col. 3 gives τ assuming no octahedral layer contraction, whereas col. 4 gives τ allowing for any such contraction.

Kaolin minerals. Since Bates, *et al.* (1950) first reported tubular morphology amongst endellites it has become increasingly evident that the kaolin minerals are not clearly divided into two distinct morphological groups. In fact Bates and Comer (1957) have proposed a continuous transition between good plates and good tubes. As Bates (1959) has pointed out, however, there is an extremely close similarity in Si:Al ratio for kaolinites and endellites, and these two minerals may in fact only differ significantly in H_2O content.

Bates, *et al.* (1950), and also Bates (1959), have explicitly discussed the curvature of endellite in terms of a supposed misfit between a larger tetrahedral layer and a smaller octahedral layer. They also have roughly calculated an expected radius of curvature from an assumed difference in dimensions between the tetrahedral and octahedral surfaces. This concept has been widely accepted since then, but cannot (in the author's opinion) be reconciled in detail with our current understanding of the layer silicate structures.

The hypothesis has now been put forward (Parts I, II, and IV) that if the tetrahedral layer of a layer silicate would, on its own, exceed the dimensions of the neighbouring octahedral layer then the former may contract, very readily and quite markedly, simply by tetrahedral rotations leading to ditrigonal rather than hexagonal surface symmetry for many such minerals. It is not claimed that these T-O-T angles (T = tetrahedral cations) can be varied without any resistance to deformation at all; but it is strongly suggested that any such force is of an appreciably lower order of magnitude than other stresses in these structures. That is, *by comparison* the resistance to deformation of T-O-T angles is much smaller than papers on kaolin morphology generally imply. The considerable amount of detailed evidence for this is discussed in Part IV.

This has two obvious implications with respect to kaolin morphology, *viz.:*

(a) The curvature of endellite cannot be explained satisfactorily solely in terms of a misfit in dimensions between the tetrahedral and octahedral layers, or their surfaces, as Bates (1959) discusses. If a tetrahedral layer can so readily reduce its sheet dimensions by becoming more ditrigonal then there either will be no mismatch with adjacent octahedral dimensions, or at least the stresses due to any mismatch will be of very secondary importance, and inadequate to explain the tubular morphology of endellites.

(b) The morphology of different kaolin minerals is unlikely to be *directly* related to subtle differences in Si/Al ratio, as Bates (1959) has sought to establish. An increase in Al substitution tetrahedrally will result primarily in slightly greater rotations in the already ditrigonal tetrahedral network—but again this should not lead to a more tubular morphology. [A change in Si/Al ratio may, however, affect the OH content and/or interlayer bonding (as Bates (1959) has already noted) and therefore be rather indirectly related to morphological changes.]

Nevertheless endellites do form tubes, and this does imply unequal stresses at two different levels in the 7 Å kaolin layers. These forces, moreover, are highly variable and are not *too* closely related to the overall crystallinity (Bates and Comer, 1957). It appears to the writer that a reasonable guess about the nature of these forces may now be made, consistent with the discussion of interatomic forces in dickite (Part IV). No attempt has been made to obtain experimental evidence to support these ideas, which are advanced in a tentative way only.

It appears likely that the unbalanced stresses are

(i) the expansion due to Al^{VI}-Al^{VI} repulsion across shared edges and (ii) a contraction within the layer of surface hydroxyls, probably by OH-OH bonds in the hydroxyl triads around vacant octahedral sites.[1]

In their classical work on the hydroxyl (*i.e.* OH-OH) bond Bernal and Megaw (1935) studied the basic and amphoteric hydroxides in detail, drawing particular attention to gibbsite, $Al(OH)_3$, as compared with the hydroxides of mono- and di-valent cations. By plotting the calculated electrostatic energy of the cation-hydroxyl bond against the hydroxyl-hydroxyl distance Bernal and Megaw showed conclusively that, for cations arranged in order of increasing polarizing power, Al is the first cation to induce OH-OH bonds between neighbouring hydroxyls.[2] An electrostatic bond strength of at least $\frac{1}{2}$ is needed to induce the necessary tetrahedral symmetry of charge distribution in the OH's.

Although the six Al-OH bonds in an octahedral group have an ideal strength of $\frac{1}{2}$ it cannot be assumed that particular bonds in a given structure also have this strength. This is emphasised by the contrasts between the diaspore and dickite structures in this respect (Part IV). Indeed it seems very likely that the polarizing power of Al in these minerals is at a critically sensitive level, so that quite subtle structural changes may produce considerable variations in OH polarisation and therefore in any surface OH-OH bonding. In dickite, for example, the Al-OH surface bonds apparently have strength around 0.6 (Part IV). Nevertheless the total configuration of bonds in dickite ensures that virtually all surface OH's form long O-H—O bonds to the adjacent tetrahedral surface. In the polymorph kaolinite, however, the O-H bonds are considered to be differently directed in relation to the superimposed oxygen network (Part IV); and the assumed arrangement is less likely to ensure that all OH's form long O-H—O bonds. In endellite the presence of interlayer water should still further disrupt such direct bonds to the next layer. Under these conditions the Al-OH bond strengths may be expected to lie between 0.5 and 0.6, and in the absence of immediate O-H—O bonds a

[1] Both types of stress are discussed fully in Part IV.

[2] See, *e.g.* Wells, A. F. *Structural Inorganic Chemistry*, Clarendon Press, Oxford, 1962, 3rd. ed., p. 546 f.

looser network of OH-OH and OH-H_2O bonds would be formed. (The surface OH's should tend towards a tetrahedral charge distribution.)

That is, in endellite there is clearly the possibility of some OH-OH distances being shortened around unoccupied sites, as in gibbsite (Bernal and Megaw, 1935). But, contrary to gibbsite, this can happen only on one side of the octahedral layer. The net result should not, therefore, be a shortening of the *b*-axis as in gibbsite, but an unbalanced pair of forces ((i) and (ii) above) leading to a tubular morphology. The relationships between any such forces, crystal structure, and mineralogical history for a given kaolin will certainly be very complex. The wide variations in morphology with respect to crystallinity are not in the least surprising. The pattern of OH-OH forces may well be systematically related to the octahedral network in *some* specimens, so that one direction, *e.g.* the *b*-axis, is a preferred tubular axis.

It is interesting to compare the *b*-axes of dickite (8.95 Å), well-crystallised kaolinite (8.95 Å), halloysite (8.92 Å) and endellite (8.90 Å). The decrease is consistent with an additional contraction in endellite, *e.g.* by OH-OH bonds, rather than an additional expansion, as the misfit of tetrahedral layers implies; but this observation cannot be given too much importance, of course.

It is not possible at present to obtain direct experimental evidence for these hypotheses, primarily because the poor crystallinity and small crystal size of kaolins (especially endellites) severely curtails the accurate measurement of interatomic distances. Whereas Bernal and Megaw (1935) confirmed the presence of OH-OH bonds on the surface of gibbsite by careful structure analysis similar data cannot yet be obtained for endellite in which such surface bonds have now been proposed. However, despite this lack of *direct* proof the *indirect* evidence to support the suggested out-of-balance forces is quite strong (*e.g.*, see Part IV). It should likewise be noted that there is, of course, no direct evidence either for the currently accepted explanation of tubular morphology, in terms of layer misfit. It is, moreover, fair to comment that the implications of the work of Bernal and Megaw (1935) on the hydroxyl bond in basic hydroxides appears to have been largely overlooked in papers on kaolin morphology. The sensitive position of the Al ion in their scale of polarizing power has not been generally realized, in the same context. This, together with the demonstration (Parts I–V) of the apparent ease with which tetrahedral layers contract, indicates the need for new approaches to problems of kaolin morphology.

ACKNOWLEDGMENT

Drs. J. V. Smith and S. W. Bailey kindly made their paper available in advance of publication.

References

Bates, T. F. (1959) Morphology and crystal chemistry of 1:1 layer lattice silicates. *Am. Mineral.* **44,** 78.

——— and J. J. Comer (1957) Further observations on the morphology of chrysotile and halloysite. *Proc. 6th. Natl. Clay Conf.*, p. 237, Pergamon Press, N. Y.

——— F. A. Hildebrand, and A. Swineford (1950) Morphology and structure of endellite and halloysite. *Am. Mineral.* **35,** 463.

Bernal, J. D. and H. D. Megaw (1935) The function of hydrogen in intermolecular forces. *Proc. Roy. Soc. London,* **A151,** 384.

Busing, W. R. and H. A. Levy (1958) A single crystal neutron diffraction study of diaspore, AlO (OH) *Acta Cryst.* **11,** 798.

Drits, V. A. and A. A. Kashaev (1960) An x-ray study of a single crystal of kaolinite. *Kristallografiya* **5,** 207 (in transl.).

Gillery, F. H. (1959) The x-ray study of synthetic Mg-Al serpentines and chlorites: *Am. Mineral.* **44,** 143.

Megaw, H. D. (1934) The crystal structure of hydrargillite, $Al(OH)_3$: *Zeit. Krist.* **87,** 185.

Nagy, B. and G. T. Faust (1956) Serpentines: Natural mixtures of chrysotile and antigorite: *Am. Mineral.* **41,** 817.

Newnham, R. E. (1961) A refinement of the dickite structure and some remarks on polymorphism in kaolin minerals. *Mineral. Mag.* **32,** 683.

Olsen, E. J. (1961) Six-layer ortho-hexagonal serpentine from the Labrador Trough. *Am. Mineral.* **46,** 434.

Radoslovich, E. W. (1959) Structural control of polymorphism in micas. *Nature,* **183,** 253.

——— (1962) The cell dimensions and symmetry of layer-lattice silicates, II. Regression relations. *Am. Mineral.* **47,** 617.

——— (1963a) The cell dimensions and symmetry of layer-lattice silicates, **IV.** Interatomic forces. *Am. Mineral.* **48,** 76.

——— (1963b) The cell dimensions and symmetry of layer-lattice silicates, V. Composition limits. *Am. Mineral.* **48,** 348.

——— and K. Norrish (1962) The cell dimensions and symmetry of layer-lattice silicates, I. Some structural considerations. *Am. Mineral.* **47,** 599.

Roy, D. M. and R. Roy (1954) An experimental study of the formation and properties of synthetic serpentines and related layer silicate minerals. *Am. Mineral.* **39,** 957.

Smith, J. V. and S. W. Bailey (1962) Second review of Al-O and Si-O tetrahedral distances. *Acta Cryst.*, in press.

——— and H. S. Yoder (1956) Experimental and theoretical studies of mica polymorphs. *Mineral. Mag.* **31,** 209.

Veitch, L. G. and E. W. Radoslovich (1962) The cell dimensions and symmetry of layer lattice silicates, III. Octahedral ordering. *Am. Mineral.* **48,** 62.

Whittaker, E. J. W. (1956) The structure of chrysotile, II. Clino-chrysotile. *Acta Cryst.* **9,** 855.

——— (1957) The structure of chrysotile, V. Diffuse reflexions and fibre texture. *Acta Cryst.* **10,** 149.

——— and J. Zussman (1956) The characterization of serpentine minerals by x-ray diffraction. *Mineral Mag.* **31,** 107.

Zussman, J. (1954) Investigation of the crystal structure of antigorite. *Mineral. Mag.* **30,** 498.

——— and G. W. Brindley (1957) Serpentines with 6-layer orthohexagonal cells. *Am. Mineral.* **42,** 666.

——— G. W. Brindley and J. Comer (1957) Electron diffraction studies of serpentine minerals. *Am. Mineral.* **42,** 133.

Manuscript received, July 27, 1962; accepted for publication, October 10, 1962.

Reprinted from "Clays and Clay Minerals"—Vol. XI
PERGAMON PRESS
OXFORD . LONDON . NEW YORK . PARIS
1963

CELL DIMENSION STUDIES ON LAYER-LATTICE SILICATES: A SUMMARY

by

E. W. RADOSLOVICH

Division of Soils, Commonwealth Scientific and Industrial Research Organization
Adelaide, South Australia

ABSTRACT

The statistical techniques of multiple regression analysis have been used to obtain more reliable formulae relating the cell dimensions (especially the *b*-axis) of layer-lattice silicates to their composition or structural formulae. This allowed the significance of each coefficient to be expressed precisely and so provided rigorous tests for certain structural concepts about the different factors affecting cell dimensions. More recently an explicit theory has been developed about the various forces controlling the layer-lattice silicate structures which (a) removes some anomalies, (b) explains many variations in accurate bond lengths and angles, and (c) has several interesting structural implications for properties such as polymorphism, composition limits, crystal morphology, and stability under weathering. This paper summarizes work now being published *in extenso* elsewhere.

INTRODUCTION

The studies reviewed in this paper have been concerned with the cell dimensions of the layer lattice silicates mainly in the sense that these data provide readily available links between known properties and the known or supposed crystal structures of these minerals. Nevertheless it is expected that many of the arguments at present primarily based on cell dimensions will eventually be confirmed (or possibly refuted) by further accurate determinations of layer-lattice silicate structures.

The re-determination of the $2M_1$ muscovite structure (Radoslovich, 1960) showed the ways by which this particular mica adjusts itself to reduce internal strains to a minimum. Some anomalies, such as the departure of the monoclinic angle from ideal, are thereby explained. In relation to other properties, however, the analysis merely revealed that this structure is suitably "distorted" from an ideal atomic arrangement, without (at that time) suggesting compelling explanations about why these "distortions" must of necessity occur.

From the clay mineral literature it seemed that any dimensional misfit between the tetrahedral and octahedral layers in muscovite should be an important key to this problem. Various formulae already existed which sought to relate the sheet dimensions (e.g. the *b*-axis) of layer-lattice silicates to their

isomorphous substitutions, both tetrahedrally and octahedrally. The most recent and comprehensive formulae were those due to Brindley and MacEwan (1953). These not only proved inadequate for the immediate muscovite problems but are not at all applicable to some layer lattice silicates of rather extreme composition. For example for the unusual brittle mica, xanthophyllite, Ca (Mg_2 Al) (Si Al_3) O_{10} $(OH)_2$, the "unconstrained" tetrahedral and octahedral dimensions and the calculated *b*-axis *each* exceed b_{obs}; i.e.

$$b_{tetr} = 9.84, \quad b_{oct} = 9.19, \quad b_{calc} = 9.49, \quad \text{but} \quad b_{obs} = 9.00 \text{ Å}$$

SURFACE SYMMETRY

Muscovite, in common with other layer-lattice silicate structures already published, proved to have a ditrigonal rather than hexagonal arrangement of surface oxygens. It was therefore suggested that the "ideal" mica structure should more properly allow a ditrigonal surface symmetry, and attention was drawn to this property in relation to mica polymorphism (Radoslovich, 1959). Smith and Yoder (1956) have proposed six simple polymorphs of micas on theoretical grounds, yet only three are at all commonly observed. These are based on 120° rotations between layers, and therefore permitted by ditrigonal surfaces on the layers. The rare or unobserved polymorphs depend on 60° interlayer rotations, which seem unlikely to occur with such surface symmetry.

In several mica structures now published (including muscovite) these ditrigonal surfaces ensure six- rather than twelve-fold co-ordination around the interlayer cation, e.g. K^+. Indeed a roughly octahedral arrangement around the cation of *six* closest surface oxygens with *direct* K–O (or Na–O or Ca–O) bonds may be expected as the normal interlayer configuration. In detail the structural and unit cell data for micas led to the hypothesis (Radoslovich and Norrish, 1962) that:

(i) the *b*-axis is controlled mainly by the octahedral layers and
(ii) the interlayer cations exert additional control through their *direct* bonds to surface oxygens, whereas
(iii) the tetrahedral layers do not affect the cell dimensions significantly but do control the surface configuration, i.e. the degree of "twist".

REGRESSION RELATIONS

Although satisfactory "*b*-axis formulae" could have been derived empirically this would not have *convincingly* shown whether the interlayer cation and/or tetrahedral Al contribute to the sheet dimensions. A multiple regression analysis of the unit cell data against the compositional data of the micas, however, allowed the statistical significance of each coefficient to be tested rigorously (Radoslovich, 1962a). The coefficient for K^+ was significant and large, but for tetrahedral Al it was non-significant—as predicted. In similar regression analyses of data for the kaolins and for the chlorites the coefficien

for tetrahedral Al was also non-significant; for the vermiculites and dioctahedral montmorillonites taken together it was significant but small. The new *b*-axis formulae not only can be applied to most minerals with rather extreme compositions but also provide a better fit for the more common minerals.

GENERAL THEORY

Various data have already hinted that the octahedral cations in these minerals may tend to be partially ordered, and a careful comparison of the regression coefficients and ionic radii also pointed to this possibility. It appeared that cations with high valence either occupy two sites, leaving the third vacant, or else they occupy one site with the other two essentially filled with mono- and di-valent cations. An attempt to test this by more elaborate regression techniques only partly succeeded (Veitch and Radoslovich, 1962), but this study did lead to an explicit new geometrical model of these octahedral layers. This shows that the octahedral are not generally regular in shape, but compressed along c^*. The average effect of substituting larger cations is to increase the thickness three to four times as fast as the sheet dimensions.

The initial justification for the model physically has since been developed into a set of general principles about the forces which are thought to control the structures of the layer-lattice silicates (Radoslovich, 1962b; 1962c). The detailed and explicit statement of these principles, and of the restrictions and limitations in their applicability (Radoslovich, 1962c), cannot safely be condensed into this brief review. The individual concepts must, of course, be consistent with current structural inorganic chemistry. The innovation is the attempt to assess which stresses dominate and which stresses are unimportant throughout this group of structures. Despite the tentativeness of such an initial study this approach appears to have been notably successful both in removing certain previous anomalies and in explaining in considerable detail the individual variations in some precisely known bond lengths and angles, e.g. in dickite (Newnham, 1961) and in muscovite.

SOME IMPLICATIONS

This general theory appears to be soundly based, but at this stage any interpretation of known physical properties in terms of these concepts must be viewed cautiously. Nevertheless, certain implications are highly interesting and merit attention in passing.

For example, the composition limits for natural micas (which have been extensively studied) are more restricted than any limits imposed solely to maintain electrical neutrality. But these observed limits are seen to be quite reasonable for natural specimens when the present principles are applied (Radoslovich, 1962d). Composition limits for the other clay mineral groups, which are of course less well defined, are also consistent in general.

The relative abundance of the different mica polymorphs is broadly known, but the reasons for the observed frequency distribution are hardly understood (Smith and Yoder, 1956). The dioctahedral nature of, and partial ordering of, tetrahedral cations in the $2M_1$ muscovite polymorph is now clearly seen to cause a complex network of stresses and strains which must impose on this structure the observed pattern of layer stacking (Radoslovich, 1962c). Similar forces will be present in other micas and other polymorphs, and the main forms of structural control over mica polymorphism should become plain fairly soon.

The morphology of both kaolins and serpentines has been widely studied, both experimentally and theoretically. The tubular morphology of endellites is generally explained as due to the tendency of the tetrahedral layers to exceed the dimensions of the octahedral layers. Although this is no longer convincing to the author in the light of these studies, other asymmetric forces now may be postulated which could cause the layers to curl (Radoslovich, 1962e).

Finally, the relative stability under weathering of $2M_1$ muscovite must be closely related to the almost unique way in which K^+ is locked into the interlayer positions in this particular mica (Radoslovich, 1962c). This suggests one direction in which future structures analyses may contribute to the study of the complex problems of clay mineral weathering and stability.

The substantial encouragement and participation of my colleagues in C.S.I.R.O. and in the University of Adelaide is gratefully acknowledged.

REFERENCES

Brindley, G. W. and Mac Ewan, D. M. C. (1953) Structural aspects of the mineralogy of clays and related silicates: *Ceramics, a Symposium*, Brit. Ceramic Soc., pp.15–59.

Newnham, Robert E. (1961) A refinement of the dickite structure and some remarks on polymorphism in kaolin minerals: *Min. Mag.*, v.32, pp.683–704.

Radoslovich, E. W. (1959) Structural control of polymorphism in micas: *Nature*, v.183, p.253.

Radoslovich, E. W. (1960) The structure of muscovite, $K\ Al_2(Si_3Al)O_{10}(OH_2)$: *Acta Cryst.*, v.13, pp.919–932.

Radoslovich, E. W. and Norrish, K. (1962) The cell dimensions and symmetry of layer-lattice silicates. I. Some structural considerations: *Amer. Min.*, v.47, pp.599–616.

Radoslovich, E. W. (1962a) The cell dimensions and symmetry of layer lattice silicates, II. Regression relations: *Amer. Min.*, v.47, pp.617–636.

Radoslovich, E. W. (1962b) Cell dimensions and interatomic forces in layer-lattice silicates: *Nature*, v.195, p.276

Radoslovich, E. W. (1962c) The cell dimensions and symmetry of layer-lattice silicates, IV. Interatomic forces: *Amer. Min.*, in press.

Radoslovich, E. W. (1962d) The cell dimensions and symmetry of layer-lattice silicate, V. Composition limits: *Amer. Min.*, in press.

Radoslovich, E. W. (1962e) The cell dimensions and symmetry of layer-lattice silicates, VI. Serpentine and kaolin morphology: *Amer. Min.*, in press.

Smith, J. V., and Yoder, H. S. (1956) Experimental and theoretical studies of the mica polymorphs: *Min. Mag.*, v.31, pp.209–235.

Veitch, L. G., and Radoslovich, E. W. (1962) The cell dimensions and symmetry of layer-lattice silicates, III. Octahedral ordering: *Amer. Min.*, in press.

SOME RELATIONS BETWEEN COMPOSITION, CELL DIMENSIONS AND STRUCTURE OF LAYER SILICATES

by

E. W. RADOSLOVICH

Reprinted from

"Proceedings of the International Clay Conference"
Volume 1, 1963

PERGAMON PRESS

OXFORD . LONDON . EDINBURGH . NEW YORK
PARIS . FRANKFURT
1964

SOME RELATIONS BETWEEN COMPOSITION, CELL DIMENSIONS AND STRUCTURE OF LAYER SILICATES

by

E. W. RADOSLOVICH

Geophysical Laboratory, Carnegie Institution of Washington, Washington 8, D.C., U.S.A., and Division of Soils, C.S.I.R.O., Adelaide, Australia

ABSTRACT

Present concepts of the "ideal" clay mineral structures are too limiting, and should be replaced by a new "ideal" structure in which tetrahedral surfaces are ditrigonal, octahedra are stretched and flattened, and interlayer cations are effectively six-coordinated. These new "ideal" structures are much more closely comparable to the structures already determined and more nearly consistent with current crystal chemistry.

Most papers concerned with relations between composition, cell dimensions and crystal structures of the clay minerals begin with a consideration of some ideal structure. This usually has the following important properties:

(i) These structures include tetrahedral layers consisting of regular tetrahedral groups of oxygens enclosing silicon or aluminium cations, and joined corner-to-corner in hexagonal networks.

(ii) The octahedral layers consist of six anions arranged in approximately regular octahedra around sites in which many different cations may substitute in an isomorphous manner. Adjacent octahedra share edges, i.e. share two anions.

(iii) The interlayer cations in the micas occupy sites enclosed by two hexagons of oxygens, so that in these ideal structures these cations are regarded as 12-coordinated.

The clay minerals are widely understood to possess their known shapes and structures largely because of the way the larger anions pack together, with the cations preserving the overall neutrality, or nearly so, by fitting into the interstices. Clay mineralogists have therefore attempted for some years to relate the cell dimensions of clays to the unit cell contents, i.e. to chemical composition. In particular the sheet dimensions seem to depend very strongly on composition, and quite good empirical formulae expressing the *b*-axis as a linear function of ionic proportions have been in the literature for 20 years. Despite the general goodness of fit of such *b*-axis formulae they are finally inadequate for two major reasons. Firstly the accepted *b*-axis formulae

(e.g. Brindley and MacEwan, 1953) almost always include a term for the effect of tetrahedral substitutions on the sheet dimensions. Secondly, these formulae do not include terms for the interlayer cations in the case of the micas. It has now been shown by Radoslovich and Norrish (1962) and Radoslovich (1962) that earlier formulae are unsoundly based on both accounts, and the fact that they cannot be applied to layer silicates of extreme composition is thereby explained, at least in part.

It is now a matter of observation that the ideal hexagonal network of oxygens on such tetrahedral surfaces is frequently distorted by the rotation of the tetrahedra about axes normal to the plane of the sheet. Such rotations have been reported in the structure analyses of more than ten layer structures, and vary in amount from 5° to 25°. Alternate tetrahedra rotate in opposing directions to give a so-called ditrigonal symmetry to the tetrahedral surfaces. It now seems desirable to discard the hexagonal model, and to formulate a more general ideal layer structure having a ditrigonal surface configuration, which may become hexagonal in particular circumstances.

Recent structural analyses of micas strongly suggest that the tetrahedral layers play a secondary role in determining the *b*-axis, not the co-equal role previously assumed. The cell dimensions of micas appear to be controlled largely by their octahedral layers and by the interlayer cations. The surface configuration, however, depends primarily on the size of the "unconstrained" tetrahedral layer relative to the actual *b*-axis. Radoslovich and Norrish (1962) have therefore proposed that

(a) In all the layer silicates the "silica" tetrahedra can rotate fairly freely to reduce the dimensions of this layer; but the relative rigidity of the tetrahedral group prevents any major extension beyond the hexagonal configuration.

(b) In all the layer silicates the octahedral layer can be extended or contracted with somewhat more difficulty, by changes in bond angles rather than bond lengths, and therefore with accompanying changes in thickness.

(c) For the micas in particular the surface oxygen triads rotate until some (probably half) of the cation–oxygen bonds have normal bond lengths, i.e. until half the oxygens "lock" on to the interlayer cation.

There is strong supporting evidence for each of these hypotheses from both unit cell data and the detailed structure analyses where these are available. As a further direct test new "*b*-axis formulae" were derived using the standard statistical techniques of multiple regression analysis. In this way the effect on the sheet dimensions of Al-for-Si substitutions tetrahedrally was shown to be non-significant, and the effect of the interlayer cations in micas was highly significant (Radoslovich, 1962).

During the course of the regression analyses of dimensions against composition some further structural restraints became obvious. That is, certain groups of minerals did not follow the general physical model implying that the *b*-axis depends linearly on the ionic radii of the substituting cations. In each case satisfactory explanations suggest themselves. For example, the sheet

dimensions of both serpentines, saponites, sauconites, talc and some rare micas are controlled by the limit to which their tetrahedral layers can be stretched. Conversely the sheet dimensions of micas (such as celadonites), having a deficiency of cations octahedrally are decreased by the mutual repulsion of unsatisfied anions along shared octahedral edges. The effect of an interlayer cation (such as K^+) on the b-axis of a mica depends on the size of that cation in relation to the cations in the octahedral positions. The valency of the cation and the exact position in the structure of the charge deficiency which it neutralizes also affects the cell dimensions. The use of multiple regression techniques and more accurate experimental data has led to more reliable relations between sheet dimensions and composition. The new "b-axis formulae" suggest that the data on several minerals which are rare or difficult to study have been misinterpreted and need revision.

If the b-axis and the composition of a layer silicate is known then the tetrahedral rotation, α, may be predicted from

$$\cos \alpha = b_{obs}/b_{tetr}$$

where b_{tetr} is estimated by assuming regular O–T–O angles and the accepted tetrahedral bondlengths for the given substitution. In structures already determined the discrepancies between α_{obs} and α_{calc} may be traced quantitatively, usually being due to departures of the O–T–O angles from ideal.

So far no attempt has been reported seeking to relate the individual regression coefficients explicitly to their ionic radius, i.e. to find some average geometrical factor between ionic radius and the increase in cell dimensions. This has now been attempted concurrently with a study concerned with the arrangement of the octahedral cations. For various intuitive reasons these appear to be largely ordered in the three possible sites of the asymmetric unit of the cell. Trivalent and quadrivalent cations appear either to occupy two sites leaving the third vacant in general, or else to occupy one site with mono- and divalent cations in the other two. Veitch and Radoslovich (1963) developed suitable multiple regression techniques for testing this hypothesis over the layer silicates generally, and to do this an explicit geometrical model was needed for such octahedral layers. We were forced to discard the restraint that the separate octahedra are required to be geometrically regular in shape. It was necessary to allow them to be squashed down in the c^*-direction, and to show a different average rate of expansion normal to the sheets from the rate as measured along the sheets. Experimentally the isomorphous substitution of larger cations octahedrally leads to average rates of expansion three to four times greater in the c-direction than in the b-direction.

The geometrical model proposed as the simplest basis for this statistical study is easily shown to be a reasonable model physically, and of course possesses ideally the several characteristic properties observed experimentally. A typical dioctahedral layer on this model shows (i) an octahedral ordering around the unoccupied and considerably larger sites, themselves arranged

hexagonally and (ii) counter-rotations of the upper and lower triads of oxygens around occupied sites, as shared octahedral edges are shortened. Both effects are clearly observed in the known structures of gibbsite, dickite and muscovite, for example.

In a subsequent study (Radoslovich, 1963a) the simple physical arguments supporting this geometrical model have been developed extensively into general statements about the interatomic forces within the layer silicate structures. Our understanding of these structures can be advanced considerably if we no longer view them primarily as "packing structures". It is now better to attempt to assess empirically the stresses and strains in bond lengths and bond angles, together with the ease of deformation of the supposedly spherical atoms or ions. Accurate structural data from other silicates (e.g. feldspars) may be used to postulate which forces will dominate and which structural elements are most easily deformed in the clay minerals. On this more realistic view the layer silicates are not simply close-packed layers of anions, with cations of the right size stuffed in the interstices, rather passively maintaining neutrality. Each mineral, indeed, represents a stable equilibrium, at the lowest possible internal energy, of bonds under tension or compression, of atoms pushed into close proximity against their mutual repulsion, and (infrequently) of directed bonds under "torsion". Interstices are of the "right size" for certain cations only in the sense that with those cations present the increased strains in the other bonds, distances and angles do not lead to obvious instability.

These structures may be discussed in detail on the basis of several explicit assumptions which appear to be consistent with current structural inorganic chemistry and to be valid for a wide range of complex ionic structures, viz.

1. Bondlengths in general vary inversely as electrostatic bond strengths.
2. Bonds are effectively non-directional, with occasional O—H bonds as exceptions.
3. Bonds increase in compliance in the order (Si—O) → (Al^{IV}—O) → (octahedral cation—O) → (interlayer cation—O).
4. Bond angles are more compliant than bond lengths, and the T–O–T angles more than the O–T–O angles.
5. Mutual repulsion between anions increases very rapidly as interatomic distances fall below the sum of their ionic radii.
6. The mutual repulsion of multivalent cations only partly shielded from each other by intervening anions may be of comparable importance with the strongest bonds.
7. Adjacent anions whose valencies are not fully satisfied by immediate bonds will mutually repel each other with observable structural effects.

On this basis the cell dimensions of an octahedral layer, either separately or in a layer silicate, correspond to an equilibrium between three different kinds of forces. These are (i) cation–cation repulsion across shared octahedral edges, (ii) anion–anion repulsion along shared edges and (iii) cation–anion bonds within the octahedra. On the available evidence these forces result in

severe deformation of all octahedral layers, except for those minerals in which they are opposed by additional and strong external forces. That is, the balance of forces *within the octahedral layer* usually dominates in the layer lattice silicates. Of these forces the cation–cation repulsion is the most influential in causing individual departures from ideal structures, with several important implications, viz.

(i) Dioctahedral structures will show strong tendencies toward regular hexagonal arrangements of cations around vacant sites.

(ii) Sheet dimensions become as large as the cation–anion bonds and O–O approach will allow; major expansions occur along edges of triads enclosing vacant octahedral sites. For example, equilibrium dimensions in pure dioctahedral Al^{3+} minerals correspond to $b = 8{\cdot}92$–$8{\cdot}94$ Å and strong forces external to the octahedral layer are needed to cause any marked variation from this.

(iii) In trioctahedral minerals containing $\approx 2{\cdot}0 R^{2+}$ and some R^{3+} the R^{2+} cations tend to be disposed hexagonally around the R^{3+}, to separate adjacent R^{3+} as much as possible.

(iv) Shared octahedral edges in layers with very different cations should be shortened to about the *same* minimum distance, below which the anions become more incompressible very rapidly.

Although the tetrahedral bonds are regarded as partly covalent (especially Si—O bonds) the O–T–O angles appear to depart readily from the ideal 109° 28′ to limits which are set by the minimum O–O approach along tetrahedral edges, rather than by any directed nature of the T–O bonds. In accurate analyses of felspar structures the individual O–T–O angles may vary from 99° to 119° at least, but tetrahedral edges are rarely shorter than 2·55 Å. It is apparently the shortening of the distances O_{apex}–O_{basal} which sets a physical limit to the stretching of tetrahedral layers in saponites, serpentines, talc and similar minerals.

Important details of the mica structures are actively controlled by the bonds between interlayer cations and the surface oxygens. Since the tetrahedral surfaces in most micas will in any case be ditrigonal there is a marked tendency for the cations to be in sixfold coordination, i.e. directly bonded to six anions arranged approximately octahedrally around the cation. It is notable that only those polymorphic forms of micas have been observed which are consistent with this interlayer arrangement. (Rare exceptions are known only amongst lepidolites in which the K^+ cannot form normal direct bonds to surface oxygens.)

The reported limits of stability (from synthesis studies) and also the observed ranges of composition for natural specimens may be used as independent checks on the validity of the present models of these structures (Radoslovich, 1963b). These models allow broad limits to be set to the strains from preferred lengths and shapes which different structural components (bonds, polyhedral groups) can reasonably tolerate in adjusting to some local dimensional misfit. The formation of micas, for example, in which such strains

should far exceed these limits should not be possible, even in the laboratory. Micas in which the strains would need to be unusually large may be expected to adjust their compositions rapidly, as soon as their environment allowed any change. They may therefore be synthesized but should—for at least this reason—be rare as natural specimens. An examination of the detailed published limits for micas shows that the present structural models are not at all incompatible with these, nor is there any discrepancy with the rather less well defined limits of other layer silicates.

In the light of the present studies the simplest explanation of halloysite tubular morphology (i.e. tetrahedral dimensions exceeding octahedral dimensions) is seen to be inadequate (Radoslovich, 1963c).

REFERENCES

Brindley, G. W. and MacEwan, D. M. C. (1953) Structural aspects of the mineralogy of clays and related silicates: *Ceramics: A Symposium, Brit. Ceramic Soc.*, p. 15.

Radoslovich, E. W. and Norrish, K. (1962) The cell dimensions and symmetry of layer lattice silicates. I. Some structural concepts: *Amer. Min.*, v. 47, p. 599.

Radoslovich, E. W. (1962) The cell dimensions and symmetry of layer lattice silicates. II. Regression relations: *Amer. Min.*, v. 47, p. 617.

Radoslovich, E. W. (1963a) The cell dimensions and symmetry of layer lattice silicates. IV. Interatomic forces: *Amer. Min.*, in press.

Radoslovich, E. W. (1963b) The cell dimensions and symmetry of layer lattice silicates. V. Composition limits: *Amer. Min.*, in press.

Radoslovich, E. W. (1963c) The cell dimensions and symmetry of layer lattice silicates. VI. Serpentine and kaolin morphology: *Amer. Min.*, in press.

Veitch, L. G. and Radoslovich, E. W. (1963) The cell dimensions and symmetry of layer lattice silicates. III. Octahedral ordering: *Amer. Min.*, in press.

Paper 2-13.

Handbuch der Bodenkunde

Vol. II. Soil Components

Section D, Part 3. "Micas"

E.W. Radoslovich

Division of Soils, Commonwealth Scientific
and Industrial Research Organisation, Adelaide,
South Australia.

Date. April, 1967.

Chapter 3. Micas.

Part A. Macroscopic micas (by E.W. Radoslovich).

Introduction.

Structure analyses of micas.

Cell dimensions and chemistry.

Polymorphism and twinning.

Infra-red analysis.

Part B. Micaceous clay minerals (by T. Kato and K. Norrish).

INTRODUCTION

This chapter on micas has been written in two parts. The first part (by E.W. Radoslovich) treats the mica minerals as they are usually understood by the petrologist - i.e. as minerals which may be found in rock systems, often in hand-specimen size, and which may be studied by optical and single-crystal x-ray methods. The second part (by T. Kato and K. Norrish) discusses 'the micas' as the term is used by many agricultural and soil scientists. These are the micaceous clay minerals (or illites) and related colloid-sized mica-like minerals. It should at once be emphasised that in spite of this editorial subdivision there is a complete gradation in all the important properties from well-crystallised mica in large sheets (as used industrially in insulators etc.) to the very poorly crystallised mixed-layer clay minerals with a (potassium-deficient) micaceous component. It is, in fact, this continuity of properties from the coarsest to the finest micas which justifies this account of recent research on the macroscopic micas in this Handbuch der Bodenkunde. In particular the detailed study of their atomic structure, of some aspects of their chemistry, weathering and alteration, of their anisotropic infra-red absorption etc. cannot be pursued effectively (or perhaps at all) on clay-sized mica particles. On the other hand, once explicit ideas and hypotheses have been developed for the macroscopic micas it is usually possible to devise relatively simple checks on the validity of their application to the fine-grained mica minerals. The discussion of the coarse-grained micas will include the brittle micas, even though these do not appear - for good crystallo-chemical reasons - to persist into the <2μ fraction of soils.

The micas are very important mineralogical components of a wide range of agriculturally significant soils. For example, the red-brown earths in Australia cover large areas of the most productive wheat-growing country. Their clay mineralogy has been systematically studied by Radoslovich (1958), who showed that illitic minerals generally make up from 40% to 60% of the clay fraction which is itself the major fraction of the whole soil. This kind of result would be typical for many soils in the main agricultural zones of the world. The micaceous clay minerals in such soils are important because of their chemistry (e.g. as sources of nutrient elements) and because of their colloidal properties (e.g. their large surface areas which may be highly reactive). Their platy morphology contributes to the physical properties of many soils having a moderate to heavy texture - e.g. the formation of 'cutans' as studied by micropedologists (Brewer, 1964).

The mica minerals embrace quite a wide range of chemistry and correspondingly of physical properties. They are all, however, silicate minerals (mostly alumino-silicates) with a markedly platy morphology, and a perfect basal cleavage, because of their characteristically layered atomic structures. The various mineral names such as muscovite, biotite, lepidolite etc. represent ideal chemical formulae, but there is a considerable range of substitutions possible in each case. A chemical formula such as $H_2\ K\ Si_3\ Al_3\ O_{12}$ is therefore rather meaningless unless it is rearranged as the structural formula $K\ Al_2\ (Si_3Al)\ O_{10}\ (OH)_2$. The use of structural formulae becomes essential for the adequate discussion of most micas other than the exceptional specimens, called 'end-member' micas showing virtually no isomorphous substitution.

The micas may be described in terms of a geometrically-ideal structure, and such a description is given in almost all standard text-books, e.g. Bragg and Claringbull (1965); Deer, Howie and Zussman (1962); and Brown (1961). This is of course the most straightforward way to introduce the reader to the results of modern structural analyses of micas, and will be used here. It is important, however, for the soils research worker to realise clearly that the true crystal structures of micas inherently depart quite substantially from this geometrical model (Radoslovich and Norrish, 1962), and that any departure from the simplest model should not be thought of as a structural aberration for that particular mineral. It is much more likely that a mica which is found to approach the simple structural model at all closely will probably have a quite unusual composition. The geometrical structure should not be called the 'ideal' mica structure because this has in the past created mental blocks - perhaps 'stylized' (or 'model') mica structure might be a more useful term.

The basic unit in this model is a sheet of linked tetrahedral groups of four oxygens surrounding Si^{4+} (or sometimes Al^{3+} cations) as shown in Figs. 1, 2, 3 and 4. Two such sheets, suitably oriented and bound together, constitute a single layer of the mica structure. The orientation is such that the lower sheet has its tetrahedral apices upward and the upper sheet has its tetrahedral apices downward. These two sheets are held firmly together by so-called Y cations (mono-, di-, or tri-valent ions such as Li^{+}, Mg^{++}, or Al^{+++}) and they are held together so that the coordination around the Y cations is octahedral. Thus each Y cation is surrounded by six anions, four of which are apical oxygens from the two tetrahedral layers and the remaining two being hydroxyls which fit into

gaps in the two arrays of apical oxygens. Finally, each such layer unit (which is to be considered of infinite extent two-dimensionally, relative to ionic dimensions) is joined face-to-face with another such layer. The 'hexagonal holes' on opposing tetrahedral layer surfaces are matched to provide a 12-coordinated site into which a monovalent ion (usually K^{+}) is fitted, except for the brittle micas in which this X cation position is occupied mainly by Ca^{++}. The central Y cations determine the relative positions of the two tetrahedral sheets so that they are displaced relative to one another by -a/3 in the [100] direction i.e. parallel to the a-axis (Fig. 5). The perfect cleavage occurs at the level of the X-cations because these interatomic bonds are the weakest in micas.

This stylised mica structure corresponds to a unit cell with approximate dimensions a = 5 Å, b = 9 Å, c = 10 Å, (Fig. 4) which is monoclinic with $\beta = 95^{\circ}$ but has a face-centred a-b plane. This model has hexagonal surface symmetry, whereas in almost all real micas the surfaces will only show pseudo-hexagonal symmetry at best, or more probably trigonal symmetry. This unit cell contains $2[Y\ (Si_3Al)\ X_2^{+++}\ O_{10}\ (OH)_2]$ units chemically, and is called a one-layer mica structure.

The micas, in common with many other compounds of pronounced layer morphology, show extensive polytypism or polymorphism*. This means,

---

* Polytypism is polymorphism in a narrow and restricted sense, and is probably the more precise term to apply to the layer silicates. But 'polymorphism' is not incorrect and has been much more widely used in the older literature; it will be retained in this article.

for the micas, that regular crystal structures are found in which the repeat distance in the c-direction is some multiple of (approx.) 10 Å. For example, muscovite most commonly occurs as a 'two-layer monoclinic' mica, with c ≈ 20 Å. This means that it can be thought of as one single-layer unit (of muscovite composition) with a second single layer unit added but with the direction of the 'monoclinic stagger' across the octahedral part of the second layer turned through -120° relative to the first. The third layer is 'turned' through +120° again, i.e. it now coincides in direction with the first layer, or in other words the repeat distance is two layers high, or roughly 20 Å. Smith and Yoder (1956) developed a very useful graphical vector notation for representing the possible arrangements of successive layers in the structurally distinct mica polytypes (Fig. 5). It should perhaps be added in warning that it is very unlikely that any physical rotation of one layer relative to another ever occurs. The 'rotations' referred to in discussion of mica polymorphism are really rotations of the vectors representing the monoclinic directions of each layer considered separately. Such a vector rotation can be achieved by relatively small movements of the Y atoms only (or even of the protons of the OH's) without requiring some major reconstructive transformation of the whole mica crystal.

As shown in Fig. 6, Smith and Yoder (1956) described six simple mica polymorphs which might be expected to occur on the basis of the hexagonal surface symmetry which the stylised mica structure possesses. In fact more complex polymorphs also exist, and even these six different stacking arrangements are not observed with equal frequency. The two-layer orthorhombic (20) polytype is extremely rare (perhaps non-existent). The

one-layer monoclinic (1M) polytype is the most common arrangement for some micas such as phlogopite ($K\ Mg_3\ (Si_3Al)\ O_{10}\ (OH)_2$), whereas the $2M_1$ polytype is the commonest form for primary muscovites ($K\ Al_2\ (Si_3Al)\ O_{10}\ (OH)_2$).

All micas may show twinning on the 'mica twin law' with composition plane {001} and twin axis [310], and well formed crystal often show {110} faces and therefore pseudo-hexagonal outline. A mica twin may be represented by a vector diagram, as for mica polymorphism, in which the twinning simply is shown by some irregularity in the otherwise regular pattern of vectors. Polymorphism and twinning are discussed further in a later section.

We have noted that all micas have an 'octahedral layer' or, in other words, certain 'Y' cations are octahedrally coordinated within the structure. A 1M mica typically has six such sites within the unit cell, although these are partly symmetry-related positions. It so happens that some micas (e.g. muscovite) only have two out of every three octahedral sites actually occupied (each by a trivalent cation) whereas other micas (e.g. phlogopite) have all sites, or three in three, occupied (each by a divalent cation). Micas of the first kind are called di-octahedral, and of the second kind tri-octahedral. For many natural micas with extensive isomorphous substitution the average occupancy over very many unit cells varies from somewhat less than two, all the way up to three (theoretical limit). There are, however, observed compositional limits for most micas such that micas with about 2.5 out of three sites occupied, (on the average) are quite exceptional. These composition limits are discussed again later.

The cell dimensions of the layer silicates depend broadly upon the effective radius of the oxygen anion in an ionic bond, since these

silicate minerals are crystal structures in which the anions are close-packed and the bonds are mostly ionic in character. The detailed differences in cell dimensions between various layer silicates (e.g. between micas) depends upon the size and valency of the cations. Empirical formulae have been developed by several authors who have sought to relate chemistry to cell dimensions in some systematic way. The more recent attempts (e.g. Radoslovich and Norrish, 1962) make use of the further insight into the detailed balance of forces within these minerals which recent structure analyses have provided.

STRUCTURE ANALYSES OF MICAS

The first complete structure analysis of a mica was made by Jackson and West (1933), and gave us the model described in the Introduction. It represented a very large advance in our understanding of the sheet silicate minerals. It was, however, widely understood that this structure was only a first approximation and it was with this in mind that Radoslovich (1960a) attempted a further refinement of the atomic coordinates using more modern crystallographic techniques. For this purpose it is essential to have available sufficient experimental data of reasonably high accuracy (Mathieson et al., 1959) and to have access to adequate high-speed computer facilities in order to carry the refinement of the structure analyses to the point where it really has converged closely towards the true structure. The techniques of crystal structure analysis need not be described here; the reader who wishes to pursue them should consult recent books such as Buerger (1960) or Lipson and Cochran (1966).

The refinement of the structural data for muscovite by Radoslovich (1960) advanced our understanding of this and other layer silicate structures considerably, even though it was later shown by Gatineau (1963) to be incorrect in one respect because the calculations had been terminated before the coordinates had fully converged to the best possible values.

The important results of this analysis are these. First, the surface network of oxygens does not have hexagonal symmetry. If we consider the triads of oxygens which make up the tetrahedral bases in the stylised mica model, then to adjust these anions to their true positions in muscovite the main displacement required would be a rotation of each triad about an axis through its centre (and normal to the layers) of roughly 13°. Since all triads are linked (they share corner oxygens) this means that neighbouring triads must turn +13° and -13° (see the crystal model by Radoslovich and Jones, 1961, and also Fig. 7). The effect of such an adjustment on each hexagonal hole in the layer surface is that three alternate oxygens move in towards the centre of the hole, and the remaining three move away from the centre, but of course towards the centre of neighbouring holes. It is again emphasised that such rotations and movements are primarily mental adjustments from the simplest model, though in fact some recent experiments in which the actual composition of muscovite has been changed must have involved physical articulation of the tetrahedral network (Burns and White, 1963). When two such surface holes are opposed to enclose the interlayer K^+ the potassium can only be 6-coordinated, not 12-coordinated - it is enclosed roughly in an octahedron of oxygens with K-O bonds of approx. length 2.81 Å. The remaining six

oxygens are at a distance of approx. 3.4 Å from the given K^+ but of course are at about 2.81 Å from neighbouring potassiums.

Second, the surface oxygens are not strictly coplanar. Each triad is slightly tilted, a similar result to that obtained by Newnham (1961) for dickite, for example. Tilting of tetrahedral groups for di-octahedral micas has been discussed extensively by Takéuchi (1966).

Third, the monoclinic angle does not only depend on the 'stagger' within the octahedral layer (Fig. 2); there is a further displacement of K^+'s from their positions in the simplest model which increases the mono-clinic angle beyond the predicted $\beta = \cos^{-1}(-a/3c)$.

Fourth, the "forbidden" 061, l-odd, reflections can now be accounted for by the displacement of the tetrahedral groups from the mean positions $y = n\,b/12$ (Radoslovich and Norrish, 1962), due to muscovite being dioctahedral.

Fifth, the octahedral layers conform strictly to Pauling's Rules in having shortened shared edges by counter-rotations of the triads making up the two faces of the octahedra which are parallel to the sheet, and in being 'squashed' in the direction normal to the sheets (Veitch and Radoslovich, 1963; Radoslovich, 1963).

Sixth, the stacking of layers which seems to imply octahedral coordination around K^+ does not in that case allow one-half of Smith and Yoder's (1956) hypothetical polymorphs. For muscovite, for example, the 20 polymorph would imply a trigonal prismatic arrangement of six oxygens around each potassium, a coordination which does not appear to be favoured by that ion. Certainly the recent comprehensive study of mica polytypes by Ross et al. (1966) has not uncovered any specimens to contravene this

limitation on polymorphism which was suggested originally by Radoslovich (1959).

Last, the structural refinement of muscovite strongly suggested, on the basis of 'Si' -O bond-lengths, that Al^{3+} did not occupy all possible tetrahedral sites with an equal probability. In fact it was claimed that half the sites were virtually only occupied by silicon, whereas the statistical occupancy of the other sites was $Si_{\frac{1}{2}}\ Al_{\frac{1}{2}}$[(1)]. This result was apparently confirmed by the less accurate refinement of the muscovite structure by electron-diffraction by Zviagin and Mischenko (1961). On the other hand Gatineau (1963, 1964a,b) has shown that had Radoslovich (1960a) had the computer facilities to fully refine his data by least-squares methods then his data would have converged to a different result in which Al^{3+} is randomly distributed in all four sites, whose average occupancy is therefore $Si_{\frac{3}{4}}\ Al_{\frac{1}{4}}$. Only one subsequent refinement of mica structures has yielded a result indicating an ordered arrangement of Si and Al in tetrahedral sites. Indeed the highly accurate refinement of a coexisting muscovite and paragonite by Burnham and Radoslovich (1963) gave 'T-O' bonds fully consistent with 4 $Si_{\frac{3}{4}}\ Al_{\frac{1}{4}}$ sites. Moreover DeVore (1963) had put forward theoretical arguments against the ordering proposed

---

[(1) It should be noted that single crystal structure analysis by classical x-ray techniques will give the positional and vibrational parameters for each atom averaged over thousands of unit cells. Si and Al can only be distinguished in the present case by the observed (average) 'T-O' bond-lengths. The occupancy of a particular site in a given cell cannot be determined if Si and Al are statistically distributed in successive cells].

by Radoslovich (1960a). On balance it appears that Gatineau (1963) is correct in assessing that the refinement had not been computed to a convergent result in this respect. His calculations do not make significant changes in the other deductions about the muscovite structure.

Gatineau (1963, 1964a, 1964b) has attempted to obtain further information about the "real" structure of muscovite by the admittedly difficult analysis on non-Bragg reflections or diffuse scattering. His work, which has been summarised by Brown (1965), is the only study reported so far on short range order in layer silicates and is particularly interesting for that reason. Gatineau "concluded that the substitutions of Al- for -Si tend to occur in rows in whch every atom is substituted. These rows favour the [10] or [11] or [1$\bar{1}$] directions in the plane of the layer which are at 120° to each other. The crystal is thus divided into domains each of which is characterized by the directions of these rows. The rows of substitutions are grouped together into bands that contain equal numbers of rows of entirely Al and entirely Si atoms but without regular alternation, that is in these bands Al/Si = 1:1. The bands alternate with bands of equal size, in which there is no Al, thereby leading to an overall ratio of 3 Si to 1 Al. Substituted and unsubstituted bands face each other across interlayers, and this leads to local charge balance around each K ion". This model does not seem unreasonable physically at first sight, though the experimental errors in the data from which it is derived must by their very nature be fairly large. It is, however, worth noting that the arrangement of tetrahedral Al's proposed by Gatineau (in which adjacent Al's share the same bridge oxygen) contravenes Loewenstein's (1954) rule viz. "whenever two tetrahedra are linked by one oxygen

bridge, the centre of only one of them can be occupied by aluminium; the other centre must be occupied by silicon, or another small ion of electrovalence four or more". This empirical rule seems to have been in agreement with the results of modern structure analyses, since it was proposed by Loewenstein, except in the case of a most unusual mineral such as the brittle mica xanthophyllite, Ca $(Al\ Mg_2)$ $(Si\ Al_3)$ O_{10} $(OH)_2$, studied by Takéuchi and Sadanaga (1959) and Takéuchi (1965). It seems that Gatineau's model should perhaps be accepted with some reservation until this anomaly is resolved.

The highly accurate structure analyses of a coexisting muscovite and paragonite by Burnham and Radoslovich (1963) has confirmed the general conclusions of Radoslovich (1960a) with the notable exception that there is no evidence at all for tetrahedral ordering. This is shown in Table 1, which also gives some idea of the accuracy of these analyses. The composition of these two specimens was determined by electron-microprobe analysis as

Paragonite $(K_{0.15}\ Na_{0.85})\ Al_2\ (Si_3\ Al)\ O_{10}\ (OH)_2$

Muscovite $(K_{0.65}\ Na_{0.35})\ Al_2\ (Si_3\ Al)\ O_{10}\ (OH)_2$

By allowing the scattering factors for the X atoms to vary during the final cycles of least squares analysis the occupancy was determined during the structure analysis as $K_{0.15}\ Na_{0.85}$ ± 0.02 and $K_{0.66}\ Na_{0.34}$ ± 0.02 - in very close agreement with the microprobe results. The way in which the two structures are collapsed around the K^+ or Na^+ ions to give these 6-fold coordination is shown in Fig. 6.

The equivalent isotropic temperature factors, B, are remarkably

similar, atom for atom, in the two structures, and the equality of the temperature factors for all four tetrahedral cations (0.65, 0.65, 0.62, 0.63) immediately suggests that the aluminium-silicon distribution is identical in all four positions. A careful consideration of the apparent anisotropic thermal motion of the surface oxygens strongly suggests that the arrangement of K^+ and Na^+ ions within either structure is completely random; there is no evidence for segregation either into different layers or to different domains within a layer.

Complete solid solution between muscovite and paragonite does not occur and in fact Zen and Albee (1964) have shown that the solvus is extremely asymmetric, the solubility of muscovite in albite being very limited. The asymmetric solid solution limits are easily explained by considering the variation of average alkali/oxygen interatomic distance with changing K/Na ratio.

This has now been followed by a similarly precise determination of the structure of a 3T muscovite. The interesting features of this structure include significant ordering both of the tetrahedral and of the octahedral cations. Of each four tetrahedral sites two are occupied only by Si, on the basis of T-O bonds of 1.620 ± 0.010 Å; the other two contain about 35% Al (i.e. $Si_{.65}\ Al_{.35}$) on the basis of T-O = 1.657 ± 0.010 Å. Likewise one kind of octahedral site is fully occupied by Al; the other Al octahedron also contains 30-35% Mg, Fe.

Structural studies have been made on some other micas. Pabst (1955) showed that the 1M (one-layer monoclinic) micas could be assigned to the centrosymmetric space group C 2/m. Zviagin (1957) determined the structure of the unusual mica, celadonite, with structural formula

essentially $K_{0.8}$ $(Mg_{0.7}$ $Fe^{2+}_{1.4})$ $(Al_{0.4}$ $Si_{3.6})$ O_{10} $(OH)_2$. The structure determination is of limited accuracy because of the difficulties inherent in electron diffraction methods at that time. Nevertheless it shows features which are consistent with our enlarged understanding of the chemistry, cell dimensions and structure of layer silicates (Radoslovich and Norrish, 1962; Radoslovich, 1962). In particular, the $Mg_{0.7}$ $Fe^{2+}_{1.4}$ ions appear to occupy only two-thirds of the octahedral sites, as predicted for the general case by Veitch and Radoslovich (1963); and the octahedral layer is quite thick, due to the residual charge carried on the anions which is not satisfied by direct bonds to nearest-neighbour cations.

Takéuchi and Sadanaga (1959) reported briefly on the brittle mica structure, xanthophyllite Ca Mg_2 Al (Si Al_3) O_{10} $(OH)_2$; and Takéuchi (1966) compared this with margarite, Ca Al_2 $(Si_2$ Al_2 O_{10} $(OH)_2$. There is no significant evidence for ordering among the cations in the silicate layer of margarite. The tetrahedral groups are 'rotated' by 23° and 21° (in xanthophyllite and margarite) from their stylised hexagonal positions (Figs. 8 and 9). The octahedral layers in margarite and muscovite are very similar. Takéuchi (1966) has again drawn attention to the fact that the tetrahedral groups are tilted - one of the three basal oxygens is elevated, and more so in margarite than in muscovite. He points out that in the trioctahedral micas the octahedral sites are more nearly equal in size and all occupied; accordingly the silicate layers are almost free from tilting (Figs. 9 and 10). One consequence of the fact that one in three octahedral sites is vacant in the dioctahedral micas is that the network of apical oxygens is no longer strictly hexagonal (Fig. 11).

As Takéuchi (1966) has pointed out the edgelengths of the oxygen hexagons remain surprisingly constant for various kinds of dioctahedral layers (Table 2) suggesting that the octahedral layers are a fundamental feature of the structures of layer silicates. Radoslovich and Norrish (1962) have similarly emphasised the importance of the octahedral layers in these structures.

Steinfink (1962) has carefully refined the structure of a phlogopite, $(K_{0.9}\ Mn_{0.1})\ Mg_3\ (Si_3\ Fe^{3+})\ O_{10}\ (OH)_2$, in which Fe^{3+} rather than Al^{3+} is found substituting for Si^{4+} tetrahedrally. It is a 1M mica and again shows a 'rotation' of each tetrahedral group of about 12° about the normal to the sheets. Steinfink allowed for the possibility of Fe^{3+} tetrahedrally or octahedrally, and also for centrosymmetry or non-centrosymmetry. His least squares refinement converged to a centrosymmetric structure with Fe^{3+} in the tetrahedral sites at random. Again the K^+ was found to be six-coordinated - the K-O distances were either around 2.94 Å or around 3.45 Å, and the latter can hardly be an effective bond.

Zviagin and Mischenko (1962) have studied the structure of phlogopite-biotite by electron diffraction; this shows a $5\frac{1}{2}$° tetrahedral 'rotation'. Franzini and Schiaffino (1963a) have reported on the crystal structures of six biotites by one-dimensional Fourier projections on C*. They deduced a mean tetrahedral 'rotation' of 10°, almost regular octahedral coordination around K^+ with K-O about 2.92 Å, and rather regular Si-O tetrahedra. These 'structure analyses' provide data on the z-coordinates only and there is considerable superposition of atoms. Their interpretation is based on the discussion of cell dimensions in relation to structure by Radoslovich (1962). In so far as Franzini and Schiaffino's

analyses lead to very reasonable bondlengths and coordination around cations this work provides further substantial confirmation of the general structural model proposed by Radoslovich and Norrish (1962).

Donnay et al (1964) have refined the structure of a synthetic iron mica $K\ Fe_3^{2+}\ (Si_3\ Fe^{3+})\ O_{10}\ (OH)_2$ which may be called ferri-annite by analogy with annite whose composition is $K\ Fe_3^{2+}\ (Si_3\ Al)\ O_{10}\ (OH)_2$. It is unfortunate that the inherent errors in the original measured intenstities did not allow the full power of modern least-squares refinement to be used, but the final positional parameters still give much more useful information about mica structures than was available a few years previously. This structure conforms to the general features of the mica structures discussed above.

One final comment may be useful to soil scientists. It has often been emphasised that the tetrahedral bonds (especially Si-O bonds) are the strongest in the micas. This is true, but it does not therefore follow that the tetrahedral groups are geometrically regular and rigid, or that the Si-O-Si bond angles are fixed, or that there are no circumstances at all under which the Si can be removed or replaced. On the first point it is worth noting that the recent precise structure analyses of the framework silicates, the felspars, have shown that the tetrahedral groups <u>may</u> be somewhat distorted (e.g. Jones and Taylor, 1961). For micas of unusual composition it seems necessary for the tetrahedral groups to be distorted from the regular shape (Radoslovich and Norrish, 1962); the limits seem to be set by the O-O interatomic distances along tetrahedral edges, which do not easily fall below 2.55 Å (Radoslovich, 1963). The actual length of the Si-O bond is very nearly constant, unless there is some isomorphous

replacement of the Si, of course.

On the flexibility of the Si-O-Si linkage it is worth noting Bernal's (1963) comment: "Where we were wrong, and I went wrong myself, was in assuming that, for instance, because a silicon-oxygen chain was chemically the strongest part of a structure it was also automatically the most rigid part of the structure". Accumulated recent data on silicate structures shows what a wide range of angles can be attained at such a bridge oxygen linkage, and we must certainly expect the micas to articulate readily at the bridging oxygen positions. The highly ditrigonal surface arrangement on the brittle micas demonstrates this - 'rotations' of as much as 23° from the hexagonal model are observed.

On the third point, H.F.W. Taylor and his colleagues has written extensively on various mechanisms for topotactic transformations (e.g. Glasser, Glasser and Taylor, 1962). Their studies suggest that it is not really very hard for a small highly charged cation like Si^{4+} to escape the oxygens coordinated around it - provided that there is a suitable crystallographic environment for it to escape to. Likewise Donnay, Wyart and Sabatier (1959) have suggested at least one simple mechanism for breaking Si-O bonds to bridge oxygens, and releasing the cation. Their "explanation of the mobility of the Si and Al ions rests on the catalytic action of protons and hydroxyl ions. We must therefore ascertain the presence of these ions whenever Si and Al are found to rearrange themselves in the solid state". Admittedly Donnay, Wyart and Sabatier were concerned with transformations in the solid-state at around 700-900°C; but it is at least worth noting that mechanisms are being proposed and studied that appear to allow reasonable mobility of the tetrahedral cations under some

conditions.

CELL DIMENSIONS AND CHEMISTRY

It has been recognized for some years that the unit cell dimensions of micas are dependent on their chemistry - i.e. when isomorphous substitutions occur in micas the cell dimensions change in ways which depend upon ionic radii and should therefore be predictable. A number of attempts have been made to develop 'cell-dimension formulae' or algebraic relations between cell parameters and the ionic proportions as expressed in the structural chemical formulae.

The reasons for seeking to establish such cell-dimension formulae are several: (1) they should provide quantitative relations between two properties determined independently, and hence give a check on each determination; (2) in some cases the cell parameters will broadly indicate the chemistry, at least by distinguishing biotites from phlogopites from muscovites; (3) the development of adequate cell formulae for all micas (including some of very unusual composition) has refined our understanding of their crystal structures.

It is hardly possible to develop such cell-dimension formulae simply by using a table of 'standard ionic radii'. The reason for this is that there is really no such thing as a single value for the ionic radius of the different cations and anions. In each structure the bond lengths (and interatomic distances where no bond is involved) are variable over quite a range of values, weaker bonds being more variable in length than stronger bonds. In fact the final bondlengths, as given by a precise crystal structure analysis, represent the equilibrium distances of the

atoms as a result of the total network of all forces in that particular structure. At the present time it is much easier to carry out a full structure analysis to determine interatomic distances experimentally than it would be to predict all the interatomic forces and the equilibrium coordinates of the atoms, as a results of these!

Cell-dimension formulae developed so far have therefore been almost entirely empirical, though it has usually been shown that the formulae make physical sense as well. The best-known formulae are probably those of Brown (1951), Brindley and MacEwan (1953), Radoslovich (1962) and Donnay, Donnay and Takeda (1964). These formulae are largely 'b-axis formulae' because $a = b/\sqrt{3}$ very closely indeed and does not require a separate expression. For the micas it has proved quite difficult to develop cell-dimension formulae relating the layer thickness (i.e. $d\ (001) = c \sin\beta$) to the isomorphous substitutions; indeed it has only been attempted by Donnay et al (1964) and then only for the one-layer trioctahedral micas.

Brown (1951), and Brindley and MacEwan (1953), adopted the approach of considering the b-axes for pairs of minerals (e.g. $Al(OH)_3$ and $Mg(OH)_2$) which have a similar layer structure to the octahedral layers of micas. This led to 'an expansion coefficient' associated with a given substitution - in this case of $3Mg^{2+}$ for $2Al^{3+}$. Whilst their formulae gave general agreement with experimental results they did not satisfactorily predict cell dimensions of some micas of extreme composition. For each pair of minerals it so happened that there was some unique structural factor modifying at least one sheet dimension, so that the differences could not be used for a general prediction formula (Radoslovich, 1962).

An alternative approach is to use multiple regression analysis* (Radoslovich, 1962) to develop the most general prediction formulae for the b-dimensions of layer silicates. It is assumed that paragonite, $Na\ Al_2\ (Si_3\ Al)\ O_{10}\ (OH)_2$, will have the smallest b-dimensions for micas. The b-dimensions and ionic proportions of as many carefully analysed micas as possible are then included in the regression analysis to determine the coefficients 'a_i' in the formula

$$b = b_o + \Sigma_i\ a_i\ x_i$$

where b = required b-dimension for a given mica in which x_i are the ionic proportions of the various substituting cations of the kind i = 1, 2, 3..... in the general structural formula for the micas. The regression constant b_o will correspond to the b-dimensions for a mica with no substitutions, viz. paragonite. The analysis therefore allows for substitutions at the octahedral, tetrahedral and interlayer sites for cations. Using data for 45 micas of different compositions produced a useful formula

$$b = 8.995 + 0.099\ K - 0.069\ Ca + 0.062\ Mg + 0.116\ Fe^{2+} + 0.098\ Fe^{3+} + 0.166\ Ti$$

This empirical formula seems to give good agreement between chemistry and cell dimensions for all naturally-occurring micas except celadonite. (For these the layer charge is largely located at the octahedral level and the

---

* Multiple regression analysis is a standard technique of mathematical statistics which has only rarely been applied to mineralogical problems in the past, mostly in connection with optical properties.

physical model underlying the regression analysis is not applicable). The agreement becomes a little poorer for some synthetic biotites of very high iron content (Wones, 1963) but these are micas in which the strains in their structures aryknown to be large.

The b-dimension formula above does not include a term for Al^{3+} substituting for tetrahedral Si^{4+}, because the coefficient was found to be not significantly different from zero. This simply reflects the ease with which a tetrahedral layer can contract by articulating at the shared or bridging oxygens.

Donnay, Donnay and Takeda (1964) have carefully reviewed the basic postulates for cell dimension formulae in the case of trioctahedral one-layer micas. For these micas Donnay et al offer formulae to enable the detailed prediction of atomic coordinates on the basis of known composition, the experimental values of b and of d (001) = c sin β, and average values of tetrahedral and octahedral metal-oxygen distances taken from the literature. Their predictions certainly give quite close agreement with atomic positions and bondlengths where these are known experimentally. Their formulae are limited in application to the one-layer trioctahedral micas; as Brown (1965) has commented, the Donnay formulae do not allow for ordering of octahedral cations or for incomplete occupancy of the octahedral sites, partly because both factors would be very difficult to deal with theoretically.

The assumption that the b-axis is a linear function of the ionic porportions is quite obviously an empirical approximation whose main virtues are that it is simple and gives reasonable cell-dimensions generally. In fact the average (Na, K) - O distance does not increase linearly with the

substitution of K^+ for Na^+ (Burnham and Radoslovich, 1963). Moreover the effect of K^+ on the b-axis of muscovite has been studied quite directly by Burns and White (1963). They treated muscovite with molten lithium nitrate, thereby forcing Li ions into the vacant octahedral sites, reducing the layer charge and removing the potassium. The b-axis decreased, as expected, and the data indicated a curvilinear relationship with at least two distinct slope values between the b-dimension and potassium content.

The composition limits amongst natural micas have been studied particularly by Foster (1956, 1960a,b,c). This kind of study does not define the equilibrium conditions and stability fields in the same way as laboratory studies under reversible hydrothermal conditions of the synthesis and stability of, say, phlogopite may do (e.g. Yoder and Eugster, 1954). But a survey of natural mica compositions, as undertaken by Foster, does indicate the maximum variations to be expected, taking into account by implication the temperature and pressure conditions under which micas are very generally formed, the availability and relative abundance of various elements during their formation, and the speed with which the various micas are altered under field conditions*. Foster has defined empirical composition limits for the different species of micas, which are summarised by triangular diagrams such as Fig. 12 and 13. She has also discussed in detail the distribution of charge between the tetrahedral, octahedral and inter-

---

* If a mica of unusual composition is very rapidly weathered then it is unlikely that specimens will be found by field geologists.

layer regions of all the micas studied, and drawn limits to the ranges of charge distribution. For example a phlogopite should, according to Foster, lie within the limits

<+0.30 -1.00 to -1.30 Total -1.00 ± 0.10 +1.00 ± 0.10

$$[(R^{3+}_{<0.50}\ Fe^{2+}_{<0.50}\ Mg_{3.00\ \text{to}\ 2.00})\ (Si_{3.00\ \text{to}\ 2.70}\ Al_{1.00\ \text{to}\ 1.30})\ O_{10}\ (OH)_2]\ K(Na,\ Ca/_2)_{1.0\ \pm 0.1}$$

3.00 to 2.85 4.00

Foster's studies really represent a broad correlation of the descriptive mineralogy and structural chemistry of the mica group. The limits appear to be fully compatible with the stresses and strains which are thought to develop within the crystal structures of the micas as different isomorphous substitutions occur (Radoslovich, 1963b).

The chemistry of individual micas species will not be discussed in detail here; excellent reviews (including many typical chemical analyses) are available in recent books on Mineralogy, e.g. Deer, Howie and Zussman (1962). The method by which structural formulae are usually calculated from the elemental analyses is worth stating, however. It is assumed that the chemical composition of a mica can be represented by $X_2\ Y_{4-6}\ Z_8\ O_{20}\ (OH,\ F)_4$ where

X is mainly K, Na or Ca but also Ba, Rb, Cs, $(H_3O)^+$ etc.

Y is mainly Al, Mg or Fe but also Mn, Cr, Ti, Li etc.

Z is mainly Si or Al but perhaps Fe^{3+} and Ti.

Moreover it is assumed that the anion network will be complete - that there are no missing oxygens or hydroxyls - and that the tetrahedral sites will be fully occupied. On the other hand the octahedral sites cannot contain more than 6Y and rarely contain less than 4Y. The number of X cations is

quite variable, but for many macroscopic micas is less than but close to 2. If the chemical analysis is given in terms of percentage of metal oxides (e.g. SiO_2 42.70% etc.) then the ionic positions of both metal ions and oxygen ions is next tabulated. The safest procedure is then to ignore any H_2O in the analyses, to equate the sum of the oxygen ions to 22 and to calculate the ionic proportions of metal ions on this basis. If, however, one can be confident of the analytical value for structural H_2O (i.e. on an oven-dry basis) then this figure can be included and the sum of the oxygen ions (+ fluorine) equated to 24. The Si and then Al ions are assigned to make up 8Z, and the remainder of the cations (apart from K etc.) assigned to the Y positions. The approximate chemical fomulae of micas is given in Table 3.

The clay micas are distinguished from the macroscopic micas in part by frequently having a lower net charge on the layers, i.e. in having considerably less than 2X cations per 24 anions. In addition evidence has been produced (e.g. Brown and Norrish, 1952) that some interlayer positions may be occupied by $(H_3O)^+$ ions replacing K^+. This is discussed further in Part II.

Not only are many different kinds of isomorphous substitution possible in the mica structures but the amounts of different elements in a particular species of mica may become quite high. For example the barium-muscovite known as oellacherite has been reported with 9.89% BaO, and the chrome-muscovite, fuchsite, with as much as 6% Cr_2O_3. Whilst these particular varieties may not be met in the course of soils research it does indicate that micas with the appropriate chemistry could, in some soils, be important sources of trace elements essential for plant nutrition.

The interlayer cations, including K^+, are the cations most easily removed from the mica structures by weathering processes and these minerals are therefore important suppliers of K^+ for plant growth. Further information on this subject will be found in the chapters on 'Weathering' and on 'Soil Potassium' in other volumes of this Handbuch.

Earlier clay mineralogists anticipated that mica chemistry could be estimated rapidly in some detail from a simple x-ray measurement of the b-dimension. It is now appreciated that there are too many independent variables involved to allow this to be successful. An alternative approach which has proved useful, however, is to attempt to estimate (for example) the octahedral Mg and Fe content of biotites from the relative intensities of a few x-ray reflections. Early studies of this problem were made by Brown (1955) and Gower (1957) and a more recent study based on new structural information is that of Franzini and Schiaffino (1965). They have claimed that, using the relative intensities of the 004, 005, and 006 reflections only, the octahedral Mg and Fe may be estimated with an error for the six octahedral sites of not more than ±0.5 atoms. Their technique seems quite satisfactory provided their recommended precautions in measuring relative intensities are observed.

POLYMORPHISM AND TWINNING

The polymorphism of the micas depends on their distinctive layered crystal structures, and on the high symmetry of the surface network of anions on each layer of the structure (see Introduction). Suppose we begin with one 10 Å unit, consisting of a tetrahedral, octahedral and tetrahedral layer. This has a unique 'direction' in the sense that there

is a layer 'stagger' of amount $^{-a}/3$ in the direction of the a-axis; the upper surface of oxygens is offset by $^{-a}/3$ relative to the lower surface of oxygens (Fig. 2). If we add a sheet of interlayer cations and begin building a second layer (10 Å thick) then it is easily possible for the 'stagger' of the second layer to be in a different direction from that of the first. All that is required for an ideal phlogopite, for example, is a slightly different arrangement of protons in the octahedral layer; an ideal muscovite would need additionally some slightly different arrangement of filled and empty octahedral cation sites.

To clarify recent discussions of polymorphism in the literature we must at this point distinguish two different approaches towards "a theory of mica polymorphism and twinning".

The first approach is typified by the now-classic paper by Smith and Yoder (1956), referred to in the Introduction. They sought to describe theoretically all simple mica polymorphs, in order to guide the search for, and description of, the range of polymorphs found amongst natural micas. They essentially ignored the internal crystal chemistry of the 10 Å layers - the whole layer is simply represented by a vector of length $^{a}/3$ corresponding to the amount and direction of layer stagger. Secondly Smith and Yoder proposed that because the tetrahedral surfaces 'ideally' are hexagonal (i.e. the interlayer cation is 'ideally' 12-coordinated) the change of direction of successive vectors representing adjacent layers must be always $\pm$ n 60° where n = 0,1,2,3 (Fig. 6).

This vector model was highly successful in predicting all possible simple stacking arrangements (and hence cell dimensions, and symmetry) for mica polymorphs with repeat distances along c* of 10, 20 or 30 Å. The

method in fact was so successful that Ross, Takeda and Wones (1966) used it ten years later, in conjunction with a computer, to examine all theoretical polymorphs systematically up to 9 layers thick (90 Å), and they also considered a number of other more complicated stacking arrangements. This approach, combined with an elegant systematic notation (Table 4) to describe different stacking arrangements has enabled Ross et al to point out unexpected similarities between complex polymorphs. For example some polymorphs consist of a single 1M 10 Å structure repeated several-fold, followed by a single stacking fault of 120°; and then the total stacking arrangement is repeated all over again. In this way the complex polymorphs 3-, 8-, 14- and 23- layer triclinic are all closely related. The $3Tc_1$ has a single layer plus a single 120° periodic stacking fault; the $8Tc_1$ has six 1M layers in parallel, followed by a single 120° stacking fault; the $14Tc_1$ has 12 parallel layers etc. and the $23Tc_1$ has 21 parallel layers. Other series of polymorphs are based on a combination of several trigonal units 30 Å high, followed by single stacking faults (Fig. 14).

Ross et al (1966) have also developed systematic criteria for the identification of polymorphs based on the presence or absence of certain classes of x-ray reflections (Table 4). These criteria are unambiguous, except for two small groups of 4-layer polymorphs. For their application, however, good single crystal photographs are needed on which the reflections can be indexed with certainty. Buerger precession photographs are probably the most suitable for this purpose.

Not all mica polymorphs proposed by this simplified theoretical approach have been observed in nature. Radoslovich (1959) has drawn attention to the fact that those which are observed almost always correspond

to theoretical polymorphs with vector rotations of 120°. Since the tetrahedral surfaces of micas have (di-) trigonal, not hexagonal symmetry, the stacking arrangements leading to vector rotations of ± 60° or 180° would then appear to give a trigonal prismatic coordination of six oxygens around the interlayer cations, instead of the essentially octahedral coordination which has been observed in mica structures determined so far. Furthermore from general crystallographic experience K^+ does not readily coordinate with six anions in the trigonal prismatic manner. Hence polymorphs corresponding to vector rotations of ± 60° or 180° require physically unrealistic coordination around the interlayer cations, and are therefore not found naturally.

Whilst this rule-of-thumb explains the virtual non-occurrence of two-layer orthogonal, or 6-layer hexagonal (2O or 6H) polymorphs it also happens to exclude twinning about the [100] and [110] axes - and such twinning has been observed occasionally for phlogopites, for example by Sadanaga and Takéuchi (1961), and by Bloss et al (1963).

This brings us to the second way of approaching a "theory of polymorphism and twinning", and that is to consider very carefully at what level the changes in layer stagger really take place, as Franzini and Schiaffino (1963) have done. The vector method of Smith and Yoder can, unfortunately, very easily be misunderstood so that we begin to imagine identical 10 Å units actually rotating relative to each other at the interlayer K^+ level. In fact the stagger (represented by their vector rotation) occurs at the octahedral level, and is due to the disposition of octahedral hydroxyls.

Franzini and Schiaffino (1963) proposed that the concept of one single layer, with a ditrigonal surface, stacked in a number of orientations,

should be abandoned. Instead they proposed six different basic 10 Å layers which they labelled A_1 A_2 A_3 B_1 B_2 B_3, all ditrigonal at their surfaces, differing essentially in which octahedral sites are filled (set A or set B, each set having 3 sites) and also differing in how the pairs of hydroxyls are disposed around the filled sites[1]. Of the six layers the A_1 A_2 and A_3 layers can be thought of as "identical" in that a simple symmetry operation (3-fold rotation about c*) will bring them into coincidence. But there is no similar symmetry operation which will bring an A-type layer into coincidence with a B-type layer.

From these six different single layers we can assemble stacking sequences which always preserve the octahedral coordination around the interlayer cations. It turns out that the commonly observed polymorphs require various stacking sequences of A_1 A_2 and A_3 layers only, or of B_1 B_2 and B_3 layers only. The alternate repetition of A and B type layers, however, leads to the formation of 2O, $2M_2$ and 6H polymorphs in which the K^+ nevertheless has an octahedral coordination. The twinning of micas about an [100] or [110] axis is then viewed as an A-type layer being followed by a B-type layer, i.e. as a single stacking mistake.

This approach is reminiscent of Newnham's (1961) discussion of polymorphism in kaolin minerals in which he pointed out that there should be two single-layer cells, kaolinite and its mirror image. These should,

---

(1) B.B. Zviagin (1962) has likewise proposed six different single layer structures, and then considered stacking sequences of these structures, in arriving at a theory of mica polymorphism.

however, give identical x-ray patterns and would only be distinguishable by anomalous dispersion experiments, optical activity, or etch patterns for example.

The non-occurrence of 20, $2M_2$ and 6H polymorphs (except for lepidolites) and the rarity of twinning about [100] or [110] suggests that the repeated juxtaposition of an A-type and a B-type layer does not lead to polymorphic forms with minimum free energies, i.e. to stable polymorphs (Buerger, 1961). Why this should be so, however, requires further study.

A recent study on polymorphism and twinning in synthetic fluorophlogopite (Bloss, Gibbs and Cummings, 1963) emphasises some of the difficulties of this subject. The variations in optical properties (e.g. anomalous interference figures) did not seem to be related to their x-ray data until it was realised that about 30% of the samples were not single crystals, as had previously be assumed. Instead they were composed of two or more 1M polymorphs twinned about a [310] axis (or, much more rarely, a [110] axis) with an irregular composition plane, and an irregular boundary at different levels in the crystal. A 120° variation in stagger was attributed to inconsistency in placement of the fluoride (or hydroxyl) ions in the phlogopite structure; such variations occur most frequently. A 60° (or 180°) variation in stagger direction is the result of an inconsistency in the occupancy of the octahedral sites. This appears to be unusual for phlogopites, as well as for micas in general, and therefore polymorphs such as 20, $2M_2$ and 6H or twins about [110] are rare or non-exisent for phlogopites.

The identification of different mica polymorphs is still further complicated by the fact that some specimens may be twinned polysynthetically,

i.e. they may be twinned repeatedly on a fine scale with parallel composition planes. Polysynthetic twinning of micas has been analysed theoretically and observed experimentally by Sadanaga and Takéuchi (1961). They have shown how to distinguish composite x-ray diffraction patterns (given by various modes of polysynthetic twinning) from the rather similar patterns given by regular polymorphs. Again this distinction requires fairly good single crystal photographs, preferably precession photographs.

Polysynthetic twins may be of the spiral or of the alternate type, or a mixture of both. When the thickness of each twin individual reduces to 10 Å they degenerate into the various polymorphs.

On the other hand Sunagawa (1964) has studied growth spirals on phlogopite crystals, and found that at least for his specimens phlogopite is 1M, but shows five-sided growth spirals. The orientation of these growth features indicated that the crystals consists of many domains which are in twin relationships to each other. The twinning is not polysynthetic, but is the ordinary rotation type of twin.

The distribution of mica polymorphs has been studied fairly extensively e.g. Hendricks and Jefferson (1939), Heinrich and Levinson (1955), Smith and Yoder (1956), Zviagin (1962), Ross et al (1966). Very broadly, most macroscopic micas appear to have crystallized in the 1M polymorph, although many examples are known of a number of the more complex forms. In particular, the muscovites which originate in primary rocks are very generally $2M_1$, whereas diagenetic muscovites, such as might be developed slowly in soils, are more often 1Md or 1M. The petrological significance of these observations has been discussed by Smith and Yoder (1956), and by Velde and Hower (1963). The latter authors suggest that the large abundance of

1Md illite in the Paleozoic sediments which they examined indicated a predominantly low-temperature origin for the illite. The admixed $2M_1$ illite was greatly concentrated in the coarse fractions, and was thought to be detrital and not diagenetic in origin. In a similar kind of study Bailey *et al* (1962) used K-Ar dating to compare the ages of the coarse $2M_1$ illite fraction and the fine 1Md fraction of several cyclothermic Pennsylvanian shales and clays. The $2M_1$ polymorph was shown to be considerably older than the Pennsylvanian sedimentation whereas the 1Md component is less than half the age. They concluded that the $2M_1$ component is definitely detrital; and for the 1Md component the explanation for the low age may be either (1) preferential loss of Ar, as a function of decreasing particle size and increasing surface area, or (2) epigenetic formation of 1Md illite over a long period of time, probably as a result of reorganisation and K-fixation in degraded mica structures or in montmorillonite by reaction with pore fluids. This emphasises the danger in using bulk samples uncritically for dating purposes.

In assessing whether a particular polymorph (e.g. $2M_1$ muscovite) is likely to be detrital when found in clay fractions of soils it would help considerably to know the pressure-temperature stability fields in which different polymorphs are stable, and the ease with which metastable polymorphs are formed. This problem has been studied for the 1Md → 1M → $2M_1$ sequence of muscovite polymorphs by Yoder and Eugster (1955) and by Velde (1965). Two main problems of study exist - firstly, the reactions can be unexpectedly slow, so that experiments are incomplete in laboratory times (e.g. Yoder and Eugster), or a fast reaction may not conveniently be reversible (Velde, 1965) so as to establish stability fields unambiguously.

Bearing this limitation of Velde's work in mind he has nevertheless obtained results of substantial interest to soil scientists from a study of the reaction

kaolinite + KOH → muscovite.

His studies confirm that under suitable conditions, notably favourable K^+/H^+ ratio, kaolinite may transform to muscovite at temperatures at least as low as 250°C, and pressures of 2 kilobars. This is a structural transformation, leading to the 1Md, then 1M and finally $2M_1$ polymorph if the temperature and pressure are high enough. The 1Md and 1M polymorphs are only metastable, though they can persist virtually indefinitely at conditions found in soils. The factors in these experiments of interest to soil scientists are the relatively low temperatures and very high speed of the laboratory reactions. Velde has gone on to argue that in natural conditions (e.g. in evaporites in playa deposits in California) there has been a rapid conversion of kaolinite to metastable 1M muscovite; this is his explanation for the depletion of both kaolinite and potassium in these lakes. The same kind of argument is used to explain low potassium-sodic ratios in sea estuaries of rivers bearing kaolinite.

We are left with the problem of identifying polymorphs and twinned specimens. Given well-crystallised single crystals and using, for example, a Buerger precession x-ray camera the complete identification of all one-, two or three-layer polymorphs and their twins is possible (Ross et al, 1966; Sadanaga and Takéuchi, 1961). For finegrained specimens Zviagin (1961) claims that the use of electron diffraction texture diagrams allows all the simple polymorphs to be identified, except that the 1M and 3T polymorphs of trioctahedral micas can be distinguished from each other only by detailed

analysis of the intensities of the reflections. For finegrained micas, not very well crystallised and in mixtures both of polymorphic type and perhaps of chemical variety, it is simply not possible in many cases to make a full identification. Smith and Yoder (1956) have discussed in detail some of the problems of identification by x-ray techniques. Radoslovich (1960b) has given one example of the difficulties of distinguishing the different polymorphs with certainty, even given good specimens and precise x-ray powder diffraction data.

INFRA-RED ABSORPTION STUDIES

The study by x-ray crystallographic methods of the bonding between atoms can be very usefully augmented by a number of optical, electric and magnetic techniques. Of these the absorption spectra in near infra-red band of wavelengths (i.e. up to 40μ in wavelength) provide substantial information about the modes of vibration-rotation and about the directed nature of certain bonds.

Infra-red absorption studies have been used in mineralogy as well as organic chemistry for the detection of certain groups (e.g. OH^+, NH_4^+). This is feasible because although the crystal lattice usually vibrates as a whole, with coupling between individual modes of vibration, the frequencies associated with specific bonds are quite similar for different mineral structures containing those bonds. For example the broad band associated with Si-O bonds at frequencies around 1100 cm^{-1} are observed in the I.-R. spectra of most layer silicates.

It is <u>not</u> especially in the identification of unknown minerals (e.g. in a batch of soil samples) that broad band I.-R. spectroscopy is at

present likely to be useful. The reasons for this are (1) that the main features of I.-R. spectra of a wide range of minerals (e.g. Si-O, or OH bands) are too similar to be used effectively in diagnosis and (2) that so many factors can affect the detailed shape of the absorption bands that we can very rarely say that, for example, all muscovites (and only muscovites) have this or that detailed feature in their spectra.

The most recent trend in I.-R. studies therefore seems to be towards a careful study of well-characterized specimens, (e.g. micas having nearly end-member chemical composition), and using I.-R. techniques of polarized radiation and high resolution (about 6 cm^{-1}) spectrographs. By the latter means the fine structure of the absorption bands can be determined. The aim is so doing is to test theoretically calculations about the interaction of possible lattice vibrations with the fundamental frequency due to, say, the OH-stretching vibration.

There have been several detailed and careful studies in this field recently[1]. For example Farmer and Russell (1964) have studied the I.-R. absorption bands arising from the structural hydroxyl groups of a number of layer silicates, i.e. in the region from 3500 to 3700 cm^{-1}. They attempted to assign the two frequencies they observed in terms of either octahedral substitutions or of Al-for-Si substitution tetrahedrally. They confirmed earlier work that in the dioctahedral micas such as muscovite the OH dipole oscillations lie at around 16° to the plane of the sheets, whereas

---

(1) A critical review of some of the problems of technique and interpretation was given by Nahin (1955).

in the trioctahedral micas the O-H bond is normal to the plane of the sheets.

Farmer and Russell also examined the Si-O band, noting that, of the micas, lepidolite and celadonite (which have little Al-for-Si substitution tetrahedrally) gave the sharpest spectra. Again they have considered modes of vibration of the Si-O sheet separately, although they point out that this implies a rather unreal separation of the Si-O stretching vibrations from the R-O-H bending vibrations. The position and appearance of each of the several modes in the 1150-960 cm^{-1} region are very sensitive to the regularity of the structure. Whereas Farmer and Russell (1964) say that their correlations between frequency shifts and structural details are not exact there is now some hope that the I.-R. examination of some micas whose structures have been determined with very high precision (e.g. Burnham and Radoslovich, 1963; Güven and Burnham, 1965) may in the future allow the assignment of wavelength shifts unambiguously.

There are even more uncertainties in the assignment of absorption bands in the region 960-550 cm^{-1} where both bending and stretching vibrations involving OH groups, octahedral cations and the Si-O framework must be considered. The strong absorption band below 550 cm^{-1} must arise principally from in-plane vibrations of the octahedral ions and their adjacent oxygen layers. These vibrations couple to give modes which can equally well be described as metal-oxygen stretching or Si-O bending. The pattern of absorption is largely determined by the nature and distribution of the octahedral cations.

Infra-red spectroscopy using grating resolution has been applied particularly to the study of hydroxyl frequencies of muscovites, phlogopites and biotites by Saksena (1964), Vedder and McDonald (1963), Jørgensen

(1966) and Vedder (1964). Their results confirm results obtained with lower resolution by Bassett (1960), and by Serratosa and Bradley (1958), for example.

The OH stretching vibrations in each of these micas give rise to a broad band of absorption extending from 2.68 to 2.75 μ. In each case this band has a fine structure of at least four peaks, due to interaction between the OH stretching vibration and the rest of structure - particularly the octahedral anions. These separate peaks are therefore quite sensitive to composition, i.e. to distortions in the mica structure, and also to the effects of lack of perfect crystallinity in some specimens. Furthermore some peaks in some micas are very sensitive to tilting of the cleavage flake relative to the infrared beam. In particular I.-R. spectroscopy has shown clearly that the OH bond in true phlogopites is normal to the cleavage flake, as would be expected since the OH anion is equidistant from 3 Mg's in the octahedral layer. In muscovites the OH bond is almost parallel to the cleavage plane; it is inclined at some angle between 16° and 23° to the plane (probably depending on the chemistry) and the O-H bond projects at an angle of around 45° to the a-axis on to this plane. This is probably because of O-H .... O hydrogen bonding across to an octahedral oxygen at a distance of 2.9 Å. Vedder (1964) presents a detailed analysis of absorption frequencies for an impure phlogopite, distinguishing between N-, I-, and V-bonds (Table 5). This is an interesting example of the kind of deduction possible, given high resolution I.-R. spectroscopy, well-characterised specimens with adequate structural information available, and a careful consideration of all relevant modes of vibration of the lattice around the particular bond. He deduces, for example, that the occasional

vacancy octahedrally (only 2.88 out of 3 sites are filled) occurs preferentially in those sites which are completely unoccupied in the muscovite structure - in agreement with the general predictions about octahedral ordering of Veitch and Radoslovich (1963).

Infra-red spectroscopy has been used by Vedder (1965) to demonstrate the presence of NH_4^+ in muscovite, substituting for up to 2% of the interlayer K^+.

Lyon and Tuddenham (1960) have claimed that the proportion of Al-for-Si substitution tetrahedrally can be determined from the shape of the Si-O absorption band in the 1150-950 cm^{-1} region. Both Farmer and Russell (1964) and Vedder (1964) have made detailed calculations of Si-O modes, including their coupling to other lattice vibration, and of force constants, taking into account the departures of micas from ideal hexagonal geometry, the isomorphous replacements throughout the structure, the sensitivity of I.-R. absorption wavelengths to crystalline perfection, crystallite size and thickness etc. Although there probably is some general correlation of the 1150-950 cm^{-1} band shape with tetrahedral substitution, as Lyon and Tuddenham have suggested, these more detailed analyses of the fine structure of the I.-R. band associated with the Si-O bond clearly suggest the need for caution in using I.-R. techniques to analyse for tetrahedral Al.

OTHER STUDIES

Some physical properties of micas have not been discussed here because they seem to have little direct bearing on the problems of soil science. These include hardness, cleavage, morphology, optics, and studies

on the spiral growth of mica crystals using optical interferometry. These are adequately discussed in standard mineralogical texts, e.g. Deer, Howie and Zussman (1962). The synthesis and stability relations of micas likewise has not been discussed, although there is an extensive literature in this field in the journals of experimental petrology (e.g. Wones and Eugster, 1965). It is simply that the ranges of temperature and pressure involved are largely far removed from conditions found in soils. Finally the discussion of surface properties of finegrained micas (e.g. cation exchange capacity), the weathering of micaceous minerals, and problems in the routine identification of micas in soil samples has been left to the second part of this Chapter, which now follows.

REFERENCES

BAILEY, S.W., HURLEY, P.M., FAIRBAIRN, H.W., and PINSON, W.H.: K-Ar dating of sedimentary illite polytypes. Bull. Geol. Soc. Amer., 73, 1167, 1962.

BASSETT, W.A.: Role of hydroxyl orientation in mica alteration. Bull. Geol. Soc. Amer., 71, 449, 1960.

BERNAL, J.D.: The importance of geometrical factors in the structure of matter. Soviet Physics - Crystallography (in transl.), 7, 410, 1963.

BLOSS, F.D., GIBBS, G.V., and CUMMINGS, D.: Polymorphism and twinning in synthetic fluorophlogopite. J. Geol., 71, 537, 1963.

BRAGG, Sir Lawrence, and CLARINGBULL, G.F.: Crystal Structures of Minerals. G. Bell and Sons, London, 1965.

BREWER, R.: Fabric and Mineral Analysis of Soils. John Wiley and Sons, New York, 1964.

BRINDLEY, G.W., and MacEWAN, D.M.C.: Structural aspects of the mineralogy of clays and related silicates. Ceramics; a symposium, Brit. Cer. Soc., 15, 1953.

BROWN, G.: In the X-ray Identification and Crystal Structures of Clay Minerals, edited by G.W. Brindley. The Mineralogical Soc., London, p. 160, 1951.

BROWN, G.: The effect of chemical composition on (001) intensities of micas and chlorites. Min. Mag., 30, 657, 1955.

BROWN, G. (Ed.): The X-ray Identification and Crystal Structures of Clay Minerals. Mineralogical Soc., London, 1961.

BROWN, G.: Significance of recent structure determinations of layer silicates for clay studies. Clay Minerals, 6, 73, 1965.

BROWN, G., and NORRISH, K.: Hydrous micas. Mineral. Mag., 29, 929, 1952.

BUERGER, M.J.: Crystal-structure Analysis. John Wiley and Sons, New York, 1960.

BUERGER, M.J.: Polymorphism and phase transformations. Fortschr. Miner., 39, 9, 1961.

BURNHAM, C.W., and RADOSLOVICH, E.W.: Crystal structures of coexisting muscovite and paragonite. Ann. Rep., Geophys. Lab., Carnegie Inst. Wash., p. 232, 1963-64.

BURNS, A.F., and WHITE, J.L.: Removal of potassium alters b-dimension of muscovite. Science, 139, 39, 1963.

DEER, W.A., HOWIE, R.A., and ZUSSMAN, J.: Rock-forming Minerals, Vol. 3, Sheet Silicates. Longmans, London, 1962.

DeVORE, G.: Compositions of silicate surface and surface phenomena. Contributions to Geol., Univ. of Wyoming, 2, 21, 1963.

DONNAY, G., WYART, I., and SABATIER, G.: Structural mechanism of thermal and compositional transformations in silicates. Zeits. Fur. Krist., 112, 161, 1959.

DONNAY, G., DONNAY, J.D.H., and TAKEDA, H.: Trioctahedral one-layer micas. II. Prediction of the structure from composition and cell dimensions. Acta Cryst., 17, 1374, 1964.

DONNAY, G., MORIMOTO, N., TAKEDA, H., and DONNAY, J.D.H.: Trioctahedral one-layer micas. I. Crystal structure of a synthetic iron mica. Acta Cryst., 17, 1369, 1964.

FARMER, V.C., and RUSSELL, J.D.: The infra-red spectra of layer silicates. Spectrochim. Acta, 20, 1149, 1964.

FOSTER, M.D.: Correlation of dioctahedral potassium micas on the basis of their charge relations. U.S. Geol. Survey Bull., 1036-D, 57, 1956.

FOSTER, M.D.: Layer charge relations in dioctahedral and trioctahedral micas. Am. Mineral., 45, 383, 1960a.

FOSTER, M.D.: Interpretation of the composition of trioctahedral micas. U.S. Geol. Survey Prof. Paper, 354-B, 11, 1960b.

FOSTER, M.D.: Interpretation of the composition of lithium micas. U.S. Geol. Survey Prof. Paper, 354-B, 115, 1960c.

FRANZINI, M., and SCHIAFFINO, L.: On the crystal structure of biotites. Zeits. f. Kristallographie, 119, 297, 1963.

FRANZINI, M., and SCHIAFFINO, L.: Polimorfismo e leggi di geminazione delle biotiti. Atti della Soc. Toscana Sc. Nat., 70A, 1, 1963b.

GATINEAU, L.: Localization of isomorphous replacement in muscovite. Compt. Rend., 256(22), 4648, 1963.

GATINEAU, L.: Real structure of muscovite. Distribution of isomorphic substitutions. Bull. Soc. Franc. Mineral. Crist. 87(3), 321, 1964a.

GATINEAU, L.: Structure réelle de la muscovite, répartition des substitution isomorphes. Thèses, Ph.D., L'Université de Paris, 1964b.

GLASSER, L.S.D., GLASSER, F.P., and TAYLOR, H.F.W.: Topotactic reactions in inorganic oxy-compounds. Quarterly Review, 16, 343, 1962.

GOWER, J.A.: X-ray measurement of the iron-magnesium ratio in biotites. Amer. J. Sci., 255, 142, 1957.

GÜVEN, Necip, and BURNHAM, C.W.: The crystal structure of 3T muscovite. Ann. Rep., Geophys. Lab., Carnegie Inst. Washington, p. 290, 1965-66.

HENDRICKS, S.B., and JEFFERSON, M.E.: Polymorphism of the micas. Am. Mineral., 24, 729, 1939.

HEINRICH, E.W., and LEVINSON, A.A.: Studies in the mica group; polymorphism among the high-silica sericites. Am. Mineral., 40, 983, 1955.

JACKSON, W.W., and WEST, J.: The crystal structure of muscovite. Zeits. Krist., 85, 160, 1933.

JONES, J.B., and TAYLOR, W.H.: The structure of orthoclase. Acta Cryst., 14, 443, 1961.

JØRGENSEN, P.: Infra-red absorption of O-H bonds in some micas and other phyllosilicates. Clays and clay minerals, 13, 263, 1966.

LIPSON, H., and COCHRAN, W.: The Determination of Crystal Structures. G. Bell and Sons, London, 1966. (Second Edition).

LOEWENSTEIN, W.: The distribution of aluminium in the tetrahedra of silicates and aluminates. Am. Mineral., 39, 92, 1954.

LYON, R.J.P., and TUDDENHAM, W.M.: Determination of tetrahedral aluminium in mica by infra-red absorption analysis. Nature, 185, 374, 1960.

MATHIESON, A.McL., RADOSLOVICH, E.W., and WALKER, G.F.: Accuracy in structure analysis of layer silicates. Acta Cryst., 12, 937, 1959.

NAHIN, P.G.: Infra-red analysis of clays and related minerals. Proc. 1st. Nat. Conf. on Clays and Clay Tech., 112, 1955.

NEWNHAM, R.E.: A refinement of the dickite structure and some remarks on polymorphism in kaolin minerals. Min. Mag., 32, 683, 1961.

PABST, A.: Redescription of the single layer structure of the micas. Am. Mineral., 40, 967, 1955.

RADOSLOVICH, E.W.: Clay mineralogy of some Australian Red-brown Earths. J. Soil Sci., 9, 242, 1958.

RADOSLOVICH, E.W.: Structural control of polymorphism in micas. Nature, 183, 253, 1959.

RADOSLOVICH, E.W.: The structure of muscovite, $KAl_2 (Si_3 Al) O_{10} (OH)_2$. Acta Cryst., 13, 919, 1960a.

RADOSLOVICH, E.W.: Hydromuscovite with the $2M_2$ structure - a criticism. Am. Mineral., 45, 894, 1960b.

RADOSLOVICH, E.W., and JONES, J.B.: Transparent packing models of layer-lattice silicates based on the observed structure of muscovite. Clay Min. Bull., 4, 318, 1961.

RADOSLOVICH, E.W., and NORRISH, K.: The cell dimensions and symmetry of layer-lattice silicates. I. Some structural considerations. Am. Mineral., 47, 599, 1962.

RADOSLOVICH, E.W.: II. Regression relations. Am. Mineral., 47, 617, 1962.

RADOSLOVICH, E.W.: IV. Interatomic forces. Am. Mineral., 48, 76, 1963.

RADOSLOVICH, E.W.: V. Composition limits. Am. Mineral, 48, 348, 1963b.

ROSS, M., TAKEDA, H., and WONES, D.R.: Mica polytypes: Systematic description and identification. Science, 151, 191, 1966.

SADANAGA, R., and TAKÉUCHI, Y.: Polysynthetic twinning of micas. Zeits. f. Krist., 116, 406, 1961.

SAKSENA, B.D.: Infra-red hydroxyl frequencies of muscovite, phlogopite and biotite micas in relation to their structures. Trans. Faraday Soc., 60, 1715, 1964.

SERRATOSA, J.M., and BRADLEY, W.F.: Determination of the orientation of OH bond axes in layer silicates by infra-red absorption. J. Phys. Chem., 62, 1164, 1958.

SMITH, J.V., and YODER, H.S.: Experimental and theoretical studies of the mica polymorphs. Min. Mag., 31, 209, 1956.

STEINFINK, H.: Crystal structure of a trioctahedral mica: phlogopite. Am. Mineral., 47, 886, 1962.

SUNAGAWA, I.: Growth spirals on phlogopite crystals. Am. Mineral., 49, 1427, 1964.

TAKÉUCHI, Y.: Structures of brittle micas. Clays and Clay Minerals, 13, 1, 1966.

TAKÉUCHI, Y., and SADANAGA, R.: The crystal structure of xanthophyllite. Acta Cryst., 12, 945, 1959.

VEDDER, W.: Correlations between infra-red spectrum and chemical composition of mica. Am. Mineral., 49, 736, 1964.

VEDDER, W.: Ammonium in muscovite. Geochim. et. Cosmochim. Acta, 29, 221, 1965.

VEDDER, W., and McDONALD, R.S.: Vibrations of the OH ions in muscovite. J. Chem. Phys., 38, 1583, 1963.

VEITCH, L.G., and RADOSLOVICH, E.W.: The cell dimensions and symmetry of layer-lattice silicates. III. Octahedral ordering. Am. Mineral., 48, 62, 1963.

VELDE, B.: Experimental determination of muscovite polymorph stabilities. Am. Mineral., 50, 436, 1965.

VELDE, B., and HOWER, J.: Petrological significance of illite polymorphism in paleozoic sedimentary rocks. Am. Mineral., 48, 1239, 1963.

WONES, D.R.: Physical properties of synthetic biotites on the join phlogopite-annite. Am. Mineral., 48, 1300, 1963.

WONES, D.R., and EUGSTER, H.P.: Stability of biotite: experiment, theory and application. Am. Mineral., 50, 1228, 1965.

YODER, H.S., and EUGSTER, H.P.: Synthetic and natural muscovites. Geochim. et Cosmochim. Acta, 8, 225, 1955.

YODER, H.S., and EUGSTER, H.P.: Phlogopite synthesis and stability range. Geochim. et Cosmochim. Acta, 6, 157, 1954.

ZEN, E-an, and ALBEE, A.L.: Coexistent muscovite and paragonite in pelitic schists. Am. Mineral., 49, 904, 1964.

ZVIAGIN, B.B.: Determination of the structure of celadonite by electron diffraction. Soviet Physics - Crystallography (in transl.), 2, 388, 1957.

ZVIAGIN, B.B.: A theory of polymorphism of micas. Soviet Physics - Crystallography (in transl.), 6, 571, 1962.

ZVIAGIN, B.B., and MISCHENKO, K.S.: Electron diffraction refinement of the structure of muscovite. Soviet Physics - Crystallography (in transl.), 5, 575, 1961.

EWR/VHR
20/6/67

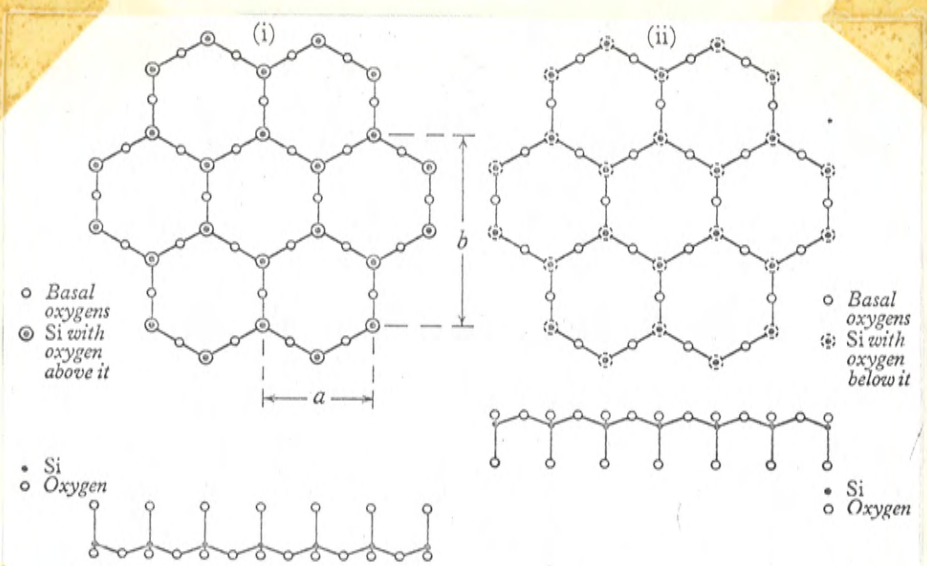

FIG. 1(i). Mica structure. Plan of tetrahedral layer (Si_4O_{10}) with tetrahedra pointing upwards, and end view of layer looking down y axis.

FIG. 1(ii). Mica structure. Plan and elevation of tetrahedral layer with tetrahedra pointing downwards. (Deer et al. 1962)

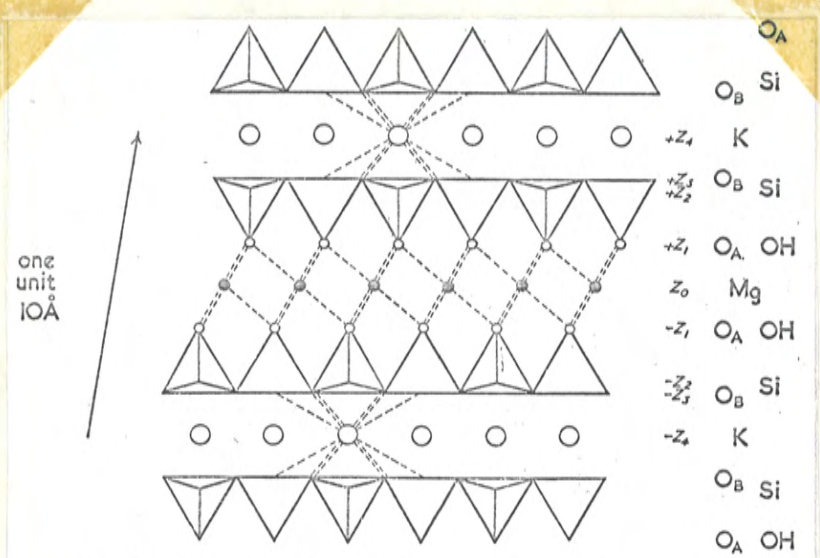

Fig. ■.2. A projection on (010) showing one phlogopite layer, together with adjacent parts of the two adjoining layers. O_A and O_B are at the vertices of the tetrahedra. The O_A oxygens overlap with the OH ions (from Smith and Yoder 1956).

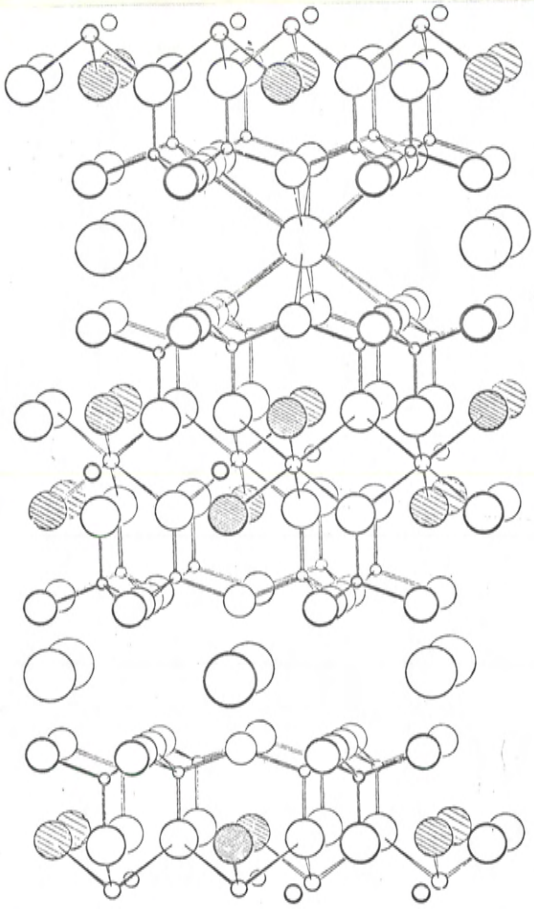

Fig. 3. The muscovite structure, viewed along the a axis. Approximately one-half of the unit cell is shown. Open circles in increasing size indicate, respectively, silicon, aluminium, tetrahedral oxygen, octahedral oxygen, and potassium. Hatched circles are hydroxyls (from Brindley and MacEwan 1953).

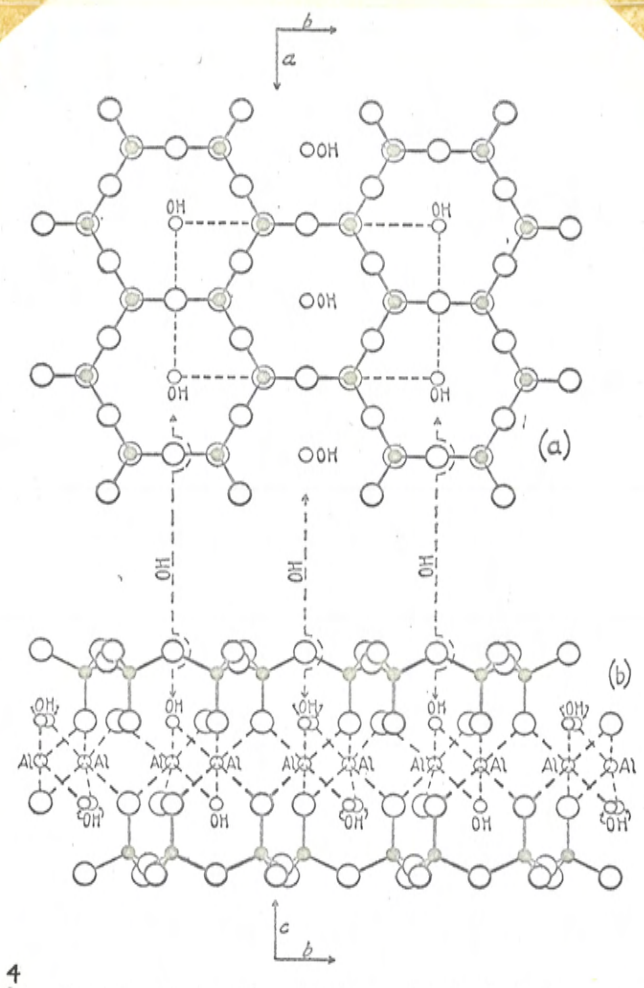

FIG. 4. Portions of the mica structure. (a) A single layer of the hexagonal network of silicon-oxygen tetrahedra with hydroxyl ions located in the plane of their vertices at the centres of every sixfold ring. (b) An edge-on view of two of these layers with inward pointing vertices showing their relative orientations and the locations of the Al (or Mg) atoms between them. (Bragg and Claringbull, 1965)

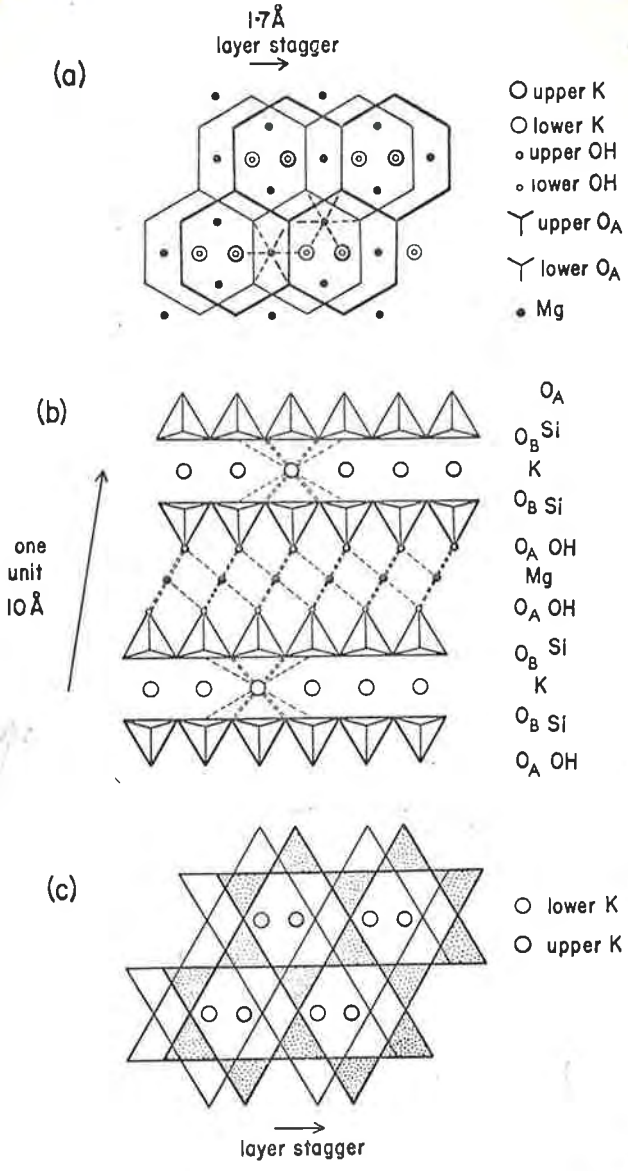

FIG. 5 (*a*) A projection normal to one mica layer showing the K (○), Mg (●), and OH (o) ions. The O_A oxygen atoms are at the corners of the hexagons. The thick and thin lines and circles in this figure and in fig. (*c*) represent the upper and lower layers of atoms in the unit. (*b*) A projection on (010) showing one layer together with the adjacent parts of the two adjoining layers. The O_A oxygen atoms overlap with the OH ions. The O_A and O_B oxygen atoms are at the vertices of the tetrahedra. The K, Si, Mg, and OH ions may be replaced by other ions. (*c*) A projection normal to one mica layer showing only the K (○) and O_B atoms. The O_B atoms are at the corners of the hexagons.

(Smith and Yoder, 1956)

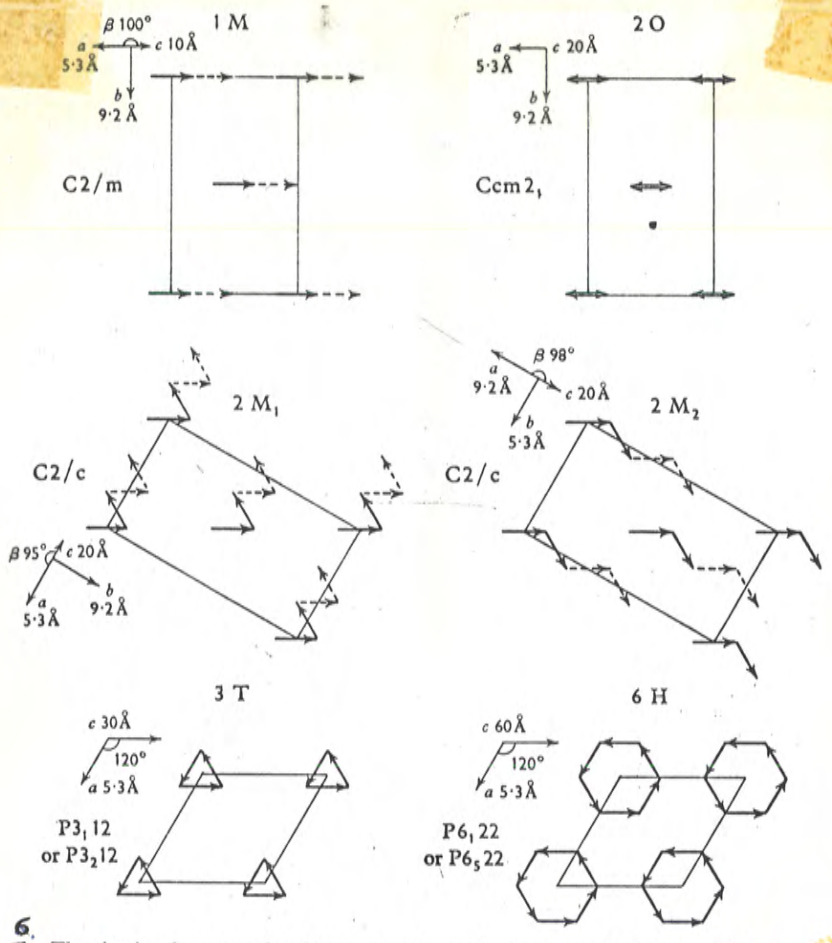

FIG. 6. The six simple ways of stacking mica layers in an ordered manner. The arrows are the inter-layer stacking vectors. Full line vectors show the layer stacking in one unit cell, whereas broken line vectors show the positions of layers in the next unit cell. The base of the unit cell is shown by thin lines, and the space group and lattice parameters are listed by the side of the diagram in each case (after Smith and Yoder, 1956).

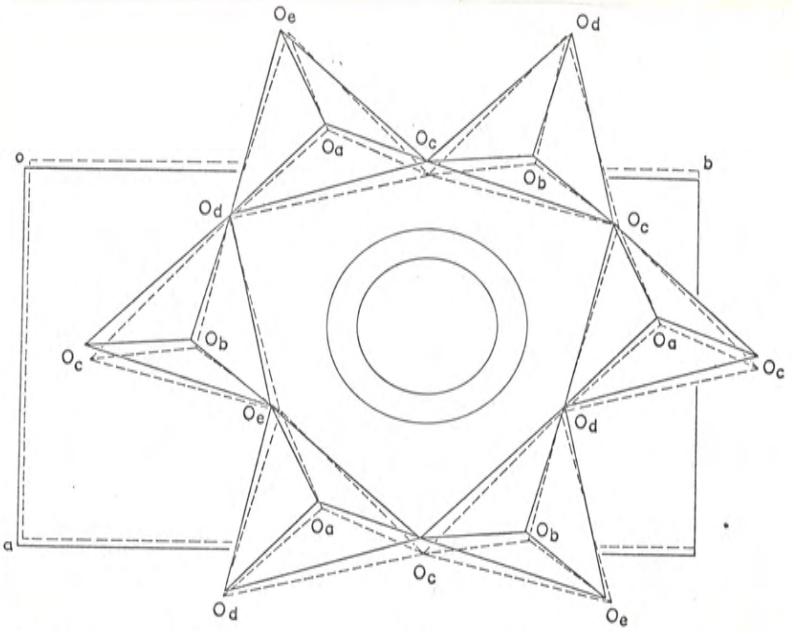

Fig. 7. Projection on (001) of one tetrahedral layer of muscovite (solid lines) and paragonite (dashed lines). The basis for superposition of layers is exact coincidence of alkali atoms. Concentric circles show the relative sizes of K (outer) and Na (inner) atoms.

(Burnham & Radoslovich 1963)

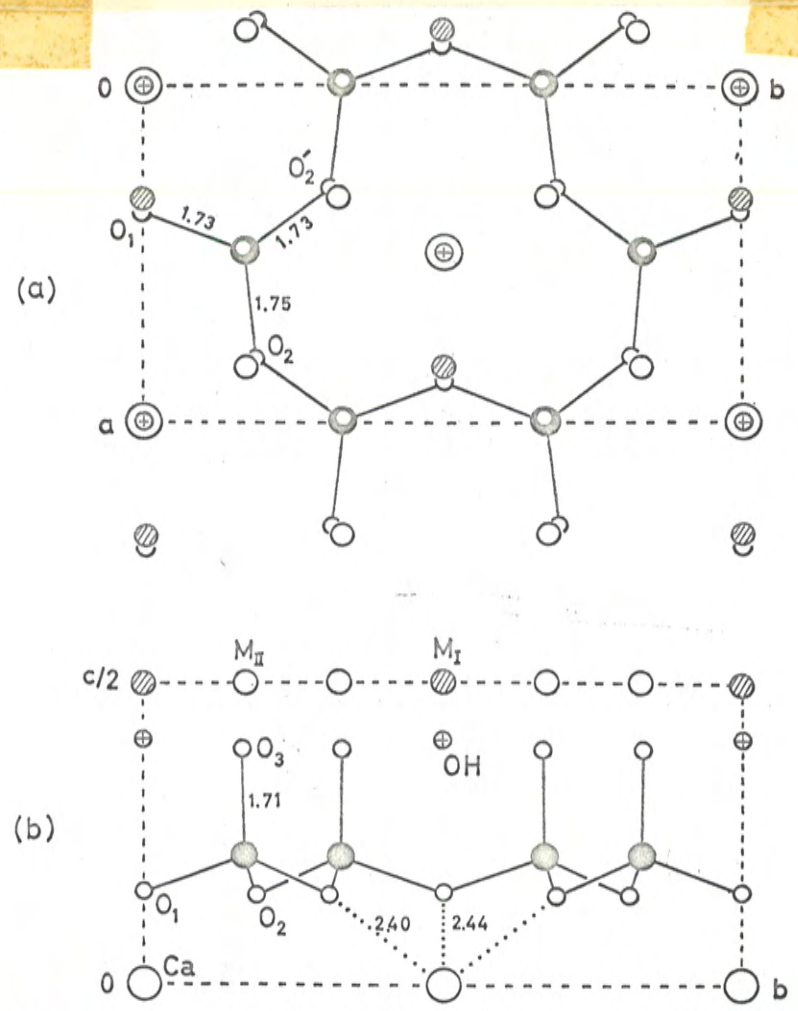

FIG. 8. The structure of xanthophyllite: (a) the projection on (001); (b) the projection along the *a*-axis.

(Takéuchi 1966)

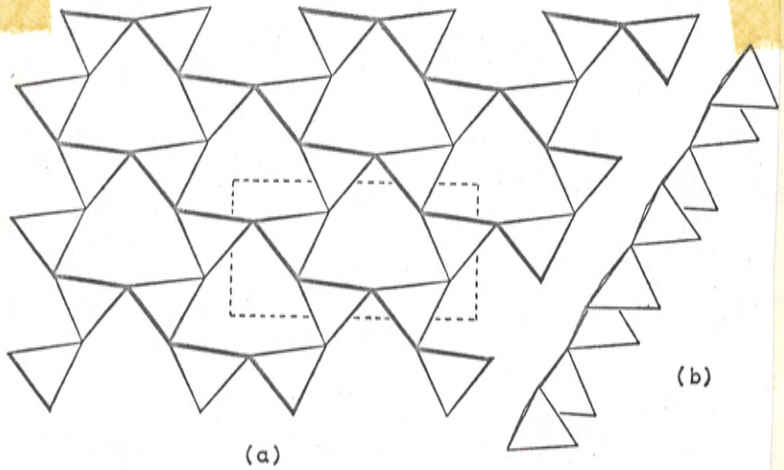

FIG. 9. A single tetrahedral layer of margarite, showing corrugation of the layer. Heavy lines indicate the elevated edges of basal oxygen triangles. The projection at (a) is on (001) and at (b) a view along [110].

(Takéuchi 1966)

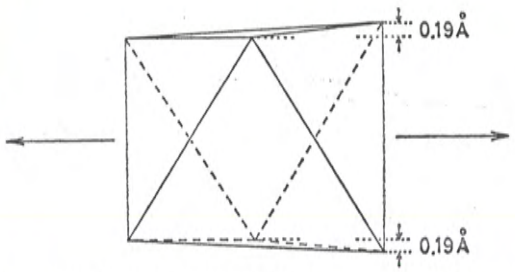

FIG. 10. Oxygen configuration around interlayer cations of dioctahedral micas as seen along the *a*-axis (the case of margarite is shown). As compared to the trioctahedral micas, where the planes of the basal oxygen triads are coplanar and parallel to the twofold axis, the basal oxygen planes in dioctahedral micas are tilted slightly, causing a displacement of the interlayer cations along the twofold axis.

(Takeuchi 1966)

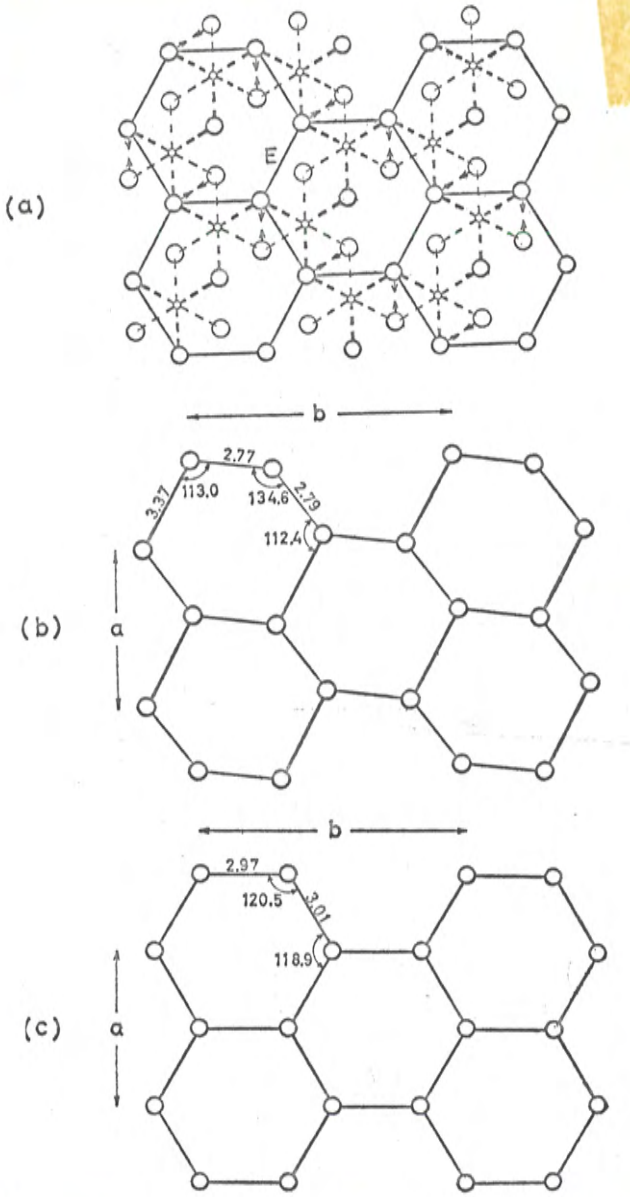

FIG. 11. (a) Al-octahedral layer. The hexagonal network of oxygen hexagons is outlined. The arrows indicate the directions of the shifts of oxygens due to shortening of shared edges. (b) The network of oxygen hexagons in margarite. (c) The network of oxygen hexagons in xanthophyllite.

(Takeuchi 1966)

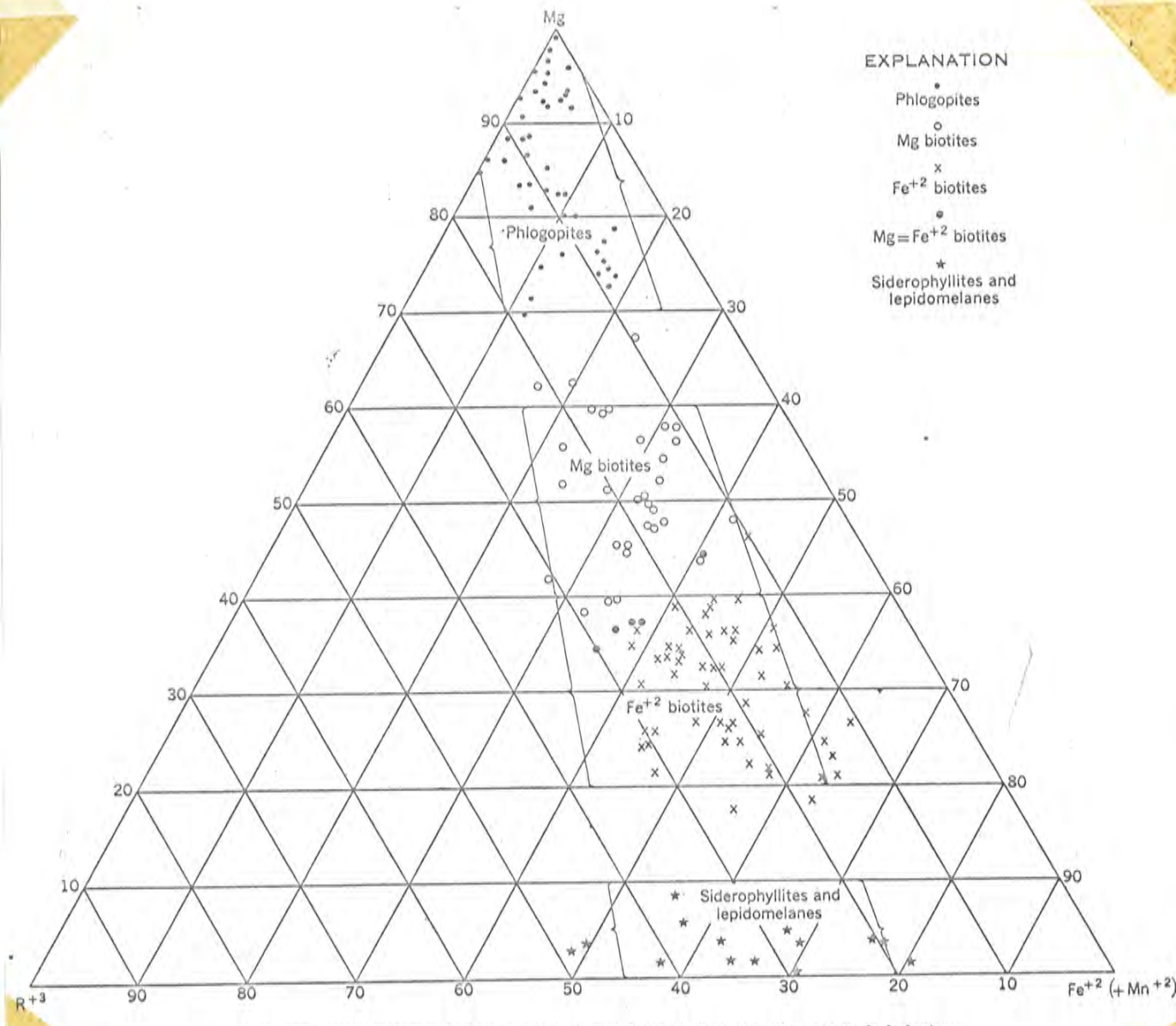

FIGURE 12.—Relation between Mg, Fe^{+2} (Mn^{+2}), and R^{+3} (Al, Fe^{+3}, and Ti) in trioctahedral micas.
(Foster 1960b)

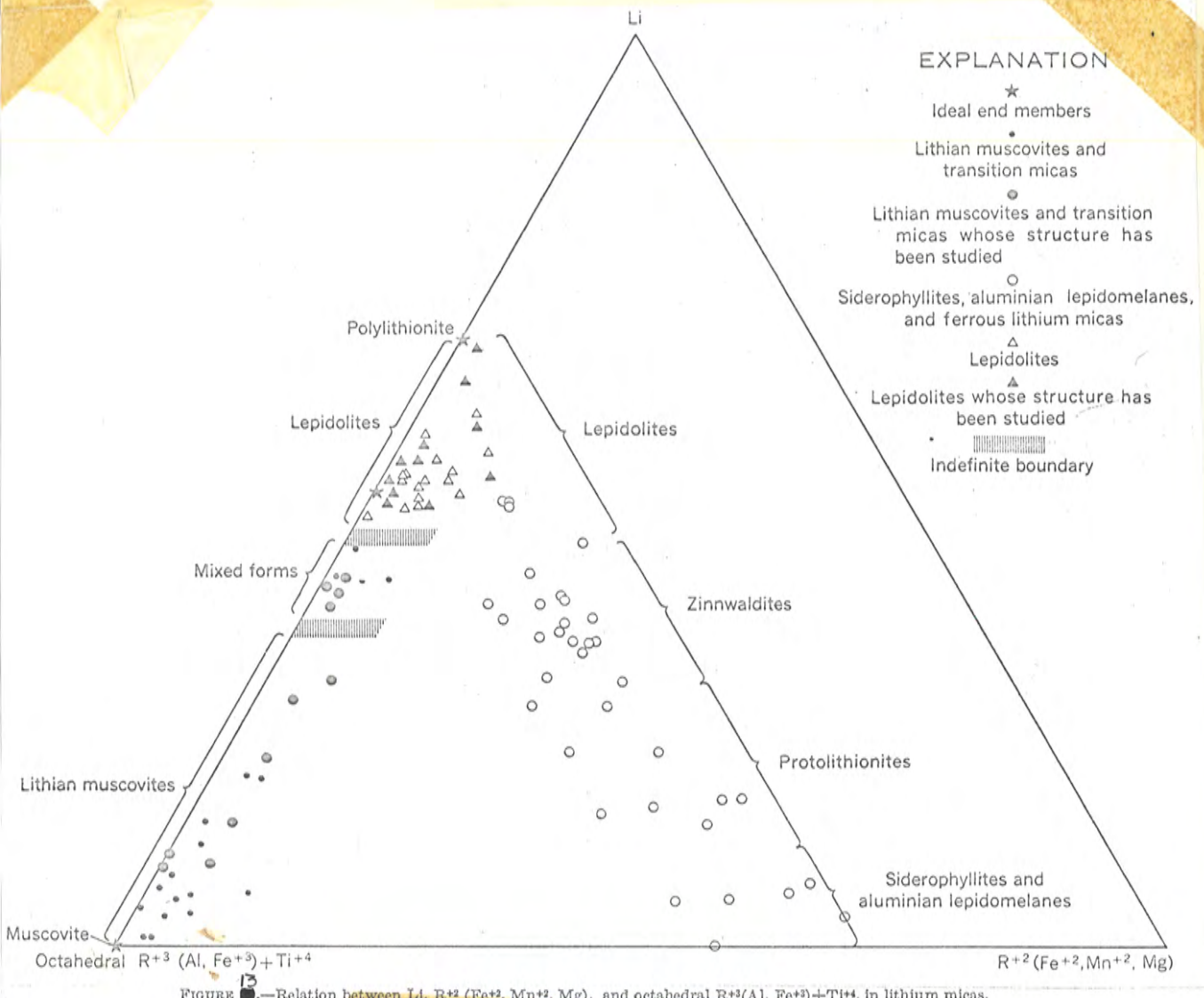

FIGURE 13.—Relation between Li, R^{+2} (Fe^{+2}, Mn^{+2}, Mg), and octahedral R^{+3}(Al, Fe^{+3})+Ti^{+4}, in lithium micas.

(Foster 1960c)

Series $(3n+1)[(222)_n 0]$,
$(3n+2)[(222)_n 2\bar{2}]$.

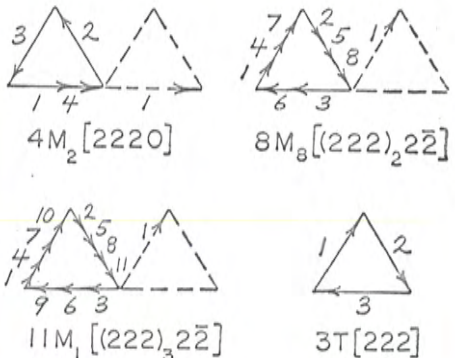

Fig. 14. The stacking sequences of the 3T, $4M_2$, $8M_8$, and $11M_1$ polytypes as represented by Smith-Yoder diagrams.

(Ross, Takeda and Wones 1966)

TABLE 11. Interatomic Distances (Å) in $2M_1$ Muscovite (Mu_{60}) and Paragonite (Mu_{15})

Atom Pair	Muscovite	Paragonite
T_1 tetrahedron		
T_1-O_a (apical)	1.642 ± 0.004	1.648 ± 0.002
T_1-O_c	1.645 ± 0.004	1.655 ± 0.004
T_1-O_d	1.643 ± 0.004	1.642 ± 0.004
T_1-O_e	1.649 ± 0.004	1.664 ± 0.003
Mean T_1-O	1.645	1.652
O_a-O_c	2.694 ± 0.005	2.706 ± 0.004
O_a-O_d	2.725 ± 0.005	2.720 ± 0.004
O_a-O_e	2.701 ± 0.005	2.709 ± 0.004
O_c-O_d	2.696 ± 0.005	2.707 ± 0.005
O_c-O_e	2.654 ± 0.005	2.685 ± 0.005
O_d-O_e	2.639 ± 0.005	2.656 ± 0.005
Mean O-O	2.685	2.697
T_2 tetrahedron		
T_2-O_b (apical)	1.644 ± 0.004	1.652 ± 0.003
T_2-O_c	1.648 ± 0.004	1.656 ± 0.004
T_2-O_d	1.644 ± 0.004	1.653 ± 0.003
T_2-O_e	1.645 ± 0.004	1.644 ± 0.004
Mean T_2-O	1.645	1.651
O_b-O_c	2.702 ± 0.005	2.709 ± 0.005
O_b-O_d	2.726 ± 0.005	2.726 ± 0.005
O_b-O_e	2.699 ± 0.005	2.707 ± 0.005
O_c-O_d	2.647 ± 0.005	2.677 ± 0.005
O_c-O_e	2.647 ± 0.005	2.650 ± 0.005
O_d-O_e	2.695 ± 0.005	2.709 ± 0.005
Mean O-O	2.686	2.696
Al octahedron		
Al-O_a	1.943 ± 0.004	1.933 ± 0.002
Al-O_a'	1.920 ± 0.004	1.914 ± 0.002
Al-O_b	1.917 ± 0.004	1.906 ± 0.004
Al-O_b'	1.946 ± 0.004	1.938 ± 0.004
Al-OH	1.907 ± 0.004	1.891 ± 0.004
Al-OH′	1.907 ± 0.004	1.899 ± 0.004
Mean Al-O	1.923	1.913
Mean of 9 unshared O-O	2.824	2.807
Mean of 3 shared O-O	2.420	2.417
Interlayer cation		
K,Na-O_c	2.762 ± 0.004	2.531 ±0. 004
K,Na-O_d	2.823 ± 0.004	2.726 ±0. 004
K,Na-O_e	2.795 ± 0.004	2.668 ±0. 004
Mean K,Na-O	2.793	2.641

(Burnham and Radoslovich, 1963)

TABLE 2. INTERATOMIC DISTANCES AND BOND LENGTHS OF ALUMINUM OCTAHEDRA

	Shared edge (Å)	Nonshared edge (Å)	Al—O(Å)
Gibbsite[1]	2.49±0.05	2.79	1.89±0.05
Dickite[2]	2.36±0.02	2.80	1.90±0.02
Kaolinite[3]	2.48±0.04	2.83	1.93±0.04
Muscovite[4]	2.55±0.03	2.83	1.95±0.02
Margarite	2.42±0.03	2.80	1.91±0.02

[1]Megaw, 1934. [2]Newnham, 1961. [3]Zvyagin, 1960. [4]Radoslovich, 1960

(Takéuchi 1966)

Table 3. APPROXIMATE CHEMICAL FORMULAE OF MICAS

Di-octahedral

		X	*Y*	*Z*
Common Micas	Muscovite	K_2	Al_4	Si_6Al_2
	Paragonite	Na_2	Al_4	Si_6Al_2
	Glauconite	$(K,Na)_{1\cdot2-2\cdot0}$	$(Fe,Mg,Al)_4$	$Si_{7-7\cdot6}Al_{1\cdot0-0\cdot4}$
Brittle micas	Margarite	Ca_2	Al_4	Si_4Al_4

Tri-octahedral

		X	*Y*	*Z*
Common micas	Phlogopite	K_2	$(Mg,Fe^{+2})_6$	Si_6Al_2
	Biotite	K_2	$(Mg,Fe,Al)_6$	$Si_{6-5}Al_{2-3}$
	Zinnwaldite	K_2	$(Fe,Li,Al)_6$	$Si_{6-7}Al_{2-1}$
	Lepidolite	K_2	$(Li,Al)_{5-6}$	$Si_{6-5}Al_{2-3}$
Brittle micas	Clintonite and Xanthophyllite	Ca_2	$(Mg,Al)_6$	$Si_{2\cdot5}Al_{5\cdot5}$

(Deer Howie & Zussman 1962)

Table 4. Crystallographic data for all possible 1-, 2-, 3-, and 4-layer mica polytypes.

Vector stacking symbol[a]	β[b] (deg)	Space group	Structural-presence criteria
1M[0]	100.0	$C2/m$	
2O[33]	90	$Cmmm$	
$2M_1$[$2\bar{2}$]	95.1	$C2/c$	$h3hl: l = 2n+h$
$2M_2$[$1\bar{1}$]	98.7	$C2/c$	
3T[222]	90	$P3_112$	$hh2\bar{h}l: l = 3n$
$3M_1$[033]	93.4	$C2/m$	$0kl: l = 3n$
$3M_2$[$11\bar{2}$]	93.4	$C2$	
$3Tc_1$[$02\bar{2}$]	95.1	$C\bar{1}$	$h0l: l = 3n$; $h3hl: l = 3n+h$; $h\bar{3}hl: l = 3n-h$
$3Tc_2$[011]	91.7	$C\bar{1}$	$0kl: l = 3n$
$3Tc_3$[123]	93.4[c]	$C1$	
$4O_1$[0303]	90	$Cmmm$	$0kl: l = 4n$
$4O_2$[$1\bar{3}13$]	90	$C2cm$	$h3hl: l = 2n$
$4O_3$[$23\bar{2}3$]	90	$Cc2m$	
$4O_4$[1212]	90	$C222_1$	
$4M_1$[$020\bar{2}$]	95.1	$C2/c$	$h0l: l = 4n$; $h3hl: l = 4n+2h$
$4M_2$[2220]	95.1	$C2$	$h0l: l = 4n$; $h3hl: l = 4n+2h$
$4M_3$[$2\bar{2}\bar{2}2$]	95.1	$C2/c$	$h0l: l = 4n$; $h3hl: l = 4n+2h$
$4M_4$[0033]	92.5	$C2/m$	$0kl: l = 4n$
$4M_5$[1122]	92.5	$C2$	
$4M_6$[$1\bar{1}11$]	90[d]	$C2/c$	$h3hl: l = 2n$
$4M_7$[$01\bar{2}1$]	90[d]	$C2$	
$4M_8$[$0101\bar{1}$]	98.7	$C2/c$	$h0l: l = 4n$
$4M_9$[1131]	94.4	$C2$	$0kl: l = 2n$; $3hhl: l = 2n+h$
$4M_{10}$[$12\bar{1}\bar{2}$]	94.4	$C2/c$	
$4M_{11}$[$1\bar{2}32$]	94.4	$C2$	
$4Tc_1$[$2\bar{2}33$]	92.5[e]	$C\bar{1}$	$0kl: l = 2n$
$4Tc_2$[1122]	92.5[e]	$C1$	$hh\bar{h}l: l = 2n+h$
$4Tc_3$[$13\bar{2}\bar{2}$]	92.5[e]	$C1$	
$4Tc_4$[0213]	92.5[e]	$C1$	
$4Tc_5$[0132]	92.5[e]	$C1$	
$4Tc_6$[$1\bar{1}33$]	90[d]	$C\bar{1}$	$h0l: l = 2n$; $h3hl, h3\bar{h}l: l = 2n+h$
$4Tc_7$[0123]	90[d]	$C1$	
$4Tc_8$[$002\bar{2}$]	95.1	$C\bar{1}$	$h0l: l = 4n$; $h3hl, h3\bar{h}l: l = 4n+2h$
$4Tc_9$[$\bar{1}\bar{1}22$]	92.5	$C\bar{1}$	$hhl: l = 2n+h$
$4Tc_{10}$[$001\bar{1}$]	92.5	$C\bar{1}$	$h\bar{h}l: l = 4n+h$
$4Tc_{11}$[$01\bar{1}2$]	92.5	$C1$	

[a] The polytypes within the large braces ($4M_1$, $4M_2$, $4M_3$ and $4Tc_3$, $4Tc_4$, $4Tc_5$) cannot be distinguished from one another with the data given in this table.

[b] The other unit-cell parameters of all of the above polytypes are $a = 5.3$, $b = 9.2$ Å, $d_{001} = 10N$ Å (where N is the layer repeat), and $\alpha = \gamma = 90°$—*with the following exceptions:* $2M_2$, $4M_8$, $4M_9$, $4M_{10}$, $4M_{11}$ ($a = 9.2$, $b = 5.3$ Å); 3T (hexagonal $a = 5.3$ Å, $\gamma = 120°$); $3Tc_1$ ($\alpha = 92.9°$); $3Tc_2$ ($\alpha = 98.7°$); $4Tc_6$, $4Tc_7$ ($\alpha = 94.4°$).

[c] Triclinic polytypes having the special feature of orthogonal (100) projections.

[d] Monoclinic and triclinic polytypes having the special feature of orthogonal (010) projections.

(Ross Takeda & Wones 1966)

TABLE 5

N-band (normal)	OH ions for which the immediately neighboring octahedral sites are all filled with divalent ions;
I-band (impurity)	OH ions for which all three closest octahedral sites are occupied, one however by a trivalent ion (*e.g.*, Fe^{3+} or Al)
V-bands (vacancy)	OH ions close to an unoccupied octahedral site.

(Vedder, 1964)

Paper 3-1

Reprinted from *Acta Crystallographica*, Vol. 7, Part 6-7, July 1954

PRINTED IN DENMARK

Acta Cryst. (1954). **7**, 513

A construction giving the projection of the point *h*00 on to the 0*kl* plane in reciprocal space, for non-orthogonal axes.

By E. W. Radoslovich, *Crystallographic Laboratory, Cavendish Laboratory, Cambridge, England*

(*Received* 15 *March* 1954)

In the course of a three-dimensional structure determination on a triclinic crystal one frequently wishes to find the projection of the point *h*00 on the 0*kl* plane in reciprocal space, in order to use the 0*kl* reciprocal net as the *hkl* net. This point can be marked on the 0*kl* net by calculating its displacement from the point 000 using well known formulae (Bunn, 1945). It is, however, interesting to note that there is a very simple geometrical construction which gives the same result, as can be shown trigonometrically.

For a net containing b^* and c^*, with angle α^* between them the construction is as follows (see Fig. 1):

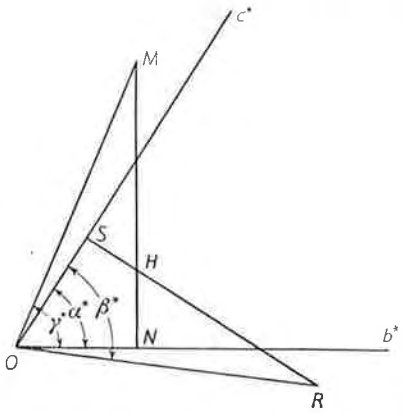

Fig. 1.

(i) Draw OM at an angle γ^* to b^*; make OM equal to ha^* in length, and draw MN normal to b^*.

(ii) Draw OR at an angle β^* to c^*; make OR equal to ha^* in length, and draw RS normal to c^*.

Then the intersection, H, of MN and RS is the projection of $h00$ on $0kl$. Usually one will put $h = 10$, say, and (having found the projection of 10,0,0) then divide the line OH into ten parts to give the projection of 100, 200, etc.

The fact that this construction does give the correct projection can be appreciated as follows:

Imagine a cone constructed around b^* with apex O, vertical half-angle γ^*. Then a^* lies in the surface of this cone. Likewise a^* also lies in the surface of a cone constructed around c^*, apex O, vertical half-angle β^*. The two cones will in general intersect along two straight lines passing through O. These are both a^*; they correspond to the two cases of right-handed or left-handed axes. The point $h00$ lies at a distance ha^* from O along the intersection of the two cones; we require its projection on the plane of b^* and c^*. We obtain this projection by making the sloping sides of the cones of length ha^*, drawing the cones in projection on the plane of b^* and c^*, and noting the point H where the projections of their respective bases intersect.

Reference

Bunn, C. W. (1945). *Chemical Crystallography*, p. 158. Oxford: Clarendon Press.

FR. BAGGES KGL. HOFBOGTRYKKERI
COPENHAGEN, DENMARK

87

Paper 3-2

Reprinted from *Acta Crystallographica*, Vol. 8, Part 2, February 1955

PRINTED IN DENMARK

Acta Cryst. (1955). **8**, 95

Calculation of Geometrical Structure Factors for Space Groups of Low Symmetry. I

By E. W. Radoslovich and (in part) Helen D. Megaw

Crystallographic Laboratory, Cavendish Laboratory, Cambridge, England

(*Received* 30 *August* 1954 *and in revised form* 15 *October* 1954)

This paper describes a simple calculator for the function cos $(hx+ky+lz)$. Values of this function can be read directly from tables of cos hx, provided that the origin of the latter can be shifted an amount $(ky+lz)$ at will. A simple mechanical device to do this is described.

Introduction

The geometrical structure factor for all space groups is

$$\sum_j \cos(hx_j+ky_j+lz_j)+i\sum_j \sin(hx_j+ky_j+lz_j)\,,$$

where the summation is over symmetry-equivalent atoms. This sum is often rewritten as a product or sum of products of cosine or sine factors, each involving only one of the coordinates x, y, z, by making use of any symmetry present; but it can equally well be calculated in the above form if we have some device which assists in rapidly tabulating cos $(hx_j+ky_j+lz_j)$ and sin $(hx_j+ky_j+lz_j)$. The present device is designed for this purpose.

The principle* of the device is as follows. Suppose that cos $(hx+ky+lz)$ is tabulated for one plane in reciprocal space at a time, working across the plane, row by row. That is, l is kept constant for a large number of (h, k); and k is kept constant for, say, h from -15 to $+15$. If we were reading values of cos $(hx+ky+lz)$ from a cosine curve then we would move a distance l_1z from the origin along the abscissa for all (h, k, l_1), and a further distance k_1y for all (h, k, l_1). From this point (k_1y+l_1z) we move a distance hx, and read off the value of the cosine; this last step is repeated for successive h.

In actual use it would be faster to move the abscissa scale relative to the cosine curve so that the zero point on the *scale* is at the position corresponding to cos (k_1y+l_1z) on the *curve*. The point hx on the abscissa scale now corresponds to cos $(hx+k_1y+l_1z)$ on the curve. If we replace the cosine curve by a table of values of cosines then it is a simple matter to move the abscissa column mechanically, relative to the cosine column, by any desired amount l_1z or (k_1y+l_1z). An immediate practical difficulty is that such a device would be too long, and therefore in any practicable design the tables must be broken up. The present device is described below.

* Bunn (1945) has described a slide-rule using the same basic principle, but with a different mechanical arrangement.

Description

Three kinds of tables are used: (1) tables of angular intervals, given as decimal fractions of a cycle, at intervals of 0·01 (i.e. 3·6°) from 0·00 to 0·99; (2) tables of sines of these angles; (3) tables of cosines of these angles.

The moving chart consists of a strip of tracing linen $4\frac{1}{2}$ in. wide, and about 45 in. long. It carries tables of sines and cosines, and one table of angular intervals under the heading '*ky*' (see Fig. 1(*a*)). The tables are

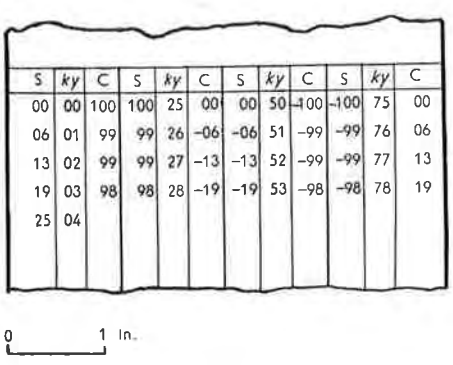

(*a*)

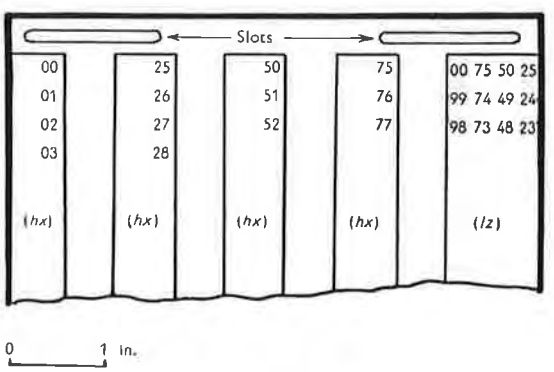

(*b*)

Fig. 1. (*a*) Section of movable chart, showing arrangement of sine (S), cosine (C), and *ky* tables. Values of *ky* given in decima fractions of a cycle; sines and cosines to two-figure accuracy, and at 3·6° intervals.
(*b*) Arrangement of *hx* and *lz* scales on perspex cover.

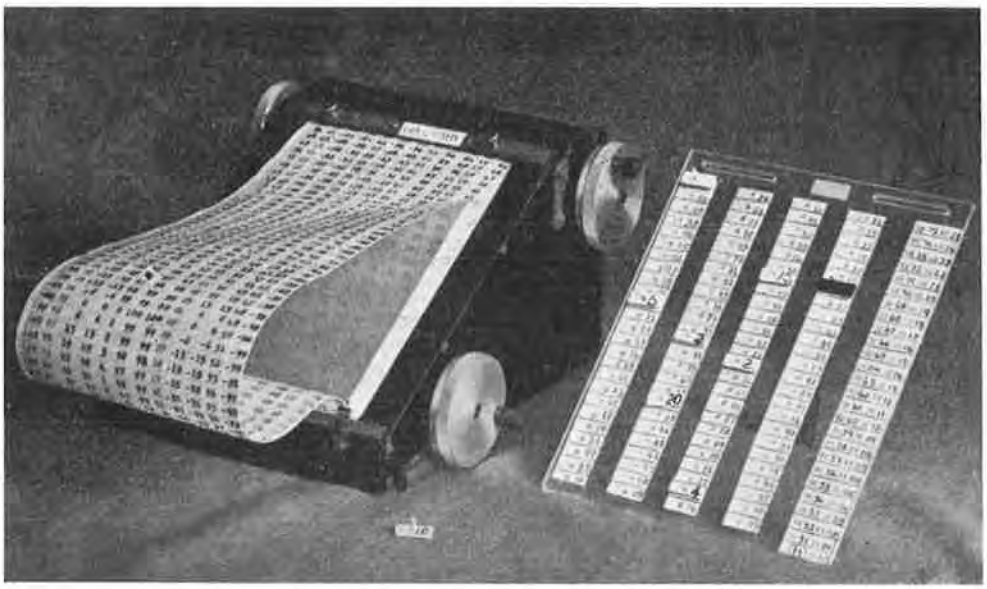

Fig. 2. Photograph of the device. The perspex cover is removed and placed (with one of the marking pins) alongside the box.

arranged vertically, the spacing between the rows being $\frac{1}{4}$ in., a spacing which can be conveniently set on a typewriter. The spacing of the columns is given in Fig. 1(*a*).

The three tables on the chart are in four blocks. In the left-hand block the *ky* table with its corresponding sine and cosine tables runs from $\theta = 0$ to $\theta/2\pi = 1{\cdot}25$; the other three blocks begin at $\theta/2\pi =$ 0·25, 0·50, 0·75, respectively, and each runs through $1\frac{1}{4}$ cycles.

The chart is mounted in a suitable box with a sloping front panel and two winding drums (Fig. 2). The drums move independently, one being used for forward and one for backward winding. Small fibre washers prevent them running too freely. A flat metal plate, curved at the ends, supports the chart close to a perspex cover, and leads it on to the drums. The box is designed so that a quarter of a cycle in each column can be seen, i.e. an area of $4\frac{1}{2}$ in. by 7 in., which is a convenient size. (In fact the sole reason for having more than one block of tables is to reduce the device to these dimensions.) Thus a full table of values of cosines (or sines, or *ky*) always appears on the visible area of the chart.

The perspex cover carries fixed scales of angular intervals, labelled '*hx*' and '*lz*' respectively, on paper glued to its lower surface (Fig. 1(*b*)). The *hx* scale is typed on four strips equally spaced ($\frac{1}{2}$ in. apart, and $\frac{5}{8}$ in. wide). The numbers on these run from top to bottom, and the strips from left to right. The *lz* scale (on the single wider strip on the right) is similar, but the numbers run from bottom to top, and from right to left. Faint horizontal lines have been ruled on the perspex to guide the eye.

The cover is loosely held by thumbscrews through horizontal slots in its upper edge, to allow sideways movement of a little more than 1 in. The clear sections of the cover, between the *hx* scales, allow the tables on the chart to be seen; and the dimensions have been chosen so that only one set of figures on the chart (i.e. *either* the cosine, *or* the *ky*, *or* the sine table) can be seen at once, depending on the position of the cover.

Small holes are drilled in the perspex at the position of each value of '*hx*', into which can be inserted flat markers mounted on a short pin. The markers are numbered 1, 2, 3, ..., corresponding to values of *h*, and there are two sets, with black and red figures on a white background, for *h* and $\bar{h}$. A similar marker painted red is used to indicate the origin. These markers are not essential, but are an aid to quick reading.

The device is used as follows. Coordinates (x, y, z) known to any desired accuracy can be used as starting-point, and the integral multiples *hx*, *ky*, *lz*, are formed to the same accuracy. These quantities are *then* rounded off to the nearest 0·01. The red (origin) marker is now placed in the appropriate hole on the cover, using the '*lz*' table on the right. Thus if l_1z is in the first column on the *lz* table then the origin marker is in the first column of holes (counting from the *right*), and in the same horizontal row as l_1z on the *lz* scale. Next the '*h*' markers are placed at the tabulated values of *hx*; and it will be noted that these '*h*' pins are not moved as long as this atom is being considered. The cover is now moved to expose the *ky* scales, and the chart is wound on until k_1y is at the origin marker (reading k_1y on the table to the right of the marker). Then the cover is shifted to expose the cosine table; the values of the cosines opposite the '*h*

markers are values of cos $(hx+k_1y+l_1z)$ for $h = 1, 2, 3, \ldots$. (Likewise the cover can be shifted, if necessary, to expose the corresponding values of sin $(hx+k_1y+l_1z)$.) Once all the values of cos $(hx+k_1y+l_1z)$ have been written down, the chart is moved to bring k_2y to the origin marker, then k_3y, etc. Finally the whole process is repeated, by shifting the origin marker, to deal with l_2z, then l_3z, etc.

Discussion

A device of this kind must be judged by considering (1) simplicity and cheapness of construction, (2) simplicity and directness in use, (3) speed in calculation, (4) universality, i.e. usefulness for many different calculations, (5) accuracy.

The present device is simple and cheap to make. It is also simple and direct to use, for two reasons. First, the structure-factor formula is evaluated in its most general, and at the same time most straightforward, form; the device simply carries out the calculations in the way represented in the formula, without prior re-arrangement in some 'sum-of-products' form. Secondly, the only accessory table needed for each calculation is a table of hx, ky and lz; and the device uses these quantities in a very simple way. (It can be used by unskilled computers as readily as a table of cosines.)

Any simple device dealing with one atom at a time must be slower than more elaborate machines which deal with atoms in groups. A test of this little box, however, showed it to be surprisingly speedy to use. An atom with coordinates $x = 0{\cdot}2777$, $y = 0{\cdot}1639$ and $z = 0{\cdot}5500$ was chosen, and cos $(hx+ky+lz)$ was tabulated for $l = 3$, $k = 0, 1, \ldots, 19$, and $h = 0, 2, 4, 6, \ldots, 20$, or $h = 1, 3, 5, 7, \ldots, 19$. The time for tabulating hx, ky and lz, and for setting the markers, was 6 min.; but this is, of course, done only once for each atom. The time for writing down cos $(hx+ky+lz)$ for the 220 values of (h, k, l) mentioned above was 16 min.; and this speed could be maintained for a long period. It seems unlikely that cos $(hx+ky+lz)$ can be calculated by hand faster than this. (It should be mentioned, however, that a larger device using the same basic principle is now being constructed which directly assists the hand computation of

$$\sum_{j=1}^{N} \cos\,(hx_j+ky_j+lz_j)$$

rather than cos $(hx+ky+lz)$; it will be described in Part II of this paper.)

The question of speed cannot be discussed without reference to the form in which the geometrical structure factor is expressed. As mentioned earlier, this direct form is often rewritten, where possible, as a single product term for purposes of evaluation. This is convenient for two reasons: (*a*) it means that one term only need be evaluated for the whole set of symmetry-equivalent atoms, (*b*) many desk machines and mathematical tables can more easily be used to evaluate a product of cosines than the cosine of a sum. If, however, the geometrical structure factor can be expressed only as the sum of two or more product terms, and the number of symmetry-equivalent atoms is low, the first advantage is reduced or disappears. This is notably the case in the triclinic system, where the sum of four product terms is needed. In this case, direct evaluation is obviously preferable. In the monoclinic system, for a general hkl structure factor, the sum of two product terms is needed, but each includes the contribution of two atoms; hence the total number of terms to be evaluated by either method is the same. In the orthorhombic and higher systems the direct evaluation of one term for each atom becomes increasingly inefficient.

It is worth specifically pointing out the universality of this device, since this is one of the advantages it has over most strip methods. The box is complete in itself, and is used *as it stands*. The use of high indices in a calculation involves no more preparation than the tabulation of hx, ky and lz—a few minutes' work. Thus the labour of any calculation is simply proportional to the number of reflexions considered, no matter how large the indices along any axes. Likewise the extra labour in changing from three-figure to four-figure accuracy in (x, y, z) lies only in the tabulation of hx, ky and lz, and is trivial.

Inaccuracies in calculations on devices of this kind arise from three causes: (1) physical inaccuracies in construction of the device, (2) inaccuracies due to 'rounding-off' hx, ky and lz, (3) inaccuracies due to finite interval-size in cosine table.

Since the box is not an analogue device no inaccuracies arise from its construction, in which, therefore, there is no necessity for fine tolerances. The other two sources of error are interdependent. It should first be noted that the maximum error introduced by the use of this device into hx, ky and lz will be no more than 0·005, whatever the value of h, k and l. In the Appendix to this paper a short account of the standard-deviations of 'rounding-off' errors has been given. This shows that the process of rounding-off hx, ky and lz separately before adding (as is done here) gives about twice the standard error when compared with rounding off the sum, $(hx+ky+lz)$; but that *both* methods are in general more accurate than using the product form.

It would be quite practicable to halve the error by constructing a slightly larger box in which the interval of the tables was 0·005 cycles, rather than 0·01 cycles, since the figures on the present tables are quite reasonably spaced out. Indeed, a box with tables at 0·002 cycles, and with sines and cosines to three figures, need not be inconveniently large; but problems requiring subdivision at smaller intervals than 0·005 probably warrant other and more powerful methods of calculation.

It is believed that this calculating device may be of

service in laboratories where larger machines are not readily available; even where they are available it is proving useful for those exploratory 'trial-and-error' calculations which arise at some point or another in most structure determinations.*

This work has been done during the tenure of a C.S.I.R.O. Overseas Studentship. The writer has pleasure in acknowledging helpful discussions with Dr Helen D. Megaw.

APPENDIX

By Helen D. Megaw

Rounding-off errors

It is assumed that angles, expressed in cycles, are rounded off to two decimal places; where the third digit is 5, it is rounded off to make the second digit even. Values of $\cos\theta$ or $\sin\theta$ are rounded off to two decimal places. We require to know the standard deviation of the geometrical structure factor. Suppose there are $2p$ symmetry-related atoms in general positions in a centrosymmetric structure.

(i) If the geometrical structure factor is evaluated by summing hx, ky, lz, rounding off the sum, and evaluating the cosine for each of the p atoms separately, the s.d. of θ for a single atom is $0{\cdot}01\times 1/\sqrt{12}$ cycles. The s.d. of $\cos\theta$ due to this is $1/\sqrt{2}\times 2\pi\times 0{\cdot}01/\sqrt{12} = 0{\cdot}013$; the effect of rounding-off errors in $\cos\theta$ itself is negligible. For $2p$ atoms, the s.d. of their sum of cosines is $2\sqrt{p}\times 0{\cdot}013$.

(ii) If the terms hx, ky, lz are rounded off before adding, then for $\cos(hx+ky)$ the s.d. is 0·019, for $\cos(hx+ky+lz)$ it is 0·022; as before, the s.d. for $2p$ atoms is proportional to $2\sqrt{p}$.

(iii) If the geometrical structure factor can be expressed in the form

$$2p\begin{Bmatrix}\cos\\ \sin\end{Bmatrix}hx.\begin{Bmatrix}\cos\\ \sin\end{Bmatrix}ky \quad \text{(one index zero)}$$

or

$$2p\begin{Bmatrix}\cos\\ \sin\end{Bmatrix}hx.\begin{Bmatrix}\cos\\ \sin\end{Bmatrix}ky.\begin{Bmatrix}\cos\\ \sin\end{Bmatrix}lz \quad \text{(no index zero)},$$

its s.d. is $2p\times 0{\cdot}013$ or $2p\sqrt{(3/2)}\times 0{\cdot}013$ respectively. If it can be expressed only as the sum of n such terms, its s.d. is $2p\sqrt{n}\times 0{\cdot}013$ or $2p\sqrt{n}\sqrt{(3/2)}=0{\cdot}013$ respectively.

The ratio of the s.d.'s resulting from methods (ii) and (iii) is thus

$$\frac{1}{\sqrt{(pn)}}\times\frac{0{\cdot}19}{0{\cdot}13} \quad \text{(one index zero)}$$

or

$$\sqrt{\left(\frac{2}{3pn}\right)}\times\frac{0{\cdot}22}{0{\cdot}13} \quad \text{(no index zero)}.$$

Where no index is zero, pn is never less than 4, and method (iii) is therefore less accurate than method (ii). The same holds good where one index is zero, except for triclinic crystals and for monoclinic crystals in the zones $hk0$ and $0kl$; here pn is 2, and the methods are of equal accuracy. The case when two indices are zero can be treated similarly, but is not of as much importance in practice.

* *Note added in proof.*—The device is now manufactured by Crystal Structures Ltd, 339 Cherryhinton Road, Cambridge, England.

Reference

Bunn, C. W. (1945). *Chemical Crystallography*, p. 270. Oxford: Clarendon Press.

FR. BAGGES KGL. HOFBOGTRYKKERI
COPENHAGEN, DENMARK

Paper 3-3

Reprinted from *Acta Crystallographica*, Vol. 8, Part 8, August 1955

PRINTED IN DENMARK

Acta Cryst. (1955). **8**, 456

Calculation of Geometrical Structure Factors for Space Groups of Low Symmetry. II

By E. W. Radoslovich

Crystallographic Laboratory, Cavendish Laboratory, Cambridge, England

(*Received* 6 *December* 1954 *and in revised form* 14 *February* 1955)

This instrument (called SUMCOS) assists in the calculation of $\sum_j \cos(hx_j+ky_j+lz_j)$ by hand. It does this by forming $\cos(hx_j+ky_j+lz_j)$ separately for ten atoms, and simultaneously presenting the values of these ten cosines ready for addition for any given (h, k, l). The final addition must be done by hand.

The values of $\cos(hx_j+ky_j+lz_j)$ are derived from a table of $\cos hx_j$ by using a simple mechanical arrangement to shift the origin of this table by (ky_j+lz_j). The values are presented for addition by switching on a small light behind the particular value of $\cos hx_j$ on the table, which is written on translucent material. New values of $\cos(hx_j+ky_j+lz_j)$ are presented for successive h simply by turning to the next position of a 24-position switch.

1. Introduction

Part I of this paper (Radoslovich & Megaw, 1955) described a device for moving the origin of a table of cosines by any arbitrary amount $(ky+lz)$ in order to read $\cos(hx+ky+lz)$ from a table of $\cos hx$. It consisted of a box carrying a fixed scale and two tables on a movable chart, so that shifts of origin could be made easily and rapidly. The usefulness of this box in calculations for triclinic and monoclinic space groups was pointed out.

Such a box speeds up calculations dealing with one atom at a time. In most calculations, however, we are concerned with several chemically identical but crystallographically distinct atoms, and we are therefore interested in the quantity

$$\sum_{j=0}^{N} \cos(hx_j+ky_j+lz_j) ,$$

where the summation is over N chemically similar atoms. This could be computed rapidly if the values of

cos $(hx_j+ky_j+lz_j)$ presented separately on N such boxes could be easily picked out simultaneously, ready for immediate addition. To achieve this it was necessary to re-design the box so that a convenient number of identical units would stack together in one instrument. A description of *one* of these units is given first; the method of combining them follows.

2. Description of instrument

(*a*) *Outline*

The new design incorporates the following changes. The fixed hx scale with its associated marking pins is replaced by a panel of bulbs. The moving scale, which is now translucent, is arranged horizontally in front of these and carries the values of cos hx printed from left to right. The bulb designated hx is required to light up when a multiple switch is at position h; by doing so it clearly marks the required value of cos $(hx+ky+lz)$. For this purpose each pole of the switch is permanently connected to a socket in a panel behind the lights, and likewise each bulb is connected to a socket on this panel. The instrument is set up for calculations with any given set of atomic coordinates by connecting the switch socket h with the bulb socket hx, a process corresponding to placing the marking-pins on the hx scale on the box.

A short subsidiary scale on the chart, reading angular intervals, can be placed so as to label the bulbs with their values of hx for the purpose of making the above connections; it is also used to fix the origin at a position determined by l_1z. By moving k_1y on the main scale up to this new origin we obtain the required displacement (k_1y+l_1z) of the origin, and hence values of cos $(hx+k_1y+l_1z)$. A second subsidiary scale is available for setting up the instrument to read values of sin $(hx+k_1y+l_1z)$.

(*b*) *Tables*

The tables of cosines and angular intervals are written on a narrow strip of tracing linen. This is held vertically in a milled channel between two sheets of perspex, and can be moved to the left or right by hand-operated drums at each end. The winding drums move independently, one being used for forward winding and one for backward winding. Small fibre washers prevent them running too freely. The lower disc of each drum, which is of large diameter and knurled, projects through a slot in the perspex, for winding purposes.

The tracing linen is $1\frac{3}{4}$ in. deep, and about 8 ft. long. It contains three blocks of tables, i.e. the main and the two subsidiary tables mentioned above. The main table (Table 1) contains eight rows of figures, i.e. four cosine tables, and four tables of angular intervals labelled ky. The latter are used only in resetting the strip, and so are in light coloured inks, whereas the cosine figures are in heavy Indian ink, since they are finally to be read off for addition. Both tables are at 0·005 cycle intervals, but as ky is linear every second figure only is recorded. The reason for having four rows of cosines (and of ky) is that the cosine cycle has been folded into a quarter-cycle length to keep the width of the box reasonable. Thus the cosine sections begin at $\theta = \pi$, 0, $\pi/2$ and $3\pi/2$ respectively; each section runs through $1\frac{1}{4}$ cycles.

The two subsidiary tables (of $\frac{1}{4}$ cycle length) also

Table 1. *Beginning of main table*

The tables are reproduced approximately actual size. The ky tables are printed in red ink.

$\overline{100}$	$\overline{100}$	$\overline{99}$	$\overline{99}$	$\overline{99}$	$\overline{99}$	$\overline{98}$	$\overline{98}$	...	→ $1\frac{1}{4}$ cycles
00		01		02		03		...	ky
100	**100**	**99**	**99**	**99**	**99**	**98**	**98**	...	
75		76		77		78		...	ky
50		51		52		53		...	ky
	0	$\overline{03}$	$\overline{06}$	$\overline{09}$	$\overline{13}$	$\overline{16}$	$\overline{19}$	...	
25		26		27		28		...	ky
	0	**03**	**06**	**09**	**13**	**16**	**19**	...	

Table 2. *Beginning of setting-up tables*

The tables are reproduced approximately actual size. The tables run for a quarter-cycle each. The lz tables are printed in red ink.

COSINES

50		**51**		**52**		**53**		... hx
00		99		98		97		... lz
00		**01**		**02**		**03**		... hx
25		24		23		22		... lz
50		49		48		47		... lz
	25		**26**		**27**		**28**	... hx
75		74		73		72		... lz
	75		**76**		**77**		**78**	... hx

SINES

50		**51**		**52**		**53**		... hx
25		24		23		22		... lz
00		**01**		**02**		**03**		... hx
50		49		48		47		... lz
75		74		73		72		... lz
	25		**26**		**27**		**28**	... hx
00		99		98		97		... lz
	75		**76**		**77**		**78**	... hx

have eight rows of figures, every row being in angular intervals. The first, third, sixth, and eight rows are labelled hx, and the other four rows lz (Table 2). In order to obtain the double shift of origin (k_1y+l_1z) it is necessary to be able to mark the position of l_1z on the front panel of the instrument, when the subsidiary tables are in position. This is done using thin perspex plates, $\frac{1}{2}$ in.$\times 1\frac{1}{2}$ in., which have a short pin in their upper edge. A row of holes has been drilled at $\frac{1}{4}$ in. intervals (the spacing of the tables) in the perspex face of the instrument, into which the pin can be pushed. Each plate has a small white dot painted on the rear surface at the height of one or other of the lz rows of figures, and a particular value of lz is marked simply by placing the appropriate plate so that the dot lies over it. This dot now becomes the 'origin' of the instrument.

(c) Bulbs

There are four rows of small electric bulbs, 25 in each row. These are mounted in standard 'screw-in' holders spaced $\frac{1}{2}$ in. apart and soldered to brass rods fixed immediately behind the perspex panel; this arrangement allows a bulb to be replaced, in case of failure, in three minutes. These rods both support the bulbs and act as the common earth throughout the instrument. The $\frac{1}{2}$ in. spacing means that values on the hx or cosine table can be lit up at 0·01 cycle intervals (though the tables can be set to twice this accuracy). A grid of black paper strips is stuck to the perspex immediately behind the charts, to leave an aperture $\frac{1}{4}$ in. square in front of each bulb. Likewise each bulb is painted black, except for a small area on top; thus any given bulb only lights up one cosine figure on the chart. The bulbs are lit by a small 6V. transformer.

(d) Sockets and switches

The bulbs are connected vertically in pairs (either a 1st- plus 2nd-row bulb, or a 3rd- plus 4th-row bulb) and each pair is connected to one socket on the rear panel. This pairing was done to keep down the number of sockets, but it introduces certain complexities considered in the next paragraph. Since there are four rows of cosines there are two rows of bulb sockets. Two further rows of 23 sockets are connected in sequence to a 48-position switch (two standard 24-pole switches in series); these will be referred to as switch sockets. Pairs of switch sockets in the upper and lower rows correspond to successive values of h, and are wired to successive switch positions, which are therefore called

$$1_a, 1_b;\ 2_a, 2_b;\ 3_a, 3_b;\ \ldots;\ h_a, h_b;\ \ldots .$$

Connections from bulb socket to switch socket are made by a short lead with a wander-plug at each end.

The two switches each have another wafer on which alternate positions are joined together and connected to a panel light, $1_a, 2_a, \ldots, h_a, \ldots$ to a white light, $1_b, 2_b, \ldots, h_b, \ldots$ to a red light, the latter marked with the word 'TOTAL'. The bulbs light up in vertical pairs, giving two values of hx differing by π (i.e. by 0·50 cycle). The top and bottom rows of figures (which begin at $hx = \pi$ and $3\pi/2$ respectively) have strips of red cellophane fixed behind them so that they appear against a red background, while the other two rows are left clear. Thus the two figures illuminated appear against a white and a red background for the first and second half-cycles respectively. If hx lies between 0 and π, the bulb socket hx is connected to the switch socket h_a (see Fig. 1); the *white* light then appears on the panel above the switch to show that the figure against the *white* background is the value required. If hx lies between π and 2π the connection is made to switch socket h_b, and the red panel light indicates the figure against the red background. Fig. 1 shows the

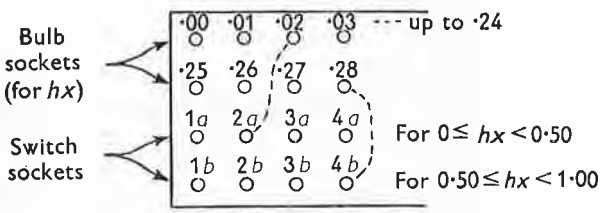

Fig. 1. Rear panel. Scheme of sockets showing connections for $2x = 0{\cdot}02$ and for $4x = 0{\cdot}78$ (i.e. 0·28+0·50).

arrangement. For a given h the connection will be made either to switch socket h_a or h_b, but not to both.

Thus the two rows of bulb sockets give half the cycle, and the two switch positions (i.e. two indicating colours) extend this to the full cycle of cosines. Experience suggests that an instrument half a cycle wide would not be too cumbersome, and this would not, of course, require two switch positions for each h.

(e) Combination of several units into one instrument

The description so far has been of one basic unit of the main instrument. Ten of these units have been mounted vertically in one frame, as a single device, with all the winding drums at either side on the same shaft (Fig. 2). As mentioned above, for any given h a selection of the ten units will show (white) values of $\cos(hx+k_1y+l_1z)$ at switch position h_a (but not at h_b) and the remainder will show (red) values at the following position h_b. These two sets of cosines are added together, as indicated by the word 'TOTAL' on the red light.

A standard design of wander-plug is used which allows several plugs to be inserted into the same socket. Thus one double row of switch sockets would suffice for the whole instrument, but only if no value of hx was repeated for two different values of h for a given atom. For triclinic space-groups, values of hx will not recur very often. This possibility is provided for, however, by having four double rows of switch

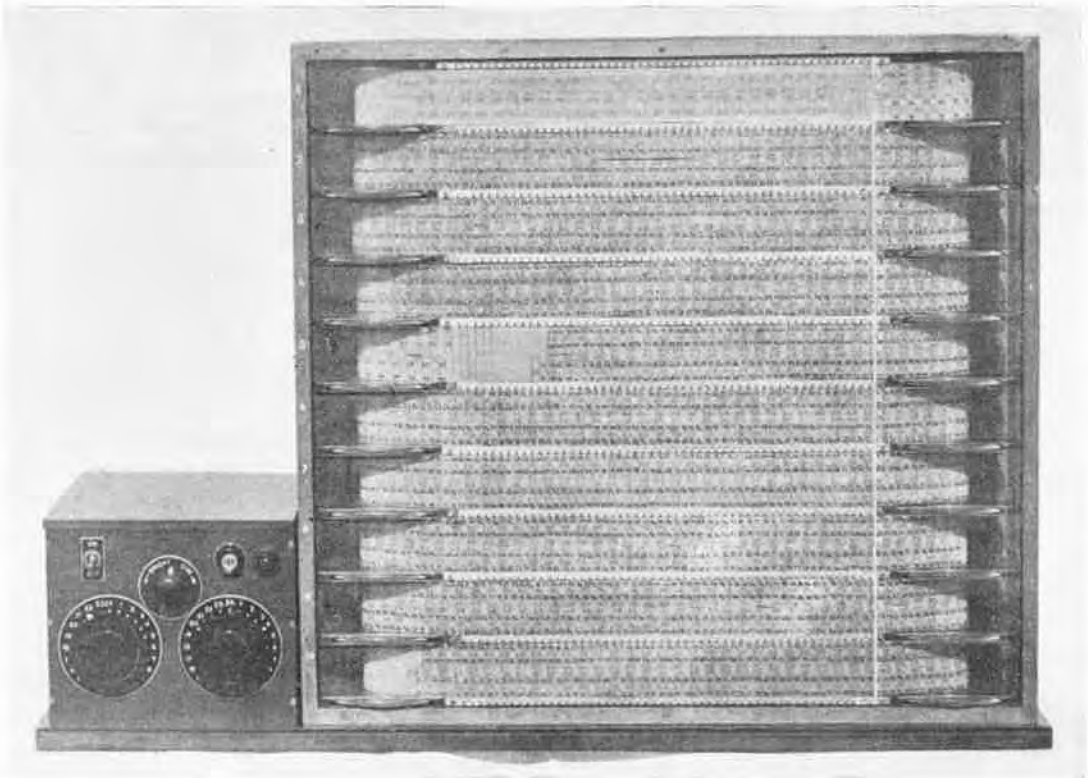

Fig. 2. Front view of SUMCOS. The sine (and part of cosine) setting-up tables are visible in the top unit (the white line on the right is for positioning these).

sockets connected to *separate* wafers of the switches (which have six wafers in all). Thus these four rows have independent circuits (see § 3(*c*)). To avoid the inconvenience of plugging the remaining six units into one double row of switch sockets a further *four* rows, permanently in parallel, have been connected to another switch wafer. The remaining wafer is required for the indicating lights.

(*f*) *Dimensions*

The overall height of the instrument is 22 in. and the width 32 in., but the significant area of figures is only 20 in. × 13 in., which is sufficiently compact for rapid reading.

3. Use of the instrument

(*a*) *Setting up*

The first step is to tabulate hx, ky and lz, for all required positive values of h, k and l, using values of x, y, z, with their maximum known accuracy. (Though this table is the only essential one it is convenient if $\bar{h}x$, $\bar{k}y$, and $\bar{l}z$ are also tabulated.) If the quantity to be calculated is

$$\sum_{j=1}^{N} \cos\,(hx_j+ky_j+lz_j)\,,$$

then the 'cosine' setting-up tables are moved into position. One unit is assigned to each atom, but this choice cannot be quite arbitrary (see § 3(*c*)).

Within each unit the bulb sockets are now connected to the switch sockets, this being done so that when the switch is at position h_a (or h_b) the value of hx, rounded off to two figures, is lit up on the table. This procedure is quite straightforward. (If the hx table is copied out and permanently fixed above the sockets on the rear panel, it considerably speeds up the wiring process.) After the connections are made, the successive values of hx are lit up simply by rotating the switch, and the correctness of the connections can therefore be promptly checked. These connections are not altered until all calculations with that atom have been completed.

(*b*) *Use of main table*

With the setting-up tables in place the small perspex plates are attached so that the origin is placed at lz for $l = l_1$ in each unit. The charts are now set so that ky for $k = k_1$ is brought up to the origin in each unit, thus giving values of $\cos\,(hx+k_1y+l_1z)$ (§ 2(*a*)). The indices (h, k_1, l_1) are the same in all units and hence we obtain

$$\sum_{j=1}^{10} \cos\,(hx_j+ky_j+lz_j)$$

by adding the ten cosines presented at the two switch positions h_a and h_b.

This sum is therefore computed for all (h, k_1, l_1) as h runs through a sequence of values, and the charts are then reset for the next value of k, e.g. (k_1+1). After computing all (h, k, l_1) the charts are moved back to the cosine setting-up tables, in order to place the perspex origin markers at new positions, e.g. $(l_1+1)z$.

Obviously we could get $\sum_1 \sin(hx_j+ky_j+lz_j)$ by subtracting 0·25 from all values of lz. The 'sine' setting-up table does this conveniently; otherwise the ky, cosine and hx tables (and hence rear connections) are used as described.

(c) *Problem of independent circuits and choice of atoms*

Because of the limited number of wafers on the switches, only four rows of switch sockets have independent circuits, so that a preliminary sorting-out of the coordinates is necessary.

When hx has been tabulated for the ten atoms the values for any atom must be looked over to see if some hx occur twice for the same atom. If so, then one of the four independent rows of switch sockets must be used for that atom. If N atoms are considered then $(N-4)$ must be found for which hx has no repeat values; but this is not a very stringent condition for triclinic space groups, where x is rarely a simple fraction. In any case the tables on the instrument have been called hx, ky and lz for convenience, and ky or lz can equally well be the quantity connected up to the switches (for all atoms) if hx proves inconvenient to use.

4. Discussion*

This machine attempts to fill a gap in the considerable range of computational aids and machines for structure factors now available. It is, by contrast with many techniques, relatively more efficient for the space groups of lowest symmetry.

The basic design is simple. It is not an analogue machine and therefore does not demand high precision in its construction. The few different components used are very reliable, so that little maintenance is needed. (The failure of a bulb is immediately obvious, since too few cosines will be lit up for a given h.) The cost of making the machine is probably less than for other machines (of comparable efficiency) suitable for use with triclinic or monoclinic space groups.

The accuracy is quite adequate for most problems. One component (hx) is rounded off to the nearest 0·01 cycle; the other two components (ky and lz) are set to the nearest 0·005 cycle. This accuracy is maintained however large h, k and l may become. In practice one index is limited instrumentally to 23 values in all, but the other two indices can run through any number of values. The index changed by switching (i.e. h) may be wired up consecutively, or in some convenient sequence such as $\ldots, \bar{6}, \bar{4}, \bar{2}, 0, 2, 4, \ldots$ followed by $\ldots, \bar{5}, \bar{3}, \bar{1}, 1, 3, \ldots$. Values of k and l can be taken in any order.

Some estimate of speed may be given. Tabulating hx, ky and lz (20 values of each) for ten atoms took 50 min., and checking for recurring values a further 10 min. The initial connections for a given problem occupied 12–15 min. per atom. An unskilled assistant using SUMCOS for the first time computed 300 values of

$$\sum_{4 \text{ atoms}} \cos(hx+ky+lz)$$

for fixed l, with $\overline{18} \leqslant k \leqslant 18$ and $h+k+l$ even, in 5 hr.; an experienced operator would take rather less than this. Many problems, however, would not require such frequent resetting of the charts as this particular one did.

A device of this kind is useful in various exploratory calculations during lengthy structure determinations. It also makes the use of three-dimensional data more feasible for laboratories without ready access to the considerably more efficient electronic computers, such as EDSAC.

The writer acknowledges with sincere thanks his indebtedness to Dr W. H. Taylor and Dr H. D. Megaw, and to the workshop staff of the Crystallographic Laboratory for their ready cooperation. The work was done during the tenure of a C.S.I.R.O. Overseas Studentship.

Reference

Radoslovich, E. W. & Megaw, H. D. (1955). *Acta Cryst.* **8**, 95.

* See also the discussion in Part I (Radoslovich & Megaw, 1955).

FR. BAGGES KGL. HOFBOGTRYKKERI
COPENHAGEN, DENMARK

Paper 3-4

COMMONWEALTH OF AUSTRALIA
COMMONWEALTH SCIENTIFIC AND INDUSTRIAL RESEARCH ORGANIZATION

Reprinted from *Acta Crystallographica*, Vol. 12, Part 1, January 1959
PRINTED IN DENMARK

Acta Cryst. (1959). **12**, 11

Calculation of Geometrical Structure Factors for Space Groups of Low Symmetry. III

BY E. W. RADOSLOVICH

Division of Soils, Commonwealth Scientific and Industrial Research Organization, Adelaide, Australia

(*Received* 27 *January* 1958 *and in revised form* 9 *September* 1958)

This paper describes a simple calculator for functions such as $\cos(hx+ky).\cos lz$. Values of these functions may be readily read off from suitably arranged tables of $\cos hx.\cos lz$, after a simple mechanical shift of origin by an amount ky.

Introduction

A simple mechanical device has previously been described (Radoslovich & Megaw, 1955) which allows values of $\left\{\begin{matrix}\sin\\ \cos\end{matrix}\right\}(hx+ky+lz)$* to be read directly from tables of $\left\{\begin{matrix}\sin\\ \cos\end{matrix}\right\}(hx)$. This is useful for space groups $P1$ and $P\bar{1}$, and for certain two-dimensional projections of the monoclinic space groups. The device has also been extended (Radoslovich, 1955) to compute $\Sigma\cos(hx+ky+lz)$. It would, however, be more useful when studying monoclinic crystals to be able to tabulate directly quantities of the kind

$$\left\{\begin{matrix}\sin\\ \cos\end{matrix}\right\}(hx+ky)\cdot\left\{\begin{matrix}\sin\\ \cos\end{matrix}\right\}(lz).$$

This is the form assumed by both A and B in the structure factor expression $F = A+iB$ for the space groups nos. 3 to 15 in the *International Tables* (1952).

The earlier device has been redesigned to permit such calculations. The tables have been enlarged to read $\left\{\begin{matrix}\sin\\ \cos\end{matrix}\right\}(hx)\cdot\left\{\begin{matrix}\sin\\ \cos\end{matrix}\right\}(lz)$ directly, at suitable intervals of lz and for integral values of h. These tables can still be moved mechanically, however, to include the term ky in the form $\left\{\begin{matrix}\sin\\ \cos\end{matrix}\right\}(hx+ky)\cdot\left\{\begin{matrix}\sin\\ \cos\end{matrix}\right\}(lz)$.

* i.e. either $\sin(hx+ky+lz)$ or $\cos(hx+ky+lz)$, as required.

Description

The three angles to be specified (viz. hx, ky and lz) are given as decimal fractions of a cycle, at intervals of 0·01 (i.e. 3·6°); values of cosines are given at the same angular intervals. There are 26 different tables of $K\cos hx$, where K has values $K = \cos lz$, and $lz =$ 0·00, 0·01 . . . 0·25, for successive tables.

The values of hx are set out on four strips of paper

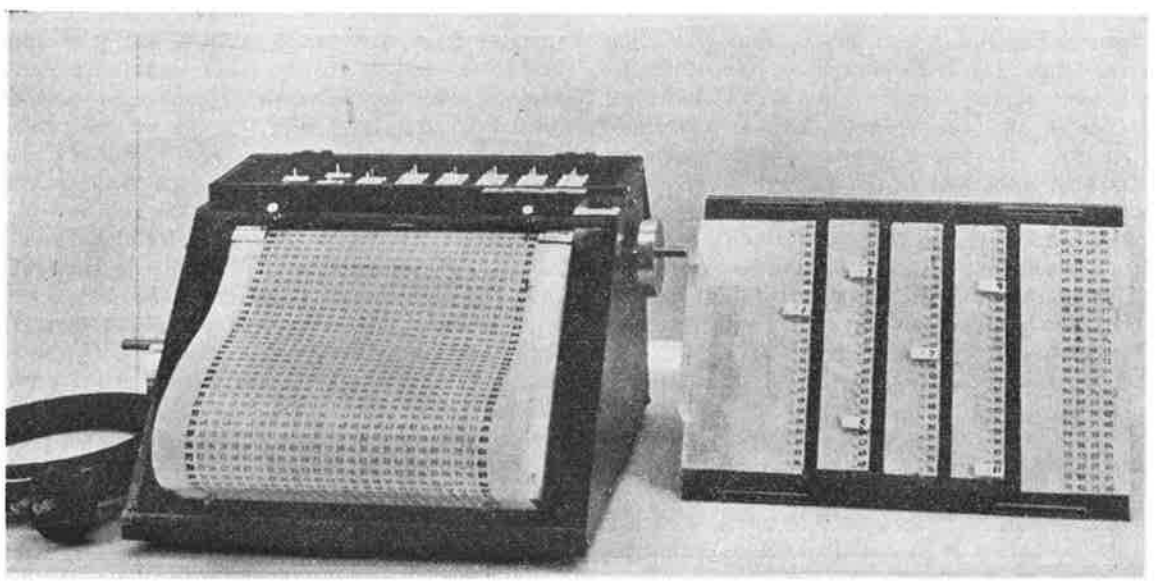

Fig. 1. General view of calculator, with cover removed. This shows the ky scales on the two edges of the chart, and the four columns of the hx scale on the cover, with some 'h' pins in place. (The block of figures on the right of the cover are for use with the cos $(hx+ky+lz)$ section of the calculator). The markers are conveniently stored in the top compartment.

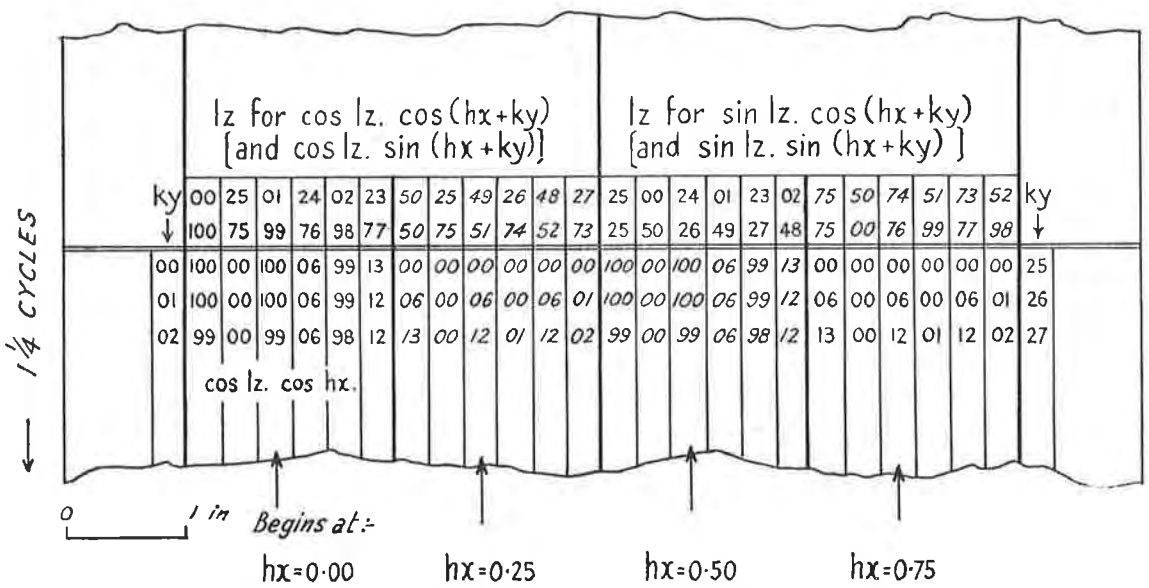

Fig. 2. First section of the movable chart. Arrows point to the table for $\cos 0{\cdot}01 . \cos hx$, which is given four times (see text). When lz values are in red (sloping figures here) then $\cos lz$ or $\sin lz$ is negative.

glued to the lower side of a perspex cover carried on the sloping face of the instrument (Fig. 1). These strips are correctly spaced to reveal, through the remaining transparent sections in the perspex cover, just one at a time of several vertical tables of cosines. The required table on the chart underneath can be chosen by moving the cover sideways, up to about two inches.

Small holes are drilled in the perspex, at the position of each 'hx', into which can be inserted flat markers mounted on a short pin. The markers are numbered 1, 2, 3, ..., corresponding to values of h, and there are two sets, with black and red figures on a white background, for h and $\bar{h}$. The markers are not essential, but are an aid to quick reading.

The values of ky and lz, and the 26 tables of $K \cos hx$ are set out (Fig. 2) on a moving chart consisting of a strip of tracing linen 8 in. wide and about 15 feet long. The ky values and the cosine tables are arranged vertically, with one space between each two-figure column, whilst values of lz are set out horizontally, as column headings to the cosine tables. Since it is impossible to accommodate all the 26 cosine tables in parallel columns across the chart they have been set out in five sections on the chart, six tables in each section, except the last. There is a blank space of about two inches between sections.

The ky values are set out vertically down the left hand edge of the chart, beginning at $ky = 0{\cdot}00$ and running through $1\frac{1}{4}$ cycles to $ky = 1{\cdot}25$ (equivalent to 0·25). This ky column is duplicated on the right-hand edge of the chart, but here the values begin at $ky = 0{\cdot}25$ and run to $ky = 1{\cdot}50$ (i.e. 0·50). This set-out of the ky values is repeated in each of the five sections of the chart mentioned above.

Two values of ky are always visible at the top left and right corners of the computer. A small bracket at the upper left corner of the chart area carries the word 'cos' and an arrow. This defines the origin with respect to the left-hand ky scale, to be used when calculating $\cos(hx+ky) \cdot \left\{\begin{matrix}\sin\\\cos\end{matrix}\right\} (lz)$. The right-hand bracket defines the origin for calculating $\sin(hx+ky) \left\{\begin{matrix}\sin\\\cos\end{matrix}\right\} (lz)$.

Now consider the arrangement of one $K . \cos hx$ table, e.g. when $K = \cos lz$ for $lz = 0{\cdot}01$. This table lies in the first section of the chart. It is set out vertically, beginning at a value 0·99 corresponding to $\cos 0{\cdot}01 . \cos hx$ for $hx = 0{\cdot}00$ and running for $1\frac{1}{4}$ cycles through to $hx = 1{\cdot}25$. The dimensions of the perspex cover of the instrument, however, permit only one quarter of a cycle to be seen at any one time, and therefore this $K . \cos hx$ table is repeated in three further columns, beginning at values corresponding to $hx = 0{\cdot}25$, 0·50 and 0·75 (Fig. 2). In this way a full cycle of one (and one only) $K \cos hx$ table is always visible through the perspex, no matter how that section of the chart is moved backwards and forwards behind it. Values of $K . \cos hx$ for which $\cos hx$ is negative are in red. The successive columns of $K \cos hx$ tables are not in order of increasing lz, but are arranged so that $\cos l_1 z . \cos hx$ and $\sin l_1 z . \cos hx$ $(= \cos(0{\cdot}25 - l_1 z) \times \cos hx)$ are in adjacent columns and hence both values can be read off with only a slight movement of the cover. Values of $\cos l_1 z . \cos hx$ and $\cos l_1 z . \sin hx$ are obviously related by a chart shift of a quarter cycle.

The value of lz (viz. $lz = 0{\cdot}01$) to which this table corresponds will appear through the clear sections of the perspex cover at the top of the left-hand $K \cos hx$ column. But this table also represents values of $\cos 0{\cdot}99 \cos hx$, $-\cos 0{\cdot}51 . \cos hx$, $-\cos 0{\cdot}49 \cos hx$, $\sin 0{\cdot}26 \cos hx$, $\sin 0{\cdot}24 \cos hx$, $-\sin 0{\cdot}76 \cos hx$, and

$-\sin 0{\cdot}74 \cos hx$. All eight values of lz, (under the appropriate heading, and in black or red, as the above products have a positive or negative sign) therefore appear at the top of the other three columns of this particular table, $\cos 0{\cdot}01 . \cos hx$. It is by this means that all values of lz from 0·00 to 1·00, and all four combinations $\begin{Bmatrix}\sin lz\\ \cos lz\end{Bmatrix} \cdot \begin{Bmatrix}\sin hx\\ \cos hx\end{Bmatrix}$ can be calculated from the 26 different tables given.

The sign of $\begin{Bmatrix}\sin\\ \cos\end{Bmatrix}(hx+ky) \cdot \begin{Bmatrix}\sin\\ \cos\end{Bmatrix} lz$, which will depend on the sign of both components, is determined from its colour (black or red) on the table. This choice is aided by a simple indicator above the perspex, consisting of a metal bar sliding behind covers. Values of lz for which $\begin{Bmatrix}\sin\\ \cos\end{Bmatrix} lz$ is negative are shown in red; and the metal bar is moved to place 'lz' on it opposite a black or red dot, depending on the colour of lz on the chart. The + and − signs on the bar then show whether all black figures (for the quantity $\begin{Bmatrix}\sin\\ \cos\end{Bmatrix}(hx+ky) \times \begin{Bmatrix}\sin\\ \cos\end{Bmatrix}(lz)$) are to be read as positive and all red figures as negative, or vice versa.

A mechanical drive* for moving the chart smoothly either forwards or backwards is included, though it is not essential. A small non-reversing electric motor is mounted on a pivot so that it can be placed in three positions determined by a standard radio switch. In the first of these the rubber driving wheel from the motor engages a knurled wheel on one winding drum, for forward motion of the chart. The middle position is neutral; and in the third position the knurled wheel on the other chart drum is engaged, for reverse motion. Spring-mounted fibre washers on both winding drums ensure that the chart is always taut. The chart may also be moved manually.

The device is used as follows. Coordinates (x, y, z) known to any desired accuracy can be used as a starting point, and the integral multiples hx, ky and lz are formed to the same accuracy. These quantities are *then* rounded off to the nearest 0·01. The value of lz for some particular calculation (involving either $\cos lz$ or $\sin lz$) is then located at the head of one of the five sections and its colour is set on the sign indicator. The perspex cover is placed so that this lz is visible through one of the transparent strips in the cover. The chart is now moved within that section so that the required value of ky lines up with the arrow, for calculating either $\cos(hx+ky)$ or $\sin(hx+ky)$. The h markers are placed at the tabulated values of hx, and are left in these positions until a further atom is being considered. The values on the chart opposite the markers are values for

$$h = \pm 1, 2 \ldots, \quad \text{of} \begin{Bmatrix}\sin\\ \cos\end{Bmatrix}(hx+ky) \cdot \begin{Bmatrix}\sin\\ \cos\end{Bmatrix}(lz),$$

depending on the position of the cover and on which ky scale is used.

Cos $(hx+ky+lz)$ *section*

In order to make one device as useful as possible two further sections of chart, both for calculating $\begin{Bmatrix}\sin\\ \cos\end{Bmatrix}(hx+ky+lz)$, are included. One of these is an exact copy of that described previously (Radoslovich & Megaw, 1955), but the tables have been more widely spaced to match the transparent strips on the new perspex cover. The other section has the same layout, but the interval used for all the tables is now 0·005 cycles, so that the accuracy is doubled. This requires twice as many values of hx, and to accommodate these the tables are set out in eight columns rather than four. The perspex cover is replaced by one carrying the hx table in eight columns, at 0·005 cycle intervals.

Discussion

The present computer retains the several advantages of the earlier device, which were discussed in detail by Radoslovich & Megaw (1955). It is, however, worth emphasizing that it is now possible to compute geometrical structure-factors for all of the triclinic and monoclinic space groups directly from the formulae in the *International Tables* (1952), so taking advantage of any symmetry relations for these space groups. Contributions of the separate atoms to the geometrical structure factor can be read off immediately by unskilled computers, using no more than a table of hx, ky and lz values to set up the device. The rounding-off errors are kept to the minimum which is possible when using trigonometrical tables at 0·01 cycle intervals.

The following example shows the speed of this device. Values of $\cos(hx+ky) . \cos lz$ were calculated for an atom for which $x=0{\cdot}938$, $y=0{\cdot}417$ and $z=0{\cdot}055$, the indices being given values $h=\overline{20}, \overline{18}, \ldots, 18, 20$; $k = 0, 1, \ldots, 6$; and $l = 3$ and 4. Eight minutes were needed to set up the h markers, and thereafter 300 values of $\cos(hx+ky) . \cos lz$ were tabulated in 23 minutes, i.e. as fast as they could be written down. It was not tiring to use the computer at this speed, which is considerably faster than can be achieved by other simple methods of calculating trigonometric products of this form.

References

Radoslovich, E. W. & Megaw, H. D. (1955). *Acta Cryst.* **8**, 95.

Radoslovich, E. W. (1955). *Acta Cryst.* **8**, 456.

International Tables for X-ray Crystallography (1952), vol. 1. Birmingham: Kynoch Press.

* The computer was constructed (and in part designed) by Messrs. K. Barrow and A. Palm in the workshops of this Division.

Printed in Denmark at Fr. Bagges kgl. Hofbogtrykkeri, Copenhagen

Paper 3-5

COMMONWEALTH OF AUSTRALIA
COMMONWEALTH SCIENTIFIC AND INDUSTRIAL RESEARCH ORGANIZATION

Reprinted from *Acta Crystallographica*, Vol. 15, Part 10, October 1962
PRINTED IN DENMARK

Acta Cryst. (1962). **15**, 1005

The Structure of Anorthite, $CaAl_2Si_2O_8$. I. Structure Analysis

BY C. J. E. KEMPSTER,* HELEN D. MEGAW AND E. W. RADOSLOVICH†
Crystallographic Laboratory, Cavendish Laboratory, Cambridge, England

(*Received* 5 *October* 1961 *and in revised form* 20 *November* 1961)

Anorthite $CaAl_2Si_2O_8$ has the same point group, $\bar{1}$, as a simple felspar, but four times the volume per lattice point; its unit cell is primitive, with a 14 Å *c*-axis, while that of albite, for comparison, is *C*-face-centred with a 7 Å *c*-axis. Anorthite approximates much more closely to a *C*-face-centred cell with a 14 Å *c*-axis than to either a body-centred cell with a 14 Å *c*-axis or a primitive cell with a 7 Å *c*-axis. The work was done in two stages. A synthesis using only main reflections gives elongated peaks or pairs of peaks whose centres of gravity define an 'average structure'. In the different subcells, atoms have displacements from the average positions whose magnitude and direction are given by the elongation (or 'splitting') and whose signs are found from the difference reflections (which also provide a check for magnitude and direction). The Ca peak has the most conspicuous elongation, and can be used for a heavy-atom method of determining the signs of the difference reflections. In the first stage, only '*c*'-type difference reflections were used, and the 14 Å *C*-face-centred approximation was obtained; a repeated application of the method using '*b*' and '*d*' reflections gave the true primitive structure. The final refinement was done by successive differential syntheses. Coordinates of the 52 independent atoms are given; their standard deviations are 0·0007 Å for Ca, 0·0015 Å for Si and Al, 0·0038 Å for O.

1. Introduction

1·1. *General approach*

Anorthite, $CaAl_2Si_2O_8$, is a member of the felspar family. The general features of the felspar structure have been known since the study of sanidine by Taylor (1933). Anorthite is one of the commonest and geologically most important members of the family, and it differs from the others in ways which made a detailed study desirable. Of the felspars whose structure has previously been studied, it is chemically most nearly related to celsian, $BaAl_2Si_2O_8$. Crystallographically, however, the triclinic symmetry and the radius of the large cation give it a closer resemblance to albite, $NaAlSi_3O_8$, and the significance of this relationship is strengthened by the occurrence of an apparently continuous series of solid solutions between the calcium and sodium felspars. It was therefore reasonable to take the structure of albite as a starting-point.

The obvious difference in chemical formula between anorthite and albite does not raise any difficulties in this approach. The scattering factors of Al and Si are so nearly identical that the difference between them could only become important at a very late stage of refinement. We write the felspar formula as AT_4O_8, *T* standing for 'tetrahedral cation', and make no attempt to distinguish the individual *T* cations as Si or Al during the analysis.

The present paper deals only with the method by which the structure was determined, the atomic coordinates found, and their accuracy. The description and discussion of the structure is left to a separate paper (Megaw, Kempster & Radoslovich, 1962). The nomenclature used throughout for the individual atoms is that proposed by Megaw (1956).

1·2. *Cell dimensions and lattice*

The cell dimensions of anorthite are given by Cole, Sørum & Taylor (1951); they are

$$a=8{\cdot}1768,\ b=12{\cdot}8768,\ c=14{\cdot}1690\ \text{Å};$$
$$\alpha=93°\ 10',\ \beta=115°\ 51',\ \gamma=91°\ 13'.$$

The *c*-axis is thus nearly double that of albite, the other dimensions being very similar. These authors also showed that anorthite has a primitive lattice, while albite is *C*-face-centred. This means that the asymmetric unit of anorthite is four times that of albite, the unit-cell content being 8 $CaAl_2Si_2O_8$. There is no evidence in the literature suggesting the absence of a centre of symmetry, and none arose in the course of this work. (The conclusions which can be drawn from the statistical distribution of intensities are discussed in § 2·3.) The space group is taken as $P\bar{1}$.

In reciprocal space, anorthite has four times as many lattice points as albite, classified for convenience as follows:

'*a*' type: $h+k$ even, l even
'*b*' type: $h+k$ odd, l odd
'*c*' type: $h+k$ even, l odd
'*d*' type: $h+k$ odd, l even.

Of these, only the '*a*' type correspond to possible reflections of albite. The rest, which arise from dif-

* Present address: Department of Physics, University of Adelaide, Adelaide, Australia.
† Present address: Division of Soils, Commonwealth Scientific and Industrial Research Organisation, Adelaide, Australia.

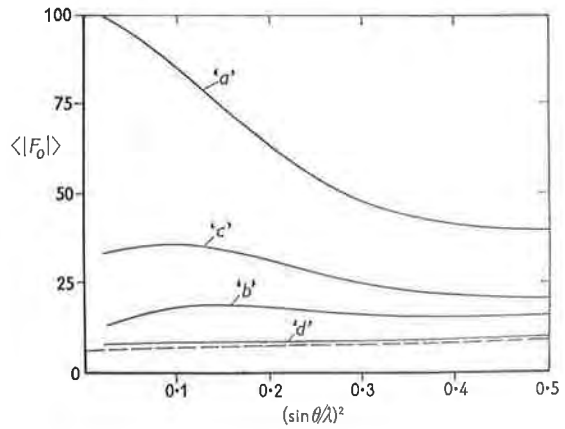

Fig. 1. Average non-zero $|F_o|$ values of four types of reflections, versus $(\sin\theta/\lambda)^2$. (The dashed line gives an estimate of the lowest experimentally observable value.)

ferences between the subcells, are on the whole very much weaker (see Fig. 1), indicating that the differences are small. The analysis of such a structure may be attempted by a method of successive approximations.

1·3. *Principle of method of solution*

It is easiest to understand the method of solution by considering a hypothetical structure with two subcells only. This is illustrated in Fig. 2(*a*), where $c/2$ is nearly but not exactly a translation vector, so that corresponding atoms in the two subcells are at slightly different positions, and the difference gives rise to weak reflections with odd l. A synthesis of reflections with even l will give a superposition of the two subcells, replacing each atom by two 'half atoms' (Fig. 2(*b*)), which in practice will probably appear as an unresolved elliptical peak (Fig. 2(*c*)). A synthesis of odd-l reflections (Fig. 2(*d*)) has to be added to this to reproduce the true structure. The mean parameters (x_m, y_m, z_m) give a reference point, shown by a dot, which is the same in each subcell. The difference parameters $\pm(\delta x, \delta y, \delta z)$ give the displacements of the actual atoms from this mean position. An illustration from the actual structure, corresponding to Figs. 2(*c*) and 2(*d*), is given in Fig. 7.

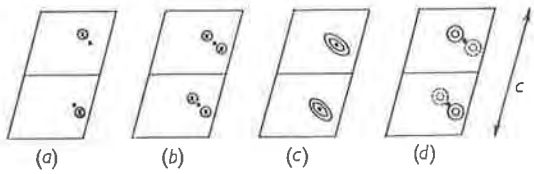

Fig. 2. Diagram illustrating effects in a hypothetical structure: (*a*) different atomic positions in two subcells, (*b*) 'average structure', showing positions of two 'half-atoms' in each subcell, (*c*) Fourier synthesis (F_o map) using main reflections, (*d*) Fourier synthesis (F_o map) using difference reflections. (Dotted lines show negative contours; contours in (*d*) are at smaller intervals than in (*c*).)

A knowledge of the approximate structure gives the signs of the even-l reflections only; hence the synthesis of Fig. 2(*c*) can be constructed, but not that of Fig. 2(*d*). From the former it is possible to deduce the mean position of the two half atoms and the magnitude of their separation or 'splitting' but not its sense, i.e. one cannot say which half atom belongs to which subcell. If there is only one 'split atom' the choice is arbitrary, but if there is more than one the question is a real one and can only be answered from the evidence of the difference intensities. The actual atomic parameters are the algebraic sum of the mean parameters and the difference parameters with correct sign. Once they are known the refinement of the structure as a whole can proceed in the ordinary way.

In principle the method is closely related to one used by Buerger (1956), but in detail the latter would have been inapplicable to our work even if we had known of it at an early stage (cf. Radoslovich, 1955). Buerger, concerned with differences of atomic *occupation* between subcells, takes the actual structure as made up of 'substructure' and 'complement structure', substructure being 'that part of the electron density which conforms to the substructure period'. We, concerned with differences of atomic *coordinates*, find a break-up into 'average structure' and 'difference structure' much more informative, even though the electron density over half the volume of the latter is necessarily represented as negative.

1·4. *Application to anorthite*

The above is a general method for structures with closely similar subcells. The determination of the signs of the difference parameters, however, remains an individual problem for each structure. One example occurred in the structure of celsian (Newnham & Megaw, 1960). In anorthite, there was the advantage that the Ca atoms were found experimentally to have the largest difference parameters, and hence a modification of the heavy-atom technique could be used. On the other hand, there was the disadvantage that the true structure had four subcells, not two, which meant that its derivation from that of albite had to proceed in two stages. Initially it was assumed that the first stage had been completed in Sørum's study of 'body-centred anorthite' (1951, 1953), and this structure was taken as the starting-point for the second stage. This soon proved not to be a good approximation, so a fresh approach was made. In this the average structure was referred to an albite-type subcell, and the strongest set of difference reflections, namely the '*c*' type (Fig. 1), was considered first, leaving the '*b*' and '*d*' types to be included at the second stage. This method proved successful, and the structure could finally be refined in the ordinary way using all four types of reflection.

It is convenient henceforward to refer to the set of difference parameters which would be zero if the '*c*' or the '*b*' reflections were systematically absent as the '*c*' *splittings* or the '*b*' *splittings* respectively.

Since this is a method of successive approximations, it is desirable to check its progress at every stage. This was done by considering not only the R-factor (which can be misleading) but also the height and shape of the peaks on Fourier maps, the amount of false detail in the background of F_o syntheses and difference syntheses, and the relative magnitude of the atomic shifts in successive syntheses. The continuous and simultaneous improvement in all these was evidence that the structure was refining truly.

2. Experimental

2·1. *Material*

The anorthite selected for analysis was from Monte Somma, Vesuvius (reference number B.M. 30744, provided by P. M. Game of the British Museum); it is from the same locality as the material (B.M. 49465) used by Taylor, Darbyshire & Strunz (1934) and Cole, Sørum & Taylor (1951). Gay (1953) points out that it is of low-temperature origin. Optical examination, using a universal-stage microscope, had shown its composition to be in the range 95–100% anorthite.

The material was found to be heavily twinned, but single-twinned cleavage flakes could be picked out from crushed samples; by cutting with a sharp knife inside a small perspex box a few small untwinned blocks were obtained. The crystal finally chosen was of square cross-section, $0{\cdot}18 \times 0{\cdot}18 \times 0{\cdot}32$ mm., elongated roughly parallel to the a-axis.

The lattice constants were taken to be those of Cole, Sørum & Taylor (1951), which are quoted in § 1·2.

2·2. *Measurement of intensities*

Three-dimensional intensity data were collected from equi-inclination Weissenberg photographs, using filtered Mo $K\alpha$ radiation and the standard techniques of visual estimation with a comparison scale. Corrections were made for spot shape; in the later stages of refinement revised values were introduced, calculated by a modification of the method of Phillips (1954) (see Appendix). Some extinction effects were apparent for low-angle reflections; as suggested by Jellinek (1958) all reflections in these regions were omitted from difference syntheses, (and elsewhere replaced by calculated values), and not just the strongest ones with obvious discrepancies. Reflections in the central region of higher layers were also omitted, because for them the spot-shape correction was very large. In all, about 18% of the observed reflections were omitted.

No correction was made for absorption, because no convenient method was available. As a check, the absorption was calculated for a few selected low-angle reflections by the method of Albrecht (1939), and was found to vary from 19% to 37%. It was decided that these differences could be ignored, since accurate values of the temperature factors were not a primary object of investigation.

2·3. *General relations between observed intensities*

The final F_o and F_c values have been tabulated and can be made available on request.

The numbers and proportions of the four types of reflections are recorded in Table 1. Statistics are also included for a restricted group of strong structure factors (>60 on an absolute scale) comprising one quarter of the observed reflections. The difference reflections are evidently both weaker and less numerous than the main 'a' reflections, and the average intensities of the classes as a whole are in the order 'a' > 'c' > 'b' > 'd', irrespective of the distance from the origin of reciprocal space (Fig. 1).

It is clear that the structure of primitive anorthite approximates more closely to a base-centred (C-face-centred) structure than to a body-centred structure. This is a geometrical fact; the physical implications cannot be discussed till the structure as a whole is completely described.

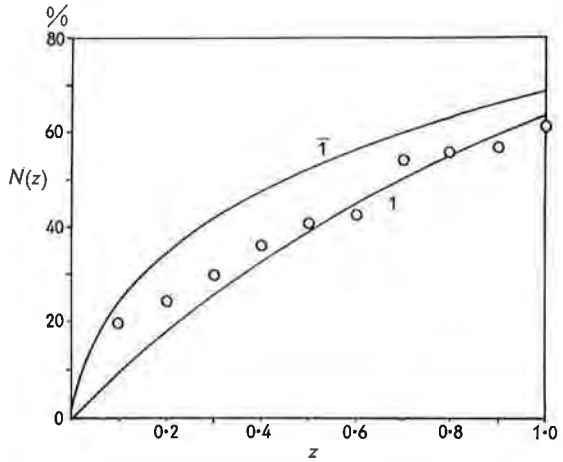

Fig. 3. $N(z)$ test applied to the 'a'-type $0kl$ reflections of anorthite.

Table 1. *Survey of anorthite structure factors*

Type of reflection	'a' $h+k$ even l even	'b' $h+k$ odd l odd	'c' $h+k$ even l odd	'd' $h+k$ odd l even	Total
No. observed	1346	478	853	114	2791
	48%	17%	31%	4%	
No. of strong reflections (>60 on absolute scale)	621	4	89	0	714
	87%	1%	12%	0	
Percentage of group below least observable	27%	71%	48%	93%	59%

The older statistical tests for the presence or absence of a centre of symmetry fail because of the large proportion of intensities below the observable limit, characteristic of this type of pseudosymmetric structure (see Table 1). If the $N(z)$ test is applied to the '*a*' reflections of the 0*kl* zone all but the first few points follow the acentric curve fairly closely (Fig. 3). This is probably due to the implicit assumption of an albite-size unit cell containing incompletely resolved quarter atoms, which is not in accordance with the random distribution of spherical atoms required by Wilson's (1949) theory. The $P(y)$ test (Ramachandran & Srinivasan, 1959), on the other hand, can and should be applied to *all* the reflections. When this is done, it speaks conclusively for centrosymmetry.

3. Outline of calculations

3·1. *Atomic scattering factors*

The scattering curves of Bragg & West (1928) were used in the early stages, but they were later replaced by others based on those of Berghuis, Haanappel, Potters, Loopstra, MacGillavry & Veenendaal (1955), modified by appropriate temperature factors (see § 3·2). An average between the curves for Al and Si was used throughout.

3·2. *Computing methods*

At the time when work on this structure was begun, no computer programme was available which was suitable for carrying out Fourier syntheses. Since it was clear that two-dimensional work would not give enough resolution, bounded projections were calculated (cf. Lipson & Cochran, 1953) using a Hollerith punched-card installation. It was thought initially that the unit cell would be covered adequately, without much overlap of atoms, by five slabs, bounded by the pairs of planes $x=0\pm\frac{1}{16}$, $x=\frac{1}{4}\pm\frac{1}{10}$, $y=0\pm\frac{1}{24}$, $y=\frac{1}{6}\pm\frac{1}{12}$, $y=\frac{1}{3}\pm\frac{1}{12}$. At a later stage thicker slabs with boundaries $x=0\pm\frac{1}{8}$, $x=\frac{1}{4}\pm\frac{1}{6}$, were found necessary.

Structure factors were computed on Edsac I.

When all the 52 independent atomic peaks had been individually located, difference syntheses in two and three dimensions were used for further refinement, calculated on Edsac I. The three-dimensional syntheses were computed in two stages, a set of generalized projections being calculated and used to give the coefficients for a series of one-dimensional syntheses scanning the whole volume. The electron-density differences near each atomic site were plotted out on a series of pieces of tracing paper representing parallel sections through the atom.

To calculate atomic shifts from the slopes in a difference synthesis it is necessary to know the curvatures of the peaks in the corresponding F_o synthesis, or to estimate these from their p-value and heights (Lipson & Cochran, 1953). The p-values are based on the assumption of a Gaussian atom, and to this approximation they are the same for the peaks in the bounded projections as in three dimensions, a fact which allows the peak height for the latter to be deduced from the former. The values adopted are given in Table 6(*c*).

Table 2. *Scattering factor coefficients*

Atom and state of ionization*	Scattering factor coefficients				
	A	*B*	*C*	*D*	*E*
Ca^{++}	5·590	1·697	8·061	13·042	4·259
Si^{++}/Al^{+}	7·612	2·857	2·249	63·642	2·128
O^{-}	4·463	7·056	3·035	36·845	1·478

* These 'states of ionization' were chosen arbitrarily, as being empirically reasonable. They make very little difference to F_c.

The final stages of refinement were done with a cyclic program on Edsac II (Wells, 1961). For this, the scattering factor curves of Berghuis *et al.* (1955) were fitted by expressions of the form

$$A \exp[-Bs^2]+C \exp[-Ds^2]+E ,$$

(Forsyth & Wells, 1959). The coefficients (Table 2) were evaluated independently because of differences in the state of ionization assumed. The isotropic temperature factors were determined from two-dimensional syntheses and thereafter left unchanged.

After rejection of reflections liable to be in error because of extinction or spot shape, 2200 remained (82% of those observed). These F_o's were stored on magnetic tape. The F_c's were calculated, and the F_o's scaled to them by a single scaling factor not varying through reciprocal space. After calculation of an R-factor, reflections for which $||F_o|-|F_c||$ was greater than 10 on an absolute scale, or $|F_o|/|F_c|$ lay outside the range $\frac{1}{2}$ to 2, were tabulated and rejected; their number dropped from 70 at the beginning to 4 at the last cycle. The rest were used to calculate the values of differential syntheses at each atomic site and the shifts, and new coordinates, were punched out as well as being fed back for a new cycle.

4. Structure analysis

4·1. *Preliminary work*

The first attempt used the structure of body-centred anorthite put forward by Sørum (1951) as a trial structure; the plan was to refine it, using '*a*' and '*b*' reflections, and then move to the true structure by including '*c*' and '*d*' reflections.

After two cycles of refinement, the Ca and T peaks were fairly clear and well defined; but the '*b*' splittings were much smaller than those determined by Sørum and for some of the T peaks they differed in direction from his (though not by appreciably more than they changed in the course of his final three-dimensional refinement). The O peaks were irregular, of varying height, and as much as 1·5 Å from their expected positions. It seemed that some of them might have moved outside the limit of the bounded projection

The Ca and T peaks were markedly elongated, as was expected because of the 'c' splittings. The magnitudes of these splittings were estimated from the peak contours by plotting out sections along the major and minor axes of the peaks; then if each atom has a cross section like that along the minor axis, the separation $2\delta r$ of two such atoms giving a cross section like that along the major axis can be found by trial.

Attempts were made to deduce the signs of the splittings, following which a synthesis gave fair agreement for Ca, but inconsistent results for T. It had become clear at this stage that the differences from Sørum's structure were too great to treat it as a reliable trial structure; if the magnitudes and directions of its 'b' splittings were not close to those of anorthite, their signs would be unreliable, and so would deductions about 'c' splittings which depended on them. This approach was therefore abandoned.

4·2. *Average structure from 'a' reflections*

The new approach started with a trial structure having an albitoid cell and thus giving 'a' reflections only. Their signs were assumed to be known fairly accurately from the preliminary work. A complete set of bounded projections was prepared; the layers at $x=0$ and $x=\frac{1}{4}$ are shown in Fig. 4.

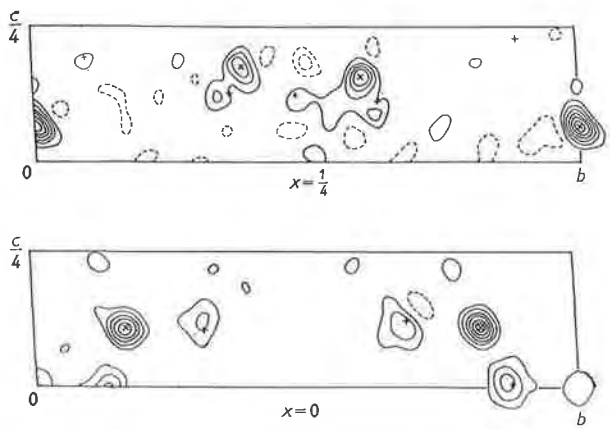

Fig. 4. First bounded projections: slabs at $x=0$ and $x=\frac{1}{4}$. Contours at intervals of 7·3 e.Å^{-3}; zero contour omitted. Cation peaks ×, anion peaks +. The strong peak near $(\frac{1}{4}, 0, 0)$ is Ca. The site of $O_D(m)$, which remained missing till a much later stage, is shown at the top right-hand corner of the slab at $x=\frac{1}{4}$.

As before, the Ca and T peaks were clear, the O peaks less good. Coordinates were obtained with fair accuracy for 11 of the 13 atoms in the asymmetric unit. The two remaining O's, $O_A(2)$ and $O_D(m)$, did not show up at all; positions were guessed for them in the gaps between the bounded projections.

Of the well-defined peaks the Ca appeared to show the largest splittings but some of the T peaks were also appreciably split.

Although each peak in this 'average structure' consists of four quarter atoms, it is necessary at this stage to assume that the 'b' splittings are negligible compared with the 'c' splittings, and so to treat each peak as if it were merely double. With the less important splittings this may give rise to indeterminacy or misinterpretation, but if the more important splittings are correctly interpreted ('important' in this context referring to the scattering factor of the atom concerned as well as the magnitude of the splitting) the errors may be expected to remedy themselves during refinement.

Since Ca, which has the largest splitting, is also the heaviest atom in the structure, it seemed likely that a 'heavy-splitting' method of solution might be effective. The fact that the difference reflections were observable as far out in reciprocal space as the 'a' type reflections agreed with the assumption that Ca made an important contribution to them. The criterion of the 'heaviness' of a heavy atom suggested by Lipson & Cochran (1953, p. 207) is the ratio $(\Sigma f^2)_{\text{heavy atoms}}/(\Sigma f^2)_{\text{other atoms}}$. For Ca in anorthite, using the Bragg–West scattering curves, this is 0·3 at low angles and 0·6 near the limit of visible reflections. If the ratio were 1·0, about 75% of all signs would be determined by the heavy atom. The effective 'heaviness' is expected to be enhanced by the large splitting.

4·3. *Location of symmetry centres*

In this first-stage reduction of symmetry, from 7 Å C-face-centred (albite-type) to 14 Å C-face-centred, half the centres of symmetry are lost, making it necessary to decide whether those retained are the set including (0, 0, 0) or the set including $(0, 0, \frac{1}{4})$ (referred to the 14 Å cell). The contribution of the Ca atoms must first be calculated for both possibilities.

The eight atoms which were originally equivalent in the double albite cell have now been divided into two sets of four, derived from atoms at

$$(x_m+\delta x,\ y_m+\delta y,\ z_m+\delta z) \quad \text{and}$$
$$(x_m-\delta x,\ y_m-\delta y,\ \tfrac{1}{2}+z_m-\delta z)$$

by the operation of the centre of symmetry and the C-face centring. Writing

$$\Theta = 2\pi(hx_m+ky_m+lz_m)$$
$$\Delta = 2\pi(h\delta x+k\delta y+l\delta z)$$

it can be shown that the structure factor contributions in the two cases are as follows:

centre of symmetry at (0, 0, 0):

'a' reflections $\quad 8f\cos\Theta\cos\Delta$,
'c' reflections $\quad 8f\sin\Theta\sin\Delta$;

centre of symmetry at $(0, 0, \frac{1}{4})$:

'a' reflections $\quad \pm 8f\cos\Theta\cos\Delta$,
'c' reflections $\quad \pm 8f\cos\Theta\sin\Delta$.

The total structure factor is obtained by summing terms of this form over all the atoms in an asymmetric

unit of albite. In this initial approximation, however, all except Ca are assumed to be negligible. Since Δ is small compared with Θ, the factor $\cos\Delta$ or $\sin\Delta$ varies slowly in reciprocal space, modulating the rapidly varying factor $\cos\Theta$ or $\sin\Theta$. The effect on the inner '*a*' reflections is very like that of a highly anisotropic temperature factor, and is independent of the choice of origin. The '*c*' reflections are modulated by the factor $\sin\Delta$, which is zero in a plane of reciprocal space normal to the direction of splitting, and on either side of it gives a set of parallel plane fringes with maxima at $\Delta = \pm\pi/2$. The magnitude of these reflections depends on either $\cos\Theta$ or $\sin\Theta$ as above.

This argument was used to determine the position of the centres of symmetry. Both Θ and Δ are calculable for every *hkl*. Since the contribution of atoms other than Ca is relatively more important at small reciprocal radii, low-angle reflections were at first excluded from the analysis, as were those for which $\sin\Delta$ was small. Division of the rest into two groups according to whether $|\sin\Theta|$ or $|\cos\Theta|$ was greater gave no significant difference of average intensity between the groups. Inspection of the strongest '*c*' reflections proved more informative, however. Of 73 which were stronger than the strongest '*b*' reflection, 59 had $|\sin\Theta| > |\cos\Theta|$, showing conclusively that the centre of symmetry was at (0, 0, 0)—a result confirmed by all subsequent work. It is interesting that this selective method succeeded when the comprehensive method including the larger sample failed.

4·4. *T splittings*

In the array of intensities of '*c*' reflections on the reciprocal lattice the strong intensities lay conspicuously on the fringes where $\sin\Delta_{Ca}$ had a maximum, but in patches consisting of from 2 to 5 strong reflections separated by weaker ones. These patches could often be identified as the intersection of fringes due to one or more *T* splittings with those due to the Ca splitting. Though the interpretation along these lines was not complete, it was sufficiently comprehensive to be very encouraging.

4·5. *Syntheses using 'a' and 'c' reflections*

The first synthesis of '*c*' reflections—a set of bounded projections—was constructed using only those of strongest intensity, about one eighth of the total number observed, with the signs determined from their Ca contributions. This 'partial-*c*' synthesis is illustrated in Fig. 5. The '*c*' splittings are here shown by a slope at the atomic position, which lies between a trough and a peak. The Ca splitting, of course, came out very strongly in the direction assumed in calculating signs. In addition, appreciable slopes appeared at many of the other peak sites. The general background was still fairly undulating.

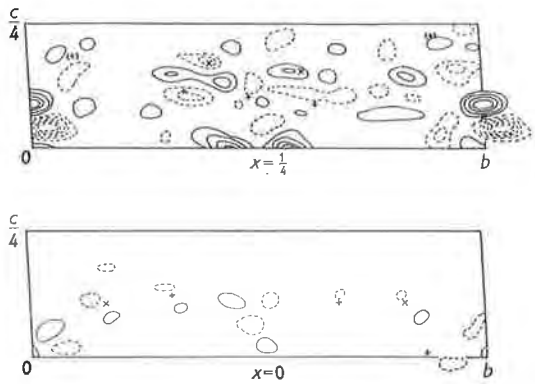

Fig. 5. 'Partial-*c*' synthesis, using only the strongest '*c*' reflections with signs determined by Ca. Diagram shows slabs of bounded projection at $x=0$ and $x=\frac{1}{4}$. Contours at intervals of 1·5 e.Å^{-3}; zero contour omitted; negative contours shown dotted. Cation peaks ×, anion peaks +. The peaks near $(\frac{1}{4}, \frac{1}{2}, 0)$ are false detail which disappears later.

This synthesis, by its construction, overemphasized the components of all splittings parallel to that of Ca. Better estimates of the magnitude and direction of the splittings were already available for some atoms from examination of the ellipticity of peaks in the synthesis of '*a*' reflections. The '*c*' synthesis, however, gave information about the signs of the difference parameters which could not be obtained from the '*a*' synthesis.

Table 3. *Proposed c-splittings for anorthite*

	Initial values			Refined values (at *C*-face-centred stage)		
Atom	δx	δy	δz	δx	δy	δz
Ca (000)	−0·0075	−0·0052	0·0058	−0·0020	−0·0174	0·0182
T_1 (0000)	0	0	0	−0·0055	0·0020	−0·0005
T_1 (*m*000)	0	0	0	−0·0018	0·0015	−0·0020
T_2 (0000)	−0·0071	−0·0031	−0·0028	−0·0076	0·0010	−0·0060
T_2 (*m*000)	−0·0057	−0·0015	0·0029	0·0032	0·0025	0·0065
O_A (1000)	0	0	0	0	−0·002	0·004
O_A (2000)	0·050	0	−0·017	0·001	0·003	0·001
O_B (0000)	0·004	−0·002	−0·004	−0·024	0·006	−0·018
O_B (*m*000)	0·025	−0·003	0·006	0·014	−0·011	0·002
O_C (0000)	0·003	0	−0·003	0·006	0	0·011
O_C (*m*000)	0	0	0	−0·020	0·001	0·002
O_D (0000)	−0·013	0·005	0·004	−0·008	0·003	0·011
O_D (*m*000)	0	0	0	0·020	0·012	−0·013

Two of the four T atoms now showed measurable splitting, as did five O atoms; for the other two T's the splitting was small and was taken as zero. The z parameters determined independently from the x and y projections agreed satisfactorily. The signs of the T splittings were checked by calculating their contributions to a number of F_c's corresponding to large F_o's. Where the Ca contribution was negligible, the T contributions were usually large; where both Ca and T contributions were large, they usually had the same sign. The difference parameters at this stage are recorded as 'initial values' in Table 3.

A second synthesis of the 'a' and 'c' reflections separately was constructed using the revised coordinates. All the peaks in the 'a'-reflection synthesis had improved, except $O_D(m)$ which was still missing. The 'c'-reflection synthesis (Fig. 6) showed much greater contrast between atomic sites and background, but was otherwise very much like the previous cycle, even at sites where it had been thought unsafe to attribute the slopes to splitting. This was satisfactory confirmation of the validity of the procedure. A further indication was provided by the behaviour (not illustrated in Fig. 6) of two oxygen atoms for which large splittings had been deduced: for $O_B(m)$ the splitting was confirmed, whereas for $O_A(2)$ it had disappeared, and in the 'a'-reflection synthesis the whole peak came up at one of the two 'half-atom' sites. It appeared that the mean position of this latter atom had been wrong by at least 0·5 Å in the earlier syntheses, and that it had not refined satisfactorily.

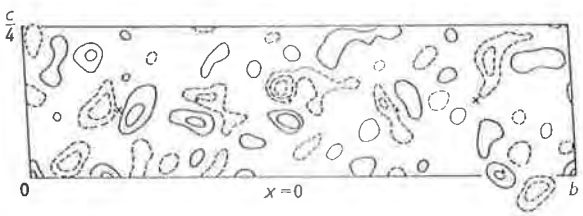

Fig. 6. First full 'c' synthesis. Diagram shows slab of bounded projection at $x=0$. Contours as in Fig. 5. Here the site of $O_A(2)$, near (0, $\frac{1}{2}$, $\frac{1}{8}$), is marked for the first time.

It seemed likely that the missing atom $O_D(m)$ was still misplaced by about 0·5 Å; a new position for it was proposed.

The sum and difference of the 'a' and 'c'-reflection syntheses were plotted for each peak, giving the electron density and atomic coordinates in the two subcells. Fig. 7 illustrates this procedure.

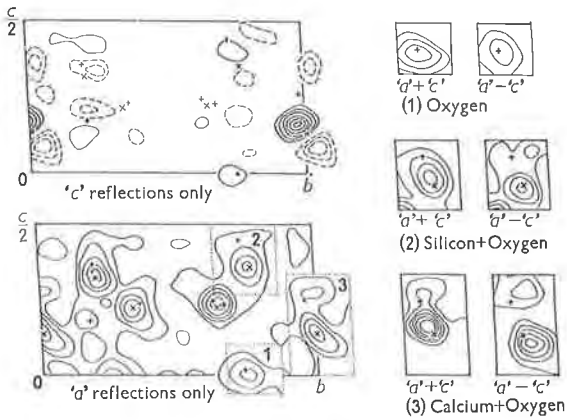

Fig. 7. Combination of 'a' and 'c' synthesis by sum and difference. Diagram shows projections on (100). Contours for 'a' at intervals of 6 e.Å^{-2}, zero and first contours omitted; contours for 'c' at intervals of 3 e.Å^{-2}, zero contour omitted. The small diagrams to the right show the effect of taking the correspondingly-numbered regions of the 'a' synthesis and adding or subtracting the electron densities in the same regions of the 'c' synthesis. Cation peaks ×, anion peaks +.

Here and throughout the analysis, adjustments to atomic coordinates were made from the evidence of the Fourier maps alone, and never from considerations of interatomic distance; the latter might have speeded up the refinement process, but might also have prejudged the bond lengths unwisely.

Next, several cycles of refinement were carried out using F_o, F_c, and (F_o-F_c) projections down the x-axis. (The y- and z-axis projections contained serious overlapping.) The R-factors at this and earlier stages are given in Table 4.

Table 4. *R-factors* (*as percentages*)

Where R-factors were calculated separately for different types of reflections, the types concerned are noted in the first column, and the separate values recorded in the later columns
From the stage illustrated in Fig. 9 onward, all types were taken together

Stage of work, and type of reflection used	$0kl$	$h0l$	$hk0$	Overall
After first 'a'+'c' bounded projections (Fig. 5): 'a', 'c'	53, 80	—	—	—
After refinement in projection: 'a', 'c'	31, 53	41, 51	45	—
After second 'a'+'c' bounded projections (Fig. 6): 'a'+'c'	32	37	34	—
After first determination of signs of 'b': 'a'+'c', 'b'	29, 50	—	—	—
After 'partial-b' (Fig. 8)	28·8	28·2	27·7	—
After final bounded projections (Fig. 9)	22·2	18·6	18·4	—
After two cycles of F_o-F_c projections	15·4	17·2	17·2	18·9
After first three-dimensional F_o-F_c synthesis	12·8	—	—	17·1
After second three-dimensional F_o-F_c synthesis	12·6	—	—	15·2
After revision of coordinates and F_o's	11·2	—	—	13·5, 12·4*
After 23 cycles of automatic refinement	9·6	—	—	(11·1), 10·2*

* These figures refer to about 82% of the reflections. The value in brackets is estimated for all reflections from the calculated value for the 82%.

Using the new coordinates of the 26 atoms, and taking '*a*' and '*c*' reflections together, a third set of bounded projections was calculated having the new limits $x=0\pm\frac{1}{8}$ and $x=\frac{1}{4}\pm\frac{1}{6}$. The general appearance was good, and the missing O atoms, $O_D(m000)$ and $O_D(m0ic)$, showed up for the first time, fairly close to their estimated positions. In estimating a new set of coordinates, rough corrections were made for the very pronounced diffraction effects.

The final difference parameters at the *C*-face-centred stage are given in Table 3. Most of them increased noticeably as the work progressed, but the x components in general decreased, though the peaks continued to show the marked elongation in the x direction which had led to the original high estimate of δx. This was clearly a diffraction effect, due to the distribution in reciprocal space of the observed data: the main collection of data was from photographs about the x axis, and layer lines with $h>8$ had not been included because of the extreme distortion of spot shape. Once recognized, this 'natural elongation' of the peaks could be allowed for, until it was eliminated by the use of difference maps.

4·6. *Second stage*: *inclusion of 'b' and 'd' reflections*

It had become clear towards the end of the first stage that one of the principal factors slowing down the refinement was failure to take account of the departures from the *C*-face-centred approximation, namely the '*b*' splittings of the 26 peaks. Replacement of each of these peaks by two half atoms is a possible first step in the second stage of the structure analysis. When this was done in the [100] projection it immediately reduced the *R*-factor by $5\frac{1}{2}$%. This approach was not followed up because of programming difficulties.

An alternative approach started from the observation that one of the two Ca peaks, Ca (00), was considerably more elongated than any other, suggesting a repetition of the 'heavy-splitting' method applied to the '*b*' reflections. (The '*d*' reflections, which are few and weak, were omitted till the final stages.)

It was necessary, as previously, to begin by determining which of the two sets of symmetry centres in the *C*-face-centred approximation is retained as such in the true structure. An analysis like that of § 4·3 shows that the '*a*' and '*c*' structure amplitudes are the same for both choices, since $h+k$ is even, but that the '*b*' and '*d*' structure amplitudes are proportional to $\sin\Theta$ for a centre at (0, 0, 0), to $\cos\Theta$ for a centre at $(\frac{1}{4}, \frac{1}{4}, 0)$. Examination of 183 strong '*b*' reflections showed that 52% lay close to a maximum of $|\sin\Theta|$, 34% to a maximum of $|\cos\Theta|$. Further, of the 16 strong '*b*' reflections in the 0*kl* zone, 13 had large contributions from Ca if the centre of symmetry was at (0, 0, 0), and 8 if it was at $(\frac{1}{4}, \frac{1}{4}, 0)$. The centre was therefore tentatively placed at (0, 0, 0); the correctness of this choice was established by the successful refinement of the consequent trial structure.

There were now 13 strong '*b*' reflections in the 0*kl* zone whose signs were known from the Ca contribution, and these were used to construct a 'partial-b' x-axis projection. Only for the Ca atoms were the pairs of peaks related by '*c*' splittings sufficiently resolved in this projection to give clear information about the '*b*' splittings.

By assuming that strong '*b*' reflections arise when the contributions from Ca atoms and the rest of the framework are *both* strong and of the same sign, it was possible to allocate signs to the '*b*' splittings of six *T* peaks, their magnitudes being estimated from the final *C*-face-centred synthesis. (The splittings of the O peaks were too small for this.) The resulting set of difference parameters (Table 5) produced large contributions to all the 16 strong *b* reflections. A difference synthesis computed with these parameters was used to improve the coordinates of the four Ca atoms.

To check these conclusions, and to extend them to include the x-parameters, an independent estimate was made of the three-dimensional splittings for the atoms of the framework as described in § 4·5 for the '*c*' reflections. The contributions of the four Ca atoms were calculated for the 183 strong '*b*' reflections. Signs were indicated for 70% of these reflections, which were then used to construct a set of 'partial-*b*' bounded projections (Fig. 8). Comparison with the final bounded projections of the approximation using '*a*' and '*c*' reflections only—an approximation which now acts as an average structure—allowed splittings to be derived for

Table 5. *Proposed b-splittings for anorthite*

	Values from x-projection		Values from first three-dimensional trial			Final values		
Atom	δy	δz	δx	δy	δz	δx	δy	δz
Ca(000)	−0·011	0·008	−0·012	As in		0·0006	−0·0112	0·0066
Ca(z00)	−0·004	0·001	−0·005	x-projection		−0·0024	−0·0021	0·0008
T_1(0000)	0	0	0·004	−0·004	0	0·0056	−0·0046	−0·0041
T_1(0z00)	0·007	0·005	−0·004	0·004	0·002	0·0004	0·0021	0·0046
T_1(m000)	−0·007	0·006	0	−0·005	0·005	−0·0053	−0·0030	0·0050
T_1(mz00)	0·006	−0·008	0	0·005	−0·005	−0·0010	0	−0·0042
T_2(0000)	0·008	−0·004	0	0·007	0	0·0056	0·0036	0·0004
T_2(0z00)	−0·011	0	−0·003	−0·005	0	−0·0044	−0·0047	−0·0018
T_2(m000)	0·008	0·005	−0·002	0·003	0·001	−0·0058	0·0019	0·0033
T_2(mz00)	0	0	−0·003	−0·003	0	0·0020	0·0042	−0·0014

each of the eight T peaks; it also suggested possible splittings for several of the O peaks, which were however disregarded for the present. The difference parameters thus obtained agreed remarkably well with the two-dimensional set.

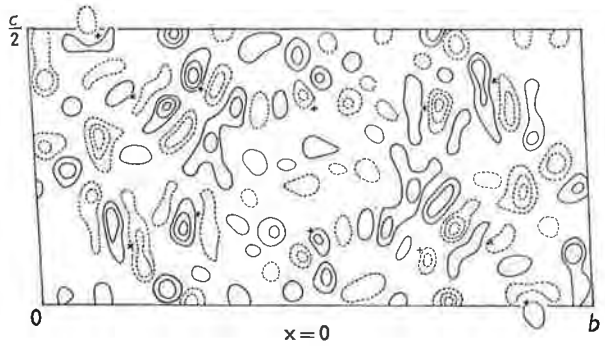

Fig. 8. Partial-b synthesis, using only the strongest b reflections, with signs determined by Ca. Diagram shows slab of bounded projection at $x=0$. Contours at intervals of 1·8 e.Å^{-3}, zero contour omitted. Cation peaks ×, anion peaks +.

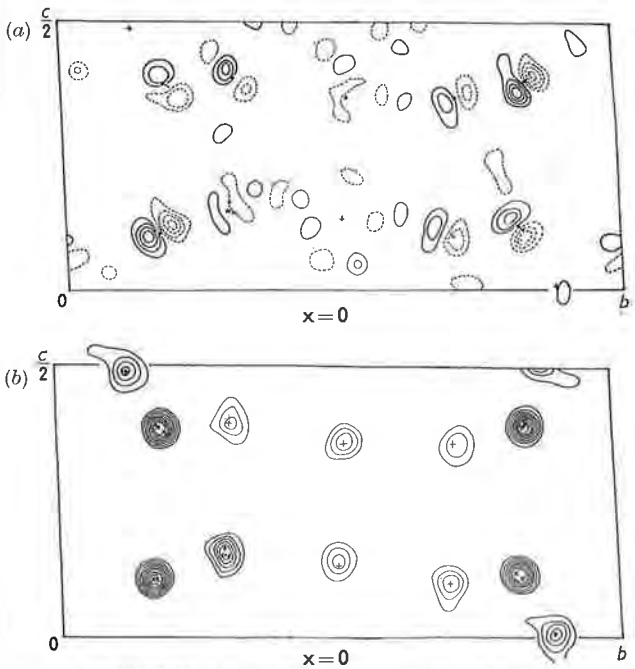

Fig. 9. (*a*) Final '*b*'+'*d*' synthesis; contours at intervals of 1·8 e.Å^{-3}, zero contour omitted. (*b*) Final '*a*'+'*c*' synthesis; contours at intervals of 8·3 e.Å^{-3}, zero contour omitted. Diagrams show slab of bounded projection at $x=0$. Compare with Fig. 4. Atoms marked × are T_1; atoms at $z=0$, $\frac{1}{2}$, are $O_A(1)$; atoms at $y=\frac{1}{2}$ are $O_A(2)$ (not visible in Fig. 4); the rest are O_C.

Combination of these difference parameters with the parameters of the C-face-centred approximation gave a trial structure with a primitive lattice.

A final set of bounded projections was calculated from the full set of observed reflections using this trial structure. Separate syntheses were constructed for the '*a*' and '*c*' reflections together, and the '*b*' and '*d*' reflections together. Both were greatly improved (Fig. 9); the ('*b*'+'*d*') synthesis was remarkably similar to the 'partial-*b*' synthesis at peak sites, but had a much tidier background elsewhere. In particular, several splittings of O atoms suggested by the earlier synthesis but not adopted in the trial structure reappeared in the new synthesis—an effect similar to that observed with the '*c*' splittings (§ 4·5). It seems that deductions from the partial syntheses were too cautious—an error on the right side in a structure of this complexity—and that the use of the Ca splitting as a 'heavy splitting', analogous to that of a heavy atom, has been fully justified.

A synthesis of the complete structure was obtained by combining the ('*a*'+'*c*') and ('*b*'+'*d*') syntheses, and this gave new coordinates for all the atoms, including all the O's. The '*b*' splittings for Ca were smaller than in the trial structure, the Ca peaks remaining somewhat elongated. The R-factors were much improved, but the calculated intensities of '*b*' and '*d*' reflections were still lower than the observed. There was very considerable scatter of bond lengths within the tetrahedra, making it impossible to detect any kind of Si/Al ordering. Nevertheless one could be confident that the structure was essentially correct and only needed refinement.

5. Refinement

5·1. *Use of difference syntheses*

Difference syntheses for the three cardinal projections were now so much improved that it was worth while using them for refinement while preparations were being made for three-dimensional syntheses. Certain interesting effects were noticed.

Two cycles of refinement of the x-axis projections

Table 6

(*a*) Isotropic temperature factors

B values in Å^2

Atom	Effective value in Bragg–West curves	First revised values from refinement of x-projection	Final values
Ca	0·4	1·0	1·0, 0·3
T	0·3	0·3	0·2
O	1·5	0·7	0·6

(*b*) Principal axes of thermal ellipsoids (direction of long axis is close to [110])

Ca(000)	0·75	1·88	0·32
Ca(zi0)	1·00	2·00	0·50
Ca(z0c)	0·40	1·18	0·50
Ca(0ic)	0·50	1·72	0·19

(*c*) p-values and peak heights

Atom	p	Peak height (e.Å^{-3})
Ca	7·2	80
T	8·3	67
O	6·8	28

Table 7. *Progress of refinement at various stages*

(*a*) Refinement by 3-dimensional ($F_o - F_c$) synthesis: Shifts in Å

	Ca	*T* Mean	*T* Max.	O Mean	O Max.
First cycle	Very small	0·021	0·039	0·046	0·085
Second cycle	Very small	0·012	0·021	0·028	0·048

(*b*) Automatic refinement programme

(δx, δy, δz are in fractions of cell edge $\times 10^4$)

	Calcium				I				O			
Cycle	δx	δy	δz	Shift (Å)	δx	δy	δz	Shift (Å)	δx	δy	δz	Shift (Å)
17	2·0	1·6	2·6	0·0046	3·8	1·9	1·9	0·0048	4·6	2·2	2·1	0·0056
18	1·4	1·4	1·9	0·0034	2·5	1·3	1·2	0·0031	3·1	1·8	1·5	0·0034
19	1·1	0·9	1·3	0·0023	2·1	0·9	0·7	0·0023	2·5	1·4	1·3	0·0032
20									2·0	1·3	1·1	0·0028
21									1·4	0·9	0·9	0·0021

reduced the *R*-factor from 22·2% to 15·4%; the '*b*' splittings for Ca increased towards their original values, the Ca peaks meanwhile becoming rounder; and the calculated intensities of '*b*' reflections increased. On all these points, therefore, the first complete F_o synthesis had been misleading, simply because more than 70% of the '*b*' and more than 90% of the '*d*' reflections were too weak to observe (Table 1). The omission of so many reflections from the ('*b*'+'*d*') synthesis meant that the observed slopes at the peak sites were lower than they should have been, and the deduced splittings therefore smaller. From this point onward, therefore, it was necessary to work with difference syntheses, even in three dimensions.

The first three-dimensional synthesis improved the coordinates but showed the inadequacy of the temperature factors implicit in the Bragg–West scattering factors. Revised values (Table 6) were obtained from two-dimensional work. A second three-dimensional synthesis gave further changes of atomic coordinates (Table 7(*a*)). The temperature factors were still not perfect, and the Ca peaks showed slight elongation, in a direction quite different from the previous splittings, but approximately the same for all four Ca's.

5·2. *Final refinement*

For final refinement, new spot-shape corrections (see Appendix) were used to give an improved set of F_o's. New techniques of computation had also become available.

An improved set of temperature factors was derived from two-dimensional data as follows. First the magnitudes of all temperature factors were adjusted till the scaling factor was constant and independent of reciprocal-space radius. Then their relative values were altered in a series of $F_o - F_c$ syntheses in the usual way. The two pairs of Ca peaks seemed to need quite different isotropic (mean) temperature factors, though all four peaks appeared to have the same elliptical shape, as judged from the *x*-axis and *y*-axis projections. These projections were used to estimate the lengths and orientations of the principal axes of the thermal ellipsoids (Table 6). The longest axis is roughly in the [110] direction for all four atoms. No three-dimensional refinements of these anisotropic effects has been attempted; more detailed examination of absorption effects would be needed before they can be taken as real.

Re-examination of the second three-dimensional synthesis suggested alterations in the coordinates of some of the O atoms. These lay at positions of moderate slope, but near regions of much steeper slope in the *x*-direction (the direction of slowest refinement). In the first interpretation of this synthesis, the shifts had been calculated from the slopes in the immediate environment of the atoms; the revised shifts were larger. It was noticed that this improved the regularity of *T*–O distances within the same tetrahedron; indeed, in some cases it was irregularities in the bond distances which called attention to the significance of features of the difference map, though irregularities were never by themselves used as criteria for shifting atoms.

These changes, together with the introduction of corrected F_o's, reduced the *R*-factor from 15·2% to 13·5%.

The revised coordinates and temperature factors were used as a starting point for the automatic refinement on Edsac II. The *R*-factor for the reflections actually used (cf. § 2·2) fell after 23 cycles from 12·4% to 10·2%, which probably corresponds to about 11·1% for the total number of observed intensities. The mean atomic shifts during the later cycles are recorded in Table 7(*b*), and the final coordinates in Table 8.

6. Errors

The errors in the coordinates were calculated using Cruickshank's formula (Lipson & Cochran (1953), equation 308·2). The curvature C_n, which appears in this formula, was calculated from the theoretical *f*-curve for the atom in question, modified by the

Table 8. *Final coordinates*

(In fractions of cell edge $\times 10^4$)

Atom	x	y	z	Atom	x	y	z
$O_A(1000)$	0276	1234	9957	$T_1(0000)$	0099	1584	1043
$O_A(1z00)$	9814	1237	4808	$T_1(0z00)$	0069	1609	6125
$O_A(10i0)$	4873	6256	4865	$T_1(00i0)$	5061	6567	6033
$O_A(1zi0)$	5129	6256	9970	$T_1(0zi0)$	4987	6675	1125
$O_A(2000)$	5724	9909	1451	$T_1(m000)$	9928	8146	1190
$O_A(2z00)$	5732	9901	6398	$T_1(mz00)$	0059	8154	6129
$O_A(20i0)$	0732	4876	6330	$T_1(m0i0)$	5078	3154	6212
$O_A(2zi0)$	0755	4925	1363	$T_1(mzi0)$	5034	3207	1091
$O_B(0000)$	8114	1027	0792	$T_2(0000)$	6841	1134	1512
$O_B(0z00)$	8071	0996	6046	$T_2(0z00)$	6818	1029	6644
$O_B(00i0)$	3363	5938	6045	$T_2(00i0)$	1906	6123	6681
$O_B(0zi0)$	2912	6036	0819	$T_2(0zi0)$	1714	6062	1504
$O_B(m000)$	8148	8516	1454	$T_2(m000)$	6749	8828	1881
$O_B(mz00)$	8090	8510	6018	$T_2(mz00)$	6799	8717	6715
$O_B(m0i0)$	2983	3575	6113	$T_2(m0i0)$	1759	3802	6744
$O_B(mzi0)$	3382	3606	1309	$T_2(mzi0)$	1865	3790	1815
$O_C(0000)$	0120	2780	1351				
$O_C(0z00)$	0177	2900	6486				
$O_C(00i0)$	5082	7778	6311				
$O_C(0zi0)$	5102	7969	1500				
$O_C(m000)$	0004	6802	1063	Ca(000)	2647	9844	0873
$O_C(mz00)$	0083	6898	6017	Ca(z00)	2684	0312	5438
$O_C(m0i0)$	5150	1794	6090	Ca(0i0)	7732	5354	5422
$O_C(mzi0)$	5067	1947	0974	Ca(zi0)	7636	5067	0740
$O_D(0000)$	1795	1072	1919				
$O_D(0z00)$	2153	1057	6862				
$O_D(00i0)$	6992	6031	6779				
$O_D(0zi0)$	6921	6014	2000				
$O_D(m000)$	2027	8723	2106				
$O_D(mz00)$	1754	8557	7170				
$O_D(m0i0)$	6861	3637	7335				
$O_D(mzi0)$	6999	3691	1993				

appropriate temperature factor, and by a cut-off in reciprocal space at the same radius as for the summation over the F's. The values of $\sigma(x_n)$ so obtained were: for Ca, 0·0007 Å; for T, 0·0015 Å; for O, 0·0038 Å. The dangers of accepting these values as trustworthy are: (i) that the method is reliable only when refinement is complete, and provides no internal check to show that this is so; (ii) that the curvatures are calculated, not derived empirically from the F_o map, and since they are very sensitive to cut-off radius they could be seriously over-estimated.

It is however possible to check the error estimate by examining the progress of refinement. If it goes smoothly, the atomic shifts should become progressively smaller; and the completion of refinement will be marked by shifts of steady r.m.s. value whose signs tend to reverse as the atoms move at random over the small volume characteristic of the random errors. If refinement is incomplete, it will depend on the program whether the atom approaches its final position steadily from one direction or by bracketing it. In the latter case, the r.m.s. value of the shifts provides an estimate of accuracy which allows for incomplete refinement. It can, however, only be safely used if it is clear that the shifts are reversing in sign; unless this is tested, there is a danger that the program may be providing too slow an advance to the final position to allow extrapolation.

Table 7(b) shows that the shifts of atomic positions are becoming small, but provides no test of their signs. In practice it was easier to examine the changes in T–O bond lengths rather than atomic coordinates. Before considering these changes some preliminary comments on the bond lengths are needed.

It was apparent from an early stage of the structure determination that the tetrahedra fell into two groups of unequal size. Though it was obvious that these must contain different proportions of Si and Al, this fact was never used at any time during the refinement; here, therefore, we shall simply distinguish the groups by the subscripts S (small) and L (large). Table 9 gives the variation of the mean bond length of each group, and their difference, in the final stages of refinement. The steady increase of the difference is very striking, and provides evidence that the refinement is meaningful. It is not safe to assume that all the bonds within a tetrahedron are equal, nor that all tetrahedral means within a group are equal. Nevertheless it is of interest to notice (Table 9) that their r.m.s. deviation from the tetrahedral mean and the group mean respectively drop during refinement until a very late stage, when they level off.

Table 9. *Refinement of T–O bond lengths, in* Å

Cycle	Mean bond length T_S–O	Mean bond length T_L–O	Difference	R.m.s. deviation from tetrahedral mean *S*	R.m.s. deviation from tetrahedral mean *L*	R.m.s. deviation of tetrahedral mean from group mean *S*	R.m.s. deviation of tetrahedral mean from group mean *L*	R.m.s. change of individual bond lengths *S*	R.m.s. change of individual bond lengths *L*
*A*1	1·635	1·720	0·085	0·044	0·062	0·024	0·013		
*B*1	1·626	1·729	0·103	0·036	0·053	0·023	0·016	0·014	0·014
14	1·622	1·739	0·117	0·028	0·046	0·019	0·009	0·021	0·020
21	1·616	1·746	0·130	0·029	0·042	0·009	0·005	0·015	0·016
22	1·615	1·748	0·133	0·030	0·042	0·008	0·005	0·007	0·008
24	1·614	1·749	0·135	0·026	0·036	0·008	0·006	0·0045	0·0041

Table 10. *Changes of bond length with* (1) *same sign,* (2) *opposite sign, in last two steps studied*

		(1)	(2)	Zero changes
No. of changes	*S*	12	17	3
	L	8	20	4
R.m.s. value of changes	*S*	0·0035 Å	0·0059 Å	
	L	0·0025 Å	0·0053 Å	

The r.m.s. changes of the individual bond lengths are recorded in the final column of Table 9; they appear to be approaching a steady low value. This is not by itself sufficient evidence to show that refinement is approaching completion, for the steps between the cycles recorded are not necessarily equal. However, Table 10 shows that the majority of the changes, particularly of the large ones, reverse sign between the last two cycles listed. Hence the atoms are oscillating about final positions; whether or not refinement is complete, the r.m.s. values of the changes estimate the overall error.

We may compare these final bond-length changes, 0·0045 Å and 0·0041 Å, with the error estimated from Cruickshank's formula, 0·0040 Å. The agreement is very satisfactory; even if its closeness is partly fortuitous, it suggests that the order of magnitude of the error estimate is trustworthy.

7. Discussion and summary

The lists of bond lengths and bond angles, and discussion of the structure itself, are left to Paper II.

Two principles have been used in solving the structure: (1) that omission of difference reflections in carrying out a Fourier synthesis is equivalent to averaging over those subcells which contribute to the difference reflections, (2) that the signs of difference reflections can be found by a heavy-atom technique. As a consequence of (1), the elongations of peaks on an F_o-map, or anomalies on a difference map, show the magnitudes of the difference parameters; as a consequence of (2), the difference reflections can be used to find the signs of the difference parameters (which must be opposite in the two subcells), and also, less accurately, to confirm the information about their magnitude. Because anorthite has four subcells, the whole process had to be repeated in two steps, the pairs of subcells that give rise to the stronger set of difference reflections being sorted out in the first step. It is essentially a method of successive approximations, and its progress can be, and has been, checked to make sure that no errors outside the permissible limits remain at any stage.

Since no assumptions about Si/Al distribution in the *T* sites, or about equality of *T*–O bonds within a tetrahedron or between tetrahedral means, have been made at any point in the analysis, the decrease in their r.m.s. deviations (Table 9) as refinement proceeds is independent evidence that no gross errors are being perpetuated. It can be seen, however, that differences within tetrahedra in the final structure are still rather large. The significance of these, and of differences between tetrahedral means and between groups of tetrahedra, will be discussed in Paper II.

We wish to record our thanks to Dr W. H. Taylor for suggesting this problem, and for constant help and encouragement during the work; to Dr P. Gay for advice and help in choosing the material; to Dr Wilkes and Mr Mutch for the facilities of the Mathematical Laboratory; to Mr M. Wells for devising the program for the final refinement; and to very many others who have helped with the computations over a period of years. One of us (C. J. E. K.) is indebted to the Department of Scientific and Industrial Research for a Maintenance Grant, and to the Nuffield Foundation for maintenance during the completion of the work; and one (E. W. R.) to the Commonwealth Scientific and Industrial Research Organisation for an Overseas Studentship.

APPENDIX

Correction for elongation and contraction of spots on higher layers was particularly important because, owing to the restricted range of the Weissenberg camera, many had been recorded on one side of the film only. Elongated and contracted reflections were handled separately. For layers $h=5$ and $h=6$, the ratio $\Sigma F_o/\Sigma F_c$ was evaluated over narrow annuli of reciprocal space, and plotted against the radius, ξ. The elongated reflections fitted the Phillips curves reasonably well; these curves were therefore used for all layers. The contracted reflections showed discrepancies; if they were fitted to the Phillips curves at

large ξ they diverged at small ξ. Hence empirical curves were drawn through the observed points, and from the curves for layers 5 and 6 those for the other layers were deduced. The corrected intensities for elongated and contracted reflections were scaled independently, layer by layer, to the calculated structure factors. When the same reflection occurred in both sets, agreement was good, and mean values were finally used.

References

Albrecht, G. (1939). *Rev. Sci. Instrum.* **10**, 221.

Berghuis, J., Haanappel, IJ. M., Potters, M., Loopstra, B. O., MacGillavry, C. H. & Veenendaal, A. L. (1955). *Acta Cryst.* **8**, 478.

Bragg, W. L. & West, J. (1930). *Phil. Mag.* **10**, 823.

Buerger, M. J. (1956). *Proc. Nat. Acad. Sci. Wash.* **42**, 776.

Cole, W. F., Sørum, H. & Taylor, W. H. (1951). *Acta Cryst.* **4**, 20.

Forsyth, J. B. & Wells, M. (1959). *Acta Cryst.* **12**, 412.

Gay, P. (1953). *Miner. Mag.* **30**, 169.

Jellinek, F. (1958). *Acta Cryst.* **11**, 677.

Lipson, H. & Cochran, W. (1953). *The Determination of Crystal Structures*. London: Bell.

Megaw, H. D. (1956). *Acta Cryst.* **9**, 56.

Megaw, H. D., Kempster, C. J. E. & Radoslovich, E. W. (1962). *Acta Cryst.* **15**, 1017.

Newnham, R. E. & Megaw, H. D. (1960). *Acta Cryst.* **13**, 303.

Phillips, D. C. (1954). *Acta Cryst.* **7**, 746.

Radoslovich, E. W. (1955). Thesis, Cambridge University.

Ramachandran, G. N. & Srinivasan, R. (1959). *Acta Cryst.* **12**, 410.

Sørum, H. (1951). *K. Norske Vidensk. Selsk. Skr.* No. 3. Thesis, Trondheim.

Sørum, H. (1953). *Acta Cryst.* **6**, 413.

Taylor, W. H. (1933). *Z. Kristallogr.* **85**, 425.

Taylor, W. H., Darbyshire, J. A. & Strunz, H. (1934). *Z. Kristallogr.* **87**, 464.

Wells, M. (1961). Thesis, Cambridge University.

Wilson, A. J. C. (1949). *Acta Cryst.* **2**, 318.

Printed in Denmark at Fr. Bagges kgl. Hofbogtrykkeri, Copenhagen

COMMONWEALTH OF AUSTRALIA
COMMONWEALTH SCIENTIFIC AND INDUSTRIAL RESEARCH ORGANIZATION

Reprinted from *Acta Crystallographica*, Vol. 15, Part 10, October 1962
PRINTED IN DENMARK

Acta Cryst. (1962). **15**, 1017

The Structure of Anorthite, $CaAl_2Si_2O_8$. II. Description and Discussion

BY HELEN D. MEGAW, C. J. E. KEMPSTER* AND E. W. RADOSLOVICH†
Crystallographic Laboratory, Cavendish Laboratory, Cambridge, England

(*Received* 5 *October* 1961 *and in revised form* 21 *November* 1961)

Anorthite has a felspar structure with the following particular features: (1) Si and Al tetrahedra alternate, so that each O atom has one Si and one Al neighbour; there is no Si/Al disorder. (2) Si–O and Al–O bond lengths show real variations within the same tetrahedron, the average value of each increasing as the number of Ca neighbours of the O atom increases from zero to 2. (3) There are 4 independent Ca atoms, 6- or 7-coordinated: pairs related (topologically, not exactly) by the *C*-face-centring translation have very similar environments, while those related by body-centring or by *z*-axis halving are very markedly different. There is no disorder of Ca position. (4) If the tetrahedra are grouped into the two topologically different types (distinguished conventionally by the subscripts 1 and 2 for their tetrahedral atoms) all tetrahedra of the same type have qualitatively similar bond-angle strains (i.e. departures from the tetrahedral angle of 109° 28′), independent of their Si/Al content. Comparison with other felspars shows that the strains are characteristic of the felspar structure, but are nearly twice as great in the felspars with divalent cations as in those with monovalent cations. (5) Most of the bond angles at O are in the range 125–145°, but there are some exceptionally large angles of about 165–170°.

These facts are explained by a model in which the building elements are nearest-neighbour bonds and bond angles, endowed with elastic moduli, acted on by the only unshielded cation–cation electrostatic repulsion, namely that acting across the centre of symmetry. The bond-angle strains at Si and Al are qualitatively predicted by it, and agree with observation. Most of the distortions of the felspar structure are common (qualitatively) to all felspars, depending on cation charge; others depend on cation size. In contrast to these, the effects of Si/Al distribution are relatively so small that discussion of them cannot usefully begin until the other larger effects have been clarified.

1. Introduction

Anorthite, $CaAl_2Si_2O_8$, is an important member of the felspar family. Other members of the family, whose structures have been determined in detail, and to which reference will be made here, are listed in Table 1. It was hoped that detailed comparison of the differences between members of the family would help our understanding not only of the felspars as a whole but also of the general character of three-dimensionally-linked framework structures. This has proved to be the case, as will be shown in what follows.

The method by which the structure was determined was described in Paper I (Kempster, Megaw &

* Present address: Department of Physics, University of Adelaide, Adelaide, Australia.
† Present address: Division of Soils, Commonwealth Scientific and Industrial Research Organisation, Adelaide, Australia.

Table 1

Composition	Name	Source	Reference
$KAlSi_3O_8$	Sanidine	Mogok, Burma (Spencer C), heat-treated	Cole, Sørum & Kennard (1949)
	Orthoclase	Mogok, Burma (Spencer C)	Jones & Taylor (1961)
	Microcline (intermediate)*	Kodarma, India (Spencer U)	Bailey & Taylor (1955)
$NaAlSi_3O_8$	Low albite	Ramona, California (Emmons 29)	Ferguson, Traill & Taylor (1958)
	Quenched high albite	Amelia Co., Virginia (Emmons 31) heat-treated	Ferguson, Traill & Taylor (1958)
$CaAl_2Si_2O_8$	Anorthite ('low anorthite', 'primitive anorthite')	Monte Somma, Italy (B.M. 30744)	Kempster (1957) and this paper
$BaAl_2Si_2O_8$	Celsian	Broken Hill, New South Wales (Segnit, 1946)	Newnham & Megaw (1960)

* A preliminary report on the structure of maximum microcline by B. E. Brown and S. W. Bailey appeared in the program of a joint meeting of the Geological and Mineralogical Societies of America in November 1961. All references in the present paper are to intermediate microcline.

Radoslovich, 1962), which includes a table of atomic coordinates and their standard deviations. No attempt was made, during that analysis, to distinguish between Si and Al atoms, which were both given the symbol T' ('tetrahedral atom').

The space group is $P\bar{1}$; the unit cell is primitive,

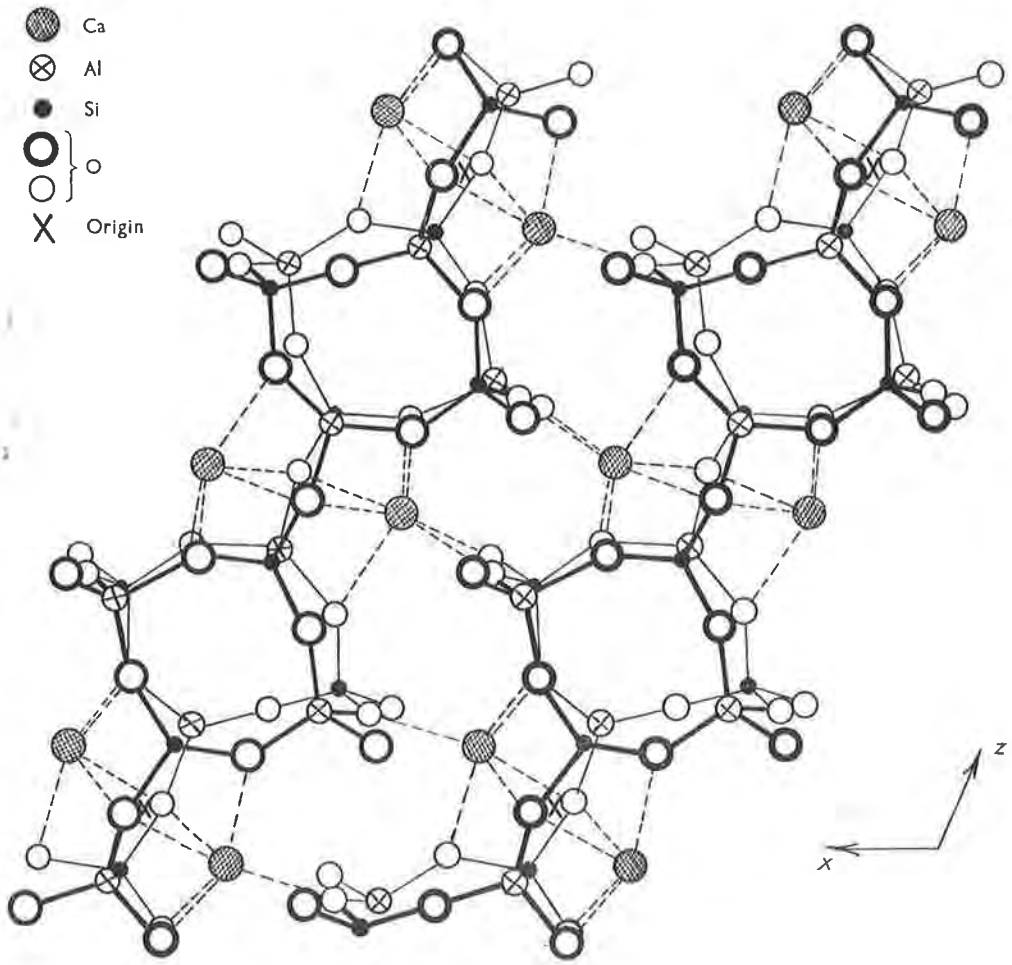

Fig. 1(*a*)

Fig. 1. Projection down [010] of parts of structure bounded roughly by the following planes: (*a*) $y = \pm 0{\cdot}3$; (*b*) $y = 0{\cdot}2, 0{\cdot}8$; (*c*) $y = 0{\cdot}1, 0{\cdot}4$. Heavy lines indicate upper part of layer shown. The projection of the corners of the unit cell (origin of coordinates) are marked with crosses in all diagrams. (*Note.* This is an *inclined* projection down [010] on (010). The drawing differs very little from an *orthogonal* projection on the plane normal to [010], but in the latter case the axes x and z would stick slightly out of the paper.)

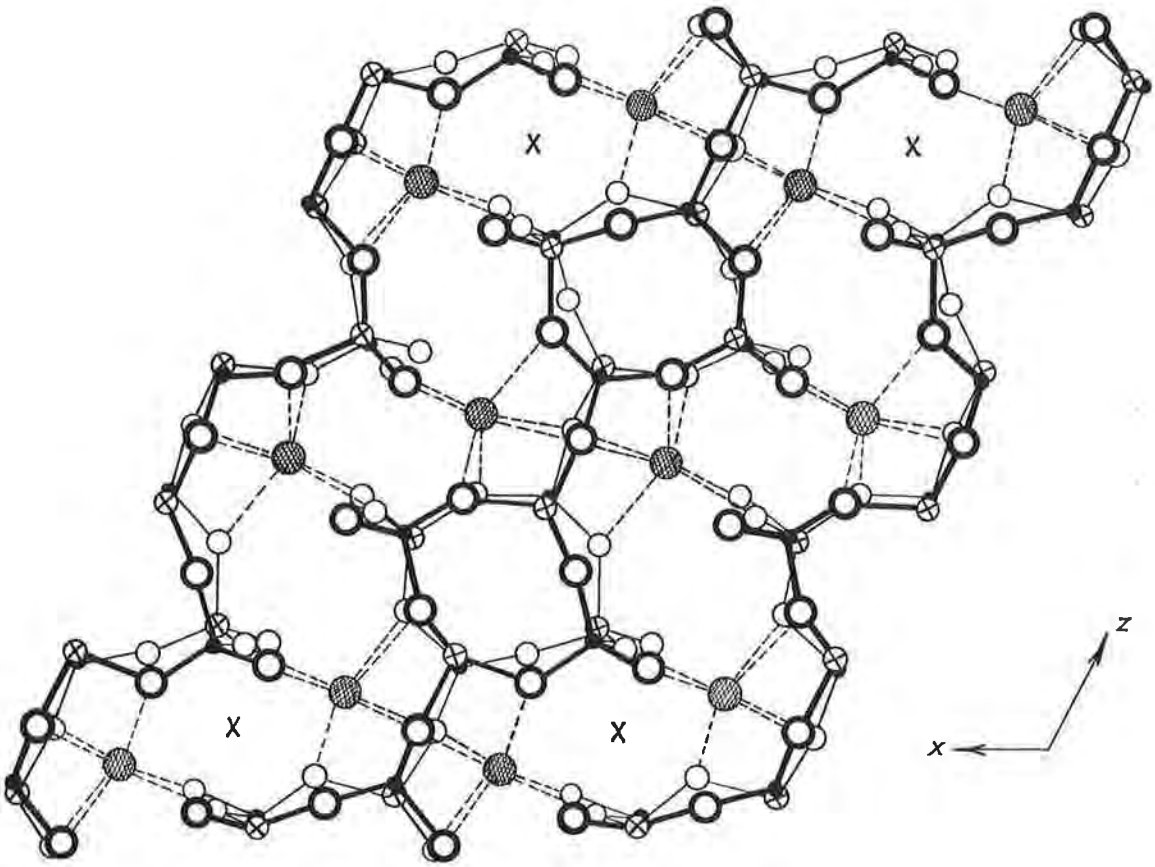
X
X
X
X
z
x

Fig. 1(*b*)

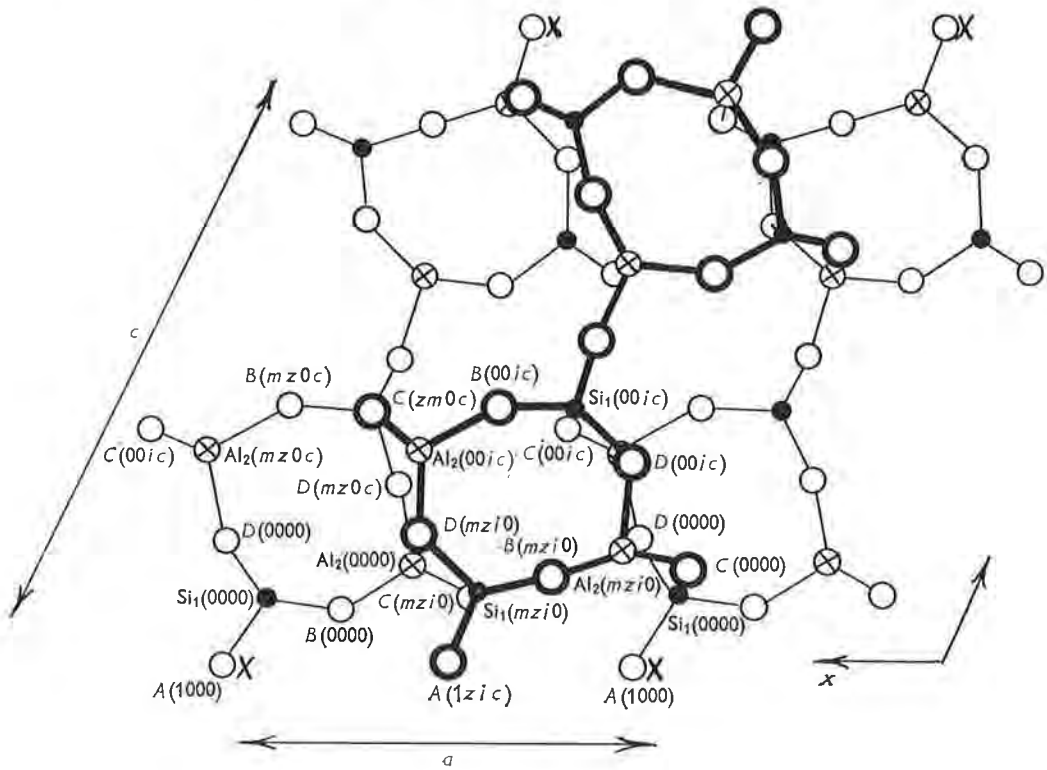
X
X
c
B(mz0c)
B(00ic)
C(zm0c)
Si1(00ic)
C(00ic)
Al2(mz0c)
Al2(00ic)
C(00ic)
D(00ic)
D(mz0c)
D(0000)
D(mzi0)
D(0000)
B(mzi0)
Al2(0000)
C(0000)
Al2(mzi0)
Si1(0000)
C(mzi0)
Si1(mzi0)
Si1(0000)
B(0000)
X
X
A(1000)
A(1zic)
A(1000)
x
a

Fig. 1(*c*)

with dimensions approximately $8 \times 13 \times 14$ Å, which means that the volume per lattice point is four times that of typical felspars such as albite. Thus the true cell consists of four subcells, equal in volume and with closely similar but not identical contents. Each subcell contains two formula units (CaT_4O_8) related by a centre of symmetry; but, relative to an origin at the corner of the subcell, corresponding atoms in the four subcells have slightly different coordinates.

It can be seen that atomic positions in subcells related by the base-centring vector (*zi*) are more closely similar than those related by the body-centring vector (0*i*) or the *c*-axis halving (*z*0).

Bond lengths and bond angles are given in Table 2,

Table 2. *Bond lengths and angles*

(*a*) Ca–O bonds in Å

Ca(000)		Ca(*zi*0)		Ca(*z*0*c*)		Ca(0*ic*)	
O_A(1000)	2·618	O_A(1*zi*0)	2·471	O_A(1*z*0*c*)	2·476	O_A(10*ic*)	2·459
O_A(100*c*)	2·500	O_A(1*zic*)	2·586	O_A(1*z*00)	2·720	O_A(10*i*0)	2·822
O_A(2000)	2·279	O_A(2*zi*0)	2·322	O_A(2*z*0*c*)	2·350	O_A(20*ic*)	2·335
O_A(2*z*0*c*)	3·491	O_A(20*ic*)	3·762	O_A(2000)	> 4	O_A(2*zi*0)	> 4
O_A(200*c*)	> 4	O_A(2*zic*)	3·746	O_A(2*z*00)	3·375	O_A(20*i*0)	3·237
O_B(0000)	3·995		> 4		> 4		> 4
O_B(000*c*)	2·368	O_B(0*zic*)	2·421	O_B(0*z*00)	2·464	O_B(00*i*0)	2·413
O_B(*m*00*c*)	3·836	O_B(*mzic*)	3·247	O_B(*mz*00)	2·491	O_B(*m*0*i*0)	2·496
O_C(0*zi*0)	3·088	O_C(0000)	3·543	O_C(00*ic*)	3·824	O_C(0*z*0*c*)	3·798
O_C(*mzi*0)	3·279	O_C(*m*000)	2·807	O_C(*m*0*ic*)	2·565	O_C(*mz*0*c*)	2·568
O_D(0000)	2·423	O_D(0*zi*0)	2·391	O_D(0*z*0*c*)	2·397	O_D(00*ic*)	2·382
O_D(*m*000)	2·532	O_D(*mzi*0)	2·771	O_D(*mz*0*c*)	3·725	O_D(*m*0*ic*)	3·876
Mean	2·544	Mean	2·538	Mean	2·495	Mean	2·496

(*b*) Individual *T*–O bonds, in Å

Key no. of tetrahedron	Atoms		Length	Key no. of tetrahedron	Atoms		Length
	T	O			*T*	O	
1.	T_1(0000)	O_A(1000)	1·647	9.	T_1(0*z*00)	O_A(1*z*00)	1·820
		O_B(0000)	1·641			O_B(0*z*00)	1·755
		O_C(0000)	1·575			O_C(0*z*00)	1·701
		O_D(0000)	1·589			O_D(0*z*00)	1·755
2.	T_1(00*i*0)	O_A(10*i*0)	1·620	10.	T_1(0*zi*0)	O_A(1*zi*0)	1·747
		O_B(00*i*0)	1·599			O_B(0*zi*0)	1·733
		O_C(00*i*0)	1·585			O_C(0*zi*0)	1·708
		O_D(00*i*0)	1·661			O_D(0*zi*0)	1·796
3.	T_1(*mz*0*c*)	O_A(1*z*00)	1·618	11.	T_1(*m*00*c*)	O_A(1000)	1·794
		O_B(*mz*0*c*)	1·626			O_B(*m*00*c*)	1·723
		O_C(*mz*0*c*)	1·617			O_C(*m*00*c*)	1·735
		O_D(*mz*0*c*)	1·571			O_D(*m*00*c*)	1·754
4.	T_1(*mzic*)	O_A(1*zi*0)	1·643	12.	T_1(*m*0*ic*)	O_A(10*i*0)	1·757
		O_B(*mzic*)	1·600			O_B(*m*0*ic*)	1·757
		O_C(*mzic*)	1·623			O_C(*m*0*ic*)	1·755
		O_D(*mzic*)	1·637			O_D(*m*0*ic*)	1·695
5.	T_2(0*z*00)	O_A(2*z*00)	1·624	13.	T_2(0000)	O_A(2000)	1·784
		O_B(0*z*00)	1·589			O_B(0000)	1·749
		O_C(*m*0*i*0)	1·629			O_C(*mzi*0)	1·723
		O_D(*m*00*c*)	1·611			O_D(*mz*0*c*)	1·730
6.	T_2(0*zi*0)	O_A(2*zi*0)	1·606	14.	T_2(00*i*0)	O_A(20*i*0)	1·782
		O_B(0*zi*0)	1·652			O_B(00*i*0)	1·792
		O_C(*m*000)	1·617			O_C(*mz*00)	1·745
		O_D(*m*0*ic*)	1·566			O_D(*mzic*)	1·692
7.	T_2(*m*00*c*)	O_A(200*c*)	1·646	15.	T_2(*mz*0*c*)	O_A(2*z*0*c*)	1·754
		O_B(*m*00*c*)	1·559			O_B(*mz*0*c*)	1·747
		O_C(0*zic*)	1·601			O_C(00*ic*)	1·706
		O_D(0*z*00)	1·603			O_D(0000)	1·769
8.	T_2(*m*0*ic*)	O_A(20*ic*)	1·634	16.	T_2(*mzic*)	O_A(2*zic*)	1·738
		O_B(*m*0*ic*)	1·628			O_B(*mzic*)	1·696
		O_C(0*z*0*c*)	1·622			O_C(000*c*)	1·780
		O_D(0*zi*0)	1·629			O_D(00*i*0)	1·792

Table 2 (*cont.*)

(*c*) T–O bonds, tetrahedral means and r.m.s. deviations, in Å

Key no.	Atom	r_t	$\varepsilon(r)$	$\lvert r_t$-group mean$\rvert$	Key no.	Atom	r_t	$\varepsilon(r)$	$\lvert r_t$-group mean$\rvert$
1.	$T_1(0000)$	1·613	0·031	0·001	9.	$T_1(0z00)$	1·758	0·034	0·009
2.	$T_1(00i0)$	1·616	0·029	0·002	10.	$T_1(0zi0)$	1·746	0·032	0·003
3.	$T_1(mz0c)$	1·608	0·022	0·006	11.	$T_1(m00c)$	1·752	0·027	0·003
4.	$T_1(mzic)$	1·626	0·017	0·012	12.	$T_1(m0ic)$	1·741	0·027	0·008
5.	$T_2(0z00)$	1·613	0·015	0·001	13.	$T_2(0000)$	1·746	0·024	0·003
6.	$T_2(0zi0)$	1·610	0·031	0·004	14.	$T_2(00i0)$	1·753	0·039	0·004
7.	$T_2(m00c)$	1·602	0·031	0·012	15.	$T_2(mz0c)$	1·744	0·023	0·005
8.	$T_2(m0ic)$	1·628	0·004	0·014	16.	$T_2(mzic)$	1·752	0·038	0·003
	Mean	1·614				Mean	1·749		
	R.m.s. value		0·024	0·008		R.m.s. value		0·031	0·005

(*d*) O–O distances in tetrahedron edges, in Å

Key no. of tetrahedron	O_A–O_B	O_A–O_C	O_A–O_D	O_B–O_C	O_B–O_D	O_C–O_D
1.	2·537	2·770	2·525	2·631	2·721	2·593
2.	2·518	2·702	2·540	2·651	2·680	2·711
3.	2·486	2·744	2·556	2·666	2·713	2·577
4.	2·598	2·709	2·564	2·696	2·678	2·669
5.	2·586	2·519	2·655	2·644	2·659	2·723
6.	2·636	2·520	2·639	2·743	2·550	2·678
7.	2·700	2·549	2·660	2·603	2·535	2·648
8.	2·618	2·613	2·651	2·706	2·663	2·697
9.	2·725	3·020	2·724	2·842	3·016	2·842
10.	2·594	3·013	2·638	2·893	2·962	2·914
11.	2·839	2·946	2·705	2·867	2·892	2·886
12.	2·679	2·914	2·819	2·935	2·871	2·818
13.	2·895	2·752	2·803	2·886	2·862	2·897
14.	2·712	2·690	2·831	2·962	2·936	2·944
15.	2·857	2·759	2·753	2·819	2·903	2·974
16.	2·791	2·797	2·840	2·876	2·870	2·980

(*e*) Other short O–O distances and Ca–Ca distances, in Å

Atoms	Length	Comment
$O_B(0z00)$–$O_B(mz00)$	3·200	Ca($z0c$) polyhedron edge
$O_B(00i0)$–$O_B(m0i0)$	3·063	Ca($0ic$) polyhedron edge
$O_B(mz00)$–$O_C(m0ic)$	3·003	Ca($z0c$) polyhedron edge
$O_B(m0i0)$–$O_C(mz0c)$	2·983	Ca($0ic$) polyhedron edge
$O_C(0zi0)$–$O_D(m000)$	3·146	Ca(000) polyhedron edge
$O_D(0000)$–$O_D(m000)$	3·054	Ca(000) polyhedron edge
$O_D(0zi0)$–$O_D(mzi0)$	2·993	Ca($zi0$) polyhedron edge
$O_A(1000)$–$O_A(100c)$	3·217	Shared edges across centres of symmetry
$O_A(1zi0)$–$O_A(1zic)$	3·245	
$O_A(1z00)$–$O_A(1z0c)$	3·260	
$O_A(10i0)$–$O_A(10ic)$	3·278	
Ca(000)–Ca($00c$)	3·983	Short cation–cation distances across centres of symmetry
Ca($zi0$)–Ca(zic)	3·880	
Ca($z00$)–Ca($z0c$)	4·055	
Ca($0i0$)–Ca($0ic$)	4·160	

using the notation of Megaw (1956). Their standard deviations, calculated from the standard deviations of the coordinates, $\sigma(x_n)$ (see Paper I, § 6), are as follows: Ca–O, 0·0039; T–O, 0·0041; O–O, 0·0053 Å; angle at T, 0·4°; angle at O, 0·6°. Projections of the structure are shown in Fig. 1.

Preliminary results, and conclusions about the Si/Al arrangement, have already been reported (Kempster, Megaw & Radoslovich, 1960).

2. Description of structure

2·1. T–O *bond lengths, and* Al/Si *distribution*

It was mentioned in Paper I that the T–O tetrahedra divided themselves into two groups, the difference between which became more marked as refinement progressed. It is obvious from inspection of Table 2(*b*) (and is confirmed below) that the difference is significant, and therefore the small and large tetrahedra

Table 2 (*cont.*)

(*f*) Bond angles at T, in degrees

Key no. of tetrahedron	Atom	Edge subtending angle at T					
		O_A–O_B	O_A–O_C	O_A–O_D	O_B–O_C	O_B–O_D	O_C–O_D
1.	$T_1(000)$	101·0	118·6	102·6	109·8	114·7	110·1
2.	$T_1(00i)$	102·9	115·0	101·4	112·7	110·6	113·3
3.	$T_1(mz0)$	100·0	116·0	106·5	110·5	116·1	107·9
4.	$T_1(mzi)$	106·4	112·1	102·8	113·5	111·7	109·8
5.	$T_2(0z0)$	107·2	101·5	110·3	110·5	112·4	114·3
6.	$T_2(0zi)$	108·0	102·9	112·6	114·1	104·8	114·6
7.	$T_2(m00)$	114·8	103·4	109·9	110·8	106·6	111·4
8.	$T_2(m0i)$	106·8	106·7	108·7	112·8	109·7	112·1
9.	$T_1(0z0)$	99·3	118·1	99·2	110·7	118·5	110·7
10.	$T_1(0zi)$	96·4	121·3	96·3	114·4	114·1	112·4
11.	$T_1(m00)$	107·6	113·2	99·3	112·0	112·5	111·6
12.	$T_1(m0i)$	99·3	112·2	109·5	113·4	112·6	109·6
13.	$T_2(000)$	110·0	103·3	105·8	112·5	110·7	114·1
14.	$T_2(00i)$	98·7	99·4	109·1	113·8	114·8	117·8
15.	$T_2(mz0)$	109·4	105·7	102·7	109·4	111·3	117·7
16.	$T_2(mzi)$	108·7	105·3	107·1	111·6	110·7	113·2

(*g*) Bond angles at O, in degrees

	O_A		O_B	O_C	O_D
1000	136·2	0000	129·4	132·8	137·8
10*i*0	140·0	00*i*0	135·9	130·8	124·6
1*z*00	135·3	0*z*00	139·6	131·2	125·2
1*zi*0	136·1	0*zi*0	128·3	130·8	132·6
2000	125·3	*m*000	170·8	130·5	140·3
20*i*0	122·5	*m*0*i*0	145·3	130·9	166·9
2*z*00	124·0	*mz*00	143·5	127·5	161·4
2*zi*0	125·9	*mzi*0	163·6	130·5	138·5

must be identified as Si-rich and Al-rich respectively. Small and large tetrahedra alternate in every direction, so that each O atom is shared by one small and one large one. Since no assumptions about the nature of the T atom were made at any stage in deriving this result, it constitutes a direct proof of the 'aluminium avoidance rule' put forward earlier (Loewenstein, 1954; Goldsmith & Laves, 1955).

The significance of bond-length differences can be examined by Cruickshank's (1949) test, based on the ratio $\delta l/\sigma$, where δl is the difference of the two quantities to be compared, σ_1 and σ_2 are their standard deviations, and $\sigma^2=\sigma_1^2+\sigma_2^2$. The mean bond lengths and deviations from the mean are recorded in Table 2(*c*).

We first notice that $\varepsilon(r)$, the r.m.s. deviation of a bond from the tetrahedral mean, is much greater than $\sigma(r)$, the standard deviation derived from $\sigma(x_n)$. The significance of this is demonstrated in Table 3 (1). It shows that the differences of bond length within a tetrahedron, though not very large, are real. At this stage we merely note their existance, without trying to discover their physical meaning.

Because of this effect, differences *between* tetrahedra cannot be regarded as real unless they are significantly greater than the average differences *within* tetrahedra. Thus significance tests for tetrahedral means must be based on comparisons of differences with $\varepsilon(r)$ rather than with $\sigma(r)$.

It is next necessary to consider whether the mean radii of tetrahedra in the same group differ significantly from one another. From Table 3 (2) it can be seen that the differences are not significant. If the test had been carried out using $\sigma(r)$ in place of $\varepsilon(r)$, the ratios would have been 7 and 4 respectively, indicating high significance. Thus we can say that, while the differences between tetrahedral means are real, they are only of the order of magnitude of differences within tetrahedra, and therefore cannot be used as evidence for different Si/Al ratios in the atoms occupying them.

By contrast, we may apply the same test, using $\varepsilon(r)$, to the difference between the group means (Table 3 (3)). This difference is seen to be highly significant.

We now use the results of Smith (1954) to examine the Si/Al ratios corresponding to the group mean bond lengths. Smith's values are $1{\cdot}60\pm0{\cdot}01$ Å for Si–O, $1{\cdot}78\pm0{\cdot}02$ Å for Al–O, and it would be reasonable to assume, for statistical study, that his estimated errors are about twice the standard deviation. However, Smith (1960) expresses doubt about the constancy of the bond lengths within these limits in all circumstances. To make some allowance for this we use the estimated errors as if they were s.d.'s

Table 3. *Significance of bond-length differences*

Key to symbols:

r_t = tetrahedral mean bond length
r_g = group mean bond length
r_{Sm} = Smith's empirical bond length
$\varepsilon(r)$ = r.m.s. deviation of single bond length
$\sigma(r)$ = s.d. of single bond length calculated from $\sigma(x_n)$
$\Delta(r)$ = Smith's estimated limit of error

	Quantities compared	σ	δl	Set of tetrahedra	Numerator	Denominator	Cruickshank ratio	Significance*
(1)	Single bond	$\sigma(r)$	$\varepsilon(r)$	(i) Small	0·024 Å	0·0044 Å	5·5	High
	Tetrahedral mean	$\sigma(r)/2$		(ii) Large	0·031	0·0044	7	High
(2)	Tetrahedral mean	$\varepsilon(r)/2$	$\lvert(r_g-r_t)_{\max.}\rvert$	(i) Small	0·014	0·013	1·1	Zero
	Group mean	$\varepsilon(r)/2\sqrt{8}$		(ii) Large	0·009	0·016	0·6	Zero
(3)	Group mean, small	$\varepsilon_{Si}(r)/2\sqrt{8}$	$\lvert(r_g)_{Si}-(r_g)_{Al}\rvert$	All	0·035	0·007	5	High
	Group mean, large	$\varepsilon_{Al}(r)/2\sqrt{8}$						
(4)	Smith's bond length	$\Delta(r)$	$\lvert r_g-r_{Sm}\rvert$	(i) Small	0·014	0·011	1·3	Zero
	Group mean	$\varepsilon(r)/2\sqrt{8}$		(ii) Large	0·031	0·041	1·5	Zero

* Significance levels are those suggested by Cruickshank (1949): 'high' and 'zero' correspond to probabilities of accidental occurrence of $<0{\cdot}1\%$ and $>5\%$ respectively, or $\delta l/\sigma > 3{\cdot}1$ and $<1{\cdot}65$.

Then from Table 3 (4) it can be seen that the differences of the group means from Smith's values for pure Si and pure Al are not significant. It is true, of course, that no significance test is more objective or carries more weight than the postulates on which it is based; however, it is certainly clear that there is no evidence from which we can reliably deduce any departure from perfect Si/Al order.

It is perhaps worth noting that, from Smith's values, one would deduce the presence of 8% Al in the Si-rich sites, 17% Si in the Al-rich sites. In view of the particular difficulty experienced by Smith in fixing the Al end of his scale, the latter estimate is quite unreliable.

It is interesting that in both forms of $BaAl_2Si_2O_8$, the felspar celsian (Newnham & Megaw, 1960) and the non-felspar paracelsian (Bakakin & Belov, 1960), there is also a high degree of Si/Al order, and no certain evidence that order is less than perfect (though neither structure is so far refined as anorthite). In celsian, the pattern of Si-rich and Al-rich sites is the same as in anorthite.

Inspection of Table 2(*c*) suggests that the tetrahedral means in anorthite differ *less* from the group mean than would be expected from their variations within a tetrahedron if the tetrahedra provided random samples. This may be tested by comparing the two estimates of the standard deviation of the group mean, namely [r.m.s. value of $\varepsilon(r)$]/$\sqrt{(32)}$ and (r.m.s. value of (r_t - group mean)]/$\sqrt{8}$. From Table 2(*c*) these are $0{\cdot}0043 \pm 0{\cdot}0006$ Å, $0{\cdot}0029 \pm 0{\cdot}0007$ Å respectively for Si–O; $0{\cdot}0055 \pm 0{\cdot}00035$ Å, $0{\cdot}0018 \pm 0{\cdot}00029$ Å respectively for Al–O. The Cruickshank ratios are therefore 1·6 for Si–O, 8 for Al–O, indicating doubtful significance for the former, high significance for the latter. Non-randomness could be caused by the pseudo-symmetry discussed later (§ 3·3), but its more conspicuous manifestation for Al–O is rather striking: it suggests that the *volume* occupied by an Al atom is more nearly constant than would be expected if it were controlled purely by the direct Al–O contacts.

The largest Si-rich tetrahedral mean in anorthite, 1·628 Å, is not far from the $Si_2(m)$–O tetrahedral mean in reedmergnerite, $NaBSi_3O_8$, (Clark & Appleman, 1960) which has the value 1·623 Å. In reedmergnerite (which has the felspar structure) there is no possibility of attributing the large value to Al substitution. This supports the conclusion previously reached that it is unsafe to do so in anorthite.

The results of this section may be summed up by saying that the structure contains a regular alternation of Si and Al tetrahedra, such that any O atom has one Si neighbour and one Al; that the ordering of Si and Al is perfect, within the limits of experimental error (which suggest that disorder is in any case less than 10%); that the individual bond lengths within tetrahedra vary slightly, but that the tetrahedral means are rather more uniform than would have been expected if the individual variations were wholly random.

2·2. *Environment of* Ca

Since there are four different subcells, there are four differently situated Ca atoms. The Ca–O distances are listed in Table 2(*a*), the seven shortest for each Ca on the left-hand side of the column, other distances of less than 4 Å on the right. The distances on the left-hand side include all up to 3·1 Å, and the O atoms concerned may be counted as neighbours; each Ca is then 7-coordinated. One of these distances, however, —the O_C bond of Ca(000)—is so much longer that any of the others that it might have more meaning physically to count it as a non-bonding contact, and take this Ca as 6-coordinated. No arguments depend critically on which choice is made; indeed with irregularly coordinated atoms like Ca there is not much significance attached to any such choice.

All other bonds are within the usual range for Ca–O, except that from Ca(000) to $O_A(2)$, which is exceptionally short. Bonds from cation to $O_A(2)$ tend to be

short in most felspars, and in anorthite the $O_A(2)$ bonds of the other three Ca's are also short.

It can be seen that the configurations round Ca($z0c$) and Ca($0ic$) resemble one another very closely; Ca(000) and Ca($zi0$), though not quite so much alike, nevertheless resemble each other much more than they do the other Ca's.

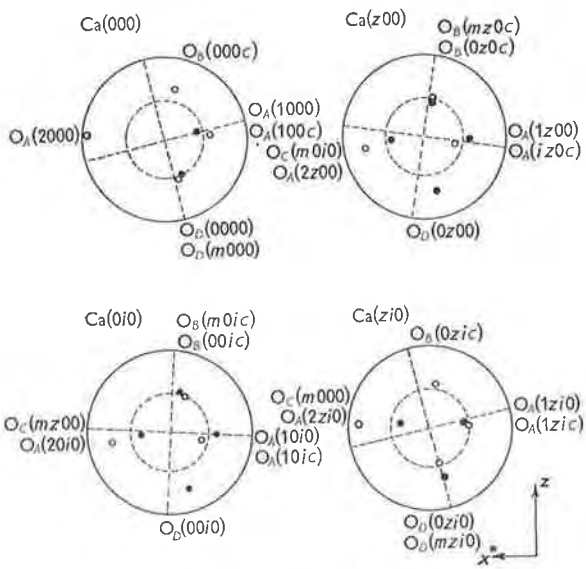

Fig. 2. Stereograms of environment of the four Ca atoms. Intersections of the small circles and diameters shown with dashed lines are at the corners of a regular cube. Where the symbols of two atoms are written together the upper symbol refers to the atom in the upper hemisphere.

Stereograms showing the directions of the Ca–O bonds are given in Fig. 2. (Note that the groups related by subscript c are related by a true centre of symmetry; it is more convenient here to consider Ca(z00) and Ca(0i0) than the equivalent (Ca($z0c$) and Ca($0ic$)). The general resemblance of the coordination to a distorted cube with one corner missing (or two corners for Ca(000), if this is taken as 6-coordinated) can be seen. In more detail, one may note that four bonds (to two $O_A(1)$ and two O_B *or* two O_D atoms) approximate rather closely to cube-corner directions, the bond to $O_A(2)$ lies roughly along the bisector of the angle between the two $O_A(1)$ bonds, and the other toms fait in as best they can. It is as if the steric necessity to fit the $O_A(2)$ atom in this direction, at a rather short distance, upset the regular angular arrangement of the neighbouring O's.

It is often said that the large cations in a felspar are situated in a 'cavity' in the Si/Al–O framework. This suggests that they are perhaps rather loosely held in place, or that there may be more than one possible position for them. It is true that there is a large cavity enclosed by 10 oxygen atoms, but in anorthite the corrugations of its walls are such as to grip each Ca atom tightly. This central interstice has two essentially different shapes, one bounded by two O_B's and one O_D, one by one O_B and two O_D's. If the coordinates of Ca in one such interstice are altered by $z=\frac{1}{2}$, it will not fit into the other interstice; one of the distances to O_B or O_D is impossibly short. The same is true of any other such interchanges (cf. Table 4).

The isotropic B value of about 1·0 Å^2 is comparable with that found for the cation in other felspars; the accuracy with which it or its anisotropy is determined is not great enough to draw elaborate conclusions. It is certainly larger than for the other atoms. Whether it represents a true thermal vibration of r.m.s. amplitude about 0·1 Å, or a random distribution of Ca atoms within about 0·1 Å of a mean position (which might result from 'frozen-in' thermal amplitudes), cannot be decided on present evidence. Outside these limits, there is no evidence for Ca disorder, and any displacement of Ca would need corresponding changes in the shape of the framework to make room for it.

Table 4. *Bond lengths (in* Å*) with* Ca *placed at 'right' and 'wrong' sites in subcell*

(A 'wrong' site is one derived by adding $\frac{1}{2}$ to all the coordinates of a Ca atom whose symbol differs by i from that of the right atom for the subcell)

	Subcell 00		Subcell $z0$		Subcell $0i$		Subcell zi	
Neighbours	Right Ca(00)	Wrong Ca($0i$)	Right Ca($z0$)	Wrong Ca(zi)	Right Ca($0i$)	Wrong Ca(00)	Right Ca(zi)	Wrong Ca($z0$)
$O_A(1)$	2·62	*2·19*	2·48	2·65	2·46	2·85	2·47	*2·30*
$O_A(1)$	2·50		2·72	2·41	2·82	*2·28*	2·59	2·87
$O_A(2)$	2·28	2·34	2·35	2·31	2·34	2·31	2·32	2·35
O_B	2·37	*2·27*	2·46	2·63	2·41	2·60	2·42	*2·30*
O_B		2·92	2·49		2·50			2·72
O_C	(3·09)	2·61	2·57	2·87	2·57		2·81	2·50
O_C								
O_D	2·42	2·68	2·40	*2·16*	2·38	*2·17*	2·39	2·67
O_D	2·53					2·93	2·77	

(Ca–O bond lengths of 2·30 Å and less are regarded as too short to be stable unless in exceptional cases, e.g. the bond to $O_A(2)$ which is abnormally short in most felspars. Unsatisfactory values are shown in italics.)

Table 5. *Electrostatic valence*

	O atoms in group	No. of Ca neighbours	Electrostatic valence
Group 1	$O_A(100)$, $O_A(10i)$, $O_A(1z0)$, $O_A(1zi)$ (4 altogether)	2	2·32
Group 2	$O_A(200)$, $O_A(20i)$, $O_A(2z0)$, $O_A(2zi)$, $O_B(000)$, $O_B(00i)$, $O_B(0z0)$, $O_B(0zi)$, $O_B(m0i)$, $O_B(mz0)$, $O_C(0zi)$, $O_C(m00)$, $O_C(m0i)$, $O_C(mz0)$, $O_D(000)$, $O_D(00i)$, $O_D(0z0)$, $O_D(0zi)$, $O_D(m00)$, $O_D(mzi)$ (20 altogether)	1	2·04
Group 3	$O_B(m00)$, $O_B(mzi)$, $O_C(000)$, $O_C(00i)$, $O_C(0z0)$, $O_C(mzi)$, $O_D(m0i)$, $O_D(mz0)$ (8 altogether)	0	1·75

Table 6. *Bond angles at oxygen in various felspars*

Angles are given in degrees, rounded off to the nearest degree
Where independent values are taken together in a group, the extreme values are recorded, and also (in brackets) the mean of the group

	Microcline	Low albite	High albite	Orthoclase	Celsian	Anorthite
$O_A(1)$	144	142	144	144	139	(137) 135–140
$O_A(2)$	140	131	133	139	135	(124) 122–126
O_B	(153) 152–155	(150) 140–160	(149) 142–155	153	(150) 150	(144) 128–171
O_C	(131) 130–132	(130) 125–135	(131) 128–134	131	(129) 127–130	(131) 128–133
O_D	(142) 140–144	(141) 134–147	(140) 136–144	142	(139) 138–139	(141) 125–167

2·3. O–O *distances, and bond angles at* Si *and* Al

These are recorded in Table 2(*d*), (*e*), and (*f*). Since the standard error in the determination of bond angle is about 0·5°, the difference of the angles from the tetrahedral value are real; their structural significance will be left for discussion in § 3·3.

2·4. *Environment of* O *atoms, and bond angles at* O

Each O atom has one Si neighbour and one Al; the angle between these two bonds is recorded in Table 2(*g*). In addition, many of the O's have Ca neighbours: each $O_A(1)$ has two, as in other felspars, and most other O's have one, but certain O's have none within what are regarded as effective bonding distances. Table 5 shows the symbols of the atoms in each group, and their electrostatic valence. (Here Ca(000) is counted as 7-coordinated; the effect of counting it as 6-coordinated would be to transfer $O_C(0zi)$ from group 2 to group 3, with negligible effect on any of the arguments for which this classification is later used).

The bond angles at O resemble in a general way those in other felspars (Table 6), but on the whole show a larger spread of values. They are of the order of magnitude of those found in other silicates (cf. Liebau, 1960). Detailed discussion is left to § 3·3.

The average temperature factor for O has a B-value of 0·6 Å² (Paper I). This, though not very accurately determined, is still appreciably lower than the values found in some other felspars (Table 7). It is an indication that we are here dealing with an ordered structure, and that the O atoms are not spread over a wide range of neighbouring positions in different unit cells, as

Table 7. *Isotropic B values in* Å²

	Microcline	Low albite	Sanidine	Orthoclase	Celsian	Anorthite	Reedmergnerite
Large cation	1·0	1·3	1·9	1·0–1·5	0·5–1·2	0·3–1·0	1·23
T	—	—	—	0·6	0·6*	0·2	0·33†
O	—	—	—	1·2	1·2*	0·6	0·67†

* These figures refer to the penultimate stage of refinement, when the structure was still being treated as if there were complete Si/Al disorder. No revised estimates were made at the later stage.

† Information kindly supplied by Dr D. E. Appleman, 1962.

must inevitably happen if Si and Al are distributed at random in the tetrahedral sites, because of their difference of radii.

3. Discussion

3·1. *Concept of structure as a framework built from elastic 'building elements'*

There is much to be gained from a consideration of the anorthite structure as if it were a construction built on engineering principles, according to the macroscopic laws of statics. We first consider the Si/Al–O framework, neglecting the large cation. Suppose all Si–O and Al–O bonds are rigid rods with lengths of 1·61 units and 1·75 units respectively, all angles at Si and Al are exactly tetrahedral, and all angles at O exactly 130°; O–O contacts, between different tetrahedra, of less than 2·7 Å are forbidden. Attempts to build a structure resembling that of felspars, and repeating itself with a parallelepiped of approximately $8 \times 13 \times 7$ units, will probably show that it cannot be done. We must endow our building elements with elasticity—the rod lengths with a Young's modulus, the hinge angles with a rigidity modulus. It may then prove possible to build the required periodic structure. The existence of the felspars proves that it *is* possible but suggests also that the structure will not be in stable equilibrium (in the sense used in statics) unless it is propped open with spacers of appropriate size, namely spheres of radius about 1 to 1·3 units. If the role of the large cation were merely to maintain electrical neutrality we should expect to find felspars in which magnesium, and possibly beryllium and lithium, could play this part. As it is, the hinged framework shears till the forces due to elastic compression of the spacer are called into play, and, when the spacer is large enough, equilibrium results. In determining the detailed nature of the shear, the electrostatic forces play their part.

In this process, all the bond lengths and bond angles are necessarily strained from their ideal values; the amount of strain adjusts itself at each, so that over the structure as a whole the energy is a minimum. Thus there are intrinsic strains in the various building elements when the structure as a whole has its equilibrium configuration.

Assuming a knowledge of the unstrained dimensions of the building units and their elastic constants, and a Hooke's law relation between stress and strain, one could in theory set up equations from which to derive the equilibrium configuration and all individual strains. In practice the mathematical solution of the equations might be too difficult. For a crystal structure there are the further difficulties (i) that we do not know our unstrained lengths and angles, because they never exist in isolation, (ii) that we cannot be sure of the validity of a Hooke's law approximation, and (iii) that the elastic constants themselves may depend on such influences as the electrostatic field of neighbouring atoms. Nevertheless an empirical examination of bond lengths and angles along these lines, taking the strains as deviations from the best estimated mean value, provides a useful starting point.

It turns out that the model needs to be adapted to allow for electrostatic attractive and repulsive forces emanating from the large cations, as well as the homopolar (or semipolar) attractive forces in the framework, and the repulsive forces within the framework and between cation and oxygen. These will be considered in more detail later.

3·2. *Framework and 'lattice' vibrations*

This girder-type model enables us to understand the doubling of the unit cell additional to that required by the Si/Al alternation. If all bond lengths and bond angles are strained in order to achieve a periodic repeat, doubling the period doubles the numbers of atoms over which the strain is to be distributed, and therefore (roughly) halves the individual strains with a consequent reduction in strain energy.

One may then ask why, if longer periods lower the strain energy, periodic structures are ever achieved? The answer lies in the fact that we have so far considered only potential energy. An actual macroscopic structure has natural frequencies corresponding to modes of vibration, and kinetic energies associated with them. The corresponding features of the crystal structure are the 'lattice vibrations' and their contribution to the free energy. Presumably this part of the energy is so much less for a periodic structure that it more than compensates for the extra strain energy. It is, however, temperature-dependent; and a transition to a structure of half the period at higher temperatures could be caused by a changing distribution of energies between the available vibration modes in a way which favoured shorter wave lengths.

The very small variations in Si–O bond lengths, and the only slightly larger variations in Al–O, show that these bonds are elastically stiff; by comparison the Ca–O bonds are elastically compliant. A similar contrast is seen for Si and Al bond angles on the one hand, Ca bond angles on the other. It is therefore to be expected that the Si/Al–O framework will vibrate as a whole, in 'lattice' modes, while Ca will vibrate more nearly independently, in Einstein modes. (This is perhaps a crude approximation, but it is only intended to give a qualitative picture). Since the force constants of the Ca–O bonds are smaller than of bonds and angles in the framework, and the effective mass concerned in the framework vibrations is greater than that of a single Si/Al or O atom, the vibration amplitudes of Ca are likely to be larger than those of Si/Al or O. This agrees with the observations of B values in anorthite, and also in reedmergnerite, the only other perfectly ordered structure for which detailed information is available.

Again, since the spread of values of bond angles

at O suggests that such angles are elastically more compliant than those at Si and Al, and since moreover the greater mass of Si/Al compared with O might tend to make them act as nodes for the standing waves, it is reasonable to expect that Si/Al amplitudes should be still less than O-amplitudes. This is observed. It may be related to the smaller difference parameters of T atoms compared with O atoms (Paper I, Table 5 and Table 9), as if the T atoms tended to stay as fixed points during the distortions of the parts of the structure round them. The B values recorded for other felspars are in accordance with these ideas (cf. Table 7); but when Si/Al disorder is believed to be present in the structure (as in the simplest interpretation of orthoclase) or is simulated by an averaging process at the stage at which the B values are computed (as was true of celsian, and is a possible interpretation of orthoclase) care has to be taken in estimating the effects of thermal vibration, because the experimental evidence does not distinguish between this and disorder broadening of the peaks. It is therefore rather surprising that in both orthoclase and celsian the B values for Si/Al are so low; it is obviously due to the same physical cause as the small size of the difference of T coordinates in anorthite. In both orthoclase and celsian the disorder broadening is manifested in B values for oxygen which are much larger than those in the ordered structures. For the A cations, if the very large anisotropy in the albites is attributed to disorder, and the smaller anisotropy in some of the others is ignored, all have isotropic B values of about 1 to 2 Å.

3·3. *Detailed examination of intrinsic strains*

We proceed to examine the intrinsic strains of individual bond lengths and bond angles, to see what regularities can be noted and how far they can be correlated with each other or with physically reasonable causes.

(i) *Bond angles at* O

Since, of all the 'building elements' of the structure, these show the greatest spread, and are therefore most compliant, it is convenient to consider them first.

Table 2(*g*) shows that a classification according to the type of atom ($A(1)$, $A(2)$, B, C, or D) is a natural one for demonstrating regularities. At O_C, the angles are all closely alike ($\sim 130°$), not only in anorthite but in other felspars (Table 6). There is similar consistency at $O_A(1)$, with slightly lower values ($\sim 138°$) for the 14 Å felspars than for the 7 Å felspars ($\sim 143°$). At $O_A(2)$ the angles in anorthite are even more consistent as a group, but conspicuously lower than in any other felspar. At O_B and O_D there is much more spread in all felspars, and in anorthite it is so great that there is not much significance in recording the mean.

The O_B and O_D atoms at which very large angles (160–170°) occur are those which have no Ca neighbour. At first glance one might try to correlate large angles with low electrostatic valence. This, however, cannot be substantiated by consideration of the other O bond angles, since comparison with Table 5 shows that (*a*) high values of electrostatic valence at $O_A(1)$ are associated with normal bond angles, and normal values at $O_A(2)$ with low bond angles, (*b*) similar values at $O_A(2)$ and half the O_C's are associated with different bond angles, (*c*) different values for two sets of O_C's are associated with similar bond angles. These qualitative comparisons can be substantiated by detailed statistics. It must be concluded either that the electrostatic field does not play a large part in controlling the bond angles or that the simple treatment of the field embodied in the Pauling rules for electrostatic valence is inadequate for evaluating its effect on bond angle.

In fact it seems much more likely that steric effects (depending on repulsive forces) play the main part in determining the oxygen bond-angle strains. One piece of supporting evidence is the fact that abnormally high angles at some O_B, O_D sites are compensated by low values at others within the same ring of four linked tetrahedra, so that the means for each ring are very much alike (Table 8). It is very noticeable that, for these angles as for the Ca environments, the closest resemblance among the four subcells is between those related by the base-centring operation *zi*. This point will be considered further below.

(ii) Si–O *and* Al–O *bond lengths*

The grouping of bond lengths to show up regularities in their strains may be tried in three ways, as follows (grouping into tetrahedral means having been shown to smooth out differences rather than emphasize them). The first way is according to the number of Ca neighbours of the O atom, as given in Table 5. The results are shown in Table 9. There is obviously a significant shortening for group 3 as compared with group 2; between groups 1 and 2 the differences for Si and Al separately are not (formally) significant,

Table 8. *Bond angles* (*in degrees*) *in the four different* O_B–O_D *rings*

Atom	Angle	Atom	Angle	Atom	Angle	Atom	Angle
$O_B(0000)$	129·4	$O_B(mzi0)$	163·6	$O_B(0z00)$	139·6	$O_B(m0i0)$	145·3
$O_D(0000)$	137·8	$O_D(mzi0)$	138·5	$O_D(0z00)$	125·2	$O_D(m0i0)$	166·9
$O_B(mz0c)$	143·5	$O_B(00ic)$	135·9	$O_B(m00c)$	170·8	$O_B(0zic)$	128·3
$O_D(mz0c)$	161·4	$O_D(00ic)$	124·6	$O_D(m00c)$	140·3	$O_D(0zic)$	132·6
Mean	143·0	Mean	140·6	Mean	144·0	Mean	143·8

Table 9

(*a*) Comparison of *T*–O bonds according to environment of O

	No. of Ca neighbours	Mean bond length		S.d. of mean bond length	
		Si–O	Al–O	Si–O	Al–O
Group 1	2	1·632 Å	1·780 Å	0·007 Å	0·015 Å
Group 2	1	1·622	1·755	0·005	0·006
Group 3	0	1·588	1·719	0·008	0·009

(*b*) Significance tests

		Group 1–2	Group 2–3
Cruickshank significance ratio c_s	Si	$10/(7^2+5^2)^{\frac{1}{2}} = 1{\cdot}16$	$34/(5^2+8^2)^{\frac{1}{2}} = 3{\cdot}62$
	Al	$25/(15^2+6^2)^{\frac{1}{2}} = 1{\cdot}56$	$36/(6^2+9^2)^{\frac{1}{2}} = 3{\cdot}33$
Probability of accidental occurrence of observed difference*	Si	0·12	< 0·001
	Al	0·06	< 0·001
	Joint	0·007	$<10^{-6}$

* Calculated from Cruickshank's expression, $P = \frac{1}{2} - \frac{1}{2}\,\mathrm{erf}\,(c_s/\sqrt{2})$.

but since the probability for their joint occurrence accidentally is the product of the separate probabilities, the combined effect is significant. (Errors in the coordinates of any O, which would affect both its bonds, would tend to do so in opposite directions, because the bond angle is greater than 90°; hence they could not give rise to systematic differences in the same direction between both kinds of bonds).

The second way of grouping bonds is according to the type of O atom, which proved effective for O bond angles. Average values for both kinds of bonds involving $O_A(1)$ are slightly larger than for those involving $O_A(2)$, and these again than for bonds involving O_B, O_C, O_D, which show no consistent trend; but none of the differences is large enough to be significant. Bonds to $O_A(2)$, which is linked by the abnormally short bond to Ca, are if anything longer than normal; hence the shortening of Ca–$O_A(2)$ is not due to stresses exerted on $O_A(2)$ by its *T* neighbours.

The third way is a comparison of *T*–O bond lengths with bond angle at O. This showed no detectable regularity, except what could be accounted for by the fact that the four atoms with largest angle have no Ca neighbour.

It therefore seems clear that the most conspicuous differences of Si–O and Al–O bond length depend on the number of Ca neighbours of the O atom. Such an effect has been suspected previously, e.g. by Smith (1960), Smith, Karle, Hauptman & Karle (1960), Radoslovich (1960); but is here conclusively demonstrated. It means *either* that there are intrinsic stresses in the *T*–O bonds due to the stresses applied to them by the Ca–O bonds, *or* that the electrostatic field of Ca acts directly on the bonds to lengthen them. Which explanation is physically more realistic cannot be decided on this evidence.

It also remains doubtful which of the lengths should be regarded as 'unstrained', since there are certainly other stresses operating besides those in the Ca–O bonds—notably those affecting the bond angles at O. It is not surprising, for example, that Si–O bonds in this structure for O atoms with no Ca neighbours should be shorter than in a structure such as quartz where *none* of the O's has any other neighbour.

No similar effects have been observed with certainty in other felspars. For intermediate microcline, orthoclase and celsian, the scatter of individual bond lengths within a tetrahedron is insignificant ($\varepsilon(r) \sim 0{\cdot}005$ Å or less). For low albite, the scatter is rather large ($\varepsilon(r) = 0{\cdot}021$ Å) but so is the standard error of determination ($\sigma = 0{\cdot}019$ Å). For high albite, with about the same σ, the scatter is small (0·008 Å). For reedmergnerite, $NaBSi_3O_8$ (with the felspar structure), the scatter is rather larger in proportion ($\varepsilon(r) = 0{\cdot}017$ Å, $\sigma = 0{\cdot}010$ Å), which suggests that the deviations are real; but the margin is too narrow to allow very definite conclusions. More detailed information from three-dimensional analysis of the albites is desirable.

(iii) *Bond angles at* Si *and* Al

Inspection of Table 2(*f*) suggests some degree of uniformity within groups of four tetrahedra. Accordingly, bond-angle strains (differences from the tetrahedral angle, 109·5°) for corresponding angles were averaged over the four atoms whose symbols are derived from any one of the set by operations 000, 00*i*, *m*00, *m*0*i*—i.e. for atoms related topologically (not exactly) by body-centring and mirror-plane operations. The results (Table 10) show clearly that corresponding angles for different atoms within a set have on the average very small differences from one another as compared with the differences between their means. (Most of these differences are large compared with the estimated experimental error, $\sim 0{\cdot}5°$). Moreover, while T_1 and T_2 tetrahedra show quite different sets of strains, tetrahedra containing Si or Al respectively (related by operator *z*) have very similar strains, except that those for Al are slightly (perhaps not significantly) larger.

Table 10. *Bond angle strains (in degrees) and* O–O *tetrahedron edge strains (in* Å)

Strains are deviations from values for a regular tetrahedron
The table lists the means over corresponding angles and edges in similar tetrahedra, and their standard deviations

Type of tetrahedron	O atoms	O–O edge in anorthite		O–*T*–O angle											
				Anorthite		Low albite		High albite	Microcline		Orthoclase		Sanidine	Celsian	
		Si	Al	Si	Al	Si	Al	Si/Al	Si	Al	Si	Si/Al	Si/Al	Si	Al
T_1	*AB*	−0·105	−0·148	−6·9	−8·4	−3·9	−5·9	−4·8	−4·8	−2·2		−3·4	−4·2	−6·5	−6·9
		±0·020	±0·004	±1·3	+2·1			±0·3							
	AC	+0·091	+0·113	+5·9	+6·7	+3·7	+5·6	+2·5	+3·5	+3·7		+5·1	+3·5	+6·7	+6·4
		±0·015	±0·027	±1·2	±1·7			±0·6							
	AD	−0·094	−0·138	−6·2	−8·5	−2·9	−6·2	−4·6	−4·3	−2·8		−3·4	−3·4	−6·5	−8·4
		±0·009	±0·031	±0·9	±2·5			±1·0							
	BC	+0·021	+0·024	+2·1	+3·1	−0·6	+2·1	−1·5	+3·2	+0·7		+0·7	+1·4	+1·8	+4·1
		±0·012	±0·019	±0·8	±0·7			±3·5							
	BD	+0·058	+0·075	+3·8	+4·9	+1·2	+0·7	+3·0	+0·2	+0·1		+0·5	+2·4	+4·2	+4·3
		±0·012	±0·038	±1·1	±1·2			±4·0							
	CD	−0·002	+0·005	+0·8	+1·6	+0·8	+2·6	+4·5	+0·9	−4·8		−0·7	−0·3	+0·1	−0·5
		±0·032	±0·022	±1·0	±0·5			±1·7							
T_2	*AB*	−0·005	−0·046	−0·4	−2·8	−1·1		−2·9	−1·0		+0·6		+0·6	−3·1	−3·0
		±0·020	±0·040	±1·6	±2·3	±1·5		±1·7	±0·4						
	AC	−0·090	−0·110	−5·9	−6·2	−5·0		−2·5	−4·3		−4·9		−4·9	−6·2	−8·4
		±0·019	±0·019	±1·0	±1·3	±0·9		±0·1	±0·3						
	AD	+0·011	−0·053	+0·9	−3·1	−1·5		−2·2	−0·9		−0·8		−0·6	−0·6	−0·6
		±0·004	±0·018	±0·7	±1·2	±0·7		±1·3	±0·2						
	BC	+0·034	+0·026	+2·5	+2·3	+3·5		−1·8	+1·2		+1·8		+0·4	+4·0	+3·3
		±0·031	±0·024	±0·7	±0·8	±0·5		±2·3	±0·2						
	BD	−0·038	+0·033	−1·2	+2·4	+1·0		+1·3	+1·2		+1·6		+2·1	+2·3	+3·3
		±0·030	±0·017	±1·5	±0·9	±0·3		±0·4	±0·2						
	CD	+0·046	+0·089	+3·6	+6·2	+2·1		+7·4	+3·3		+1·3		+2·3	+2·9	+4·3
		±0·015	±0·018	±0·7	±1·0	±1·7		±0·2	±0·9						

Exactly similar effects are shown by an analysis of the O–O bond-length strains, i.e. the differences from the values 2·640, 2·860 Å, corresponding to regular tetrahedra with T–O distances 1·614, 1·749 Å respectively. These are also shown in Table 10. The consistent differences between the edges $T_1(AC)$ and $T_2(AC)$ in a number of felspars was earlier noted by Jones & Taylor (1961), who pointed out that it could not be due to a difference in Si/Al ordering but must 'be due to the general balance of forces as between Si/Al and O on the one hand, and K (or Ba) on the other.'

The more detailed analysis of the present paper allows us to go further. Table 2(f), or its analysis in Table 10, shows that in anorthite all tetrahedra of the same type (T_1 or T_2) tend to have the same shape, i.e. the same angular strains, whatever their position or orientation in the structure, and whatever the nature of T. These tetrahedra are not related by symmetry, though of course their general arrangement is not far from the symmetrical sanidine structure. It therefore seems that the strains, and consequently the stresses producing them, are not on the whole very sensitive to the detailed coordinates of the atoms and their departure from the higher symmetry. (In so far as bond-length strains may be associated with any of the same regularities as affect bond-angle strains, similarity between tetrahedra of the same type will have the effect of making their T–O tetrahedral means more nearly alike than would have been expected from a random distribution of the bond lengths throughout the structure, thus tending to explain the observation noted in § 2·1.)

Some striking facts emerge from comparison of the bond angles with those in other felspars (Table 10). The largest strains, those in $T_1(AB)$, $T_1(AC)$, $T_1(AD)$, $T_2(AC)$, are observed in *all* the felspars studied; they do not vary greatly within a structure, and the mean value of each for a given structure is roughly constant for all the felspars with cations of similar valency (Table 11), the ratio of the strains for divalent and monovalent cations being about 1·7. The strains must therefore be due (like the T–O bond-length elongations) to the effect of the A cations. The stresses causing them must, like the strains, be relatively insensitive to small differences in atomic coordinates and configuration round A. Since the A atom is nearly on a mirror plane of symmetry, and is nearly repeated by a body-centring translation, this explains the close resemblance in shape between different tetrahedra in the same structure as well as between different structures. The relative insensitivity of the strain to the departure from overall monoclinic symmetry is particularly striking: the monoclinic (or nearly monoclinic) potassium felspars are only slightly different from the distinctly triclinic albites, but quite different from monoclinic celsian.

3·4. *Bond-angle strain as a consequence of electrostatic repulsion*

The mechanism by which the cation affects the O–T–O bond angle must be treated in terms of electrostatic forces, because even if homopolar forces contribute to the Ca–O bond we have no means of estimating them. As a nearest-neighbour effect, the electrostatic field of Ca polarizes each neighbouring O and thereby influences both the attractive and repulsive forces between O and its other neighbours. For second-nearest-neighbour effects, we must consider Ca–Ca and Ca–T electrostatic repulsions; this looks formidable at first glance but is greatly simplified if one recognizes the shielding of Ca by its surrounding O's. Since these are polarizable, one may represent them in a crude model by conducting spheres of radius about 1·5 Å. For this purpose one must include *all* O's at distances not greater than the cation–cation distances to be studied, since it is not merely O's in contact with Ca which serve to shield it. Then only where there are gaps in the shell of O's is cation–cation repulsion likely to be important. This effect can be visualized using lines of force. The ideas used here are the same as those underlying Pauling's electrostatic-valence concept.

Table 11. *Comparison of bond angles showing large strain: mean values over all similar tetrahedra*

Large cation	Felspar	Mean bond-angle strain (degrees)			
		$T_1(AB)$	$T_1(AC)$	$T_1(AD)$	$T_2(AC)$
Na^+	Low albite	−4·9	+4·6	−4·6	−5·0
Na^+	High albite	−4·8	+2·5	−4·6	−2·5
K^+	Microcline	−3·5	+3·6	−3·5	−4·3
K^+	Orthoclase	−3·4	+5·1	−3·4	−4·9
K^+	Sanidine	−4·2	+3·5	−3·4	−4·9
Ca^{++}	Anorthite	−7·7	+6·3	−7·3	−6·1
Ba^{++}	Celsian	−6·7	+6·5	−7·5	−7·3
1-valent	Mean	−4·2 ±0·3	+3·9 ±0·4	−3·9 ±0·3	−4·3 ±0·4
2-valent	Mean	−7·2 ±0·4	+6·4 ±0·1	−7·4 ±0·1	−6·7 ±0·4
Ratio $\frac{2-\text{valent}}{1-\text{valent}}$		1·7	1·6	1·9	1·6

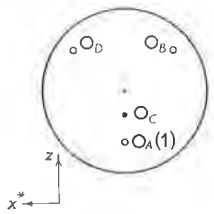

Fig. 3. Sketch stereogram of the environment of $T_1(0000)$.

The fact that the largest O–T–O strains are those involving the three angles round T_1–$O_A(1)$ is sufficiently striking to provide an empirical starting point for study. The geometrical consequence of these strains can be seen from Fig. 3. As compared with a regular tetrahedron, angles AB and AD are too small, AC too large; in other words, T–$O_A(1)$ is tilted further downwards. To restore regularity, it would be necessary to increase the y coordinate of $O_A(1)$, and hence (because of the centre of symmetry and pseudo-symmetry axis) to increase the edge $O_A(1)$–$O_A(1)$ and the bond angle at $O_A(1)$. The latter is already slightly too large (135° instead of the unstrained 130°), but in view of the softness (high compliance) of T–O–T angles, further changes are hardly likely to give prohibitive energy increase. On the other hand, $O_A(1)$–$O_A(1)$ is a shared edge between two Ca polyhedra; its length, ~3·2 Å, is also rather high for such an edge. It seems that there are strong forces tending to make it contract.

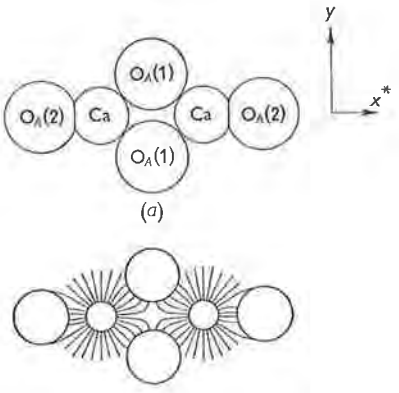

Fig. 4. Environment of a pair of Ca atoms related by a centre of symmetry; section in plane perpendicular to [001]. (*a*) Packing diagram, with radii drawn to scale; (*b*) lines of force, with atomic centres as in (*a*), but radii reduced to show effect more clearly.

The electrostatic origin of the forces tending to shorten $O_A(1)$–$O_A(1)$ can be shown as follows. The shielding shell of Ca comprises ten O's (two each of $O_A(1)$, $O_A(2)$, O_B, O_C, O_D). The only serious gap in it is at the edge $O_A(1)$–$O_A(1)$, across which there is another Ca at a distance of about 4 Å. Fig. 4(*a*) shows a section in a plane perpendicular to [001], drawn approximately to scale. The abnormally short Ca–O distance is shown by the cut-off of the circles at a common chord. Assuming the $O_A(2)$–$O_A(2)$ distance to be fixed by other parts of the framework not shown (cf. below, § 4·1), the Ca–O distances could be made more nearly normal by moving the Ca's nearer together and the $O_A(1)$'s further apart, thus relieving the strain in the angles at T_1 and $O_A(1)$ also. But the Ca's are kept apart by their electrostatic repulsion, and this also draws together the two $O_A(1)$'s, as shown in Fig. 4(*b*). Not only the interrelation of the three largest strains, but their independence of the detailed symmetry of the felspar, and their dependence on cation valency, are thus explained simultaneously. (It may be noted in passing that since $O_A(2)$ is abnormally close to Ca it is in a strong electrostatic field and is polarized accordingly, with consequent effect on its other bonds).

4. Linkages and stability of structure

4·1. *Monoclinic approximation*

We now consider the linked framework as a whole, to see how the details hitherto examined fall into place. Figs. 5(*a*), (*b*), (*c*), are stylized diagrams of parts of the structure; (*a*) and (*b*) are viewed down [010], and may be compared with the scale diagram in Fig. 1,

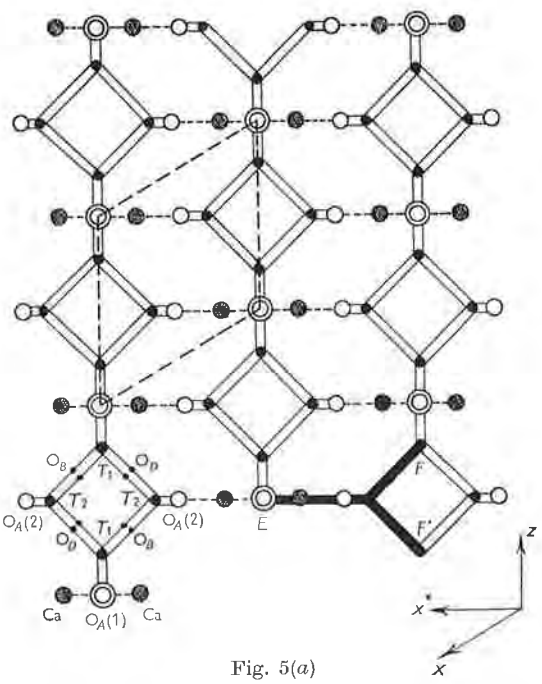

Fig. 5(*a*)

Fig. 5. Stylized diagrams of parts of structure. (*a*) Projection on (010) of slab bounded approximately by $y = \pm 0{\cdot}3$, (*b*) projection on (010) of slab bounded approximately by $y = 0{\cdot}1$, 0·4, (*c*) projection down [001] of whole 7 Å cell. In (*a*) and (*b*) the 7 Å cell is outlined by dashed lines. Pairs of atoms and bonds which are superposed in projection are shown by double lines. Heavy lines E–(F, F') and G–H indicate links affecting x^* repeat distance. Labelling of atoms is given in bottom left-hand corner.

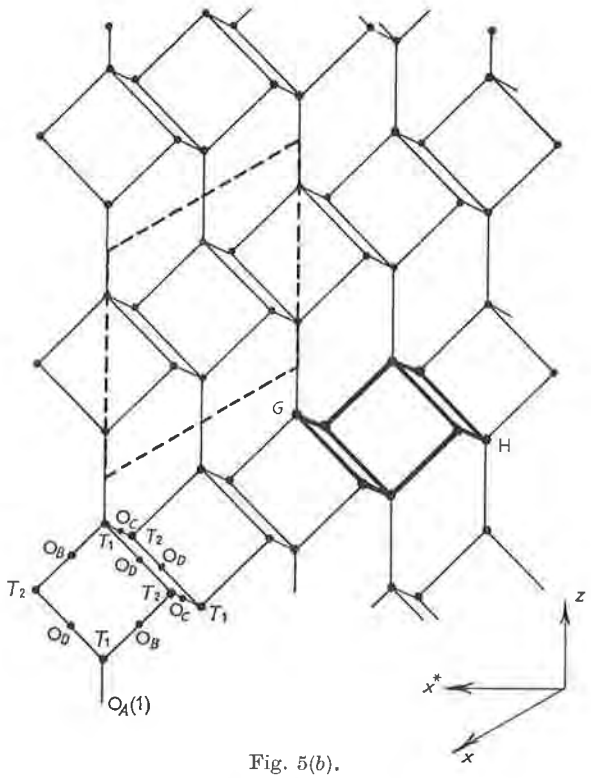

Fig. 5(*b*).

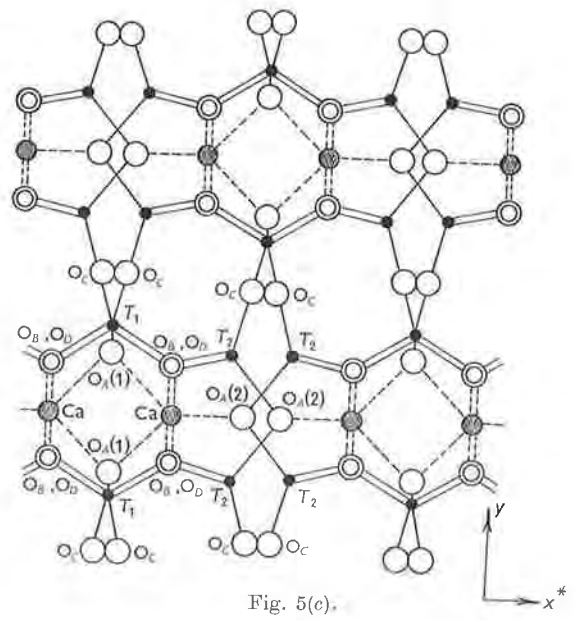

Fig. 5(*c*).

and (*c*) is viewed down [001]. Neither in Fig. 5 nor in the following discussion is any distinction made between Si and Al, because, as has been shown above, their difference gives only second-order effects. The full sanidine symmetry is retained for this first stage of the discussion.

Fig. 5(*a*), which includes all atoms except O_C, shows the striking pseudosymmetry which exists within a (010) slab of the structure bounded approximately by $y = \pm 0{\cdot}2$. To this approximation, atoms O_B and O_D are equivalent, and the symmetry is orthorhombic, atoms Ca, $O_A(1)$ and $O_A(2)$ each lying at the intersection of two mirror planes. The slab is built from a double sheet of *T*–O tetrahedra, each sheet containing four-membered rings bound tightly to rings in the other sheet by a complex system of cross-girders emanating from Ca and $O_A(2)$ (Fig. 5(*c*)). Obviously the whole slab forms a fairly rigid unit.

Fig. 5(*b*) shows the linkage between one slab and the next, between the upper rings of the slab in 5(*a*) (centred on $y=0$) and the lower rings of the one above it (centred on $y=\frac{1}{2}$). The linkage is through O_C. The orthorhombic pseudosymmetry has completely disappeared. Atoms O_D are topologically distinguished from O_B by their participation in a four-membered ring with O_C, which stands in a vertical plane linking the layers.

The repeat distance in the x^* direction is determined by two different sets of links, shown in Figs. 5(*a*) and (*b*) by the heavily-drawn lines *E*–(*F*, *F*′) and *G*–*H* respectively. Other links are negligible, tending mainly to produce shear. For equilibrium, the stresses in *E*–(*F*, *F*′) and *G*–*H* must be equal and opposite.

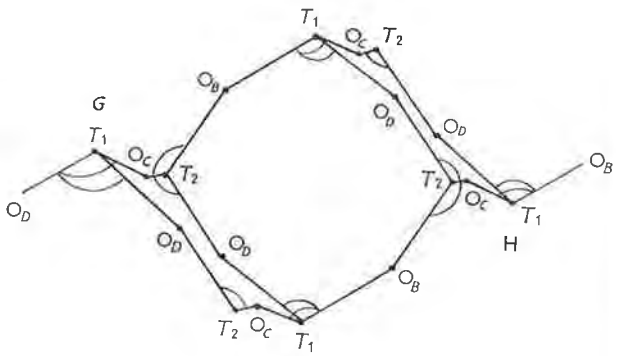

Fig. 6. Stylized diagram showing detail of linkage in region *G*–*H* of Fig. 5(*b*).

But we have seen that *E*–(*F*, *F*′) is in compression, shown by the shortness of the bond Ca–$O_A(2)$. Hence *G*–*H* must be in tension. This is shown in more detail in Fig. 6 (cf. also 5(*c*)). Assuming that the stress manifests itself more in bond angle strains than in *T*–O bond length strains, we expect positive strains in the angles marked in Fig. 6, and negative strains in $T_2(BD)$ and $T_2(AC)$, the latter rotating the bond T_2–O_C downwards towards the plane of the paper. The angle $T_1(BD)$ is also concerned in the link *E*–(*F*, *F*′), where a negative strain is required, but its effect on this length is only half its effect on *G*–*H*, and may therefore be ignored; on the other hand, $T_2(BD)$ should have a positive strain in *E*–(*F*, *F*′) and we cannot predict whether this or the negative strain required for *G*–*H* will predominate. Table 12 shows a comparison of predicted and observed strains

Table 12. *Comparison of observed and predicted bond angle strain in x* repeat distance*

	Mean bond-angle strain (degrees)					
	$T_1(BC)$	$T_1(BD)$	$T_2(AC)$	$T_2(BC)$	$T_2(BD)$	$T_2(CD)$
Predicted	+	+	−	+	Indeterminate	+
Anorthite	+2·6	+4·4	−6·1	+2·4	+0·6	+4·9
Celsian	+3·0	+4·2	−7·3	+3·0	+2·9	+3·6
Low albite	−0·6	+1·2	−5·0	+3·5	+1·0	+2·1
High albite	−1·5	+3·0	−2·5	−1·8	+1·3	+7·4
Microcline	+3·2	+0·2	−4·3	+1·2	+1·2	+3·3
Orthoclase	+0·7	+0·5	−4·9	+1·8	+1·6	+1·3
Sanidine	+1·4	+2·4	−4·9	+0·4	+2·1	+2·3

for these angles in all felspars. The agreement is very good for anorthite and celsian, and the same trend can be seen in the other felspars, though with more irregularities. Possibly this good agreement, and the regular distribution of strain it entails, are associated with the stability of the anorthite structure.

Fig. 5(*c*) shows part of the structure viewed down [001]. The complexity of the linkages in the double layers near $y=0$ and $\frac{1}{2}$ is very evident, and contrasts with their paucity between double layers. One would expect to find the structure amenable to shear in this plane. The observed lack of strain in the O_C angles (Table 2(*g*)) suggests that they can adjust themselves independently of internal changes in the double layers, at the cost of lateral displacement, resulting macroscopically in changes of α and γ angles.

4·2. *Distortion from monoclinic symmetry*

The next step is to examine what distortions follow as a result of the small Ca radius.

In Fig. 3(*a*) it was shown that the x^* coordinate of Ca is rather rigidly determined. In the (001) plane, however, the approximation of Fig. 5(*a*) shows that Ca has four equidistant O_B and O_D neighbours, which cannot all come into contact with it because they are impeded by $O_A(1)$ and $O_A(2)$. For the larger cations K and Ba, they can do so, and the cation remains on, or very close to, the symmetry plane. But the smaller Ca moves off the symmetry plane along one diagonal of the square $O_BO_DO_DO_B$, and these O's readjust themselves so that three make good contact and one is pushed right out, its bond angle increasing to about 170° in the process.

These displacements of O cause stresses in the framework which cannot be entirely accommodated by strains in the nearest *T*–O bonds and *T* bond angles. The tetrahedra are rotated or displaced, and so transmit part of the strain to their neighbours. If the next Ca atom is fairly close, its direction of displacement may be determined by that of the first. In this way the displacements may be cooperative either over closed groups of atoms or over the whole periodic structure.

The detailed pattern of Ca displacement in anorthite can be predicted qualitatively with the help of two general principles: (i) that when strong internal stresses are related by symmetry or pseudosymmetry in the ideal structure, this symmetry will be retained, at least locally, in the distorted structure, (ii) that all periodicities will remain as small as is compatible with (i). In anorthite, there are strong oppositely-directed electrostatic repulsions acting along Ca–Ca across the centre of symmetry at (0, 0, 0); this centre is retained. There is a strong compression along Ca–$O_A(2)$; this direction remains, locally, an axis

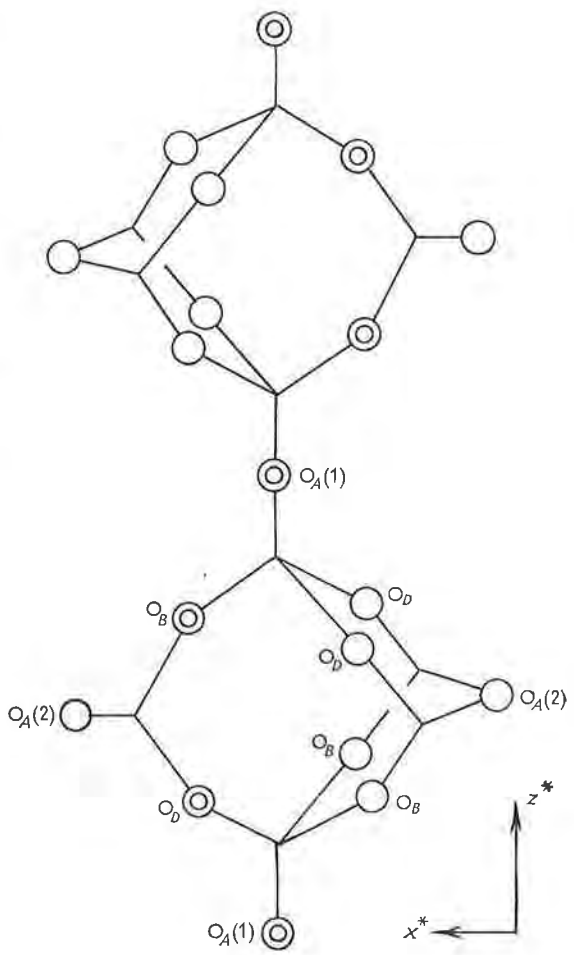

Fig. 7. Schematic projection of double layer on (010), showing distortion from original symmetry due to small Ca.

of pseudosymmetry, and the plane defined by T_2–$O_A(2)$–T_2 tilts about it, out of the vertical, giving equal rotations (or displacements) to the two T_2 octahedra and their adjacent O's (Fig. 7). In this way large bond-angle strains can be introduced at O_B and O_D, without change of bond length. Since there is one large O-angle for every Ca, and two are associated with every $O_A(2)$, half the $O_A(2)$'s are unaffected. Those affected are (like everything else) centrosymmetric about (0, 0, 0) (Fig. 7). Hence successive double rings in the z direction cannot be true repeats; exact repetition occurs only after twice the original c distance. There is nothing in the sideways linkage to forbid the original C-face-centred arrangement, which is therefore retained. A body-centred arrangement would have the disadvantage, because of its centre of symmetry at $(\frac{1}{4}, \frac{1}{4}, \frac{1}{2})$ (referred to the cell in Fig. 5(a) and (b)), of introducing two 170° angles into the same vertical 4-membered ring, which looks unlikely.

The features illustrated schematically in Fig. 7 can be seen in the projection of the actual structure, Fig. 1 (best shown in 1(a)).

The argument thus predicts a 14 Å C-face-centred structure, having the environments of Ca(000) and Ca(zi0) identical with each other and different from those of Ca(z00) and Ca(0i0). This result, as was made clear in Paper I, is a very good approximation to observed fact. The Si/Al alternation, however, does not satisfy the C-face-centring condition, and the consequent atomic displacements result in small differences between members of each of the above pairs.

The argument would apply equally to albite, except that the electrostatic forces and their resultant strains are smaller, and mistakes of sequence therefore more likely. This point will be discussed elsewhere.

No use has been made here of the individual bond-angle strains at T which show departures from monoclinic symmetry. These, and the individual bond angles at O, may contain much useful information. The structure also offers opportunities for studying lattice parameters in terms of interatomic forces, along the lines suggested in § 4·1. On both these points, it would be particularly valuable to trace the changes of structural detail which accompany macroscopic changes and changes of composition. Structure determinations of other felspars in the plagioclase series are in progress (Chandrasekhar, Fleet & Megaw, 1960; Kempster, 1957; Waring, 1961), and further discussions may wait till anorthite can be compared with them.

5. Summary

The unit cell of anorthite consists of four subcells of equal volume in which the atoms have nearly but not quite identical configurations. The structure is perfect, with no disorder, within the limits of accuracy of the work, which are fairly narrow. Si and Al tetrahedra alternate so that every oxygen has one Si neighbour and one Al. This distribution means that pairs of subcells related by the body-centring vector have the same Si/Al distribution; nevertheless their atomic coordinates are not as closely similar as pairs which have unlike distribution, and are related by C-face-centring. The tetrahedra are not perfectly regular—an effect observed in earlier felspar studies concerning bond angles, and here extended to their bond lengths. Small differences in tetrahedral mean bond lengths are rather less than would have been expected from the scatter of lengths within tetrahedra, but greater than is allowed for in Smith's original discussion of bond lengths.

One Ca atom is perhaps best considered as 6-coordinated, though with a 7th more distant neighbour; the other three are 7-coordinated. All the Ca bond lengths are fairly normal; the closest contact is to $O_A(2)$, which is a short bond in other felspars. Though the Ca environments (the 'cavities' in the structure) are of different shapes, there is no evidence that any of them has a possible alternative site giving reasonable bond lengths to the oxygens surrounding.

The temperature factors, though not determined with great accuracy, are informative. The low values of B for Si/Al and O are characteristic of a perfect structure (as contrasted with the B value for oxygen in felspars with Si/Al disorder, which includes a 'broadening factor'). The high value for Ca is comparable with that in other felspars, and may represent either a true or a frozen-in thermal amplitude.

The 'strains' (departures from ideal values) of bond length and bond angle give important information. Individual Si–O and Al–O bonds show, on the average, significant decreases as the number of Ca neighbours of the O drops from 2 to zero. The bond angle strains at all T atoms of the same crystallographic type (T_1 or T_2) show marked similarity, independent of symmetry or Si/Al ratio in different felspars; the three largest, in particular, can be shown to depend on cation charge rather than cation size. The role played by cation–cation repulsion across the symmetry centre (0, 0, 0) is very important. It controls not only the distortions of the tetrahedra compatible with monoclinic symmetry, but also the pattern of displacements and rotations consequent on the relatively small size of Ca. Consideration of its effect on the x^* repeat distance leads to a qualitative prediction of bond-angle strain in the other Si and Al angles which agrees with that observed. Consideration of its effect on Ca displacement predicts the close approximation to a C-face-centred lattice which is also found experimentally.

It is rather surprising that the explanation of the structure can be carried so far without any need to invoke the effects of differences between Si and Al in either radius or charge. Obviously these must play a part; but it would appear that the part is smaller than has often been tacitly assumed. Deviations of

individual values of bond lengths and bond angles from their group averages give a basis for further study.

It is a pleasure to express our indebtedness to Dr W. H. Taylor for suggesting this work, and for his support and guidance throughout its execution. It will be obvious how much it owes to his forethought and wise planning, by which detailed structural studies of the key members of the felspar family have been made available for comparison with each other. We are grateful to Mr P. H. Ribbe for carrying out the bond angle calculations.

References

Bakakin, V. V. & Belov, N. V. (1960). *Kristallografiya*, **5**, 864.
Bailey, S. W. & Taylor, W. H. (1955). *Acta Cryst.* **8**, 621.
Chandrasekhar, S., Fleet, S. G. & Megaw, H. D. (1960). *Abstract, Congress of International Mineralogical Association*, Copenhagen, 1960.
Clark, J. R. & Appleman, D. E. (1960). *Science*, **132**, 1837.
Cole, W. F., Sørum, H. & Kennard, O. (1949). *Acta Cryst.* **2**, 280.
Cruickshank, D. W. J. (1949). *Acta Cryst.* **2**, 65.
Ferguson, R. B., Traill, R. J. & Taylor, W. H. (1958). *Acta Cryst.* **11**, 331.
Goldsmith, J. R. & Laves, F. (1955). *Z. Kristallogr.* **106**, 3.
Jones, J. B. & Taylor, W. H. (1961). *Acta Cryst.* **14**, 443.
Kempster, C. J. E. (1957). Thesis, Cambridge University.
Kempster, C. J. E., Megaw, H. D. & Radoslovich, E. W. (1960). *Acta Cryst.* **13**, 1003.
Kempster, C. J. E., Megaw, H. D. & Radoslovich, E. W. (1962). *Acta Cryst.* **15**, 1005.
Liebau, F. (1960). *Silikattechnik*, **11**, 397.
Loewenstein, W. (1954). *Amer. Min.* **39**, 92.
Megaw, H. D. (1956). *Acta Cryst.* **9**, 56.
Newnham, R. E. & Megaw, H. D. (1960). *Acta Cryst.* **13**, 303.
Radoslovich, E. W. (1960). *Acta Cryst.* **13**, 919.
Smith, J. V. (1954). *Acta Cryst.* **7**, 479.
Smith, J. V. (1960). *Acta Cryst.* **13**, 1004.
Smith, J. V., Karle, I. L., Hauptman, H. & Karle, J. (1960). *Acta Cryst.* **13**, 454.
Waring, J. (1961). Thesis, Cambridge University.

Printed in Denmark at Fr. Bagges kgl. Hofbogtrykkeri, Copenhagen

Paper 3-7

X-RAY STUDIES OF THE ALTERATION OF SODA FELDSPAR

G. W. BRINDLEY AND E. W. RADOSLOVICH

Reprinted from
Proceedings of Fourth National Conference on CLAYS AND CLAY MINERALS
National Academy of Sciences — National Research Council
Publication 456, 1956, pp. 330-336
Made in United States of America

X-RAY STUDIES OF THE ALTERATION OF SODA FELDSPAR[1]

By

G. W. Brindley and E. W. Radoslovich
Department of Ceramic Technology,
The Pennsylvania State University, University Park, Pennsylvania

ABSTRACT

Studies have been made of the alteration of pure albite single crystals and powders. No structural modification of the feldspar itself has been detected. No evidence has been obtained for any preferential orientation of an alteration product in relation to the initial feldspar. Under hydrothermal conditions at 280° C and 430° C, albite flakes and powders have been subjected to attack by 0.1 *N* HCl for periods ranging from a few hours to 52 days. The flakes changed mainly to boehmite, the powders to a variety of products, including a well-defined kaolinite. This difference of behavior is interpreted in terms of Correns' ideas on the weathering of silicates.

INTRODUCTION

This paper reports exploratory work undertaken to elucidate the formation of clay minerals from feldspars. An attempt has been made to study the process at three stages of development, namely (i) the initial stage when the alteration of the feldspar commences, (ii) an intermediate stage, and (iii) the final stage when clays and/or other products are fully developed.

Feldspars are formed of three-dimensionally linked SiO_4 and AlO_4 tetrahedral groups. Clay minerals consist mainly of two-dimensionally linked SiO_4 and AlO_4 tetrahedra, together with octahedral groups containing Al and other cations. A considerable structural rearrangement is involved, therefore, in passing from feldspar to clay mineral and it is not obvious how the transformation takes place. We have therefore looked for evidence which may show how a feldspar alters in the initial stage of the transformation, and also for evidence of any crystallographic relation between an alteration product and the initial feldspar. Various x-ray diffraction techniques have been applied, involving both single crystals and powdered materials. The work began with a study of some naturally altered feldspars, but progressed towards laboratory-controlled alterations. Various physical and chemical environments have been used and the nature of the end products determined.

EXAMINATION OF SOME NATURALLY ALTERED FELDSPARS

Eleven rock specimens, mainly granites, containing weathered feldspars from the surface and apparently unweathered feldspars from below the surface were first examined. They appeared to be well suited for the present investigation. Microscopic examination showed small surface cavities containing crumbly or

[1] Contribution no. 55-25 from the College of Mineral Industries.

clayey materials, commonly white in color. These were carefully hand picked and examined by x-ray powder methods. They revealed no obvious clay minerals and appeared to be essentially feldspar material broken down to small particle size.

Comparison of the surface feldspar with the interior feldspar by x-ray powder and single crystal methods gave disappointing results. The apparently fresh, interior feldspars seemed to be variable, probably even within single crystals, so that no reliance could be placed on comparisons between weathered surface material and fresh interior crystals. Since it was an essential condition for the present work that it should be possible to interpret the x-ray data unambiguously, attention was directed towards well-defined feldspars, the alteration of which could be followed under laboratory-controlled conditions.

SINGLE-CRYSTAL TESTS FOR FELDSPAR ALTERATION

Soda feldspar (albite) was chosen as being the most suitable for preliminary experiments. It is more easily altered than potash feldspar and is more easily obtainable in good crystalline condition than lime feldspar. Experiments were carried out principally on two albites: (a) from Court House, Amelia Co., Virginia; and (b) a cleavelandite from Auburn, Maine. These gave identical x-ray powder diagrams in good agreement with the data of Goodyear and Duffin (1954), and from the lattice spacing-composition diagram[1] of Tuttle and Bowen (1950, fig. 5, p. 581) it appears that they are low-temperature forms with less than 3 percent of lime feldspar. Tuttle and Bowen state: "Low-temperature albite apparently cannot tolerate more than very small amounts of potash. Crystals which have formed side by side with potash feldspar usually contain only a few tenths of a percent of K_2O." On the basis of this evidence, we consider that the materials used in the present experiments were pure or almost pure soda feldspar.

Under the microscope, the Amelia albite showed liquid inclusions and the cleavelandite a few solid inclusions and possibly a trace of muscovite. The specimens cleaved readily on (010) and cleavage flakes about $6 \times 4 \times 0.5$ mm in size were easily obtained.

An x-ray examination of cleaved flakes was made before and after various treatments. It was expected that any marked extraction of alkali or aluminum ions by an alteration process would modify the relative intensities of the $0k0$ reflections; a one-dimensional Fourier synthesis should then give an indication of the nature of the change taking place. Flakes were carefully mounted on goniometer arcs on a G.E. XRD3 Geiger counter diffractometer and the intensities of the $0k0$ reflections were accurately measured. The experiments failed to show any changes in the *relative* intensities of the $0k0$ reflections, even though these were practically destroyed by some of the treatments.

Additional experiments were carried out in which the $0kl$ reflections of fresh and of partially altered albite crystals were recorded on Weissenberg photographs. No reflections became markedly weakened or diffused by the treatments applied.

The outcome of all these experiments is that no evidence was obtained for any

[1] In this diagram, the angular interval 2θ should be given as $13\bar{1}$–131.

systematic alteration of the feldspar lattice as a first step towards the breakdown of the mineral.

ABSENCE OF ORIENTATION RELATIONSHIPS BETWEEN SODA FELDSPAR AND ITS ALTERATION PRODUCTS

The possibility was envisaged that alteration of a feldspar may proceed by chemical breakdown followed by an oriented development of the new products on the surface of the feldspar. Partially altered flakes were observed to develop a shell of altered material around a core of apparently unchanged feldspar. Glancing-angle photographs of slightly altered flakes were recorded with a flat plate camera and pinhole collimation. No positive evidence was obtained for an oriented development of an alteration product. However, as will be shown in the following section, it was only rarely that claylike products were formed in the experiments with albite flakes. We cannot therefore exclude the possibility that oriented growth may sometimes occur. It can only be stated that we have not so far detected any such effect.

ALTERATION PRODUCTS FROM FELDSPARS TREATED HYDROTHERMALLY WITH 0.1 *N* HCl

Preliminary attempts to alter albite with acid and alkali treatments up to 100° C proved extremely slow. Hydrothermal treatments were therefore applied. Experiments with powdered albite and $H_2O + CO_2$ in a steel bomb at around 400° C yielded a mica-like product, probably of biotite type, and a chlorite-like material, but the products were not well crystallized and there was contamination by reaction with the steel bomb.

All subsequent experiments were carried out with 20 cc gold-lined Morey bombs charged with 10 cc of 0.1 *N* HCl together with the specimen, either a (010) cleavage flake of albite weighing about 10 to 20 mg, or a similar amount of powdered material. In some experiments, the particle size was reduced to less than 5 microns. The bombs were maintained at about 280° C and saturation pressure, or at 420 to 435° C and about 10,000 psi for periods of 2 hours to 52 days. There was a large excess of HCl in these experiments; the initial pH was about 1 and the final pH about 1.2 after a run.

Table 1 summarizes the main experimental results. The product obtained from the flakes was most commonly boehmite, AlO(OH). Kaolinite was obtained in experiment 56 when <5 micron cleavelandite was kept at 285° C for 52 days. In experiment 40, finely powdered Amelia albite after 24 hours at 285° C yielded a rather doubtful kaolin-type mineral. Occasionally the product hydralsite was obtained; this has been described previously by Roy and Osborn (1952, 1954) and appears to have a composition approximating to $2Al_2O_3 \cdot 2SiO_2 \cdot H_2O$. As these authors state, previous workers have probably obtained hydralsite, but have confused it with pyrophyllite. In addition, an unknown product *X* was obtained on several occasions. This yields a rather simple x-ray powder diagram of sharp lines (Table 2). The material has not been identified so far and may possibly be a new phase.

TABLE 1. — ALTERATION OF ALBITES BY HYDROTHERMAL TREATMENTS WITH 0.1 *N* HCl (A = ALBITE FROM AMELIA, VIRGINIA; C = CLEAVELANDITE FROM AUBURN, MAINE)

Expt. no.	Albite	Temp.	Time	Results
I. *Experiments with albite flakes*				
37	C	285°C	2½ days	Boehmite and residual albite.
28	A	285°	17 days	Boehmite, strong sharp x-ray diagram.
55	A	275°	52 days	Boehmite predominant, but diagram less sharp than no. 28. Component showing lines at 7.2, 3.6, 2.65, 1.57 A may be a kaolin-type mineral.
56	C	285°	52 days	Flake disappeared completely; data for powder, see below.
22	A	420°	2 hours	Boehmite; weak unidentified x-ray lines which may be hydralsite; residual albite.
34	C	430°	1 day	Hydralsite, nearly pure; a few additional x-ray lines.
26	A	420°	2 days	Boehmite.
29	A	420°	13 days	Boehmite, strong sharp x-ray pattern.
II. *Experiments with powdered albites*				
40	A, $<5\mu$	285°	1 day	Kaolin mineral, rather doubtful; unknown component, *X*.
55	A, $<5\mu$	275°	52 days	Uncertain product resembling a disordered pyrophyllite.
56	C, $<5\mu$	285°	52 days	Good kaolinite; small amount of boehmite; additional lines not identified including a sharp line at 12.5 A. Also a glassy deposit giving no crystalline pattern.
30	A	435°	1 day	Boehmite and hydralsite in comparable proportions.
31	C	430°	2 days	Unknown *X*; a little boehmite.
38	A	435°	2½ days	Unknown *X*; boehmite; other lines not identified.

Boehmite, AlO(OH); hydralsite, $2Al_2O_3 \cdot 2SiO_2 \cdot H_2O$ (Roy and Osborn, 1954); kaolinite, $Al_2Si_2O_5(OH)_4$; unknown product *X*, x-ray pattern given in Table 2.

DISCUSSION OF THE HYDROTHERMAL RESULTS

The results obtained with the two kinds of albite from Amelia and from Maine are not quite consistent. Also, what is less surprising, the results obtained with flakes and powders are different. The present results may be compared with results obtained by Gruner (1944) who, in certain of his experiments, used conditions closely similar to those employed in the present work. Using a powdered soda feldspar containing 87 percent albite and 0.1 *N* HCl in gold-lined bombs, Gruner obtained after 17 days at 300° C pyrophyllite and some kaolinite and after 14 days at 400° C pyrophyllite and some unchanged feldspar. The pyrophyllite which he recorded may have been the hydralsite which we have observed. Boehmite was seldom observed by Gruner, but this may be attributed to his use of powdered material rather than flakes. It appears that in experi-

TABLE 2.—X-RAY POWDER DATA FOR UNKNOWN PRODUCT, *X*

d, A	I (est.)	d, A	I (est.)
5.95	vw	1.900	w
3.22	s	1.801	vw
3.06	vw	1.664	m
2.770	vs	1.595	m
2.350	m	1.450	vw
2.170	vw	1.425	vw
1.957	vs	1.380	wm

ments of this kind it is rather easy to obtain variable results, probably because all the factors influencing the reactions are not fully appreciated or fully under control.

With the data so far available, it appears that feldspar flakes are changed principally to boehmite, although if the experiment is continued sufficiently long (c.f. Expts. 55 and 56) the boehmite itself may change. Finely powdered materials tend to pass quickly through the boehmite stage, but the full course of the transformation is not yet clear. It appears that unknown *X*, hydralsite, and possibly other products may be intermediates before a clearly recognizable kaolinite is obtained.

A result not brought out in Table 1 is that throughout the experiments with flakes (with Expt. 56 as the only exception) the flakes retained their size and shape during the hydrothermal treatment. They became porous and chalky in appearance, and lost a considerable fraction of their weight. Except for the shortest treatments, the feldspars were completely altered; in cases of incomplete alteration, the inner core remained as unaltered feldspar so far as we could ascertain by x-ray tests (see section on single-crystal tests).

The alteration to boehmite is noteworthy. This mineral may not be the final reaction product but it appears to be a significant stage in the alteration. It is observed more clearly with flakes than with fine powders. The boehmite shows no detectable preferential orientation. It is probably not strictly valid to compare this result with the equilibrium studies of Ervin and Osborn (1951) on the system Al_2O_3—H_2O, according to which we would expect corundum or diaspore as the most likely product under the temperature-pressure conditions of our experiments. However, we do not have the simple Al_2O_3—H_2O system, since HCl, SiO_2, and Na_2O are also present, and in addition it is probable that equilibrium has not been reached in many of the present tests. However, the significant fact is that alumina rather than silica remains behind within the confines of the flake. This appears to rule out entirely any hypothesis which requires that the HCl shall attack the feldspar and form $AlCl_3$ which then hydrolyzes to $Al(OH)_3$ and subsequently transforms to $AlO(OH)$. In one experiment (no. 26 in Table 1), the flake lost 51 percent of its initial weight, and an approximate chemical analysis by Dr. R. C. Vanden Heuvel gave the following data:

	Before treatment	After treatment
Al_2O_3	19.5%	49%
SiO_2	68.7%	16%

This confirms the marked extraction of SiO_2 from the flake by the acid treatment.

The different behavior of flakes and fine powders may be interpreted in terms of a mechanism similar to that considered by Correns (1940) and his co-workers. This has been summarized conveniently by Van Schuylenborgh and Sänger (1950). The outer layer of a weathering particle consists predominantly of the more slowly dissolving components. Dissolution of the components within a particle is then determined by their rates of diffusion through the surface layer. The thickness of the leached layer grows until there is an equilibrium between the rates of diffusion through it and its own rate of dissolution. Under the conditions of the present experiments, it is clear that silica dissolves more readily than alumina from the albite flakes, so that a leached layer deficient in silica, and a concentration of alumina within the flakes, are to be expected. We cannot, however, offer any explanation why boehmite rather than other forms of alumina is the product. In the case of fine powders, however, we may picture the bulk of the material as residing in the surface layer, so that no appreciable segregation of alumina takes place. The whole system then becomes reactive and the products approach equilibrium in considerably less time.

During the course of the experiments described here, Dr. G. W. Morey (1955) of the Geophysical Laboratory, Washington, gave an account (at a meeting of the Geophysical Union) of experiments on the decomposition of albite and microcline by a continuous flow of water at 350° C and 5000 psi for long periods. In the case of albite he recorded the formation of boehmite together with paragonite; analcite was formed at the exit tube from the bomb. The two latter products have been recognized in the present experiments.[1]

ACKNOWLEDGMENTS

We gratefully acknowledge that a grant-in-aid from the Gulf Research and Development Company has made possible the participation of one of us (E. W. R.) in this research and has provided equipment necessary for the work. We also thank Mr. E. W. Westrick of the Dominion Gulf Co., Toronto, who supplied the naturally altered feldspars, and our colleagues Dr. Rustum Roy and Dr. R. C. Vanden Heuvel for assistance with the hydrothermal techniques and chemical analysis respectively. We also thank Dr. G. W. Morey for advance information on his experiment.

REFERENCES

Correns, C. W., 1940, Die chemische Verwitterung der Silikate: Die Naturwiss., v. 28, p. 369-376.

Ervin, Guy, Jr., and Osborn, E. F., 1951, The system Al_2O_3–H_2O: J. Geol., v. 59, p. 381-394.

Goodyear, J., and Duffin, W. J., 1954, The identification and determination of plagioclase feldspars by the X-ray powder method: Min. Mag., v. 30, p. 306-326.

Gruner, J. W., 1944, The hydrothermal alteration of feldspars in acid solutions between 300° C and 400° C: Econ. Geol., v. 39, p. 578-589.

Morey, G. W., 1955, The action of hot water on some feldspars: Abstracts of papers presented at 36th annual meeting of the Amer. Geophys. Union, p. 15.

Morey, G. W., and Chen, W. T., 1955, The action of hot water on some feldspars: Amer. Min., v. 40, p. 996-1000.

Roy, Rustum, and Osborn, E. F., 1952, Studies in the system alumina-silica-water: in Problems of clay and laterite genesis, Am. Inst. Min. Met. Eng., p. 76-80.

[1] Since this was written, a detailed account of these experiments has been published; see Morey and Chen (1955).

Schuylenborgh, J. Van, and Sänger, A. M. H., 1950, On the origin of clay minerals in the soil: Landbouwkundig Tijdschrift, v. 62, no. 4/5.
Tuttle, O. F., and Bowen, N. L., 1950, High-temperature albite and contiguous feldspars: J. Geol., v. 58, p. 572-583.

Paper 3-8

COMMONWEALTH OF AUSTRALIA

COMMONWEALTH SCIENTIFIC AND INDUSTRIAL RESEARCH ORGANISATION

EFFECT OF BIOTITE ON THE FIRING CHARACTERISTICS OF CERTAIN WEATHERED SCHISTS

By K. NORRISH and E. W. RADOSLOVICH

Reprinted from *Clay Minerals Bulletin*
Vol. 3, No. 18, Pages 189-192

Reprinted from Clay Minerals Bulletin, Vol. 3, No. 18

EFFECT OF BIOTITE ON THE FIRING CHARACTERISTICS OF CERTAIN WEATHERED SCHISTS

By K. NORRISH and E. W. RADOSLOVICH
Division of Soils, C.S.I.R.O., Adelaide, South Australia.

[Read 13th April, 1957.]

ABSTRACT

A study was made of five clays used for brickmaking to determine the reason why certain clays crumbled on firing. Partially weathered biotite was found to be a constituent of the clays which crumbled and the crumbling was due to this mineral exfoliating and so disrupting the bricks at a comparatively low temperature. Fresh biotite and highly weathered biotite do not have this adverse effect.

INTRODUCTION

The present investigation was concerned with the problem of why certain clays used by the Onkaparinga Brickworks, South Australia, crumbled on firing while adjacent clays were satisfactory.

To enable a mineral comparison to be made between the satisfactory and unsatisfactory clays five samples were taken from the quarries of the Onkaparinga Brickworks and the following are notes on their firing characteristics.

No. 78. White fireclay. Short and friable. Very refractory with a low shrinkage on firing. Used for blending with the materials for making bricks. No. 119. Red clay. Good strong clay which binds well and is moderately plastic. Medium shrinkage on firing. Fuses at 1350°C. Makes satisfactory bricks. No. 120. Decomposing fine grained mica schist. Less plastic than 119 but binds fairly well. High shrinkage on firing. Fuses at 1200°C. Good for making bricks. No. 203. Decomposing fine grained mica schist. Rather short. Does not bind and tends to crack on drying. Crumbles on firing. Useless for brickmaking. No. 204. Decomposing fine grained mica schist. Coarser texture but behaviour similar to 203.

According to Gaskin and Samson (1951) the white clay, 78, "is a bed of decomposed slate, 75 ft. thick, occurring between two beds of mica schist, and forms part of the Middle Adelaide Series." Sample 119, a soil, overlies 204, 203 and 120 in that order; the clay, 78, is 100 yards away.

Results

The results of laboratory analyses are recorded in Tables 1-3 inclusive. The X-ray data are in good agreement with the chemical analyses. Table 4 gives the approximate mineral composition of the samples, calculated from the data of Tables 1-3. X-ray diffraction patterns of the mica present in the schists indicate the presence of biotite. However, chemical and physical data indicate that the

Table 1—Particle size analyses.

Size in microns	(Sample number with % material in each grain-size)				
	78	119	120	203	204
2000–200	0·20	0·36	2·00	0·84	29·44
200– 20	59·44	18·08	56·76	86·80	60·24
20– 2	29·76	22·38	36·02	9·37	7·22
<2	7·24	55·90	4·17	4·75	3·35
Moisture loss % (at 110°C)	0·25	3·10	1·10	0·45	0·60

Table 2—Chemical analyses.

	78	119	120	203	204
SiO_2	73·11	70·13	59·08	61·87	64·13
Al_2O_3	18·38	15·64	19·30	17·21	18·10
Fe_2O_3	0·40	5·45	4·19	6·19	5·82
FeO	—	0·16	1·82	0·94	0·29
MgO	0·18	0·16	5·13	4·34	2·51
CaO	0·04	0·20	—	0·04	0·04
Na_2O	trace	0·29	0·62	0·26	0·34
K_2O	—	0·43	2·46	2·51	2·26
TiO_2	1·46	1·19	1·57	1·24	1·09
SO_2	—	0·02	0·02	0·01	—
Cl	—	—	0·03	0·02	0·03
H_2O+	6·63	6·22	5·77	5·38	5·12
Total	100·20	99·89	99·99	100·01	99·73

Analyses by Assay Dept., School of Mines, S. Australia.

micas have undergone varying degrees of weathering. Chemically, some of the micas are altered from biotite in that most of the iron has been oxidised to the ferric state; there has probably been a loss of potassium also, coupled with some hydration. Physically the micas have changed so that the flakes from 204 are golden coloured, soft and pliable. (Golden micaceous flakes represent an early stage in the weathering of biotite, (Walker, 1949) hydration not having proceeded sufficiently to increase the interlayer spacing beyond

10 Å). This mica is termed "weathered biotite" in Table 4. Where weathering and hydration have proceeded sufficiently to increase the interlayer spacing to about 12 Å, the mica is termed hydrobiotite.

All the mica of the coarse sand of sample 204 is weathered biotite while the mica of the same fraction of No. 203 contains only a small percentage of golden flakes and in No. 120 it is practically absent. The ratio of ferrous iron to total iron in the samples also suggests that the biotite of sample 204 has weathered more than that in No. 203 and this more than that of No. 120. The golden flakes of

TABLE 3—X-ray diffraction analyses of separate size fractions.

	78	119	120	203	204
Whole sample	K c Q c	K c Q c	K c M c Q c	K c M c Q c	K c M c Q c
200–20μ		Q c	Q c M c K l C m	Q c M c K l C ?	Q c M c K m
<20μ	K	K c H m Q<5%	K c H l M l Q<5%	K c H l M l Q<5%	K c H l M l Q<5% G l
<2μ	K	K c S l H l	K c S m H l M l Q 2%	K c S m H l M l Q 2%	K c G l H l M l Q 2%

K=kaolinite S=montmorillonite G=goethite
M=mica Q=quartz H=hydrobiotite
C=chlorite m=moderate
c=considerable amount l=little

weathered biotite exfoliated on heating and Table 5 shows the increase in volume of some 200-20μ fractions when rapidly heated to 850°C. The volume increase in these samples appears to depend on their weathered biotite content.

Walker (1949) has studied weathered biotites, similar in many respects to these, which also exfoliate on heating. Furthermore, many of the Australian commercial "vermiculites" studied by the authors were found to be biotites in an early stage of weathering. They expanded greatly on heating but had an ignition loss only a little greater than that of biotite.

The mechanism of exfoliation restricts the phenomenon to particles of moderate particle size so that silt and clay size micaceous minerals do not exhibit exfoliation. For this reason the hydro-biotite which is in the finer fractions of the samples, would not be expected to cause any volume increase on heating.

The properties of the samples can now be viewed in relation to their mineralogy. The high kaolinite content of sample 78 is consistent with it being a good fireclay. The good binding and plasticity of No. 119 is due to the high clay content (partly montmorillonite).

TABLE 4—Approximate mineralogical composition of samples in per cent.

	78	119	120	203	204
chlorite	—	—	15	5	—
biotite	—	—	34	20	—
weathered biotite	—	—	—	20	40
hydro-biotite	—	15	10	5	5
montmorillonite	—	5	1	—	—
kaolinite	47	45	15	20	25
quartz	52	35	25	30	30
goethite	—	—	—	—	2

TABLE 5—Volume increase on rapid heating in per cent.

	120	203	204
Increase in volume	3·2	8·6	13·4
Weight loss on ignition	3·5	4·5	4·0

Samples 120, 203 and 204 have low clay contents with correspondingly poor plasticities. The crumbling on firing of samples 203 and 204 is due to the exfoliation of the weathered biotite. Since this volume increase takes place below 800°C (*i.e.*, before there is any sintering) the expanding flakes are able to disrupt the mould while it is mechanically weak. On the other hand the mica of sample 120 has not weathered sufficiently to give a serious volume change on heating.

It appears from this study that both the relatively unweathered and the highly weathered schists form suitable raw material for brick-making, whilst the partially weathered schists are unsuitable.

Acknowledgement.—We wish to thank Mr H. Ellerton, of the Cement and Ceramics Section, C.S.I.R.O., who brought this problem to our notice, and who provided the notes on firing characteristics.

REFERENCES

Gaskin, A. J. and Samson, H. R. 1951. *Bull. geol. Surv. S. Aust.*, (28).
Walker, G. F. 1949. *Miner. Mag.*, **28**, 693.

COMMONWEALTH SCIENTIFIC
AND INDUSTRIAL ORGANIZATION
Reprinted from 'JOURNAL OF SOIL SCIENCE'
Volume 9, No. 2, Pp. 242–251, September 1958

CLAY MINERALOGY OF SOME AUSTRALIAN RED-BROWN EARTHS

By

E. W. RAOSLOVICH

(Division of Soils, Commonwealth Scientific and Industrial Research Organization, Waite Institute, Adelaide, South Australia)

OXFORD
AT THE CLARENDON PRESS
Subscription (for 2 numbers) 30s. post free

CLAY MINERALOGY OF SOME AUSTRALIAN RED-BROWN EARTHS

E. W. RADOSLOVICH

(*Division of Soils, C.S.I.R.O., Waite Institute, Adelaide, South Australia*)

Summary

The clay mineralogy of Australian red-brown earths has been investigated by X-ray diffraction techniques supported by chemical analyses.

A brief description of the morphology of this group of soils is given, and their geographical distribution indicated. Profiles have been studied from each of the major areas in which red-brown earths are found.

A large number of samples were examined by X-ray diffraction. The results showed relatively little variation in clay mineralogy from one profile to another, or from one horizon to another within a profile. The dominant clay minerals in typical red-brown earths in southern Australia are illite and kaolin, but in Queensland kaolin predominates.

Chemical data (cation-exchange capacity, SiO_2:Al_2O_3 ratio) are consistent with the X-ray results. There is evidence, however, that the illites in these soils are deficient in structural potassium, having K contents between 2·5 and 4·1 per cent. K approximately. There is a consequent increase in the exchange capacity of these 'degraded' illites.

The variations in the clay mineralogy of these soils appear to depend mainly on the parent materials from which the soils are derived. Those red-brown earths developed on alluvial and similar materials contain more illite than kaolin; those soils developed on materials such as granite, granodiorite, and basalt contain mainly kaolin in the clay fraction.

PRESCOTT (1944) has discussed the distribution of red-brown earths in Australia, with special emphasis on South Australia, Victoria, and New South Wales. Representatives of the group are also found in Queensland. The suggested distribution is from tropical to sub-temperate regions over a range from 20° to 45° S. latitude. Prescott states that red-brown earths 'occur in zones of seasonal rainfall, whether of the Mediterranean type with rain in winter, or of the tropical type with rain in summer. At the height of the wet season, however, conditions are such that leaching is effective for a limited period.' These soils typically carry open savannah woodland vegetation, and are generally found in a zone with an annual rainfall between 14 and 25 in. The average daily mean temperature ranges from 60° to 75° F.

The morphology and chemistry of a number of red-brown earths from southern Australia have been described in detail by Piper (1938), Smith *et al.* (1943), Stephens *et al.* (1945), Smith (1945), Downes (1949), and Aitchison *et al.* (1954). The group has been compared with the reddish chestnut soils of the U.S.A. by Smith (1949) and Stephens (1950). Their relationship with other Australian soils has also been discussed by Stephens (1956).

Red-brown earths have a characteristic morphology. The A horizon is invariably brown to red-brown in colour, but may vary in texture from

sand to clay loam, with loams predominant. This horizon varies in depth from 6 to 24 in., but is commonly around 12 in. deep. There is a marked texture contrast between the A and B_1 horizon, which is always brighter and redder than the A horizon. The texture of the B_1 horizon is most commonly clay, but is occasionally sandy clay. The B_2 horizon consists of similarly-textured material, generally browner in colour and containing slight to large amounts of lime in soft or concretionary form,

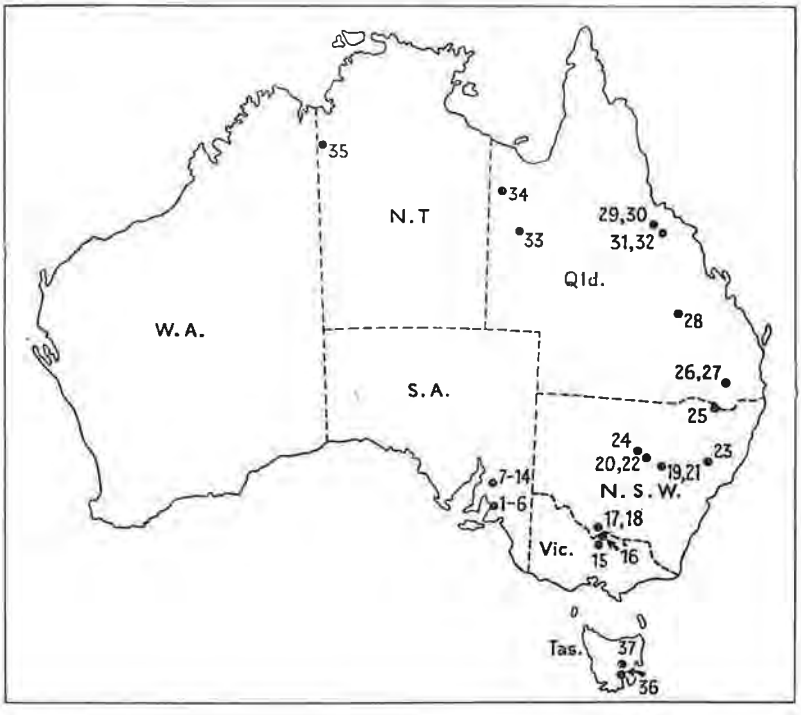

FIG. 1. Sketch map of Australia showing approximate locations of soils studied.

or both. The lime of the B_2 horizon usually persists into the C horizon. The C horizon, which often begins between 40 in. and 50 in. from the surface, consists of parent material of very diverse character. This may be either sedimentary or igneous rock, alluvium or colluvium, calcareous or non-calcareous. Chemical data reported by Piper (1938) for a number of red-brown earths in South Australia appear to correspond with data for red-brown earths from other localities, including those soils studied here.

Soil Profiles Studied

Soil samples taken from various horizons in 37 red-brown earth profiles have been studied. The geological origins of these profiles are described in Table 1 and their approximate geographical locations are shown in Fig. 1.

TABLE 1

Description of Some Red-brown Earth Profiles Studied

Profile no.	*Description*	*Approximate location*	*Soil no.*	*Leaching index*	*Parent material and reference*
1	Urrbrae fine sandy loam	Adelaide, S.A. (Waite Institute)	12721–6	1·18	Developed on an alluvial-colluvial apron derived mainly from adjacent Pre-Cambrian slates, shales, and quartzites. Aitchison *et al.* (1954).
2–6	..	Adelaide, S.A.	..	0·88	..
7	Light Pass fine sandy loam	Barossa Valley, S.A.	15144–9	1·01	Pleistocene to Recent proluvium derived from Pre-Cambrian calcareous rocks. Northcote *et al.* (1954).
8–12	..	Barossa Valley, S.A.	..	1·00	..
13	..	Clare, S.A.	3743–7	1·06	Developed on Pre-Cambrian shales, slates or schists or on alluvial material from same. Piper (1938).
14	Belalie loam	Booboorowie, S.A.	3805–9	1·06	On colluvial and older alluvial material; rocks of area are Pre-Cambrian in age. Piper (1938).
15	Lemnos loam	Dookie, Vic.	V6188–93	1·11	Fine-grained Tertiary alluvium. Downes (1949).
16	..	Barooga, N.S.W.	11423–8	1·11	Sedimentary material of river plains of western N.S.W.
17	Finley loam	Berriquin, N.S.W.	10300–8	0·68	Sedimentary fine channel deposits of 'prior streams'.
18	Deniboota loam light profile phase	Deniliquin, N.S.W.	13464–72	0·68	Solonchakous parent sediments laid down by 'prior streams'. Johnston (1953).
19	..	Trangie, N.S.W.	11700–4	0·70	Fine-grained alluvium.
20	..	County Narromine, N.S.W.	16204	0·59	On late Pleistocene alluvium.
21	..	Trangie, N.S.W.	16191	0·70	Fine-grained alluvium.
22	Summervale clay loam	Nyngan, N.S.W.	16168–73	0·59	Pleistocene alluvial deposits derived from metamorphosed Silurian sedimentary rocks.
23	Overton loam	Muswellbrook, N.S.W.	12891–5	0·97	Upper Coal Measures, Branxton Beds.
24	..	County Oxley, N.S.W.	17871–7	0·59	Pleistocene alluvium.
25	..	Dirranbandi, Qld.	16546	0·74	..
26	Oakey area red-brown earth	Jondaryan, Qld.	9887–9	1·12	Transported material, partly basaltic in origin.
27	Oakey area red-brown earth	Jondaryan, Qld.	16559–65	1·12	Alluvium of mixed origin, some from basalt, mostly from Mesozoic sedimentaries, silty and calcareous sandstones.
28	..	Springsure, Qld.	16886–90	0·91	..
29	Towers sandy loam (deep solum)	Charters Towers, Qld.	16554–8	0·85	Granodiorite mass intruded by some basic rocks as dykes.
30	Towers sandy loam (deep solum)	Charters Towers, Qld.	13156–9	0·85	On an acidic granite exposure.
31	Dalrymple sandy loam (*c*)	Burdekin Valley, Qld.	16549–53	1·25	Fine-grained basic igneous rock, probably of a dyke swarm through a granitic-dioritic mass.
32	Dalrymple loam	Lower Burdekin Valley, Qld.	14812–17	1·25	Low stony rises underlain by metamorphic sediments intruded by basic dykes.
33	Equivalent to Georgina r.b.e.	21° 48′ S., 138° 55′ E. (Kallala H.S.), Qld.	14020–3	0·38	Moderate textured basic alluvium.
34	Equivalent to Gulf Alluvial r.b.e.	On Riversleigh-Lawn Hill Road, Qld.	14050–3	0·38	Basic alluvium.
35	..	17° 37′ S., 127° 37′ E. (Hall's Creek—Wyndham Rd.), N.T.	15546–8	0·53	Biotite granite.
36	Kimbolton clay loam	County Buckingham, Tas.	12022-5	1·69	Residual and colluvial material, from dolerite intrusion of Jurassic Age, in form of dykes and sills.
37	..	Brighton, Tas.	16945–7	1·69	Jurassic dolerite.

Soils selected by Dr. C. G. Stephens, Soil Survey and Pedology Section, Division of Soils, C.S.I.R.O.

Prescott (1949) has suggested the use of a climatic index as an indication of the leaching factor in soil formation. This index takes the form

$$P/E^m,$$

where P = annual rainfall in inches,

E = annual evaporation from a free water surface in inches,

and the value of the exponent m is determined experimentally. The best value of m appears to be about 0·75.

The values of this index reported in Table 1 have been calculated from data taken from *Climatic Averages, Australia*, prepared by the Bureau of Meteorology, Melbourne. There are meteorological stations reasonably close to most of the profiles studied. Profiles 1 to 24 in south-eastern Australia occur in climatic areas which are either cool with winter rains, or have moderate temperatures and uniform rains. The northern profiles, i.e. 25 to 35, are subject to moderate to high temperatures, with predominantly summer rains.

Several profiles were examined in the Adelaide area, and also in the Barossa Valley, S.A.; only one profile is described for each area, since the variation within a given area is small. Individual descriptions of relief have not been given since all the profiles studied are found on flat or gently sloping land.

The soils examined were chosen as typical red-brown earths, and included representative profiles from the major areas in which these soils have been mapped.

X-ray Studies

The X-ray diffraction methods used were similar to those described by Brindley (1951). Soil suspensions were prepared by dispersion, using sodium-hexa-meta-phosphate ('Calgon') and sodium hydroxide; no acid pretreatment was used during the dispersion procedure (Hutton, 1955). A clay-sized fraction ($< 2\mu$) was sampled by a pipette after a suitable sedimentation period. Care was taken to wash the pipette samples thoroughly before adding calcium chloride to Ca-saturate the clays; otherwise a significant amount of amorphous calcium phosphate may be precipitated with the clay fraction. Powder specimens (in cellulose-acetate tubes) and oriented-flake specimens were prepared from the suspensions; the flakes were usually saturated with glycerol. Where necessary various pretreatments were used (e.g. heating to 500° C.; H_2O_2 treatment for removing organic matter; reduction with H_2S to remove free iron oxide).

A 5·73-cm. diameter powder camera was used, in which there is no effective air-scatter up to 30Å. The minerals were usually identified by comparison with standard patterns set up in this laboratory.

Normal kaolin, illite, and montmorillonite were readily identified, but sometimes an oriented-flake (air-dry or glycerol-saturated) gave continuous central scattering from approximately 10Å up to 30Å (limit of camera). This cannot at present be ascribed to any particular mineral, and has been termed 'mixed-lattice minerals' in Table 2. This does not, however, preclude the possibility that the scatter is associated with minerals already identified, in particular with illite.

The results of the X-ray diffraction analysis of these soils (195 samples) are summarized in Table 2. These results are not reported in detail as most profiles show no significant variation in clay minerals with increasing depth. Furthermore the results from a number of profiles

are closely comparable, and hence are not recorded separately. Diffraction photographs show that many soils contain calcite, quartz, and iron oxide in small amounts. Generally the amount of well-crystallized iron oxide present is insufficient to identify it more specifically, though both

TABLE 2

X-ray Analyses of Some Red-brown Earths (< 2μ fraction)

Profile	*No.*	*Horizon*	*Depth (in.)*	I	K	M	M.L.	*Others*	*Comments*
1	12723	B_1	13–30	mod.	l.	..	..	Chlorite?	Chlorite increasing with depth.
2–6 Similar.									
7	15147	B_1	12–27	m.	mod.	..	l.	..	..
8, 9, 14, 21, and 24 Similar.									
13	3745	B_1	10–20	m.	mod.	..	l. to mod.	..	M.L. increasing slightly with depth, in general.
10, 11, 12, 15, 16, 17, 19, 20, and 22 Similar.									
18	13469	B	19–24	mod.	l.	l.	mod.	..	M. increasing with depth, but absent in surface soils.
23	12893	B_1	8–16	mod.	mod.	..	..	Chlorite or vermiculite?	..
25	16546	..	24–27	m.	mod.	l.	..	..	M. not well crystallized.
26	9889	B	18–33		m.	..	l.	..	Probably kaolinite.
27 Similar.									
28	16889	B	24–30	..	v.m.	?	l.	..	K. probably partly hydrated halloysite.
29	16555	B	6–18	l.	m.	..	l.	..	K. mineral similar to halloysite or 'fireclay'.
30	13158	B	13–19	..	m.	..	l.	..	K. probably halloysite.
31 Similar.									
32	14814	B_2	8–23	..	m.	..	mod.	..	K. probably halloysite.
33	14022	B	18–24	mod.	mod.	mod.	l.	..	M. increasing, and M.L. decreasing depth.
34	14052	BC	20–27	l.	m.	..	?	..	..
35	15548	BC	26–34	..	m.	mod.	l.	Chlorite or vermiculite (l.)	..
36	12024	B	8–13	..	..	mod.	l.	..	M. does not give very sharp basal spacing.
37	16947	B	9–18	..	l.	l.	mod.	..	K. probably halloysite.

I, illite; K, kaolin (specific minerals of this group identified where possible); M, montmorillonite; M.L., mixed-lattice minerals; v.m. very much, > 80%; m., much, 50–80%; mod., moderate, 20–50%; l., little, 10–20%; v.l., very little, 2–10%; tr., trace, 2% (these percentages very approximate); ?, identification doubtful.

haematite and goethite have been found in red-brown earths. These minerals are omitted from Table 2.

The X-ray results show that the dominant clay minerals in typical red-brown earths in South Australia, Victoria, and New South Wales are illite and kaolin, with the former representing from 40 to 60 per cent. of the < 2μ fraction (profiles 1 to 18). The dominant clay mineral present in the red-brown earths from eastern Queensland is kaolin, and this appears to be kaolinite in the south but a 'fireclay' or halloysite in the Charters Towers area. One soil from western Queensland, one from

Northern Territory and one from Tasmania contain montmorillonite as a major component.

Chemical Data

The cation-exchange capacities (at pH 8·4) for 90 soils have been obtained from the records of this Division. Data which were obviously affected by the presence of organic matter were disregarded in relating the cation-exchange capacity of the clay fraction of the soil to clay mineral composition. The method used to determine the sum of the metal ions and exchangeable hydrogen was essentially that described by Piper (1942). The data are given in a histogram (Fig. 2).

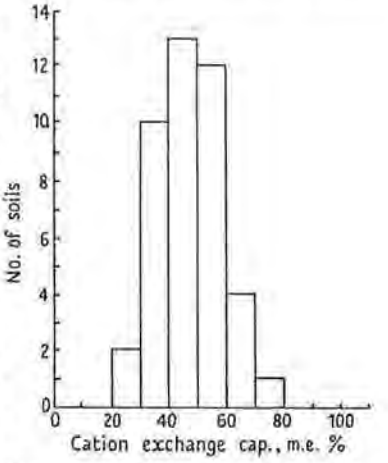

FIG. 2. Histogram of cation-exchange capacities (m.e. per 100 g clay) of some Australian red-brown earths. The data for two horizons only from any one profile are included here; they are taken from the records of the Soil Chemistry Section, Division of Soils, C.S.I.R.O.

These data are consistent with the X-ray results, since the presence of 'mixed-lattice' minerals (including 'degraded' illite) would raise the exchange capacities of both the soils which are illite-kaolin mixtures, and the soils which are predominantly kaolin, to values between 30 and 60 m.e. per 100 g. of oven-dry clay.

Piper (1938) has shown that the molecular ratios of SiO_2 to Al_2O_3 for the clay fraction of a number of red-brown earths in South Australia generally lie between 2·90 and 3·40. The present study has shown that for red-brown earths in the same area (including two profiles examined by Piper) the clay fractions are composed of 60–70 per cent. illite, 20–30 per cent. kaolin, and a little mixed-layer mineral. A mixture of 70 per cent. illite and 30 per cent. kaolin has a $SiO_2:Al_2O_3$ ratio of 3·10 approximately, and the X-ray analyses are therefore in general agreement with the chemically determined ratios of $SiO_2:Al_2O_3$.

Piper also reported that these soils show a strong correlation of K_2O content with the quantity (clay percentage $+\frac{2}{3}$ silt percentage). X-ray studies show that illite is the only mineral present in the clay fraction which contains potassium. The above calculation thus suggests that the proportion of illite in the clay fraction remains fairly constant since the ratio of silt to clay is usually below 1 : 4.

Potassium Content of Illitic Minerals in Some Red-brown Earths

Recently a number of workers (e.g. Grim *et al.* (1949), Vivaldi and Garcia (1955), and Droste (1956)) have reported finding 'degraded illite', which Grim (1953) describes as 'material which has been partially leached of its constituent alkalis and alkaline earths, but not sufficiently to transform it into new minerals'. Droste records that the X-ray pattern of such material shows 'asymmetry on the high side of the 10Å peak, and

the loss of this asymmetry in the heated and glycolated slide implies that some of the illite layers are now hydrated'. Such material should not show the further reflections which characterized either regularly or randomly interstratified minerals, but may show increased central scatter.

The potassium content of the illite described by Grim *et al.* (1937) lies between 5 and 6 per cent. If all illites contained this proportion of potassium then the potassium content of an illite-kaolin mixture should be directly proportional to the amount of illite present. Since illites appear to vary in potassium content, however, this direct relationship does not always hold. For illites in some solonized brown soils in

TABLE 3

Potassium Content of Illite in Some Red-brown Earths

	Clay fraction		*Calculations*		*X-ray*
Soil no.	*K* (%)	*Ex. Cap* (*m.e.* %)	*K in Illite* (%)	*Illite* (*y*) (%)	*Illite* (*y*) (%)
3745	2·1	46	3·4	61	70
3807	2·4	40	3·8	63	70
10302	2·2	39	3·9	58	70
11425	3·4	40	4·1	82	90
12893	1·7	34	3·8	43	50
13466	2·4	46	3·6	68	80
14051	0·7	40	2·5	30	25
12723	1·7	50	3·0	58	70

Cols. 2–5 were recalculated from data supplied by Mr. A. D. Haldane and Mr. J. T. Hutton, Division of Soils, C.S.I.R.O.

Australia, Norrish (1949) has suggested that the following approximate relationship holds between exchange capacity and potassium content:

potassium content + exchange capacity = a constant.
(m.e. per cent.)* (m.e. per cent.)

This constant was of the order of 150 m.e. per cent. for illites in these soils, and has been assumed to be of the same order for the red-brown earths.

This relation was used as follows by Mr. A. D. Haldane† and Mr. J. T. Hutton† to determine the proportion (y) of illite, and also the potassium content (K_I) of this illite, in eight red-brown earths examined by X-ray diffraction by the author.

$$C_s = 20(1-y)+150y-K_s,$$
$$K_s = K_I.y,$$

where C_s = exchange capacity of the clay sample,
K_s = potassium content of the sample in m.e. per cent.,
and 20 m.e. per cent. is accepted as the exchange capacity of kaolin.

The values obtained for K_I from the chemical data (Table 3) lie between 2·5 per cent. and 4·1 per cent. K. The values of the illite

* Milli-equivalents per 100 g. clay. † Chemist, Division of Soils, C.S.I.R.O.

content estimated from the X-ray patterns are included for comparison with values of y calculated from chemical data. The soils in Table 3 were chosen because their X-ray patterns indicate that they are essentially illite-kaolin mixtures showing only some central scatter in addition to the lines normally due to illite and kaolin. (It should be noted that the presence of moderate amounts of minerals other than illite and kaolin will invalidate the above approximate relationships.) The agreement between the two values of the illite content is reasonable for these soils, suggesting that they contain illite deficient in potassium.

Foster (1954) has emphasized that removal of potassium from illite does not immediately change it to montmorillonite. It is therefore not unreasonable to suppose that some illites occurring in soils may give the standard illite pattern without additional lines, even though they are partially leached of potassium. The above results suggest that this is the case for some Australian red-brown earths. The exchange capacities of such illites will be rather higher than that for illite containing 5 to 6 per cent. potassium.

Pedogenesis

The two principal factors influencing the clay mineral composition of these soils are parent material and climate, since the drainage status is uniformly good for the red-brown earths. Of these the climate will probably be the less important. Prescott (1949) suggested that the index $\frac{P}{E^{0\cdot75}}$ assumes values* between 0·74 and 1·43 for red-brown earths. This study has shown that for red-brown earths in South Australia, Victoria, New South Wales, and eastern Queensland (profiles 1 to 32) the leaching index $\frac{P}{E^{0\cdot75}}$ ranges from 0·59 to 1·25. It is interesting to observe that all these soils have values of Prescott's leaching index within the same range, even though the average daily mean temperature and the annual rainfall figures are somewhat higher in eastern Queensland. Variations in the clay mineralogy of red-brown earths in these areas (which are the major occurrences of this soil group) do not, therefore, appear to be due to variations in climate from one profile to another.

On casual inspection of the X-ray data the proportion of kaolin in the $< 2\mu$ fraction appears to increase with mean annual temperature. On closer examination, however, this is seen to be due to a fortuitous correlation between mean annual temperature and parent material.

Parent material is undoubtedly the main factor in determining the clay mineralogy of Australian red-brown earths. Those soils which are formed on the alluvial, sedimentary, and/or loessial deposits of the river plains extending inland from the Mt. Lofty Ranges in South Australia, and from the Great Dividing Range in Victoria and New South Wales, have clay fractions which are very largely mixtures of illite and kaolin. The relative proportions of the two minerals are fairly constant, both

* Prescott (1949) used an exponent $m = 0\cdot70$, giving limits 0·92 to 1·70 for these soils. He has since recommended $m = 0\cdot75$ as a better value, and for this exponent the limits are approximately 0·74 and 1·43.

within a given profile and from one profile to the next. Red-brown earths formed on other parent materials—granite, granodiorite, basalt, basaltic alluvium—show quite different clay mineralogy. Kaolin is the dominant clay mineral of these soils, whereas illite has not in general been observed as a major component. This is probably because these parent materials are unable to contribute sufficient potassium for the formation of illite.

Profiles 33 to 37 need further discussion. The two profiles in western Queensland (33 and 34) show some illite, and 33 shows montmorillonite. These soils have the typical morphological features of the red-brown earth group. Their parent materials ('basic alluvium') are not known precisely enough to explain the presence of illite, which is rather unexpected; but they must contribute a little potassium during weathering, which is not removed by the lower than usual degree of leaching these two profiles experience.

After the X-ray data were obtained the field descriptions for profiles 35 to 37 were re-examined, and it was found that all three soils are doubtful red-brown earths. The northern profile 35 was sampled in an area where there are no soils with clearly defined texture contrasts, though red earths and skeletal red soils are reported. The two Tasmanian soils, 36 and 37, which Prescott (1944) mapped as red-brown earths, have recently been remapped as brown earths. They also have leaching indices significantly higher than is usual for red-brown earths. It is therefore interesting that of the thirty-seven profiles studied these two alone contain only a little kaolin and in addition do not contain illite at all.

Practically all of the profiles examined show clay-mineral compositions which are fairly constant with increasing depth. The climatic and leaching conditions under which the red-brown earths are generally formed apparently have been insufficient to cause much weathering of the clay minerals in the profile even though they have caused the profile development.

It is not possible from the results of the present study to relate the clay mineralogy of the particular red-brown earth profiles more closely to their parent materials than has been attempted here, since the original samples did not include samples of the parent materials. In addition the sediments, &c., which form the parent materials of many red-brown earths are themselves ill defined and heterogeneous.

Acknowledgements

The author acknowledges with thanks the advice and assistance of various officers of the Division of Soils during the course of this work, particularly Mr. J. K. Taylor, Dr. K. Norrish, and Mr. J. T. Hutton for helpful criticism, and Mr. J. Pickering for technical assistance in the X-ray studies.

REFERENCES

Aitchison, G. D., Sprigg, R. C., and Cochrane, G. W. 1954. Dept. of Mines, South Australia, Bull. 32.

BRINDLEY, G. W. (Ed.) 1951. X-ray Identification and Crystal Structures of Clay Minerals. Mineralogical Society, London.
DOWNES, R. G. 1949. Coun. Sci. Ind. Res. (Aust.), Bull. 189.
DROSTE, J. B. 1956. Bull. Geol. Soc. Amer. **67**, 916.
FOSTER, Margaret D. 1954. Proc. 2nd Nat. Conf. on Clays and Clay Minerals, p. 386. (Nat. Res. Coun., Wash., U.S.A.)
GRIM, R. E., BRAY, R. M., and BRADLEY, W. F. 1937. Amer. Min. **22**, 813.
—— DIETZ, R. S., and BRADLEY, W. F. 1949. Bull. Geol. Soc. Amer. **60**, 1785.
—— 1953. Clay Mineralogy, p. 352. McGraw-Hill, N.Y.
HUTTON, J. T. 1955. C.S.I.R.O. (Aust.) Div. Soils Div. Rep. 11/15.
JOHNSTON, E. J. 1953. C.S.I.R.O. (Aust.) Soil Pub. No. 1.
NORRISH, K. 1949. (Unpublished report.)
NORTHCOTE, K. H., RUSSELL, J. S., and WELLS, C. B. 1954. C.S.I.R.O. (Aust.), Div. Soils, Soils and Land Use Series No. 13.
PIPER, C. S. 1938. Trans. Roy. Soc. Sth. Aust. **62**, 53.
—— 1942. Soil and Plant Analysis, p. 185. Univ. Adelaide.
PRESCOTT, J. A. 1944. Coun. Sci. Ind. Res. (Aust.), Bull. 177.
—— 1949. J. Soil Sci. **1**, 9.
SMITH, R., HERRIOT, R. I., and JOHNSTON, E. J. 1943. Coun. Sci. Ind. Res. (Aust.), Bull. 163.
—— 1945. Coun. Sci. Ind. Res. (Aust.), Bull. 189.
—— 1949. Soil Sci. **67**, 209.
STEPHENS, C. G., HERRIOT, R. I., DOWNES, R. G., LANGFORD-SMITH, T., and ACOCK, A. M. 1945. Coun. Sci. Ind. Res. (Aust.), Bull. 188.
—— 1950. J. Soil Sci. **1**, 123.
—— 1956. A Manual of Australian Soils. 2nd ed. C.S.I.R.O. (Aust.), Melbourne.
TREWARTHA, G. T. 1943. An Introduction to Weather and Climate. McGraw-Hill, N.Y.
VIVALDI, J. L. M., and GARCIA, S. G. 1955. An. Edafol. Fisiol. **14**, no. 2.

(*Received 12 November 1957*)

PRINTED IN
GREAT BRITAIN
AT THE
UNIVERSITY PRESS
OXFORD
BY
CHARLES BATEY
PRINTER
TO THE
UNIVERSITY

Reprinted from the *Journal of Scientific Instruments*, VOL. 39, pp. 559–563, NOVEMBER 1962

A curved-crystal fluorescence X-ray spectrograph

K. NORRISH and E. W. RADOSLOVICH
Division of Soils, Commonwealth Scientific and Industrial Research Organization, Adelaide, South Australia

MS. received 13*th March* 1962, *in revised form* 7*th August* 1962

This curved-crystal fluorescence x-ray spectrograph has been used successfully for about eight years as a routine analytical instrument; its performance compares favourably with other spectrographs. Several novel features of the design so simplify the instrument mechanically that it can be constructed inexpensively by workshops with modest facilities. The sample is placed near the analysing crystal, rather than on the focusing circle. This avoids the usual need for the precise relative movement of both detector and sample (or detector and crystal); accurate movement of the detector alone is required. The geometry allows this to be achieved quite simply—an ordinary centimetre scale being linearly related to wavelengths.

The practical performance is discussed with particular reference to the associated x-ray and counting equipment.

1. Introduction

A focusing fluorescence x-ray spectrograph has been used very successfully in these laboratories for about eight years for the elemental analysis of a variety of materials. The instrument has operating characteristics which compare favourably with those of other designs in common use. Moreover it possesses some novel mechanical features which make it possible for a workshop with only modest facilities to construct a similar spectrograph simply and inexpensively. The counting equipment may be obtained commercially.

2. Geometrical design

Birks and Brooks (1955) have discussed two designs of spectrographs using curved crystals in the reflecting position. In their designs a small sample is placed at the correct position on the focusing circle, or alternatively a larger sample is mounted behind a slit in this position. The detector is then placed on the focusing circle symmetrically opposite the sample. Adler and Axelrod (1956) used a similar geometry for analysing small samples. Indeed any *very* small sample must be placed on the focusing circle to obtain sufficient sensitivity. A larger sample, however, can be placed with advantage nearer the crystal without loss of sensitivity, and this is the arrangement used here.

Sandstrom (1934) pointed out that fluorescence radiation will be correctly focused by a curved crystal for a sample placed anywhere between lines C_1S and C_2S (figure 1). A line source S may therefore be replaced by an extended source S_1S_2. There is then no loss of sensitivity provided that the sample S_1S_2 occupies the whole angle C_1SC_2 and that all of S_1S_2 is irradiated as brightly as the corresponding line sample S would have been. Since most x-ray tubes provide beams of several square centimetres quite close to the window these conditions may easily be met. In the present instrument a larger sample is placed close to the crystal because of the several inherent advantages of this geometry (Radoslovich 1951), viz.:

(i) The sample now subtends a considerable angle at C enabling quite a range of wavelengths to be recorded without moving S_1S_2. This is practically essential if a range of wavelengths is to be recorded simultaneously on a film in a cassette placed along the focusing circle. However, this geometry also considerably simplifies the mechanical design if counting techniques are used. In order to scan the spectral lines of several neighbouring elements, *only* the detector need be moved. Moreover it is not at all necessary to locate an extended specimen with precision, provided that it is in the (broad) primary beam. Other designs—both for curved or flat crystals—require the precise location of the sample (or the slits) and/or the precise relative movement of at least two mechanical components. Thus the designs of Birks and Brooks (1955) require the precise relative movement of the counter and the sample or sample slit; that of Adler and Axelrod (1956) needs precision reduction gearing between detector and analysing crystal.

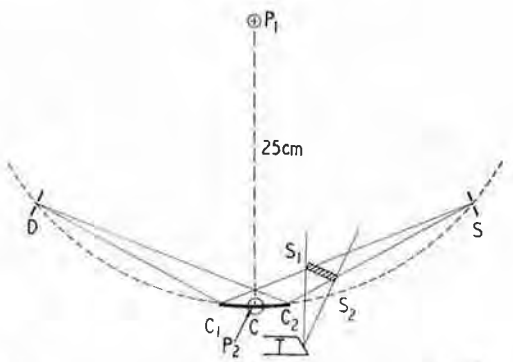

Figure 1. Diagram of a reflecting focusing curved crystal fluorescence x-ray spectrograph using a line source S or extended source S_1S_2.

(ii) The path length from sample to detector is thereby decreased to the minimum possible for any geometry, so reducing the air or gas absorption.

(iii) With a heterogeneous sample a more representative portion is analysed using an extended source S_1S_2, rather than a line source weighing milligrams at S. Polished rock sections may be placed at S_1S_2 without grinding, for example.

It appears that the geometry adopted by Sandstrom (1934) has not been widely noticed, since few people seem aware that the sample can be placed *within* the focusing circle in

this way. This arrangement is not mentioned in the review by Birks, Brooks and Friedman (1956) nor in the books by Birks (1959) and by Liebhafsky *et al.* (1960), but surely deserves to be considered more generally for its merits.

In this spectrograph the sample is a disk (diameter = 1·27 cm) placed about 8 cm from the x-ray tube target T, and 6 cm from the crystal C_1C_2 (figures 1 and 2). The radius of the focusing circle, centre P_1, is $CP_1 = 25$ cm, and the counter views C_1C_2 through a slit D moving on this circle. Then

$$\lambda = 2d \sin\theta = 2d(CD/2)/CP_1 = 0{\cdot}04d\ CD\ \text{Å}$$

and the measurement of CD by a suitable vernier centimetre scale gives λ very simply for each crystal used; no precise angular scales or conversion tables are needed. The recording range is from $\theta = 8°$ (i.e. CD = 7 cm, $\lambda \simeq 0{\cdot}25d$) to $\theta = 30°$ (i.e. CD = 25 cm, $\lambda = d$), so that three suitable crystals could cover from 0·3 to 3·6 Å which includes the K or L spectra of all elements heavier than Ca ($Z = 20$). The resolution of λ is adequate for $\theta < 30°$, and higher angles, leading to lower intensities and greater path lengths, are avoided. Wavelengths less than 0·3 Å are also avoided.

The dispersion is the same as that of a non-focusing spectrograph of equal radius, i.e. 25 cm. At the midpoint of the CD scale the Kα or Lα lines of elements of neighbouring atomic number are separated by about 1 cm, which is adequate for an analytical instrument.

3. Mechanical design

The parts of the spectrograph are fixed to a solid base which is itself mounted in slots on a subplatform to allow some freedom for alignment in front of the x-ray tube. Two pillars P_1 and P_2 (figures 1 and 2) are fixed 25 cm apart and the crystal was originally mounted over P_2 with the following adjustments for aligning it.

(i) The whole assembly can rotate about P_2 to bring the centre of curvature of the crystal on to the line P_1P_2.

(ii) A platform above P_2 has a screw adjustment for moving the crystal along P_1P_2 until the crystal surface is exactly 25 cm from P_1.

(iii) The crystal holder was supported above this platform by three levelling screws, for aligning the crystal axis parallel to axis of the focusing circle. Experience has shown that this adjustment is not needed if the spectrograph is constructed with reasonable precision; it is omitted in figure 2. Since (i) and (ii) are made only rarely the mounting could be made very simply by clamping the crystal block directly on to a plate on top of P_2. Movement together of screws B and C gives the radial adjustment (ii), and in opposition the angular adjustment (i).

The specimen is supported on a small table T (figure 2) carried on arm A_2 (length 6 cm) pivoted about P_2. A pointer on A_2 shows the average angle θ on a scale on the baseplate. The base of T (which can rotate about a vertical axis on A_2) is graduated so that the approximate angles to the sample of the incident and emergent beams can be noted. The specimen holders, generally of Perspex, slip into a brass block on T.

Initially the fluorescence spectral lines were photographed using a film cassette on the focusing circle from $\theta = 7°$ to 30° (Radoslovich 1951). Although this is still available, counting techniques are used exclusively as they are more sensitive and better adapted to quantitative analysis. The arm A_1, pivoted about P_1, carries a bearing exactly 25 cm from P_1 (centre to centre), and the receiving slits are mounted on a block B fitting over this bearing. A rod R passes through P_2, and then through B above the centre of the supporting bearing. Thus A_1 and R together constrain the receiving slit D so that it moves around the focusing circle but is always normal to the beam from the crystal C. The

Figure 2. Actual instrument, removed from x-ray tube and omitting all lead shielding. 1, crystal holder; 2, specimen in holder; 3, centre of focusing circle; 4, slits for counter, moving on focusing circle; 5, centimetre scale, linearly proportional to λ; 6, counting tube; 7, clamp for sample holder, for making absorption measurements; 8, holder for absorption foils. (See text also.)

distance CD is measured by a scale rigidly fixed parallel to R, an accurate steel rule being quite suitable after the centimetre scale had been changed to read CD directly. A vernier attached to B gives readings to 0·05 cm and is mounted through slotted holes for adjusting the origin. The slits can be locked by a clutch from B on to R, after which a simple screw device allows vernier movement (over a range of 1·5 cm) along CD. This screw may be driven by a synchronous motor, giving automatic traverse over a small range of wavelengths.

The receiving slits are made of tantalum and adjusted in width using feeler gauges—the slits are usually set at 0·2 mm. The detector is attached to B by two thumbscrews. The centres of the sample, crystal and receiving slits (all at the same height above the base-plate) are set level to the x-ray tube window. A slit assemblage on the latter limits the dimensions of the primary beam on to the sample. The slits are tantalum plates mounted in brass housing which also carries a tantalum shutter for the tube window. The housing further provides a slot for holding absorption foils, and beyond this a clamp for holding the Perspex sample holder when the absorption of the direct beam by the sample needs to be measured. The absorption coefficients of the sample for particular monochromatic wavelengths are measured when necessary and for this purpose a clamp for the sample holder is provided above R near to the crystal holder. Absorption foils can be placed in a slot in front of the receiving slits.

The crystal holders* consist of two pieces between which the crystal is clamped. For perfect focusing a crystal ground cylindrically to a radius of curvature of 50 cm should be bent by the holder to 25 cm (Johannson 1933). Cylindrically ground quartz crystals are readily available and therefore used, but most other suitable crystals cannot be ground satisfactorily and are simply bent elastically in a holder of 50 cm radius. The focusing is no longer theoretically perfect, but there is almost no difference in line width (using approximate and perfect focusing) which is due mainly to aberrations

* Available from Charles Beaudouin, 13 Rue Rataud, Paris 5. The central portion of the convex piece, containing the aperture screw, is reduced in size by filing to increase the aperture to $\theta = 30°$,

from other causes, e.g. height of the beam, and depth of penetration in the crystal. The crystal holders necessitate using crystals of about 45 mm × 12 mm × 0·2 mm although the reflecting area is only 45 mm × 5 mm. The intensity would be considerably increased if the slot height (5 mm) were enlarged, or if the crystal were cemented to the back block and the front block removed, to utilize the whole crystal face.

The following crystals have given satisfactory results.

Gypsum (010)	$d = 7{\cdot}58$ Å	for $\lambda > 1{\cdot}8$ to $3{\cdot}4$ Å
Quartz ($10\bar{1}1$)	$d = 3{\cdot}345$ Å	for λ from $0{\cdot}85$ to $3{\cdot}35$ Å
LiF (200)	$d = 2{\cdot}012$ Å	for λ from $0{\cdot}5$ to $2{\cdot}00$ Å
LiF (400)	$d = 1{\cdot}006$ Å	for $\lambda < 1{\cdot}0$ Å.

All are readily available. Certain organic crystals may be better than gypsum for the longer wavelengths.

4. Specimens

The specimen holders are normally made from Perspex with dimensions 1·25 in. × 1·0 in. × 0·125 in., and have a 0·500 in. hole drilled through them. Powder specimens are pressed into this hole using a closely fitting plunger which is guided vertically by a cylindrical metal jig. If the holder is laid on a strip of Terylene plastic and a Perspex plunger is used the specimen may be pressed into the mount without contacting any metal; this is desirable for the analysis of trace elements. The pressure needed to form a sample which is self-supporting depends a great deal on the nature of the sample. Pressures up to 8000 lb in^{-2} are obtained by a hydraulic jack, and specimens weighing from 0·02 to 0·2 g are used. Very small powder samples (<0·02 g) are either diluted and mounted in the normal way or else pressed into a shallow recess machined into a Perspex plate. Sample holders for fluorescence and absorption measurements on liquids are made with a hole identical with the powder holders, using Perspex of different thicknesses between 0·15 and 1·5 cm. Thin Terylene windows, 0·01–0·1 cm thick, are cemented over the hole and the cell so formed is filled and emptied via two capillary holes with the aid of a hypodermic needle.

Samples are normally made comparatively thin and without backing—or with the minimum window thickness for the liquid cell—for several reasons. (i) All irradiated instrument parts, including any support behind the sample, are potential sources of contaminating wavelengths at the counter. (ii) A thick sample or backing material may increase the background more rapidly than the line intensity, reducing the sensitivity. (iii) For absorption and absorption–fluorescence spectrography the absorption coefficient of the sample is required, for which the sample must have a uniform thickness and known area.

5. X-ray generator and counting equipment

The primary beam is obtained from a Raymax demountable self-rectifying x-ray tube, capable of operating at 1500 w and up to 100 kv (peak). The input voltage is stabilized to within ±0·5% and the x-ray tube current is stabilized by the feed-back circuit (Lees and Armitage 1950). A fine control and milliampere meter are mounted beside the scaler so that the tube current can be monitored continuously. These factors ensure adequate stability over periods of several hours. In a typical test, under working conditions, the times for twenty consecutive counts of 10^6 were recorded; this gave a coefficient of variation of 0·17% (in the times for 10^6 counts). Since a counting error of 0·1% is associated with 10^6 counts the overall stability of the generator and counting equipment was about 0·15%. The long-term drift of the x-ray output (due to changes in the focus and to deposition on the target) can be compensated for by regularly checking against standards. Additions to the vacuum line of the x-ray tube allow the changing or cleaning of the target within a few minutes. The tube has an 0·2 mm thick beryllium window. Targets of Ag and Au electroplated from high purity reagents are used for certain analyses of trace elements where less pure targets give spurious lines at the detector. Other targets include Cr, Fe, Co, Ni, Cu, Mo and W.

The wavelength range covered by the instrument is from about 0·3 to 3 Å for which a scintillation counter proved to be the most generally satisfactory single detector. The scintillation crystal is a small piece of NaI (Tl) mounted in a cell with a 0·1 mm beryllium window.

The photomultiplier feeds through an adjacent head amplifier to the main linear amplifier (total gain used from 10^4 to 2 × 10^5) and then to a single channel pulse analyser (figure 3). This is followed by a gating circuit operated

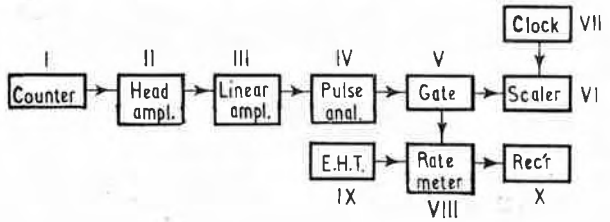

Figure 3. Block diagram of electronic components, viz.: I, sodium iodide scintillation crystal and photomultiplier tube (Dumont, type 6291); II, head amplifier and III, linear amplifier (both EKCO, N 568); IV, pulse analyser (Dynatron, N/101); V, gating circuit (designed here); VI, scaler (Austronic Engineering Laboratory, SC 4/4 Px); VII, stopwatch and 'start-count' switch (Venner, A 40); VIII, ratemeter (Austronic, R X 1); IX, h.t. supply (Austronic, H 52); and X, recording potentiometer (Philips, PR 2210 A/21).

from the mains in such a way that pulses are passed only for that portion of the a.c. cycle when the primary beam is being produced (about one-third). Thus no background is counted when there is no useful beam. Pulses finally go to a scaler and also to a chart recorder via a ratemeter. The scaler is controlled for preset times (10 to 10^3 sec) or for preset counts (10^3 to 10^6) in which case the time is read from a built-in stop-watch to within 0·02 sec.

The resolution time of the counting equipment is limited by the pulse analyser. Though this has a nominal *input* resolution time of 1 μsec it is in fact somewhat longer, and depends on the integration and differentiation time constants of the amplifier. Furthermore since coincidence losses occur at the *input* to the analyser, but only pulses *transmitted* by the channel are counted, the apparent resolution time will exceed the input resolution time by the ratio of pulses received to pulses transmitted. The *effective* resolution time for the pulses counted therefore varies with the channel width setting of the pulse analyser, with the energy distribution of the input pulses, and with the time constant settings of the linear amplifier. This variability is intolerable because it is the *effective* resolution time which must be used to correct for counting losses. It has been overcome by adjusting the resolution time at the input of the scaler to about 3 μsec, a value exceeding normal variations in resolution time due to changing conditions. X-rays are only produced for a fraction f of each cycle; actual counting rates during

that part of the cycle are $1/f$ times the average rate. The correction to be applied for coincidence losses then becomes

$$C = \frac{C'}{(1 - C')dt}$$

where C' = the measured rate in counts per second, C = the rate, corrected for losses, and dt = effective resolution time divided by f. The resolution time of the scaler has been adjusted so that $dt = 10$ μsec which further simplifies the above formula.

In routine analyses the quantity measured is the line t for a fixed number of counts N for which the above formula becomes

$$t = t' - Ndt$$

where $N = Ct$. This provides an even more convenient correction for losses, when $dt = 10$ μsec. The correction is then very simply made by subtracting 10 sec from the elapsed time for $N = 10^6$, 1 sec for $N = 10^5$ and 0·1 sec for $N = 10^4$.

6. Performance

As mentioned earlier the dispersion is satisfactory for analytical purposes. Focusing spectrographs are inherently capable of very high resolution, but in practice the use of large crystals and approximate focusing (crystals bent but not cylindrically ground) gives rise to line broadening. In the present instrument penetration of the crystal is the main source of aberration. Perfect focusing depends on reflection taking place *at the surface* of the crystal. This condition is fulfilled for the longer wavelengths, but the shorter wavelengths penetrate to an appreciable depth l giving a broadening of $l/\sin\theta$. As θ decreases l increases and $\sin\theta$ decreases, so that broadening increases rapidly in the region where the lines of neighbouring elements lie closest together.

The difficulties of making crystals less than 0·1 mm thick (to limit this broadening) would be considerable. The actual width of the lines at half height varies from about 0·10° for long wavelengths (2 Å) to about 0·4° for shorter wavelengths (0·7 Å). This compares well with other focusing and non-focusing spectrographs. Barstad and Refsdal (1958) have described a curved crystal spectrograph employing slits in front of the detector and sample with line widths of 0·4° for 2 Å and 1·0° for 0·5 Å. Line widths on a commercial non-focusing spectrograph are constant at about 0·5°.

Because a comparatively small crystal is used absolute intensities are less than given by some other focusing or non-focusing instruments. Nevertheless the sensitivity is comparable with, and sometimes exceeds, that for other instruments, mainly because of the good line to background ratio (due to sharper lines). The aperture control on the crystal holder and various lead shielding ensure that only crystal reflected radiation reaches the detector.

In the present design the sample is near the crystal, not on the focusing circle. Since this geometry theoretically can increase the background the main sources of background are now considered, as follows.

(i) *Non x-ray background.* This includes natural radiation, noise from the photomultiplier and amplifier and spurious counts due to interference from outside sources. This can be minimized by using pulse height analysis and by gating (for a half wave generator); the rate is 0·3 c/s in this spectrograph.

(ii) *Radiation diffracted by the crystal.* This lies near to the fluorescence beam in wavelength, and originates as white radiation from the x-ray tube, and is both coherently and incoherently scattered by the sample. It cannot be removed by pulse height analysis, and, because it is diffracted, its intensity depends on the brightness of the sample in the same way as the fluorescence beam. Line to background ratio is therefore unaffected by moving the sample off the focusing circle. This constitutes a major fraction of the background normally.

(iii) *Radiation from, but not diffracted by, the crystal.* A small fraction of all the radiation falling on the crystal will be scattered (coherently and incoherently) over a large angular range. Most of the radiation will be that originating as white radiation from the x-ray tube and scattered by the sample, but fluorescence radiations originating in the sample will contribute, sometimes in a major way. Radiation falling on the crystal can cause the crystal elements to fluoresce, occasionally increasing the background considerably.

These sources of background depend on the *total* radiation falling on the crystal; increasing the area of the sample (as in this geometry) might be expected to raise this fraction of the total background significantly. Normally, but not always, this fraction is small compared with that diffracted by the crystal. The wavelengths will generally differ from the required spectral line and so can be effectively removed by pulse height analysis. All fluorescence radiation arising in the crystal, except CaKα from gypsum, will be absorbed by the air in a non-evacuated spectrograph.

For the radiation listed as (ii) and (iii) above, the line to background ratio will increase directly with resolution, i.e. inversely with the angular width of the lines.

A consideration of (i), (ii) and (iii) above suggests that, with pulse height analysis, backgrounds should be little affected by moving the sample from the focusing circle, and this is confirmed experimentally. The line and background intensities for several elements in $CaCO_3$ (see table) are compared with data for an instrument with a slit on the focusing circle in front of the sample (Barstad and Refsdal 1958). Their use of a Geiger counter undoubtedly reduced both the absolute intensities and the line to background ratios.

Comparison of line intensities and line-to-background ratios for two spectrographs, for 0·1% of element in $CaCO_3$

Element	Author*	Line	Order	Filter	Background (c/s)	Peak less background (c/s)	Line background
Ni	B & R	Kα	1	Br	16	126	8
Ni	N & R	Kα	1	—	4	40	10
Sr	B & R	Kα	2	Mo	12·2	44	3·6
Sr	N & R	Kα	1	—	90	1000	11

* Data from Barstad and Refsdal (1958) marked B and R; other data obtained by authors.

The range of elements is from $Z = 20$ (Ca) to $Z = 92$ (U), as for all non-evacuated x-ray spectrographs. The instrument has been used in this laboratory for about eight years on a wide range of elements and samples. For accurate quantitative analyses calibration curves are used where possible, but for variable materials an absorption–fluorescence method is used which does not require calibration curves, dilution or internal standards. This will be described by one of us (K.N.). The following typical analyses confirm the performance characteristics.

(i) *Solutions*

For Fe in soil extracts (Norrish and Taylor 1961).

For U in metallurgical specimens, both in major and minor amounts (K. Norrish and T. R. Sweatman 1961, Divisional

Report 11/61 of the Division of Soils of the Commonwealth Scientific and Industrial Research Organization). High U contents were determined by fluorescence or absorption spectrography with an error of about 2% (relative); minor amounts were determined by fluorescence spectrography with an error of ± 4 parts per million in several minutes.

(ii) *Powder specimens*

For major amounts of Pb, Zn, Fe and other elements in ores minerals and soils with relative accuracies to 1%.

(iii) *Trace elements*

Analyses of Sr in plant materials and their ashes showed agreement internally and with independent assays (David 1962). All three results on a variety of plant materials agreed to within about 1 part per million in the range 2–100 parts per million.

Soils and rocks may be analysed for various trace elements. For example the standard rocks G1 and W1 have been analysed for V, Ga and Zr and the results compare satisfactorily with those obtained by other methods (McKenzie, Oertel and Tiller 1958).

Acknowledgments

We are grateful to Mr. A. W. Palm and other members of this Division's workshop for careful construction of the spectrograph.

References

ADLER, I., and AXELROD, J. M., 1956, *Amer. Min.*, **41**, 524.

BARSTAD, G. E. B., and REFSDAL, I. N., 1958, *Rev. Sci. Instrum.*, **29**, 343.

BIRKS, L. S., 1959, *X-ray Spectrochemical Analysis* (New York: Interscience).

BIRKS, L. S., and BROOKS, E. J., 1955, *Analyt. Chem.*, **27**, 437.

BIRKS, L. S., BROOKS, E. J., and FRIEDMAN, H., 1956, *Norelco Reporter*, **3**, 44.

DAVID, D. J., 1962, *Analyst*, **87**, 567

JOHANNSON, I., 1933, *Z. Phys.*, **82**, 507.

LEES, C. S., and ARMITAGE, M. D., 1950, *J. Sci. Instrum.*, **27**, 300.

LIEBHAFSKY, H. A., PFEIFFER, H. G., WINSLOW, E. H., and ZEMANY, P. D., 1960, *X-ray Absorption and Emission in Analytical Chemistry* (New York: John Wiley).

MCKENZIE, R. M., OERTEL, A. C., and TILLER, K. G., 1958, *Geochim. et Cosmoch. Acta*, **14**, 68.

NORRISH, K., and TAYLOR, R. M., 1961, *J. Soil Sci.*, **12**, 294.

RADOSLOVICH, E. W., 1951, *M. Sc. Thesis* (Adelaide).

SANDSTROM, A., 1934, *Z. Phys.*, **92**, 622.

UNWIN BROTHERS LIMITED, WOKING AND LONDON

Paper 3-11

Handbuch der Bodenkunde

Vol. II. Soil Components

Section D, Part 12. "Felspars"

E.W. Radoslovich

Division of Soils, Commonwealth Scientific
and Industrial Research Organisation, Adelaide,
South Australia.

Date. June, 1966.

Chapter 12. Felspar minerals.

Introduction.

Crystal structures.

a) Albite-orthoclase felspars.

b) Plagioclase felspars.

c) Barium felspars.

Chemistry, Optical Properties.

Felspars as Geologic Thermometers.

Weathering of felspars.

Identification of Felspars in Soils.

INTRODUCTION

The felspars are amongst the most important, abundant and widely occurring minerals to be found in various types of rocks. They are of direct concern to the soil scientist because (i) they are important primary minerals from which soil components (especially clay minerals) are formed during the weathering cycle, (ii) they are direct sources of some plant nutrients, and (iii) they are major constituents of the sand and silt fractions of soils, and as such may provide useful pedological information. The felspar minerals have not, however, been widely studied in soils laboratories, partly because for the more highly weathered soils they are not commonly found in the <2μ particle size range (i.e. the highly reactive clay fraction, which is of the greatest interest in soils problems). There are also inherent difficulties in their adequate identification when they are finely divided and admixed with other felspars and other minerals.

The felspars have, however, been very intensively studied in geological and mineralogical laboratories in the last two decades. More intensive and more precise crystallographic studies have probably been made on this group than on any other mineral group, and these have been matched by detailed investigations of both their optical properties and their chemistry. The stability fields for different felspars at different pressures and temperatures have been widely investigated, and the resultant phase equilibrium diagrams compared in considerable detail with the known physical properties (e.g. "melting curves") and paragenesis of different natural rock systems. The external morphology and the twinning of these minerals have also received much attention, particularly as their crystal structures have become known in detail. The changes in both crystal structure and optical properties with heating have also been the subjects of many recent papers. Some work has

been reported on the alteration of felspars both in the field and under laboratory conditions. A few papers have also appeared on their place in $^{40}K/^{40}Ar$ dating techniques, and their use as geologic temperature indicators.

It would not be appropriate to discuss the large volume of work in these various fields in any detail here, since much of the data is primarily of geological interest.* In this article, rather, only a sufficient number of main conclusions will be set out briefly to draw attention to some of the complexities involved in identifying and studying felspars as components of soils.

The felspars are alumino-silicate minerals having a framework type of crystal structure in which the cations Na^+, K^+, Ca^{2+} and Ba^{2+} play important roles. They are often called tectosilicates in geochemical literature. They may be subdivided into several categories according to their physical and chemical properties or their optical or structural characteristics. For a felspar of given composition both its optical constants and the details of its crystal structure depend extensively upon its initial temperature of crystallization and its subsequent thermal history. A felspar which has been rapidly quenched usually retains the structure which it had at its high temperature of formation, and is therefore called a "high-temperature felspar". Another felspar with identical chemistry and a similar (but significantly

---

* Those with particular interests should refer to the appropriate literature in geology and mineralogy. An excellent comprehensive review in English is given in "Rock Forming Minerals, Vol. IV" by W.A. Deer, R.A. Howie and J. Zussman (Longmans, London, 1963), pages 1-178.

different) structure may be formed either directly at low temperatures, or else by slow cooling from the high temperature melt. Natural felspars are also found with structures corresponding to intermediate temperatures of formation.

The majority of felspars may be classified chemically in terms of the molar proportions of the three end-member minerals, albite Na Al Si_3O_8, orthoclase K Al Si_3O_8 and anorthite Ca $Al_2Si_2O_8$. Barium felspars form a rather separate group. Felspars with all compositions between albite and orthoclase are known as the alkali felspars, and generally contain <5% of the anorthite "molecule". The plagioclase felspars may have all compositions between albite and anorthite (Fig. 1). As an example of the interdependence of structure, optical properties, crystal symmetry and formation temperature, the pure end-member KAl Si_3O_8 may exist as a high-temperature monoclinic form (sanidine), or a lower temperature monoclinic form (orthoclase). The lowest temperature forms of KAl Si_3O_8 (microcline) are, however, triclinic but the "obliquity" of the unit cell depends on the thermal history of the specimen. Adularia is a further potassium felspar recognized by its habit and paragenesis rather than structural properties.

Within a given felspar series (e.g. low-temperature plagioclases) the crystal structure varies with the chemistry, and the felspars generally are no longer considered to form continuous series of solid solutions between the end-member minerals, at least in the low temperature forms. Since variations in crystal structure are so closely related to physical properties and to problems in identifying finegrained specimens their structures are

discussed first, in the next section.*

CRYSTAL STRUCTURES

In this section we must consider the alkali felspars either low or high in K, in low-, intermediate- and high-temperature forms; the plagioclase felspars, in low- and high-temperature forms, and at several points in the composition range between albite and anorthite; and the barium felspars.

a) Albite - orthoclase felspars

The first felspar structure determined was that of sanidine K Al Si_3O_8 by Taylor (1933), and this structure was found to be typical for all felspars. The structure consists of a "framework" of (Si, Al) $-O_4$ tetrahedral groups in which neighbouring tetrahedra are linked together in a three-dimensional array by sharing corner oxygens. The tetrahedral groups form long chains throughout the structure but these chains are not discrete; neighbouring chains are crosslinked through "bridge oxygens", in two directions approximately perpendicular to their length. In this way the tetrahedra are joined into four-membered rings which are only roughly normal to the chain axis, and are twisted successively clockwise and anticlockwise about that axis. The rings are linked in directions roughly about their own plane to form larger eight-membered rings of tetrahedra (in black, Plate I). Below this network of four and eight-member rings lies a second similar network

---

* A recent review of felspar structures by W.H. Taylor has appeared as Chapter 14, of "The Crystalline State, Vol. IV. Crystal Structure of Minerals" edited by Sir Lawrence Bragg (G. Bell and Sons, London, 1965).

(in red, Plate I); and these two networks are linked by oxygens such as P, Q (Fig. 2) and also Fig. 3 to form vertical four-membered rings. The resultant framework of four-membered rings of tetrahedral groups encloses large interstices which may be occupied by K, Na, Ca, Ba and other cations. These sites are occupied by K in sanidine, orthoclase, microcline and adularia; the K-O distances (about 3Å) indicate an irregular nine-fold coordination for the K^+ ion.

If the general felspar formula is written as AB_4O_8 then we can distinguish in the structure the A sites, occupied by the larger cations in six- to nine-fold coordination, and the B sites, with Si and Al in four-fold coordination. The polymorphism of felspars (e.g. sanidine - orthoclase - microchine, all K Al Si_3O_8) is at least in part a result of the detailed distribution of Al and Si ions amongst the available B sites. In some cases the observed spacegroup, symmetry, and composition imply that the available Al must be distributed randomly amongst the B sites; e.g. sanidine has eight B sites which are required by symmetry to be equivalent, and which must accommodate 6 Si and 2 Al ions. The occupancy of <u>each</u> of these sites, averaged over many unit cells, must be $Si_{3/4}$ $Al_{1/4}$. An accurate structure analysis (Cole et al, 1949) confirmed that all (Si, Al) -O distances are equal to 1.64 Å, within experimental error. This may be compared with a detailed structure determination of orthoclase (Jones and Taylor, 1961). In both sanidine and orthoclase there are two such sets of eight sites (above) called set B_1 and set B_2. For sanidine the structure analysis showed equal bond lengths in <u>both</u> sets. For orthoclase the bond lengths in set B_1 are greater than in set B_2, with the tentative conclusion that each B_1 site is occupied by (0.30 Al + 0.70 Si) and each B_2 site by (0.19 Al + 0.81 Si). The potassium electron density peak shows some anisotropy in each of the three

potassium felspars, suggesting that the potassium may vary in position from cell to cell probably depending on the local (Si, Al) ordering. Other interpretations of the bond length data are argued strongly, especially those involving submicroscopic twinning or domains in which the symmetry is triclinic (Laves and Goldsmith, 1961). The lowest temperature form of K Al Si_3O_8 is microcline which has been shown (e.g. MacKenzie, 1954) to consist of a continuous series of structures from monoclinic microcline to "maximum microcline" which is triclinic with $\gamma = 87.8°$. In the latter case we have four sets of four equivalent sites in which to arrange 12 Si and 4 Al. These continuous changes in obliquity (i.e. in γ) may be related both to (Si, Al) order amongst the four sets of B sites, and to the amount of Na in solid solution in microcline (MacKenzie, 1954). The obliquity can be estimated from the separation of the $1\bar{3}0$ and 130 lines in x-ray powder patterns; but this measurement cannot be correlated with (Si, Al) order, (i.e. with thermal history of the specimen) unless the Na content is known.

The sodium analogue of orthoclase etc., viz. albite Na Al Si_3O_8, also occurs in a low-temperature and high-temperature form. The general structural features of albite and sanidine are compared in Fig. 4, showing the greater distortion of the structure around Na, with the consequent loss of symmetry to become triclinic. As with microcline the difference between low- and high-albite seems to reflect a different distribution of Al between the four non-equivalent tetrahedral (or B) sites. The Al is largely concentrated in one of these set of sites in low-albite but is about equally distributed between the four independent sites in high-albite (Ferguson et al, 1958). The anistropic shape of the Na electron density peak could be interpreted in terms of two Na sites separated by about 0.6 Å along y; in any

given cell Na would occupy one of these, probably in response to local (Si, Al) order in that cell.

A tentative summary of the available evidence on the structures of the alkali felspars in relation to (Si, Al) ordering is given below, with acknowledgement to J.B. Jones:-

High sanidine	Complete local and distant disorder.
Low sanidine	Partial local order but distant disorder.
Orthoclase)	Increasing local and distant order.
Intermediate microcline)	
High albite	Very slight local and distant order.
Low albite	Complete local and distant order.

For soil scientists it is interesting to note the careful structure analysis by Finney and Bailey (1964) of an authigenic microcline "believed to have grown directly in the ordered state at a very low temperature during the diagenetic history of the sediment". The ordering of tetrahedral Si, Al atoms is nearly complete and there is no significant difference from an igneous maximum microcline.

Most natural alkali felspars are "unmixed" in the sense that they contain both Na-rich and K-rich phases, but the highest-temperature forms of alkali felspar do form a complete series of solid solutions. On the basis of their optical properties four separate series of minerals are recognised, viz.

high-albite - high-sanidine

high-albite - low-sanidine

low-albite - orthoclase

low-albite - microcline

Although the cell dimensions (and therefore a particular spacing such as $\bar{2}01$ in an x-ray powder diagram) vary systematically with composition within any series this cannot be widely used analytically, since the degree of unmixing on a very fine scale is highly dependent on the thermal history of the specimen. Even if single crystal data are available it is difficult to estimate composition from unit cell data due to extensive twinning in some of the unmixed phases (Smith and MacKenzie, 1955). Nor can bulk compositions be estimated satisfactorily from powder data or optic axial angle by homogenizing the samples by prolonged heating (MacKenzie and Smith, 1956).

The significance of these recent structural results in soil studies is that is is probably insufficient to characterise a specimen as, say, K-felspar if in subsequent experimental studies the detailed bonding forces around the K^+ ions are likely to be significant. Conversely, in some pedological problem the identification of an "alkali felspar" felspar may be useful, but more detailed information (if obtainable) about its structural state, submicroscopic twinning, chemistry, thermal history etc. may become a critical key to whole study. The soil scientist studying the felspars in the sand fractions in future should therefore be prepared to make detailed and precise optical, chemical and x-ray measurements, preferably on small single crystals, before interpreting his results in pedological or geochemical terms in any great detail.

b) Plagioclase felspars

The plagioclase felspar series extends between the two end-members albite, Na Al Si_3O_8, and anorthite, Ca $Al_2Si_2O_8$, this composition range being somewhat arbitrarily divided into six mineral names. Although plagioclases of all possible compositions are known, and the variation of refractive

indices of the low-temperature series is continuous many other properties do not vary continuously from albite to anorthite; the plagioclases are no longer regarded as the classic example of an isomorphous series of minerals. This is well illustrated by the complexities of their structural variations which are slowly and with much difficulty being revealed (Taylor, 1962; Gray, 1962).

Their structures are triclinic and similar to albite, i.e. essentially a sanidine framework distorted to conform fairly closely around the smaller Ca and Na ions substituting in place of K in sanidine. The plagioclase structures show both low- and high-temperature forms, as well as intermediate structural states. There is evidence of complete solid solution in the high-temperature series from albite to anorthite, but there are a number of complex structural changes or discontinuities in the corresponding low-temperature series (Fig. 5 4). If all of these structures are described in terms of approximately the same orientation of the crystallographic axes then anorthite is related to body-centred anorthite and to albite by a loss of half the centres of symmetry and a doubling of the c-axis. (Fig. 6) This is readily shown by indexing the x-ray reflections from single crystals on the basis of a cell with a ∿ 8 Å, b ∿ 13 Å and c ∿ 14 Å ("primitive anorthite cell") and forming groups as follows:- (a) (h + k) even, l even (b) (h + k) odd, l odd (c) (h + k) even, l odd and (d) (h + k) odd, l even. All types of reflections are present and sharp for an anorthite with <10% of the albite molecule (Ab_0An_{100} to $Ab_{10}An_{90}$) which is also low-temperature in structural form. Reflections of types (c) and (d) are missing in the case of body-centred anorthites, and these are found the composition range from $An_{90}Ab_{10}$ to $An_{70}Ab_{30}$ for low-temperature materials. On the other hand high-temperature

material near An_{100} gives the "transitional anorthite" pattern in which (d) reflections are absent and (c) reflections are diffuse rather than sharp. Plagioclases of composition between $An_{70}Ab_{30}$ and $An_{25}Ab_{75}$ give patterns (also dependent on thermal history) which are characteristic of the imperfectly understood "intermediate anorthite structures". No (c) or (d) reflections are observed, and on c-axis photographs the (b) reflections are replaced by pairs of spots defining a pair of weak subsidiary layer lines, the position of which (relative to the principal layer lines) varies linearly with composition. The tentative explanations for these reflections are based on hypothetical sodium-rich and calcium-rich regions intermixed in some regular manner, or alternatively on regularly distributed stacking faults (i.e. lattice disorder), the occurrence and nature of which are dependent on the Si:Al ratio (Gay, 1962).

The primitive anorthite structure (i.e. for low-temperature material close to An_{100}) shows a complete ordering of Al and Si in the tetrahedral sites, with each Al surrounded by 4 Si, and vice versa. The tetrahedral groups are by no means geometrically regular in shape; this is an important feature of the <u>real</u> structures of both framework and layer silicates, in contrast to the <u>ideal</u> structures so frequently discussed in soil science. This means that in the anorthite structure some oxygens may be linked to 2 Ca, some to 1 Ca and some to no Ca atoms, with marked variations in Si -O and Al -O bond-lengths (due to variations in bond strengths). Each Ca atom is located within an irregular cavity bounded by about 10 oxygen atoms, of which seven are close neighbours to the Ca's. In primitive anorthite there are four distinctly different kinds of Ca sites, with different environments. The effect of substituting Na for some of the Ca is to reduce these four

different sites to two pairs of sites, in one of which the cations are six-coordinated and in the other seven-coordinated; this is the body-centred anorthite structure.

The effect of heating the low-temperature plagioclases is again to produce disorder in the distribution of the cations amongst essentially identical sites. For example the Ca ions become disordered (in their four different kinds of "holes") when primitive anorthite, An_{100}, is heated; i.e. heating and quenching primitive anorthite produces a body-centred anorthite structure, as confirmed by the systematically absent reflections. Further heating of anorthite disorders the Si and Al amongst the tetrahedral sites, to produce a high-temperature albite type of structure (Fig. 5).

c) Barium felspars

These include celsian, Ba $[Al_2\ Si_2\ O_8]$ and hyalophane, (K, Na, Ba_x) $[Al_{1+x}, Si_{3-x}\ O_8]$, both of which are structurally very similar to the potassium felspars. In celsian, which is truly monoclinic, the Al and Si are ordered into alternate tetrahedral sites (Newnham and Megaw, 1960).

CHEMISTRY

The majority of felspars may be classified as members of the ternary system, $K\ Al\ Si_3O_8$ - $Na\ Al\ Si_3O_8$ - $Ca\ Al_2\ Si_2\ O_8$, in which there is less than 5 to 10% of the "anorthite molecule" in the potassium felspars, or of the "orthoclase molecule" in the calcium felspars. Comprehensive tables of relatively recent and reliable chemical analyses of felspars which are representative of a wide range of rocks are given by Deer, Howie and Zussman (1963, Vol. 4 pp. 36-45, 108-120, 170-171).

The alkali felspars may show substitutions in limited amounts of

Ba for K; of Mg, Fe^{2+}, Sr and Mn for Ca (in the anorthite phase) and of Fe^{3+} and Ti for Al. The distribution of trace elements in felspars has been reviewed in considerable detail by Heier (1962). Of the elements that occupy the "alkali position" in potash felspars it can be deduced that they enter the lattice in the following order:-

Univalent Na>Rb>Tl>Cs

Bivalent Ba>Sr>Ca>(Pb)

The plagioclase felspars may include very limited amounts of Ti, Fe^{3+}, Fe^{2+}, Mn, Mg, Ba and Sr; of these the Ti and Fe^{3+} are thought to replace Al, with Sr, Fe^{2+}, Mg and Mn replacing Ca, whilst Ba replaces K in any orthoclase phase which may be present in the plagioclase specimen.

Up to date at least eight elements have been found which probably substitute in trace amounts (a few p.p.m.) for Al or Si in the tetrahedral positions in the felspar lattice; these include B^{3+}, Be^{2+}, Fe^{3+}, Ga^{3+}, Ge^{4+}, P^{5+}, Ti^{4+} and Ti^{3+}.

Barth (1961) has studied the distribution of Rb, Cu, Pb, Li, Ca, Sr and Ba between coexisting felspars and has found some interesting relationships with respect to temperature.

A great deal of careful laboratory work has been done in determining the phase equilibrium diagrams of various felspars and related mineral systems; this has been critically reviewed by Deer, Howie and Zussman (1963, Vol. IV). Although much of this work has necessarily been restricted to binary or ternary systems the results have been carefully correlated with geological field observations (see, e.g., Yoder and Tilley, 1962 or Muir, 1962). In this way our detailed understanding of the conditions (of temperature, pressure, and composition of melt) under which various rocks have formed has

been substantially enlarged. The experimental techniques and the detailed results are of rather specialized interest to the petrologist, however, and would be out of place in the present volume; the interested reader should consult some recent textbook dealing with experimental petrology, such as Deer, Howie and Zussman, Vol. IV.

The optics of the various felspars have turned out to be quite complicated and are only slowly being unravelled. For any particular specimen the various optical properties depend quite critically on both composition and thermal history or structural state. For soil scientists it seems pertinent to remark that one should not attempt to characterize closely the felspars in sand fractions by their optical properties without a considerable amount of experience and/or the advice of a highly skilled petrologist who is used to peculiarities of these minerals. As an example of their complexities, consider the twin-laws for felspars which Burri (1962) has recently surveyed. There are now more than twenty of these, and although not all of them are commonly observed it is generally true that twinning of some form or another is very frequent amongst the felspars. Since this twinning is sometimes on a very fine scale it may very easily complicate the optical properties of a given specimen. Schiller effects due to interference from planes of segregation in the perthitic textures (or to diffusion of light by neighbouring small domains with different optical properties) add to the difficulties of examining felspars with the petrological microscope.

The main optical properties which are studied, and have been found useful for diagnostic purposes in conjunction with other kinds of data, are optic orientation (of optic axial plane relative to crystallographic axes), optic axial angle 2V, refractive indices and extinction angles. For example

the optic axial angle (2V) has frequently been plotted against weight per cent for alkali felspars with compositions from orthoclase to albite, and for the plagioclases from albite to anorthite (Tuttle, 1952; MacKenzie and Smith, 1955; J.R. Smith, 1956). On the basis of these plots it is possible to distinguish four series of minerals among the alkali felspars viz.

a. high sanidine - high albite
b. sanidine - anorthoclase
c. orthoclase - low albite
d. microcline - low albite

By contrast the 2V for plagioclases is always large but changes sign twice between albite and anorthite for low temperature plagioclases and changes both sign and magnitude substantially on heating these specimens to convert them to the high temperature structural state (J.R. Smith, 1956). The optic axial angle can therefore be used to determine composition if the thermal history of an alkali felspar is known; but the same measurement may only be used to determine thermal state if the composition of a plagioclase is otherwise known, and not vice versa.

On the other hand the curves of refractive index can be used to estimate the composition of a plagioclase, especially if it is possible to invert the specimen to the maximum high temperature form first (J.R. Smith, 1958). For the alkali felspars, however, the values of the refractive indices are quite sensitive to small amounts of the anorthite molecule in solid solution (or to traces of Ba, Sr, Rb and Fe^{3+}), and furthermore this property is fairly dependent on the thermal state or history of the specimen. Refractive index is not a particularly suitable optical property for estimating chemical composition for the alkali felspars, but is fairly useful

for the plagioclases.

This suffices to show, for the purpose of the present article, that the optics of felspars can yield information of considerable importance provided the investigator has a substantial degree of experience, and is skilful with the petrological microscope, including the use of universal stage techniques. For a detailed account of the considerable volume of recent work in this field the reader should consult Deer, Howie and Zussman (1963, Vol. IV) or similar books. As a final warning for the soils investigator it should be noted

(i) that felspars in fine sand fraction are often incipiently altered and that this interferes significantly with a proper determination of the refractive index;

(ii) that felspars in this fraction are not infrequently coated with silica (in particular) which leads to a different apparent R.I.; and

(iii) the standard staining tests for felspars do not work with reliable consistency below about 150 μ particle diameter.

These factors further complicate the use of felspar optics on fine sand fractions (H.W. Fonda, personal communication, 1966).

FELSPARS AS GEOLOGIC THERMOMETERS

The geologist and the soil scientist must observe rocks far removed from the temperatures at which they have formed; and yet if we wish to interpret correctly the partition of chemical elements between the different mineral phases in a rock system we may very well need to know quite closely the thermal history of the rocks. Fortunately the rapid or moderately rapid cooling of many systems has resulted in a "quenching" of the mineral phases

in a chemical or a structural state which is related to some former high temperature rather than present-day atmospheric temperatures. In particular the sensitivity of the felspar structures, optical properties and chemistry to temperature (and the fact that the felspars are very commonly occurring and widespread minerals) allows them to be used as geological thermometers. Various felspar thermometers have been proposed (e.g. Barth, 1962; Christie, 1962) and these proposed thermometers are slowly being refined in their reliability and general applicability.

The felspar thermometers so far proposed include the so-called "two-felspar thermometer" discussed in detail by Barth (1962). The sodium felspar albite is soluble in both the potassium felspar (orthoclase) and the calcium felspar (anorthite). During crystallisation of a rock the albite is distributed between the orthoclase and anorthite phases. The coefficient of distribution is, in fact, a constant at constant temperature and this allows one to draw up a suitable curve of temperature against the composition of the two felspar phases in a rock. That is, on the basis of the composition of these two felspars a series of rocks may be arranged reliably according to increasing temperature. It is important to note (see Barth, 1962) that the temperature given by a geologic thermometer is not necessarily the highest temperature to which the rock has been subjected. The important prerequisite is that chemical equilibrium at some definite temperature was established in the rock, prior to quenching. The quench temperature may be related in quite a variety of ways to the maximum temperature achieved.

The order/disorder transitions in plagioclase felspars (as detected by the separation of certain powder lines such as 131 and $1\bar{3}1$) have been linked with the anorthite content by Christie (1962) and others to provide

yet another geologic thermometer. The utility of this thermometer has not been fully worked out, and (like all such thermometers) the results must be used with care. Thus this plagioclase thermometer is based on structural state, in particular Si/Al order-disorder, whereas the two-felspar thermometer is based on the partition of Na between plagioclase and K-felspar. Although the two phenomena are closely related they cannot necessarily be expected to yield the same temperatures when applied to a whole series of rocks. Differences in the physico-chemical conditions of rock formation may very easily result in one thermometer reading either above or below the other - with both values being fully valid, once we can really understand precisely what temperature they are each indicating.

OCCURRENCE AND WEATHERING OF FELSPARS

A detailed discussion of the paragenesis of felspars lies within the field of geology (see, e.g., Deer, Howie and Zussman (1963)). Very briefly it can be said that "the alkali felspars are essential constituents of alkali and acid igneous rocks and are particularly abundant in syenites, granites, granodiorites, and their volcanic equivalents; the alkali felspars are also major constituents in pegmatites and in many acid and intermediate gneisses". Potassium felspar occurs in a variety of thermally metamorphosed sediments, including shales, impure sandstones, impure limestones and dolomites. Plagioclase felspars are the most common minerals of many basalts. The plagioclase in pegmatites is generally albite, and this is also the most distinctive mineral of the spilites (basic lavas). Albite is a very abundant constituent of some schists, and is also a common authigenic mineral forming contemporaneously with sedimentation.

All felspars are very apt to undergo alteration, both from hydrothermal solutions in rock systems and from the normal processes of weathering which result in primary rocks being converted to soils. There have been many field studies of rock alteration by geologists, and in parallel with this a number of studies in the laboratory of the alteration of felspars under hydrothermal conditions. For example Morey and Chen (1955) studied the action of hot water under pressure on felspars; Tchoubar and Oberlin (1963) experimentally weathered albite by water containing CO_2 in solution, and observed oriented overgrowth of boehmite using electron optical techniques; and Brindley and Radoslovich (1956) also observed the formation of boehmite on albite under mildly acidic hydrothermal conditions.(1)

The general result of these studies (in so far as they are applicable to soils) is that it is at present very difficult to predict the end-products, in a soil, of the weathering of a given felspar under certain natural conditions. The decomposition products commonly include kaolinite, halloysite, sericite, quartz, gibbsite or allophane. As Brewer (1964) discusses in some detail, however, the course of weathering depends in each case on the micro-environment - on the leaching factor locally, on the chemical micro-environment, on the accessibility to weathering for each grain. The total number of variables makes it very difficult at present to give detailed pedological explanations, even in situations where we know both the composition of the primary

---

(1) The experimental study of felspar alteration is fully summarised in Deer, Howie and Zussman (1963), Vol. IV, pp. 54-55, 127-129. The recent thesis by Pedro (1964) contains an extensive review and bibliography.

felspars and the end-products of their weathering.

Several authors have attempted to draw up tables of the comparative stability of mineral species during weathering processes leading to soil formation. Brewer (1964) has summarised these tables and has pointed out how there is a certain amount of disagreement between them due to the large number of somewhat imponderable factors operating during weathering and soil formation. Within the restricted group of felspathic minerals, however, there is general agreement with the sequence of increasing stability proposed originally by Goldich (1938), viz. calcic plagioclase, calcic-alkalic plagioclase, alkali-calcic plagioclase, alkalic plagioclase, potassium felspars, muscovite, quartz.

It is also worth noting that sodium felspar is a common authigenic mineral, forming contemporaneously with sedimentation, and that authigenic albite generally shows greater purity than albite from other sources.

There is very little written about felspar minerals in soils literature generally, and in fact most papers which have appeared have been concerned with the alkali felspars as sources of potassium for plant nutrition. A more detailed study of the reactivity of finely divided felspar particles in the presence of neutral salt and acidic solutions was made by Nash and Marshall (1957). They concluded that the apparent exchange capacity of the surface layers was a sensitive function of the ions concerned, and that (under the conditions of their experiments, at least) any poorly organized surface layer is not more than a few unit cells in depth.

The study of all the forms of potassium in soils will no doubt be an important topic in the forthcoming volume on soil chemistry of the present Handbuch. There have, however, been a reasonable number of laboratory studies

on the extraction and availability of K^+ from felspars and micas under varying conditions of temperature, pH and buffering, and over various particle size ranges. A typical recent paper is that by Stohlberg (1959), and a recent summary of forms of potassium in the soil is that of Wiklander (1955). The results of these studies can be very broadly summarized as follows. Potassium in felspars is a major source of the potassium required for plant growth in many soils. It is, however, virtually non-exchangeable K^+ by comparison with the potassium in the micaceous clay minerals, and it is acid-extractable only with considerable difficulty. Some plants (e.g. sugar cane) appear to be able to extract K^+ from felspars more readily than some of the techniques used in the laboratory; measurements of "acid-extractable" K^+ on these minerals in the laboratory are not very closely correlated with the nutrient requirements of plants in a given soil-plant-climatic environment. Potassium is more easily removed from finely divided felspars. In general, in fact, the felspars appear to make a major contribution to plant nutrition mainly by breaking down completely and fairly readily under most conditions of weathering. But an analysis for total K^+ will not be too meaningful for plant growth if the K^+ is present very largely in the form of unweathered felspars. As Jeffries et al (1956) put the matter after studying 650 surface soils in Pennsylvania:- "The most valuable soils agriculturally are those where the felspar of the very fine sand is greater than 17% and the predominant clay mineral is a low fixer of potassium".

It is almost trite to add that these are the results to be expected when the positon of the large K^+ ion in the felspar framework structures is considered in relation to the migration of K^+ through the lattice which would be necessary if there was to be any effective exchangeable K^+ available from

felspars in soils.

IDENTIFICATION OF FELSPARS IN SOILS

Brown (1962) has given tables recently of x-ray powder diffraction data for several typical plagioclases and alkali felspars, and (following Goodyear and Duffin (1954)) has suggested that a plagioclase can be distinguished from an alkali felspar by

(i) two very strong reflections in the region 3.17 - 3.22 Å

(ii) a medium reflection of spacing 6.4 - 6.5 Å

(iii) three medium to strong reflections with spacings 4.03 - 4.05, 3.74 - 3.78, and 3.61 - 3.67 Å.

Whilst these criteria are sufficient for a gross identification they certainly do not allow any more definite characterisation, e.g in terms of anorthite content and structural state for the plagioclases. This latter problem has been discussed in considerable detail by Smith and Gay (1958) (pp. 758-761) for the plagioclases. They point out that in the range from $Ab_{100}An_0$ to about $Ab_{30}An_{70}$ it is possible to determine both An content and structural state with considerable confidence by a combination of optical (universal-stage) and x-ray powder techniques (essentially the measurement of γ^* by the separation of line pairs). Both methods are relatively rapid and non-destructive. Single-crystal x-ray methods can be used to determine structural state from An_{40} to An_{100}, but these are tediously slow for general application. Finally, a more recent paper by Doman, Cinnamon and Bailey (1965) has drawn attention to some previously unsuspected ambiguities which can arise in the range An_{30} to An_{50} if the separation of line pairs on x-ray powder photographs is used to determine composition and structural state for

the plagioclase felspars. Previously it was thought that for a given composition the high and low structural states differ primarily in their γ^* values. The data of Doman et al indicate that plagioclases of very similar compositions can have differences in γ^* of 0.4° to 0.5° in the immediate vicinity of An_{33} and An_{50} and still belong entirely within the low structural state.

As Smith and Gay (1958) have emphasised, the detailed study of a plagioclase specimen requires single-crystal, powder diffraction, chemical analysis, refractive index and optical orientation data at least. This is similarly true for the alkali felspars, especially since some optical properties are sensitive to compositional impurities as much as structural state. It would seem that such a careful study of felspars in the fine sand fraction may repay handsome dividends in some particular pedological problem. It is equally true that important deductions should not be made on the basis of the observed felspar mineralogy unless the investigator is closely aware of the many inter-related complexities which are to be found in the optical, chemical and structural properties of these very interesting minerals.

REFERENCES

BARTH, T.F.W.: The felspar geologic thermometers. Norsk Geol. Tids. 42, 330 (1962).

BREWER, Roy: Fabric and Mineral Analysis of Soils. John Wiley and Sons, N.Y. (1964).

BRINDLEY, G.W., and RADOSLOVICH, E.W.: X-ray studies of the alteration of soda felspars. Clays and Clay Minerals, 4, 330 (1956).

BROWN, G. (ed.): The x-ray identification and crystal structures of clay

minerals. Mineral. Soc., London, (1961).

BURRI, C.: A survey of felspar twinning. Norsk Geol. Tids. 42, 193 (1962).

CHRISTIE, O.H.J.: Observations on natural felspars: Randomly disordered structures and a preliminary suggestion to a plagioclase thermometer. Norsk Geol. Tids. 42, 383 (1962).

DEER, W.A., HOWIE, R.A., and ZUSSMAN, J.: Rock-forming Minerals, Vol. 4. Framework Silicates. Longmans, Green and Co. London (1963).

DOMAN, R.C., CINNAMON, C.G., and BAILEY, S.W.: Structural discontinuities in the plagioclase felspar series. Am. Mineral. 50, 724 (1965).

FERGUSON, R.B., TRAILL, R.J., and TAYLOR, W.H.: The crystal structures of low-temperature and high-temperature albites. Acta Cryst. 11, 331 (1958).

FINNEY, J.J., and BAILEY, S.W.: Crystal structure of authigenic maximum microcline. Zeits. f. Krist. 119, 413 (1964).

GAY, P.: Subsolidus relations in the plagioclase felspars. Nordsk Geol. Tids. 42, 37 (1962).

GOLDICH, S.S.: A study in rock weathering. J. Geol. 46, 17 (1938).

GOODYEAR, J., and DUFFIN, W.J.: The identification and determination of plagioclase felspars by the x-ray powder method. Min. Mag. 30, 306 (1954).

HEIER, K.S.: Trace elements in felspars - a review. Norsk Geol. Tids. 42, 415 (1962).

JEFFRIES, C.D., GRISSINGER, E., and JOHNSON, L.: The distribution of important soil forming minerals in Pennsylvania soils. Soil Sci. Soc. Amer. Proc. 40, 400 (1956).

JONES, J.B., and TAYLOR, W.H.: The structure of orthoclase. Acta Cryst. 14, 443 (1961).

LAVES, F., and GOLDSMITH, J.R.: Polymorphism, order, disorder, diffusion and confusion in the felspars. Instituto Lucas Mallada, Cursillos y Conferencias fasc 8, 71 (1961).

MacKENZIE, W.S.: The orthoclase-microcline inversion. Min. Mag. 30, 354 (1954).

MacKENZIE, W.S., and SMITH, J.V.: The alkali felspars: I. Orthoclase microperthites. Am. Mineral. 40, 707 (1955).

MacKENZIE, W.S., and SMITH, J.V.: The alkali felspars: III. An optical and x-ray study of high-temperature felspars. Am. Mineral. 41, 405 (1956).

MOREY, G.W., and CHEN, W.T.: The action of hot water on some felspars. Am. Mineral., 40, 997 (1955).

MUIR, I.D.: The paragenesis and optical properties of some ternary felspars. Norsk Geol. Tids. 42, 477 (1962).

NASH, V.E., and MARSHALL, C.E.: Cationic reactions of felspar surfaces. Soil Sci. Soc. Amer. Proc., 21, 149 (1957).

NEWNHAM, R.E., and MEGAW, H.D.: The crystal structure of celsian (barium felspar). Acta Cryst., 13, 303 (1960).

PEDRO, G.: Contribution a l' étude expérimentale de l' altération géochimique des roches cristallines. Ann. Agron. 15, 13 (1964).

SMITH, J.R.: Effects of heating natural plagioclases. Carnegie Inst. Washington, Yx. Book, No. 55, 188 (1956).

SMITH, J.R.: Optical properties of heated plagioclases. Am. Mineral. 43, 1179 (1958).

SMITH, J.V., and GAY, P.: The powder patterns and lattice parameters of plagioclase felspars. II. Min. Mag., 31, 744 (1958).

SMITH, J.V., and MacKENZIE, W.S.: The alkali felspars: II. A simple x-ray technique for the study of alkali felspars. Am. Mineral., 40, 733 (1955).

STÅHLBERG, S.: Studies on the release of bases from minerals and soils. I. Release of potassium from potassium felspar and micas at contact with synthetic ion exchangers. Acta Agric. Scand., 9, 361 (1959).

TAYLOR, W.H.: The structure of sanidine and other felspars. Zeits. Krist., 85, 425 (1933).

TAYLOR, W.H.: The structures of the principal felspars. Norsk Geol. Tids., 42, 1 (1962).

TCHOUBAR, C., and OBERLIN, A.: Alteration de l´ albite par action de l´ eau. J. de Microscopie 2, 415 (1962).

TUTTLE, O.F.: Optical studies on alkali felspars. Amer. J. Science, Bowen vol., 553 (1952).

WIKLANDER, L.: Forms of potassium in the soil. Potassium Symposium, 109 (Kungl. LantbrHögsk, Uppsala, Sweden 1955).

YODER, H.S., and TILLEY, C.E.: Origin of basalt magmas: An experimental study of natural and synthetic rock systems. J. Petrol., 3, 342 (1962).

EWR/VHR

3/3/67

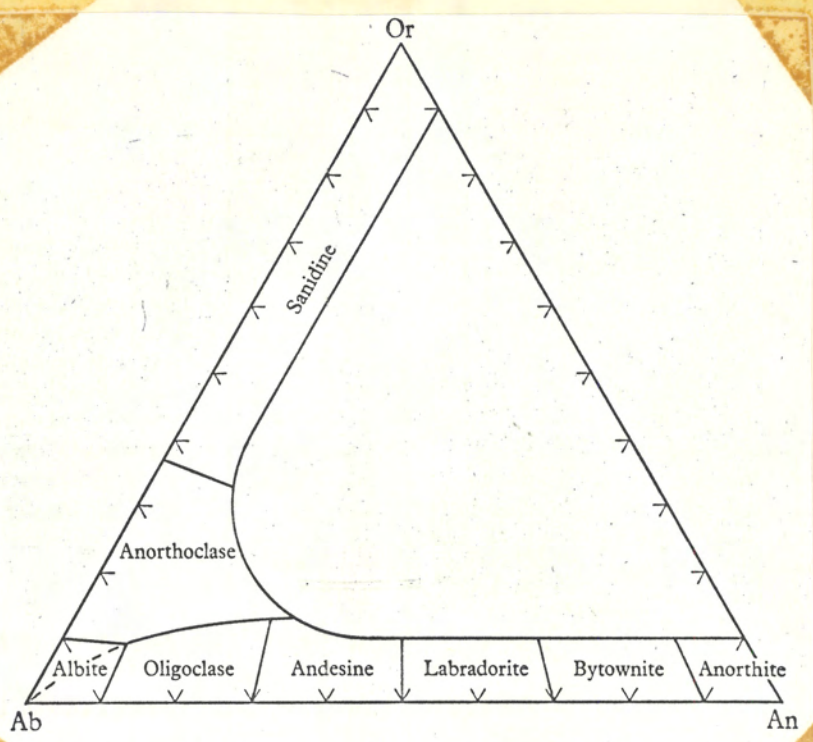

FIG. 1. Illustrating solid solution in the felspars. The nomenclature of the plagioclase series and the high-temperature alkali felspars is also shown.

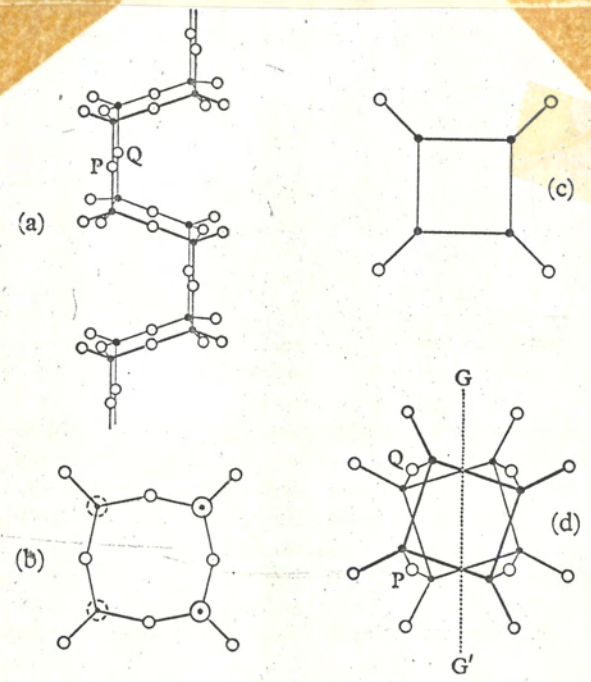

FIG. 2. Idealized illustrations of the felspar "chain" (see text) (after Taylor, 1933).

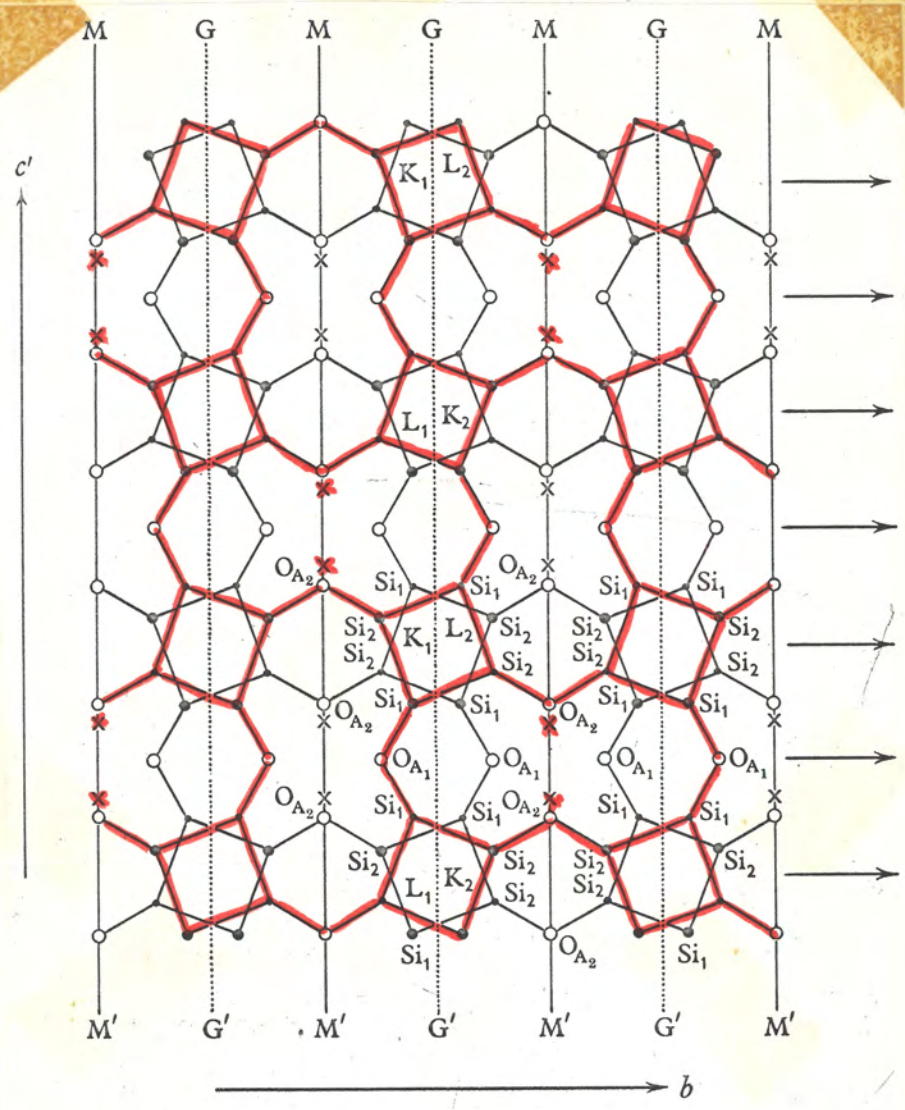

Plate 1. In black: schematic illustration of the cross linkage of the felspar "chains" to form a "sheet" in the plane $K_1L_1K_1$ of Fig. 3.
In red: similar "sheet" to that shown in black but $a/2$ below it and related to it by a vertical glide plane. This "sheet" lies in the plane $L_2K_2L_2$ of Fig. 3. Oxygens linking tetrahedra within the "chains" are not shown on this diagram. (After Taylor, 1933.)

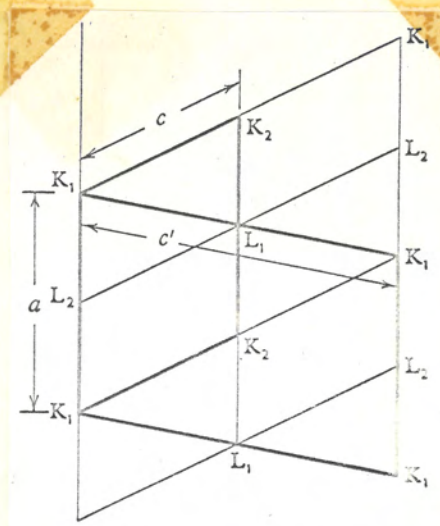

FIG. 3. (010) projection illustrating the relation of Plate 1 to the cell by which felspars are usually described. Plate 1 shows the plane $K_1L_2K_1$ as viewed along a and also shows $L_2K_2L_2$. The cell normally referred to has edges c and a.

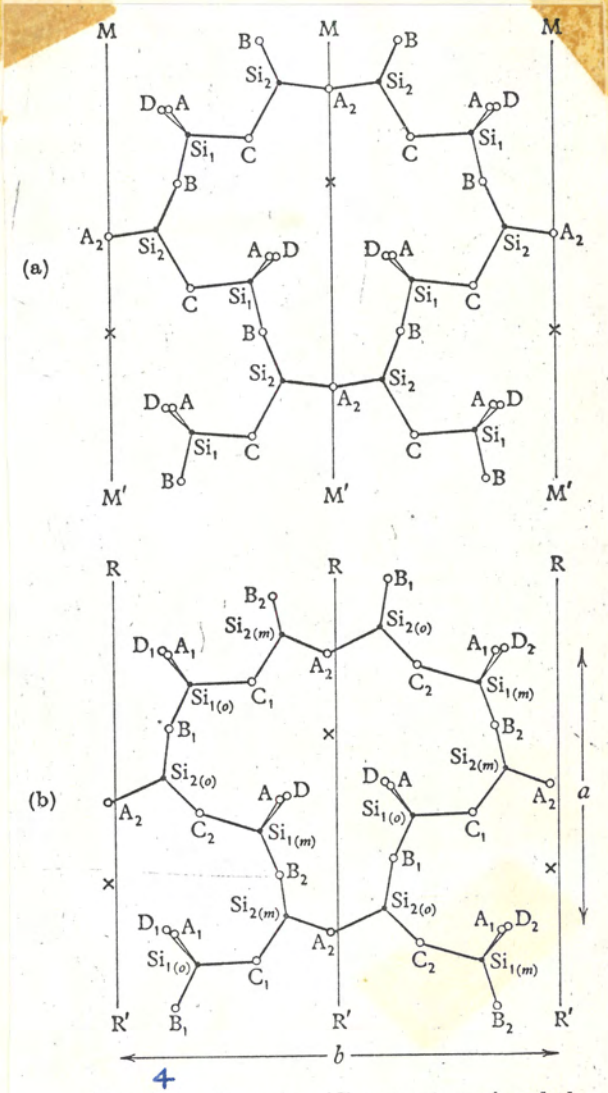

FIG. 4. Part of sanidine structure viewed along normal to (001). MM′ are mirror planes (after Taylor, 1933). (b). Part of albite structure viewed along normal to (001). RR′ are not mirror planes (after Taylor *et al.*, 1934).

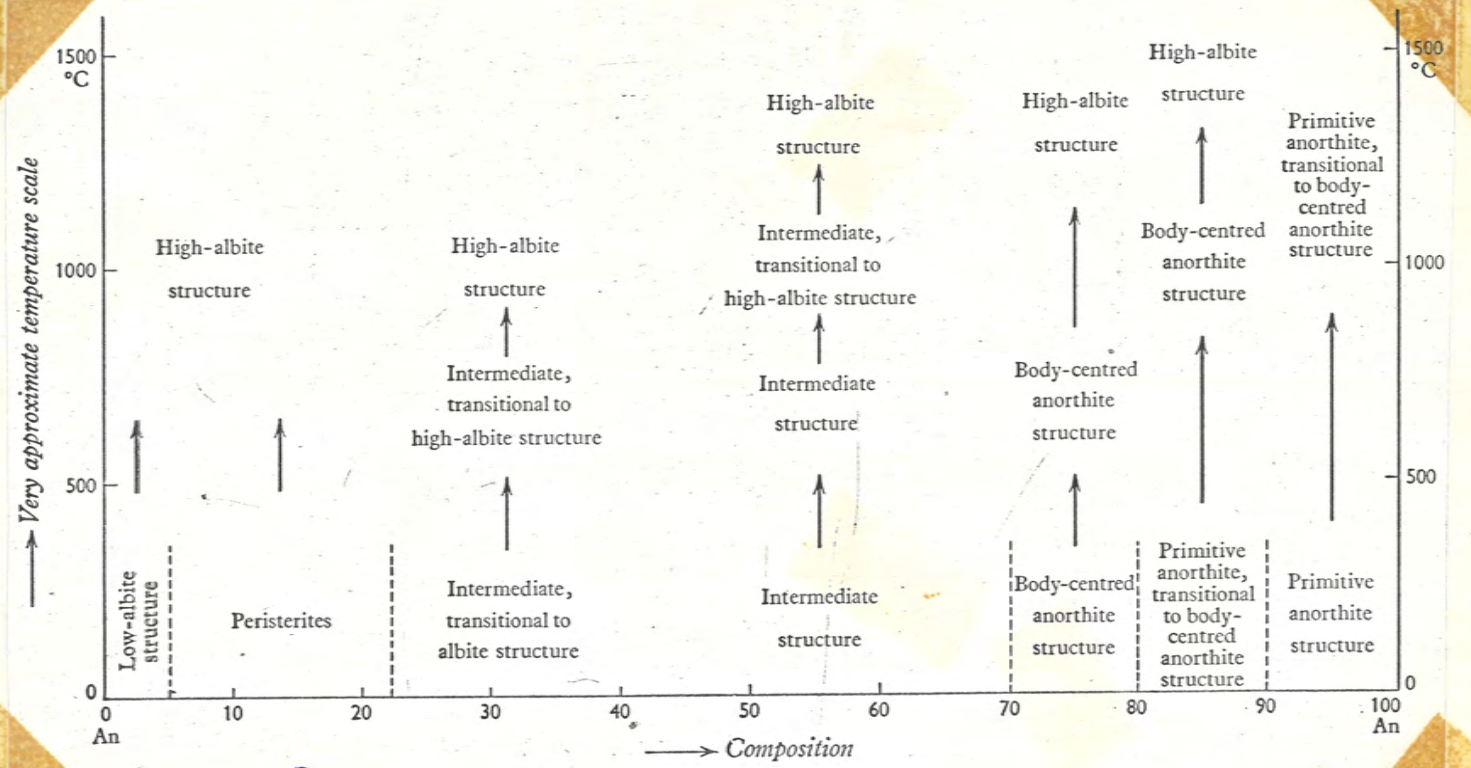

FIG. 5. Sequence of structural changes with temperature for plagioclases of various compositions.

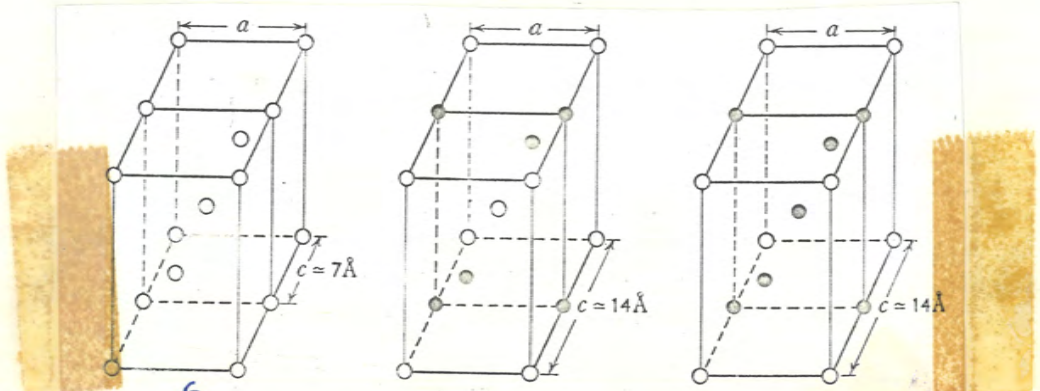

FIG. 6. Relationship between lattices of plagioclases (after Cole *et al.*, 1951). Left to right: Albite, body-centred anorthite, primitive anorthite.